Controls on slope channel-levee evolution in the Amazon Fan

Carlos Manuel de Assis Silva

Submitted in accordance with the requirements
for the degree of Doctor of Philosophy

The University of Leeds
School of Earth and Environment

October 2011

The candidate confirms that the work submitted is his own and that appropriate credit has been given where reference has been made to the work of others.

Acknowledgements

My supervisors Douglas Paton and Bill McCaffrey have given me much appreciated support and guidance throughout the past three and a half years. Advice has always been provided with optimism and enthusiasm for my research and for this I am very grateful.

I would like to acknowledge PETROBRAS for sponsoring this research, allowing me the opportunity to undertake a PhD at the University of Leeds. I would further like to thank Turbidite Research Group (TRG) for sponsoring my participation at numerous international Conferences and Claire Keevil for her continued help. My colleagues from E&P (Margem Equatorial) of PETROBRAS have been very helpful in providing useful information and data for this thesis. I owe much gratitude to them.

I acknowledge BP for donating the 3D data to the University of Leeds and ANP for selling me the 2D data. Without these data, it would not be possible to develop this research.

I offer many thanks to the precious friends that I made in Leeds: Joanna Hansford, Phill Kellman, Claire McDonald, Joana Costa, Bruno Simoes, Mariagrazia Berloco, Serena Rapisarda, Arthur Galamba, Marina Campelo, Dulce Vargas and Karen Pascal, who have all provided me with many happy memories of England.

Special thanks go to my dearest friends Francesco Giorgio-Serchi and Luciana Genio for the pleasant and happy work environment that we had in the "Latin Quarter" during the last year.

I would like to thank my great friend, Viviane Santos, for always giving me incentive to go on and for solving all my problems in the Southern Hemisphere, hence making it possible for me to carry on "life" in Brazil during these years.

Finally, but by no means least, I am grateful for my whole family in Brazil, who motivated and helped me to keep going. Particularly, I thank my parents Francisco e Cely, for their love and support throughout my life wherever they are, to whom I dedicate this thesis.

Abstract

Submarine channel-levee architecture is a result of interaction between turbiditic flows and the bathymetry that they encounter on the slope and that they themselves construct. However, the spatio-temporal evolution of channel-levee systems, i.e., their manner of spatial accretion is not fully understood. In addition, the controls on the patterns of channel distribution and stacking remain relatively poorly understood.

The results presented in this thesis are based on the interpretation of a 3D seismic survey located in water depths of about 1000 to 2000 m on the upper slope of the Amazon Fan. The analysis of the data includes two different approaches: on a larger scale, the interpretation of the tectono-stratigraphic analysis of the data; and on a smaller scale, the characterization of the evolution of the channel-levee systems and associated deposits. The methods of analysis used included the mapping of significant horizons and the extraction of sequences horizon slices across the channel-levee systems. The horizon slices allowed visualisation of the vertical distribution of the channel-levee elements and interpretation of their evolution.

The seismic data can be divided in two main packages, separated by an unconformity. The pre-unconformity package is characterized by a predominant sub-parallel seismic facies (characterized by continuous, homogeneous and sub-parallel reflections), and is strongly folded and faulted due to gravity tectonics. In this interval, no channel-levee systems were identified, but canyon-like channels with dimensions as large as 2600 m wide and 220 m deep were observed. Conversely, the post-unconformity package comprises a heterogeneous arrangement of seismic facies, and is less strongly deformed. Three upslope-stacked channel-levee systems of Middle Pleistocene age can be distinguished in this interval. Each channel disperses obliquely down the slope, resulting in levee size asymmetry, with the downslope levee being of greatest size. The upslope stacking of channel-levee systems results from a sequence of avulsions on the upslope levees. Bathymetric influence of the older channel levee system is interpreted to dictate the slope-oblique orientation of the new channel.

Two main architectural styles were identified, each one associated with different models of spatio-temporal development of channel-levees. A pattern of upstream accretion of the aggradational (channel-levee) component of the channel is associated with the channel narrowing and becoming more sinuous upward. This style is characterized by an onlapping pattern of channel and levee reflections. Downstream accretion of channel-levee is associated with a trend of channel widening and becoming less sinuous upwards. This style is characterized by a downlap pattern of the channel and levee reflections. Each style is related to different evolutionary histories of the turbidite flows and thalweg configuration in relation to the equilibrium profile.

Three styles of channel distribution on slope can be distinguished: structurally controlled erosive channels, aggradational channels obliquely oriented to the slope and agradationally confined channels that are vertically stacked. The pre-unconformity erosive channels are diverted and possibly owe their erosive character to active anticlines that kept the paleo-slope above the equilibrium profile. The oblique direction of each channel in the post-unconformity interval was inherited from the previous one in a sequence of upslope stacking after systematic avulsion through the left-hand levee. The vertical stacking of channel-levee elements is due to the confinement of the channel between the outsize downslope levee and an upslope anticline which inhibited avulsion in the area. It is probable that each stacked channel-levee element corresponds to a downstream channel avulsion.

This study provided important information about the architecture and distribution of channels on the upper-slope of submarine fans subject to gravitational tectonics. Therefore, it can be used as an analogue and help the prediction of sand prone areas in other submarine fans which are not so well imaged.

Contents

List of Figures

List of Tables

1 INTRODUCTION

1.1 Thesis Rationale

Large submarine fans are constructed by the vertical and lateral stacking of channel-levee systems, and associated deposits combined with variable degree mass wasting deposits (Kolla and Coumes, 1987; Leeder, 1999; Schwenk et al., 2005; Weimer, 1990). Submarine channels have been recognized as important depositional elements of large submarine fan systems, allowing the conduction of gravity flows, which carry sediments to deep basins and build up the submarine fans (Damuth et al., 1988). Pelagic and hemipelagic sediments deposit with relatively low deposition rates when the fan becomes inactive during highstand (Leeder, 1999), hence they are not volumetrically important constituents of the majority of submarine fans. The architecture of the channels records both erosion and deposition related to gravity flows whose characteristics (e.g. magnitude, composition, density) may vary, combined with changes in the slope morphology induced by tectonics, channel avulsions, and aggradation (Kneller, 2003; Pirmez et al., 2000). Channel evolution, therefore, can provide evidence of gross submarine fan evolution through their temporal and spatial alterations in geometry. These changes may be controlled by sea level changes, sediment flux variations, tectonics and climate change (Flood and Piper, 1997; Pirmez et al., 2000).

Submarine channels have economic importance in that they are a target of hydrocarbon exploration and production (Deptuck et al., 2003; Kolla et al., 2001; Mayall et al., 2006; Mayall and Stewart, 2000; Posamentier and Kolla, 2003; Prather, 2003). Although there have been numerous studies focused on channel-levee architecture, the spatio-temporal evolution of slope channels and the controls on patterns of channel distribution on slope are still not fully understood (Clark and Cartwright, 2009).

Some studies describe an upward transition from an erosional channel style to an aggradational channel-levee style on the slope (e.g. Deptuck et al., 2003). Kneller (2003) suggests that theoretically channels may evolve from being erosional to aggradational and *vice* versa, under the influence of changes in flow parameters on the equilibrium profile (with channels being either

erosional, at grade or aggradational, depending on whether the inherited profile is above, at, or below the equilibrium profile, respectively). These authors, however, do not show how the transitions spatially occur, i.e., the way the channel evolves passing from erosional to aggradational along its length in a determined time interval, and what the architectural record of this transition may be. Moreover, channel-levee systems are normally interpreted to accrete downstream, taking into account the upstream source of flow and their downstream tendency of becoming thinner. However, the internal architecture of the channel-levee systems that illustrate downstream accretion and the upstream limit of the channel-levee (the transition to the feeder erosive channel/canyon) are not satisfactorily described. Some questions emerge from these observations: could an upstream accretion of the channel-levee occur? If so, which channel-levee geometries and associated controls (flow characteristics and changes in equilibrium profile) would account for downstream *versus* upstream accretion?

Controls on patterns of channel distribution on the slope have been commonly been associated with sea-floor relief, which in most of the cases has a tectonic origin (Babonneau et al., 2004; Damuth, 1994; Gee and Gawthorpe, 2006; Hodgson and Haughton, 2004; Morgan, 2004; Smith, 2004a). However, the timing of slope deformation and the implications on channel orientation and/or style, however, have not been described in detail (though see Clarke and Cartwright, 2010). For instance, the channel orientation on slope can be oblique to the main slope dip. Channel obliquity on the slope has been attributed to structural controls (e.g. Kane, 2007) but other controls such as marine currents and paleo-bathymetry inheritance from previous deep marine deposits should also be considered and discussed.

The Amazon Fan has been extensively mapped using seismic-reflection profiles, long-range side-scan sonar (GLORIA) and Sea Beam multibeam bathymetry. This mapping has shown that it was built by a complex pattern of submarine channel-levees and large debris flows (Damuth and Flood, 1983, 1985; Damuth et al., 1988; Damuth et al., 1983b; Flood and Damuth, 1987; Flood et al., 1991; Manley and Flood, 1988). Most of the sedimentological studies on the Amazon Fan, however, are located downslope from the study area which samples part of the regime of compressional structures mainly

developed in the upper and mid slope. Therefore, the study 3D seismic data offers an exceptional opportunity to understand the interrelationships of slope deformation and channel evolution. The turbidite systems are additionally extremely well imaged in seismic reflection profiles, allowing a detailed analysis of channel-levee architecture together with their relationships to other slope deposits.

1.2 Thesis objectives

The aim of this thesis is to characterize styles of channel-levee architectures and the controls on their evolution. There are three specific objectives:

i) Establish an evolutionary history of slope deposition during the Quaternary, using the upper slope of the Amazon Fan as a case history. This study includes the investigation of the following aspects:

a) The tectono-stratigraphy of the area;

c) Characterization of channel styles;

d) The interplay between structures and channels;

e) The relationship between the channel-levees, the associated mass transport deposit (MTD) and high amplitude reflection packets (HARPs).

ii) Identify variability in the spatio-temporal development of channel-levee systems on slope and relate them to interpreted forcing mechanisms. This includes the following:

a) To demonstrate how changes in the equilibrium profile might favour or not the development of each model;

b) To interpret how the evolution of flow parameters with time (magnitude, grain-size composition, flow efficiency) might influence the development of each model.

iii) Identify controls on patterns of channel distribution (orientation and stacking) on the slope, including:

a) To explain how the growing structures can affect channel styles and orientation;

b) Elucidate why the Middle-Pleistocene channels are orientated oblique to the main slope dip;

c) Establish possible controls on the observed patterns of channel-levee stacking.

In order to accomplish these objectives, a detailed analysis of a 3D seismic data set from the upper slope of the Amazon Fan was performed. Moreover, analysis of the seismic volume was put into the structural-stratigraphic context of the Fan by tying the 3D data into a 2D seismic line across the slope and by correlation with the literature.

Although the Amazon Fan is one of the best studied submarine fans in the world, previous studies focused on areas downslope of the current study area, where the slope gradients are small and there are only minor gravity tectonic effects (Fig. 1.1). The study area, however, is appropriate for study because it is located in the upper slope and not only presents very well developed channel-levee systems but also shows gravity induced deformation. Therefore, the analysis of this 3D seismic data allows the interpretation of the channel-levee system evolution and a better comprehension of the interaction between tectonics and channel-levee development, which are objectives of this research.

The unavailability of boreholes piercing the seismic volume or that could be reliably tied to the 2D line did not allow the direct calibration of the seismic facies with the lithology. Therefore, the calibration of the seismic facies with the correspondent lithofacies was indirect and based on the description of the Quaternary package of the Amazon Fan in the Ocean Drilling Program leg 155 (Normark et al., 1997). Although there is some imprecision on the characterisation of the lithology of each seismic facies, the geometry of the seismic reflections and relative amplitude identified (e.g. HARs, levee reflections, HARPs, etc) have been recognized not only in Amazon Fan but also in many other submarine fans such as the Niger Delta, Indus, Bengal and Zaire (Babonneau et al., 2002; Deptuck et al., 2003; Heiniö and Davies, 2007; Schwenk et al., 2005). Hence, the lack of a precise rock calibration of the seismic reflections is interpreted to not strongly hinder the current work because the lithological and process significance of each depositional element could be interpreted by analogy with the literature. Ideally, an accurate calibration of the rock characteristics would allow a better interpretation of the flow variability

during the build up of each of the channel-levee architectures and their patterns of accretion and this represents a limitation to the current analysis. Details of the description of the seismic facies and lithotologic meaning are presented in Chapter 4.

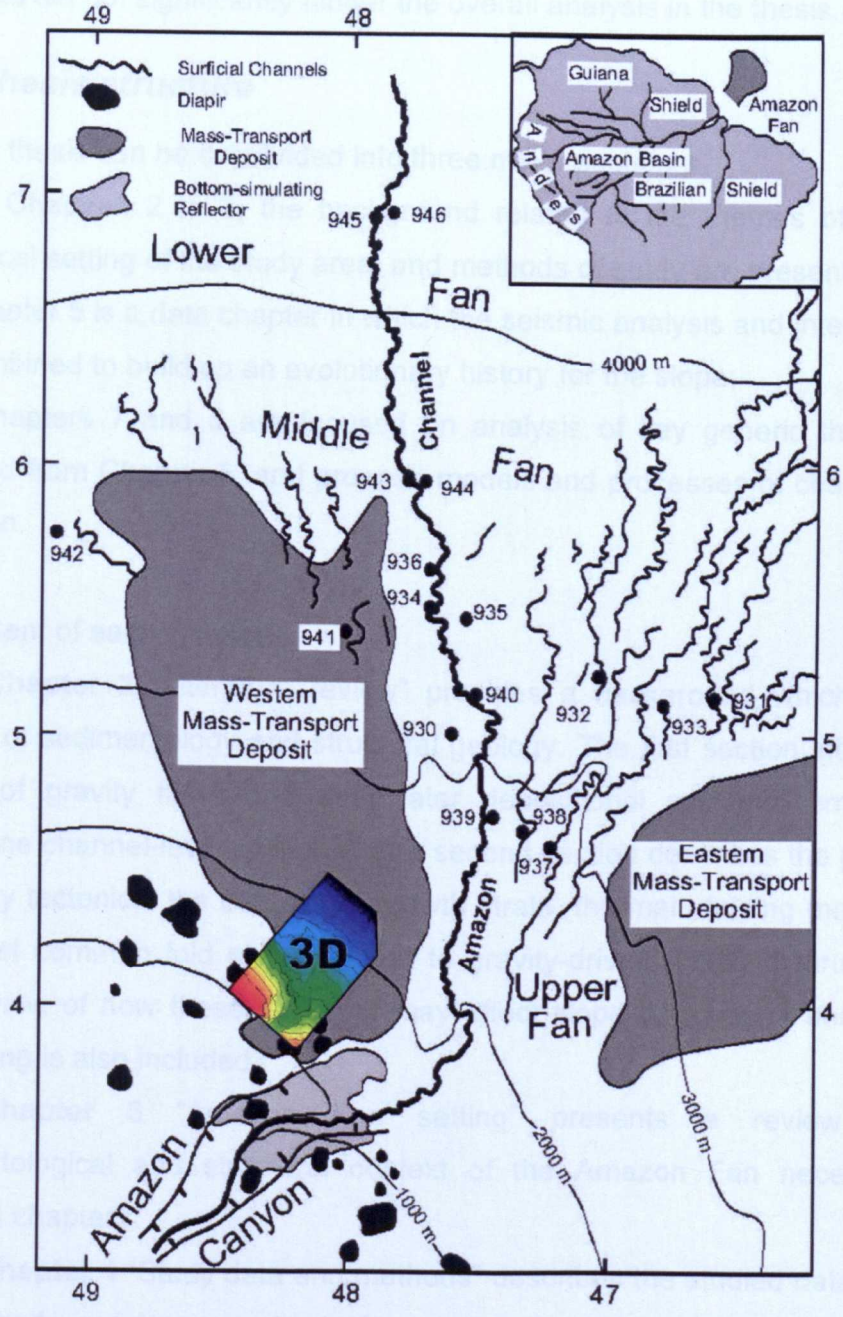

Figure 1-1 – Location of the 3D seismic data in the Upper Amazon Fan. The map also shows the location of the boreholes (used in ODP Leg 155), and the main surficial fan components, e.g., channel systems, Amazon Canyon and mass transport deposits. The Amazon Channel is the most recently active channel on the Amazon Fan (modified from Normark et al., 1997).

The seismic reflections located upslope or underneath the Quaternary channel-levee systems could not be correlated to any lithologic data because no typical geometry was identified and related to calibration examples elsewhere. These areas, however, were not the principal focus of study, thus they also did not significantly hinder the overall analysis in the thesis.

1.3 Thesis structure

- The thesis can be subdivided into three major sections:

I – In Chapters 2 to 4, the background related to the themes of research, geological setting of the study area, and methods of study are presented;

II – Chapter 5 is a data chapter in which the seismic analysis and interpretations are combined to build up an evolutionary history for the slope;

III – Chapters 7 and 8 are focused on analysis of key generic themes that emerged from Chapter 5, and propose models and processes of channel-levee evolution.

- Content of each chapter:

Chapter 2 "Literature review" provides a background which includes themes of sedimentology and structural geology. The first section introduces a review of gravity flows and deepwater depositional systems, emphasizing submarine channel-levee systems. The second section describes the processes of gravity tectonics, the concept of growth strata, the main folding mechanisms and most common fold styles related to gravity-driven fold and thrust belt. A brief review of how these tectonics may affect slope bathymetry and channel positioning is also included.

Chapter 3 "Amazon Fan setting" presents a review of the sedimentological and structural context of the Amazon Fan necessary for following chapters.

Chapter 4 "Study data and methods" describes the studied data set, and the methods used (e.g. seismic interpretation). This chapter also gives an overview of the tectono-stratigraphic framework, outlining the mapped horizons, and the geological implications of the main seismic facies identified.

Chapter 5 "Slope evolution in the study area" describes the local tectono-stratigraphy, the structural framework and the different styles of

submarine channels, emphasizing the channel-levee architectures. This chapter provides an evolutionary model for the stacked channel-levee system of the Middle Pleistocene in the study area.

Chapter 6 "Spatio-temporal evolution of channel-levee/architecture" details the architectural styles of the identified channel-levee systems and proposes two models of channel accretion on slope. Distinct controls to the upstream and downstream models of channel-levee accretion are proposed by relating the models to different configurations of the equilibrium profile and changing flow parameters.

Chapter 7 "Controls on patterns of channel distribution" describes how the channels may be oriented, distributed and stacked on slope, taking into account controls such as the presence of tectonic structures, marine currents and of autocyclic depositional processes (e.g. avulsion).

Chapter 8 – "Discussion" brings together the themes presented in previous chapters, providing a broad overlook of the thesis and debates the aspects of theories developed as a result of the detailed analysis and interpretation. This also includes a discussion of the complete evolution of the slope and suggestions for further work.

Chapter 9 'Conclusions' provides a summary of the conclusions of this study.

2 LITERATURE REVIEW

The literature review for the current research must necessarily include both tectonic and sedimentary components of the deep-marine slope environment. Bearing this in mind, the review is divided in four sections which include submarine channel development, gravity-driven deformation on submarine slopes, interaction between the channels and the deformation and final remarks, focussing upon areas that are not yet fully understood.

2.1 Submarine channels: processes and architectures

2.1.1 Introduction

Submarine channels are the most important pathway for sediment transported by turbidity currents from the shelf to the basin. Their dimensions and internal architecture supply information about the gravity flow processes involved in channel body build-up and about related submarine fan development. Their architectures may record both erosion and deposition, with the erosional or depositional tendency arising both from the transmission of different types of submarine gravity flows (which may vary in volume, sediment composition and rheology) and from changes in slope induced by regional or local structural deformation and by channel avulsions. Moreover, submarine channel-levees are economically important because they have been recognized as important hydrocarbon reservoirs, and their study has applications in both exploration and development scenarios (e.g., Beaubouef, 2004; Deptuck et al., 2003; Hickson and Lowe, 2002; Mayall et al., 2006; Mayall and Stewart, 2000).

Research on modern submarine channel-levee systems has revealed important insights regarding depositional processes, geometries and lateral facies relationships, but relatively little insight regarding the vertical stacking patterns and internal facies architecture of these deposits (Hickson and Lowe, 2002). On the other hand, outcrop studies of ancient deposits can be used to better evaluate the facies and architecture of submarine channel-levee fill (Cronin et al., 2000a; Hickson and Lowe, 2002; Walker, 1985). Therefore, during recent years, the understanding of channel-levee depositional systems has been driven by intense research on both ancient and recent/modern

channels, using high quality 3D seismic (e.g., Abreu et al., 2003; Deptuck et al., 2003; Deptuck et al., 2007; Gee and Gawthorpe, 2006; Klaucke et al., 1997; Kolla et al., 2001; Mayall et al., 2006; Mayall and Stewart, 2000; Pirmez et al., 2000) and outcrop analysis (e.g., Clark and Pickering, 1996b; Eschard et al., 2003; Gardner et al., 2000; Kane et al., 2007; Kneller and McCaffrey, 2003; McCaffrey et al., 2002) together with other data sources such as acoustic imaging of sea floor side scan sonar (Hickson and Lowe, 2002; Klaucke et al., 1997) and laboratory experiments (e.g., Kane, 2007; Kneller and Buckee, 2000; Kneller and McCaffrey, 1999; Peakall et al., 2000).

In this section the main characteristics of submarine channels, including geometry, sinuosity, stacking pattern and internal architecture will be discussed, taking into account possible controls such as gravity flow processes, structural features and slope bathymetry, with reference to both modern and subsurface channel-levee systems.

2.1.2 Gravity flows

Types and classification

Gravity and friction are the main controlling factors on channelized flow (Clark and Pickering, 1996b). The outcome of the interaction of these factors (further influenced by the volume and density of suspended sediment) can lead to either the erosion and/or additional incorporation of sediment in the flow, deposition (such as overbank or channel fill sedimentation) or bypass without erosion.

Based on their rheology, sediment-fluid mixtures display either fluid or plastic behaviour. In the influential classification scheme of Lowe (1979), the associated flows are denominated fluidal and debris flow; a further subdivision of gravity flows can be made, into turbidity currents in which the sediment is supported by flow turbulence; fluidized flows in which the sediment is fully supported by upward moving pore fluid; liquefied flows in which the sediment is not fully supported but settles through the pore fluid that is displaced upward; grain flows in which the sediment is supported by dispersive pressure arising from particle collisions; and cohesive flows in which the sediment is supported by cohesion (Table 2-1 and Table 2-2).

Table 2-1– Nomenclature of laminar sediment gravity flows based on flow rheology and particle support mechanisms (Lowe 1979).

FLOW BEHAVIOUR	FLOW TYPE		SEDIMENT SUPPORT MECHANISM
FLUID	FLUIDAL FLOW	TURBIDITY CURRENT	FLUID TURBULENCE
		FLUIDIZED FLOW	ESCAPING PORE FLUID (FULL SUPPORT)
		LIQUEFIED FLOW	ESCAPING PORE FLUID (PARTIAL SUPPORT)
PLASTIC (BINGHAM)	DEBRIS FLOW	GRAIN FLOW	DISPERSIVE PRESSURE
		MUDFLOW OR COHESIVE DEBRIS FLOW	MATRIX STRENGTH MATRIX DENSITY

Table 2-2 - Nomenclature of both laminar and turbulent sediment gravity flows (Lowe 1979).

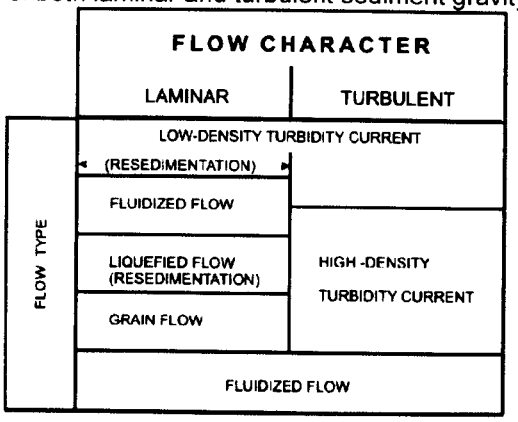

In fact there has been much debate around the classification of gravity flows and related deposits (Kneller, 1995; Middleton, 1993; Mulder and Alexander, 2001; Shanmugam, 1996). Another influential scheme (Mulder and Alexander, 2001) is a classification of density flows based on cohesivity of particles and particle support mechanisms, related to likely deposit characteristics (Fig 2.1). In this scheme subaqueous density flows are divided into cohesive flows and frictional or non-cohesive flows. Cohesive flows are divided into debris flow and mud flows on the basis of the sediment size distribution, whereas mud flows are subdivided into clay-rich and silty mud flow. Non-cohesive flows are subdivided into hyperconcentrated density flows, concentrated density flows and turbidity flows, and these are further subdivided on the basis of duration into surges, surge-like flows and quasi-steady currents. It is worth mentioning that flow transformations can occur with distance (down and across flows) and with time (Fig. 2.2).

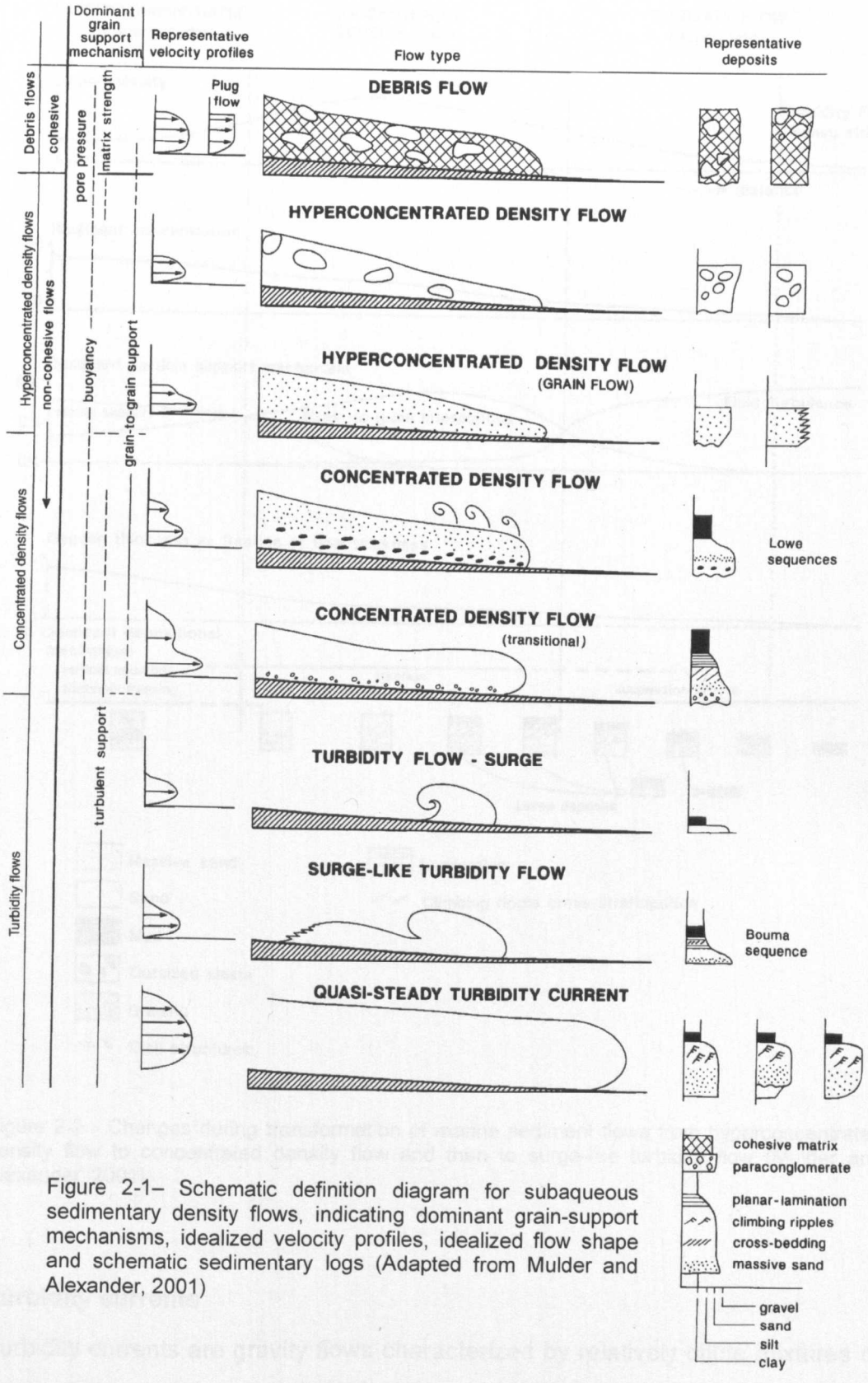

Figure 2-1– Schematic definition diagram for subaqueous sedimentary density flows, indicating dominant grain-support mechanisms, idealized velocity profiles, idealized flow shape and schematic sedimentary logs (Adapted from Mulder and Alexander, 2001)

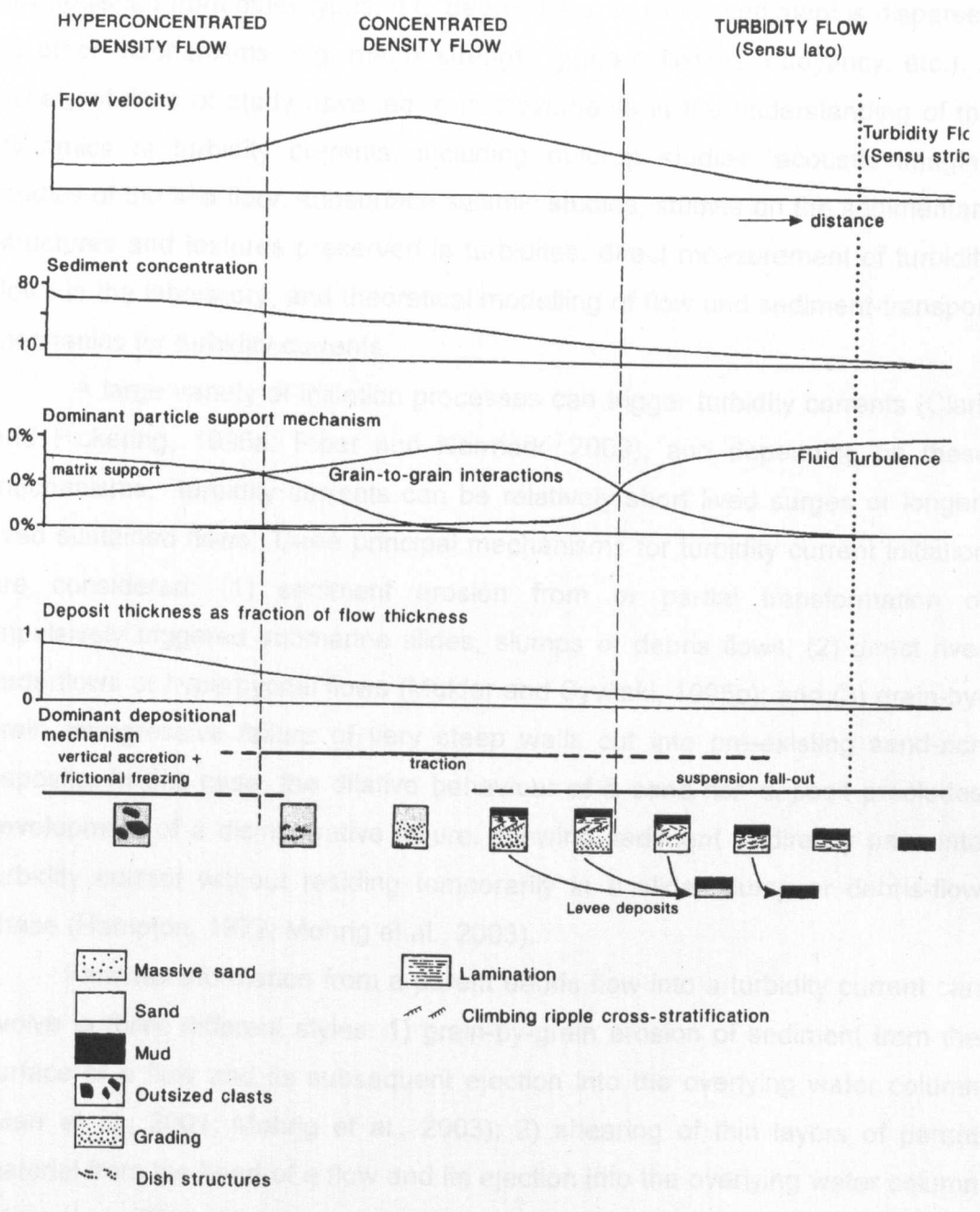

Figure 2-2 - Changes during transformation of marine sediment flows from hyperconcentrated density flow to concentrated density flow and then to surge-like turbidite flow (Mulder and Alexander, 2001).

Turbidity currents

Turbidity currents are gravity flows characterized by relatively dilute mixtures of water and sediment in which most of the particles are suspended in the flow by upward directed turbulent eddies (Mohrig et al., 2003). They can be

distinguished from other types, e.g. debris flows, in which sediment is dispersed by other mechanisms (e.g. matrix strength, grain collisions, buoyancy, etc.). A variety of lines of study have led to improvements in the understanding of the dynamics of turbidity currents, including outcrop studies, acoustic imaging studies of the sea floor, subsurface seismic studies, studies on the sedimentary structures and textures preserved in turbidites, direct measurement of turbidity flows in the laboratory, and theoretical modelling of flow and sediment-transport mechanics for turbidity currents.

A large variety of initiation processes can trigger turbidity currents (Clark and Pickering, 1996a; Piper and Normark, 2009), and depending on these mechanisms, turbidity currents can be relatively short lived surges or longer-lived sustained flows. Three principal mechanisms for turbidity current initiation are considered: (1) sediment erosion from or partial transformation of impulsively triggered submarine slides, slumps or debris flows; (2) direct river underflows or hyperpycnal flows (Mulder and Syvitski, 1995b); and (3) grain-by-grain retrogressive failure of very steep walls cut into pre-existing sand-rich deposits. In this case, the dilative behaviour of a sand-rich deposit precludes development of a disintegrative failure, allowing sediment to directly pass into turbidity current without residing temporarily in a slide, slump or debris-flow phase (Hampton, 1972; Mohrig et al., 2003).

Flow transformation from a parent debris flow into a turbidity current can evolve in three different styles: 1) grain-by-grain erosion of sediment from the surface of a flow and its subsequent ejection into the overlying water column (Marr et al., 2001; Mohrig et al., 2003); 2) shearing of thin layers of parent material from the head of a flow and its ejection into the overlying water column (Marr et al., 2001; Mohrig et al., 2003); and 3) the turbulent mixing of ambient water into the head of a parent flow causing dilution and local transformation to a turbidity current (Hallworth et al., 1993; Marr et al., 2001; Mohrig et al., 2003).

Turbidity flow characteristics

Many turbidity currents are unsteady surges, while others are long-lived, more or less steady flows; both are capable of erosion or deposition (Middleton, 1993). Flows range from hundreds of meters thick, carrying many cubic kms of sediment, to thin dilute currents. They experience drag on the upper and lower

bounding surfaces, in contrast to open-channel flows which experience insignificant drag on the upper surface. This dictates the position of the maximum velocity and hence the sediment distribution within the flow (Fig. 2.3). Based on gravity surge experiments, a typical gravity current can be divided into three parts, head, body and tail (Middleton, 1966a, b, 1967).

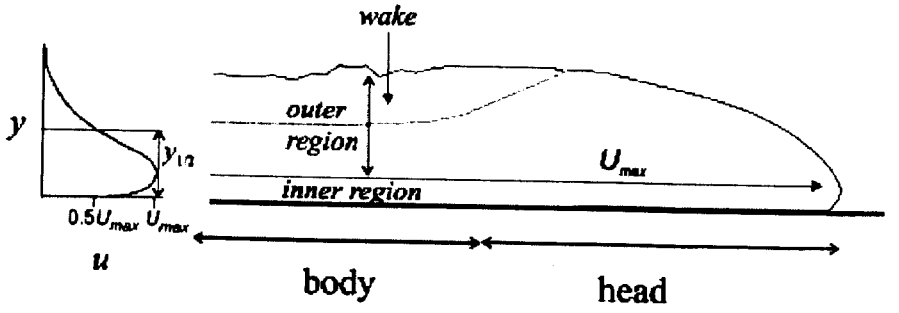

Figure 2-3 – Schematic diagram of the head and body of a turbidity current, showing the typical downstream velocity profile (Kneller and Buckee, 2000)

The dynamics of the head are important, in that they may set a condition for the current as a whole (Simpson & Britter, 1979, cited in Kneller and Buckee 2000); the head may commonly be erosive, when the rest of the current is not. The downstream velocity within the body of the current is dependent on the slope, and has been shown to be up to 30-40% faster than the head velocity (Kneller and Buckee, 2000; Kneller and McCaffrey, 1999; Kneller et al., 1997). This is because, for the head to advance it has to displace the ambient fluid. The ambient fluid is generally at rest and has a resistance to the flow which is larger than the friction on the bed of the current or the upper interface with the surrounding fluid (Middleton, 1993). As a consequence, the head of the current is generally thicker than the current behind the head and its height increases with slope, as the body velocity increases and material moves more quickly into the head (Middleton, 1993, Hopfinger and Tochon-Danguy, 1977; Britter and Linden, 1980; Simpson, 1997 in: Kneller and Buckee, 2000).

Several studies have evaluated the development and significance of density stratification of flows (produced by vertical gradients in suspended-sediment concentration (Kneller and Buckee, 2000; Kneller and McCaffrey, 1999; Middleton, 1993; Peakall et al., 1998), because it is important for understanding submarine channel process, and consequently, channel

evolution. Turbidity currents are density stratified, e.g., there is a vertical gradient in concentration, entailing a denser basal layer of fluid and sediment with a less dense, portion above, although a range of patterns of concentration are recognised (Kneller and Buckee, 2000; Peakall et al., 2000). Turbulence intensities are highest at the top of the turbidity current, and related to large scale shearing and mixing at the upper boundary. Low turbulence intensities and low kinetic energy are observed around the level of the highest velocity or the high density gradient near the base of the current (Kneller and Buckee, 2000).

2.1.3 Deep marine depositional systems

Deep marine sedimentary environments may be defined as those sedimentary systems, which extend from the shelf break towards the basin. The largest deep marine depositional systems occur on passive margins, which normally have very low slope-gradients, e.g., the Mississipi and Niger systems (O'Grady et al., 2000). The Louisiana Slope has a regional gradient of 0.5° (Pratson and Haxby, 1996) and the Amazon Fan slope averages 0.8° in the upper fan, 0.3° in the middle fan and 0.1° in the lower fan (Damuth et al., 1988).

The primary controls on the development of deepwater depositional systems are sediment supply, regional basin tectonics and sea level fluctuations (Fig. 2.4). This implies that submarine fans reflect a wide variety of allocyclic and autocyclic controls (Reading and Richards, 1994; Richards and Bowman, 1998; Richards et al., 1998; Stow et al., 1996). These result in a large number of fan types, such that no single model can be used to describe their variability in facies, sandbody geometry, reservoir architecture and seismic signal.

A basic assumption of depositional models in the context of sequence stratigraphy is that sedimentation increases within deep water systems during relative sea-level lowstands (Posamentier and Vail, 1988; Wagoner et al., 1990). It is assumed that during periods of relative sea-level fall, there is erosion of the exposed shelf and also the transport of sediment by fluvial systems with deposition in deep-marine environment beyond the shelf-break, instead of deposition on the shelf. During sea-level fall, therefore, there are enhanced rates of deep-marine deposition, mainly increasing the sand content. Although this assumption is widely applied (Mitchum et al., 1994), there is some evidence

of turbidite deposition during the Holocene transgression in the Mississppi Fan and Navy Fan (Piper and Normark, 1983a). Turbidite deposition also occurs throughout the Holocene transgression and highstand on the Bengal Fan (Kuehl et al., 1989; Weber et al., 1997). On the Zaire Fan, the Zaire Canyon cuts across the shelf into the Zaire River estuary hence the canyon is connected to the river mouth, even at the present time of high sea level. In this case, recent turbidity currents or gravity flows within the modern Zaire Canyon-Channel have been documented (Khripounoff et al., 2003). Thus in these cases, local conditions such as high fluvial discharge or headward erosion of submarine canyons promote sediment transport from the shelf into deep water even at sea-level highstand.

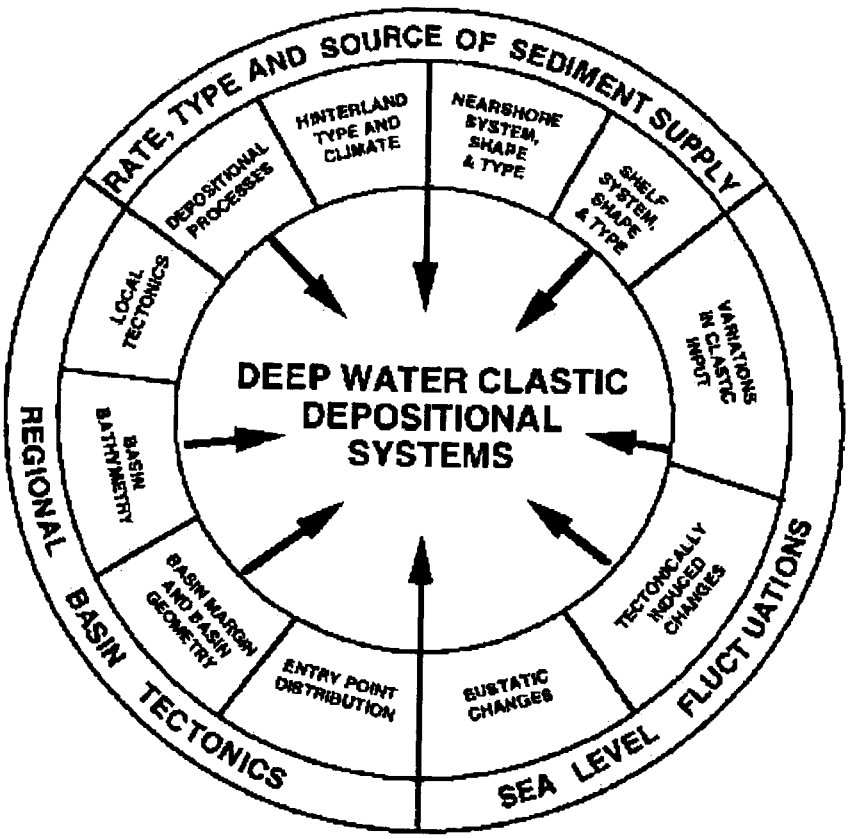

Figure 2-4 - Controls on the development of deep-marine clastic systems, from Richards et al. (1998). The deep-marine clastic systems are the product of a complex interaction between allocyclic and autocyclic controls. They are rarely mutually exclusive but normally independent of each other.

In the case of the Amazon Fan, during the Holocene the sediment brought from the Amazon River and delivered by buoyant plumes was and still is redistributed along the South American Atlantic Shelf by marine current. Thus the shelf transport dynamics substantially reduce shore-normal delta progradation and further delivery to the Amazon Canyon (Nittrouer et al., 1986). The reconstruction of the bottom water circulation in the Southern Hemisphere (Sykes et al., 1998) shows that since the Early Miocene there was a Northwestward marine current along the Brazilian coast. Therefore, the build up of the Amazon Fan (late Miocene age) may have occurred mainly during lowstand sea level.

2.1.4 Common seismic facies within submarine slope systems

The seismic facies that commonly occur in most of slope systems are mainly related to channel-levee systems and associated deposits such as inter-channel lobes ("high amplitude reflection packages": HARPs) and mass transport deposits (MTDs). The geometric configuration of the reflections in seismic facies of channel-levee systems is presented in Weimer (1991) (Fig.2.5).

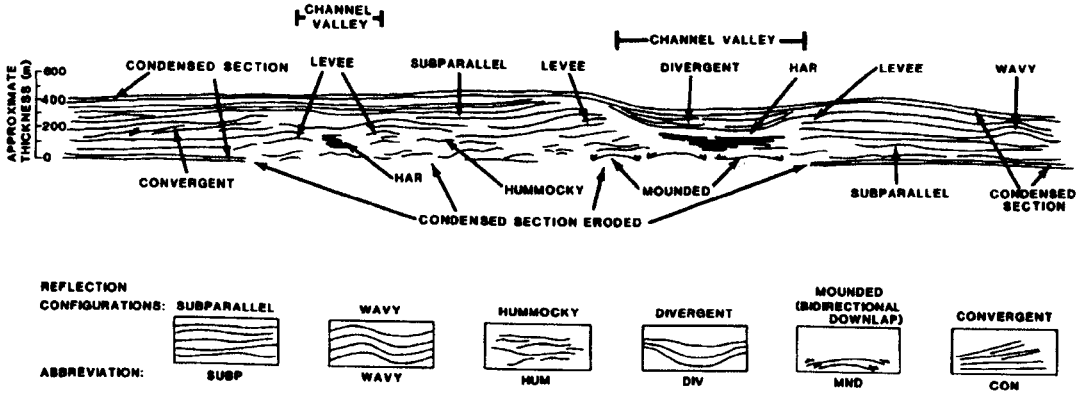

Figure 2-5 – Line drawing of a seismic profile illustrating seismic facies of channel-levee systems, and condensed sections, from Weimer (1991).

It is worth mentioning that the association of seismic facies with the depositional facies is not only based on the amplitude attribute but also on the geometry of the deposit. Channel-levee systems are large, acoustically semitransparent, lens-shaped overbank deposits with a channel close to the centre (Fig. 2.6). The levees are seismically characterized by low to moderate

amplitude, continuous to discontinuous reflections, and in some cases are completely transparent. The term high amplitude reflections (HARs) is commonly used to describe high amplitude seismic reflections located within the channel-belt (Deptuck et al., 2003) (Fig. 2.6). Stacked sets of high amplitude reflections (HARs) can mark channel axes. The HAR pattern commonly appears to extend deep within the channel-levee system and its presence and distribution within the levee has been used to map the evolution of the channel-levee system (Kastens and Shor, 1986; Stelting, 1985). This facies has been associated with sands and gravels in the channel axis which can be massive to graded sand sequences, e.g. Mississipi and Amazon fans (Lopez, 2001; Stelting et al., 1985).

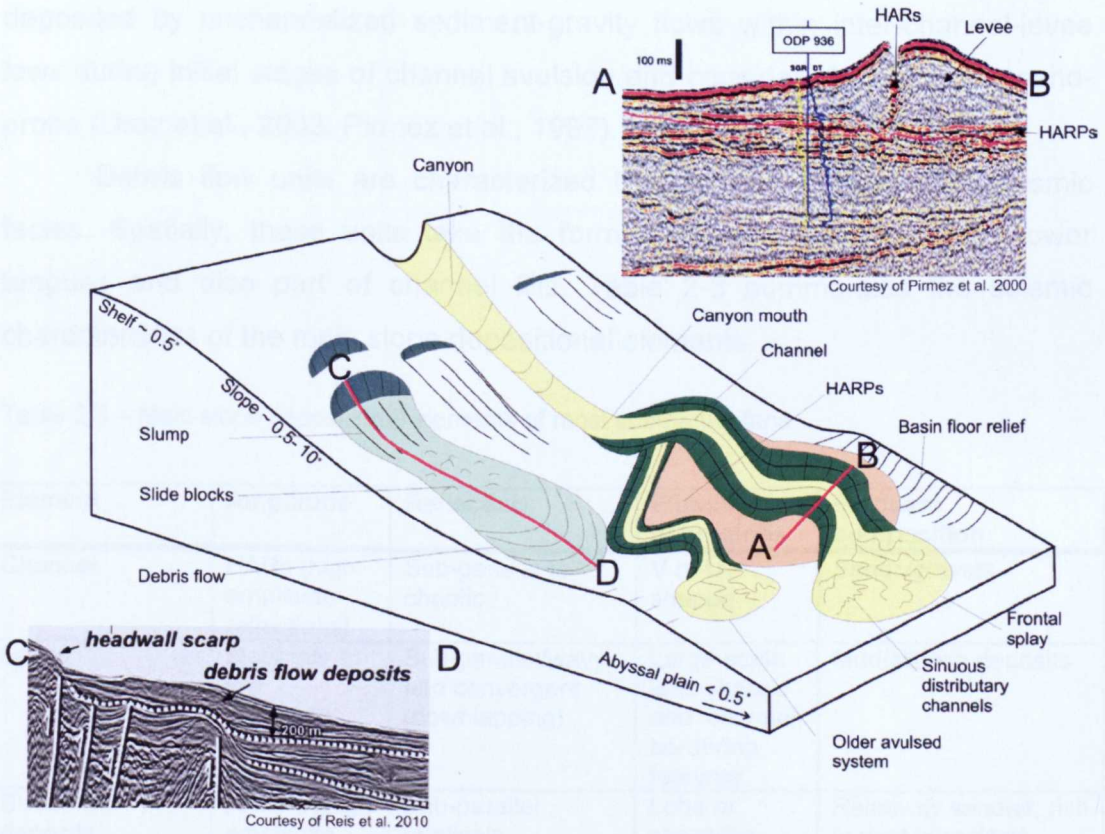

Figure 2-6 – Schematic diagram illustrating the main sedimentary systems and features of the continental slope to basin floor transition. Modified after Kane (2007). The seismic sections across the channel-levee (AB) and the MTD (CD) show some of the main seismic facies described in the Amazon Fan: HARs, HARPs, lower amplitude, continuous to discontinuous reflections of the levee and almost transparent facies of the MTD.

High amplitude reflection packets (HARPs) consist of seismically high-amplitude units composed of relatively continuous to somewhat discontinuous reflections (Droz et al., 2003; Flood et al., 1991; Kenyon et al., 1995; Pirmez et al., 1997; Schwenk et al., 2003) (Fig. 2.6). The top of a HARP unit constitutes a downlap surface for a overlying channel-levee system and its base may conform to the underlying unit or truncate it (Droz et al., 2003; Flood et al., 1991). HARPs infill relative lows located in positions inter-channel-levee systems. These deposits can have thicknesses ranging from less than 20 m to a few hundred meters; they can extend for several hundreds of kilometres toward downslope and their width depends on the widths of the pre-existing inter channel-levee lows (Kolla, 2007). These units are interpreted to be deposited by unchannelized sediment-gravity flows within inter-channel-levee lows during initial stages of channel avulsion and considered to be highly sand-prone (Droz et al., 2003; Pirmez et al., 1997).

Debris flow units are characterized by chaotic to transparent seismic facies. Spatially, these units take the form of widespread sheets, narrower tongues and also part of channel fills. Table 2-3 summarizes the seismic characteristics of the main slope depositional elements.

Table 2-3 – Main slope depositional elements of most submarine fans

Element	Amplitude	Reflection	Element geometries	Frequent composition
Channel	HARs (high amplitude reflections)	Sub-parallel to chaotic	V or U-shaped	Sands/gravels
Levee	Moderate to low amplitude reflexions	Sub-parallel/wavy and convergent (downlapping)	Large-scale lens-shaped and channel bordering features	Mud/silt rich deposits
Sheet-like deposits between channel-levee systems	HARPs (high amplitude reflection packets)	Sub-parallel relatively continuous	Lobe or sheet-like The top boundary is a downlap surface	Relatively sandier, rich in mud intraclasts
MTD (mass transport deposits)	Moderate to low amplitude	Chaotic to transparent	Widespread sheets to narrower tongues	Slump and Debris flow deposits
Pelagites and hemipelagites	High amplitude reflection	Sub-parallel and continuous	Pervasive thin reflections	Carbonate rich muds - condensed section

2.1.5 Canyon

Submarine canyon systems are common features of continental slopes. They are large-scale incisions (hundreds of meters deep, up to several kilometers wide and hundreds of kilometers long), affecting the morphology and connecting the upper slope directly to the shelf edge (Lewis & Barnes1999; Canals 2004; Baztan et al. 2005). They are generally narrow and V-shaped incised in lithified rock or sediment (e.g. Zaire Canyon, described in Babonneau et al. 2002) (Fig. 2.7) and display greater cross-sectional areas and higher axial gradients than channels (Wynn et al., 2007).

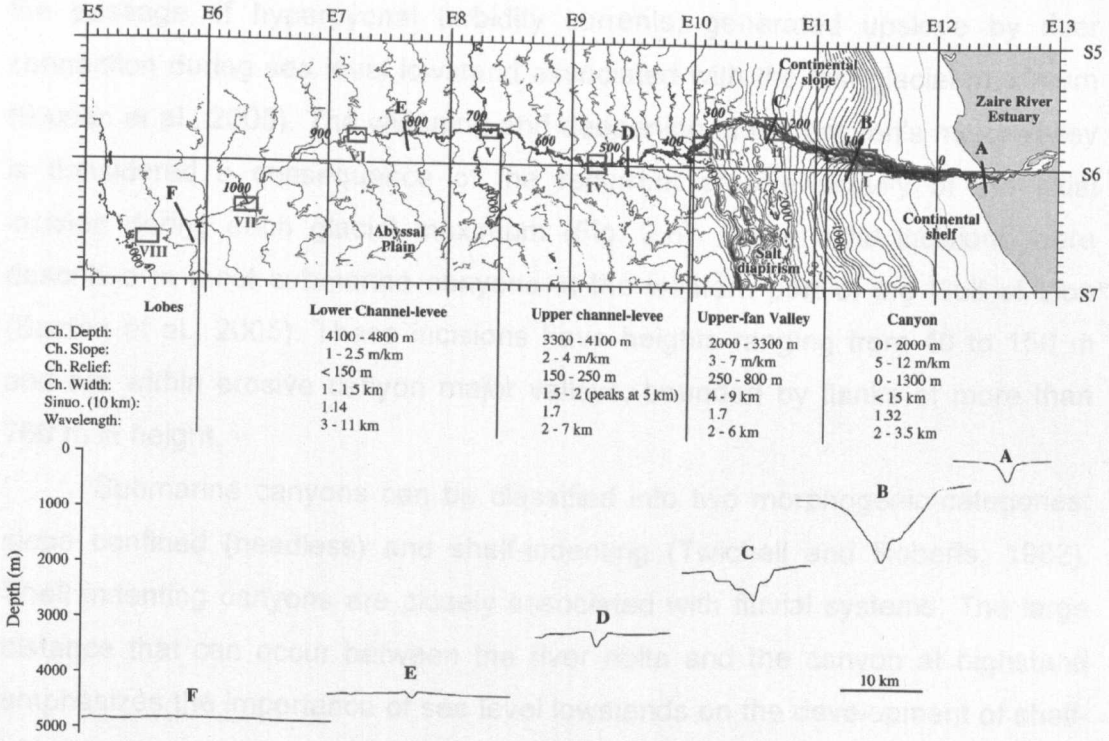

Figure 2-7 – Bathymetric contour map showing the morphology changes of the canyon/channel from the Zaire River mouth to the distal lobe, from Babonneau et al. 2002.

The erosive processes involved in creating canyons have been studied with increasing detail for several decades using marine geological and geophysical techiniques (Mitchell, 2005; Pratson et al., 1994a; Twichell and Roberts, 1982). Fluvial incision during sea-level lowstands may initiate canyon growth, e.g. Trinity Canyon and others on the northern California continental slope which have been initially incised during the lowstand associated with the last glacial maxima (Spinelli and Field, 2001). Canyon incision due to erosional passage of turbidity currents (Daly, 1936) has been proposed in modern

canyons of the New Jersey continental slope (Pratson and Coakley, 1996; Pratson et al., 1994b). Twichell and Roberts (1982) proposed that canyons are eroded by turbidity currents but also by retrogressive mass wasting of the slope. Wilmington Canyon in eastern USA is an example of retrogressive slope failure of relatively unconsolidated sediments (Pickering et al., 1989). Other possible occurrences are canyons cut by tsunamis (Bucher, 1940), submerged glacial valleys (Shepard, 1933) and structurally controlled canyons (Berryhill, 1981; Kenyon et al., 1978).

Axial incision within canyons is interpreted as the erosive path related to the passage of hyperpycnal turbidity currents, generated upslope by river connection during sea level lowstand associated with the last glacial maximum (Baztan et al., 2005). The widening and deepening of the canyon's major valley is considered a consequence of the recurrent erosive activity of the axial incision during each glacial maximum (Fig. 2.8). Some axial incisions were described in most submarine canyons in the western part of the Gulf of Lion (Baztan et al., 2005). These incisions have heights ranging from 40 to 150 m and are within erosive canyon major valleys, bounded by flanks of more than 700 m in height.

Submarine canyons can be classified into two morphogenic categories: slope confined (headless) and shelf-indenting (Twichell and Roberts, 1982). Shelf indenting canyons are closely associated with fluvial systems. The large distance that can occur between the river delta and the canyon at highstand emphasizes the importance of sea level lowstands on the development of shelf-indenting submarine canyons. Thus, fluvial down-cutting in association with turbidity currents is often considered to be the main cause of canyon generation (Fig. 2.8). On the other hand, slope-confined canyons require alternative mechanisms of formation because many are located hundreds of meters below the shelf break, and therefore, beyond the influence of lowstand shelf incision. Causes such as retrogressive landsliding e.g. Wilmington Canyon, eastern USA (Pickering et al., 1989), fluid venting and tide bottom currents have been considered (Ridente et al., 2007; Shanmugam, 2003).

Canyons are conduits of sediments captured in the shelf or slope through a variety of mechanisms, which are not mutually exclusive. They can be fed by sediment eroded due to submarine slides, slumps or debris flow, which may

transform into turbidity current toward downslope (Heezen, 1952; Weaver et al., 1992). Canyons can also be fed by direct river underflows (hyperpycnal flows) (Mulder and Syvitski, 1995a). Rivers with extremely high sediment load can develop continuous hyperpycnal turbidity currents when entering a body of standing water. The Zaire Canyon is an example which transports turbidity currents mainly generated by the hyperpycnal flow fed from the estuary of Zaire River (Fig. 2.7). Finally, longshore currents and coastal advection of mud to canyon heads are source of sediments captured by the canyon. There are many examples in the Californian borderland including Hueneme, Mugu, Dume, La Jolla, Santa Monica, Redondo and San Pedro canyons (Moore, 1965; Normark et al., 1998; Paull et al., 2005; Piper et al., 1999).

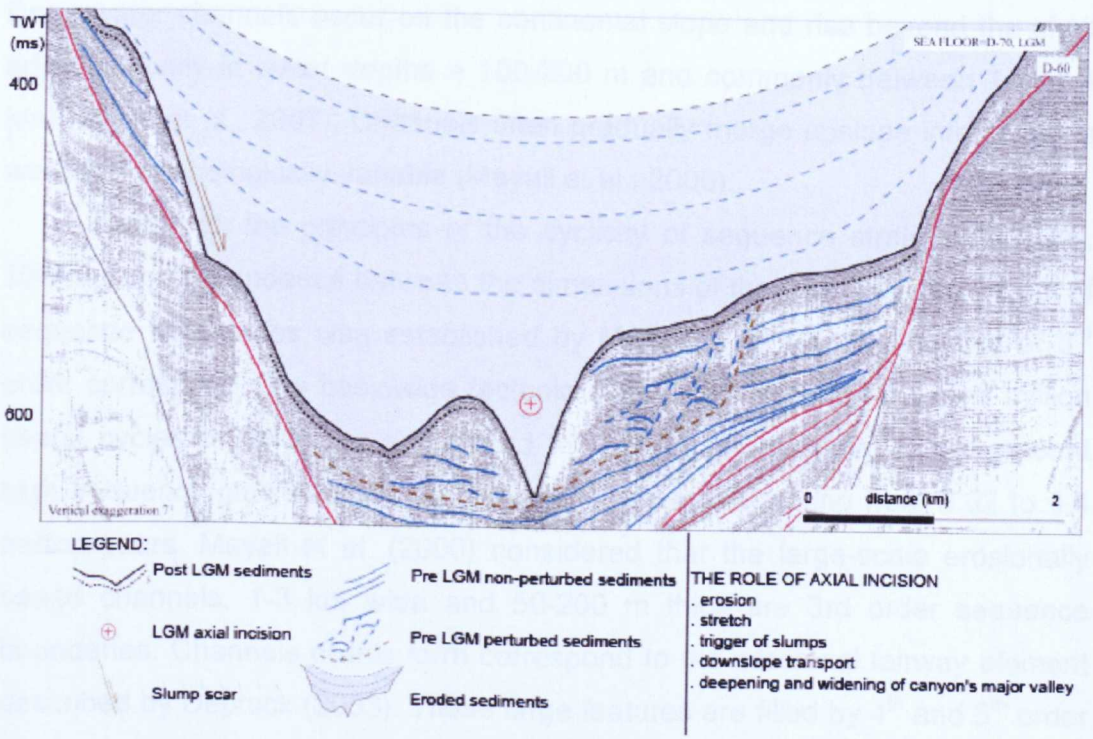

Figure 2-8 - Detail of seismic line showing the role of the axial incision (reproduced from Baztan et al., 2005). The axial incision induces instabilities in canyons through erosion. In the vicinity of the axial incision, there are perturbed stretched sediments related to the axial incision activity. This perturbation triggers major slumps. Those slumps have eroded a large amount of sediments that have been subsequently transported downslope by the axial incision. Notice that LGM is "Last glacial maximum".

At the canyon mouth flows may spill out onto splays or terminal lobes, with or without distributary channels (Babonneau et al., 2002) or they may feed into channel systems that may travel significant distances across the continental rise and abyssal plain (Chough and Hesse, 1976; Horn et al., 1971).

2.1.6 Channels

Channels are considered by Abreu et al. (2003) to be long-term conduits for sediment downslope, as defined also by Mutti (1977), regardless of the degree of erosion or confinement. They were also previously defined by Mutti and Normark (1991) as elongate depressions on the sea floor that are long-term pathways for sediment transport. Channels and their flanking levees, are commonly referred to as channel-levee systems (Flood and Damuth, 1987). Deep-water channels occur on the continental slope and rise beyond the shelf edge (typically in water depths > 100-200 m and commonly between 1 and 4 km) (Wynn et al., 2007). Channels often gradually merge upslope into canyons and are morphologically variable (Mayall et al., 2006).

Based on the principles of the cyclicity of sequence stratigraphy (Vail, 1987), a correspondence between the dimensions of the channels and orders of sequence boundaries was established by Mayall et al. (2006). Cycles of 3rd order correspond to a basinwide tectonic origin, and last from 0.4 to 3 million years; cycles of 4th order correspond to parasequence cycles that represent high frequency glacio-eustatic or autocyclic processes lasting from 0.02 to 0.4 million years. Mayall et al. (2006) considered that the large-scale erosionally based channels, 1-3 km wide and 50-200 m thick are 3rd order sequence boundaries. Channels of this form correspond to the erosional fairway element described by Deptuck (2003). These large features are filled by 4th and 5th order minor channels with recurring characteristics that can be used to predict the distribution of facies inside these 3rd order channels (Fig. 2.9).

Based on studies of submarine channel architecture, Clark & Pickering (1996) described the two end-members of a range of depositional models that have been described and fit between erosional architecture and aggradational (or depositional) channel models. These two end-members (erosional and aggradational channels) are discussed and illustrated in the section 2.1.10.

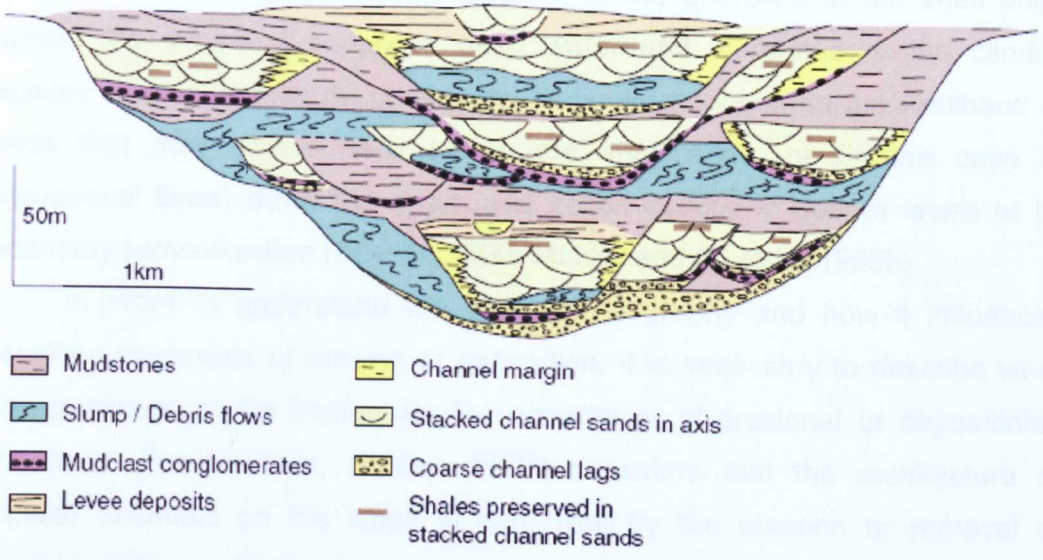

Figure 2-9 - Summary model showing the potential reservoir distribution and heterogeneity patterns in a large 3rd-order erosional channel. Each channel is unique but can be interpreted by considering: the sinuosity, the 4 main facies (basal lags, slumps, high N/G channels, channel levee), repeated cutting and filling, stacking patterns (Mayall et al., 2006).

2.1.7 Equilibrium profile

It has been noted that in common with subaerial systems, turbidite systems generally develop a graded profile in which the axial gradient of the system progressively decreases, asymptotically approaching zero (e.g., Pirmez, 2000 and references therein). The concept of the equilibrium gradient embodies the idea that the boundary conditions of the system dictate an idealised profile, and that the system evolution from an inherited profile can be interpreted as an attempt to develop such a profile. An important aspect of this study is the recognition that changes in flow properties can cause changes in the equilibrium profile of the whole system, that in turn that can affect the architectural evolution of turbidite channel systems (Kneller, 2003). Properties such as flow size, grain size of the transported particles and flow density are fundamental controls on channel evolution. In the absence of external factors such as base level and tectonics, or whether channels are erosional or depositional depends on variations in flow properties alone (Kneller, 2003). However, as the flow magnitude is dependent on the sediment availability, the sediment volume delivered to deep water and the ratio of sand and mud are strongly influenced by the base level and climate changes, flow character is strongly related to sea level and climate (Kneller, 2003). Flow character is

related to sea level because the distance of the shoreline to the shelf edge impacts the sediment supply in deep water and is related to the climate because of its influence on continental sediment supply, and the likelihood of floods that may deliver sediment to the shelf edge, or (in the case of hyperpycnal flows) down the slope, and hence directly to deeper levels or by secondary remobilisation (Kneller, 2003; Mulder and Syvitski, 1995b).

In order to understand the slope physiography and how it influences prevailing processes of erosion or deposition, it is necessary to describe what the equilibrium profile implies for the occurrence of erosional or depositional processes. For instance, Kneller (2003) considers that the architecture of turbidite channels on the slope is controlled by the creation or removal of accommodation, which is the gap between the equilibrium profile and the inherited sediment surface (Fig. 2.10).

Flow density, flow thickness and maximum settling velocity have been considered to be the main factors that determine flow efficiency, and hence the ideal equilibrium profile. Discrepancies between the inherited and ideal slope profile cause process responses that tend to bring the actual profile closer to the equilibrium profile (Kneller, 2003).

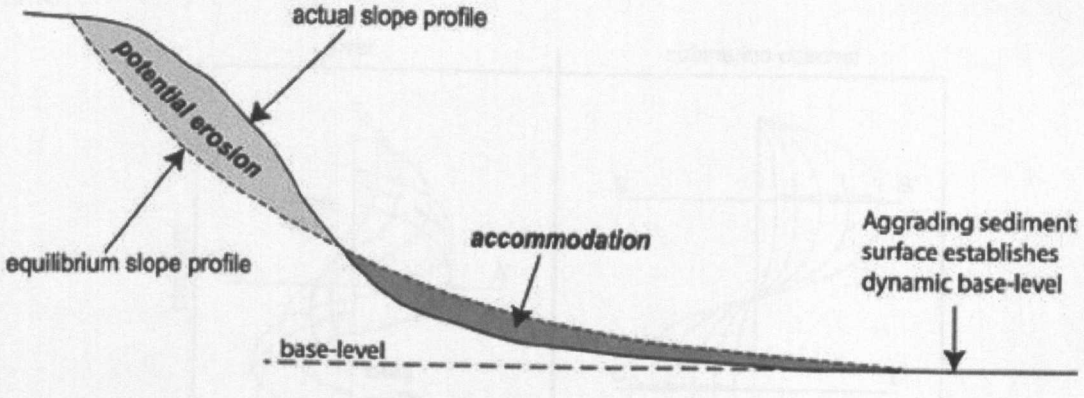

Figure 2-10 - Equilibrium profile in relation to actual slope profile (modified from Samuel et al., 2000, cited in: Kneller, 2003).

Channels aggrade if there is accommodation, which is generated by decreasing the flow density or thickness, or increasing the grain size which steepens the gradient. On the other hand, increasing the flow density or thickness, or decreasing the grain size reduce the slope gradient and remove accommodation, allowing the development of subsequent erosional channels

(Kneller, 2003). Therefore, "at grade" channels are those at or close to the equilibrium profile and represent a system that approximates to a steady state condition; both aggradational and erosional channels evolve in response to changes in flow size, density and/or grain-size. In other words, depositional gradients vary with transported grain-size distribution, flow density (concentration), thickness, rates of lateral flow expansion, and degree of containment by bounding slopes (Smith, 2004b).

2.1.8 Planform evolution

Channel sinuosity is measured as the ratio between the channel axis (centre line) length, and the overall down-channel distance for a given segment of a channel (Wynn et al., 2007). It has been recognized that the planform patterns of many leveed channels range from moderate to high sinuosity (Clark et al., 1992; Damuth et al., 1988; Flood and Damuth, 1987; Posamentier and Kolla, 2003). On the basis of the seismic data of the Mississippi channel (Kastens and Shor, 1986; Peakall et al., 2000; Stelting et al., 1985) it was suggested that the presence of both lateral (swing) and down-system (sweep) channel drift (Fig. 2.11), coupled with aggradation, accompanies increased channel sinuosity with time.

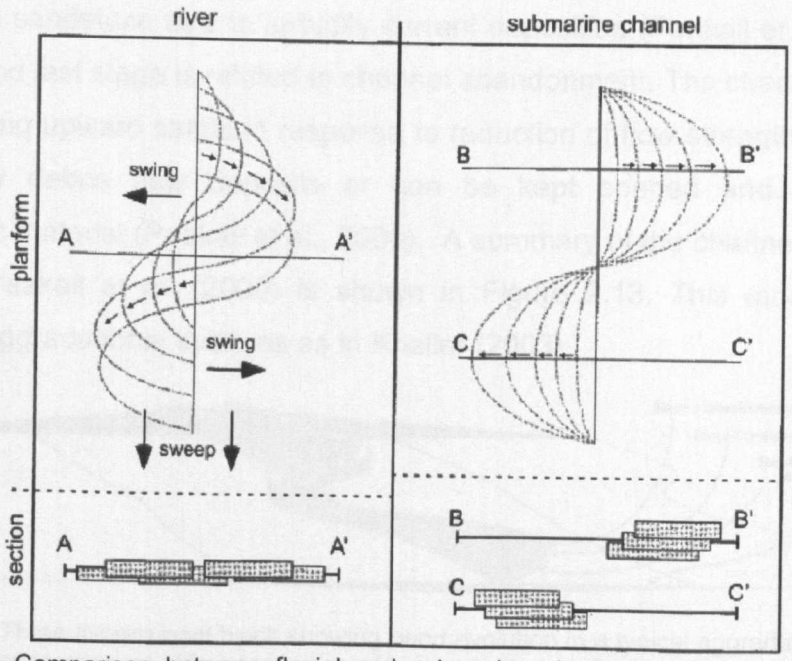

Figure 2-11 – Comparison between fluvial and submarine channel evolution (from Peakall, 2000). River channels initially have approximately straight thalwegs but start increasing amplitude by lateral translation (swing) and downstream bend translation (sweep).

Peakall et al. (2000) proposed a three stage model of submarine channel architecture) (Fig. 2.12). The first stage, when there is bend growth, lateral deposition of channel thalweg deposits occurs at bend apices, i.e. development of point bars with lateral accretion surfaces well defined.

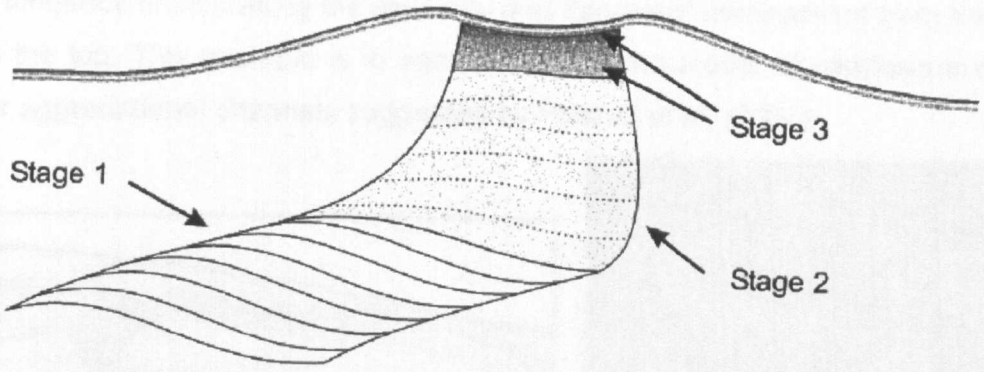

Figure 2-12 – Three stages of development of submarine channel. 1) Lateral migration at bend apices, characterized by clinoforms; 2) equilibrium phase, aggradational when the channel is working as a bypass zone; 3) channel abandonment, fining up sequence with a cape of hemipelagic, from Peakall et al.,(2000).

The second stage starts when the channel reaches the equilibrium planform, with almost vertical aggradation and the channel acts only as a bypass zone. During this stage, it is thought that lag deposits are deposited (i.e., mud clast-rich deposits, following channel wall erosion and levee collapse) and graded sandstone due to turbidity current deposition (Peakall et al., 2000). The third and last stage is related to channel abandonment. The channel can be filled by fining upward sands in response to reduction of flow strength, it can be plugged by debris flow deposits or can be kept opened and filled with hemipelagic material (Peakall et al., 2000). A summary of the channel evolution model of Peakall et al. (2000) is shown in Figure 2.13. This model strictly applies to aggradational systems as in Kneller (2003).

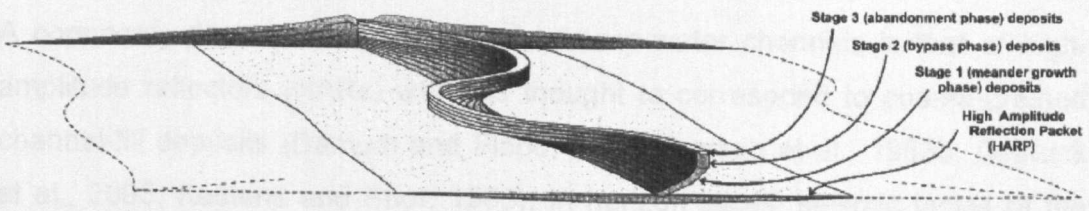

Figure 2-13 – Three dimensional block showing bend evolution in a typical aggradational highly sinuous submarine channel. After deposition of high amplitude reflection packages and levees development the channel axis aggrades forming a continuous ribbon-like body with high vertical and lateral connectivity, from Peakall et al. (2000).

Based on 3D seismic data analysis, Mayall et al. (2006) show a planform evolution of a channel that was strongly levee confined and highly aggradational, with the sinuosity increasing along a series of lateral step-wise shifts during its evolution (Fig. 2.14). The superimposed time maps demonstrate a tendency of increasing the sinuosity and degree of confinement from the base to the top. This example is in agreement with the model of planform evolution for aggradational channels suggested by Peakall et al. (2000).

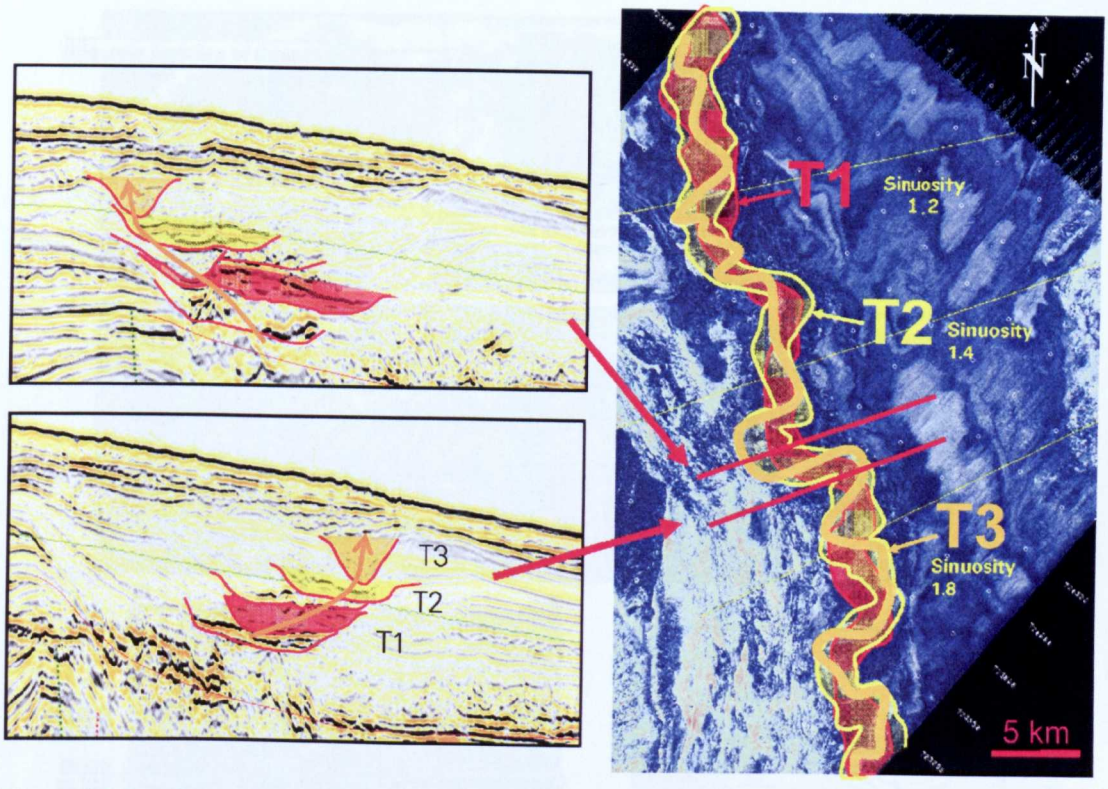

Figure 2-14 – Sinuosity due to lateral stacking of channels. Channel migrates in a series of discrete steps, increasing the sinuosity and the confinement towards the top (from Mayall et al., 2006).

2.1.9 Intra-channel seismic facies

A commonly described facies related to deep-water channels is that of high-amplitude reflectors (HARs) which is thought to correspond to coarse-grained channel-fill deposits (Damuth and Flood, 1985; Damuth et al., 1983b; Deptuck et al., 2003; Kastens and Shor, 1985). In horizon slices, seismic facies of the basal portions of channel-levee complexes show high-amplitude, multiple sinuous threads (or thread-like features) or sinuous bands (Kolla et al., 2007) (Fig. 2.15A). These features are interpreted to be due to relatively continuous

lateral channel shifts or migrations that occurred during evolution of sinuous loops (Kolla et al., 2007) (Fig. 2.15C). In the seismic sections, facies corresponding to multiple-threaded channel features may be seen in the form of off-setting, onlapping or shingled relatively discontinuous reflections (Kolla et al., 2007) (Fig. 2.15, cross section Y'Y). Here, channel forms are thought to reflect channel deposition at conditions which are close to equilibrium (e.g., Kneller, 2003): see below.

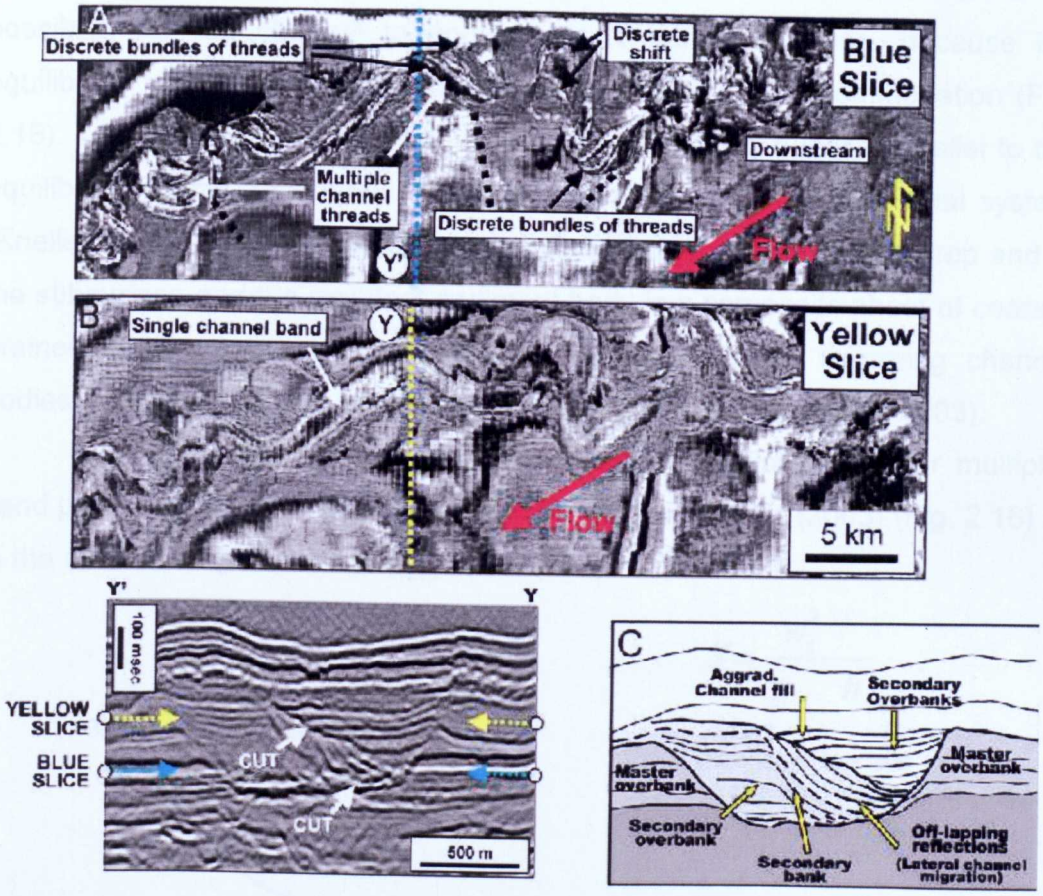

Figure 2-15 – Two amplitude horizon slices, A and B of the same channel-levee system. The blue and yellow dashed lines on the profile locate the positions of slices A and B, respectively, from Kolla et al. (2007). Slice A from the lower part of the system with multiple thread–like features. Seismic section Y'Y exhibits off-setting shingled reflections, shows lateral migrations (shifts) and some aggradation. Slice B from the upper part of the channel-levee system displays a single band-like or thread-like feature. The seismic profile C exhibits significant channel fill aggradation with some lateral migration for the upper interval. Red arrows indicate paleo-flow directions.

In contrast to the multiple threaded and laterally shifted channels in basal portions, fills in the upper sections channel-levee systems are mainly aggradational with some lateral shifting (Kolla et al., 2007). Horizon slices

across these upper sections may normally exhibit a single sinuous channel thread or band (Fig. 2.15B).

2.1.10 Channel types

Graded (neutral) channel

The channel is at grade where the gradient of the channel is in equilibrium with the flows passing down it (Kneller, 2003). Strictly, this means that there is no possibility for the channel to aggrade or tendency to erode, because the equilibrium profile remains the same with no creation of accommodation (Fig. 2.16). These channels are constrained to migrate within a plane parallel to the equilibrium profile, analogous to the meander belt in a sinuous fluvial system (Kneller, 2003). These channels show little or no aggradation at outcrop and in the subsurface and the resultant sediment body is a composite sheet of coarse-grained sediment consisting of laterally amalgamated or migrating channel bodies (Kolla et al., 2001; Mayall and Stewart, 2000; Samuel et al., 2003).

Graded channels normally present sinuous multiple-thread or multiple-band plan form shown in the conceptual diagram of Kneller (2003) (Fig. 2.16) or in the seismic amplitude slice (Fig. 2.15A).

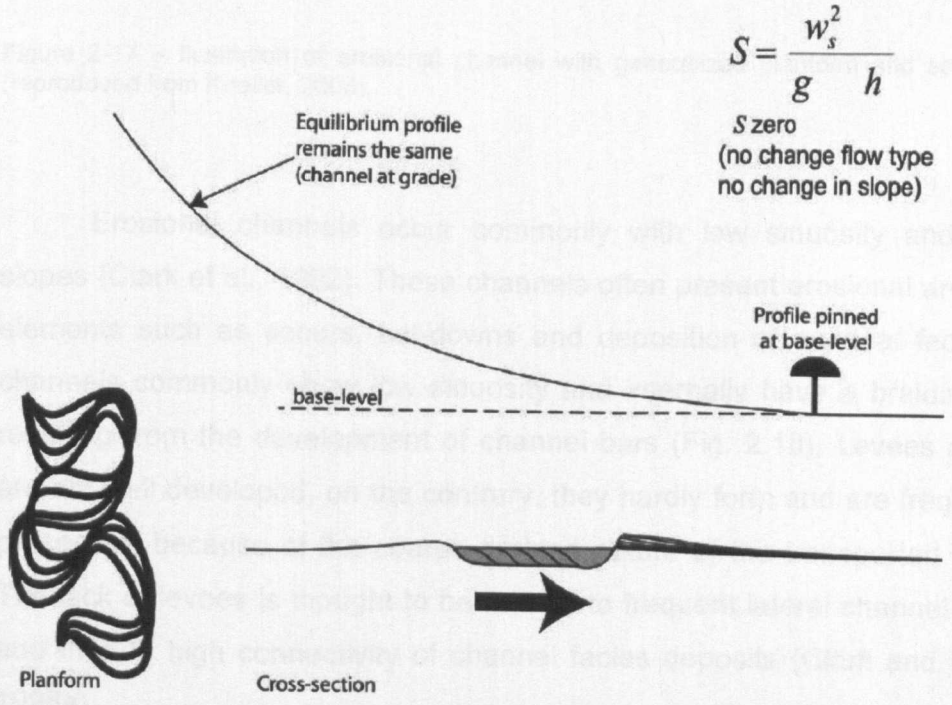

Figure 2-16 – Ilustration of graded channel with generalized planform and sectional view (Kneller, 2003).

Erosional channels

Erosional channels are created when the flow parameters change in order to reduce the local gradient (Fig. 2.17) because the channel floor is above the equilibrium profile and must therefore erode down to reach it (Kneller, 2003).

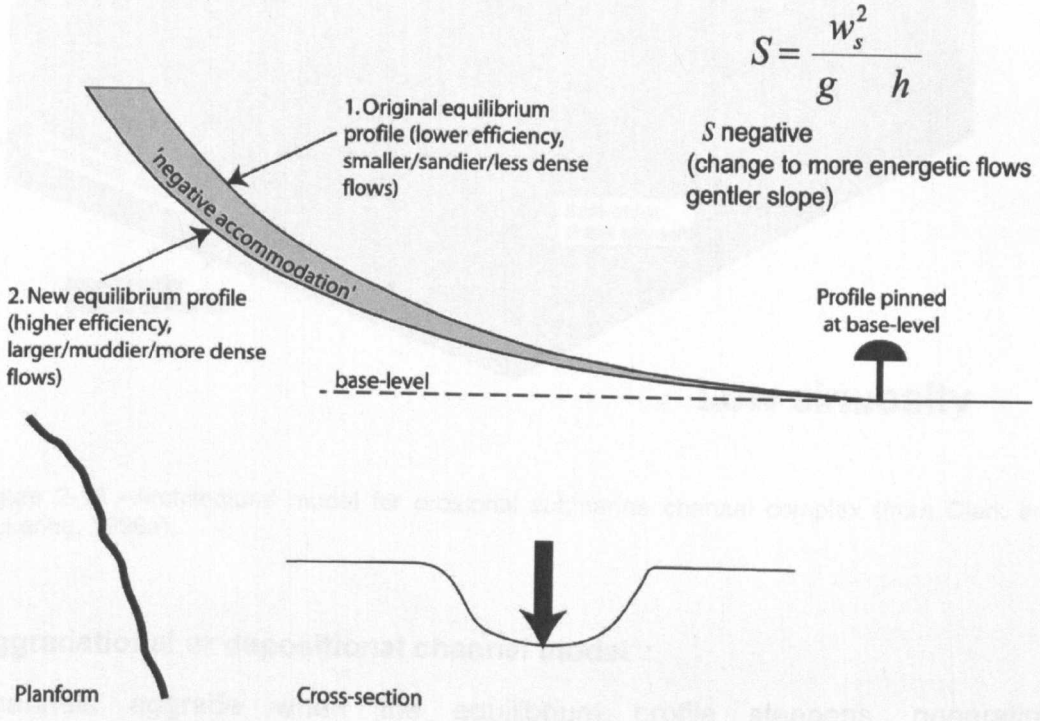

Figure 2-17 – Ilustration of erosional channel with generalized planform and sectional view (reproduced from Kneller, 2003).

Erosional channels occur commonly with low sinuosity and in steep slopes (Clark et al., 1992). These channels often present erosional architectural elements such as scours, cut-downs and deposition of residual facies. Such channels commonly show low sinuosity and internally have a braiding pattern resulting from the development of channel bars (Fig. 2.18). Levees commonly are not well developed, on the contrary, they hardly form and are frequently not preserved, because of the coarse grained nature of the transported sediment. The lack of levees is thought to be related to frequent lateral channel migration and thus to high connectivity of channel facies deposits (Clark and Pickering, 1996a).

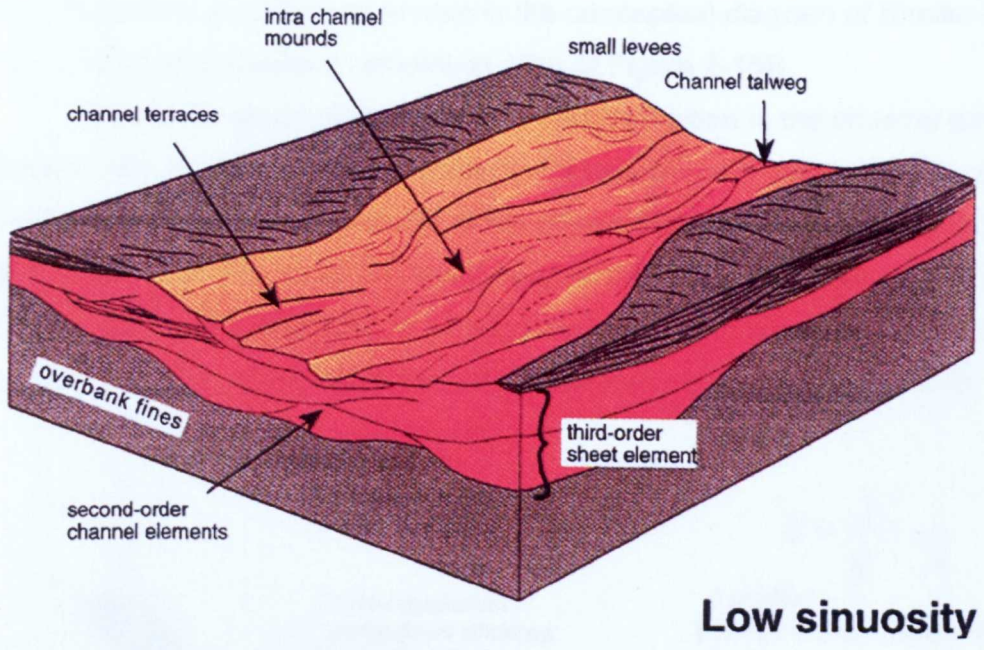

Figure 2-18 –Architectural model for erosional submarine channel complex (from Clark and Pickering, 1996a).

Aggradational or depositional channel model

Channels aggrade when the equilibrium profile steepens, generating accommodation due to change in flow parameters, resulting from the channel floor being below the equilibrium profile (Fig. 2.19).

Channel-levee systems are common depositional elements in slope and basin-floor environments. Contrasting with erosional channels, aggradational channels are associated with highly sinuous channels and gentler slopes (Clark et al., 1992). These channels mainly transport finer grained sediment, which aids sediment suspension in turbidity currents and are related to fans associated with larger drainage basins, such as the Amazon, Mississippi and Indus channels (Clark and Pickering, 1996a). The Amazon River, for instance, is an important source of fine grain sediment to the fan. The river has an annual sediment discharge of about 1.2×10^9 tons (Milliman and Meade, 1983) with 85% to 95% of the suspended sediment composed of mud (silt and Clay) (Meade et al., 1985) under present highstand conditions. Aggradational channels normally present sinuous single-thread or single-band plan forms

(e.g., Peakall et al., 2000) as shown in the conceptual diagram of Kneller (2003) (Fig. 2.19) or in the seismic amplitude slice of Figure 2-15B.

Clark & Pickering (1996a) believe that deposition in the channel axis (i.e., channel lag deposits) occurs contemporaneously with deposition of levees, leading to the vertical aggradation of the channel-levee complex (Fig. 2.20). The generally stable nature of the levee causes the channel to grow vertically. In these systems, the aggradation of large channel-levee complexes is related to avulsion of earlier channels forming discontinuous channel-body deposits.

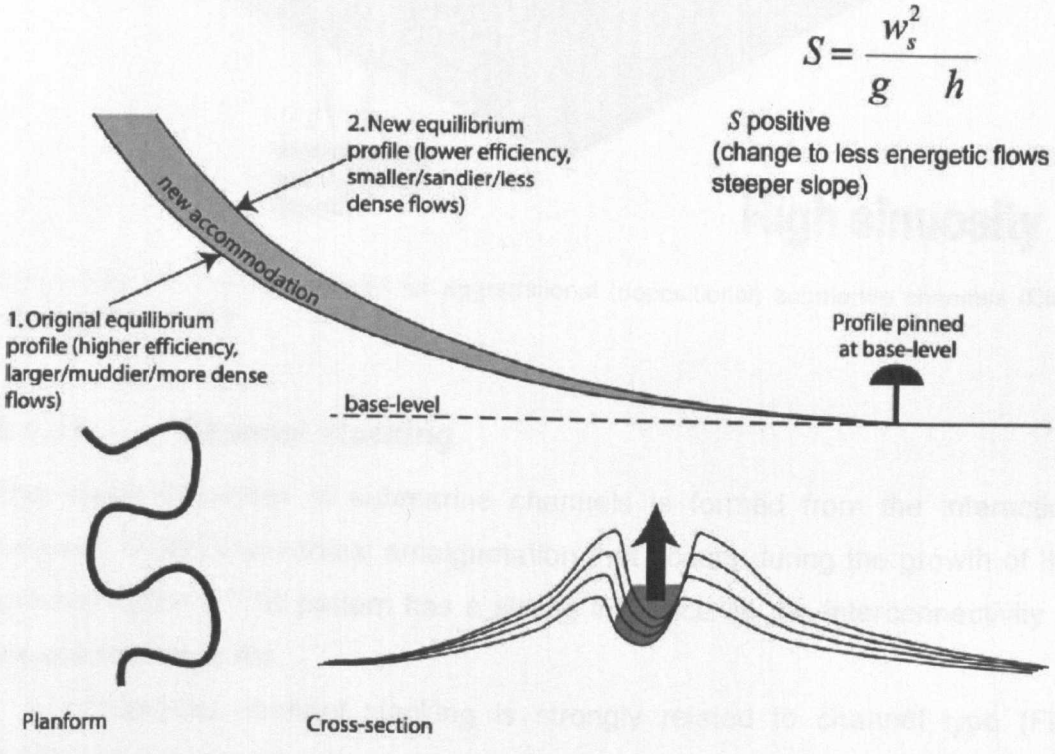

Figure 2-19 –Architectural model for aggradational with generalized planform and sectional views (from Kneller, 2003).

Leveed channels can range in width from 3 km to less than 250 m and in sinuosity between 1.2 and 2.2 (Posamentier and Kolla, 2003). Many leveed channels show evidence of having grown by lateral and down system migration, whereas other channels seem to have remained fixed in one location through large periods and are characterized by vertical stacking.

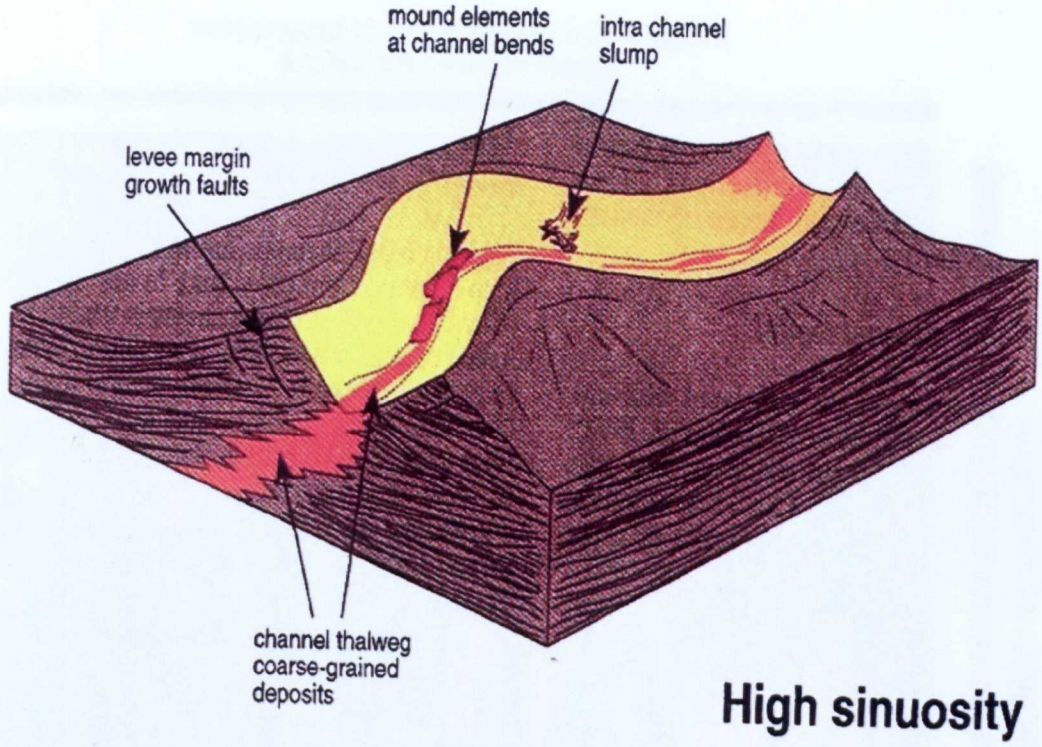

Figure 2-20 – Architectural model for aggradational (depositional) submarine channels (Clark and Pickering, 1996a).

2.1.11 Channel stacking

The stacking pattern of submarine channels is formed from the interaction between lateral and vertical amalgamation that occurs during the growth of the channel system. This pattern has a strong influence on the interconnectivity of the channel body fills.

Autocyclic channel stacking is strongly related to channel type (Fig. 2.21). For instance, the development of levees in mud rich systems will strongly favour the occurrence of vertical aggradation, whereas in sand rich systems there is a high probability that lateral migration patterns will develop due to effective absence of mud-rich levees (Clark and Pickering, 1996a).

This association between the net to gross and the amalgamation/lateral migration of the channels has been described by some authors, i.e. the greater the net to gross, the higher the degree of amalgamation of the channel complex, (e.g., Mayall et al., 2006). Moreover, the channel stacking pattern is also dependent of the rate of sediment deposition.

Figure 2-21 – Stacking pattern models of submarine channels related to confinement degree, channel dimensions (width/depth ratio), rate of deposition, aggradation and sinuosity (from Clark and Pickering, 1996a).

Analyzing erosionaly confined systems, Mayall et al. (2006) interpreted vertical stacking to be the result of focusing cutting and filling with strong differential compaction of the enclosing mud-rich rocks, and that lateral stacking occurs commonly with systematic stacking in one direction or alternating on both sides of the preexisting channel (Fig. 2.22). Additionally, the stacking pattern can change along the channel length over short distances. According to Mayall et al. (2006), although this is a common occurrence along the channel length, the cause of variations in stacking pattern is difficult to determine and can be related to local subtle changes in sea-floor relief and/or subsidence.

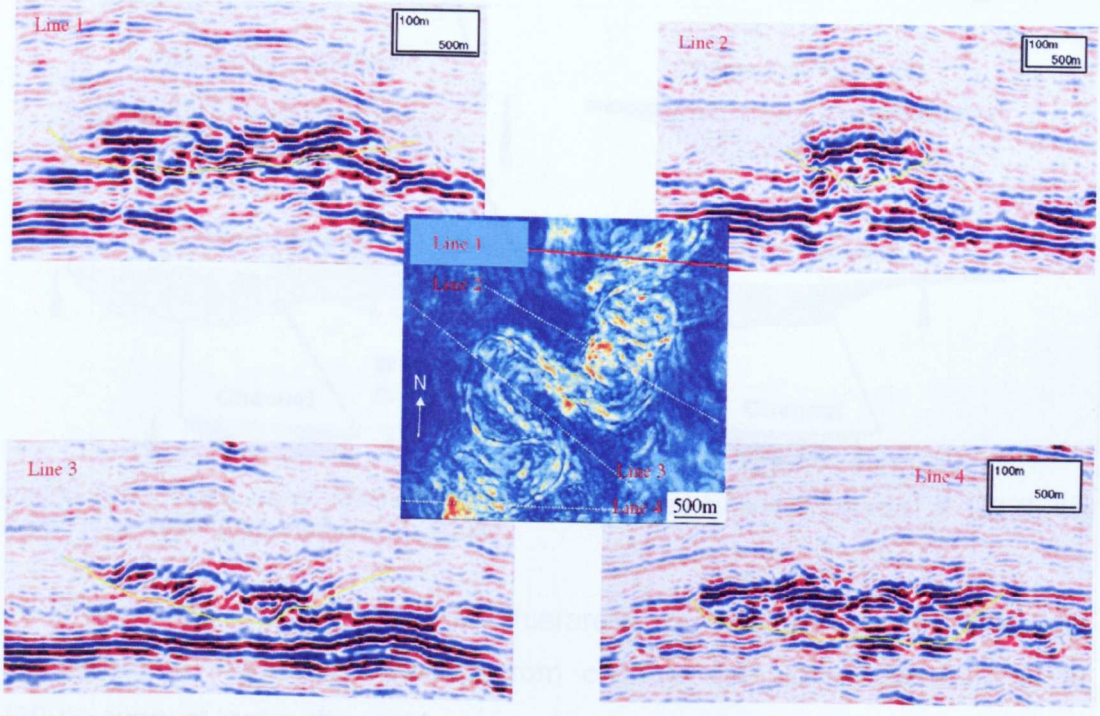

Figure 2-22 – Rapid change in stacking pattern style over short distances within a large erosional confining channel (yellow pick). Map is an RMS amplitude extraction over 30 ms window in the middle of the channel fill (from Mayall et al., 2006). Line 1 shows mostly lateral stacking in different directions, line 2 shows strong vertical stacking, line 3 shows lateral stacking in one direction, line 4 shows return to lateral stacking in different directions.

2.1.12 Channel hierarchy

Sprague et al. (2002) proposed a hierarchical scheme that could be applied to seismic-reflection profiles and on some large outcrops (Fig. 2.23). This classification is applied to confined channels, from a single channel element, to a complex of elements, to a complex set of elements, and finally to a complex system. Another classification was proposed by Abreu et al. (2003) (Fig. 2.23). They defined channel fills as the result of a single cycle of channel cutting, filling, avulsion or abandonment, channel complexes as the product of two or

more channel-fills with similar architectural style; channel complex sets as two or more channel complexes each bounded at the base by a basinward shift in facies and at the top by a surface of abandonment, and a channel complex system as comprising genetically related, stacked channel complex sets.

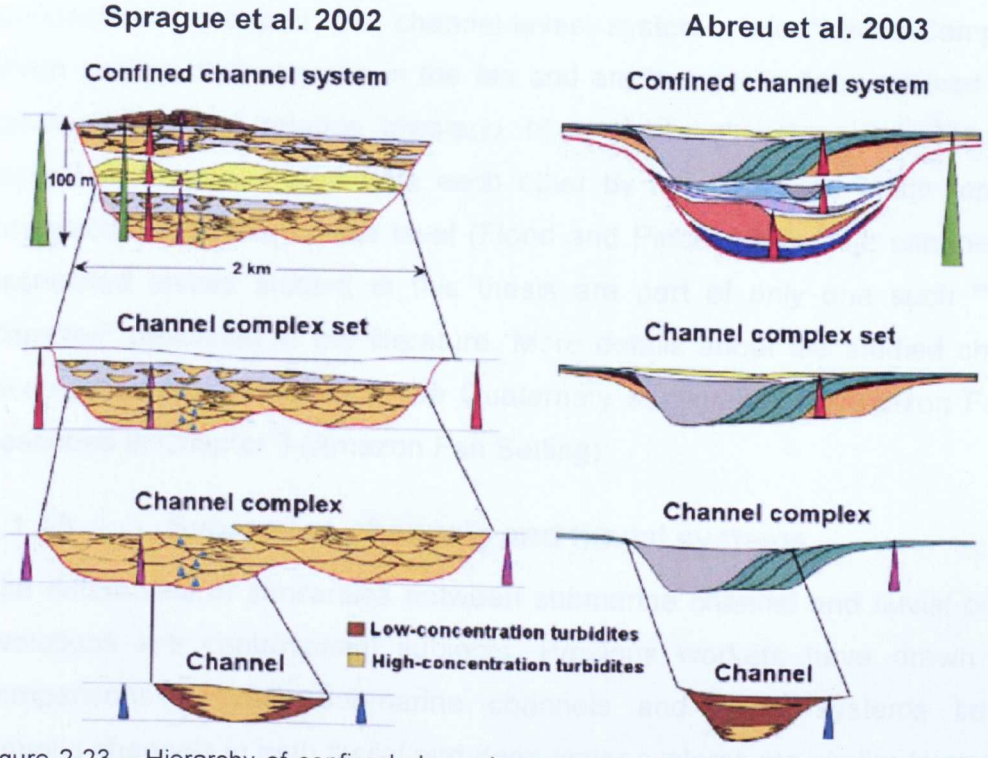

Figure 2-23 – Hierarchy of confined channels as proposed by and Sprague et al. (2002) and Abreu et al.(2003) (from Abreu et al., 2003).

In order to establish the hierarchy of occurrences of channels, distinguishing individual channels from channel complexes, Deptuck et al. (2003) suggest that a channel-levee system is a single channel belt bordered by outer levees and a channel-levee complex is a sequence of stacked channel-levee systems connected to the same canyon. Incision of a new canyon, therefore, results in the deposition of a new channel-levee complex. Similar nomenclature is used in the Amazon Fan in the ODP Leg 155 Proceedings, but instead of being called a channel-levee complex, a group of channel-levee systems connected to the same canyon is called a levee complex (Flood and Piper, 1997).

In this thesis, channels and their bordering levees are named 'channel-levee systems' (Flood and Damuth, 1987; Wynn et al., 2007). The system can be composed of one channel-levee element or of many stacked elements. In

order to be in agreement with the terminology used in previous works on the Amazon Fan and to fit the studied channel-levee systems with the stratigraphy proposed for the area, the present study uses the same nomenclature described in Damuth et al. (1988) and Manley and Flood (1988). This nomenclature grouped the channel-levee systems into "Levee-Complexes" which occupy distinct areas in the fan and are thought to have evolved during sea-level fall and relative lowstand of a single glacial period. The levee complexes are separated from each other by hemipelagites which represent interglacial highstand of sea level (Flood and Piper, 1997). The channels and associated levees studied in this thesis are part of only one such ""Levee Complex" described in the literature. More details about the studied channel-levee systems with regard to the Quaternary stratigraphy of Amazon Fan are described in Chapter 3 (Amazon Fan Setting).

2.1.13 Submarine channels and fluvial systems

The differences or similarities between submarine channel and fluvial channel evolutions are controversial subjects. Previous workers have drawn some comparisons between submarine channels and fluvial systems because sinuous channels in both fluvial and deep-water systems are similar in planform. Moreover, turbidite slope channels have been also considered analogous to fluvial channels in that they tend towards equilibrium profiles (Kneller, 2003). Several workers have shown that the morphological characteristics of deep-water sinuous channel such as sinuosity, radius of curvature, meander wavelength, amplitude, avulsions and cutoffs, are similar to those of fluvial channels (Clark et al., 1992; Flood and Damuth, 1987; Pirmez, 1994).

Fluvial-style inner-bend deposits within submarine channels had been identified not only in subsurface examples but also in modern examples (Klaucke and Hesse, 1996; Schwenk et al., 2003) and in outcrop analogues (Arnott, 2007; Martinsen et al., 2003). Posamentier identified features of meander loops migrating downstream (Fig. 2.24) and isolated examples of meander loop cutoffs and oxbows (Fig. 2.25) very similar to those described in fluvial systems based on analysis of seismic data from Gulf of Mexico.

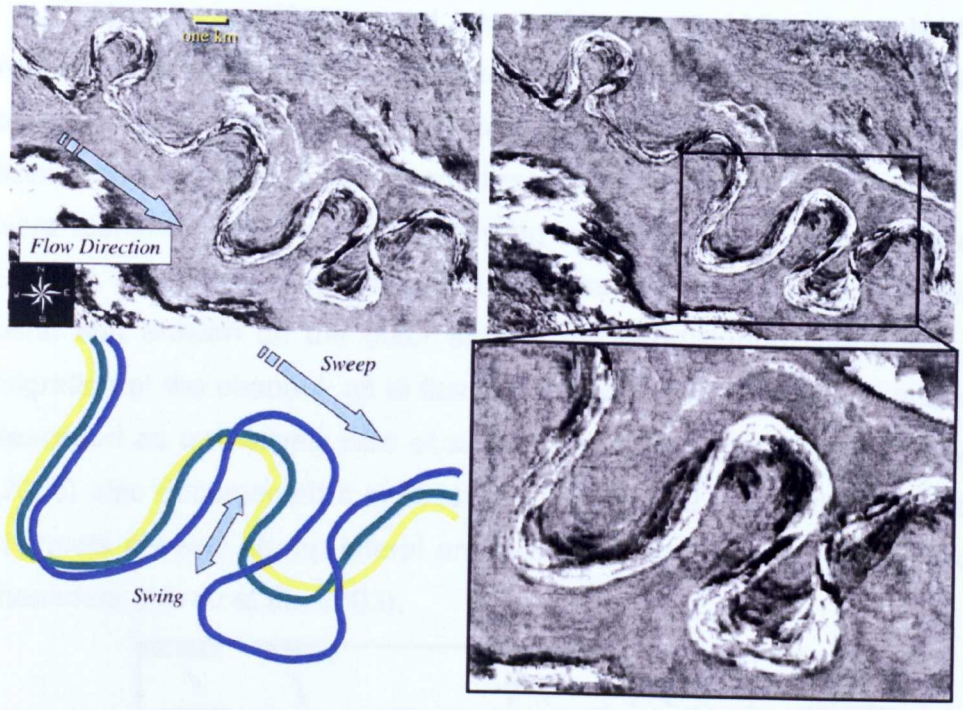

Figure 2-24 – Meander loop expansion (swing) and meander loop down-system migration (sweep). Yellow represents the oldest position and the purple the youngest position in the channel evolution .

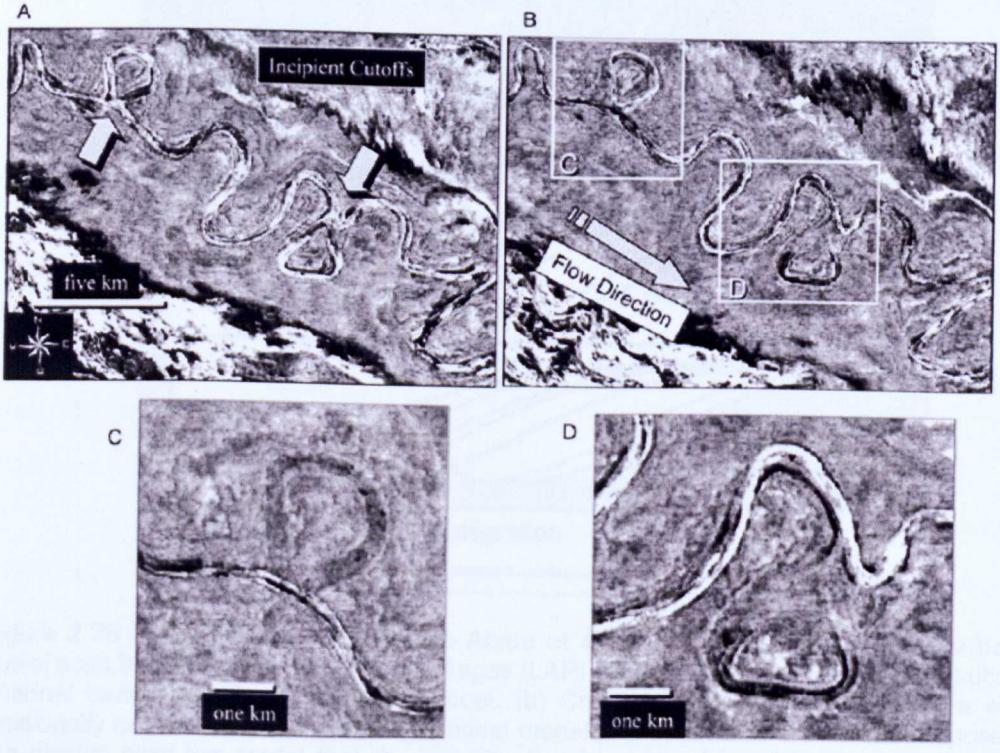

Figure 2-25 – Detail of meander loop cutoffs and oxbows of the Joshua channel, Gulf of Mexico (from Posamentier, 2003).

Abreu et al. (2003) stated that the Miocene turbidite channels of offshore Angola showed lateral accretion revealing a channel-fill style very similar to that of meandering rivers (Fig. 2.26). Additionally, reflectors dipping into the channel from the inside of meander bends resembling fluvial lateral accretion surfaces were identified in seismic data showing a highly sinuous channel (Mayall and Stewart, 2000). This suggests that there was deposition in the inner side of the bend and erosion on the outer side of the bend during lateral and downdip migration of the channel, as in fluvial point bars. Although lateral accretion was described as a relatively rare occurrence in submarine channels, Mayall et al. (2006) also documented it in seismic data (Fig. 2.27). Additionally, the studied channels showed strong lateral and downdip migration and frequent cut-off of meanders (Abreu et al., 2003).

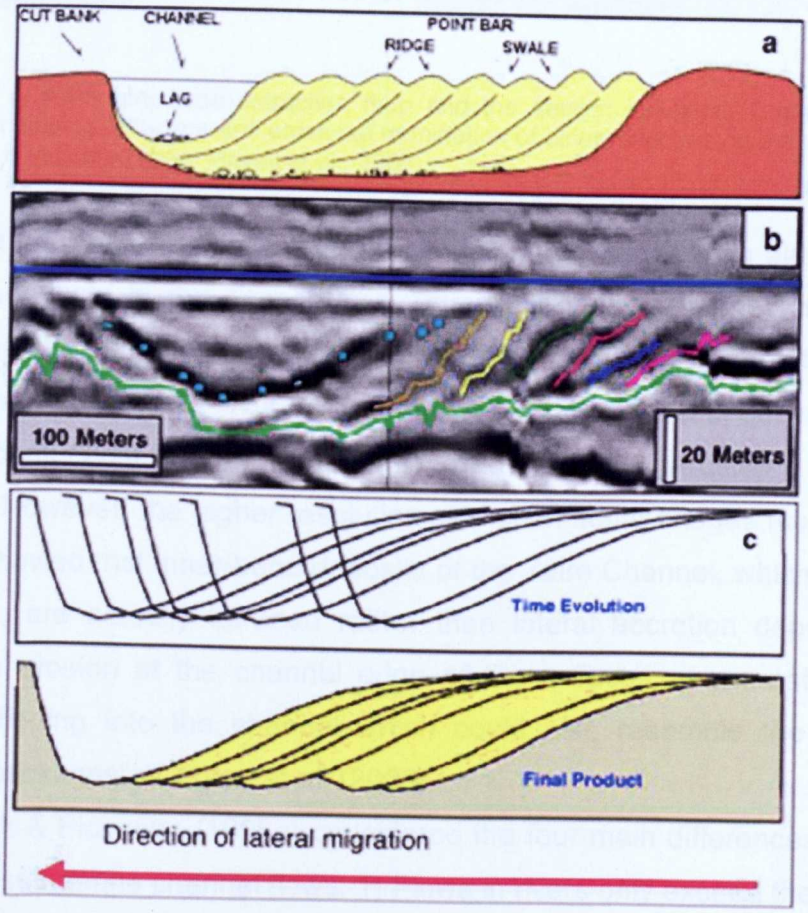

Figure 2-26 – Illustration extracted from Abreu et al. (2003), showing the similarity between fluvial point bar and lateral accretion packages (LAP) developed on the inner bank of submarine channel bends. (a) Fluvial point-bar model. (b) Cross section view of a LAP in a sinuous erosionally confined channel. (c) Depositional model proposed for LAPs. It was proposed, like the classic point-bar model that the accretion surfaces are formed by lateral sweep of the channel bends by erosion of the outer banks and deposition on the inner banks.

Both fluvial and depwater channel systems show channel shifting and sinuosity increase interpreted to result from interaction of flows, sediments and alluvial plain or seafloor gradients in attempts to build equilibrium profiles over a period of time (Kolla et al., 2007).

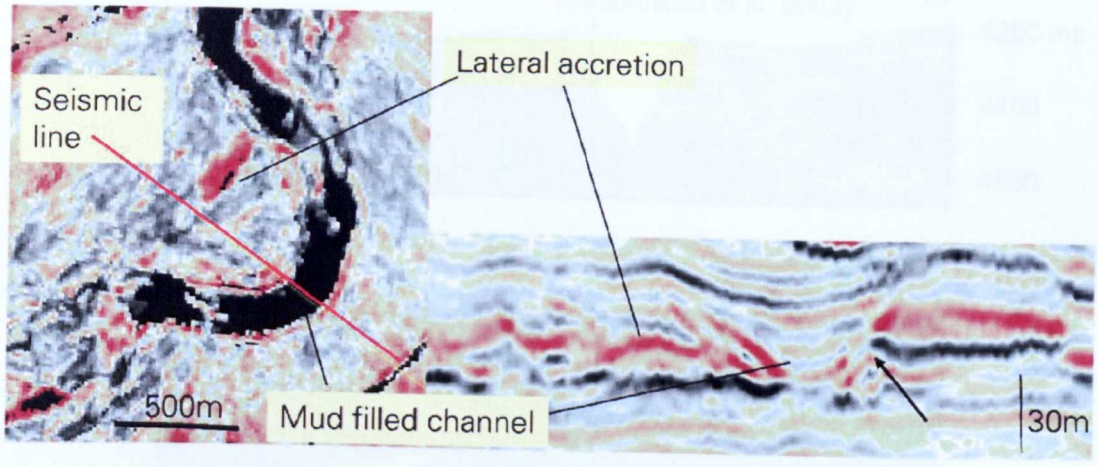

Figure 2-27 – RMS amplitude extraction map and the section indicated. Channels accrete laterally with dipping reflectors and erosional termination of older reflectors on the outer bend of the channel is indicated (from Mayall et al., 2006).

The fact that the channel can be wider at the bends than along straight sections suggests in the case of the Zaire Submarine Channel that highest rates of erosion on the outer edge of the meander due to centrifugal force (Babonneau et al., 2002). This outer bank erosion together with deceleration on the inner bank could explain the formation of depositional structures like lateral accretion. However, the higher resolution side-scan sonar images (compared to seismic) showed that inner-bend deposits of the Zaire Channel, which resemble point bars, are actually terraced rather than lateral accretion deposits (Fig. 2.28). The erosion at the channel edge of the terraces may create inclined surfaces dipping into the channel which could also resemble the "shingled reflection packages" of Abreu et al. (2003).

Clark & Pickering (1996a) considered the four main differences between fluvial and submarine channel flows: 1) Flows in rivers only exceed the levees in flood conditions whereas in turbidity currents they commonly exceed the height of the channel levees. 2) In rivers there is no incorporation of the overlying fluid (air) into the flow, whereas this process is inherent to submarine turbidity currents. 3) Most fluvial channels have continuous flow conditions, but

submarine flows are ephemeral. 4) In submarine channels, flow-stripping is a usual occurrence at channel bends whereas in rivers it is not so common.

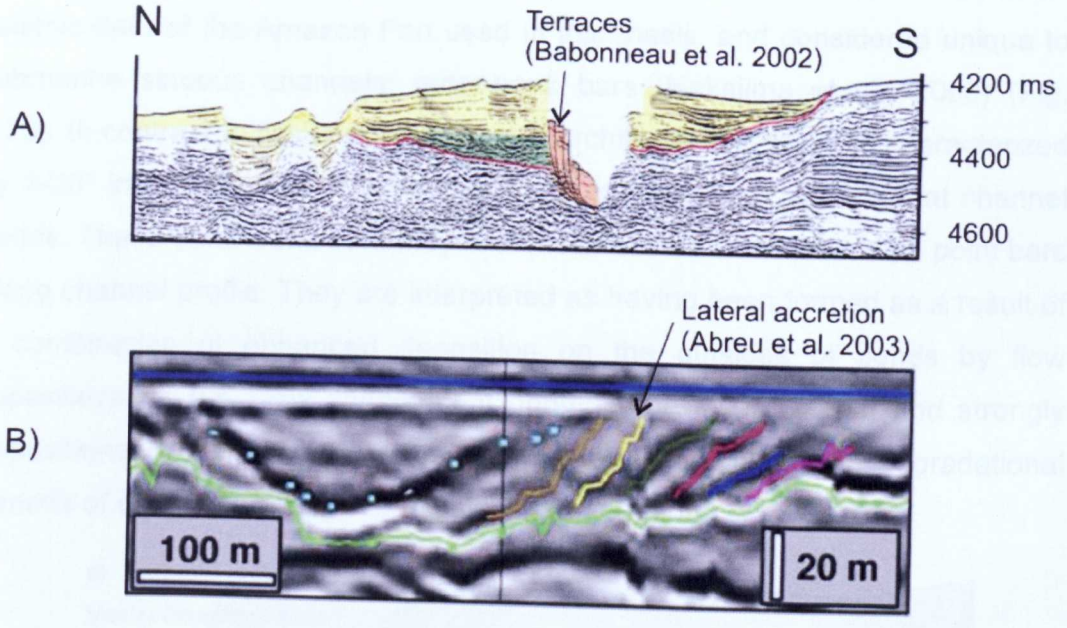

Figure 2-28 – A) Terraces in the Zaire Channel Babonneau et al. (2002) and B) Lateral accretion sets in the inner bend (from Abreu et al. 2003).

Among the comparisons between fluvial and submarine channels that have been done taking into account the sinuosity of the channels and their evolution, Peakall et al. (2000) stated that submarine channels undergo much slower bend growth than alluvial rivers and may reach planform equilibrium, in contrast to meandering rivers, where bends progressively migrate downstream. Apparently, submarine channels are less susceptible to sweep and have a greater tendency to aggrade after reaching equilibrium than fluvial channels (Peakall et al., 2000). There are also some morphological differences (Pirmez, 1994; Pirmez et al., 1997), in deepwater systems channel width and depth decrease downstream in contrast with fluvial systems where the opposite occurs (Flood and Damuth, 1987; Posamentier and Kolla, 2003). In addition, the degree of agradation is much higher in submarine channels than in fluvial systems (Kastens and Shor, 1986; Kolla et al., 2001; Posamentier and Kolla, 2003; Stelting et al., 1985). Moreover, seismic analysis of Tertiary sinuous channels on offshore Angola (Kolla et al., 2001) suggests that high sinuosity in

deepwater channels generally developed through repeated channel aggradation and subsequent lateral migration.

A new intra-channel architectural element was identified in the same 3D seismic data of the Amazon Fan used in this thesis, and considered unique to submarine sinuous channels: outer-bank bars (Nakajima et al., 2009) (Fig. 2.29). In contrast to fluvial point bars, this architectural element is characterized by 1-20° inward-dipping accumulations due to outer-bank accretion at channel bends. These outer-bank bars may in some cases be continuous with point bars along channel profile. They are interpreted as having been formed as a result of a combination of enhanced deposition on the outsides of bends by flow superelevation (i.e., >5x confinement depth: Kane et al. (2008)) and strongly depositional flows caused by flow volume reduction during the aggradational periods of channel development (Nakajima et al., 2009).

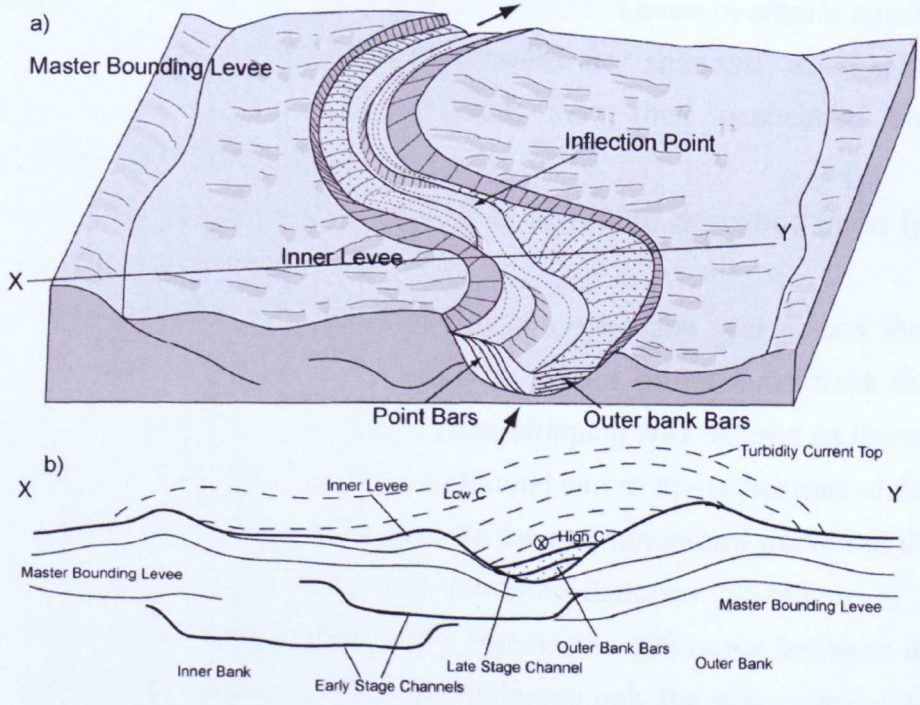

Figure 2-29 - Conceptual model of the geometry of the outer bank bars extracted from Nakajima et al. (2009): A) in 3D perspective; B) in cross section. Flow direction within the channel is perpendicular to the section away from the observer.

In summary, the main difference between fluvial and deep-water channels in terms of their internal architectures and spatial patterns of evolution (lateral migration vs. aggradation) can be interpreted to be caused by differences in density contrasts of the channelized flows relative to the ambient

fluid, together with flow frequency, volume and duration, and mode of sediment transport (Kolla et al., 2007). Sea level changes can affect the equilibrium profile in the case of fluvial systems because it constitues the base level for the system. Within deep water systems, sea level changes can affect flow parameters and grain size, indirectly controlling the equilibrium gradient (and hence system responses to non equilibrium conditions) via the flow efficiency.

2.1.14 Levees

The occurrence and properties of levees related to deepwater channels are relatively well documented in modern submarine fans e.g. Mississippi (Garrison et al., 1982; Kastens and Shor, 1986; Prior et al., 1983) and the Amazon (Damuth et al., 1988; Piper and Deptuck, 1997). Levees are the deposits laterally bounding submarine channels built by deposition from turbidity currents that spill out of the channel (Skene et al., 2002). Levee-overbank construction is mainly associated with aggradational deepwater channels. Such levees are an order of magnitude or more wider than their associated channels (Posamentier and Kolla, 2003).

Based on previous work, Peakall et al. (2000) described three types of overbank flows:

1) Inertial overspill is described as the overbank flow across the outer levee of a channel bend due to greater curvature of the outer bank than the channel axis (Hay, 1987) (Fig. 2.30). Flow stripping was defined as the splitting of the turbidite flow at tight bends in a channel where the upper part of the flow, above the levee crest, does not follow the lower channelized portion of the flow through the bend but goes on in the pre-bend direction (Peakall et al., 2000; Piper and Normark, 1983b) (Fig. 2.31). Hence, the difference between the two processes is that in the case of the flow stripping only the upper part of the flow spills out whereas in the inertial overspill, the entire flow may leave the channel. Lab studies have shown that overbank flow can not only build thicker but also coarser and steeper levees on the outer banks relative to the inner banks of the bends (Straub et al., 2008).

2) Continuous overspill is the process described in the literature that can account for the levee growth along the entire channel extension, including the inner bends, bend inflection points and straight channel segment (Hiscott et al.,

1997; Peakall et al., 2000) (Fig. 2.32). Continuous overspill occurs when there is equilibrium between sediment losses, entrainment of ambient fluid and variation in channel depth or channel cross-sectional area (Hesse, 1995) (Fig. 2.32). The process of continuous overspill, however, does not explain the occurrence of levee asymmetry over extended channel reaches in which one levee is larger than the other (see "levee asymmetry" below).

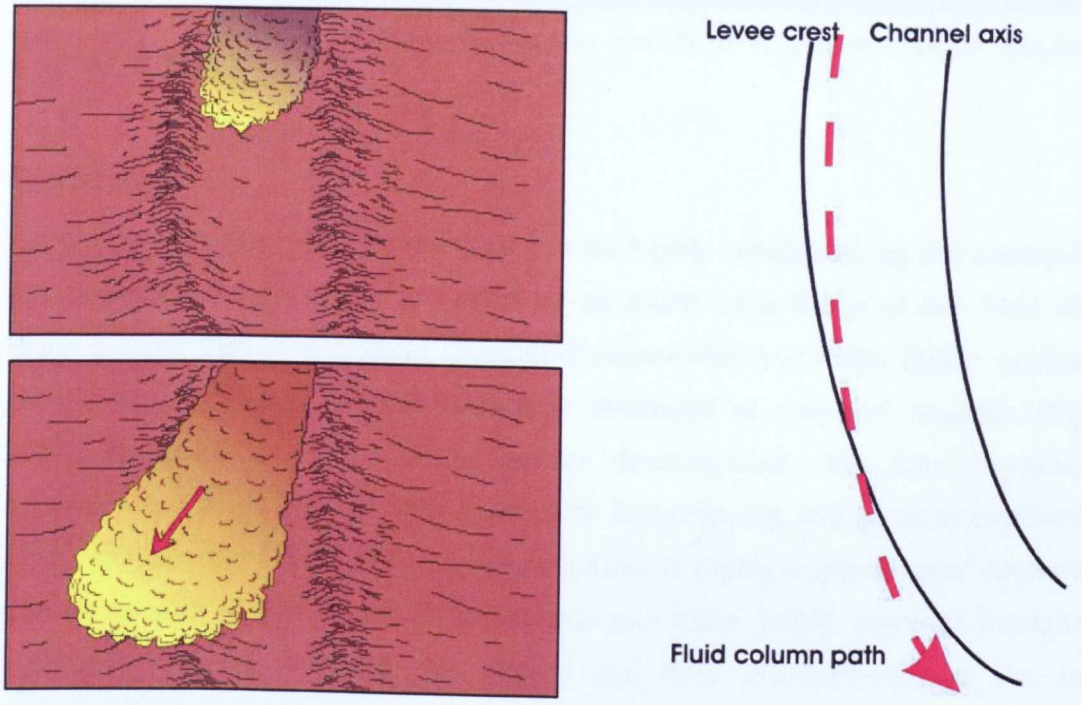

Figure 2-30 – Schematic diagram showing the process of inertial overspill. If curvature degree of the outer bend is higher than the inner one, the entire flow leaves the channel and becomes unconfined. Diagram adapted from Kane (2007).

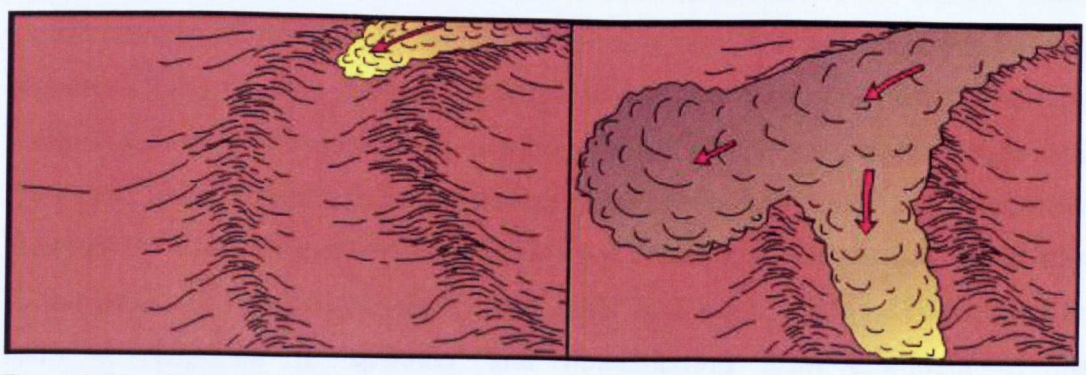

Figure 2-31 – Schematic diagram showing the process of flow stripping. The flow splits into two parts with the spilling out part forming overbank deposits mainly on the outerbank side. Due to a loss of momentum with the overbank spill, there is deposition of channel fill downstream just after the bend. Diagram adapted from Kane (2007).

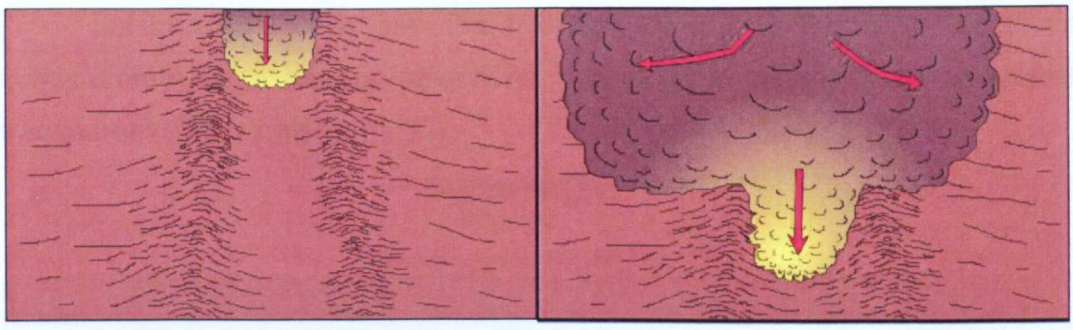

Figure 2-32 – Schematic diagram showing the process of continuous overspill. Diagram adapted from Kane (2007).

Morphology

Levee height above the channel floor can be highly variable along the course of the channel, and may vary in height by as much as a factor of two from the inner to outer bends of a given channel (Posamentier and Kolla, 2003). Levees commonly diminish in height from their landward to seaward reaches (Fig. 2.33), because as flow travels farther down-system, the flow becomes impoverished of its original mud content by flowstripping and general overbank spillover (Hiscott et al., 1997). Levee thickness in highly aggradational systems can be as high as 120-160 m (Posamentier and Kolla, 2003), whereas in highly erosional systems, they can be absent and then channelized flow can be completely confined by erosional walls of the channel (or canyon). Some levees are characterized by extensive sediment-wave development (Fig. 2.34). Typical dimensions of overbank-related sediment waves as illustrated are up to 20 m high with wavelengths of 0.5 to 0.8 km (Posamentier and Kolla, 2003). These waves are deposited by turbidity flows escaping the confinement of the leveeed channel by the process of flowstripping toward outer bends of channels due to superelevation of turbidity flow resulting from centrifugal forces (Piper and Normark, 1983a). Figure 2.34 shows the wave crests and troughs in a sediment wave field. The trends of the sediment-wave crests and troughs are subparallel to the adjacent channel bends (Posamentier and Kolla, 2003). These features form in response to spillover and flowstripping from channels of the predominantly dilute to fine-grained upper part of turbidity flows (Migeon et al., 2000; Normark et al., 1980; Piper and Normark, 1983a).

Seismically, levees are characterized by low to moderate amplitude, continuous to discontinuous reflections, and in some instances are completely transparent (Figs. 2.33 and 2.34).

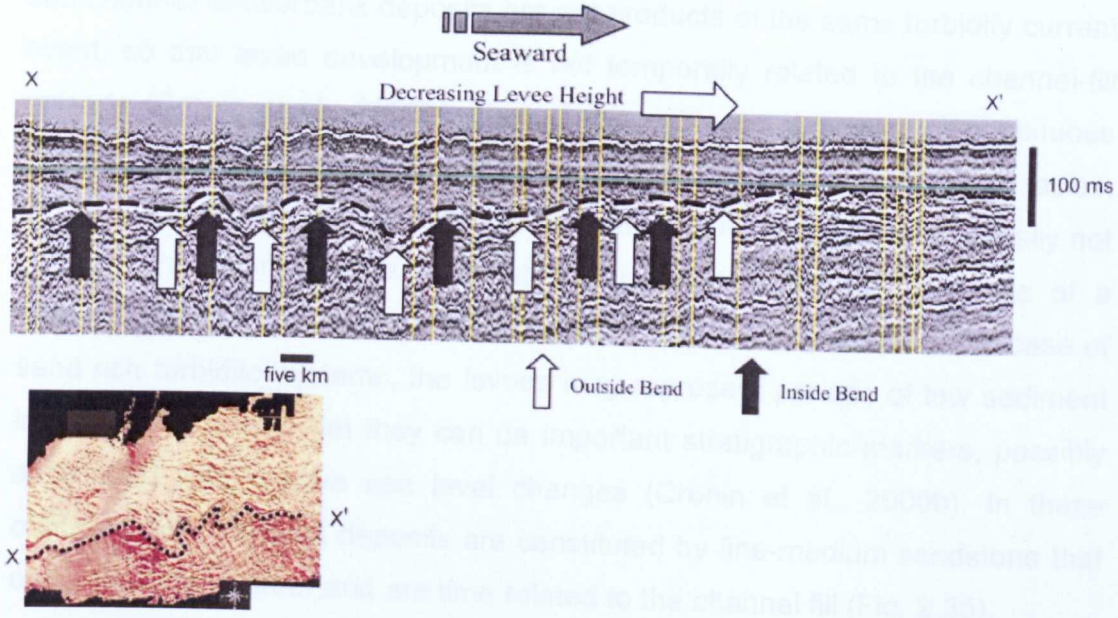

Figure 2-33 – Seismic section along the levee crest. The levee seismic facies is characterized by low amplitude discontinuous seismic reflections. Overall, the seismic thickness decreases down system (from Posamentier and Kolla, 2003).

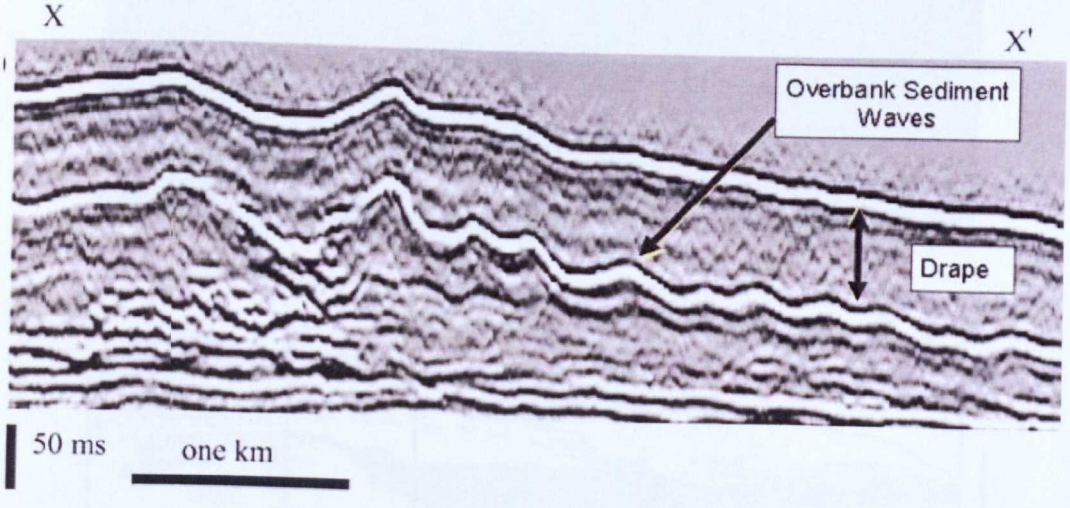

Figure 2-34 – Seismic section oriented normal to a sediment wave field, offshore eastern Borneo, Indonesia. Sediment waves are observed within as well as at the top of the levee wedge (from Posamentier and Kolla, 2003).

In the absence of contemporaneous deposition within the channel, levee deposition increases the local channel depth making the subsequent overbank flow less likely (Skene et al., 2002). There is some evidence showing that levee and channel-fill/overbank deposits are not products of the same turbidity current event, so that levee development is not temporally related to the channel-fill episode (Cronin et al., 2000b). Part of this evidence is based on continuous outcrop analysis showing the temporal/spatial relation between the facies. Although the leeves are spatially related to the channel, they are temporally not related. The channel incision is later. This implies that the presence of a channel should not lead necessarily to the occurrence of a levee. In the case of sand rich turbidite systems, the levees may represent periods of low sediment input in such a way that they can be important stratigraphic markers, possibly associated with relative sea level changes (Cronin et al., 2000b). In these outcrops, the overbank deposits are constituted by fine-medium sandstone that onlap the levee border and are time related to the channel fill (Fig. 2.35).

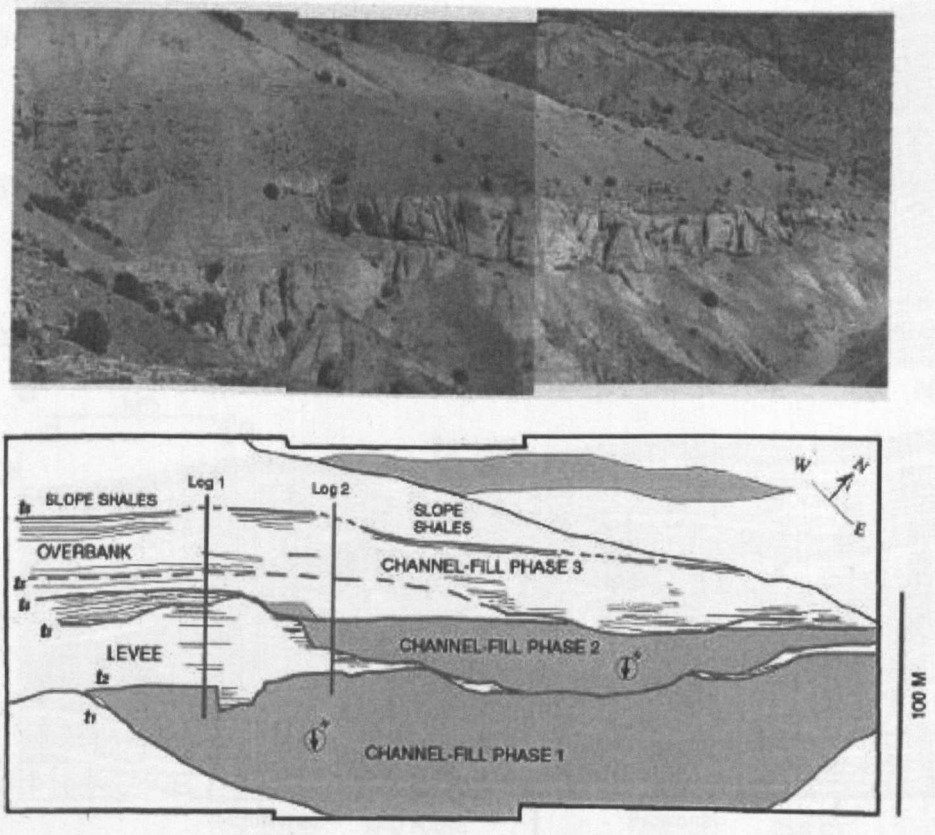

Figure 2-35 – Cross-section through the Tinker Channel (from Cronin et al., 2000b): a) Photomosaic of the Tinker Channel; b) line-drawing of the Tinker Channel including time lines: reconstruction of the temporal and spatial associations in the Tinker Channel.

Some authors subdivide the levees in outer and inner, based on seismic data features (Fig. 2.36). Outer or master levees are deposited by flows overspilling the main channel, while the less common inner or secondary levees are related to local flow overspill from flows confined within a larger channel complex (Deptuck et al., 2003; Kolla et al., 2007; Posamentier and Kolla, 2003). This distinction between inner and outer levee is important because the inner levees may be sinuous as they track a sinuous channel thalweg but outer/master levees may be not so sinuous (Kane et al., 2007). The channel thalweg may meander within a wider channel belt bounded by the master bounding levees (Posamentier, 2003). Therefore, master bounding levees may be much less sinuous than the levees of an individual channel-levee system as they do not follow a particular channel but are the product of overspill from channels or channel-levee systems meandering within the wider channel belt (Deptuck et al., 2003; Posamentier, 2003).

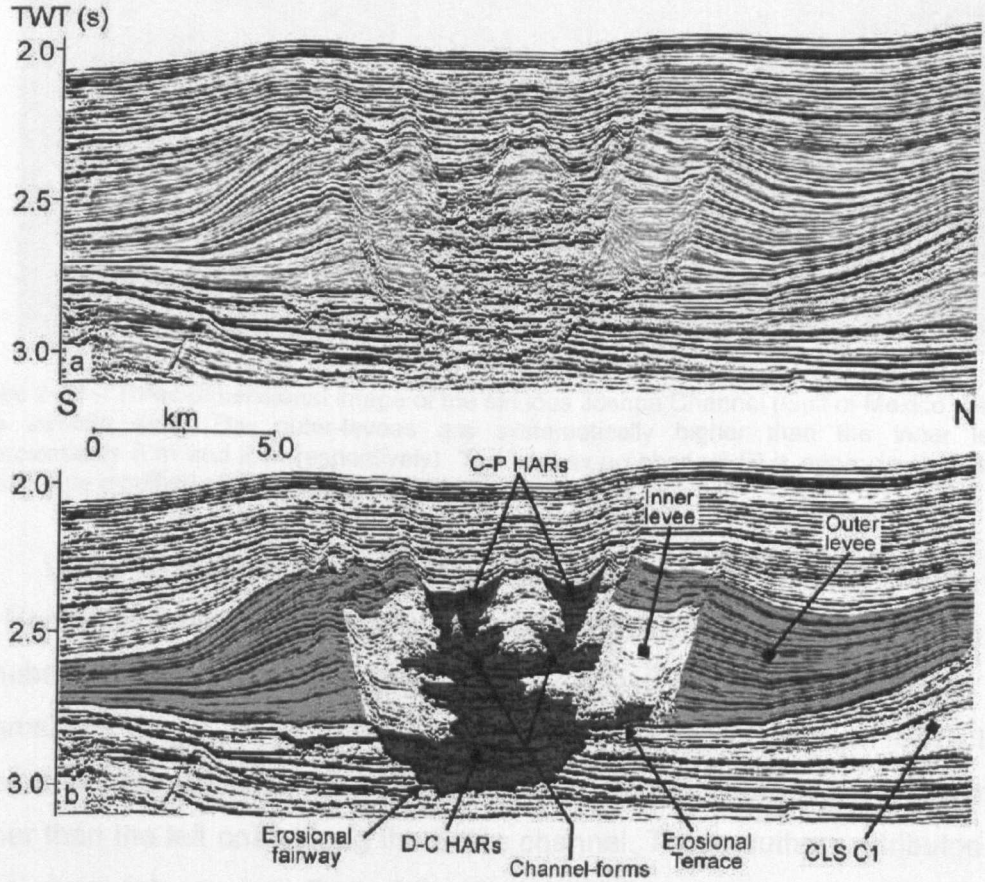

Figure 2-36 – Uninterpreted and interpreted cross section in a channel-levee system in the Indus Fan (from Deptuck et al., 2003). Notice the inner and outer levee and the high amplitude reflections (HARs) of the channel fill.

Levee asymmetry

Levees of the subsurface Joshua channel in the Gulf of Mexico, imaged from seismic data, show meaningful height differences between the outer and inner banks, reaching approximately 8 and 2 m in height respectively (Posamentier, 2003) (Fig. 2.37). This observation supports the hypothesis that flow stripping prevails at outer-bends (Piper and Normark, 1983b).

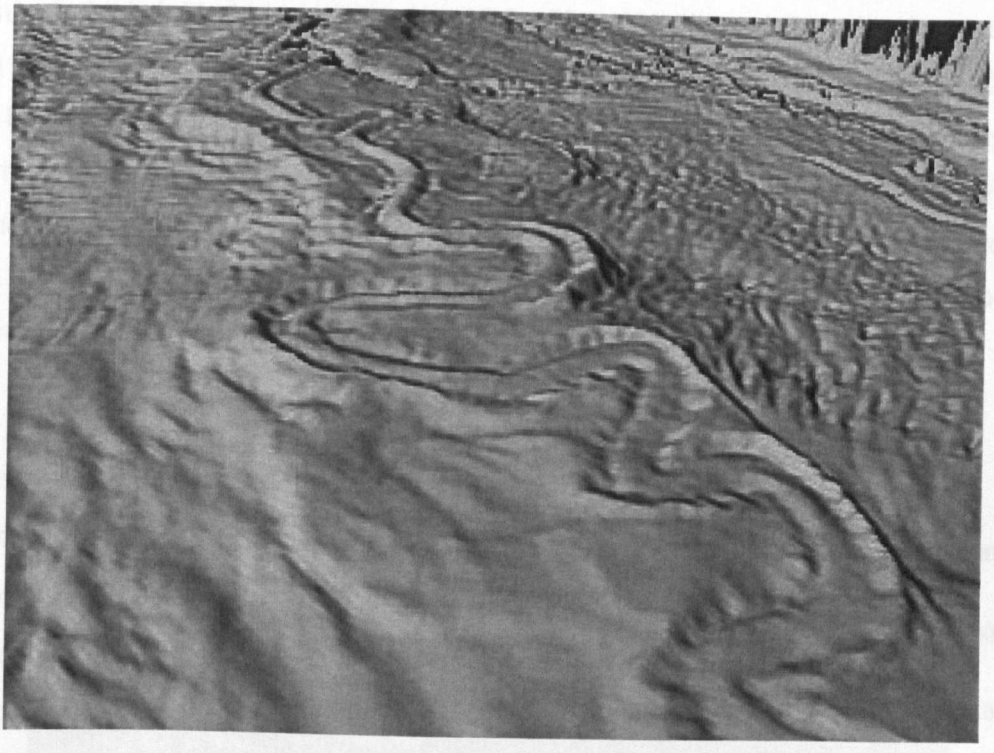

Figure 2-37 – Three-dimensional image of the sinuous Joshua Channel (Gulf of Mexico) derived from seismic data. The outer-levees are systematically higher than the inner levees (approximately 8 m and 2 m respectively). The convex-up channel fill is approximately 625 m wide. Figure modified after Posamentier (2003)

Levee asymmetry has been identified in other submarine channels, e.g., the Northwest Atlantic Mid-Ocean Channel (NAMOC) (Klaucke et al., 1997), the Danube Deep-Sea Fan (Popescu et al., 2001) (Fig. 2.38), the Bengal Fan (Emmel and Curray, 1981) and the Indus Fan (Kolla and Coumes, 1987). In all these deep-sea systems, the right-hand levees (looking downstream) are much higher than the left ones along the entire channel. These authors attributed this levee asymmetry as an effect of the Coriolis force acting on the flow overspill along the channel systematically causing overbank deposition preferentially on the right side, if the channel is located in North Hemisphere. Thus, in contrast

with fluvial systems (in which Coriolis force effects are negligible compared with centrifugal forcings), in submarine systems both forces may be important affecting overbank flow and deposition (Imran et al., 1999; Kolla et al., 2001). In the northern hemisphere Coriolis and centrifugal forces reinforce each other in left turning meander bends and oppose each other in right turning meander bends (this is reversed in the southern hemisphere) (Klaucke et al., 1997). Some of the submarine fans which present asymmetrical levees are located in relatively high latitudes such as NAMOC (50 - 60° N) and Danube Deep-Sea Fan (43 – 44° N), and others in relatively lower latitude such as Indus Fan (24 - 15° N) and Bengal Fan (20 – 5° N). An example in the Southern Hemisphere, in the middle fan channels of Wilkes Land, Antartica, the left-side channel levee is higher than the right–side levee indicating higher rates of overbank deposition in that direction (Escutia et al., 2000), consistent with Southern Hemisphere Coriolis forcing of sediment gravity flows to the left.

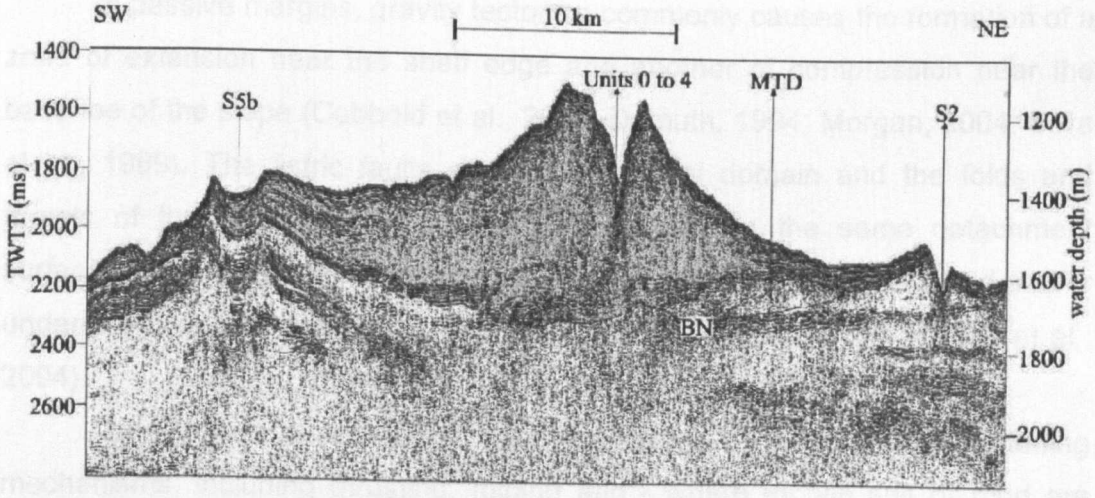

Figure 2-38 – Seismic reflection line across a channel in Danube Deep-Sea Fan showing strong levee asymmetry attributed to the influence of Coriolis Force. The larger left-hand levee is viewed looking up-channel in this section. Image obtained from Popescu et al. (2001).

On the contrary, in the Zaire Fan, the channel-levees are relatively small and very symmetrical (Migeon, 2004). This symmetry can be attributed to the small influence of the Coriolis force on the overbank flow close to Equador (5 – 7° S) (Wynn et al., 2007).

2.2 *Gravity tectonics*

2.2.1 Introduction

The majority of studies and models concerning turbidity current behaviour, channel evolution and submarine fan build-up have essentially considered unconfined deposition, resulting in fan-shaped deposits (e.g.,Bouma et al., 1985; Damuth and Normark, 1991; Flood et al., 1991; Kolla, 2007; Normark et al., 1997; Pirmez et al., 1997). Nevertheless, numerous studies have shown that, in many basins, sediment dispersal patterns and depositional geometries have been affected by the sea floor topography (e.g., Morgan, 2004; Smith, 2004a; Smith, 2004b). Tectonic activity has an important role in the creation of basin-floor relief, as it can affect the shelf width, slope gradients, position of canyon incisions, and can trigger mass failure in the shelf margin and slope. It can also be responsible for dictating the distribution pathways of turbidity currents and related flows.

In passive margins, gravity tectonics commonly causes the formation of a zone of extension near the shelf edge and another of compression near the base/toe of the slope (Cobbold et al., 2004; Damuth, 1994; Morgan, 2004; Silva et al., 1999). The listric faults of the extensional domain and the folds and thrusts of the compressional domain are rooted on the same detachment surface, which could be induced by a layer of weak salt or overpressured and/or undercompacted shales due to fast burial (Cobbold et al., 2004; Rowan et al., 2004).

Deepwater fold and thrust belts are formed by a variety of shortening mechanisms, including thrusting, folding and - where mobile salt or mud are present - in diapir development and salt/mud nappe extrusion. In passive margins, examples of deepwater fold belts with detachment on salt layers include the Missisippi Fan and Perdido fold belts of the northern Gulf of Mexico; the fold belts of the Campos, Santos, and Espirito Santo Basins in Brazil; fold belts of Benguela, Kwanza, Congo, Gabon, and Rio Muni Basins in West Africa and many others (Rowan et al., 2004). Examples of fold belts connected to a detachment surface on overpressured shales include the Mexican Ridges and Port Isabel fold belts of the western Gulf of Mexico; fold belts in Sergipe-Alagoas, Pará-Maranhão and Foz do Amazonas Basins of Brazil; and fold belts

in the Niger Delta (Damuth, 1994; Reis et al., 2010; Rowan et al., 2004; Sultan et al., 2007; Zalan, 2004).

Development of gravitational fold-thrust belts at the front of deltas of large rivers is common, due to the instability generated by the large amount of sediments piled up at the edge of continental margins combined with seaward tilting due to thermal flexural bending (Zalan, 2004). Significant amounts of sediment can slide down-slope over a ductile lithology, detaching the upper rocks from the autochtonous rocks underneath. When the gradient of the detachment surface decreases, or a physical barrier is encountered, the resulting contraction/compression generates the fold-thrust belt. The failure occurs when the vertical stresses due to overburden are weakened relative to horizontal stresses due to overpressured shales or ductile flow in salt. Thus the gravity tectonic process generates three domains of deformation linked by the detachment surface: extensional, translational and compressional (Fig. 2.39). The dimensions of the three domains can vary significantly. In practice it can be difficult to balance the compressional deformation downdip with the amount of extension updip, because of the amount of deformation that is not resolvable by seismic data (Zalan, 2004).

Shale-detached, gravitational fold and thrust belts in areas of high sedimentation and deformation rates (e.g., the Amazon Cone) may develop intense folding, mainly expressed as detachment and fault-propagation folding (Zalan, 2004). These structures commonly have very high structural relief and can reach the sea floor. Gravitational fold-thrust belts in passive margins where low rates of sedimentation/deformation prevail show fault-bend folding in the more external parts passing landwards through zones of fault-propagation folding and to detachment folding landwards. Important oil discoveries have been achieved in these compressional provinces in the deep waters of the Gulf of Mexico, Nigeria, Angola and Brazil (Corredor et al., 2005; Morgan, 2004; Zalan, 2004).

The objective of this review is to better understand the capability of tectonic activity to affect slope geomorphology in passive margins, which in turn may control channel-levee development. To achieve this aim this literature review focuses mainly on the mechanisms and causes of fold belt formation where the detachment is guided on overpressured shales, as this is inferred to

be the principal deformation mechanism in the Foz do Amazonas Basin, the area of study.

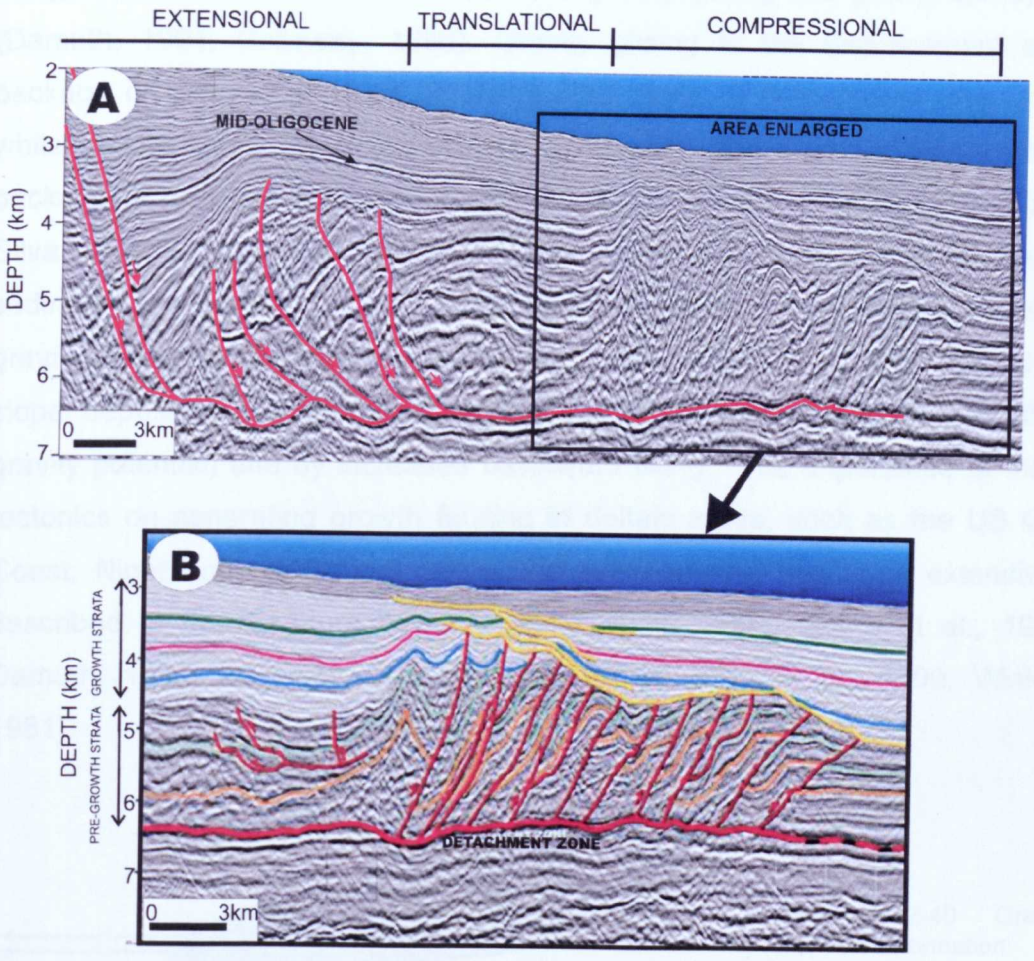

Figure 2-39 - Seismic section from Pará-Maranhão Basin, Brazilian continental margin, adapted from Zalan (2004): A - The major components extensional-compressional system, extensional, translational and compressional linked by a detachment surface. B – Detail of the fold and thrust belt formed in the compressional area highlighting pre and syntectonic bedding.

2.2.2 Driving mechanisms of gravity tectonics

The importance of gravity tectonics on the origin of growing faults in deltaic areas has been described in, amongst others, the US Gulf Coast Province and the Niger and Mississippi deltas (e.g., Cobbold et al., 2004; Crans et al., 1980; Damuth, 1994; Galloway, 1986; Morgan, 2004; Rowan et al., 2004; Silva et al., 1999). Many passive margins have deepwater, contractional fold belts formed above a basal layer of ductile material, such as salt or over-pressured shale. In this case, fluid overpressure may carry part of the weight, reducing the frictional

resistance at the base. The formation of fold belts down-slope in passive margins is the result of a mixture between gravity gliding and gravity spreading (Damuth, 1994; Galloway, 1986). Gravity gliding is the displacement of a package of rocks downslope parallel to the plane of detachment (Fig. 2.40) while gravity spreading is the vertical contraction and lateral extension of a package of rock due to gravity action on its own weight (Rowan et al., 2004; Silva et al., 1999). The increase of sedimentary weight on the slope due to sediments that bypass the shelf creates favorable conditions for the onset of gravity tectonics. Continued deformation is driven primarily by shelf and upper slope deposition (which maintains the bathymetric slope and the resulting gravity potential) and by increased basinward tilting. The importance of these tectonics on generating growth faulting in deltaic areas, such as the US Gulf Coast, Niger and Mississippi deltas and Amazon Fan has been extensively described in the literature (e.g., Cobbold et al., 2004; Crans et al., 1980; Damuth, 1994; Galloway, 1986; Morgan, 2004; Silva et al., 1999; Winker, 1981).

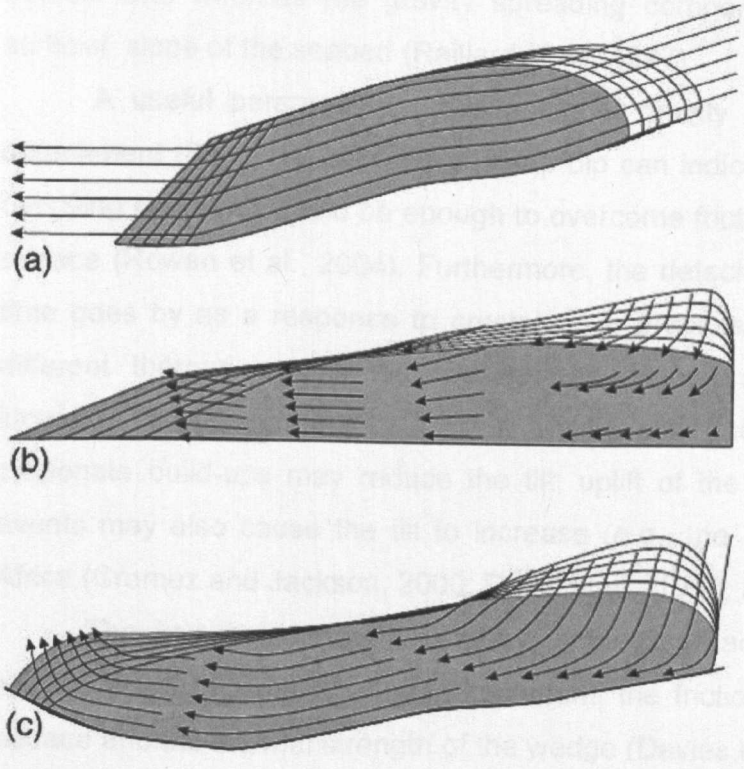

Figure 2-40 Gravity driven deformation:
a) Gravity gliding – a package of rock slide on a detachment;
b) Gravity spreading – a package of rock deform due to its own weight and by vertical collapse and lateral spreading;
c) mixed-mode deformation (from Rowan et al., 2004)

Gravity driven tectonics, with detachment on an overpressured shale layer, will have a basinward limit of deformation where there is a decrease in overpressure, increasing the frictional resistance to sliding, thus preventing lateral movement (Rowan et al., 2004). Moreover, the boundary between overpressured and normally pressured shales can migrate basinward as the point of rapid burial moves seaward. The limit of deformation can also be delimited as the front of a progradational wedge (Rowan et al., 2004).

In passive margins, the term gravity gliding has been applied to describe the detachments that are basinward-dipping (Demercian et al., 1993; Mauduit et al., 1997), whereas gravity spreading has been applied in prograding deltas, where the detachments can be landward-dipping (Worrall and Snelson, 1989). Gravity spreading and gliding are both characterized by proximal thin-skinned extension on the shelf and upper continental slope and by distal contraction on and in front of the lower slope (Vendeville, 2005). As many margins are mixed-mode (gliding and spreading), it is useful to apply gravity gliding as the component of the deformation controlled by any basinward slope of the detachment, whereas the gravity spreading component is controlled by the surficial slope of the seabed (Raillard et al., 1997).

A useful parameter for evaluation of gravity gliding is the dip of the detachment (Fig. 2.41) because a steep dip can indicate that the weight of the overlying rock body could be enough to overcome friction along the detachment surface (Rowan et al., 2004). Furthermore, the detachment dip can change as time goes by as a response to crustal-scale processes (Rowan et al., 2004): different thermal subsidence between continental and oceanic crust may increase the tilt; differential flexural subsidence due to progading delta or carbonate build-ups may reduce the tilt; uplift of the "craton" due to tectonic events may also cause the tilt to increase (e.g., the Tertiary uplift of West of Africa (Cramez and Jackson, 2000; Duval et al., 1992; Spathopoulos, 1996)).

The key parameters controlling gravity spreading are the dip of the surface slope, the dip of basal detachment, the friction along the detachment surface and the internal strength of the wedge (Davies et al., 1983; Dahlen et al. 1984, in Rowan, 2004). However, deformation onset and cessation are strongly dependent on sediment deposition (Fig. 2.42): progradation on the outer shelf and upper slope increases the surficial slope and therefore promotes spreading

(Fig. 2.42a); upper-slope bypass and distal deposition on lower slope and basin reduces the surficial slope (2.42b), slowing or stopping spreading (Fig. 2.42c). Experimental models have also shown that the deposition of a sediment wedge basinward initiates a slope that promotes seaward gravity spreading of the overburden (Vendeville, 2005). Spreading is accommodated by grabens, normal growth faults, slip along diapir margins, and the development of fault-bounded troughs and folds. The fundamental mechanical characteristics and kinematic history of spreading in prograding systems are also described by Vendeville (2005): spreading occurrence demands only a surface slope, e.g., sea floor spreading causes proximal extension and distal contraction; the displacement vectors are parallel to the direction of the local slope; timing of spreading is controlled by regional depositional events.

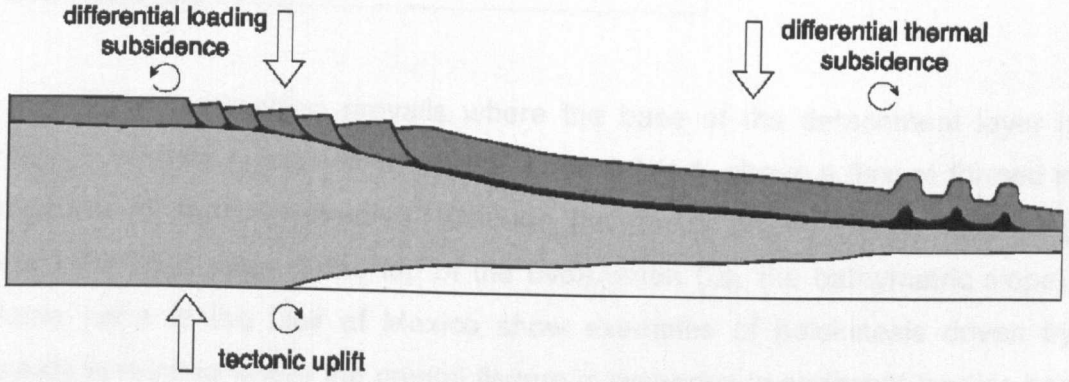

Figure 2-41 - Passive margin showing basinward tilting being enhanced by differential thermal subsidence and continental uplifting being reduced by proximal loading subsidence, from Rowan et al. (2004).

Although gravity gliding and spreading are characterized by the same three structural domains (extension/translation/contraction), they have different triggering mechanisms and generate different structural styles. The structures are multidirectional where gravity spreading prevails, e.g. faults bounding minibasins, whereas the structures are perpendicular to the slope dip where gravity gliding prevails, as described in the eastern and western portions of the Nile deep sea fan (Loncke et al., 2006) . Down-slope gliding takes place when the base of the detachment layer and the top of the overburden dip seaward. Gliding is accommodated by normal faults in the proximal region and by contractional folds or faults in the distal region (Vendeville and Cobbold, 1987,

in Loncke et al., 2006). The traces of normal faults forming during gravity gliding tend to be subparallel.

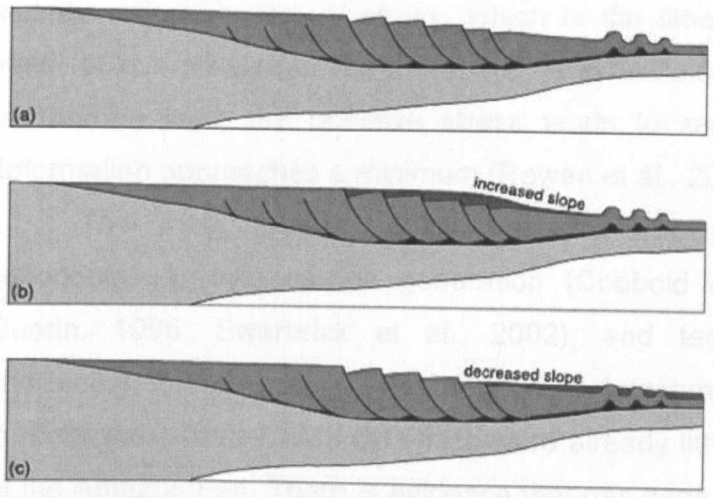

Figure 2-42 Passive margin with failure dominated by gravity spreading (a); progradation on the outer shelf and upper slope increases surficial slope and further spreading (b); upper slope bypass and distal deposition reducing the surficial slope and so slowing or stopping spreading (c), from Rowan et al. (2004).

Gravity spreading prevails where the base of the detachment layer is nearly horizontal or even slightly tilted landward (e.g. above a flexure formed in response to sediment loading, although the forces driving gravity spreading result from the slope of the top of the overburden (i.e. the bathymetric slope). Some parts of the Gulf of Mexico show examples of halokinesis driven by gravity spreading where the crustal flexure in response to sediment loading has tilted the base of the evaporate landward, making seaward gliding impossible (Vendeville, 2005). Where the surface slope is simple, traces of proximal normal faults are all parallel and sublinear (generally parallel to the coastline). Where local slope directions diverge or converge, several sets of normal faults having multidirectional traces form (Gaullier and Vendeville, 2005).

Overall, gravity driven foldbelts present structural styles mainly controlled by the nature of the décollement layer, not on the driving forces in passive margins. Foldbelts detached on overpressured shale characteristically include basinward-vergent thrusts and related folds because of the relatively high strength and frictional behaviour of plastic shale (Rowan et al., 2004); deformation does not occur until a large thickness of overburden is deposited rapidly enough to create fluid overpressure in the detachment shale. On the other hand, salt can promote early deformation, just after deposition because it is a viscous material almost without strength (Rowan et al., 2004).

2.2.3 Shale detachament

As shale is a plastic material, it deforms when the deviatoric stress overcomes its strength. The shear stress of shale is the product of the coefficient of friction and the effective vertical stress, which is the lithostatic pressure minus the effect of overpressure. Therefore, as the pore-fluid pressure approaches the overburden load, the effective stress tends to zero, and the resistance to deformation approaches a minimum (Rowan et al., 2004).

The main causes of overpressure are: extremely high rates of sedimentation, hydrocarbon generation (Cobbold et al., 2004; Morley and Guerin, 1996; Swarbrick et al., 2002), and tectonic compaction during shortening. In the Amazon Fan, the level of detachment is around 10 km deep, in rocks more than 70 Ma old which were already lithified before the deposition of the Amazon Fan. There is evidence that gas generation is the main cause of overpressure. Thus Cobbold et al. (2004) lists the presence of gas in some wells, noting that Cenomanian-Turanian source rocks are widespread on the shelf, and that modeling suggests that the rocks had reached the gas window by the time that the detachment was more active.

2.2.4 Growth strata

Growth strata are stratigraphic intervals deposited during deformation so that the ages of the strata constrain the timing of deformations. Around folds related to contractional faults, growth strata typically thin on fold limbs. The patterns of deformation of growth strata above the fold limbs may correspond to the type of folding mechanisms (Shaw et al., 2005). Hence, the geometries of growth structures in seismic images can be used to recognize the folding mechanisms and relative rates of sedimentation and uplift.

In fact, the specific geometry of the fold within the growth strata strongly depends on the history of sedimentation relative to the history of deformation (Suppe et al., 1992). Where the deposition rates exceed the uplift rates, the growth strata are the interval of reflectors that thin on the limbs of the structures (Fig. 2.43). Where the uplift rate exceeds the sedimentation rate, the growth strata onlap the limbs of the structure (Fig. 2.44).

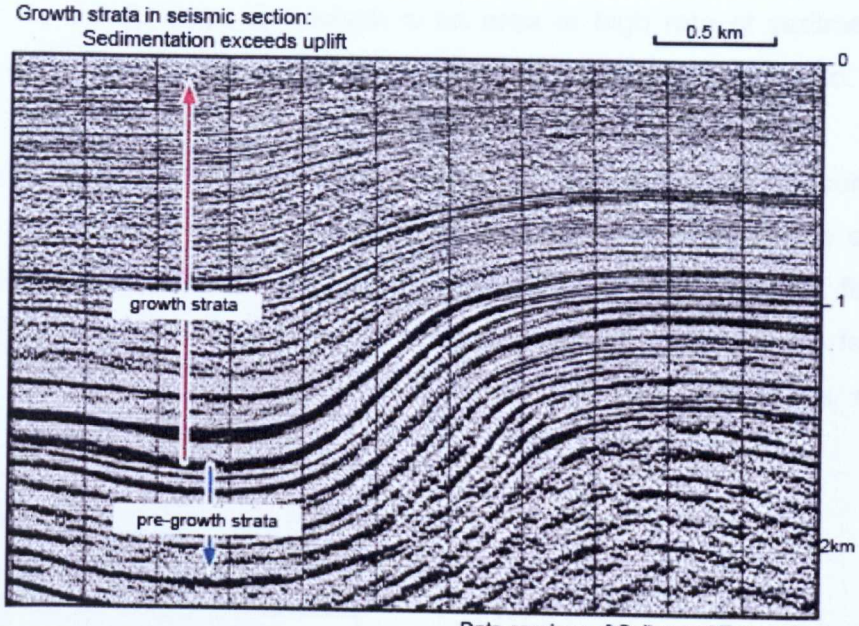

Figure 2-43 - Seismic example of growth strata where the rate of sedimentation exceeds the uplift rate, showing the bedding thinning toward the limb of the structure.

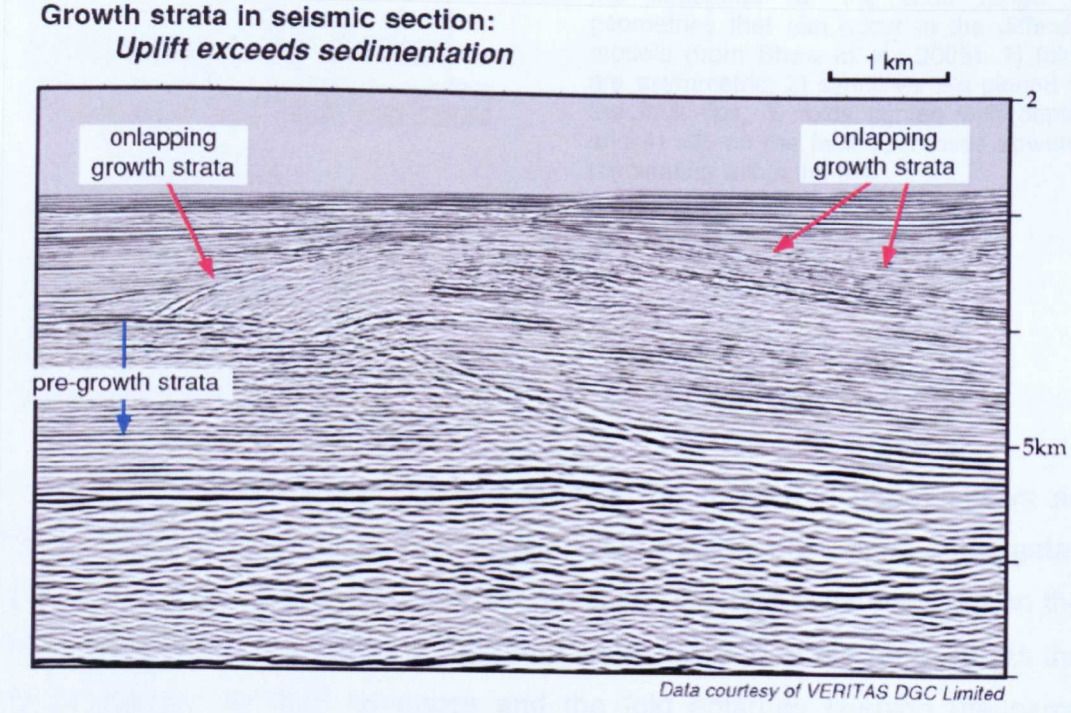

Figure 2-44 - Seismic example of growth strata where the uplift rate exceeds the sedimentation rate, showing the growth strata onlapping the limb of the structure.

2.2.5 Folding mechanisms

Three main classes of folds have been described in gravity driven fold-thrust belts: fault-bend folds, fault-propagation folds and detachment folds (Shaw et

al., 2005). In the Amazon fan, which is an area of high rate of sedimentation, detachment and fault-propagation folds are the most common fold classes identified (Zalan, 2004).

Fault propagation folds form at the tips of faults and consume slip. Although they present a wide range of geometries, they show some common characteristics (Fig. 2.45): 1) they are generally asymmetric with forelimbs steeper and narrower than back limbs; 2) synclines are pinned to the fault tips; 3) folds tighten with depth; and 4) slip on the fault decreases upward, terminating within the fold.

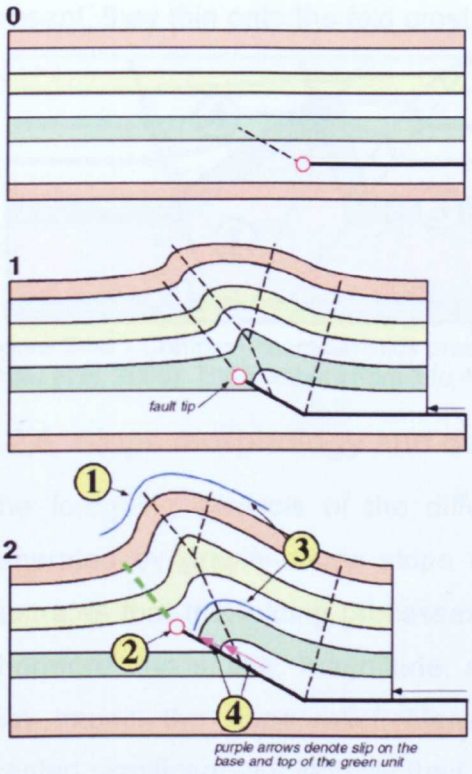

Figure 2-45 - Generic and schematic fault-propagation fold model showing the common characteristics present in most of the structures for the wide range of geometries that can occur in the different models (from Shaw et al., 2005): 1) folds are asymmetric; 2) synclines are pinned to the fault tips; 3) folds tighten with depth; and 4) slip on the fault decreases upward, terminating within the fold.

The schematic model of fault-propagation folds (Fig. 2.45) shows an asymmetric fold develop in the hanging wall as the fault ramp propagates upward, with vergence in the transport direction. The fold consumes slip on the ramp, with slip being greatest at the ramp base and zero at the ramp tip. As the slip increases, the fault advances and the fold enlarges keeping the same geometry.

Detachment folds are formed when the displacement along a bedding-parallel fault is transferred into a folding of the hanging wall layers. They differ from fault-bend and fault-propagation folds because they are not directly related to thrust ramps but to deformation distribution above the detachments. They

form across a large range of scales and can occur as isolated structures or in long fold trains (Shaw et al., 2005). Commonly, they form above a relatively thick ductile layer with a basal detachment (Shaw et al., 2005).

The common characteristics presented by detachment folds are presented in Shaw et al. (2005) (Fig. 2.46): 1) the presence of one incompetent, ductile basal unit thickened in the core of the fold, with no visible thrust ramp; 2) a detachment surface at the base of the ductile unit which defines the downwards terminations of the fold; 3) when there are competent pre-growth layer units, they have a constant layer thickness; and 4) when growth units are present, they thin onto the fold crest and exhibit the fanning of limb dips.

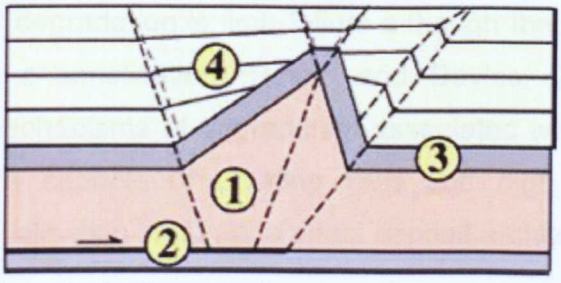

Figure 2-46 - Common characteristics presented by the detachment folds in most styles (from Shaw et al. 2005). The numbers from 1 to 4 refer to the characteristics mentioned in the text.

2.2.6 Slope morphology and degradation

The foregoing analysis of the different types of fold geometry that can be generated by gravity-driven slope deformation in deepwater fold thrust belts illustrates that the folding processes can significantly affect slope morphology. Therefore, the shape, magnitude, symmetry and uplift rates of the anticlines may impact the slope relief. Moreover, not only are the bathymetric highs created significant: additionally their manner of degradation can be an important factor on the development of syn-kinematic depositional systems, influencing the development of both canyons and channel-levees.

In deepwater, unless the folds are in an environment where sedimentation rates are high enough to cover anticlines as they grow, the anticline crests are uplifted above the surface (sea floor). Anticlines grow and accumulate thin, fine grained and poorly lithified sediment on their crests during their early stages of development, in the interlimb angles of 180° to ~140° (Morley, 2007). With the decrease of the interlimb angles during continued anticline growth, syn-kinematic sediments tend to be removed by sliding,

slumping, debris flow, turbidity currents and all the range of gravity processes (Heinio and Davies, 2006; Nigro and Renda, 2004). Thus, for instance, thrust-propagation folds in an area of Niger Delta have generated an asymmetric slope bed relief of up to 200 m, with a long and shallow backlimb with 6° dip and a steeper forelimb with 15° dip (Heinio and Davies, 2006). During the degradation of this fold both erosional and depositional features have affected the slope morphology (Fig. 2.47): backlimb and forelimb failures cause debris flows and thin related deposits; large slumps with evidence for internal deformation; failures associated with ovoid depressions; degradation by channel erosion and channel margin slumping. The most common mechanism of degradation is limb failure although the most erosive, at least volumetrically, is channelisation (Heinio and Davies, 2006). In conclusion, syn-tectonic mechanisms of degradation associated with growth fold are important, as they are capable of creating lows and high that drive the submarine channel localisation and hence affect deposit architecture.

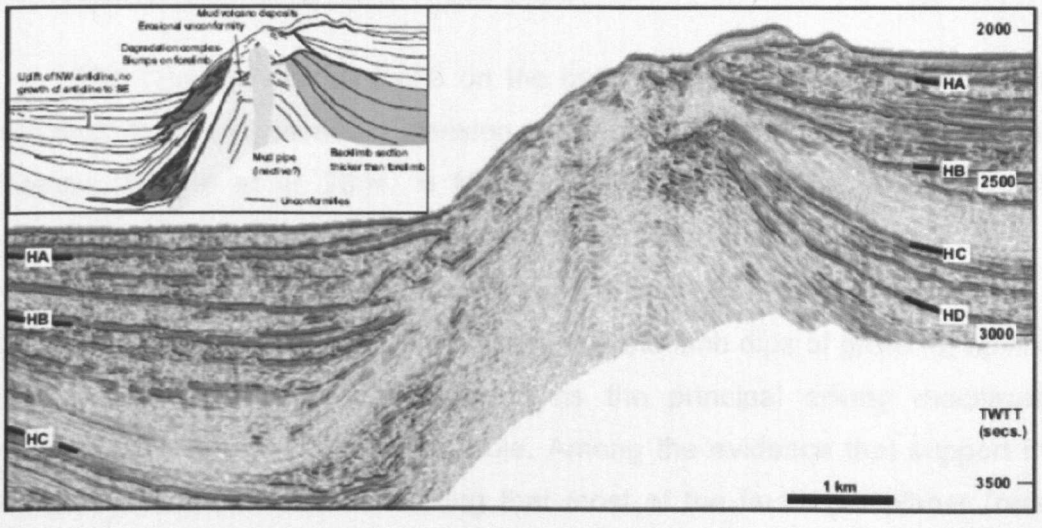

Figure 2-47 – Seismic section showing a degradation complex, multiple unconformities and mud pipe, and a strong thinning of section from the back limb to the forelimb. Notice the erosion, mass movement and mass wasting of material from the crest and forelimb of the fold. The material is re-deposited at the base of the forelimb, creating chaotic deposits or wedge-shaped units (from Morley 2007).

2.2.7 Crestal normal faults associated with fold growth

Minor fault systems that run along the crests of anticlines are commonly associated with fold growth (Grando and McClay, 2004; Morley, 2007). These

fault systems can be characterized by small offsets normally up to 30 m and though can reach as large as 50 m; many such faults are on the limit of seismic resolution (Morley, 2007). These faults propagate over vertical distances from 200 m to 800 m, with backlimb-dipping faults occurring less frequently than forelimb-dipping faults (Fig. 2.48). Fault traces in map view vary from straight, to anastomosing to curved, with complex cross-cutting pattern and these seem to reflect change in slope dip direction and steepness.

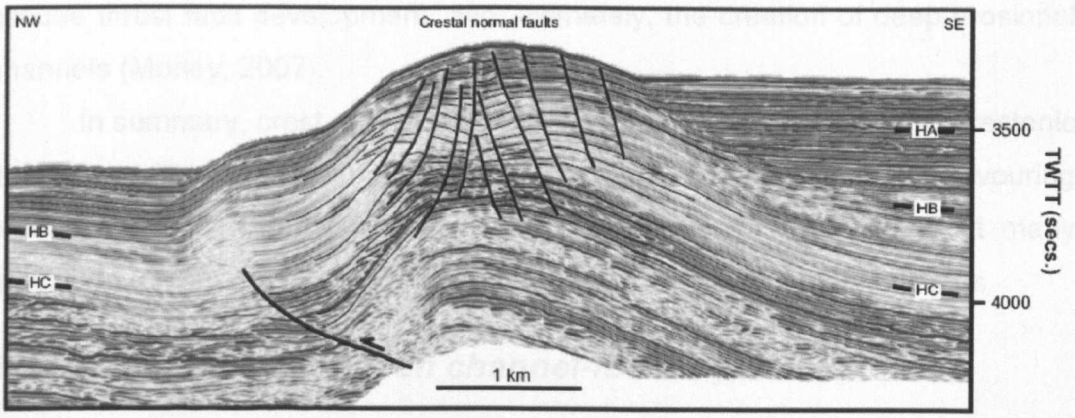

Figure 2-48 – Seismic section showing crestal normal faults with backlimb-dipping faults and forelimb-dipping faults diverging (from Morley 2007).

The origin of normal faults on the crest of growing anticlines has been attributed to several causes: extension in the outer arc of a fold due to bending stresses (Strayer et al. 2004, in Morley, 2007); collapse features due to the withdrawal of a mobile unit or intrusions of salt or overpressured clays; a component of strike-slip or oblique slip motion action along the anticline and to gravity sliding associated with the topography and limb dips of growing, uplifting folds. Of these, gravity is recognised as the principal driving mechanism whereas bending has a secondary role. Among the evidence that support this interpretation, it is worth mentioning that most of the faults are planar (rarely listric) and die out downwards at different depths and horizons, dip in the direction of the steeper limb and the number of faults increases as fold amplitude increases. Such normal faults are considered by Morley (2007) as a "deep seated, non-basal slide, mass movement phenomenon". The occurrence of the faults is constrained to a range of gravity-driven phenomena that affect the folds as they tighten and increase amplitude (Morley, 2007). Therefore, the normal faults in the crest of growth faults mark a period of syn-kinematic fold

evolution when folding initially impacts sea topography. They occur during times that sediments accumulate on the top of growing anticlines and before the crests of anticlines become eroded by gravitational processes.

Normal fault crests contribute to the complex shallow geometry of anticline crests and they record the direction of shallow local stress during folding. As the fold evolves, normal faults change orientation and may cross-cut earlier faults and therefore record such effects as fold amplitude increase, oblique thrust fault development, and, ultimately, the creation of deep erosional channels (Morley, 2007).

In summary, crest growth faults play an important role during syn-tectonic deposition. They induce the sculpturing of the slope topography, favouring processes of fold limb failure and erosion. Additionally, they conduct many gravity driven deposits and can affect the localisation of channel thalwegs.

2.3 Structural controls on channel-levee systems

On many of the major slope systems, gravity tectonics and related fold and faults create subtle to significant sea-floor topography. Slope systems can present complex topography generated by faulting, folding and, salt or mud tectonics and are characterised by coeval sedimentation and deformation. As channels cross the slope there is inevitably a control on their geometry exerted by contemporaneous sea floor topography. Therefore, considerable attention has been given to the stratigraphic architectures and patterns of channel dispersion on topographically complex submarine slopes (Booth et al., 2003; Demyttenaere et al., 2000; Grecula et al., 2003; Mayall and Stewart, 2000; Prather, 1998; Smith, 2004b; Winker and Booth, 2000). The most substantial topographic effects control the downslope route and can cause major diversions of the channel orientation (Mayall and Stewart, 2000). Examples of submarine channel systems described from such settings include the Niger Delta (Adeogba et al., 2005; Deptuck et al., 2003; Heiniö and Davies, 2007), the Gulf of Mexico (Pickering et al., 1986; Posamentier and Mutti, 2003), the Nile Delta (Samuel et al., 2003), Brunei (Demyttenaere et al., 2000), Offshore West Africa (Abreu et al., 2003; Gee and Gawthorpe, 2006) and Eastern Mediterranean Sea (Clark and Cartwright, 2009).

Analysis of 3D seismic data has contributed to the understanding of submarine channels mainly related to their architecture and temporal evolution (Deptuck et al., 2003; Deptuck et al., 2007; Posamentier and Mutti, 2003). There are relatively few studies, however, that address the interactions between submarine channel evolution and deformation and they normally focus only on a specific aspect of channel development, such as channel axis (Clark and Cartwright, 2009). Such studies have noted that increases in slope gradient caused by structural highs result in increased submarine channel incision, with channel down-cutting being localised where the gradient increase is highest (Ferry et al., 2005; Gee and Gawthorpe, 2006; Huyghe et al., 2004). The influence of basin floor bathymetry on channel axis location can explain vertically - stacked channel architectures as described by Clark and Pickering (1996). Features such as submarine canyons, salt, mud or igneous diapir activity, or syn-sedimentary faulting can cause the vertical stacking of channels (Fig. 2.49).

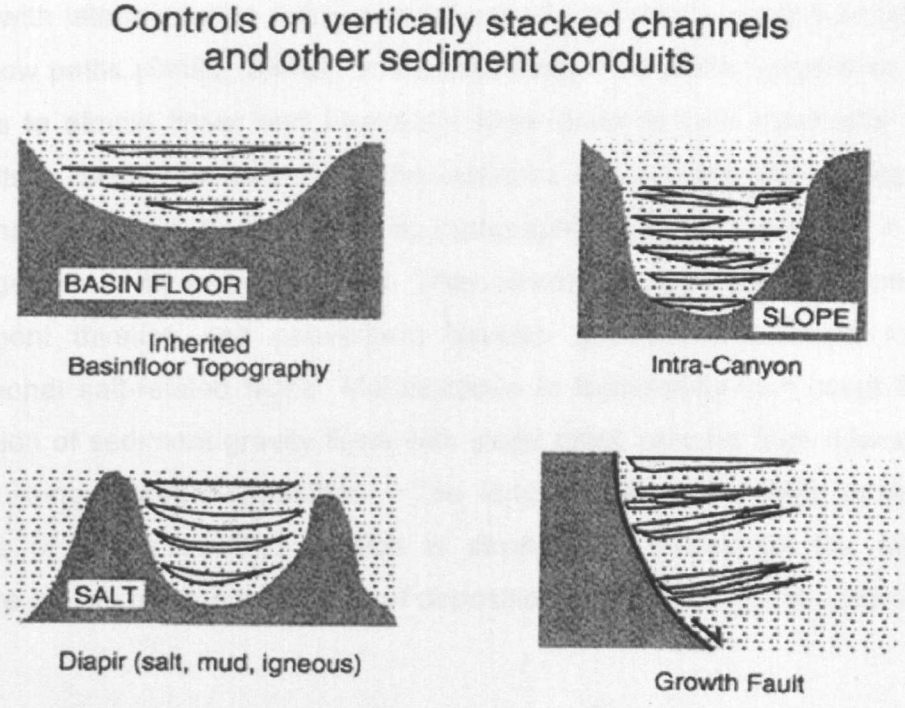

Figure 2-49 – Controls on vertically stacked channels and other sediment conduits. From Pickering et al. (1995b), in Clark & Pickering (1996).

Previous studies have also shown that development of submarine channel sinuosity is a key factor in the development of potentially sand-rich

lateral accretion packages (Abreu et al., 2003). In structurally complex slope settings, submarine channel sinuosity can vary according to changes in gradient: higher sinuosity channel reaches tend to be localised where the underlying slope gradient increases (Ferry et al., 2005; Gee and Gawthorpe, 2006).

Bathymetric features on slope can distribute the sediment through two main systems: cascades of silled sub-basins (Fig. 2.50) and connected tortuous corridors (Fig. 2.51), which are scenarios for deposition and erosion on the slope (Smith, 2004b). Silled sub-basins were described as closed topographic depressions, whereas connected tortuous corridors occur as elongate, variably tortuous, laterally confined depressions on a topographically complex slope (Smith, 2004a). Good examples of these models are present in the Gulf of Mexico for silled sub-basins and on the South Atlantic continental margins of Brazil and in West Africa for connected tortuous corridors. In addition, complex slope topography was divided in three classes: silled sub-basins, partially silled basins with lateral escape paths and tectonically induced bounding slopes that guide flow paths (Smith, 2004b). In the third class, flow paths range from highly tortuous to almost linear and frequently show portions with lower and higher gradients. These flow paths are characterized by complex slope topography and consist of corridors delimitated by topographic highs on the slope, in many cases generated by salt movement. They commonly show seismic facies with convergent thinning and convergent baselap geometries adjacent to syn-depositional salt-related highs. Modifications to topography can occur by the interaction of sediment gravity flows with slope relief, ranging from downcutting to upbuilding through deposition. The longevity of topographic control on patterns of deposition and erosion is strongly dependent on the rates of structure growth relative to the rate of deposition and erosion (Smith, 2004b).

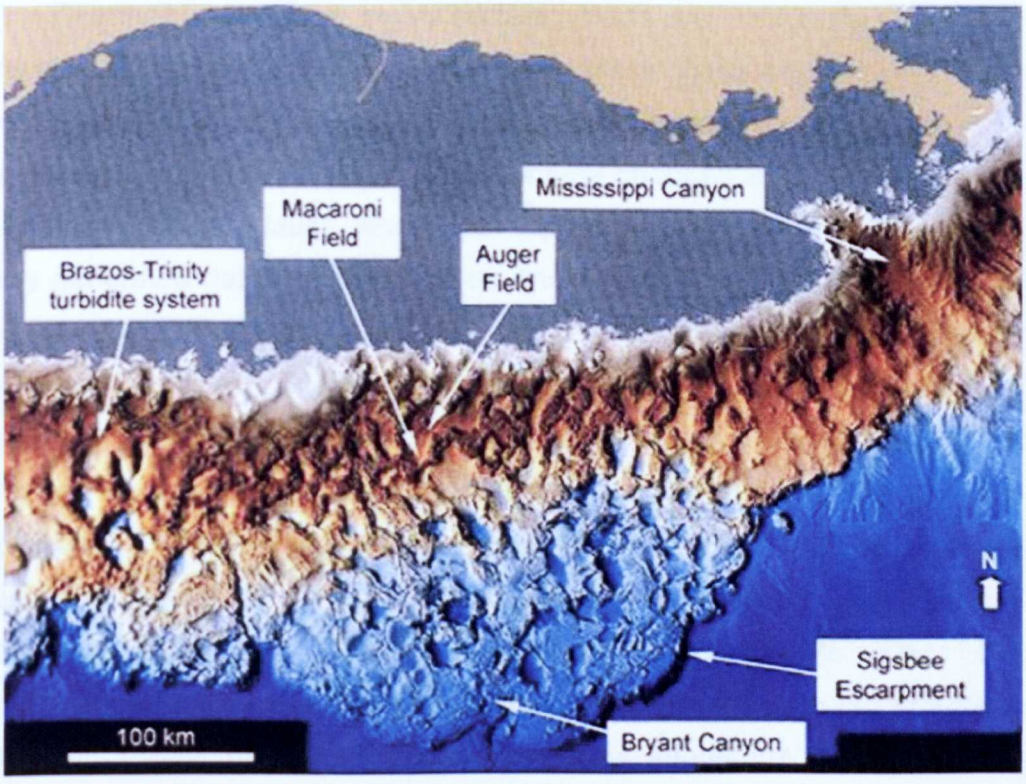

Figure 2-50 – Seafloor image of the Gulf of Mexico salt-based slope, examples of silled sub-basins. Notice the circular an elliptical salt-withdrawal intraslope basins with diameters ranging between approximately 5 and 20 km (from Smith, 2004).

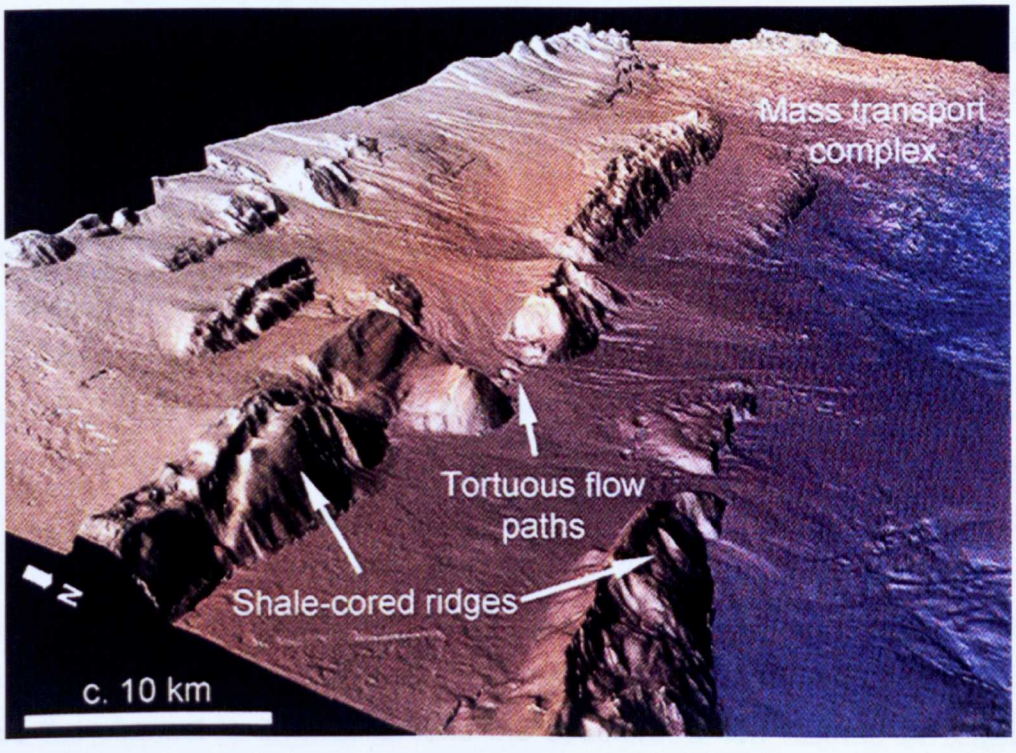

Figure 2-51 – Tortuous corridor paths, between shale-cored ridges on the northwest Borneo slope (Image courtesy Petroleum Geo-Services, in Smith, 2004).

Channels evolving in highly tectonic areas are constantly subjected to dynamic adjustments in their long profile and cross channel geometry (Gee and Gawthorpe, 2006). For example, avulsions in submarine channels of offshore Angola are interpreted to result from structural changes in the maximum slope dip direction, close to faults, where fault slip may cause a channel to seek out a newly generated bathymetric low (Gee and Gawthorpe, 2006). These authors also observed that the disruption of the channel equilibrium profile is pronounced close to salt structures where channels deposit sediment in slope depressions. Abrupt transitions between erosional and depositional channel behaviour occur where confined channels exit into the lower gradients of slope depressions. Channel aggradation and levee buildup can occur directly downslope of constrictions in salt walls and might be related to hydraulic jumps (Gee and Gawthorpe, 2006). The geometry of channels within slope depressions is complex and records the uplift pulses of the adjacent salt diapirs. Clark and Cartwright (2009) define some key submarine channel-structure interactions:

Unconfined channel development – Channel development is unaffected by underlying deformation. It is associated with channel levees that thin exponentially away from the channel axis (Skene et al., 2002) (Fig. 2.52). The channel axis is confined between the contstructional relief of the levees and not physically constrained by the underlying slope.

Confinement – Confinement of a submarine channel is described as the restriction of the course of a channel and its overbank deposits as a result of pre-existing structures (Fig. 2.53A). Confinement limits the ability of the channel to laterally migrate and develop sinuous planform geometry because of structures constraining the channel course (Clark and Cartwright, 2009).

Diversion - Diversion is defined as a change in channel course resulting from a pre-existing structure or structures obstructing the flow pathway of the channel by modifying the slope gradient (Fig. 2.53B). Diversion is normally induced by a pre-existing structure that is orientated at a high angle to the channel flow pathway which causes the channel to flow around the obstacle. Once the channel is diverted around the structure, it can resume its original downslope course.

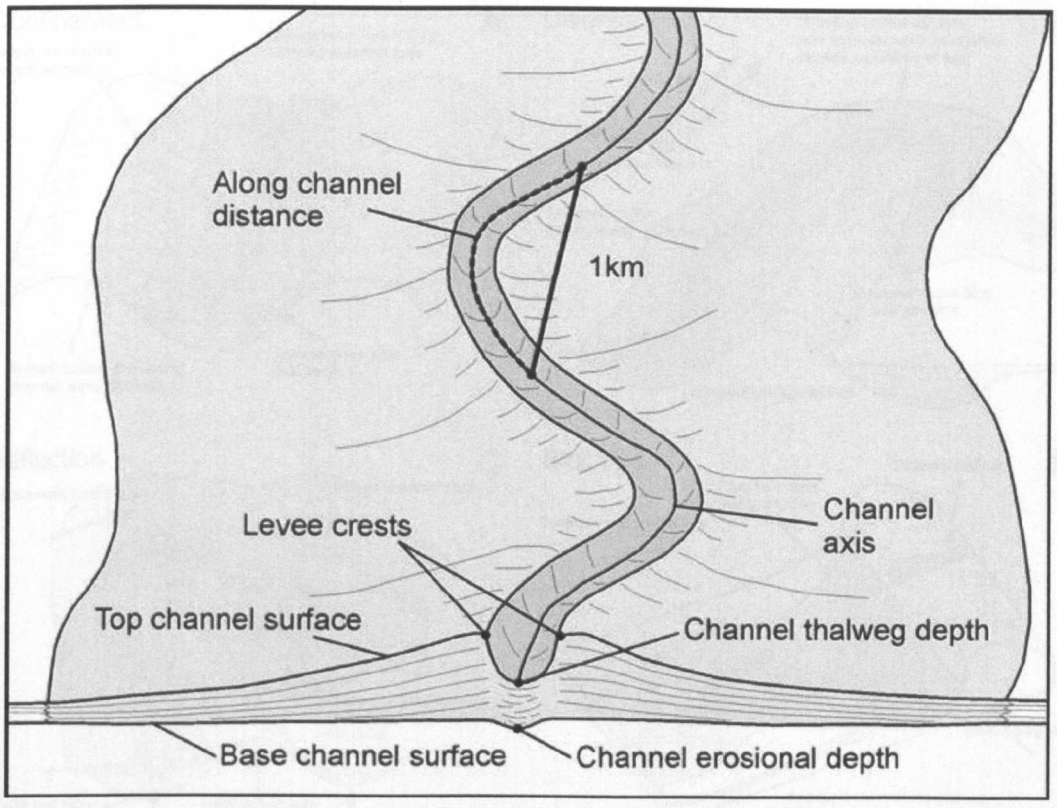

Figure 2-52 – Block diagram showing elements of an "unconfined" channel-levee system (from Clark and Cartwright, 2009).

Deflection – Deflection is defined as a progressive shift in channel position away from the axis of uplift of an adjacent growing structure, causing a shift in channel position to occupy the newly forming topographic low point. Deflection causes successive changes in channel course over time (Fig. 2.53C). This is different from diversion, which involves a single lateral shift in channel position around a passive obstacle to flow. The two types of interaction are therefore similar, with the relative timing of channel development and deformation being the key factor which sets diversion and deflection apart. Lateral accretion surfaces on the side of the channel adjacent to the structure, and erosion on the opposite side are indications that the channel path way is being shifted away from the adjacent structure. Deflection by an uplifting structure such as a growing fold may result in channel abandonment or accretion surface being perched above the present channel thalweg.

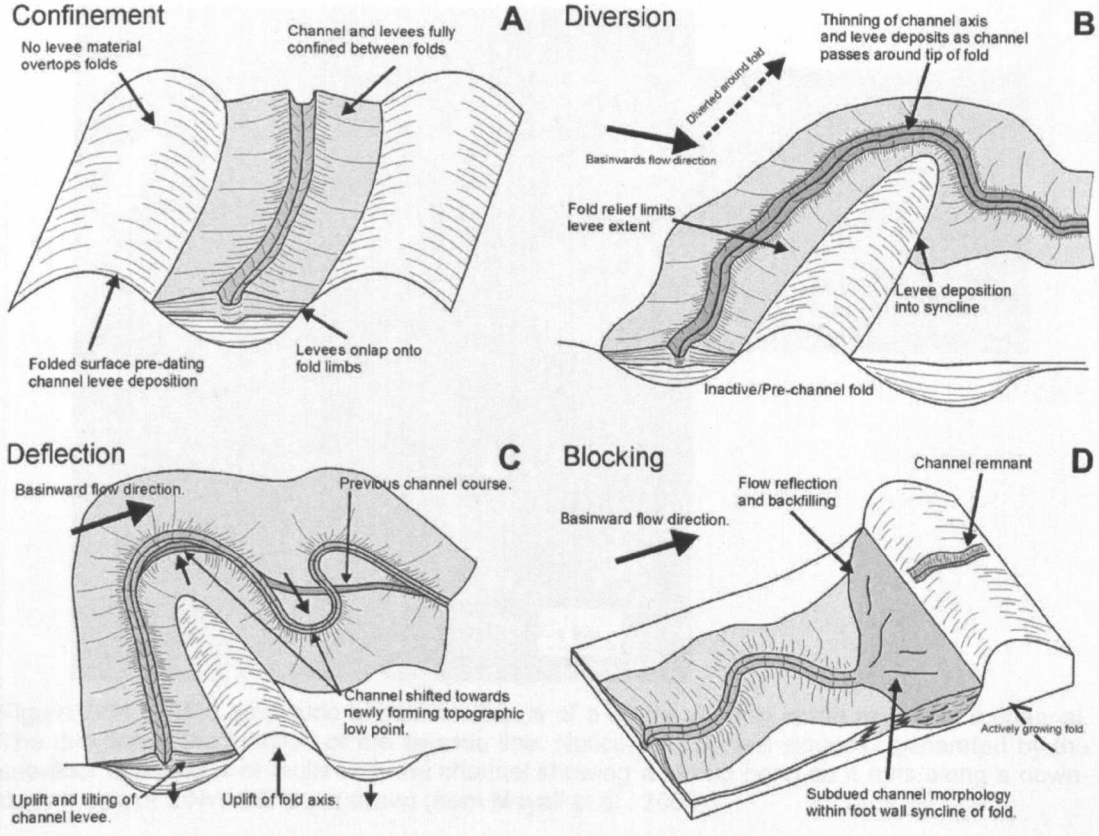

Figure 2-53 – Block diagrams illustrating the four end-member interactions between submarine channel development and underlying deformation (from Clark and Cartwright, 2009).

Not only structures genetically related to gravity tectonics but also extra structures such as transfer faults (Fig. 2.54 and 2.55), related to ocean floor drifting, can affect the channel position on slope. In the Niger delta, for instance, submarine canyons feed aggradational channel-levee systems on the lower slope which are distributaries for large deep sea fans (Morgan, 2004). Here, stacked and sinuous channels developed in larger, low sinuosity, channel complex corridors flanked by huge levees. Both recent and sub-surface channel complexes have been deflected by obstacles on the slope formed by thrusts and folds and have followed the transfer faults down-slope using offsets in the thrust zone relief to reach deeper areas (Fig. 2.56). The apparent facility with which channels cut across the sea-floor relief is due to simultaneous formation of channel-levee and fold growth.

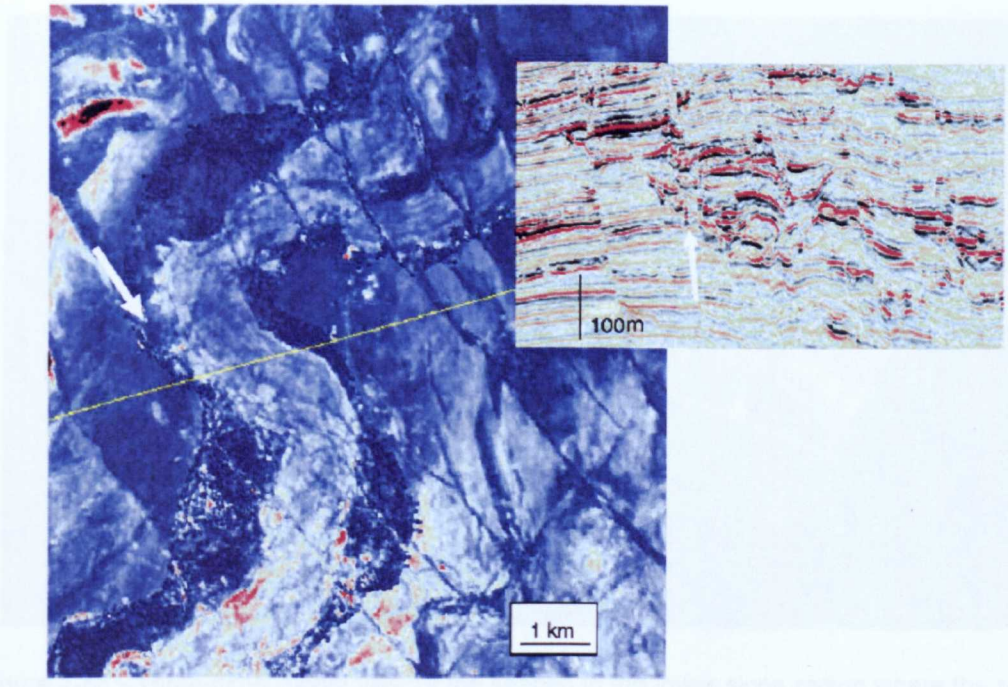

Figure 2-54 – RMS amplitude extraction map is of a 30 ms window in the middle of a channel. The thin line is the location of the seismic line. Notice the channel sinuosity generated by the sea-floor expression of faults with the channel showing a strong bend as it runs along a down-thrown side of a NW-SE fault (arrow) (from Mayall et al., 2006).

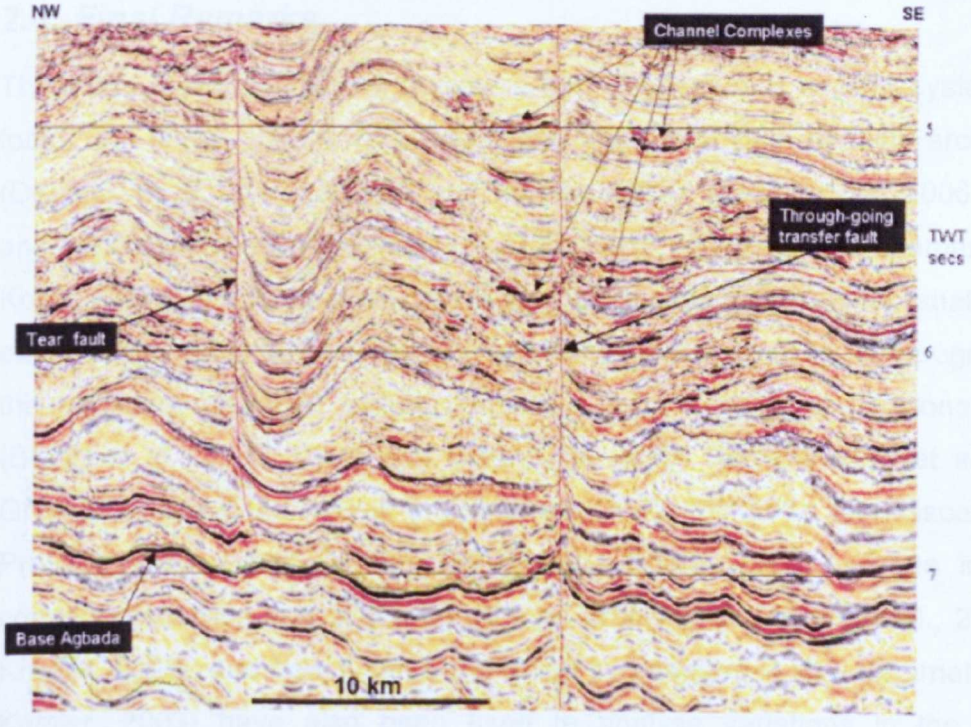

Figure 2-55 - The seismic section shows steep to vertical transfer/tear faults trending NE-SW, a fault rooting at the semi-regional detachment level at the base of Agbada formation and another going on to deeper levels offsetting the detachment level, suggesting that there is an influence of the basement on faulting. The channels are around the transfer fault (from Morgan, 2004).

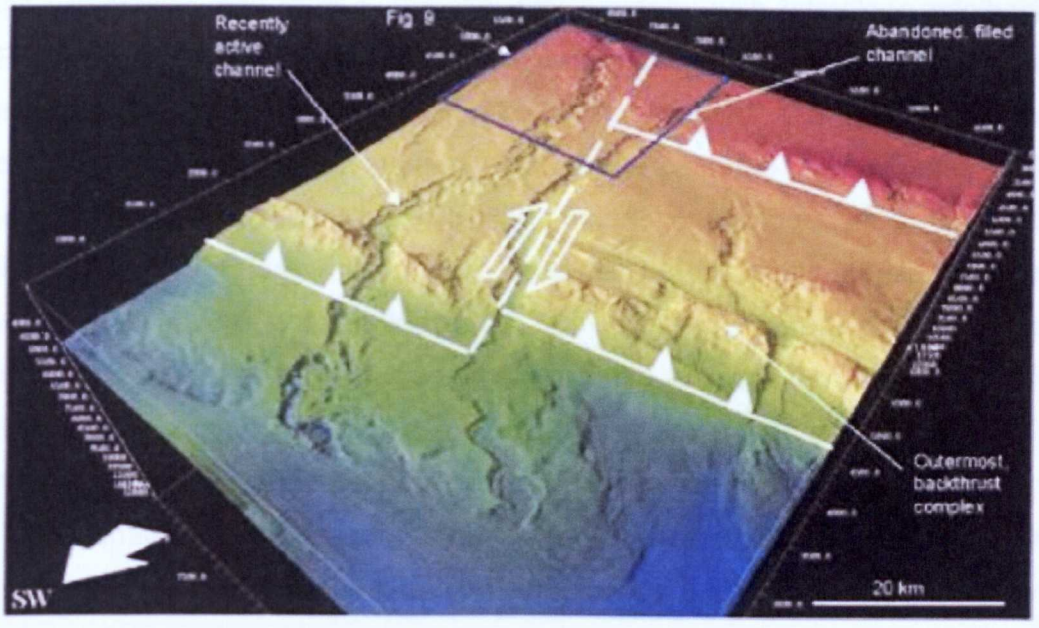

Figure 2-56 - Three-dimensional view of the seabed in the lower slope region where the ridges formed by the underlying thrusts as well as the offset generated by the transfer faults are visible. The recent channel captured by the transfer fault used the offset in the seafloor ridge to reach the outer slope area (from Morgan 2004).

2.4 Final Remarks

There are a large range of studies in both modern and ancient systems that focus on deep marine processes and their resulting deposit architecture (Deptuck et al., 2003; Kneller and Buckee, 2000; Mayall et al., 2006; Mulder and Alexander, 2001; Peakall et al., 2000; Posamentier, 2003; Posamentier and Kolla, 2003). A subset of studies, based in seismic data, outcrop analysis and experiments, have given more attention to the influence of slope topography on the sediment dispersal patterns and the geometries of depositional bodies (Booth et al., 2003; Clark and Cartwright, 2009; Demyttenaere et al., 2000; Grecula et al., 2003; Mayall and Stewart, 2000; Pickering and Hiscott, 1985; Prather, 1998; Smith, 2004b; Winker and Booth, 2000). Some important concepts, such as that of the equilibrium profile (e.g. Pirmez et al., 2000 and Kneller, 2003), and how it can be affected by changes in flow parameters (e.g. Kneller, 2003) have also been used to analyse variations in the channel architecture.

The sea floor topography in areas of halokinesis can be different from that generated by deformation triggered on overpressure shales. In the first case,

salt withdrawal may form a complex physiography with intraslope minibasins (Fig. 2-50) whereas tortuous corridors, *sensu* Smith (2004) commonly prevail in areas of shale - induced tectonics (Fig. 2.51). Moreover, the halokinesis tends to start earlier than a shale-cored deformation because overpressure shales need deeper burial to develop the ductile behaviour which promotes deformation. Therefore, the turbidite flows can be differently affected by these two contrasting styles of sea floor topography. For example, the western African submarine fans may be better analogues for the Amazon Fan than the Gulf of Mexico fans because they have the same style of deformation, driven by overpressured shale and hence more similar slope topography.

The analysis of the literature showed that the integration of modern seismic data (which shows channel planform morphology and spatial distribution) with outcrop data (which shows internal deposit character and vertical organization) is an effective method of study to clarify structural controls on slope topography and, consequently the dispersion of the submarine channels on the slope. However, although there is a significant amount of literature on submarine channel styles and evolution there are still some gaps that need to be investigated and that form the focus of this thesis:

- Previous studies show the transition from an erosional base to aggradational channel-levee vertically (e.g. Deptuck et al., 2003) but do not show how the transition evolves spatially in time. In this regard a key question is whether there is any upstream or downstream migration of the transition point between erosional and aggradational channels, and how such migration might be recorded in the architectural elements which build channel-levee systems.
- Most of channel avulsions documented in the literature of deep marine systems are related to levee breach of a perched aggradational channel. The avulsion of an erosive or at grade channel is still a theme for discussion.
- Channel-levee systems are inferred to accrete downstream, as the levees size reduces in this direction. Can a system also accrete upstream? How is it recorded in the channel-levee style? How is the transition between the leveed channel and the upstream erosive channel configured?

- The Amazon Fan literature does not mention any effect of slope tectonics on channel-levee evolution. Did the tectonics affect the channel development and dispersion in this fan?
- The upward transition from a basal HARP to a channel-levee system is described to result mainly as a result of a reduction of the flow grain size (Pirmez, 2000). However, this model does not account for the development of an erosive channel at the base of the channel-levee systems (originally described in Amazon fan in the current thesis) cutting through the HARPs in the study area.
- Levee asymmetry has been explained as a result of Coriolis Force in the majority of the cases, when it is not related to flow stripping or inertial overspill. In the case of a channel located close to the Equator, where Coriolis forcing is negligible, how can levee asymmetry develop along the whole length of channel?
- Most of the studies on the effects of tectonics on slope sedimentation focus on the role of tectonics on the bathymetry. The relative timing of the slope structures in relation to the channel formation (pre, syn or post-depositional), however, is discussed in only few articles (e.g., Clark and Cartwright, 2009). Therefore, the relative timing of structuring and channel development, which may determine channel architectural styles and location, requires further analysis.
- Few studies have addressed the role of equilibrium profile on slope channel evolution (Ferry et al., 2005; Kneller, 2003; Pirmez et al., 2000). There remain some open questions about the applicability of this concept to submarine systems, in terms of where to define effective base levels, at what scale (local or basinal) the equilibrium surface should be analsysed, and the what role syn-deposition tectonics play in perturbing equilibrium profiles of slope channels.

3 AMAZON FAN SETTING

The Amazon Fan is one of the largest deep-sea fans in the World, and is located in the Foz do Amazonas Basin in the extreme northwestern part of the Brazilian Equatorial Margin between the parallels 3° N and 9° N (Fig. 3.1). The basin covers an area of about 268,000 km^2 (Figueiredo et al., 2007), and evolved in a context of both wrench tectonics (kinematically linked to ancient Atlantic spreading – related transform faulting), and compressional tectonics (related to the history of Andean uplift, which reorganized the catchment basin of the Amazon River (Hoorn et al., 1995)).

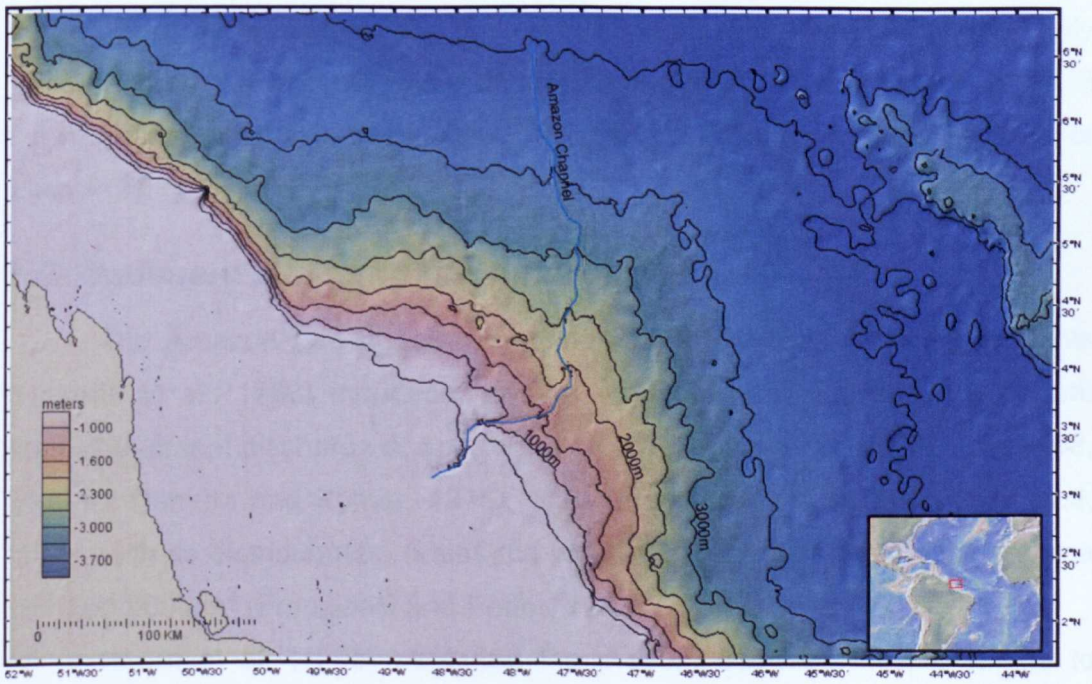

Figure 3-1 – Bathymetric map of the area of Amazon Fan obtained from the Marine Geoscience Data System.

3.1 Stratigraphy of the Foz do Amazonas Basin

A stratigraphic chart for the basin fill is presented in Figure 3.2. The syn-rift sequence is composed of Neocomian to Albian fluvio-deltaic, lacustrine and marine strata (Caciporé Formation), infilling a pull-apart half-graben (Figueiredo et al., 2007). Open-marine clastic deposition started in the Late Albian (102 Ma) with deepwater mudstones and siltstones (Limoeiro Formation) and persisited

until the Late Palaeocene. These sediments are followed by a Selandian to Tortonian mixed carbonate–siliciclastic platform succession (Marajó and Amapá Formations), deposited between 62 and 11.3 Ma, with equivalent deep-water calcilutites and mudstones (Travosas Formation). Increasing rates of Andean uplift and an associated strong increase in sediment supply by the river drove the deposition of a thick siliciclastic sequence up to 10 km thick from the Middle–Late Miocene (11.8–11.3 Ma) (Figueiredo et al., 2007). This sequence comprises shoreline facies (Tucunaré Formation) and the Amazon Fan which is composed of continental slope fine sand, clay facies (Pirarucu Formation) and deep-water mud facies (Orange Formation) (Figueiredo et al., 2007).

The final sequence, which includes the Amazon Fan, corresponds to more than 50% of the volume of the post-rift sediments although it represents only 10% of the time of deposition (Figueiredo et al., 2007). The slope sediments of the Quaternary, which are included in Pirarucu Formation, are the focus of study in this thesis.

3.2 Sediment supply to the Amazon Fan

The Amazon Fan is composed primarily of Andean-derived sediments (Damuth et al., 1988) introduced by the Amazon River which has a current annual sediment discharge of approximately 400 million tonnes (Holeman 1968, cited in: Damuth and Kumar, 1975). The Amazon river is 6770 km long and, along with its distributaries, drains the world's largest river basin, with an area of 7,050,000 km^2 (Franzinelli and Potter, 1983).

Hoorn et al. (1995) attributed the present eastward river drainage to geomorphologic changes related to Andean Uplift during Middle-Late Miocene, dated between 11.8 and 11.3 Ma (Figueiredo et al., 2009). Before, the headwaters of the river flowed northward to the Caribbean margin (Fig. 3.3). The onset of the transcontinental Amazon River supplied high volumes of siliciclastic sediments to Atlantic the shelf, causing the shut down of the Neogene carbonate platforms (Brandao and Feijo, 1994), forming the deep marine Amazon Fan.

Figure 3-2 – Stratigraphic Chart of Foz do Amazonas Basin (Figueiredo et al., 2009). The studied interval is in the Pirarucu Fm which is part of the thickest (9000 m) and latest 2nd order depositional sequence (N40-N60) which includes the Amazon Fan sediments.

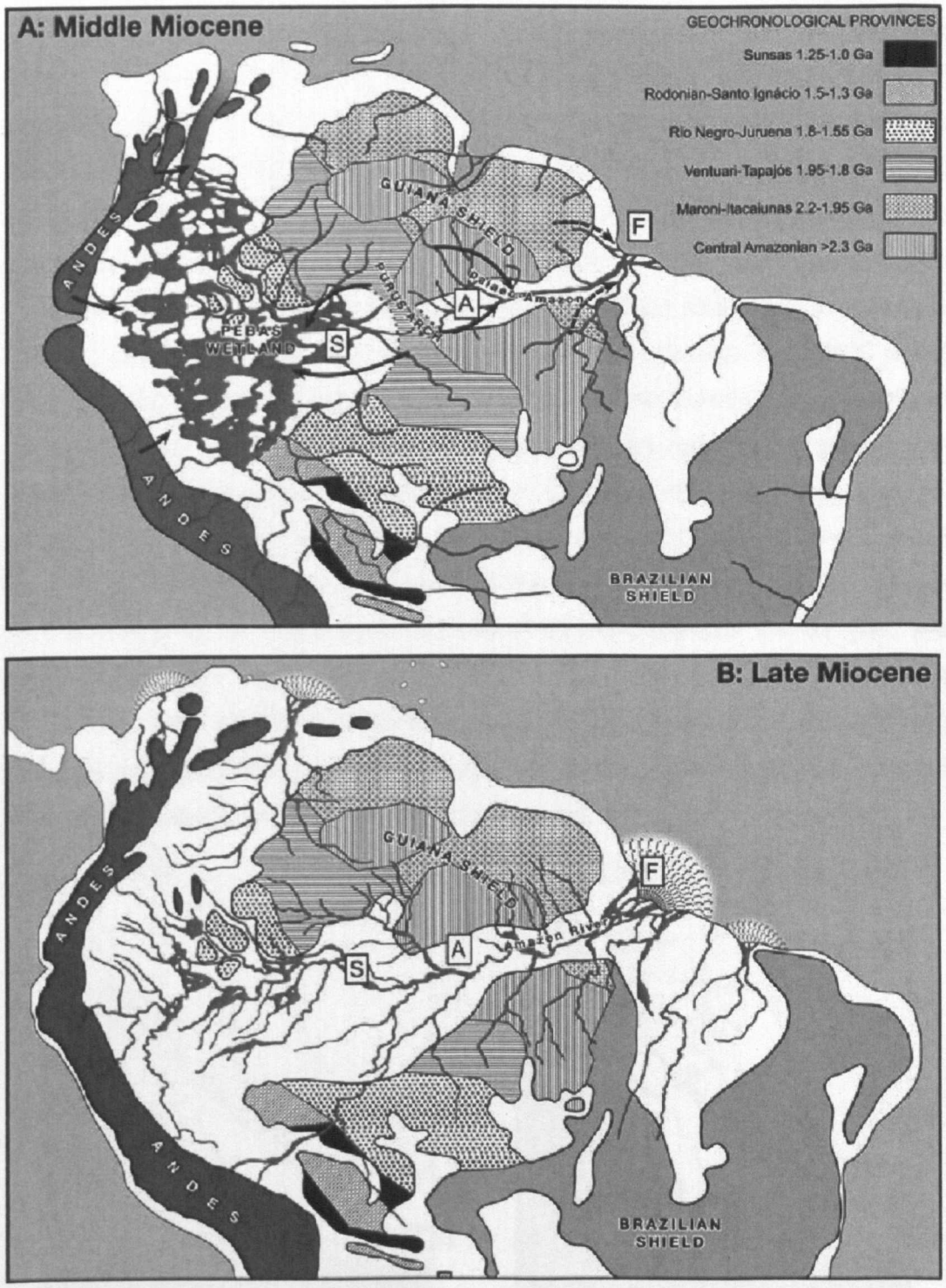

Figure 3-3 – Paleogeographic maps of the paleo Amazon hydrographic basin during Middle and Late Miocene (from Figueiredo et al., 2009). **A** - During the Middle Miocene the Solimoes River (S) flowed northward to the Caribean Sea. **B** – During the Late Miocene, due to stronger Andes uplift and sea level fall, the Solimoes connected to the Amazon River (A) forming a transcontinental river.

3.3 Marine currents

By the mid-Holocene sediment deposition in the Amazon fan was interrupted because the rising sea level prevented the transport of sediment across the shelf feeding the Amazon canyon. This sediment has been deviated northward along the South American Coast by the North Brazil Coastal Current (NBCC) (Flood and Piper, 1997) (Fig. 3.4). During lowstand, however, the NBCC would have circulated close to the slope as shown by the reconstruction of surface water composition based on oxygen isotope data from foraminifera (Maslin, 1998) (Fig. 3.5). This raises the question of whether the NBCC could have affected slope sedimentation, dictating the N/NW direction of channelized slope deposits. If so, as soon as the turbidite currents came out of the canyon mouth, they would have been driven toward NW/N and formed the channel-levee systems with that orientation. At present, the NBCC or NBC (North Brazil Current, Johns et al., 1998) is weak (less than 20 cm/s) in water depths greater than 200 m (Fig. 3.6), whereas currents of 50 cm/s towards the SE (i.e., the opposite direction) were measured in depths of 1400 m and deeper (Johns et al., 1998). Although the configuration of the Pleistocence current is not known, these data suggest that marine currents were probably unlikely to have dictated submarine channel orientations during this period.

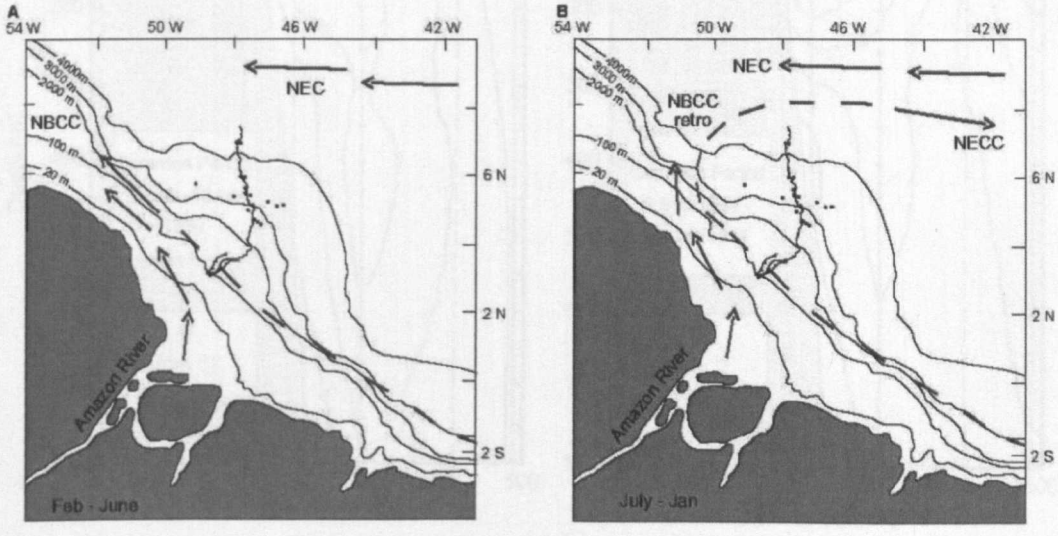

Figure 3-4 – Schematic map showing the present ocean circulation over the Amazon Fan. NBCC = North Brazil Coastal Current, NEC = North Equatorial Current, NECC = North Equatorial Counter Current, retro = retroflection of NBCC, small dots are the locations of Leg 155 sites. A) Surface circulation from February to June. B) Surface circulation from July to January. From Flood and Piper (1997).

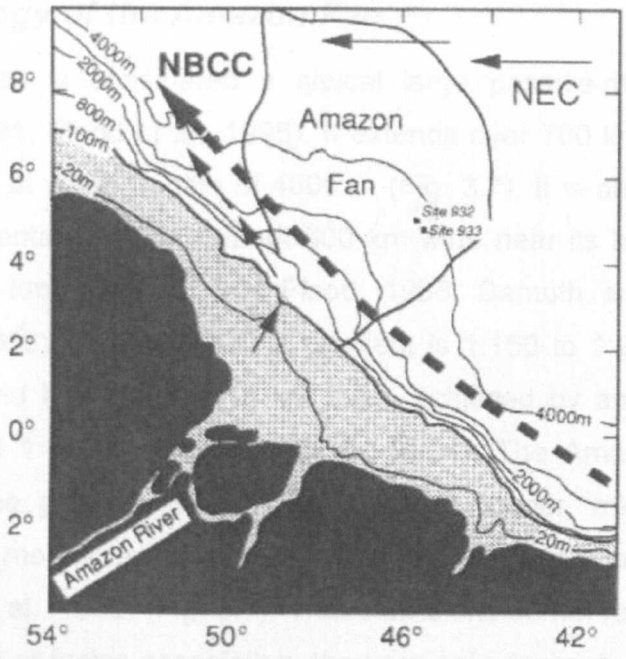

Figure 3-5 – Schematic map showing the possible glacial winter ocean circulation with peak Amazon River discharge, during the last glaciations, from Maslin (1998). NBCC = North Brazil Coastal Current, NEC = North Equatorial Current. Notice the glacial coastline of Brazil moved to the contour curve of 100 m due to lower sea level.

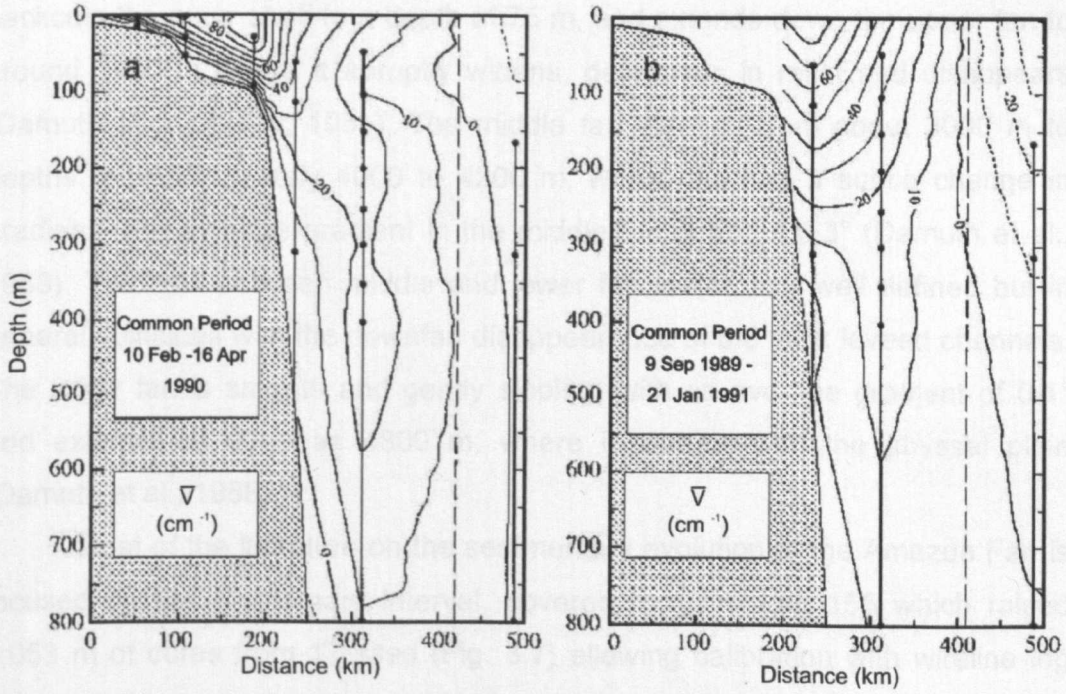

Figure 3-6 – Cross sections of mean alongshore (positive northwest) velocity for (a) common period (Feb-Apr 1990) and (b) common period (Sep1989-Jan 1991). Notice that in both cases that at 800 m water depth the current is smaller than 10 cm/s. Diagrams from Johns et al. (1998).

3.4 Morphology of the Amazon Fan

The Amazon Fan is considered a typical large passive-margin muddy-fan (Flood et al., 1991; Flood et al., 1995). It extends over 700 km seaward of the continental shelf at water depths of 4800 m (Fig. 3.7). It is about 380 km wide along the continental shelf and about 600 km wide near its base, covering an area of 330000 km^2 (Damuth and Flood, 1983; Damuth and Kumar, 1975; Pirmez et al., 2003). The longitudinal gradient is 1:150 to 1:200 (Damuth and Kumar, 1975) and it can reach 10 km thick, achieved by an average rate of sedimentation of 1 mm/yr (Cobbold et al., 2004). The Amazon Fan can be divided into three general morphologic divisions (upper, middle, and lower) based on broad morphologic and acoustic characteristics (Damuth and Flood, 1985; Damuth et al., 1988) (Fig. 3.7). These divisions do not reflect different fan subenvironments or facies association, they are only descriptive. The upper fan extends from the shelf break to depths of about 3000 m where there is a noticeable break in slope. The average gradient is approximately 0.8°. The upper fan includes the Amazon Canyon, which is up to 600 m deep and backcuts the outer shelf to a depth of 75 m, and extends down the upper fan to around 1400 m where it abruptly widens, decreases in relief and disappears (Damuth and Embley, 1981). The middle fan extends from about 3000 m to depths of approximately 4000 to 4200 m, where there is a subtle change in gradient. The average gradient in the middle fan is about 0.3° (Damuth et al., 1988). The limit between middle and lower fan is not very well defined but in general coincides with the downfan disappearance of the thick leveed channels. The lower fan is smooth and gently sloping, with an average gradient of 0.1° and extends as deep as 4800 m, where it merges with the abyssal plain (Damuth et al., 1988).

Most of the literature on the sedimentary evolution of the Amazon Fan is focused on the Quaternary interval, covered by ODP Leg 155 which raised 4,053 m of cores from 17 sites (Fig. 3.7) allowing calibration with wireline log data and selected seismic data (Flood et al., 1995). In spite of the fact that the fan is mud-rich, the Ocean Drilling Program (ODP) shallow seismic profiling and high-resolution sonar images of the sea floor have demonstrated that sand is still an important constituent of the fan, as a component of channel-fill, the

ponded sheet-like deposits (high amplitude reflection packets) and the lower-fan deposits (Damuth and Kowsmann, 1998; Flood and Piper, 1997).

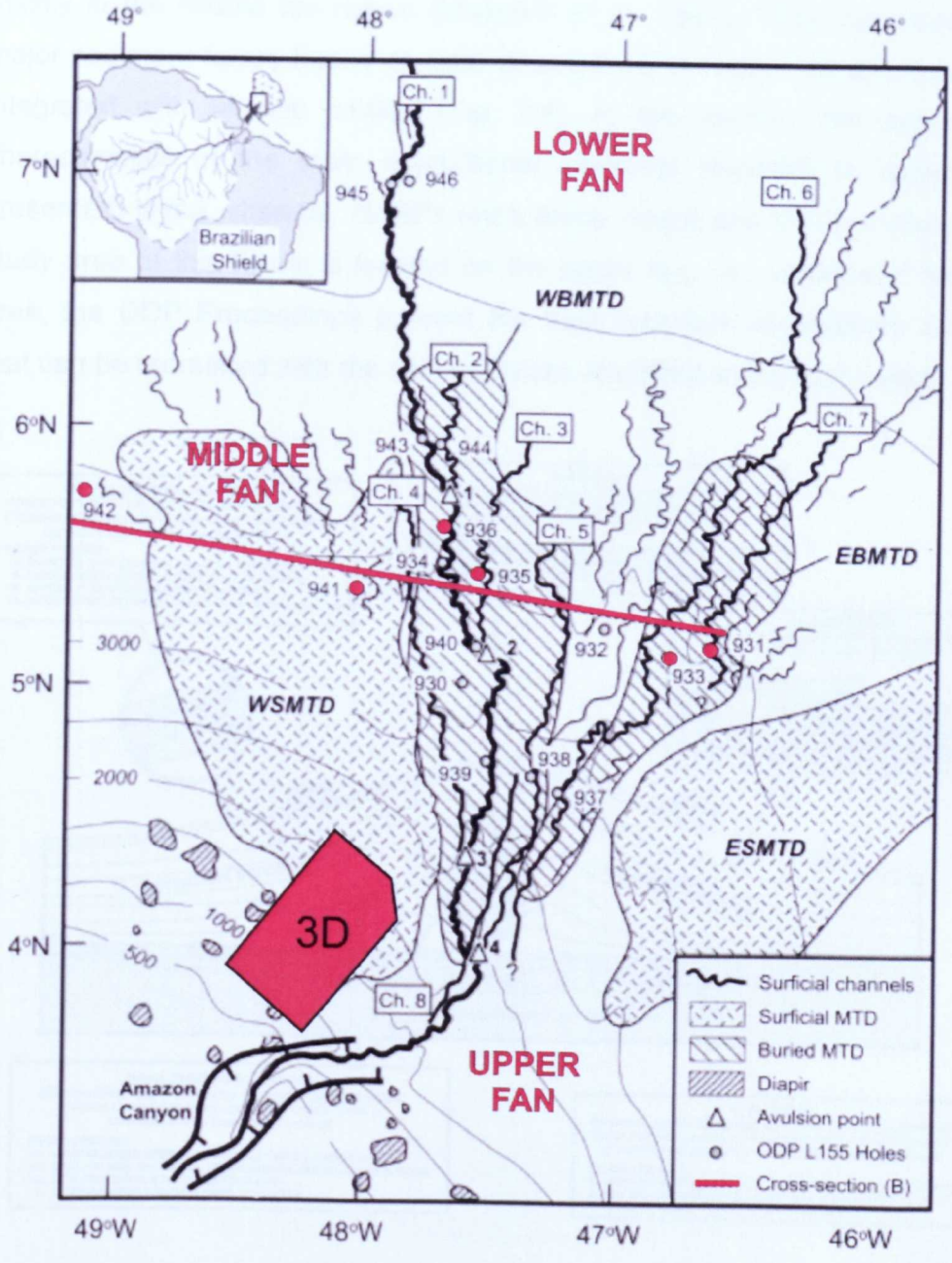

Figure 3-7 - Amazon Fan showing the 17 sites drilled during Ocean Drilling Program Leg 155. The meandering channels on the fan surface were imaged by long-range side-scan sonar (GLORIA) and multibeam bathymetry. The location of the Surficial Mass-Transported Deposits (SMTD) is from Flood et al. (1995) and the Buried Mass-Transported Deposits (BMTD) from Piper et al. (1997). The Red line shows the position of the cross-section shown in Fig. 3.9 (Adapted from Lopez, 2001). The 3D survey area and the boreholes included in the cross section (Fig. 3.9) are also indicated in red.

The most detailed sediment descriptions in the Amazon Fan are presented in the ODP Leg 155 Proceedings, focused on sediments recovered mainly in the middle fan region (Normark et al., 1997). They summarized 15 major sediment facies based on core descriptions of recovered sediments and integrated with seismic profiles (Fig. 3.8). In this section, the sedimentary characteristics of the main depositional elements identified in seismic are presented: levee, channel, HARPs (intra-slope lobes) and MTDs. Although the study area of this thesis is located on the upper fan, i.e., upslope of the ODP area, the ODP Proceedings present the best sediment descriptions available that can be correlated with the seismic facies identified in the study area.

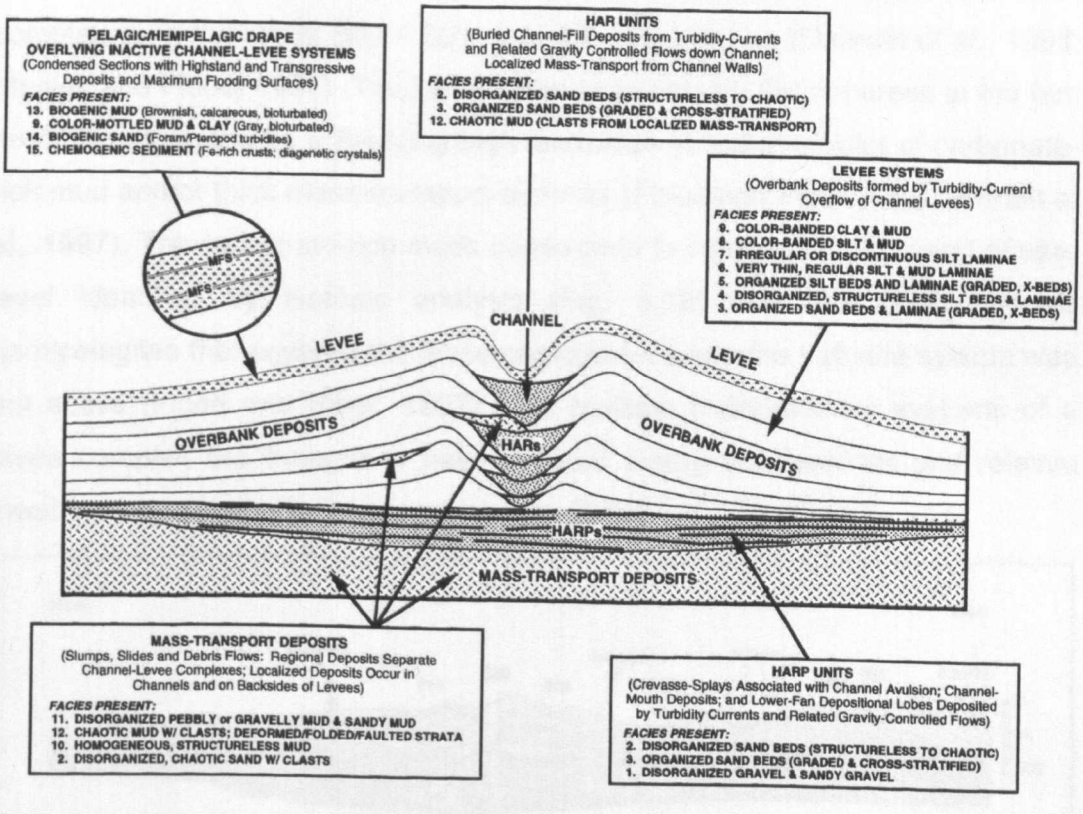

Figure 3-8 – Schematic diagram showing the distribution of sedimentary facies within acoustic units (e.g., HAR units, HARP units), mass-transport deposits and channel-levee architectural elements in the Amazon Fan. The diagram shows a typical channel-levee system, which is the elemental stratigraphic unit of the fan, and the underlying regional scale MTD. This stratigraphic relationship is typical of the upper and middle fan (Damuth et al., 1988; Flood et al., 1995; Manley and Flood, 1988). From Normark et al. (1997).

3.4.1 Channel-levee systems: dispersion, lithofacies, architecture

The middle and the upper fan were constructed mainly by the deposition of a distributary network of overlapping channel-levee systems, with thickness range between 100 and 200 m that were formed by periodic channel avulsions (Damuth et al., 1983a; Jegou et al., 2008; Manley and Flood, 1988). This complex network of meandering channel-levee systems has been mapped with swath bathymetry, side-scan sonar and high resolution seismic data to about 4300 m of water depth (Damuth et al., 1988; Damuth et al., 1983a; Flood et al., 1991; Manley and Flood, 1988).

The channel-levee systems have been grouped into four larger units, called levee complexes (Fig. 3.9), the upper, middle, lower and bottom levee complexes, in the upper 500 – 800 m of the Amazon Fan (Damuth et al., 1988; Manley and Flood, 1988). The levee complexes occupy distinct areas in the fan, normally separated by a flat-lying high amplitude reflector couplet of carbonate-rich mud and/or thick mass-transport deposits (Flood and Piper, 1997; Hiscott et al., 1997). The carbonate-rich muds correspond to interglacial highstand of sea-level identified by isotopic analysis (Fig. 3.10) and are interpreted as hemipelagites that covered the levee complexes, when the turbidite system was not active (Flood and Piper, 1997). The multiple channel-levee systems of a levee complex are thought to have evolved during sea-level fall and relative lowstand of a single glacial period (Lopez, 2001).

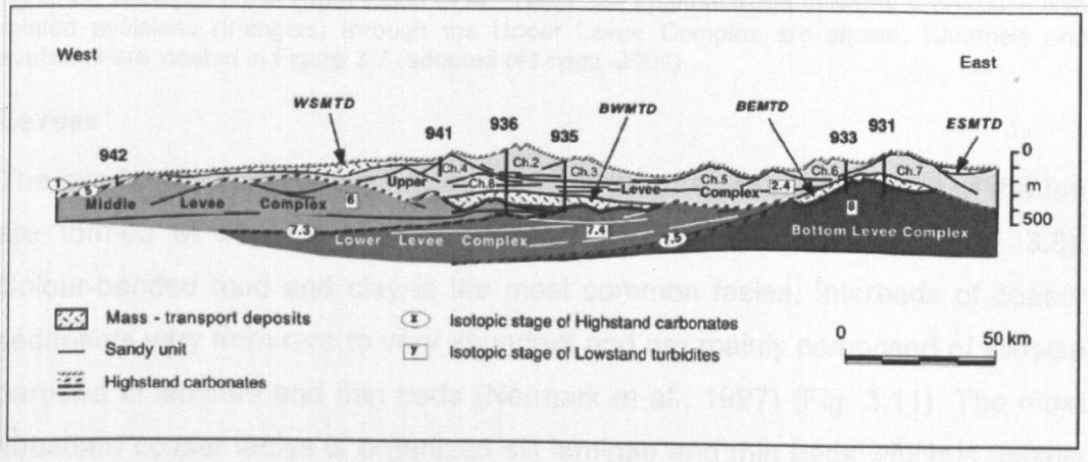

Figure 3-9 – Schematic cross-section with location as visualised in Fig. 3.7 Levee Complexes, Surficial and Buried Mass-Transported Deposits and highstand carbonate units with respective isotopic stage assignments are shown (from Lopez, 2001).

The placement of the channel-levee systems is determined by the inherited relief generated by precursor channel-levee systems and mass-transport deposits derived from the continental slope (Flood et al., 1995) and is also affected by structural features such as anticlinal folds related to gravitationally induced deformation of the fan (Nakajima et al., 2009). In the middle fan area, channel avulsion occurred frequently causing channels to switch position downstream of this area (Manley and Flood, 1988).

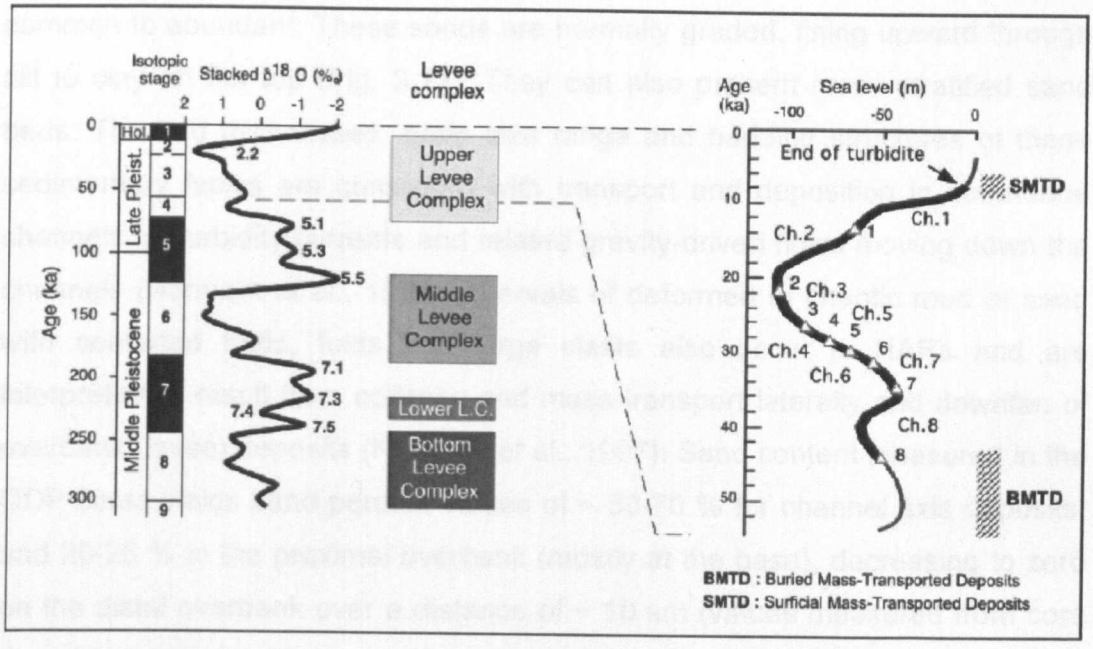

Figure 3-10 – Time distribution of the quaternary sediments of the Amazon Fan. On the left, the isotopic curve of Imbrie et al., (1984) related isotopic stages and relationships to the Upper Quaternary Levee Complexes of the Amazon Fan, obtained from Flood and Piper, 1997. On the right, the sea-level curve (from Flood et al., 1995) and channel-levee systems succession with related avulsions (triangles) through the Upper Levee Complex are shown. Channels and avulsions are located in Figure 3.7 (adapted of Lopez, 2001).

Levees

The overbank deposits which constitute the volumetrically major part of the fan are formed of seven interbedded facies (Normark et al., 1997) (Fig. 3.8). Colour-banded mud and clay is the most common facies. Interbeds of coaser sediments vary from rare to very abundant and are mainly composed of silt-size particles in laminae and thin beds (Normark et al., 1997) (Fig. 3.11). The most abundant coaser facies is organized silt laminae and thin beds which is usually present as parallel and cross laminated laminae and thin beds, rarely with normal grading or with climbing ripples (Normark et al., 1997).

Channel-fill

The modern Amazon Channel and the underlying HARs units contain much more abundant thicker bedded, coarse facies than do the levee deposits (Normark et al., 1997) (Fig. 3.8). The predominant facies is thick-bedded, disorganized structureless to chaotic sand. These beds commonly contain abundant large mud clasts and consist of poorly sorted fine to coarse sand. Medium to thick intervals of sands of grain size fine to medium are also common to abundant. These sands are normally graded, fining upward through silt to clay on the top (Fig. 3.11). They can also present cross stratified sand beds. The bed thicknesses, grain size range and bedding structures of these sedimentary facies are consistent with transport and deposition in submarine channels by turbidity currents and related gravity-driven flows moving down the channels (Normark et al., 1997). Intervals of deformed to chaotic mud or sand with contorted beds, folds and large clasts also occur in HARs and are interpreted to result from collapse and mass-transport laterally and downfan of overbank (levee) deposits (Normark et al., 1997). Sand content measured in the ODP cores yields sand percent values of ~ 50-70 % for channel axis deposits, and 20-25 % in the proximal overbank (mostly at the base), decreasing to zero on the distal overbank over a distance of ~ 10 km (values measured from core descriptions and well logs in Flood et al. (1995) and Pirmez et al. (1997)). Although the channel axis deposits have relatively high sand content, their contribution to the total volume of channel-levee sediments is small. The average sand content of the entire channel-levee system is estimated by measuring the cross-sectional areas of axial and levee deposits weighted by the average and content for the axial, proximal overbank and distal overbank areas. This yields ~ 10 % sand and 90 % mud for typical cross-sections in the middle part of the fan.

Intra-slope lobes (HARPs)

The coarsest grained facies in the Amazon Fan are found in the HARP layers (base of levee sands) which include disorganized gravel and sandy gravel, disorganized sand beds (structureless and chaotic) and organized sand beds (graded and cross stratified) (Fig. 3.8). The HARPs contain 70-90 % sand in medium to thick beds (Pirmez et al., 1997). Thick beds (>1 m) are massive and

often contain mud clasts. The typical succession has a sharp base and top, with the upper contact with thin-bedded overbank deposits characterized as a pronounced downlap surface on seismic (Pirmez et al., 1997; Pirmez and Flood, 1995) (Fig. 3.11). The sand beds do not appear to have any particular vertical trend but are clustered in bed packets 5-20 m thick separated by thin-bedded turbidites.

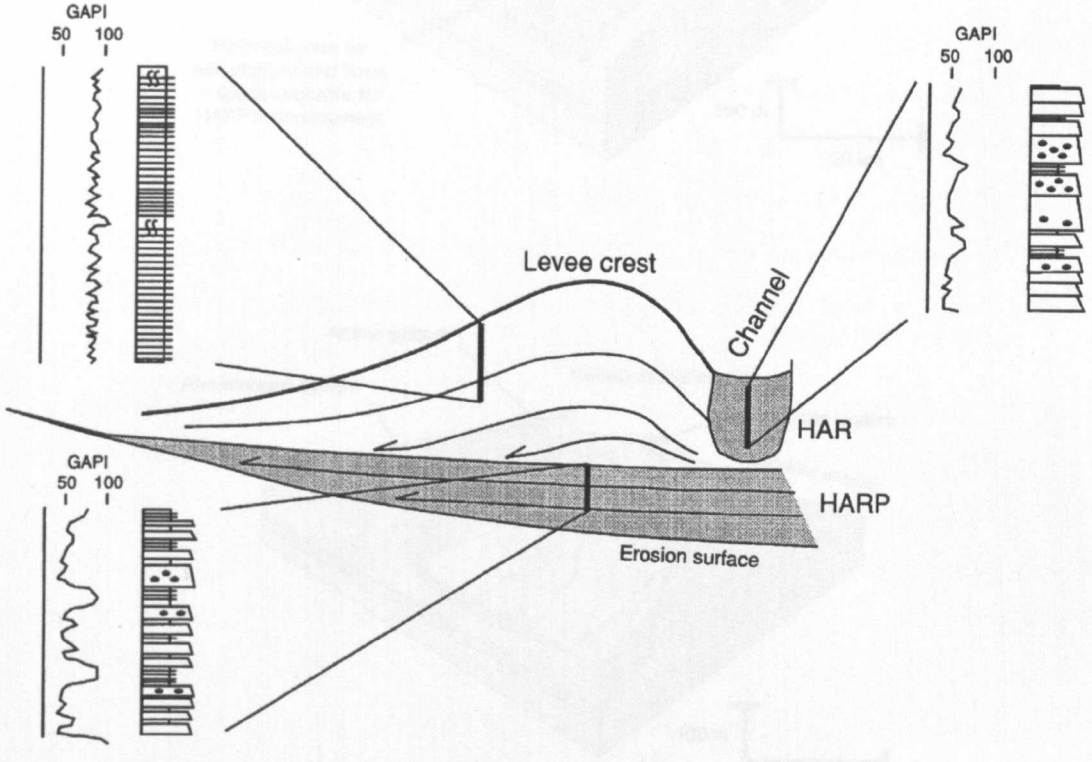

Figure 3-11 – Summary of the geometry, stratigraphy, lithofacies and gamma-ray signature of components of Amazon Fan channel-levee systems based on seismic, profiles, cores and wireline logs (from Pirmez et al., 1997).

These intra-slope lobes represent deposits related to levee breaching corresponding to the first step of avulsion (Lopez, 2001; Pirmez et al., 1997). A lobe first forms when a levee is breached. After the levee is broken, the flow path is deviated from the existing channel and goes through the breach into the inter-channel-levee space. Once there, the flow spreads and reconcentrates. The reconcentration generates a loss of turbulent energy and a quick deposition of the sand material that forms the initial base of the next channel-levee system (Fig. 3.12). The high acoustic impedance of these sandy deposits generates high-amplitude reflector packets (HARPs) (Pirmez et al., 1997).

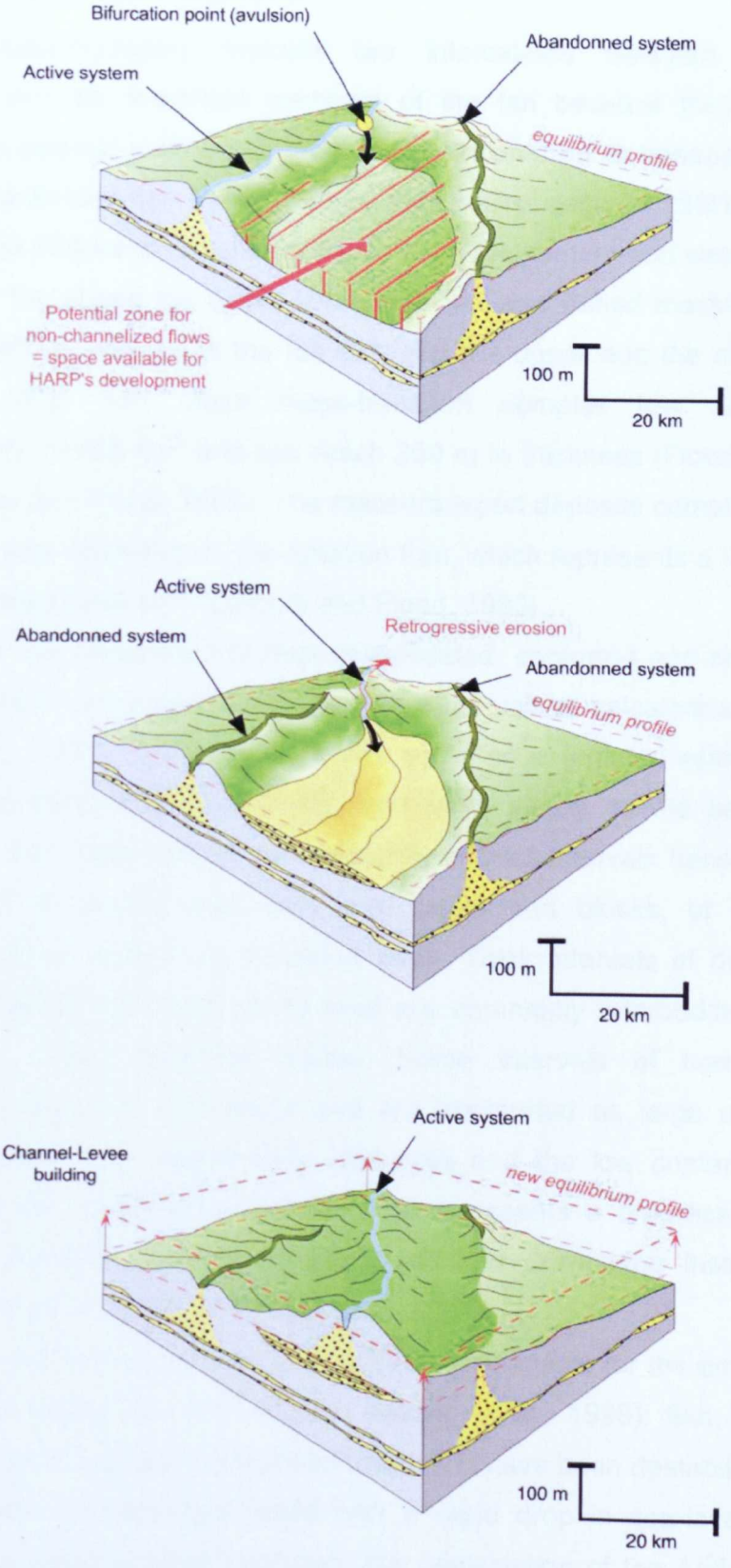

Figure 3-12 – Schematic block diagrams illustrating avulsion lobe formation and the following channel-levee development in the Quaternary of the Amazon Fan (from Lopez, 2001).

3.4.2 Mass-transport deposits

Regional mass-transport deposits are intercalated between the levee complexes and are important elements of the fan because they are easily identified on seismic sections by acoustically incoherent to transparent facies. They are subdivided into surficial mass transported deposits (SMTD), located just below the Holocene interglacial deposits on the eastern and western side of the modern fan above the upper levee complex and buried mass-transported deposits (BMTD), centred in the fan between the upper and the middle levee complexes (Fig. 3.9). Each mass-transport complex has an area of approximately 15,000 km^2 and can reach 200 m in thickness (Flood and Piper, 1997; Manley and Flood, 1988). The mass-transport deposits comprise of up to 14 % of the total sediment on the Amazon Fan, which represents a total volume of approximately 2500 km^3 (Damuth and Flood, 1983).

MTDs are constituted of over-consolidated, contorted and sheared clay and silty clays of variegated colour and with intervals of calcareous mud-chips (Flood et al., 1995). These deposits can occur on a regional scale, e.g., the Western and Eastern surficial MTDs, and more locally on the backsides of levees (Fig. 3.8). They consist predominantly of thick intervals (tens of meters) of deformed or chaotic mud with mud clasts and blocks, or discordant, contorted, folded, faulted, or truncated beds. Thick intervals of disorganized pebbly or gravelly mud and sandy mud are commonly interbedded with the predominant facies described earlier. Some intervals of homogeneous, structureless mud can also occur and are interpreted as large undeformed displaced blocks. The sedimentary structures and the low content of water suggest that the formation of these MTDs represents a progressive sliding, folding and creeping of slope deposits stacked downslope instead of an instantaneous catastrophic process (Lopez, 2001).

There are two mechanisms considered responsible for the emplacement of the MTDs during sea-level change (Maslin et al., 1998): first, during the interglacial-glacial transition, slope deposits could have been destabilised by the release of gas hydrates associated with a rapid drop in sea-level; second, during the glacial-interglacial transition, the deglaciation of the Andes and the following flooding of the Amazon river could have caused sediment over-loading

on the slope, and hence the sliding of slope deposits. According to Reis et al. (2010), the MTD sliding can also be tectonically-triggered due to disruptions on the sea-floor topography created by the fold-thrust belt in the Amazon Fan.

3.4.3 Channel mouth lobe

Channel-mouth lobes are the final place where gravity currents deposit, after travelling for several hundreds of kilometres through a channel. They correspond to areas where there is a transition between confined and less confined environments. Therefore, these deposits are different from the intraslope, inter-channel, or avulsion lobes intensively described in the literature of the Amazon Fan (e.g., Pirmez et al., 1997). Channel-mouth lobes are convex upward, lens-shaped (cross section), and lobate (plan view) deposits (Deptuck et al., 2008; Shanmugam and Moiola, 1991) (Fig. 3.13). Relatively small sand dominated or mixed systems have been described, with the channel-mouth lobes equivalent to one third to the half of the whole fan area (Deptuck et al., 2008; Fildani and Normark, 2004; Gervais et al., 2006; Kenyon and Millington, 1995; Klaucke et al., 2004; Piper et al., 1999; Zaragosi et al., 2000). These lobes are located from between a few tens of kilometres to up to 100-300 km off the coast (Jegou et al., 2008).

Contrasting with the small and middle size submarine fans, channel-mouth lobes in giant deep-sea fans have been poorly studied due to their distal location in very deep sea water (around 4800-5000 m) and their relatively small thicknesses, which are at the limit of the resolution of conventional geophysical tools (Jegou et al., 2008; Twichell et al., 1992). Giant fan systems such as the Mississipi or Zaire fans present channel-mouth lobe complexes as a minor proportion of the entire fan area, which are located farther from the coast and in deeper sea water. Erosional features such as scours and distributary channels commonly occur in channel-lobe transition zones (Fildani and Normark, 2004; Klaucke et al., 2004; Mutti and Normark, 1987; Mutti and Normark, 1991; Wynn et al., 2002). In large mud-rich systems with long meandering channels, the initial low proportion of the sand fraction of the flow is efficiently separated from the silt and clay fraction, which are deposited by the overflow on the levees, whereas the coarser sand particles are transported in the channel to distal areas of the system (Pirmez et al., 2003). Therefore, the sand rich channel

flows end up depositing into channel-mouth lobes as observed in the Zaire channel-mouth lobe (Babonneau et al., 2002).

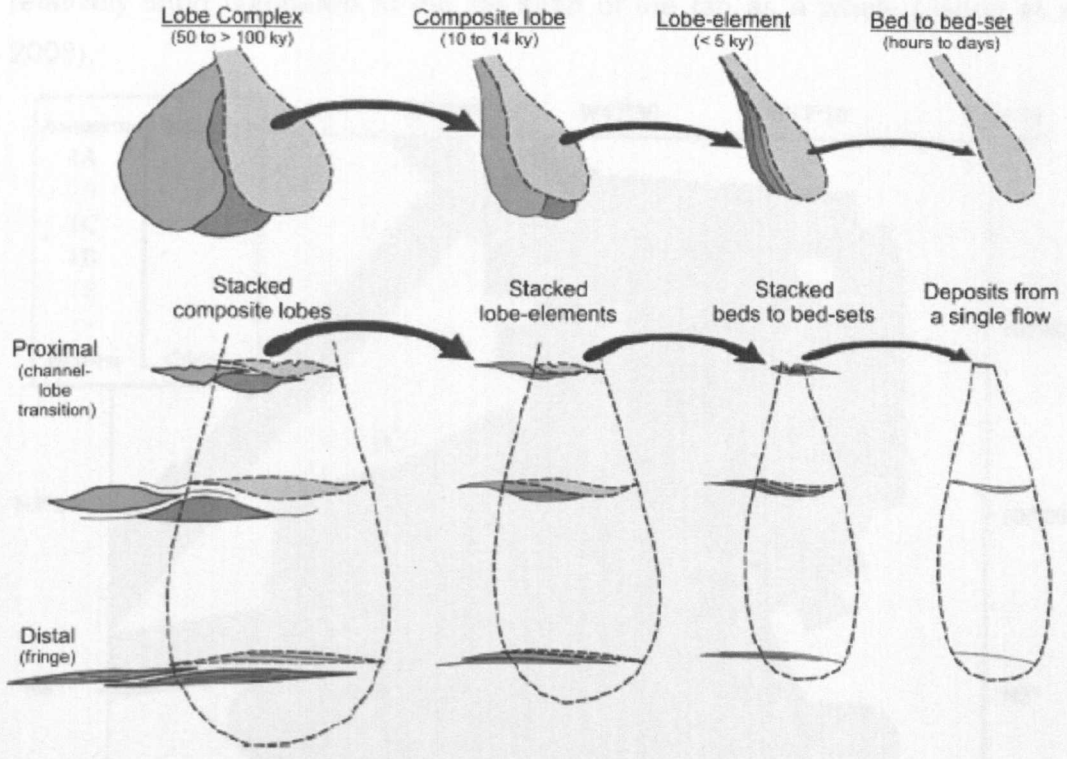

Figure 3-13 – Schematic diagram showing the hierarchy of channel-mouth lobes in the Pleistocene of northern margin of East Corsica (from Deptuck et al., 2008). It shows the lobate form in plan view and the lens shape in cross section. The lobe hierarchy is not further discussed in this thesis because channel-mouth lobes do not occur in the study area, and therefore, are not focus of this research.

Jegou et al. (2008) were the first to investigate the youngest Amazon channel-mouth lobe complex. Previous studies were focused on the upper and middle part of the fan. In the Amazon Fan, the youngest channel-mouth lobe systems were identified at the termination of the channel-levee systems of the Upper Levee Complex, 680 km from the Brazilian Coast (Jegou et al., 2008) (Fig. 3.14). Two types of lobes with distinct shapes were identified: (1) elongated and narrow lobes with branching patterns like the veins of a leaf and a width to length ratio (W/L) of less than 0.33 and (2) radial lobes with crescent-shaped features opening in the downstream direction, that do not have an organization within the lobe and a W/L ratio of over 0.35. The eight channel-levee systems and associated lobes were built during a time of ~10 ka and the

average time between successive avulsions was 1250 years. High rates of channel-levee progradation have been estimated at around 50 km per 100 years and the life span of lobes in Amazon system is around 600 years which is relatively short compared to the life span of the fan as a whole (Jegou et al., 2008).

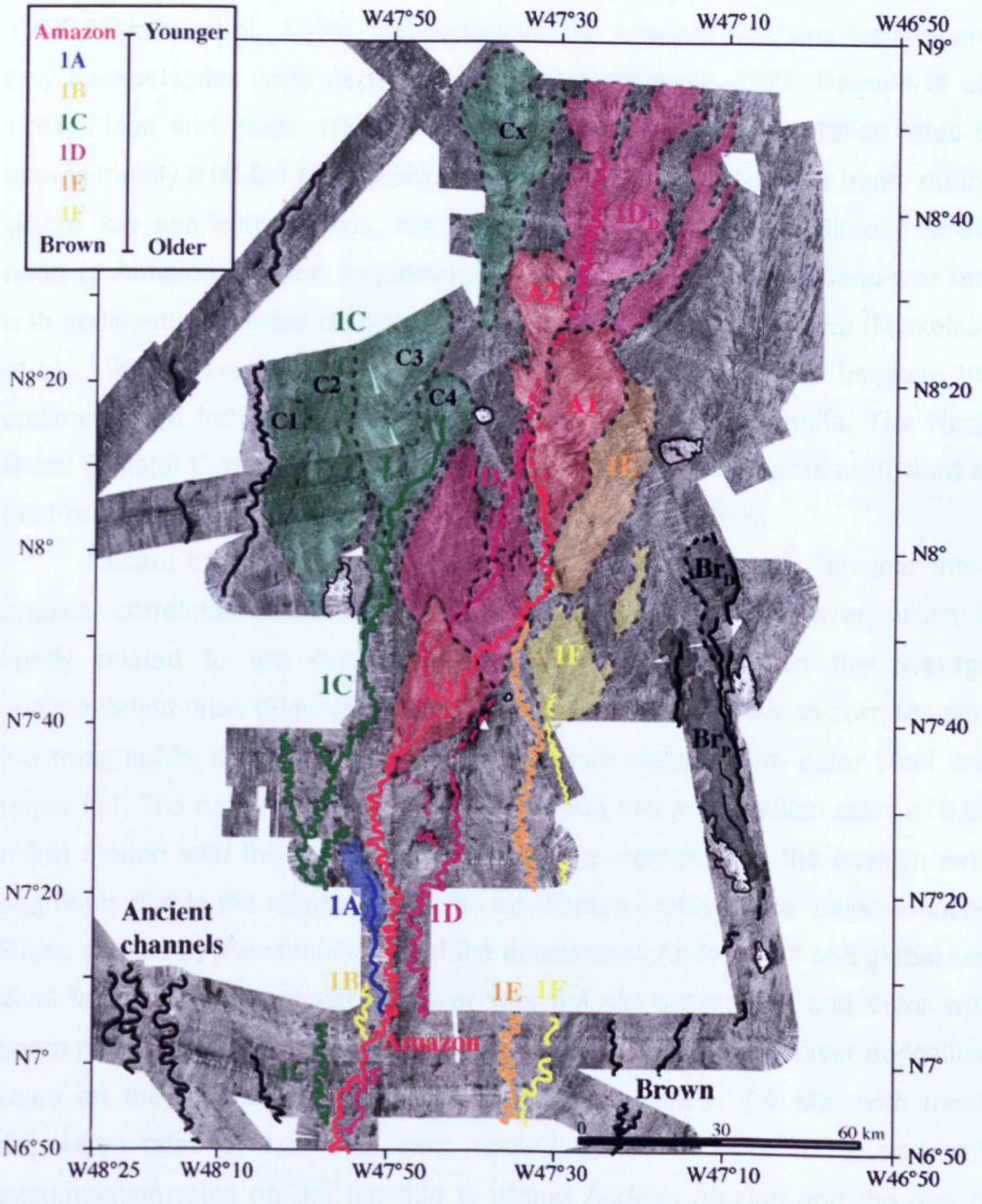

Figure 3-14 Interpretation of acoustic imagery of the Amazon channel-mouth lobe complex showing the successive channel-mouth lobe systems of Brown, 1F, 1E, 1D, 1C, 1B, 1A and Amazon channels (from Jegou et al., 2008).

3.5 Amazon Fan evolution

The development of the Amazon Fan during the Quaternary was controlled by an alternation of sediment supply between glacial and interglacial periods. During the interglacial high sea-level periods, most of the sediments brought by the river were deposited near the river mouth and on the inner shelf (Gibbs, 1967; Milliman et al., 1975). Consequently, the Amazon Fan was inactive and only hemipelagites were deposited on the fan (Damuth, 1977; Damuth et al., 1988; Flood and Piper, 1997; Flood et al., 1995) with sedimentation rates of approximately 0.05-0.1 m/ka (Mikkelsen et al., 1997). On the other hand, during glacial low sea-level periods, the sediments were channelled directly to the head of Amazon Canyon, bypassing the shelf and feeding the deep-sea fan, with sedimentation rates ranging from 1 m/ka to more than 50 m/ka (Mikkelsen et al., 1997). Nowadays, the Amazon fan is essentially inactive because the sediments are trapped on the shelf, forming a subaqueous delta. The North Brazil Coastal Current (NBCC) transports fine-grained sediments northward to the French Guiana shelf and upper slope (Jegou et al., 2008).

Recent study divides the evolutionary history Amazon Fan into three phases, correlated to different stages of development of the river, which is tightly related to the evolution of Andes uplift, based on the average sedimentation rates (Figueiredo et al., 2009). These rates were calculated using biostratigraphic, isotopic and well log data from wells on the outer shelf and upper fan. The onset phase (11.8 - 6.8 Ma, with mean deposition rates of 0.05 m/ka) started with the connection between the western and the eastern river segments due to the adjustment of the equilibrium profile of the paleo-Amazon River, caused by the combination of the accelerated Andes uplift and global sea level fall. During this phase the river was not yet entrenched and there was some deposition in the continental basins leading to relatively lower deposition rates on the submarine fan. The middle phase (6.8 – 2.4 Ma, with mean deposition rates of 0.3 m/ka) was marked by an increase in the sediment accumulation rates on the fan due to strong Andean erosion and the end of deposition on continental basins despite the coincidental rise in global sea level. During this phase the river was already entrenched, and had its main sediment input from Andes. The late phase (2.4 to present, with mean deposition rates of

1.22 m/ka) is characterised by the overprint of additional sediment sources to the Andes supply caused by a possible peripheral uplift due to basin subsidence in response to the sedimentary load on the fan. During this phase the river reached its present shape after a period of alternation of incision and aggradation during glacial and interglacial periods, respectively.

3.6 Structural Setting

There are few published works on Amazon Fan tectonics. The structural framework of the Amazon Fan is characterized by a variety of thin-skinned structures, including faults and folds (e.g., Reis et al., 2010; Silva et al., 1999) (Fig. 3.15). These contractional structures were formerly interpreted as diapirs by Castro et al. (1978), during the first studies of the structural framework of the Amazon Fan. It was only after the acquisition of new seismic data with new processing procedures, that the former diapirs could be reinterpreted as folds and thrust faults and new tectonic models based on gravity gliding and spreading (Galloway, 1986) were defined. This framework is characterized by extensional faults near the shelf margin linked by a relatively non-disturbed zone to downslope fold-thrust belts (Fig. 3.16) (Cobbold et al., 2004; Reis et al., 2010; Silva et al., 1999; Zalan, 2004). In terms of water depth, the structures occurring in less than 500 m water depth are extensional whereas those between 1000 and 1500 m water depth are contractional (Cobbold et al., 2004). The gravitationally-deformed area is about 190 km wide and 300 km along strike, totalling an approximate area of 40,000 km^2 (Reis et al., 2010). The Amazon Fan can be subdivided into two structural compartments which include a larger and structurally more complex Northwestern compartment and a shorter and less complex Southeastern compartment (Cobbold et al., 2004).

In the extensional domain there are listric normal faults dipping seaward with associated rollover anticlines and stratigraphic wedges (Fig. 3.17). The growing rollovers generated by hanging wall block rotation along fault planes created accommodation for deposition of stratigraphic wedges. There are large rollovers between conjugate pairs of faults dipping seaward and landward (Fig. 3.17). The compressional domain characterized by a thrust-fold belt formed by a sequence of thrusts which can vary in geometry and structural style along strike. In the NW compartment these thrust-cored folds can affect the whole

overlying sediments inducing the creation of ponded basins (piggy-back basins) (Reis et al., 2010).

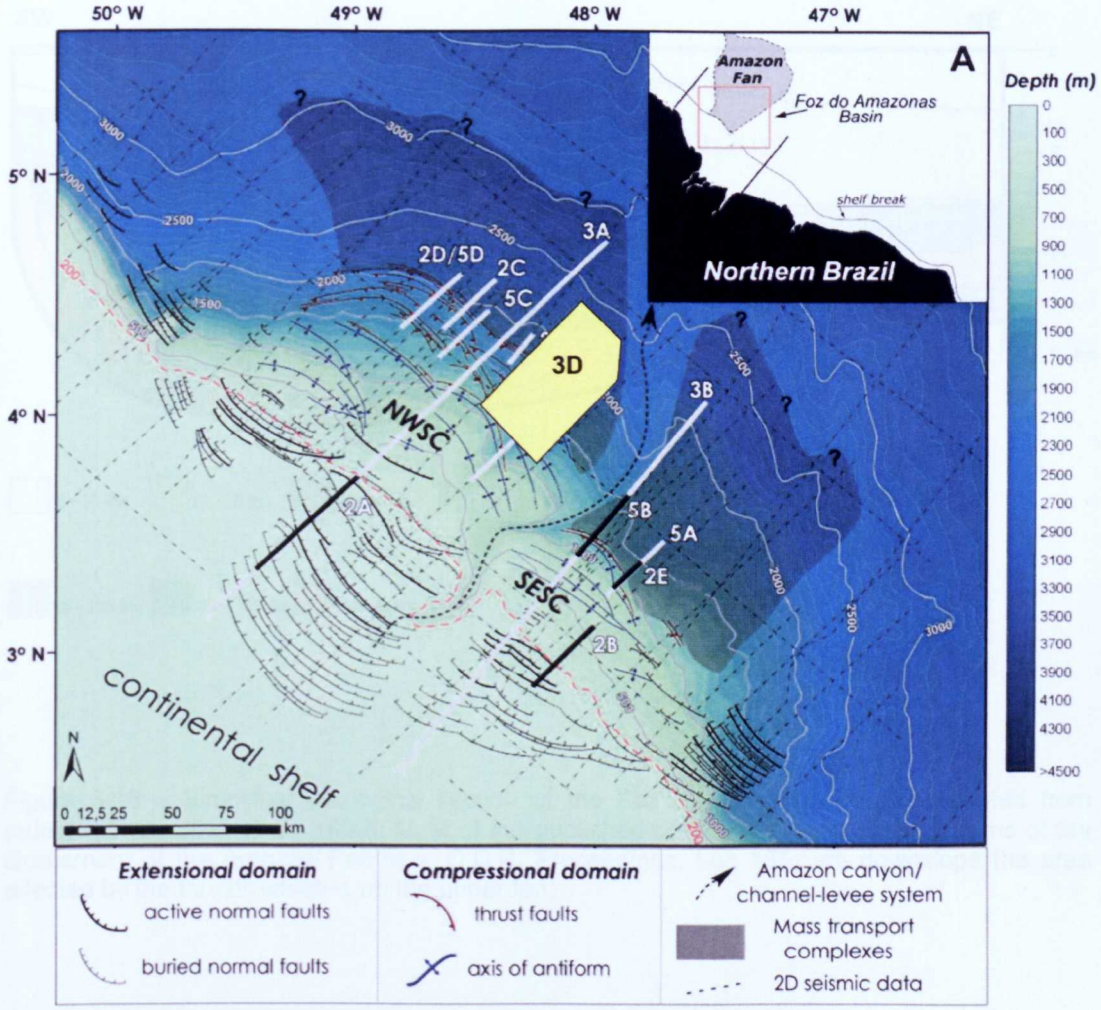

Figure 3-15 – Structural map of the gravity tectonics structures on the Amazon Fan (adapted from Reis et al., 2010). Notice the location of the 3D data used in the current thesis (yellow area) and the location of the 2D line (3A) presented in Figure 3-17.

The thin-skinned structures present in the Amazon Fan are attributed to slope instability due to gravity-driven stresses (Cobbold et al., 2004; Silva et al., 1999). The extensional and compressional domains are linked by at least two distinctive basal detachment surfaces (Fig. 3.17). Although few listric faults located on the mid continental shelf area are rooted at the base of the Late Cretaceous marine sequence, most of the listric faults located at the shelf

border and upper slope root in a detachment surface close to the top of the Cretaceous (Figs. 3.17) (Cobbold et al., 2004).

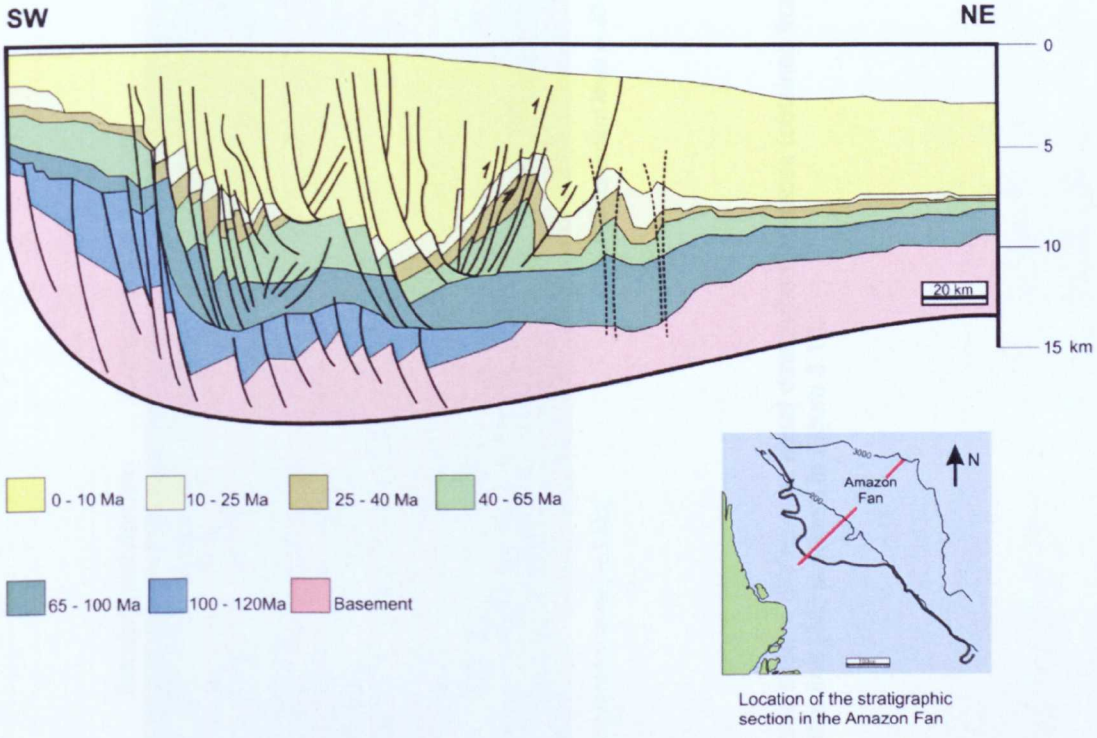

Figure 3-16 – Simplified geological section of the Foz do Amazonas Basin, adapted from (adapted from Silva et al., 1999). Most of the published data about deep water systems of the Quaternary of the Amazon Fan (e.g. O.D.P. Proceedings, Leg 155) are downslope the area affected by the thrusts which is on the upper fan.

The linked extensional-compressional domains were formed by the gliding of sedimentary sections on weak overpressured shales induced mainly by gravity spreading due to high depositional rate on the Amazon Fan since Late Miocene (Cobbold et al., 2004; Silva et al., 1999). The overpressured shales were formed due to intense gas generation in the regionally widespread Cenomanian-Turonian interval (Cobbold et al., 2004). According to Silva et al. (1999), the seaward verging folds and formation of thrust faults were favoured by the topography created in the transition between continental and oceanic crust which resisted downslope translation.

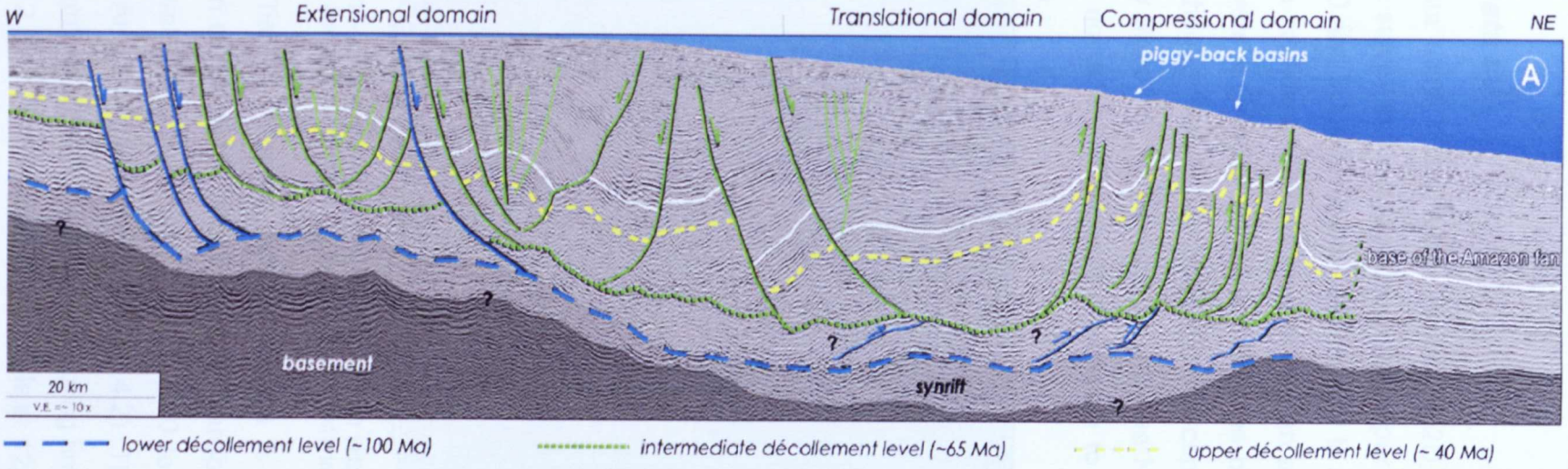

Figure 3-17 – Dip seismic line showing the linked extensional-compressional system gliding over basal detachment surfaces (obtained from Reis et al. 2010). There are rollovers associated with listric faults. The location of this line (3A) is shown in Figure 3.15.

4 STUDY DATA AND METHODS

4.1 Data set

The data used in this study include a 2D reflection seismic line and a 3D seismic survey that are located on the upper slope of the Amazon Fan System. Both 2D and 3D seismic data extend only to 5 sec two-way-time. The 2D line is used to provide a regional view of the fan and has a NE-SW orientation. The line covers a distance of 190 km from the mid shelf to the upper slope of the fan. Although the 2D line does not intercept the 3D survey, the most North-easterly extent of the line lies close to the NW border of the survey (Fig. 4.1) and as documented below, it is possible to correlate key reflections between surveys.

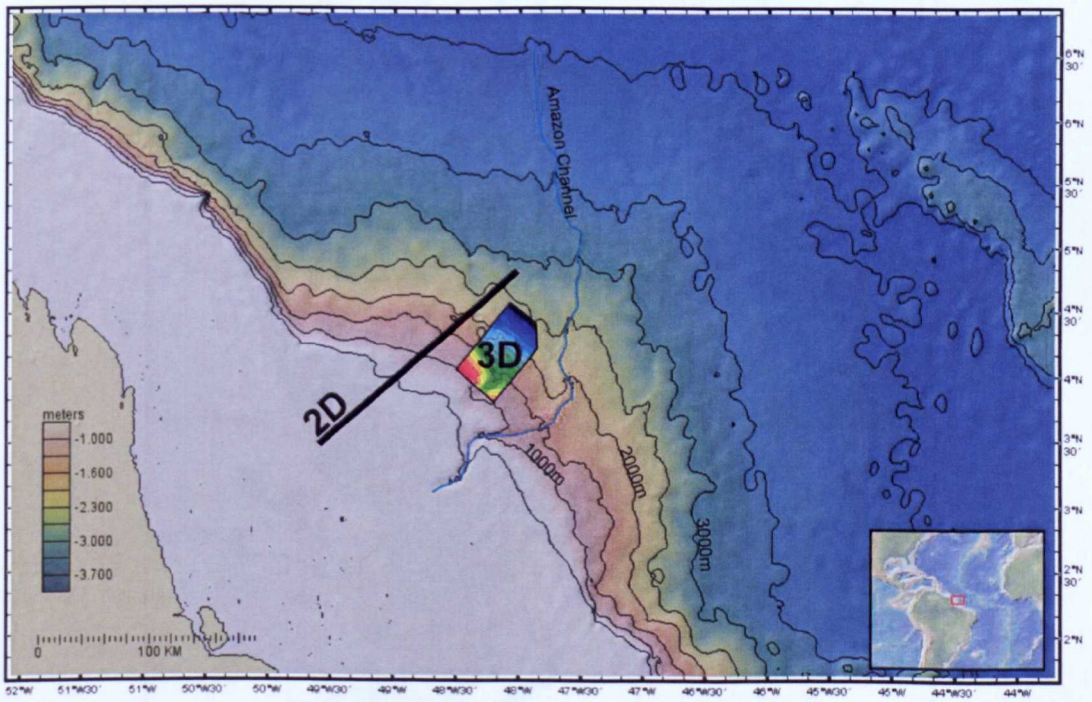

Figure 4-1 – Bathymetric map of the Amazon Fan with the location of the data set (2D seismic reflection line and 3D survey). Map adapted from Marine Geoscience Data System.

The 3D reflection seismic volume is located in the upper fan, at the southern extent of the Western Mass-Transport Deposit (Fig. 4.2). This region lies in water depths ranging around 1000 to 2000 meters and is close to the current Amazon Canyon mouth (Fig. 4.2). The 3D data set covers an area of 23000 km^2, and has a maximum recording time of 5s TWT with a bin spacing of 12.5 x 12.5 m^2. The frequency cut-off is at 125 Hz with a dominant frequency of

32 Hz at 2800 ms TWT giving a vertical resolution of approximately 22 m. Since the data has been migrated, then the Fresnel zone for the horizontal resolution is approximately ¼ wavelength which is also ~ 22 m. This study focuses on the channel-levee systems which are described in detail.

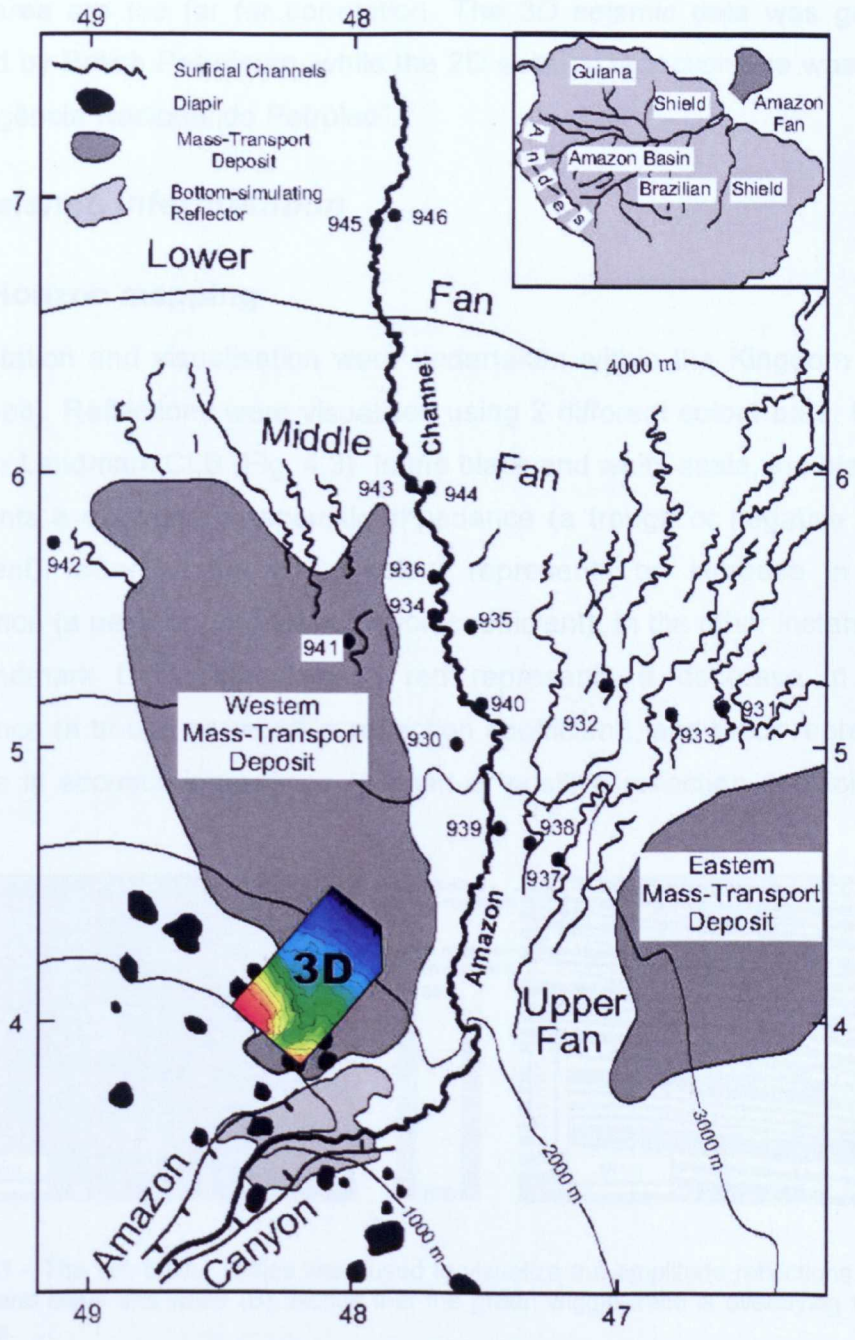

Figure 4-2 – Location of the 3D seismic data in the Upper Amazon Fan. The map also shows the boreholes (ODP Leg 155), and the main surficial fan components, e.g., channel systems, Amazon Canyon and mass transport deposits. The Amazon Channel is the most recently active channel on the Amazon Fan (modified from Normark et al., 1997).

The seismic data used in this study could not be directly tied to lithological and chronological data from boreholes. This is because all the well sites from ODP Leg 155 are located downslope of the study area (Fig. 4.2) and there are no boreholes in the area covered by the 3D survey. The closest wells in the area are too far for correlation. The 3D seismic data was generously supplied by British Petroleum, while the 2D seismic reflection line was obtained from "Agência Nacional do Petróleo".

4.2 Seismic interpretation

4.2.1 Horizon mapping

Interpretation and visualisation were undertaken within the Kingdom Software 8.1 (32-bit). Reflections were visualised using 2 different colour bars: black and white, or Landmark CLB (Fig. 4.3). In the black and white scale, the black colour represents a decrease in acoustic impedance (a trough or negative reflection coefficient), whereas the white colour represents an increase in acoustic impedance (a peak or positive reflection coefficient). In the other instance, using the Landmark CLB colour scale: red represents a decrease in acoustic impedance (a trough or negative reflection coefficient); and black represents an increase in acoustic impedance (a peak or positive reflection coefficient) (Fig. 4.3).

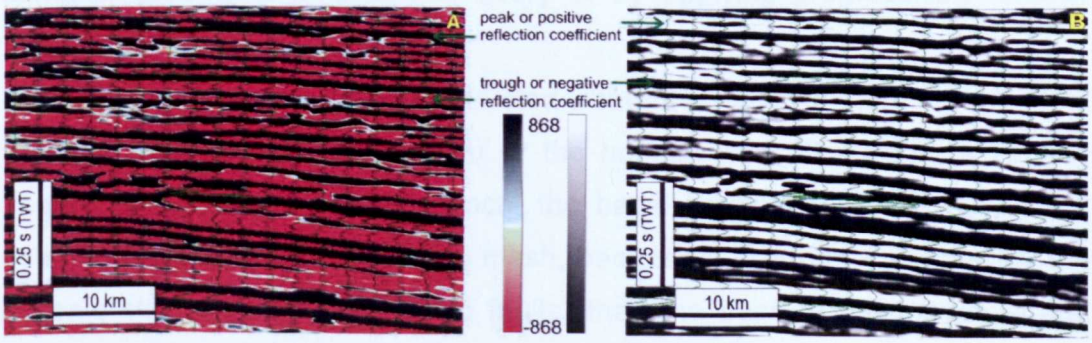

Figure 4-3 – The two colour scales were used to visualize the amplitude reflections: Landmark CLB (A) and black and white (B). Notice that the green wiggle trace is overlaying the seismic reflections.

The two-way-time maps were constructed following the work flow described below in Figure 4.4 using the tectonic-stratigraphic framework outlined in section 4.2.2. A target reflection was chosen depending upon the nature of the reflection; either a peak or a trough of the wavelet was used. The

reflection was manually picked (point to point), with a subsequent time window length of typically 0.03 s for a picking snap. A seed grid was created by picking a number of widely spaced and perpendicular in-lines and cross-lines, always tying around loops (Fig. 4.5), in such a way that at the intersection between a cross-line and an in-line, the reflection should be at the same two-way travel time, otherwise, it resulted in a mis-tie. The seed grids were constructed using at least three different line sample sizes: coarse, fine and composite grids (Fig. 4.5). The coarse grid was constructed in the examples where the picked reflection had high coherency between wavelet. In these grids, initial picks were carried out every 50 inlines/crosslines, although they were frequently reduced to 25 (Fig. 4.5). The base of growth strata is an example of a relatively coherent reflection, which was mapped using a coarse grid (Fig. 4.5).

Alternatively, the fine grid was constructed in areas of lower coherence of wavelet, e.g., in the base of incisional channels, or in areas of a higher degree of geological complexity and poorer seismic resolution. For instance, the unconformity that occurs throughout the area was mapped using a fine mesh grid because of the occurrence of discontinuities made by incisions of later channels and the occasional truncation of the underlying horizons that substantially increased the difficulty of tracking (Fig. 4.5). In this grid, the initial picks were carried out every 10 inlines/crosslines, and were reduced in the most complex case to a minimum of every 1, by applying progressively smaller sampling intervals.

Composite grids were constructed where the reflection normally presents variable coherence of the wavelet or the horizon was affected by a varying degree of deformation. For instance, the basal horizon (Fig. 4.5) required a composite grid of coarse and fine mesh, because it was more affected by the tectonic structures (anticlines and faults) than the base of the growth strata. Therefore, although this reflection regularly presents a coherent wavelet, the reflection tracking demanded application of a finer grid across the structures.

In all of the three seed grid sizes, the occurrence of misties commonly required the local reduction of the mesh size. After checking that the seed grid (generated by point to point picking) was completely tied, the TWT map was completed by using the polygon hunt tool. Using this tool, the interest area of the grid is delimited, within which Kingdom Suite auto picks the geometry of the

horizon, interpolating at all points in the grid. After the production of each TWT map, a quality control was manually performed, checking each gap in the map, and editing any anomalies. The maps were generated using Transverse Mercator/Gauss-Kruger Projection System, South America 1969 – Brazil as Geodetic Datum and latitude/longitude format in decimal degrees.

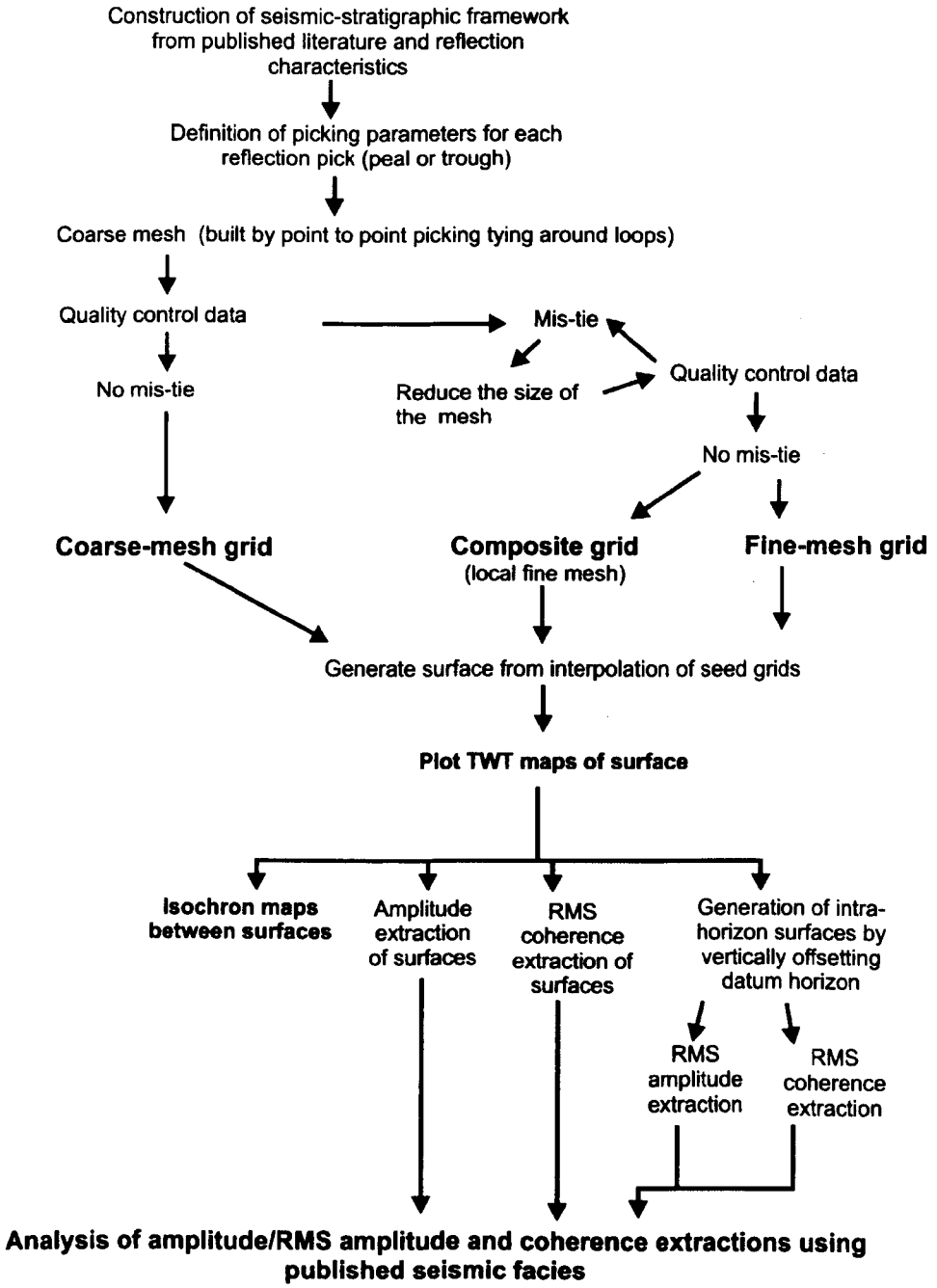

Figure 4-4 – Diagram showing the workflow used in the analysis of the studied seismic data.

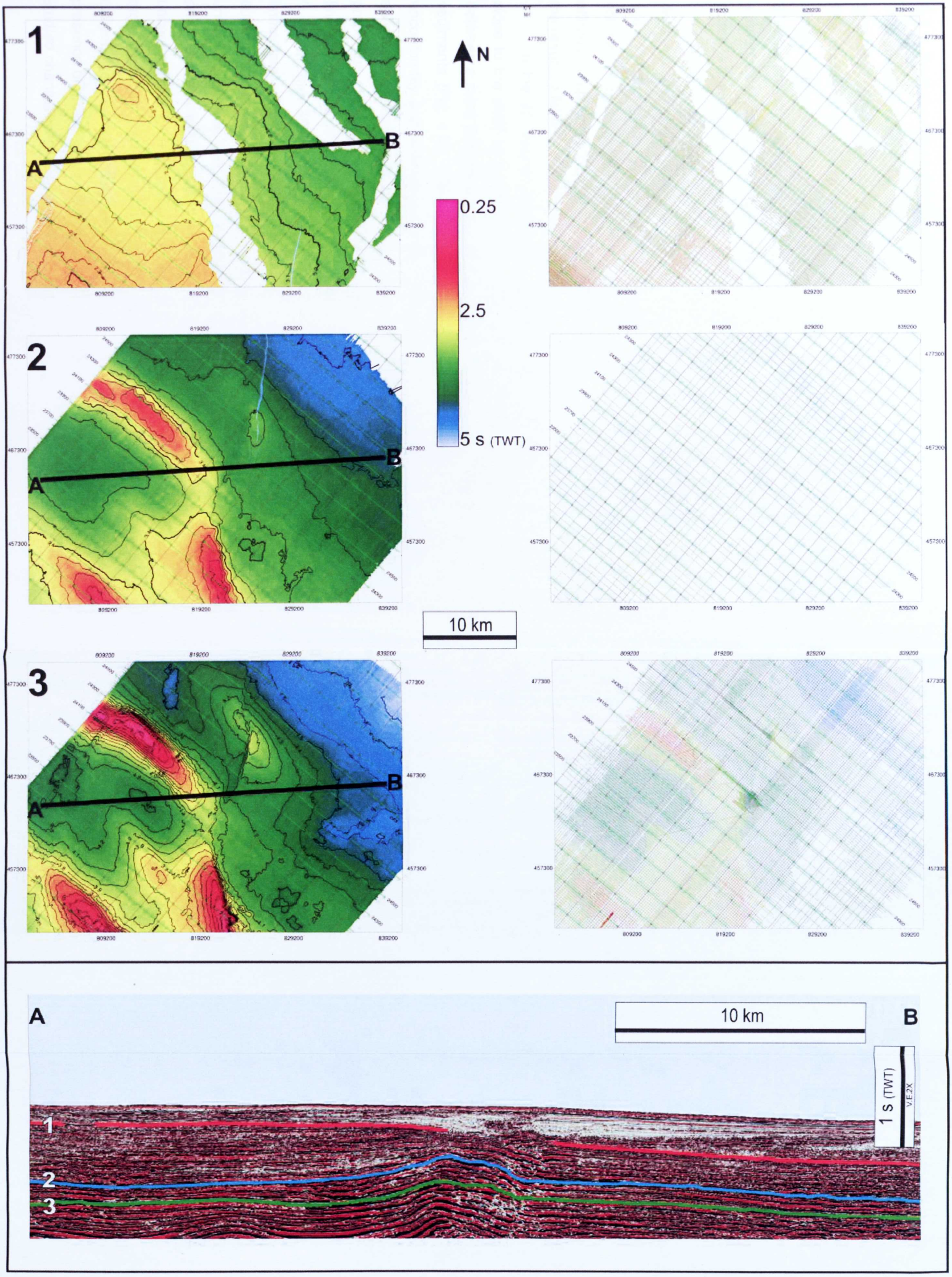

Figure 4-5 – Two-way-time maps and respective grids with different mesh size: 1) fine-mesh grid with picked horizon every each 10 to 5 lines and or less (unconformity); 2) coarse-mesh grid with picked horizon every each 50 lines or reduced to 25 (base of the growth strata); 3) composite grid with areas showing coarse mesh (SE of the area) and areas with fine mesh which in some cases was reduced to every line in the central portion of the area). The maps correspond to the three horizons presented in the section. The elongated discontinuities in the map 1 represent incisions made by later channels. Notice that the greenish grid in three maps is the displayed survey lines by the software output.

4.2.2 Tectono-stratigraphic framework

The interpretation of the seismic facies was based on reflection character, geometry, termination and amplitude, in accordance with Hubbard et al. (1985). The choice of the horizons to map was based on the tectono-stratigraphic interpretation of the seismic data outlined in the Chapter 5. Although the 2D and 3D data are not directly coincident, the seismic reflection character of the mega-sequences (separated by a basin-wide unconformity) is distinct enough that it is possible to correlate the horizons between the two surveys (Fig. 4.6).

Clearly there is a significant role of faults in controlling the margin deformation (Fig. 4.6). However, as the 3D volume had a maximum recording of 5 s TWT the geometry of the faults were poorly constrained within the data volume (Fig. 4.6). The faults themselves were therefore not mapped out although mapping of the pre-unconformity sequences revealed the geometry of the resultant folds.

In the 2D seismic line, the unconformity was tracked from the upper slope to the shelf by picking the reflection corresponding to the unconformity between a more deformed lower interval and a less deformed upper interval of sediments (Fig. 4.6). Five channel-levee systems were identified above the unconformity and downslope of the outer anticline in the 2D line. By contrast only three systems were identified in the 3D data. The 2D line covers a larger proportion of the slope, and therefore shows that at least two further channel-levee systems exist in the area and are not covered by the 3D data (Fig. 4.6).

In the 3D seismic survey, although the post-unconformity interval immediately downslope of the most eastern anticline is the main focus of the current research, two other intervals were analysed underneath the unconformity. This was done in order to understand the structural framework and the characteristics of the erosional canyon-like channels prior to the main unconformity (Fig.4.6, surface 1a). Hence, the seismic volume was divided into three packages: the lower package, which is characterized by the occurrence of canyon-like channels; the middle package, which is characterized by the presence of growth strata; and the post unconformity package which include the studied channel-levee systems (Fig. 4.6).

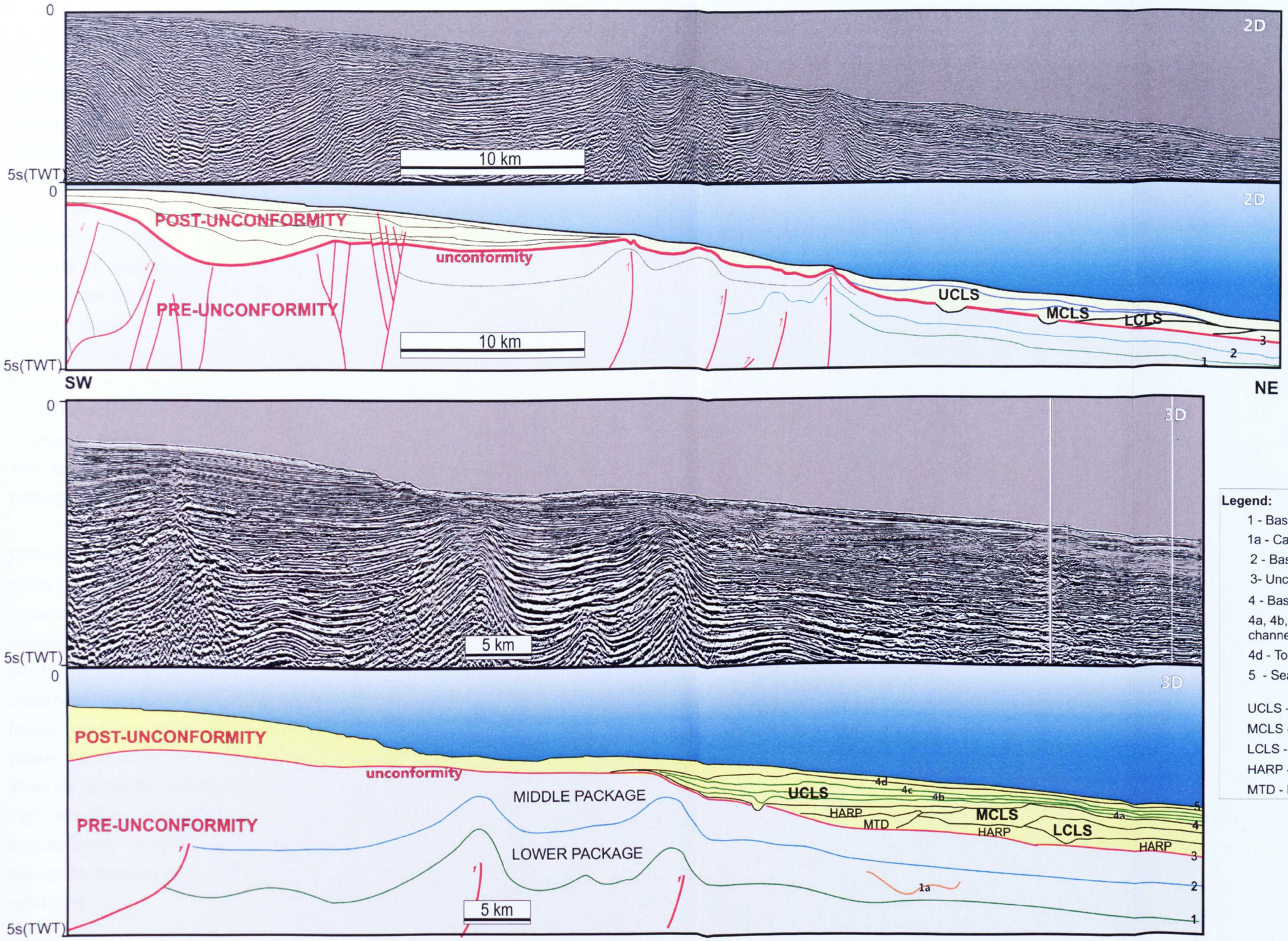

Figure 4-6 – Schematic diagrams showing the tectono-stratigraphy of the area, outlining the portion of the 2D seismic reflection line covered by the 3D survey. In total 10 horizons were picked in either the 2D or 3D surveys, the picking parameters are summarized in Table 4.1.The seismic data are divided in 2 main intervals, pre-unconformity (in grey) and post-unconformity (in yellow). In the 3D section, the seismic is divided in 3 packages: lower, middle and post-unconformity. In this section is also emphasized the mapped horizons in the current work, which are: the boundaries of the 3 packages (horizons 1,2,3 and 5), the base and top of the UCLS and the internal boundaries of the stacked channel-levees, components of the UCLS.

The sediment sequence from the base of the lower package down to 5 s (TWT) was not considered in this study. The geological interpretation of the 3D survey, therefore, required the mapping of four main horizons that are the boundaries of the studied packages: the base of the lower package; the base of the middle package; the unconformity and the sea floor (Fig. 4.6). The post unconformity package divides into three systems: the UCLS, MCLS and LCLS.

The analysis of the Upper Channel-Levee System (UCLS), which comprises a sequence of stacked channel-levee elements, required the mapping of reflections corresponding to its base and top, and a further three intermediate horizons (surfaces 4, 4a, 4b, 4c, 4d in Figure 4.6). In the intervals between these horizons, extraction of the RMS (root mean square) amplitude and coherence in horizon slices in the middle of each channel-levee element was undertaken using a time window of 20 ms.

Isochron maps of the three packages were constructed for each package in order to determine variations in sediment accumulation, which was used to infer the timing of the growing structures in relation to the deposition of each package.

The evolution of Lower Channel-Levee System (LCLS) and the Middle Channel-Levee System (MCLS) was based on the analyses of several horizon slices taken across these systems using the base of the right levee of the upper system as a reference (Fig. 4.7). This surface was chosen as reference (datum) because it dips approximately in the same direction as the channel systems, which are dipping towards the N-NW. The other surfaces, such as those underneath the unconformity and the seafloor are dipping towards the NE and, hence, were not appropriate (Fig. 4.8). RMS extraction of the reflection coherence (in a time window of 20 ms) was chosen because the same horizon slices cut across the ponded high amplitude reflection packets (HARPs) and the high amplitude reflection HARs of the channel fill, either erosional or aggradational. Therefore, the amplitude alone could not be used to fully distinguish between these two deposits because they have similar amplitude reflections.

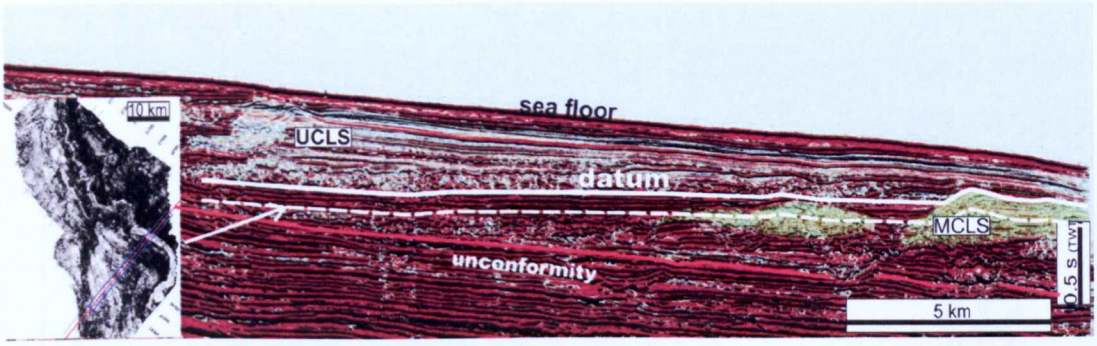

Figure 4-7 – Seismic section across the MCLS showing a horizon slice (RMS of coherence extraction) highlighted with the dashed white line parallel to base of the levee of UCLS (continuous white line), used as a datum.

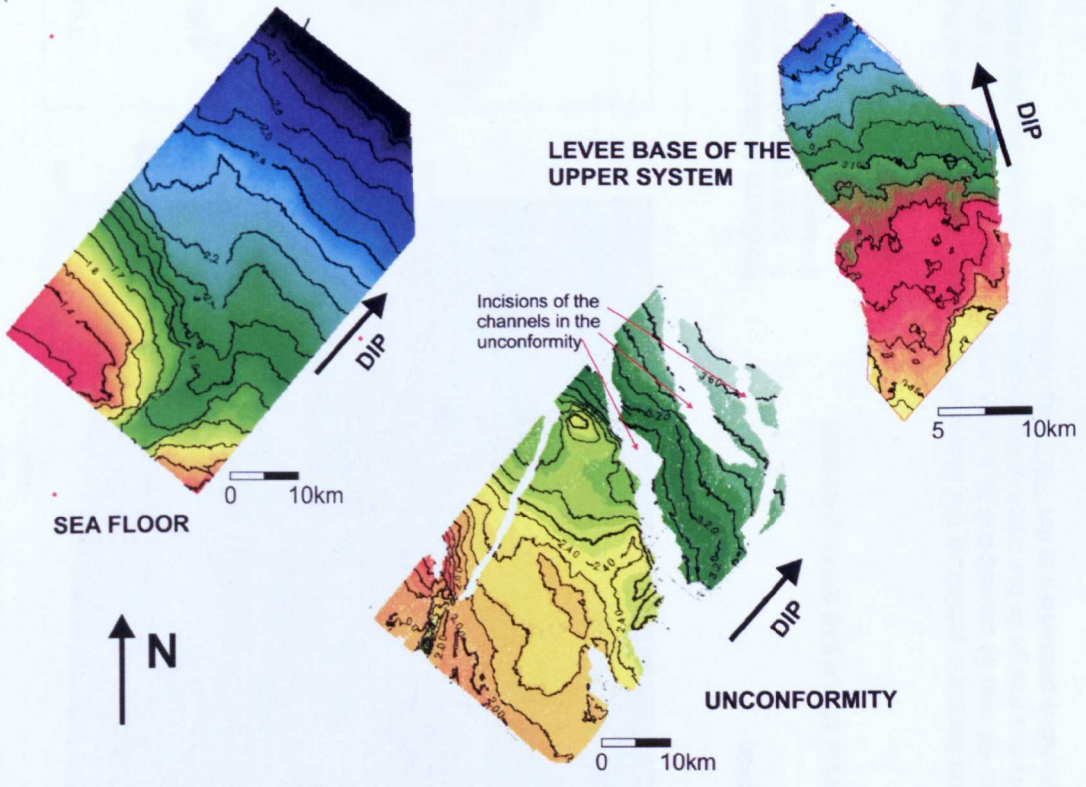

Figure 4-8 – Two-way-time maps of the seafloor, the unconformity and the base of the right levee in the Upper Channel-Levee System. The seafloor and the unconformity dip towards different directions than the channels whereas the base of the right levee of the UCLS dips towards the same direction as the channels.

Most of the horizons, including the erosional incisions, the unconformity and the seafloor were mapped by picking the peak (black in Landmark CLB colour scale) (Fig. 4.9), because there was more continuity. On the other hand, the bases of the lower and middle packages were mapped by picking the trough. The seismic character and the consistency of each picked reflection are shown in Table 4.1.

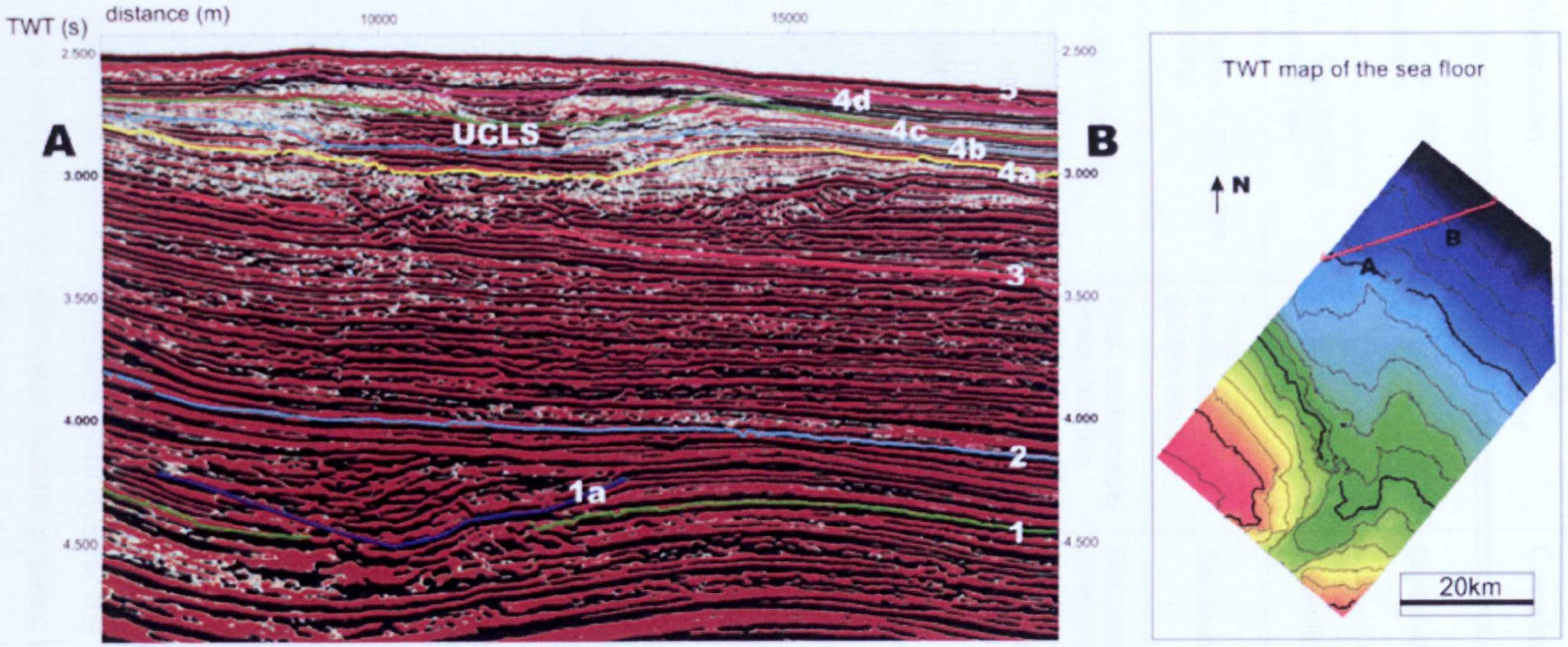

Legend

Horizons (picked peak):

1a - Canyon-like channel base
3 - unconformity
4 - base of UCLS
4a, 4b, 4c (internal boundaries of stacked channel-levees)
4d - top of UCLS
5 - seafloor

Horizons (picked trough):

1 - base of the lower package
2 - base of the middle package

Figure 4-9 – Detail of the mapped horizons exhibiting the nature of the picked reflection (peak or trough). Notice that most of the horizons (1a, 3, 4, 4a, 4b, 4c, 4d and 5) correspond to a peak reflection whereas horizons 1 and 2 are trough reflections. The base of the UCLS (horizon 4) is a merge of the maps of the erosive basal channel and the maps of the left and right-hand levees. The location of the section AB is presented in the TWT map of the sea floor.

Table 4-1 – Seismic characteristics of the mapped reflections.

Reflection	Seismic character	Consistency	Grid type
1 - Base of the lower package	Trough, high amplitude, conformable	Continuous, high coherence	Composite
1a - Canyon-like channel base	Peak, truncation	Discontinuous, low coherence	Fine
2 - Base of the middle package	Trough, high amplitude, conformable	Continuous, high coherence	Coarse
3 - Unconformity	Peak, conformable, onlap, downlap	Discontinuous, variable coherence	Fine
4 – Base of UCLS	Base of the levees, downlap, truncation	Continuous, variable coherence	Coarse
	Erosive channel base, truncation	Discontinuous, low coherence	Fine
4a, 4b, 4c, 4d internal subdivisions and top boundary of the UCLS	Channel: Peak, high amplitude, truncation	Moderate coherence, truncation	Fine
	Levee: Peak, low amplitude, downlap,	Discontinuous and with low coherence in the levee reflections close to the channel, truncation.	Fine
		Continuous an high coherence in levee reflections farther from the channel, downlap	Coarse
5 - Seafloor	Peak, high amplitude	Continuous, high coherence	Autopick

For all analyses that required depth values, an interval velocity of 1500 m/s for the water column and 2000 m/s for the shallow subsurface seismic data were assumed. For sediment burials greater than 500 m the published curve showing the relation between travel times and sediment thickness in offshore northern Brazil was used (Fig. 4.10).

Exact determination of stratigraphic unit, lithology, and age was not possible due to the absence of relevant borehole data in the area. The lithology of the seismic facies identified in the post unconformity package of the 3D data, therefore, is inferred by analogy with the sedimentary facies, e.g., MTD, HARPs and the architectural elements of the channel-levee systems described in the literature of the Amazon Fan, particularly the results of the Ocean Drilling Program leg 155 (Damuth et al., 1988; Flood et al., 1995; Manley and Flood, 1988; Normark et al., 1997; Pirmez et al., 1997) (Fig. 3.8, Chapter 3).

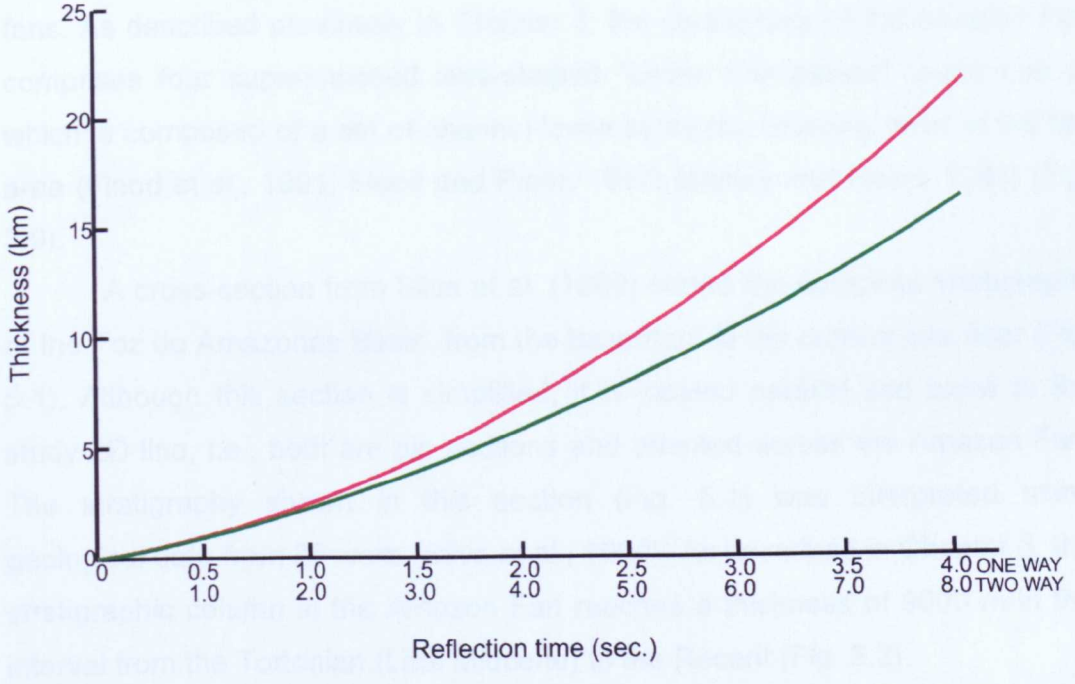

Figure 4-10 – Curves showing relation between one-way and two-way travel times and sediment thickness in kilometres for offshore northern Brazil. Curves apply to areas beyond shelf edge only; the green curve is applicable for the area west of 43°W (which includes the studied area) and the red curve is applicable for area east of 43°W. Diagram adapted from Kumar (1978).

5 TECTONO-STRATIGRAPHY

5.1 Introduction

The objective of this chapter is to describe the tectonic-stratigraphy of the studied area, focusing mainly on the channel-levee systems which occur in the uppermost interval of the northeastern portion. These constitute some of the most important depositional elements of the Quaternary interval, which corresponds to the upper 500-800 m of the Amazon Fan. The channel-levee systems are considered important because they are the largest proportion of the whole fan area in giant fan systems, such as Mississipi, Zaire or Amazon fans. As described previously in Chapter 3, the Quaternary of the Amazon Fan comprises four superimposed lens-shaped "Levee Complexes" (each one of which is composed of a set of channel-levee systems) covering most of the fan area (Flood et al., 1991; Flood and Piper, 1997; Manley and Flood, 1988) (Fig. 3.9).

A cross-section from Silva et al. (1999) shows the complete stratigraphy of the Foz do Amazonas Basin, from the basement to the current sea floor (Fig. 5.1). Although this section is simplified, it is located parallel and close to the study 2D line, i.e., both are dip sections and oriented across the Amazon Fan. The stratigraphy shown in this section (Fig. 5.1) was interpreted using geological data from 26 wells (Silva et al., 1999). As described in Chapter 3, the stratigraphic column in the Amazon Fan reaches a thickness of 9000 m in the interval from the Tortonian (Late Miocene) to the Recent (Fig. 3.2).

In this chapter a description of the inter-related deposition and tectonics of the upper slope of the Amazon Fan is given, based on the interpretation of 3D seismic data, in the context of regional tectonic-stratigraphy as given by a dip-oriented 2D line. Two generic academic themes arise from observation of the submarine channel-levee systems in the Amazon Fan and are pursued in later chapters. Thus, the spatio-temporal evolution of channel-levees is discussed in detail in Chapter 6, including discussion of flow property controls on their development. Patterns of channel distribution are discussed in Chapter 7 with a detailed analysis of the controls on channel spatial distribution and stacking.

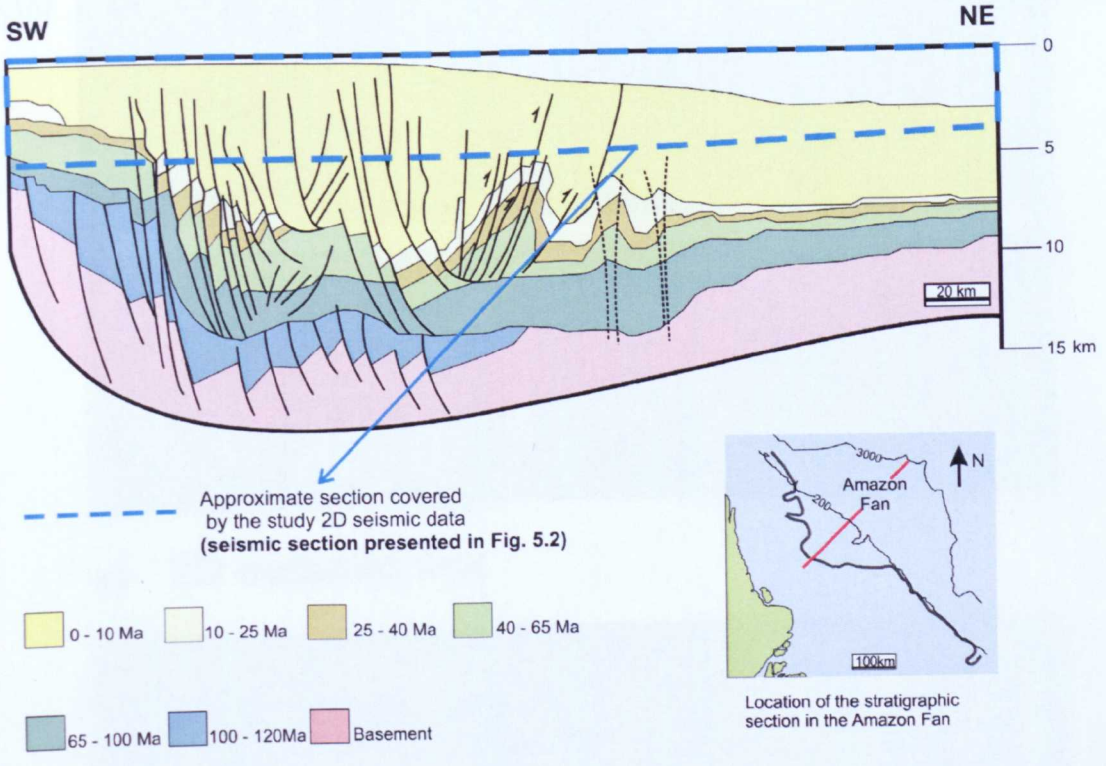

Figure 5-1 – Simplified geological section of the Foz do Amazonas Basin, adapted from Silva et al. (1999). Notice in the location map that the section is sub-parallel to the study 2D line (Fig. 5.2) and also located Northwest of the Amazon Canyon Mouth. The dashed blue line delimitates the approximate section covered by the study 2D line shown in Figure 5.2 (calculated by using interval velocity of 2000 m/s in the sediments and 1450 m/s in the water). Therefore, most of the analysed sediments in the current work were deposited since the Late Miocene and correspond to the sediments of the Amazon Fan.

5.2 Regional setting (based on 2D data)

Analysis of the 2D seismic reflection line is necessary to provide the regional tectono-stratigraphy for the 3D seismic survey. The 2D seismic reflection line is oriented downslope and shows a section from the shelf border to the upper slope in the Amazon Fan (Fig. 5.2). The lack of well data prevented an exact tie of the seismic data to the stratigraphy of the area. Therefore, the study data were fitted to the local stratigraphy by comparing the identified horizons and structures with the available data from the literature (Reis et al., 2010; Silva et al., 1999). Thus, the stratigraphic framework of the study data was established by comparing the 2D seismic reflection line with the stratigraphic section presented in Silva et al. (1999) (Fig. 5.1).

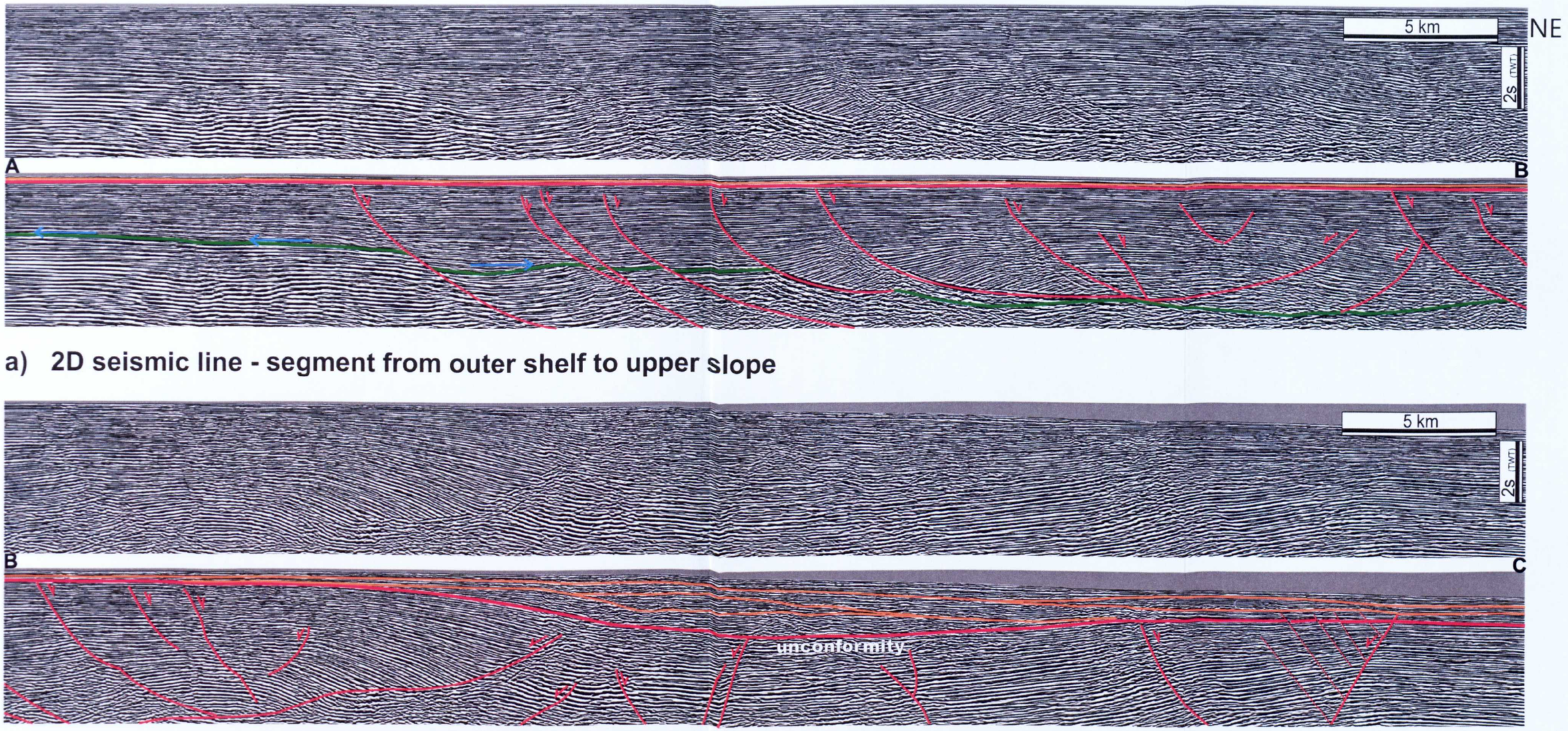

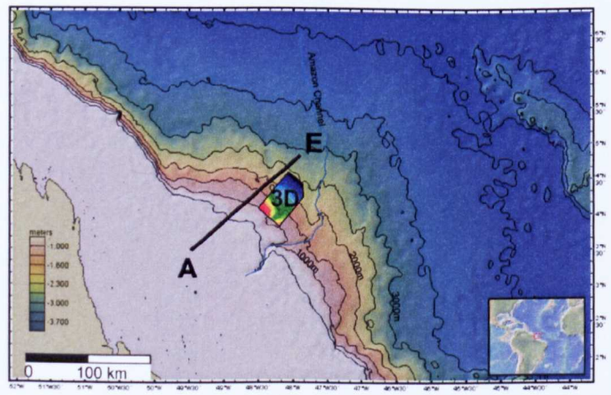

Bathymetric map of the Amazon Fan exihibiting the location of the 2D (AF) and 3D data

Legend:
AE - 2D seismic line
AC - Outer shelf and upper slope with a set of normal faults
- Early Paleocene detachment surface
- 3D seismic survey

Figure 5-2 - Non-interpreted and interpreted 2D seismic line (AE) located NW of the study 3D data cutting across the outer shelf and upper slope seen in the bathymetric map of the Amazon Fan. a) On the shelf edge (on the segments, AB and BC) the prevailing structures are listric normal faults.

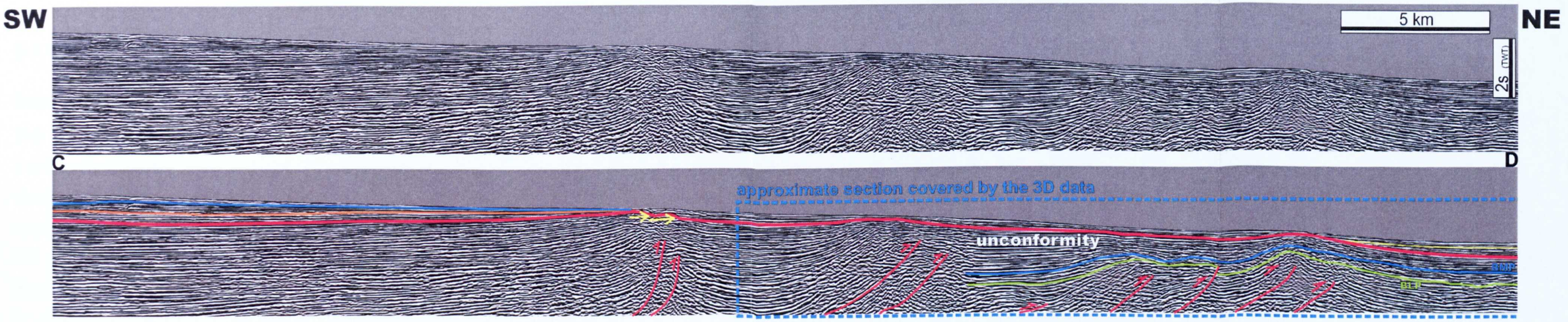

b) 2D seismic line - upper slope

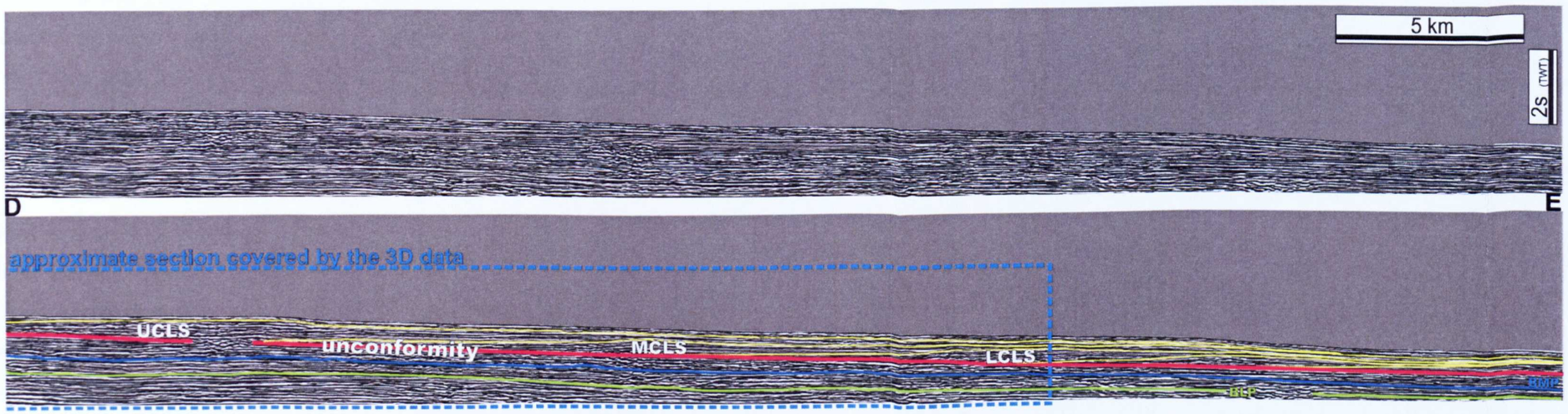

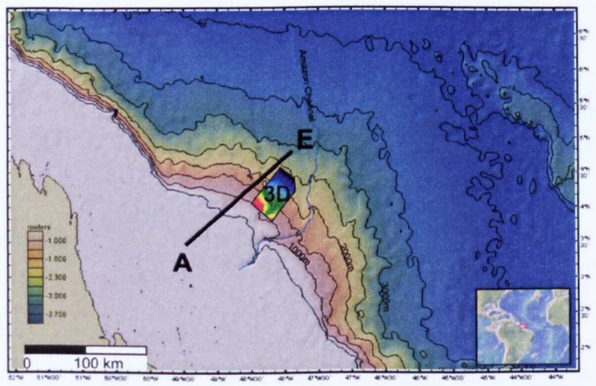

Bathymetric map of the Amazon Fan exihibiting the location of the 2D (AE) and 3D data

Legend:
AE - 2D seismic line
CD - Upper slope exhibiting a fold-thrust belt
DE - Upslope stacked channel-levee systems
UCLS - Upper Channel-Levee System
MCLS - Middle Channel-Levee System
LCLS - Lower Channel-Levee System
BMP - Base of Middle Package
BLP - Base of Lower Package
- 3D seismic survey

Figure 5.2 - 2D seismic line (AE) located Northwest of the study 3D data cutting across the outer shelf and upper slope seen in the bathymetric map of the Amazon Fan. b) Segment CD shows a fold and thrust belt and segment DE shows the unconformity and the overlying three channel-levee systems, the focus of this study, (LCLS, MCLS, UCLS). Notice that the approximate section covered by the 3D seismic data is highlighted with the dashed blue line.

5.2.1 Regional Structural Framework

Description

The 2D seismic line shows two areas with distinct structural styles separated by a relatively non-deformed section 27 km long (Fig. 5.2). On these time data, the shallowest deformed section is characterised by sets of normal faults that appear to be listric, and that dip both seaward and landward (syn/antithetic) and link at their bases (Fig. 5.2a, segment AB). The deformed area covers a distance of 75 km and extends seaward to an approximate water depth of 560 m. The normal faults are not regularly spaced, with the distance between sea floor fault traces (or near sea floor fault tips) ranging from 1 to 10 km in their uppermost extremities. They generally converge downward with their dips decreasing with depth, defining a listric shape. The surface into which the listric normal faults sole out corresponds to the detachment surface in the Early Paleocene sequence described in the structural analysis of the Amazon Fan realized by Reis et al. (2010) (Fig. 3.17).

The fold and thrust belt is characterised by a series of thrusts and associated anticlines that occur on the upper slope, extending for 25 km in the 2D line, between approximately 1000 and 1700 m of water depth. These anticlines are asymmetric, have NE vergence and are irregularly spaced. The wave-length of the successive anticlines can be as long as 7 km between the two upslope anticlines and very short in the most downslope anticlines, where they are coalescent (Fig. 5.2b, segment CD). Only the top extremities of the thrusts were sampled in the seismic data because the study 2D line is relatively shallow and the thrusts are rooted deeper than the lower seismic limit (Fig. 5.2b). These sampled thrust segments dip at around 45° toward the SW. The fault-related folds above these thrusts are characterised by long back limbs that have a lower dip than the underlying fault ramps. The forelimbs are shorter than the backlimbs and generally dip more steeply. Deeper in the same 2D line, Reis at al. (2010) show the thrusts root in the detachment surface that was identified on the shelf linking the bases of most of the listric faults in the Lower Paleocene (Fig. 3.17). Therefore, this detachment surface links the set of extensional listric faults in the shelf/shelf border to the upper slope fold and thrust belt.

Interpretation

The set of listric normal faults (syn and antithetic) linked by the detachment surface to the downdip fold-thrust belt corresponds to an extensional-compressive system typical of gravity driven sliding described not only in the Amazon Fan (Cobbold et al., 2004; Reis et al., 2010; Silva et al., 1999) but also in other passive margin systems such as the Niger Delta (Damuth, 1994; Rowan et al., 2004), the Gulf of Mexico (Peel et al., 1995; Rowan et al., 2004) and the Pará-Maranhão Basin (Zalan, 2004). The analysis of the 2D seismic line showed three structural domains, from the shelf to upper slope, approximately to 1700 m of water depth: extensional, translational and compressive. This type of structural compartmentalization is also described in the Niger Delta (Damuth, 1994) as typical of gravity driven deformation on submarine slopes.

In the extensional domain, the three uppermost slope listric faults are rooted beyond the lower limit of the seismic data (Fig. 5.2a, segment AB). In the deeper section adapted from Reis (2010), they sole out into a lower detachment surface, i.e., at the base of Late Cretaceous (~100 Ma). These faults are interpreted to have been active earlier than the listric faults occurring toward the shelf break, which are rooted on the shallower Early Paleocene (~65 Ma) detachment surface. This is because such detachment surfaces are associated with the kinetics of mobile overpressured shales (Cobbold et al., 2004; Silva et al., 1999) and are strongly dependent on depth (Morley and Guerin, 1996), i.e., the deeper surfaces were active earlier than the shallower ones. The faults rooted in the Early Paleocene surface show a tendency to remain active for longer toward the upper slope since the growth strata involved in the extensional deformation are thicker and shallower seaward (Fig. 5.2).

Rollover anticlines occur associated with the listric growth fault. These structures are interpreted to be generated by hanging wall sediments sliding, rotating and warping along the curved plane of the listric normal faults (Fig. 5.3).

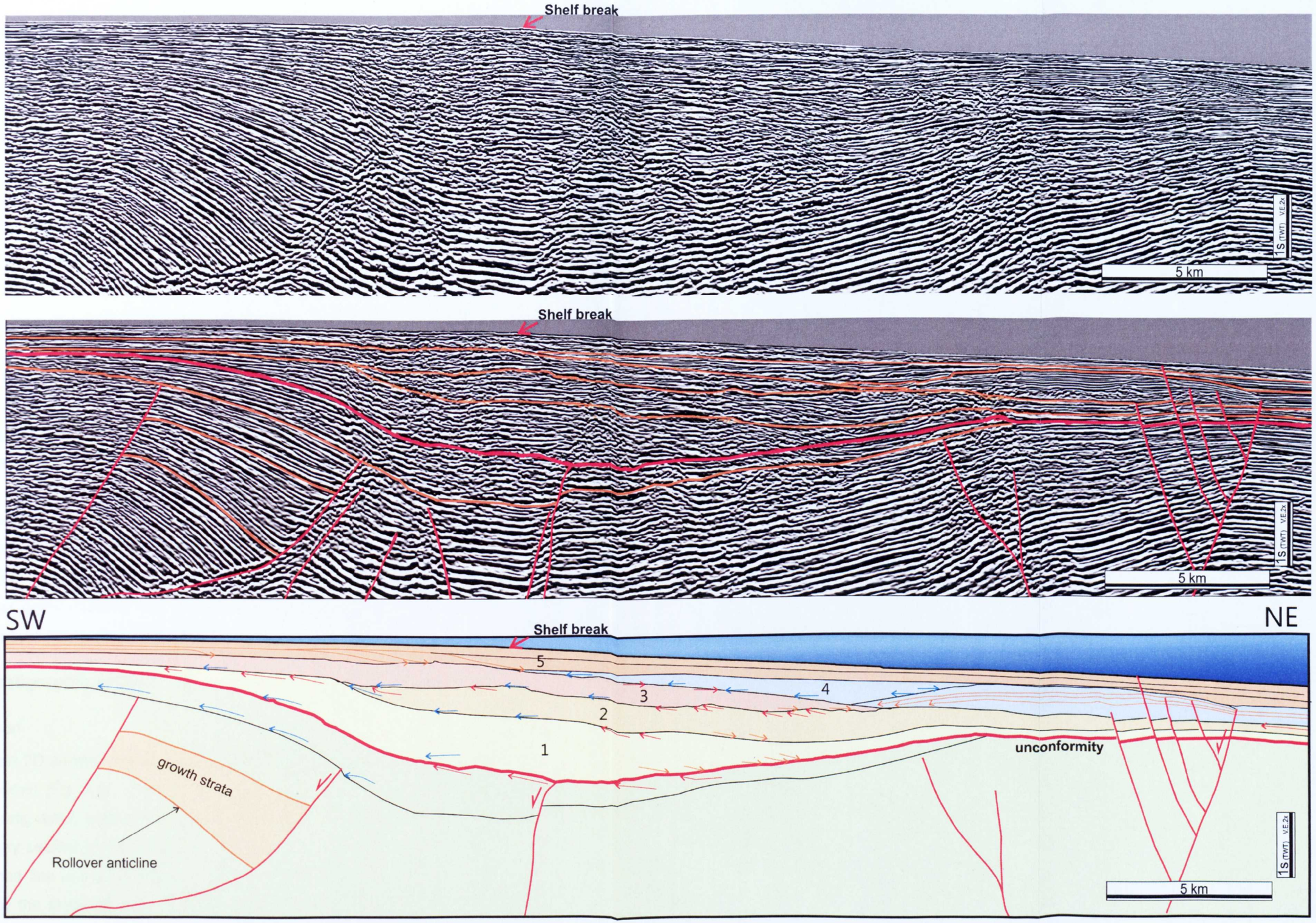

Figure 5-3 – Seismic section covering detail of the shelf border in the 2D seismic reflection line, approximately the same segment BC showed in Figure 5.2a, but here it is presented with vertical exaggeration of 2 times. At least 5 intervals of sediments (numbers) were recognized based on stratal geometry and reflection coherence and terminations. Notice that the lower 3 intervals present truncation on their boundaries which implies erosion. In interval 4 a platform shaped feature occurs with aggradational internal reflections and borders with slope. Observe the growth strata related to the listric normal fault and associated rollover anticline. The orange picks (boundaries of sediment packages) correspond to the orange picks in the Figure 5.2. Notice that the blue arrows are onlaps, orange arrows are downlaps and the red arrows are truncation.

The topographic depression of the unconformity at the shelf break seems to have been formed by the collapse of overlying sediments due to underlying listric fault activity (Fig. 5.1). The growth strata in the upper sediment layers of the pre-unconformity interval close to the shelf break and a set of small faults offsetting the unconformity are also evidence of this phenomenon (Fig. 5.3). Therefore, the listric faults close to the shelf break (Fig. 5.2, segment BC) were active until the formation of the unconformity. The faulting described here created the accommodation space necessary for the accumulation of post unconformity shelf sediments (Fig. 5.3).

In the compressional domain, the fold thrust belt is interpreted as detaching from the Early Paleocene surface (~65 Ma) by Reis (2010) (Fig. 3.17). These structures were still active after the unconformity formation because the unconformity is folded on the top of the anticlines (Fig. 5.2, segment CD). This deformation seems to have been related to the same tectonic activity that deformed the unconformity at the shelf break, taking into account that the thrust-cored anticlines and the listric faults are genetically related.

Comparatively, the extensional domain is much larger than the compressional one. The variability of the dimensions of the apparent extensional, translational and compressional domains is mentioned in the literature as being possibly caused by the amount of the deformation that is not resolvable by seismic data (Zalan, 2004).

5.2.2 Stratigraphic setting

Description

The studied 2D seismic data is relatively shallow, extending downw only to 5 s (two-way-time) (Fig. 5.2). Therefore, the study 2D line did not cover most of the deeper stratigraphic units of the Foz do Amazonas Basin (considering that the sedimentary section of the Amazon Fan is up to 9 km thick). In Figure 5.1, the blue dashed line is the approximate area of the stratigraphic section which is covered by the study 2D line. It is possible to infer that most of the section in the study 2D seismic line is part of the sedimentary package deposited during the last 10.7 Ma and equivalent to an interval from the Late-Miocene to the

present day. The southwestern-most portion of the section extends deeper (Fig. 5.1); this portion of the 2D line also covers part of the older sediments of mixed carbonatic-siliciclastic deposition, the Amapá Formation (Figueiredo et al., 2007), which lasted from Late-Paleocene to Late-Miocene (Fig. 3.2, Chapter 3).

Two horizons with significant stratigraphic relevance were identified in the study 2D line. The earlier one is a boundary evidently separating higher amplitude reflections underneath from lower amplitude reflections above. This horizon (dark green colour) is an onlap surface and occurs on the southwestern segment of the 2D line (Fig. 5.2a, segment AB). This horizon seems to be the same Early Paleocene detachment surface as that identified by Reis et al. (2010) (Fig. 3.17).

The later horizon is interpreted as an unconformity, identified and illustrated across the whole 2D line by the red horizon in Figure 5.2. The unconformity is conformable with the underlying reflections in some places but also appears locally truncating underlying reflections on the crest of the anticlines (yellow arrows in the CD segment, Fig. 2b) and on the shelf border (Fig. 5.3). This unconformity is a significant horizon in the structural-stratigraphic framework because it separates strongly deformed sediments underneath from slightly deformed sediments above.

Above the unconformity and close to the shelf border (Fig. 5.2, segment CD), at least 5 seismic-stratigraphic units were identified filling the relative paleo-low (Fig. 5.3). These units were defined using reflection terminations and strata geometries (e.g., Hubbard, 1985). The lowest units 1, 2 and 3 show coastal onlap and downlap reflections and truncation along their upper boundaries. Unit 4 shows a platform-shaped seismic feature on the shelf border, approximately 10 km long and 500 m high, and has internal sub-horizontal reflections and lateral slopes (Fig. 5.3). Moreover, Unit 4 also presents reflections onlapping the paleo-slope and the platform structure. Unit 5 is predominantly formed by sub-parallel reflections and locally, by sigmoidal downlaps.

On the upper slope and below the fold and thrust belt at least five channel-levee systems appear to be stacked in an upslope sequence, above the unconformity (Fig. 5.4). The three upper and stacked channel-levee

systems correspond to the Upper, Middle and Lower systems, identified in the northeastern portion of the 3D seismic survey and described late in this chapter.

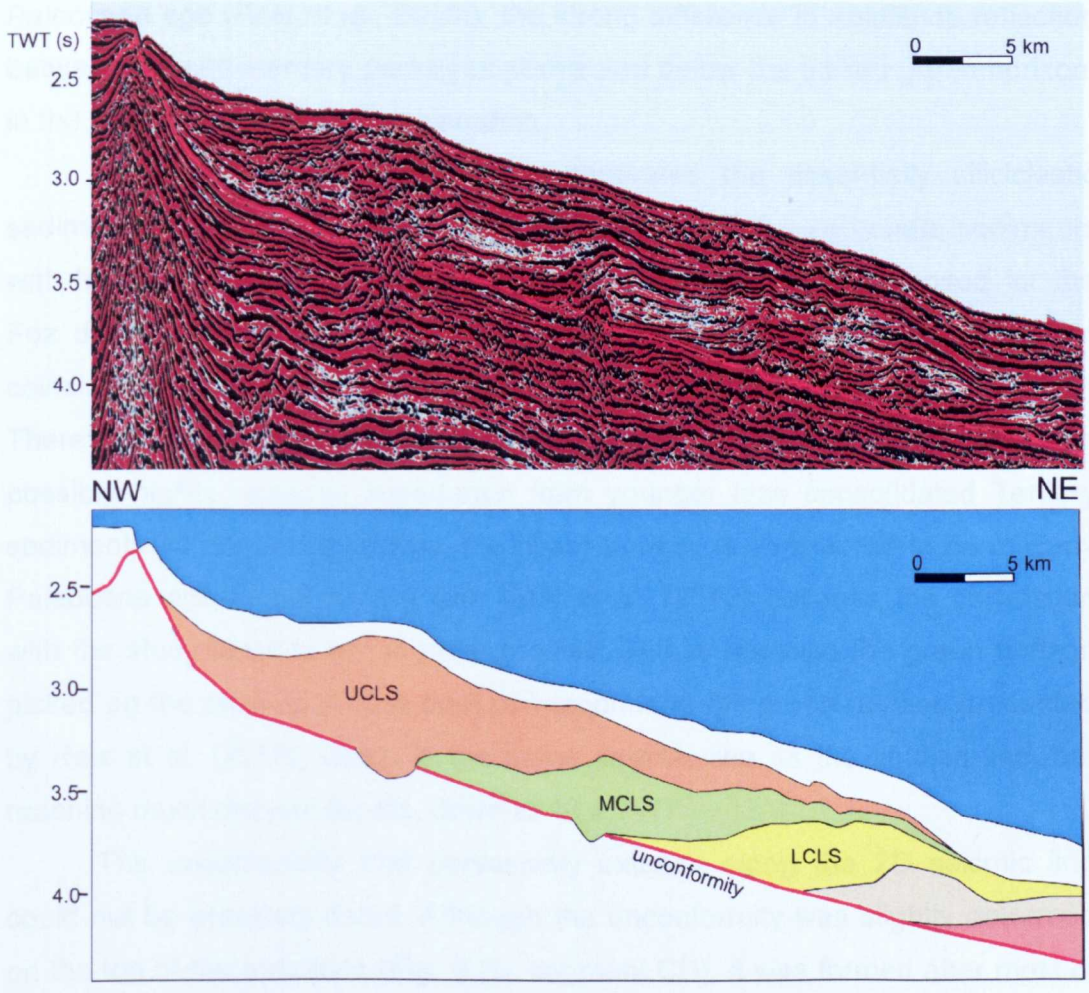

Figure 5-4 – Non-interpreted and interpreted detail of the 2D seismic line corresponding approximately to the segment DE of the figure 5.2.b with vertical exaggeration (10x). This section shows 5 stacked channel-levee systems immediately downslope from the fold and fault belt. The 3 channel-levee systems identified also in the 3D seismic data are identified (UCLS, MCLS and LCLS).

Interpretation

The age of the earlier (green) horizon which separates higher amplitude reflections from overlying lower amplitude reflections in the southwestern border of the 2D is controversial (Fig. 5.2a, segment AB). The approximate area covered by the study 2D line in the simplified stratigraphic section of Silva (1999) (Fig. 5.1) implies that the horizon that is the base of the yellow interval, which corresponds to the base of the Amazon Fan, dates from around 10 Ma. On the other hand, the green horizon (in the studied line) corresponds to the

green horizon present on the seismic line of Reis et al. (2010) (Fig. 3.17) which dates from around 65 Ma and is equivalent to the Early Paleocene. In either case (i.e., a Late Miocene interpreted age (Silva et al., 1999) or an Early Paleocene age (Reis et al., 2010)), the strong difference in amplitude reflection between the sedimentary packages above and below the picked green horizon, in the study 2D line require explanation.

In the first case, the horizon separates the essentially siliciclastic sediments of the Amazon Fan from extensive underlying carbonate sediments with higher acoustic impedance (see the stratigraphic chart proposed for the Foz do Amazonas Basin; Fig. 3.2). In the second case, the green horizon coincides approximately with the transition from the Cretaceous to the Tertiary. Therefore, it separates older and more consolidated Cretaceous sediments with possibly higher acoustic impedance from younger less consolidated Tertiary sediments. In the current thesis, the green horizon is considered to be of Early Paleocene age in agreement with Reis et al. (2010) because the correlation with the study seismic line is more precise. This is because the green horizon picked on the studied 2D line best corresponds to the green horizon presented by Reis et al. (2010), which is the same seismic line as the studied line, but reaching much deeper depths, down to 10 s TWT.

The unconformity that pervasively extends along the 2D seismic line could not be precisely dated. Although the unconformity was slightly deformed on the top of the anticlines (Fig. 5.2b, segment CD), it was formed after most of the slope deformation. This is evidenced by the relatively few normal faults that cut across the unconformity in the shelf with no or subtle offsets (Fig. 5.3). It marks roughly the end of strong gravitationally driven tectonic activity in the fan. Therefore, the whole sediment package can be vertically divided into units strongly and slightly affected by the structures, i.e., underneath and above the well marked unconformity (Fig. 5.2).

The five sedimentary units characterised above the unconformity were deposited in a topographic low close to the shelf border which created accommodation space for the sedimentary stacking (Fig. 5.3). This accommodation was possibly generated by the extensional tectonics (normal faults) that affected the pre-unconformity sediments. Unit 4 presents a structure characterized by internal aggradational reflectors bordered laterally by slopes,

and are here interpreted to resemble carbonate platforms (reefs/shoals). However, in the absence of well data no further discussion of the genesis or any stratigraphical significance of these units will be raised here. This is because the understanding of their stratigraphical meaning does not impact the study of the submarine channels which are the focus of the current research.

5.3 Unconformity

5.3.1 Description

The unconformity divides the seismic data into two main packages, with distinctive seismic facies and degree of deformation. It occurs widely, with changing characteristics across the study area. The unconformity is commonly found to be locally conformable with the underlying sediments (i.e., forming a disconformity), although it is often erosive, generating a local truncation of the underlying layers on the crest of the anticlines and on the shelf (Fig. 5.5). In these areas, the erosion could have removed sediment thicknesses greater than 430 m. The unconformity is an onlap surface for the turbidite systems deposited immediately above, but also may have thin layers of hemipelagites lying parallel and immediately above it.

In the study 3D survey, the average dip of the unconformity is around 1.4° NE and with steeper dips near the limbs of the anticlines. The elongate discontinuities exhibited on the unconformity map with N-NW directions represent incisions made by the later channel systems (Fig. 5.5).

5.3.2 Interpretation

This unconformity may represent an important gap in deposition during the Pleistocene as it is angular and erosive at the fold crests, and was therefore generated after most of the slope deformation and also marks a significant change in the style of the turbidite systems, from essentially erosive, canyon-like channels underneath to predominantly channel-levee systems above. The geological significance of this unconformity is further discussed in Chapter 9 (Discussion).

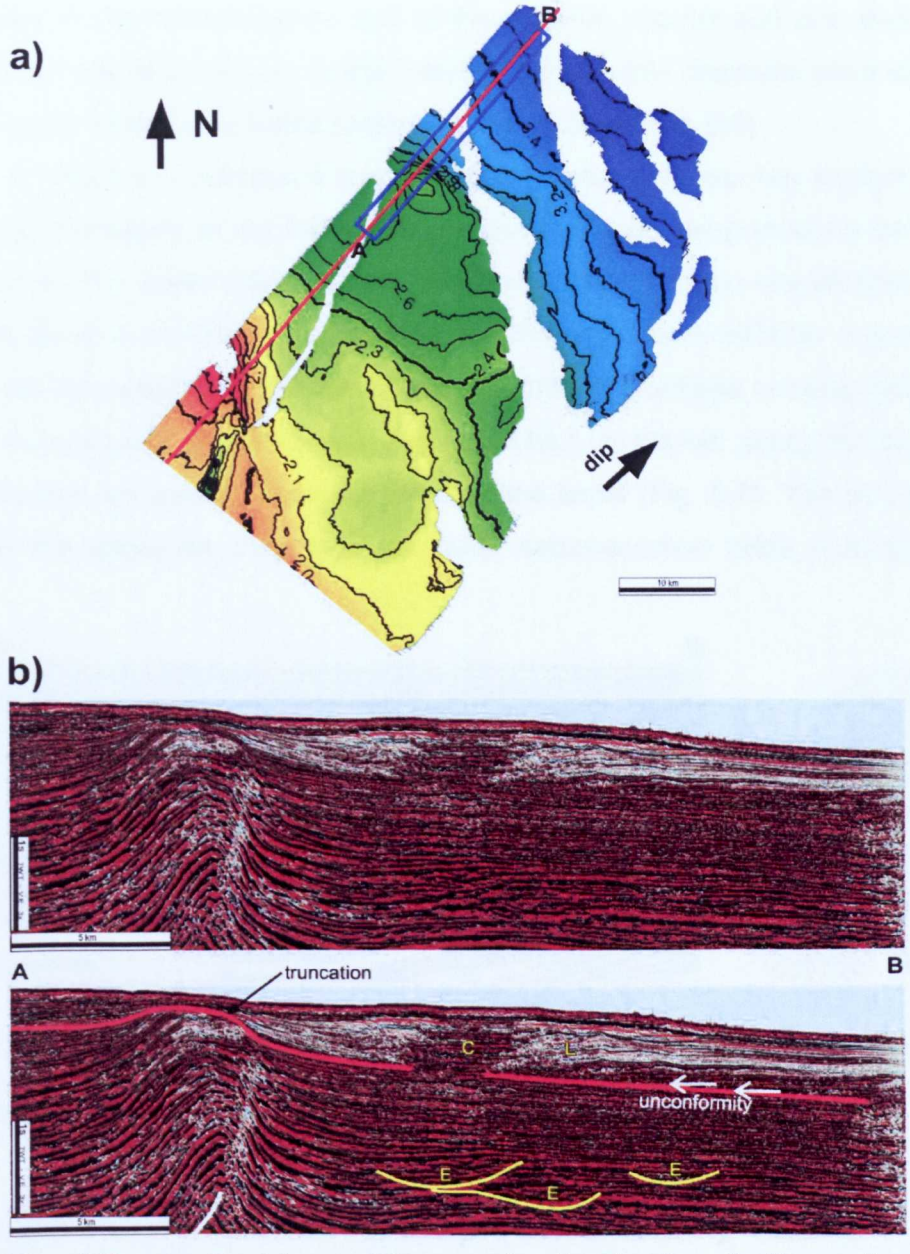

Figure 5-5 – a) Two-way-time(s) map of the unconformity. The discontinuities on the map are due to erosion by later channels; b) Non-interpreted and interpreted cross section AB, the unconformity is the red horizon, truncating underlying reflections on the crest of the fold. The white arrows indicate the onlap character of the horizons above. The unconformity also separates the upper sediment package with dominantly aggradational channel-levee systems (C-L) from the lower sediment package with essentially erosive canyon-like channels (E).

5.4 Pre-unconformity interval

5.4.1 Introduction

The prevailing seismic facies in the pre-unconformity interval are formed by tectonically deformed sub-parallel reflectors (Fig. 5.5). Thrust-cored folds form

anticlines in the Southwestern half of the seismic volume and are responsible for most of the deformation. In this interval, canyon-like channels were identified as the most common turbidite pathways (Fig. 5.5 and Fig.5.6).

In order to understand the structural framework, two key horizons were mapped: the bases of the lower and middle packages, as previously defined in chapter 4. The lower package includes the studied canyon-like channels (Fig. 5.7). Its base is a relatively continuous and high amplitude reflector at a depth to delineate the majority of the structures. The middle package corresponds to the most conspicuous growth strata interval, which is thicker along the synclines and pinches out laterally towards the anticline limbs (Fig. 5.7). The pinching-out toward the anticlines may indicate lower sedimentation rates than the uplift rates.

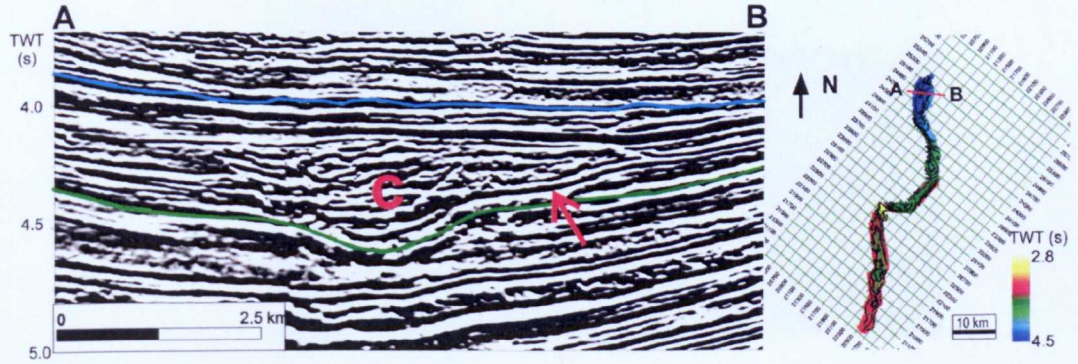

Figure 5-6 – Cross section AB showing a canyon-like channel C (the red arrow indicates the base of the channel). The section is located in the two-way time map of the base of the channel. The green and blue horizons are the base and the top of the lower package.

5.4.2 Structural framework of the pre-unconformity interval

This structural analysis is based on the 3D seismic data which cover the upper slope segment of the 2D seismic line (Fig. 5.2b). The tectonic structures can be visualized in plan view in the maps of the bases of the lower and middle packages (Figs. 5.7 and 5.8). These maps show the position of the fault-related folds and a fault with directional offset (i.e., a kink in its' intersection with the mapped key horizon).

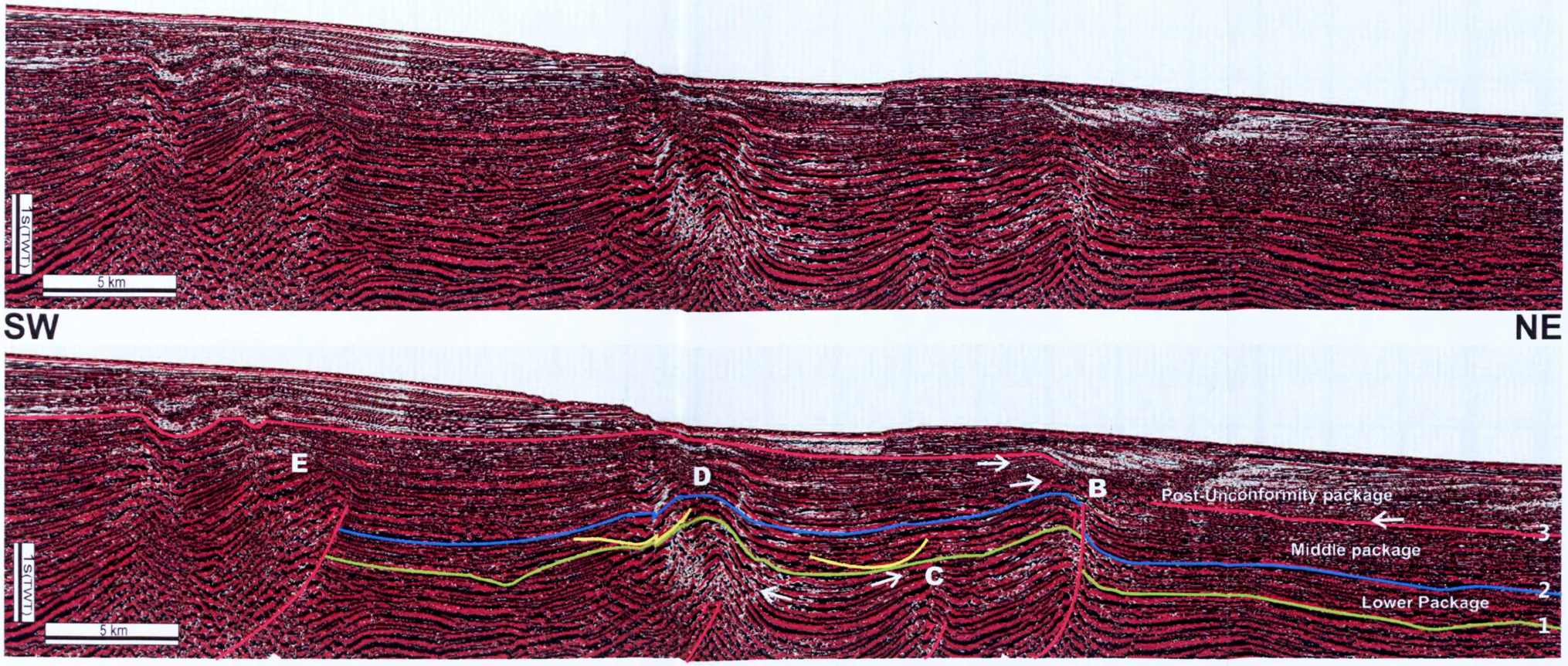

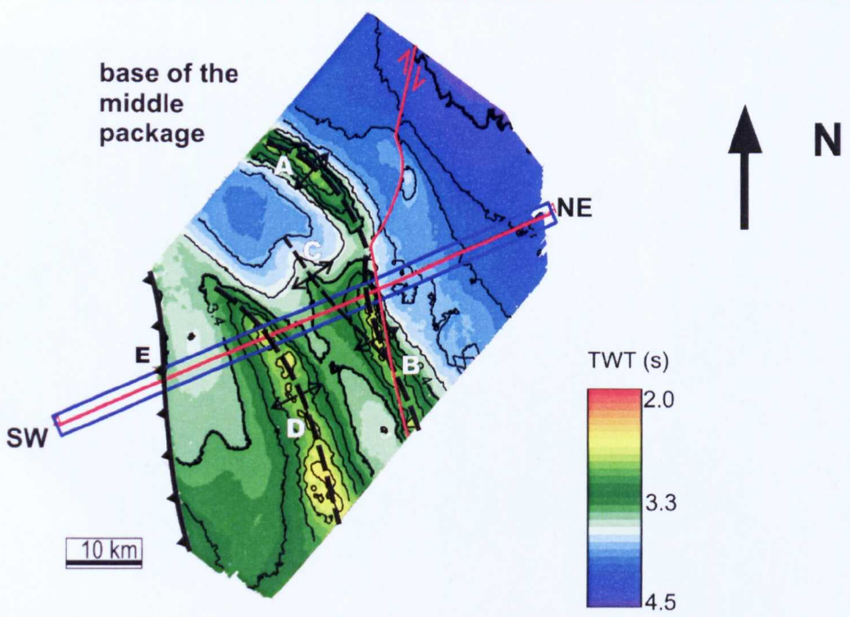

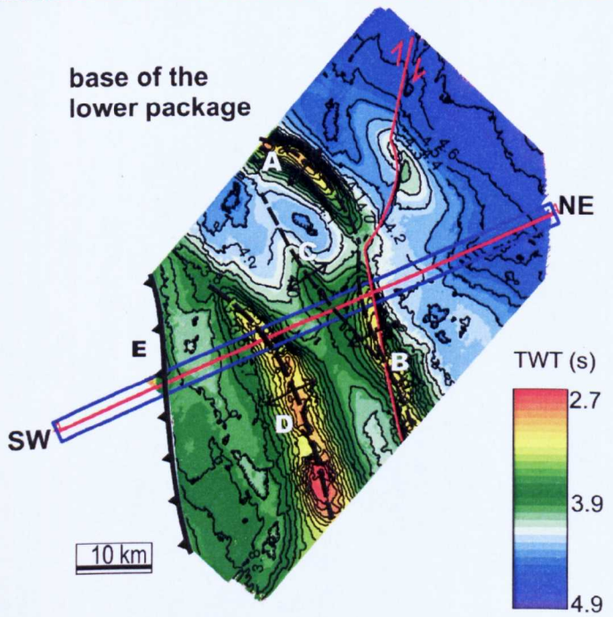

Legend:

1- base of lower package

2- base of middle package

3- unconformity

A, B, C, D and E - anticlines

Figure 5-7 – Non-interpreted and interpreted seismic sections across study area. The cross section shows 4 thrusts and related folds and the mapped horizons: unconformity (red), base (green) and top (blue) of the Basal Interval. Crescent-shape yellow structures are sections of the mapped canyon-like channel. The white arrows are onlaps onto the anticlines limbs. The two-way time maps of the base of the growth strata package and the basal horizon show the structures and the location of the seismic section.

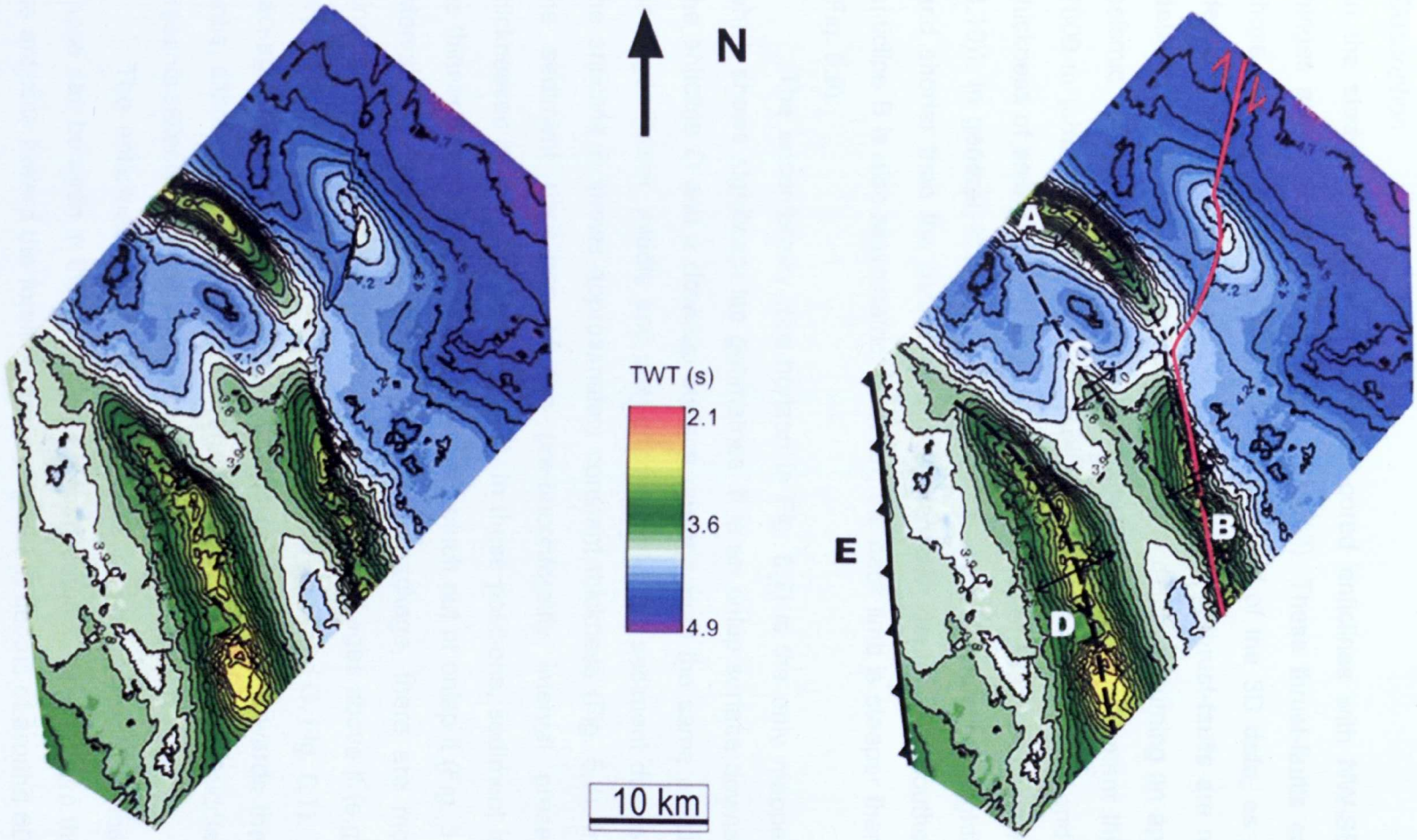

Figure 5-8 – Non-interpreted and interpreted two-way-time map of the base lower package. Notice the anticlines axes A, B, C and D are represented by black dashed lines. The anticline E is outside the SW border of the area because the horizon could not be mapped across the structure. A discontinuity interpreted as a tear fault is indicated by the red line.

Fold and thrust belt

Description

In the study area, there are 5 thrust-cored anticlines with NW-SE oriented hinges and northeasterly vergence (Fig. 5.7). These thrust-faults correlate to those seen in the 2D seismic line located NW of the 3D data, as previously described (Figs. 5.2b). Figure 3.17 shows that the thrust-faults are rooted in a detachment surface at approximately 8950 m depth, assuming an approximate seismic velocity of 1450 m/s in the water and using a sediment thickness of 7500 m (obtained from the curves relating two-way-travel times and sediment thickness of areas beyond shelf edge in off northern Brazil (Kumar, 1978) (Fig. 4.10)). In general, the folds are asymmetric with the forelimb slightly steeper and shorter than the backlimb, and tighten with depth. The Southern half of anticline B is also asymmetric, however, the back limb is steeper than the front (Fig. 5.9).

The unconformity (red horizon in Fig. 5.7) is the only mapped horizon which shows significant lap geometries. It is an onlap surface downslope from the anticline D and a downlap surface upslope from the same anticline. In all packages (lower, middle and post-unconformity) the sediment downslope from the anticline B shows approximately constant thickness (Fig. 5.7). In general, the sediment packages of the pre-unconformity interval present major thicknesses in the synclines (Fig. 5.7). In these positions, sediment layers can be thinner towards the anticline crest, can pinch out or onlap it (Fig. 5.7). In the interval underneath the base of the lower package, there are more layers pinching out towards the anticlines than in the packages above it (e.g., see the segment of the seismic section between anticlines D and C, Fig. 5.7). The lower package does not show reflection onlaps or pinch outs towards the anticline limbs, although it is slightly thinner on the anticline crests. The middle package presents reflection onlaps and pinch outs against the anticlines.

The anticlines commonly exhibit sets of normal faults in their crests. These can be seen in the anticline as planar features, dipping from the crest of the anticline toward the forelimb and dying out at depths of around 600 m (Fig. 5.10).

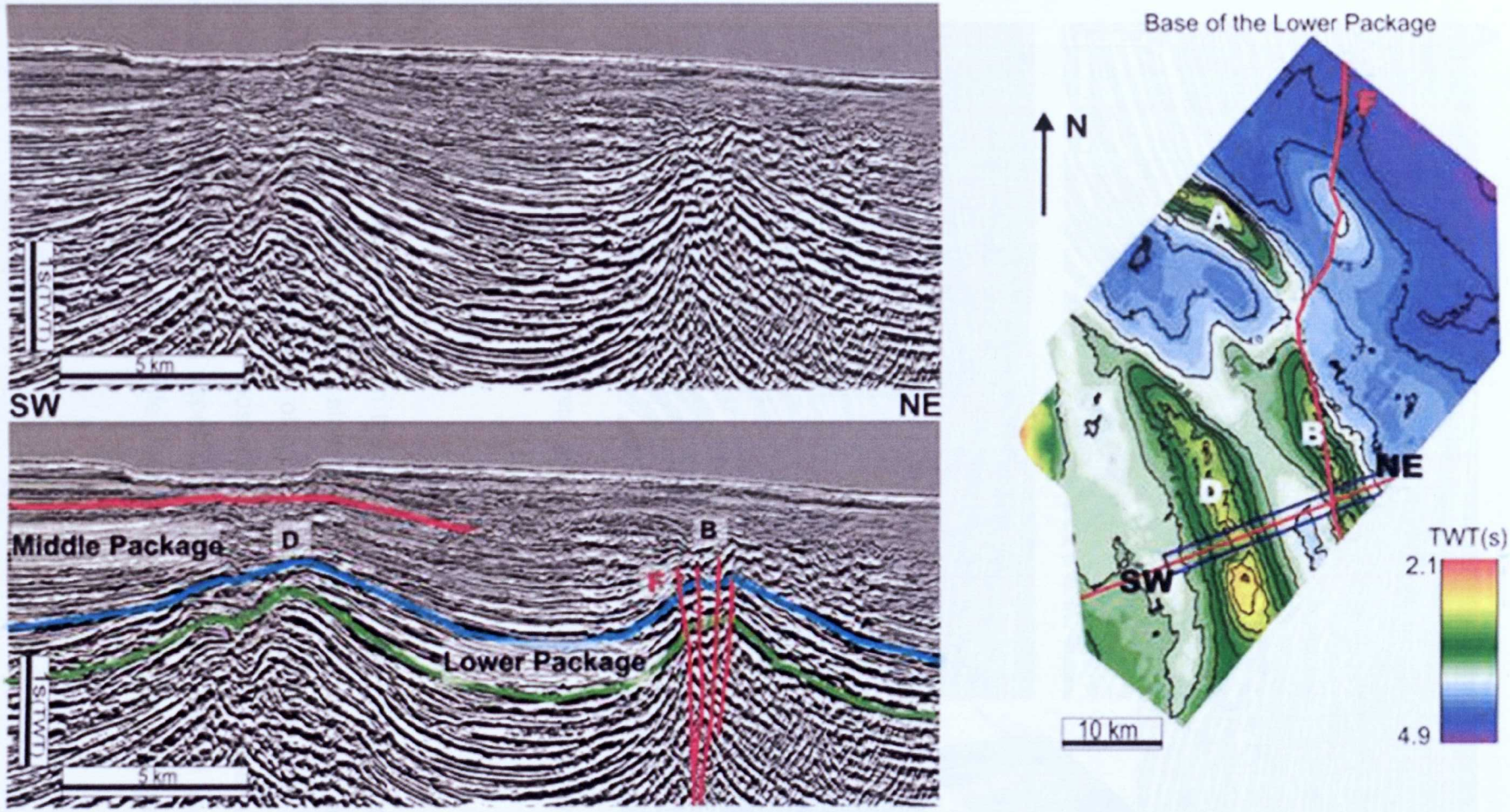

Figure 5-9 – Non-interpreted and interpreted seismic section across the anticlines B and D. Notice that anticline B in this segment is asymmetric, with its back limb steeper than the forelimb. The cross section is located on the two-way-time map of the base of the lower package.

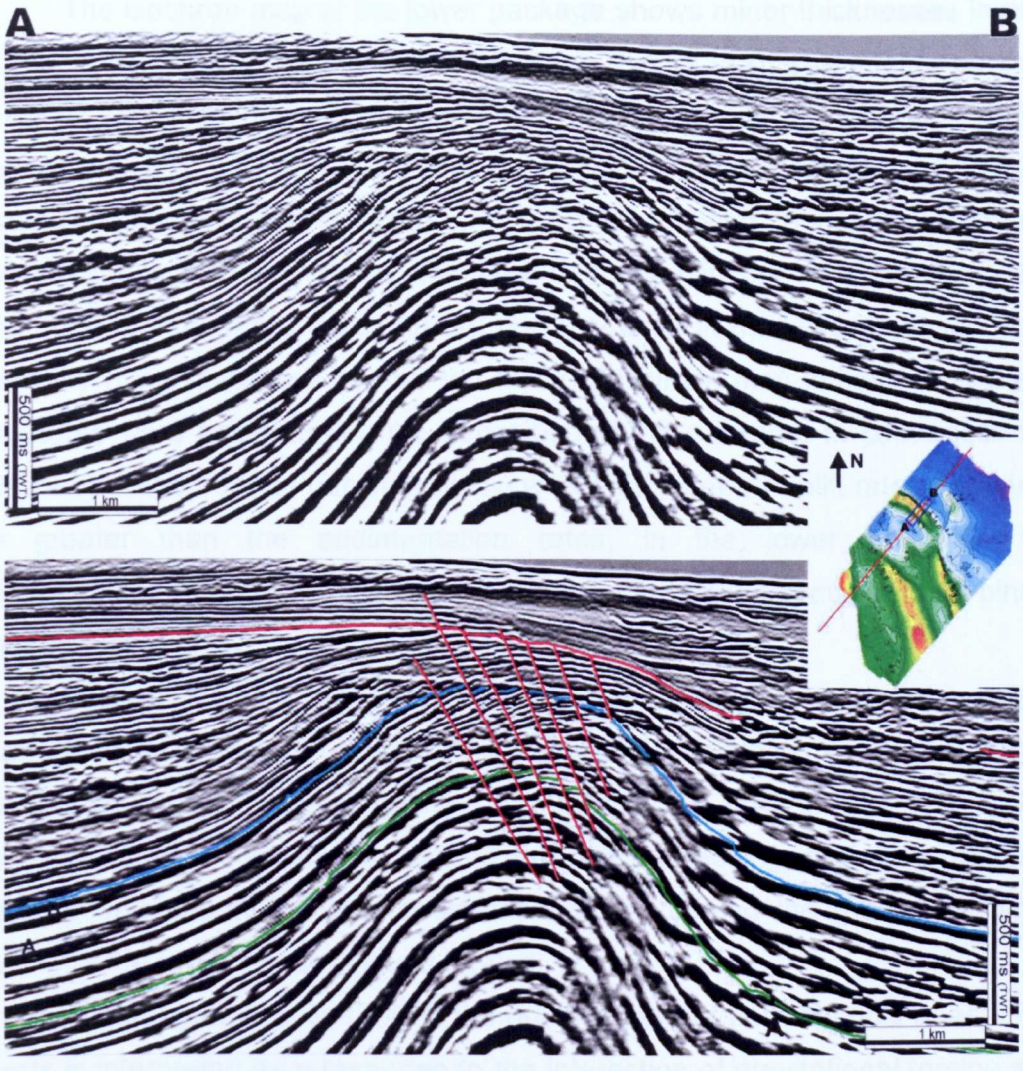

Figure 5-10 – Non-interpreted and interpreted seismic section showing crestal forelimb-dipping normal faults.

Interpretation

The occurrence of thicker strata in the synclines and layer pinch outs against the anticlines are typical of growth strata. It follows that the anticlines may have been active during the deposition of most of the sediment packages but less active during the deposition of post-unconformity sediments. The structures were more active mainly during deposition of the sediment interval underneath the lower package and the middle package, where growth strata are more conspicuous.

The isochron map of the lower package shows minor thicknesses in dark blue and the major thicknesses in dark green (Fig. 5.11a). The thinner portions coincide with the crests of the anticlines (compare with the locations of the anticlines in Fig. 5.8) and the thicker portions are distributed along ribbon-like features with N/NE orientation (Fig. 5.11a). These ribbon-like features correspond to the canyon-like channels described in the next section 5.4.3. Therefore, although growth strata are not very clear in the lower package, their relatively minor thickness on the top of the anticlines may indicate that these structures were active during the deposition of the package. In contrast to the middle package and the package below where the inferred uplift rates appear to be greater than the sedimentation rates, in the lower package, the sedimentation rates were probably greater than the uplift because stratal pinch-outs are not seen.

The isochron map for the middle package also shows minor thicknesses (dark blue) on the crests of the anticlines but the major thicknesses (orange) in the SW section of the area, upslope of the anticlines (Fig. 5.11b). The thicker strata between the anticlines indicate not only syntectonic deposition (growth strata development) but also sediment trapping behind the grown anticlines such that the synclines are almost healed.

According to Morley (2007) the development of normal faults at anticline crests is interpreted as a response to the interaction of gravitational forcing and fold growth within the syn-kinematic section. Their importance lies in the fact that they mark the moment when the folding effectively affected the sea floor topography. They occur when sediments accumulate on the tops of the growing structures (Morley, 2007). Their occurrence may favour the erosion of the anticlines by channel or mass wasting processes. In the current work, however, they are not focus of study because in the study area these faults do not appear to affect the channel-levee systems.

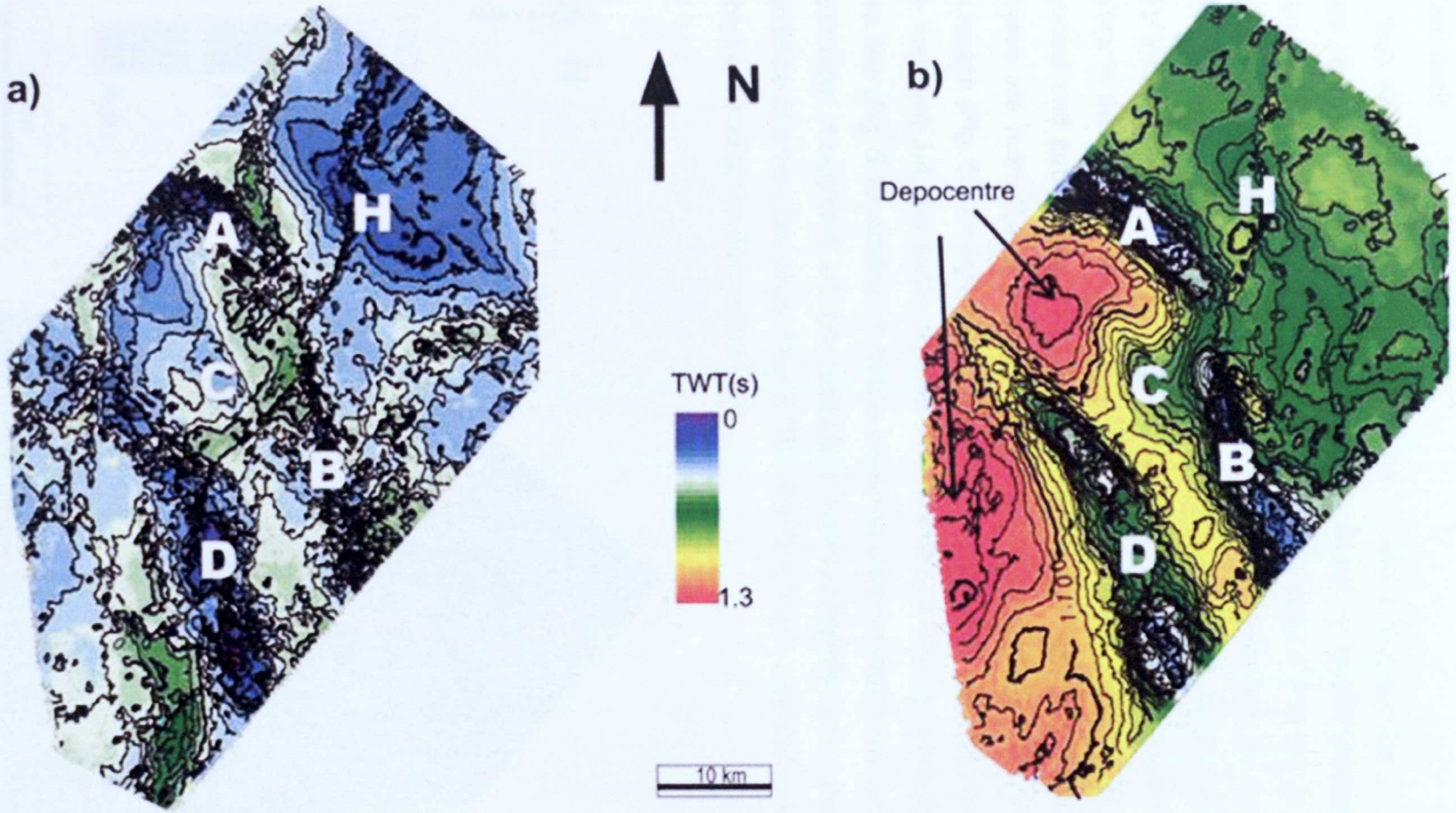

Figure 5-11– Isochron maps with the approximate location of the anticlines (A, B, C and D) and the high (H) at the fault bend indicated. The hot colours imply thicker intervals and the cold colours thinner. b) Isochron map of the lower package. a) Isochron map of the middle package. Notice that the sediment cover on the fold crests is thinner in each case. The larger thicknesses occur upslope of the anticlines.

Tear fault

A fault exists with approximate N/NE strike, with a sinuous trace in plan view and characterised by a dextral offset along strike. It is best visualised on the two-way-time map of the base of the lower horizon (Fig. 5.12). The fault geometry varies along length in the studied area, depending on the fault trace orientation. In segment 1-2 (Fig. 5.13, map) the fault has N-NE direction and a dip slip component toward the SE (Fig. 5.13, section a). In this case, the East block is the hanging wall. In segment 2-3, the fault is sub-vertical in its lower portion and cuts across a bathymetric high. In this high, the deeper sediment layers are more tightly arched, and growth strata can be found in the lower package (Fig. 5.13, section b), indicating that there was uplift during deposition. In segment 3-4, the fault has a NE direction and a dip slip component toward the NW (Fig. 5.13, section c). In this case, the western fault block is the hanging wall side. In segment 4-5, the fault trace has NW direction and cuts across the anticline at a very low angle (Fig. 5.13). The fault trace is almost coincident with the front limb of the thrust-cored fold.

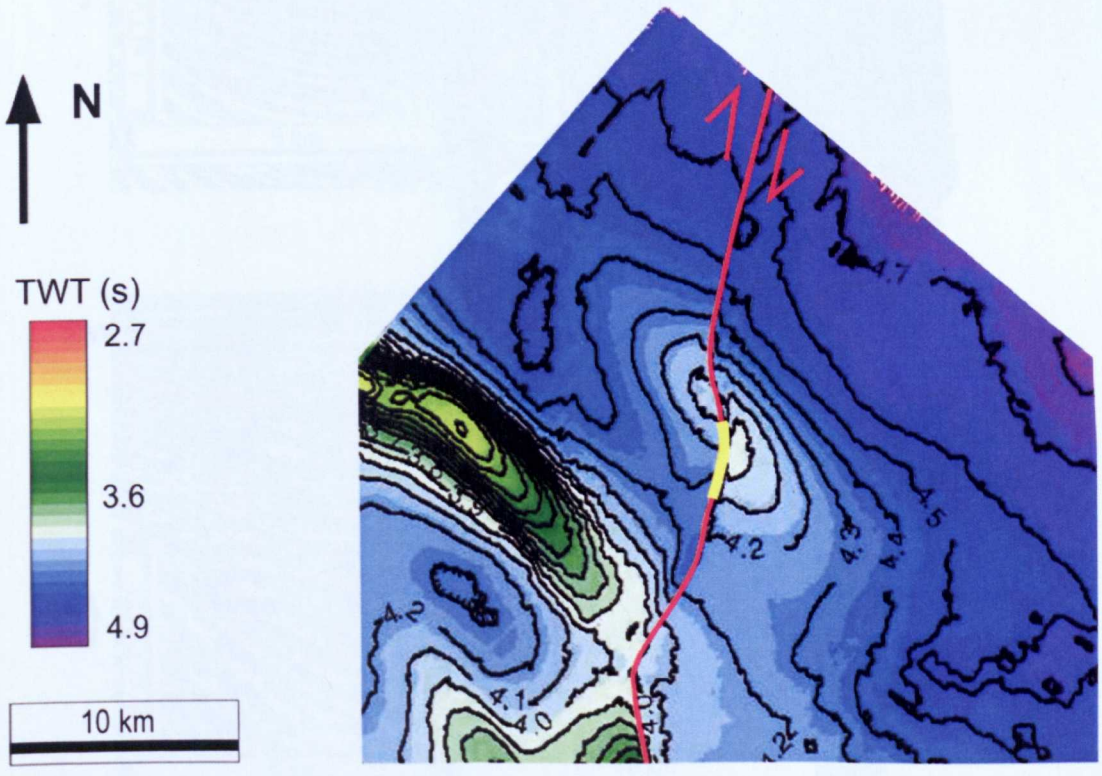

Figure 5-12 – Detail of the two-way-time map of the base of the lower package showing the fault with directional offset. The offset of the contour curve of 4.1 s is highlighted in yellow.

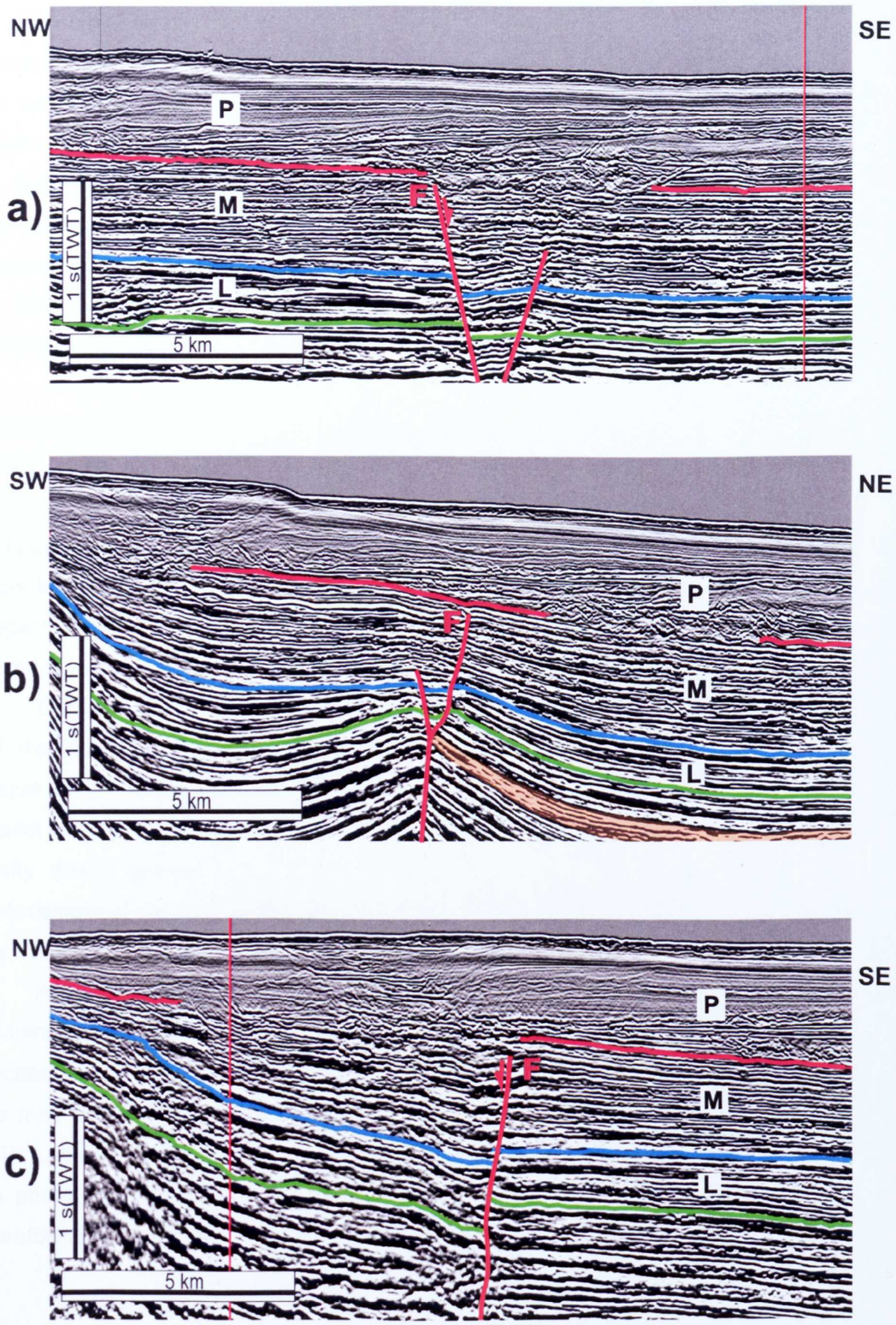

Figure 5-13 – Seismic sections across the tear fault and in different positions along the fault axis, as seen on the map of the base of the middle package. In **a** and **c** sections the hanging walls moved downward relative to the footwall, indicating extensional behaviour. In **a**, a small graben was formed. The **b** section is across the fault bend and cuts arched sediments showing growth strata (highlighted in orange) and the faults bifurcate upward showing a small minigraben characterizing extensional character in its upper half. The GH section cuts across the anticline. In map view the fault shows strike offset, better seen on the fault bend.

In cross section the fault plane may be sub-vertical at the position where it cuts the anticline (Fig. 5.13, section d). Section d outlines the juxtaposition of two fold apices ("twin peaks") that suggest that the fault is displacing fold B, creating an offset along the fault trace. In segment 4-5 the superimposition of the deformation due to folding and faulting causes added complexities in fault characterisation. The fault segments with NE direction have extensional characteristics with dip-slip offsets (Fig. 5.13, sections a and c). Conversely, in the NW fault segments the sediment layers are arched upward, indicating compressional characteristics (Fig. 5.13, sections b and d).

Fault kinematics

Growth strata are associated with the arched structure (Fig. 5.13, section b) forming a bathymetric high. Here the reflections pinch out toward the high at the fault bend, indicating that the sediment layers arched upward syndepositionally. In the lower package, growth strata can be seen in section b (Fig. 5.13). This suggests that the paleo-bathymetric high at the fault bend may have been formed by compression at a restraining bend (transpression) (Fig. 5. 14).

Complex variation of deformation style along the fault trace may indicate that the relative movement between the two plates separating the fault is oblique to the fault trace, as opposed to a typical strike-slip fault which is parallel to the fault trace (Fig. 5.14). This deformation may be related to the gravity driven gliding of the upper fan sediments downslope, with major displacement of the West portion. The difference in displacement along the fault may have promoted the tearing apart of the two blocks.

Although the faulting seems to be related to the process of gravity tectonics in the slope, the fault cuts anticline B and thus suggests an alternative direction for the main compressive stress ($\sigma 1$) to that inferred from the anticline. This may indicate that the fault postdates development of the anticline B (Fig 5.14). Above the unconformity, however, the fault remained almost inactive, with post-unconformity sediments slightly affected. Apparent offset above the unconformity is not clearly visible at the scale of seismic resolution.

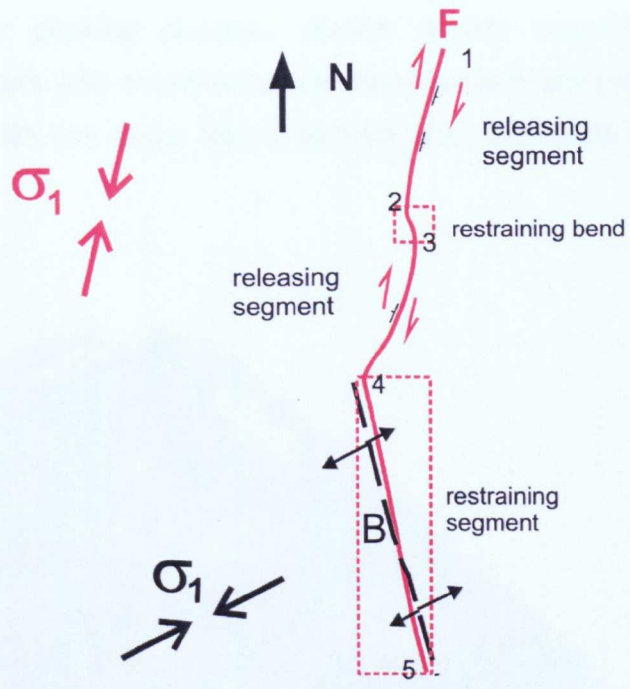

Figure 5-14 – Diagram with the trace of the tear fault (red) and the anticline B (dashed line). The releasing segments and the restraining bend are indicative of transtension and transpression, respectively. Notice the approximate direction of the interpreted major compressive stress axis ($\sigma 1$) for the fault (red) and for the anticline (black) deformations.

5.4.3 Structurally confined canyon-like channels

Description

Incised channels occur commonly in the pre-unconformity interval whereas there is no clear evidence of levee-confined channels. In the lower package, incised channels are inferred to be the main pathways of turbidity currents (Fig. 5.6 and 5.7). At least three channels were identified dipping toward the Northeast, incised in a background of continuous tabular sub-parallel reflections with amplitude similar to the channel fill (Fig. 5.15, 5.16 and 5.17). An isochron map was the best way to show the erosive channels in plan view, to focus on their geometry, distribution, and their relationship with the structures (Fig. 5.15); the thicker portions of the interval are mainly along the channel axes and the thinner are coincident with the anticline crests. In cross section, the channel bases are frequently sharp, deeply erosive and present lenticular geometry with flat or convex top layers (Fig. 5.16). The channels are sinuous because they divert and/or deflect (see Clark and Cartwright, 2009) (Fig. 2.53) from the pre-

existing and/or growing structure (further details regarding the interaction between tectonics and erosive-channel development are presented in Chapter 7). Channel width can range from 2 to 5 km (Fig. 5.16) and thickness from 200 to 280 m.

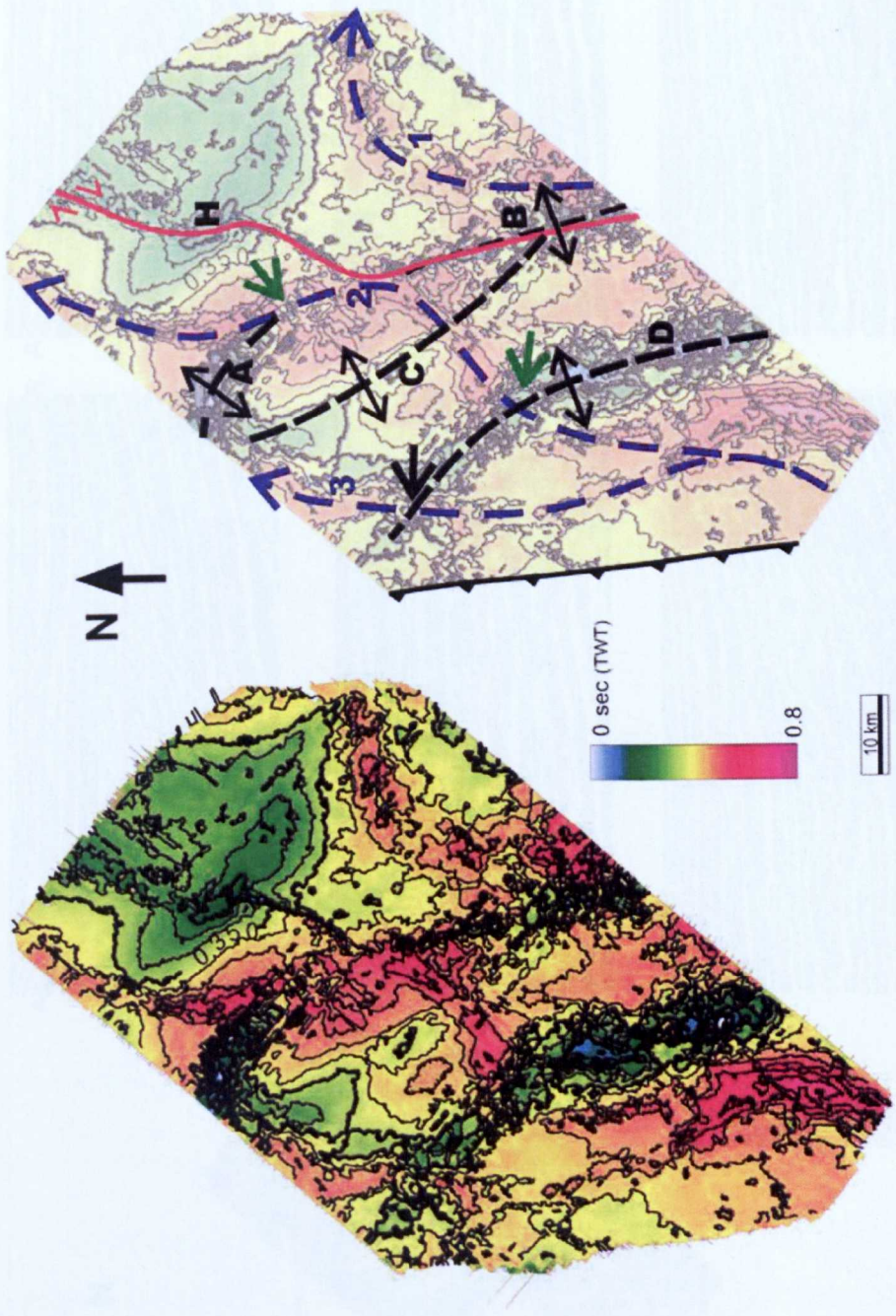

Figure 5-15 – Non-interpreted and interpreted isochron map of the lower interval calculated between the green and blue horizon (Fig. 5.7). This map shows the wider time interval with major thicknesses (warm colours) coincident with the channel axes (dashed blue lines) and the minor thicknesses (cold colours), the crests of the folds (dashed black lines, A, B, C and D) and the top of the bathymetric high (H) at the fault bend (the same one as seen in the blue horizon structural map). The green arrows indicate channels cutting through the anticlines. Channel 2 is the same as that seen in figures 5.6, 5.7, 5.16 and 5.17.

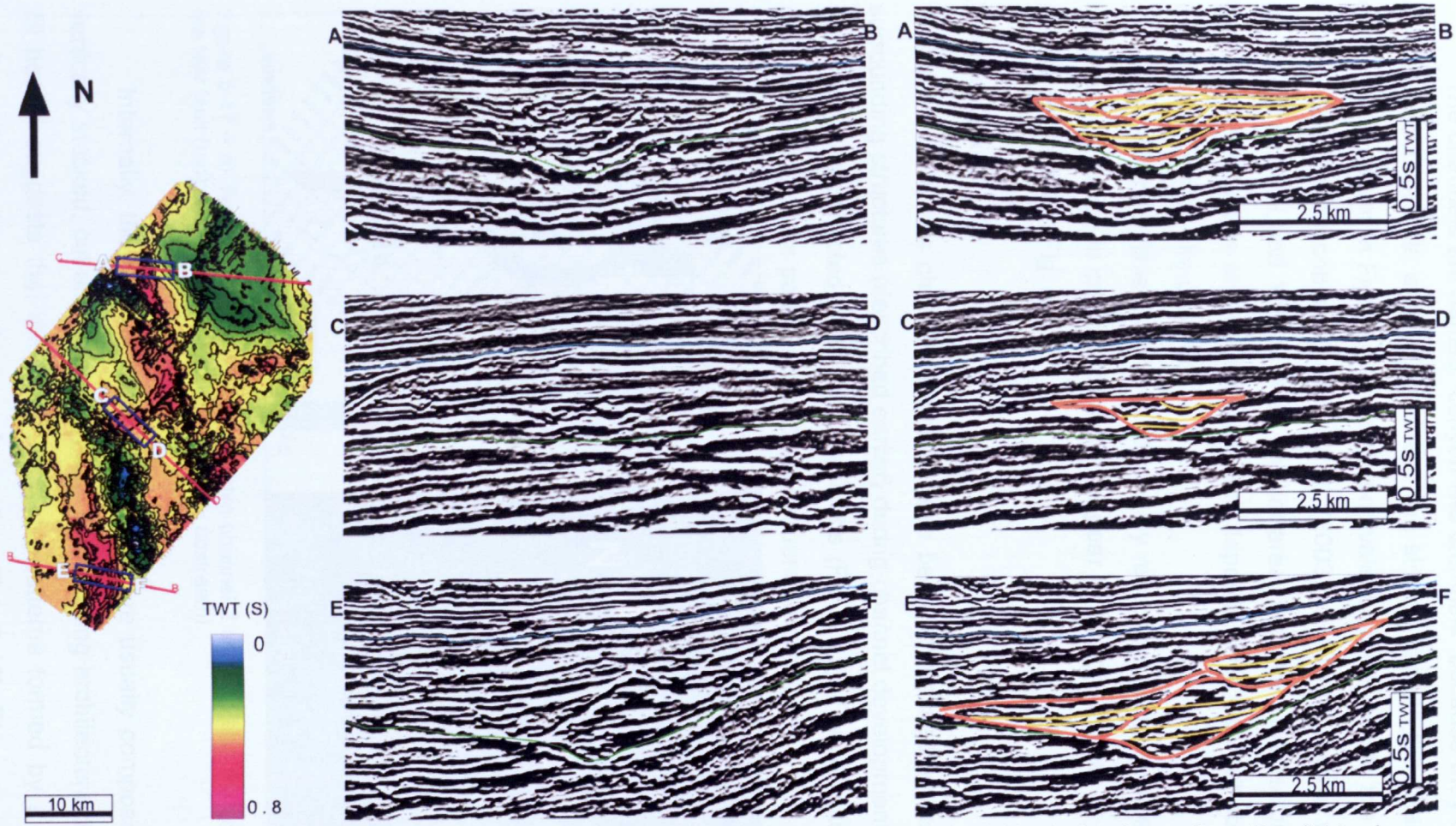

Figure 5-16 – Cross sections along channel 2 in the lower package. The channel exhibits an incisional lenticular shape often with a flat top layer but sometimes with a convex upward top layer (section AB). The thickest channel segments show an oblique stacking of cut and fill (sections AB and EF). The channel fill exhibits trough (AB-lower cut), tabular (CD and EF) or lateral accretion (AB-upper cut) reflections. Following the scheme of Sprague (2002), sections EF and AB are channel complex composed of elements (i.e., each orange coloured channel unit).

The channels are named "canyon-like channels" because they can be as large as 2600 m wide and 150 m deep. The studied canyon-like channels, for example as shown in Figure 5.17, have equivalent dimensions to the confining erosive features described by Abreu et al. (2003) in offshore Angola which are up to 200 m thick and 1-5 km wide. In that area, however, the features frame the sinuous channels and related overbank deposits. This was not observed in the studied canyon-like channels.

The channel fill is commonly formed by reflections with variable levels of organisation, which in cross section can appear as trough, tabular or sigmoidal (lateral accretions) (Fig. 5.16).

Interpretation

The sinuosity of this channel seems to have been determined by the growing surrounding structures (described earlier) during channel development because the channel is deflected at the anticline limbs (Fig. 5.15). The variation of axis gradient also appears partially due to subsequent deformation.

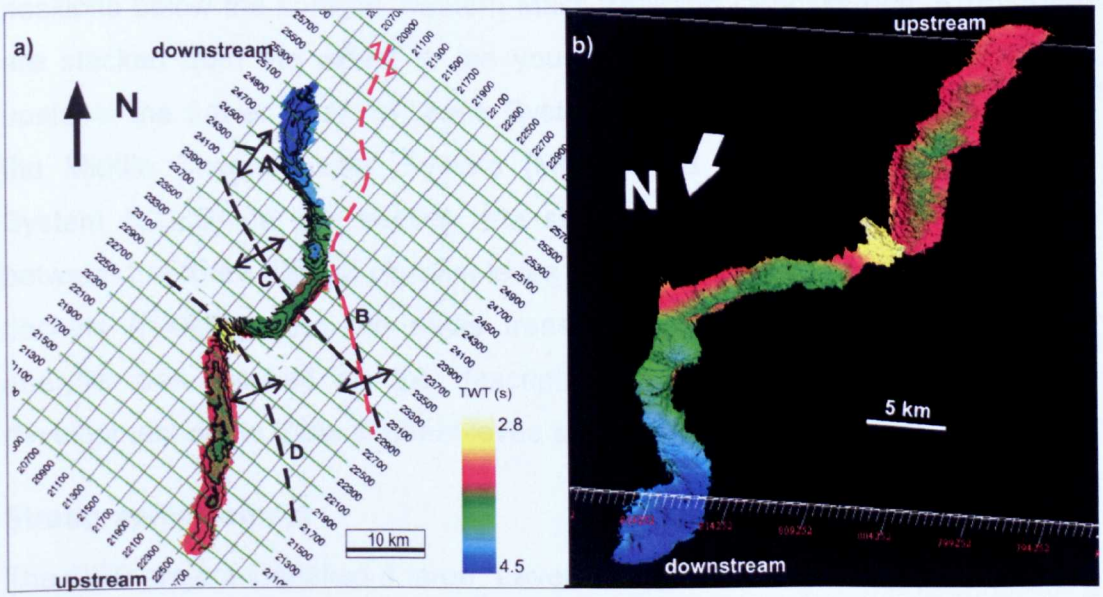

Figure 5-17 – a) Two-way-time map of the erosive channel 2 showing also the anticlines and the tear fault (red); b) 3D view of the channel 2 (view upstream).

Internally, the thickest channel segments are usually composed of sub-vertically stacked, cut and fill geometries. The stacking architecture of channel-fill bodies suggests that the channel growth patterns formed by a combined process of lateral and vertical amalgamation (Fig. 5.16). Thus, section EF in

Figure 5.16 shows an amalgamation of stacked channel cuts and fills composed of multiple channel elements, which can be classified as "channel complex, after Sprague et al. (2002) (Fig. 2.23). Each cut and fill element is considered a channel element in the proposed hierarchy. This hierarchical scheme is recognisable on seismic reflection profiles and some large outcrops (Sprague et al., 2002).

5.5 Post-unconformity interval

5.5.1 – Introduction

The post-unconformity interval can reach a thickness of 900 m in the studied area, corresponding to part of the interval analyzed by the Ocean Drilling Project (ODP Leg 155) which included the uppermost 500-800 m of the Amazon Fan (Flood and Piper, 1997; Hiscott et al., 1997). In this interval, the sediments are less tectonically disturbed than the sediments below the unconformity.

Three channel-levee systems were identified in distinctive stratigraphic positions below the surficial Western Mass-transport Deposits (Fig. 5.18). They are stacked from the oldest to the youngest and from East to West toward upslope: the Lower Channel-Levee System (LCLS) that only clips the survey, the Middle Channel-Levee System (MCLS) and the Upper Channel-Levee System (UCLS). In this section, the stacking and the genetic relationships between the three distinct channel-levee systems, the high amplitude reflection packets (HARPs), and the mass transport complexes are discussed. The analysis was focused on the description of the principal controls on the development of the three channel-levee systems.

Stratigraphic context

The ODP project identified 4 large "Levee Complexes" in the Quaternary of the Amazon Fan (Flood et al., 1995; Hiscott et al., 1997; Piper et al., 1997) (Fig. 5.19). Although well data were unavailable to tie the 3D seismic survey with the local stratigraphy proposed by ODP Leg155, the location of the 3D data in the Amazon Fan suggests that the post-unconformity channel-levee systems are components of the Middle Levee Complex.

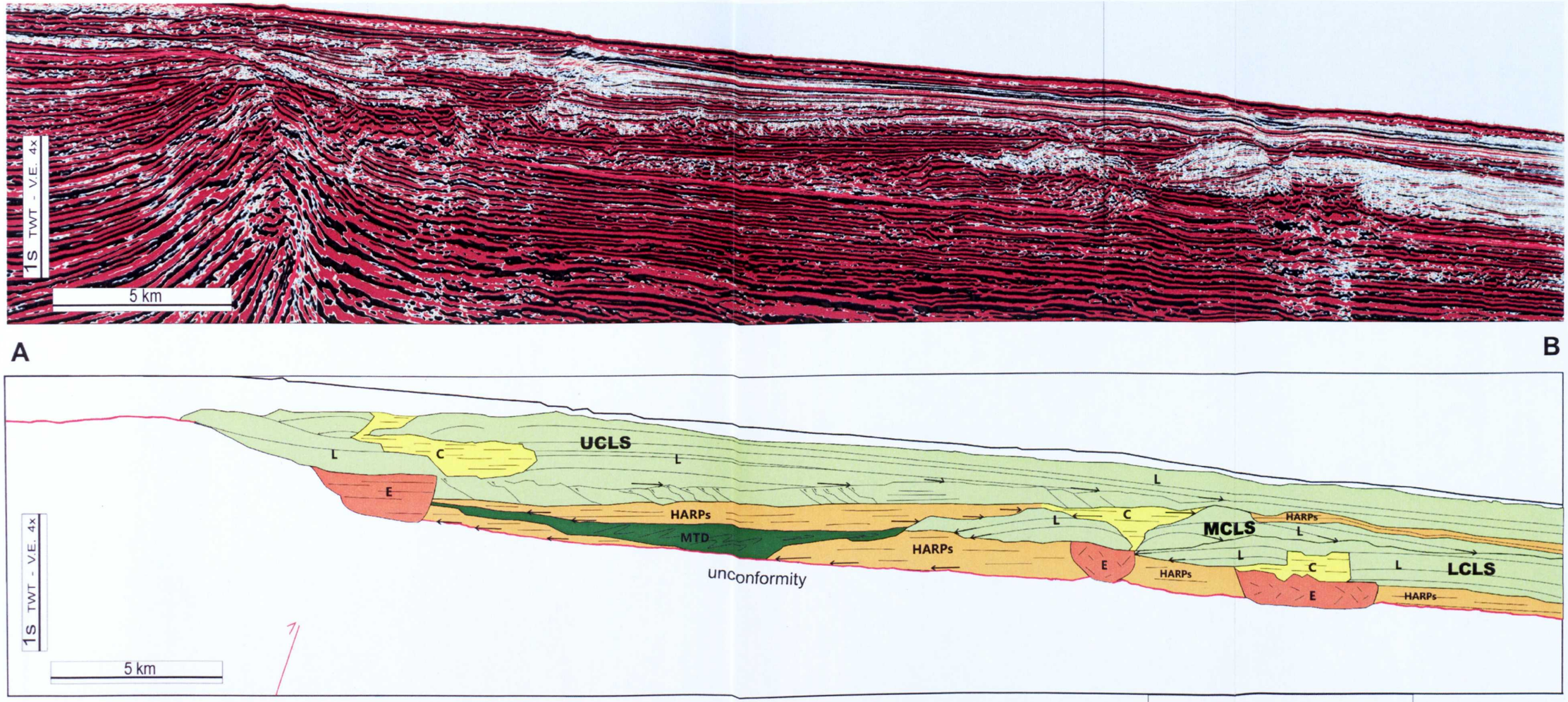

Legend:

UCLS - upper channel-levee system
MCLS - middle channel-levee system
LCLS - lower channel-levee system

HARPs - high amplitude reflection packets

MTD - mass transport deposit

C - channel (HARs)

L - levee

E - erosive basal channel

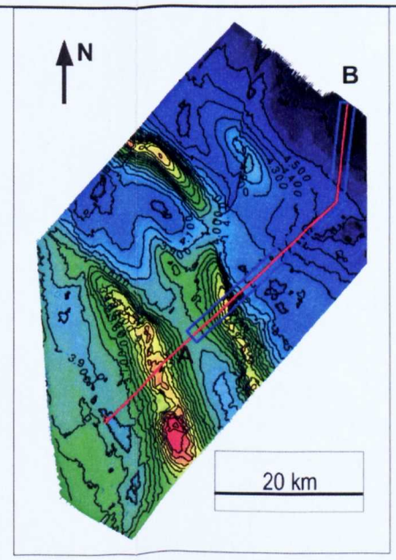

Figure 5-18 – Non-interpreted and interpreted cross section showing the three upslope-stacked channel-levee systems identified above the unconformity of the study area. Slope deposits and channel-levee architectural elements were identified based on the seismic facies which were characterized using the amplitude intensity and the terminations of reflections. The white arrows highlight the levee reflection downlaps and the HARPs onlaps. The location of the seismic section is shown on the structural map of the green horizon.

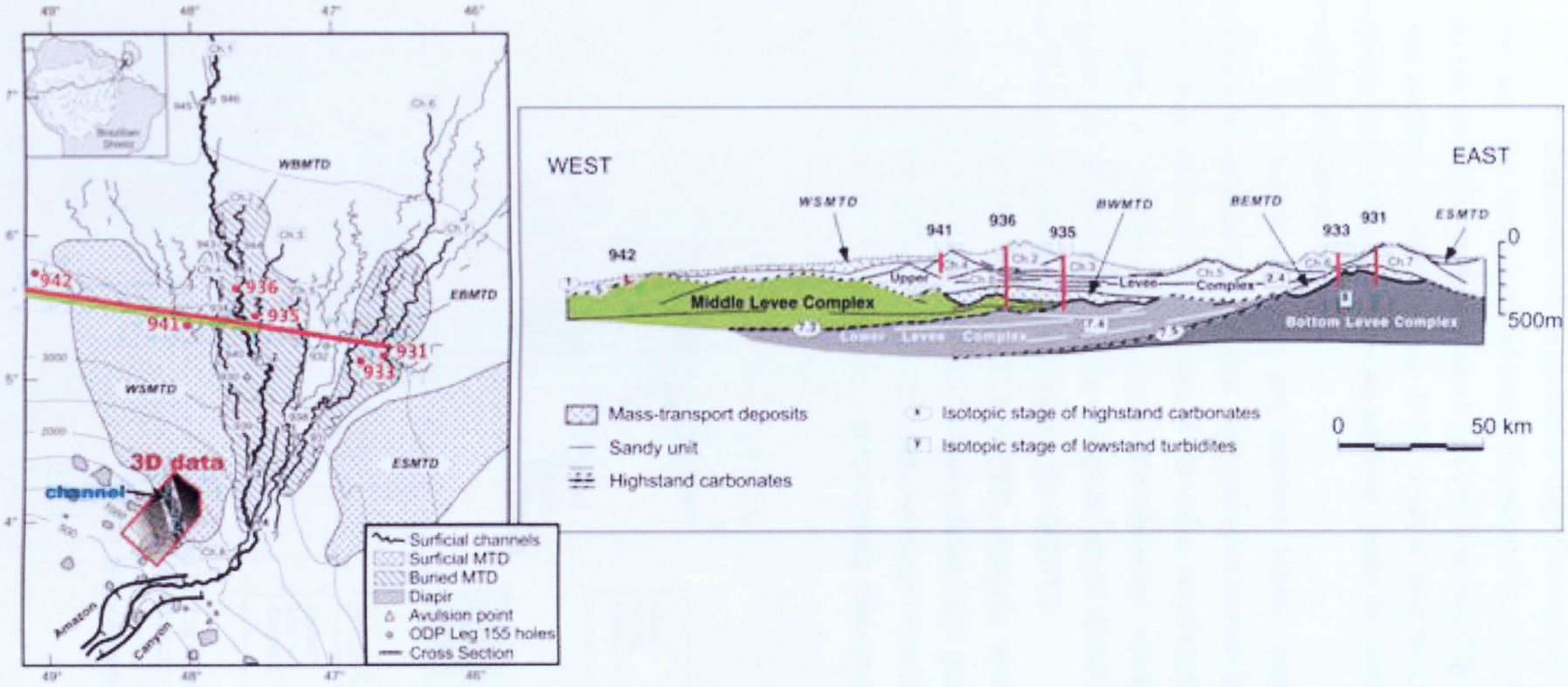

Figure 5-19 - The base map of the Amazon Fan shows the study 3D data close to the Amazon Canyon Mouth and the location of the cross section and boreholes highlighted in red. The segment of the section covered by the Middle Levee Complex (MLC) is highlighted in green beside the cross section trace. Notice that a downstream extrapolation of the Pleistocene channel (blue) shown in the 3D data indicates it would be included in the MLC domain. The MLC is highlighted in green in the cross section (Figures modified from Lopez 2001).

The 3D seismic data is located on the West side of the Amazon Channel, underneath the West Surficial Mass Transport Deposit (WSMTD) and upslope from the section between the boreholes 941 and 942 (Fig. 5.19). Although close to the position of Well 941 (Fig. 5.19), most of shallow channel-levee systems underneath the WSMTD occurring between wells 941 and 942 may be included in the Middle Levee Complex.

The studied channels are oriented N/NW, hence, the downstream extrapolation of the study channel, highlighted in blue in the 3D data (Fig. 5.19), would likely fit in the West portion of the cross section where the Middle Levee Complex is. Therefore, the study channel-levee systems are likely to be components of the Middle Levee Complex, which is the westernmost complex and is located immediately underneath the WSMTD.

The integration of biostratigraphic, isotopic and paleomagnetic data suggests that the Middle Levee Complex dates from glacial Stage 6 (Piper et al., 1997). Therefore, the study channel-levee systems might have been deposited during this glaciation, approximately between 125 and 170 ka BP (Fig. 5.20).

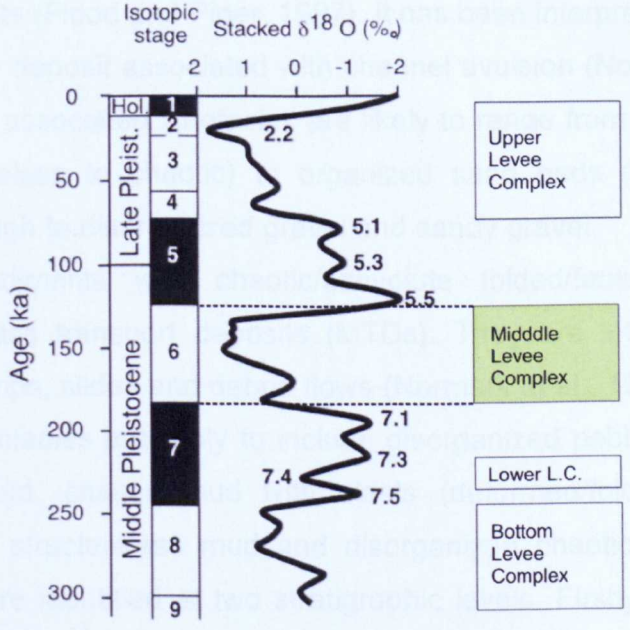

Figure 5-20 – Diagram showing four "Levee Complexes" in the Quaternary of the Amazon Fan (Flood et al., 1995) with respective isotopic stages. The isotopic curve of Martinson et al. (1987) is used as a proxy for eustatic sea level (adapted from Piper et al. (1997)). Notice that the Middle Levee Complex which includes the studied channel-levee systems was deposited approximately between 125 and 170 Ka.

Seismic facies and sedimentologic interpretation

Description

Four main seismic facies were identified in the post-unconformity interval: high amplitude reflection packets (HARPs), chaotic/convolute folded/faulted reflectors, high amplitude reflections (HARs) and downlapping, low amplitude reflections. These were correlated to the four main acoustic units previously described in the Amazon Fan by ODP Leg 155 (Manley et al., 1997) (Fig. 3.8) in order to indicate the probable lithology. The seismic facies were determined based on not only the amplitude intensity, but also on the geometry of the deposits and the geometry and termination style of the seismic reflections (Fig. 5.18).

Interpretation

All the following interpretation of the seismic facies in the study area was made by analogy with the ODP Leg 155 description on Figure 3.8:

The sub-parallel high amplitude reflection packets (HARPs) onlap the unconformity. This facies was described in the downslope areas of the Amazon Fan as sand rich ponded sheet-like deposits formed by unconfined high density turbidity currents (Flood and Piper, 1997). It has been interpreted as indicating a crevasse-splay deposit associated with channel avulsion (Normark et al., 1997) (Fig. 3.8). The associated lithofacies are likely to range from disorganized sand beds (structureless to chaotic) to organized sand beds (graded and cross stratified) through to disorganized gravel and sandy gravel.

The sediments with chaotic/convolute folded/faulted reflectors are considered mass transport deposits (MTDs). They are interpreted as being formed by slumps, slides and debris flows (Normark et al., 1997) (Fig. 3.8). The associated lithofacies are likely to include disorganized pebbly or gravelly mud and sandy mud, chaotic mud with clasts (deformed/folded/faulted strata), homogeneous structureless mud and disorganized chaotic sand with clasts. The MTDs were identified at two stratigraphic levels. Firstly, there is an MTD flanking the middle channel-levee system. It is thought to be formed by large scale gravity-driven slumping and/or sliding of sediments on the paleoslope. Secondly, another MTD exists at the base of the right-hand levee (looking downstream) and is interpreted as a slumped levee.

The channel axis facies consists of high amplitude reflections (HARs) roughly sub-parallel and enclosed by the levee reflections. According to Normark et al. (1997) they can be associated with disorganized sand beds (structureless to chaotic), organized sand beds (graded and cross stratified) and/or chaotic mud (clasts from localized mass transport) (Fig. 3.8). A HAR unit was sampled in the modern Amazon Channel and is composed of the coarsest and best-sorted sand rich sediments sampled within the Amazon Fan (Manley et al., 1997).

The levee facies comprises low amplitude reflections downlaping onto the base of the system. The levee deposits are volumetrically the most important seismic facies in the post-unconformity interval. They are considered to be overbank deposits formed by turbidity current overflows. Sampled levees consisted of mud with thin beds and laminae of silt and sand (Manley et al., 1997). They may exhibit the lithofacies of colour-banded clay and mud, colour-banded silt and mud, irregular or discontinuous silt laminae, very thin regular silt and mud laminae, organized silt beds and laminae (graded, cross-beds), disorganized silt beds and laminae and organized sand beds and laminae (Normark et al., 1997).

5.5.2 – Basal Erosive Channel

Description

An erosive channel occurs at the base of each of the three channel-levee systems identified above the unconformity. These channels form elongate features dipping towards the N-NW (Figs. 5.21 and 5.22) with variable dimensions; channel widths range from 1.6 to 4.2 km and approximate depths from 40 to 300 m. Their incision cuts through the high amplitude packages (HARPs) and the underlying unconformity (Figs. 5.21 and 5.22). The channel boundaries are often crescent-shaped forms in the horizon slices and are interpreted to be formed by rotated blocks sliding toward the channel axis along small normal faults (Fig. 5.22, section M). The basal erosive channel of the Upper Channel-Levee System is shallower than the others, ranging approximately from 50 to 150 m of depth and tends to be shallower upstream than downstream (Fig. 5.22).

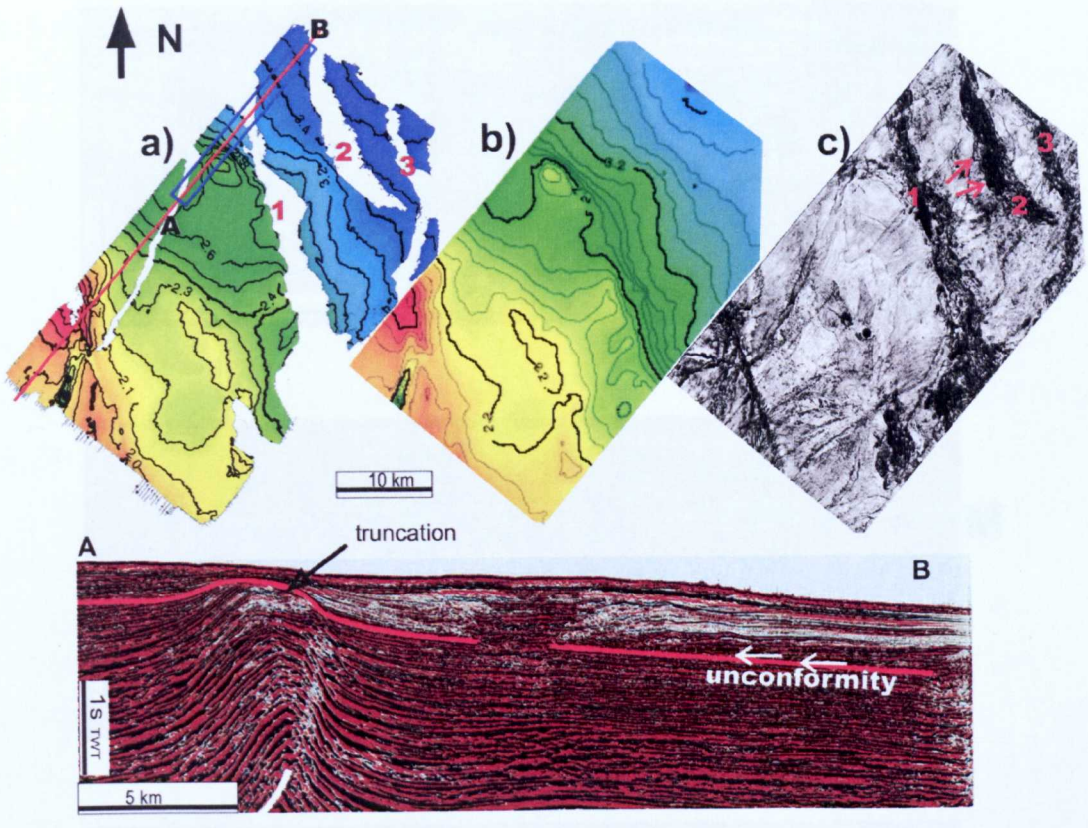

Figure 5-21 – a) Two-way time map of the unconformity (discontinuities are due to erosion by later channels 1, 2 and 3). The unconformity is shown in the cross section AB; b) extrapolated two-way-time map of the unconformity used for the construction of the map of the RMS of coherence (c). The extraction of coherence attribute was in the interval from 10 ms below to 10 ms above the unconformity. Channel 1 corresponds to the basal incision of the UCLS, 2 to the basal incision of the MCLS and 3 to LCLS. The red arrows indicate crescent-shaped borders of the erosive base in the MCLS.

The basal erosive channel of the middle system has two segments. The lower segment abruptly pinches out and becomes very shallow upstream close to the connection with the upper segment (Fig. 5.21a and c). The upper segment coincides with the upstream segment of the erosive channel of the LCLS. In the same erosive channel, the fill facies can vary from chaotic to ordered and from high to low amplitude reflections, with the chaotic reflections prevailing close to the channel base (Fig. 5.22).

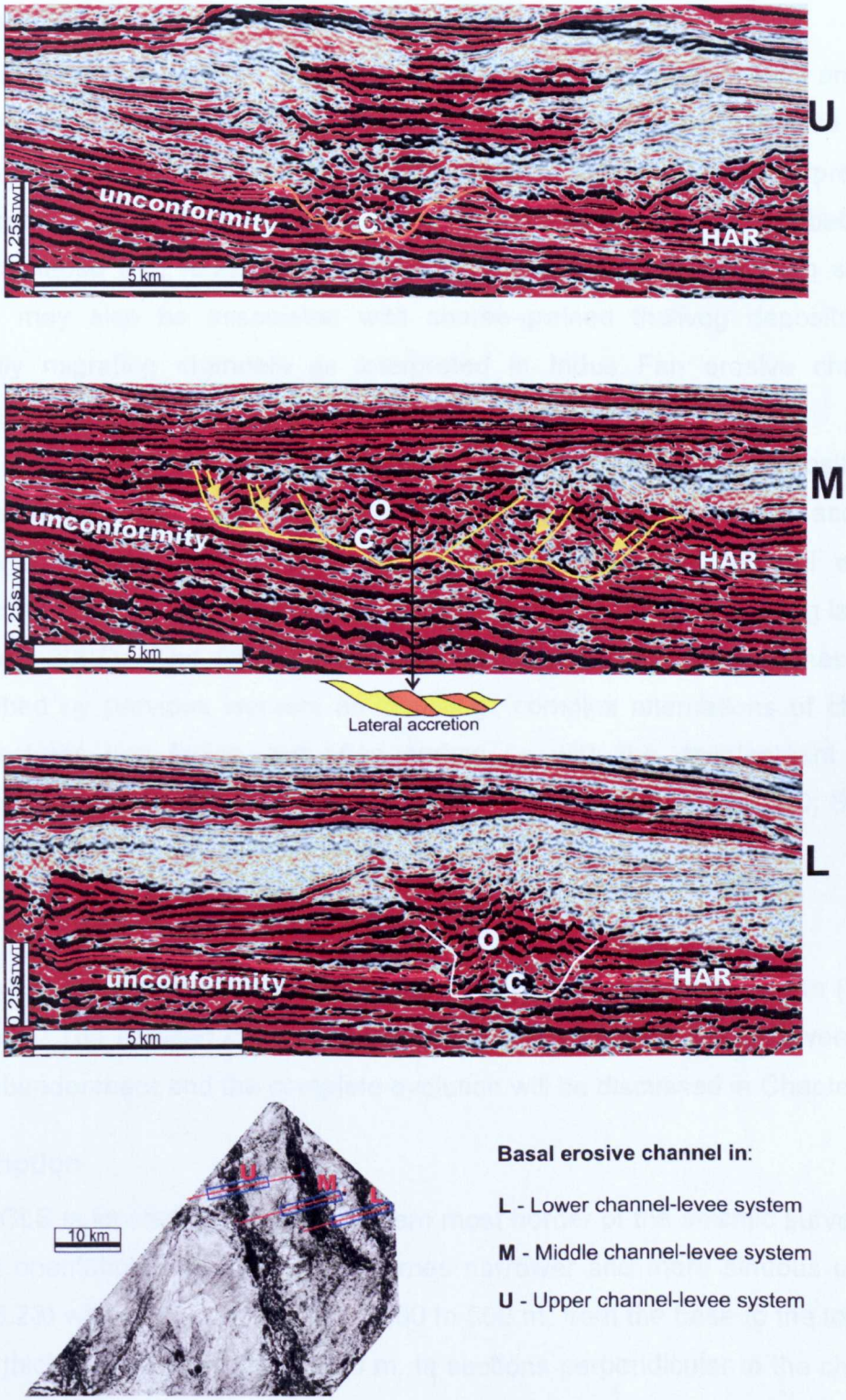

Figure 5-22 – Basal erosive channels (highlighted in orange in the UCLS, yellow in the MCLS and in white in the LCLS) occur in the three channel-levee systems identified in the study data. They exhibit diverse fills with a tendency of more chaotic reflections (C) close to the bottom and more organized reflections (O) on the top of the channel. In the erosive channel of the MCLS (M), bank collapse toward the channel axis formed a sequence of rotated blocks delimited by appropriately spaced normal faults. In plan-view, these rotated blocks appear with crescent shape as seen in Fig. 5.22. Lateral accretion packets occur close to the erosive channel base of the MCLS.

Interpretation

The chaotic low amplitude reflections of the basal erosive channel fill are here interpreted to be associated with slump deposits, which prevailed close to the channel base, whereas the chaotic high amplitude reflections are interpreted to represent the remobilization products of the enclosing HARPs, probably via bank collapse (Fig. 5.22). The chaotic and high amplitude reflection seismic facies may also be associated with coarse-grained thalweg deposits from laterally migrating channels as interpreted in Indus Fan erosive channels (Deptuck et al., 2003).

The ordered high amplitude reflectors may be channel axis deposits, and the laterally dipping reflections (Fig. 5.22) are possibly lateral accretion packages (Abreu et al., 2003) that developed when the channel was in equilibrium (i.e., without aggrading or eroding, and instead, meandering laterally (Kneller, 2003)). The filling of this kind of initial erosive channel has been described by previous workers as involving complex alternations of channel architectures and facies, but often ending up with the development of an aggradational channel levee (Kneller, 2003; Mayall and Stewart, 2000; Samuel et al., 2003).

5.5.3 – Lower Channel-Levee System

In this section a general overview of the Lower Channel-Levee System (LCLS) is shown. The detailed characteristics of the planform, channel fill, levee style, final abandonment and the complete evolution will be discussed in Chapter 6.

Description

The LCLS is located in the Northeastern most border of the seismic survey with N/NW orientation. The channel becomes narrower and more sinuous upward (Fig. 5.23) with width ranging from 1200 to 500 m, from the base to the top, and levee thickness reaching up to 280 m. In sections perpendicular to the channel, the channel fill reflectors appear to be continuous with the levee layers (Fig. 5.23). In the section along the thalweg, the channel fill is characterised by the stacking of retreating sets of reflections that pinch out upstream (Fig.5.24). Each set, however, is formed by a group of discontinuous prograding reflections.

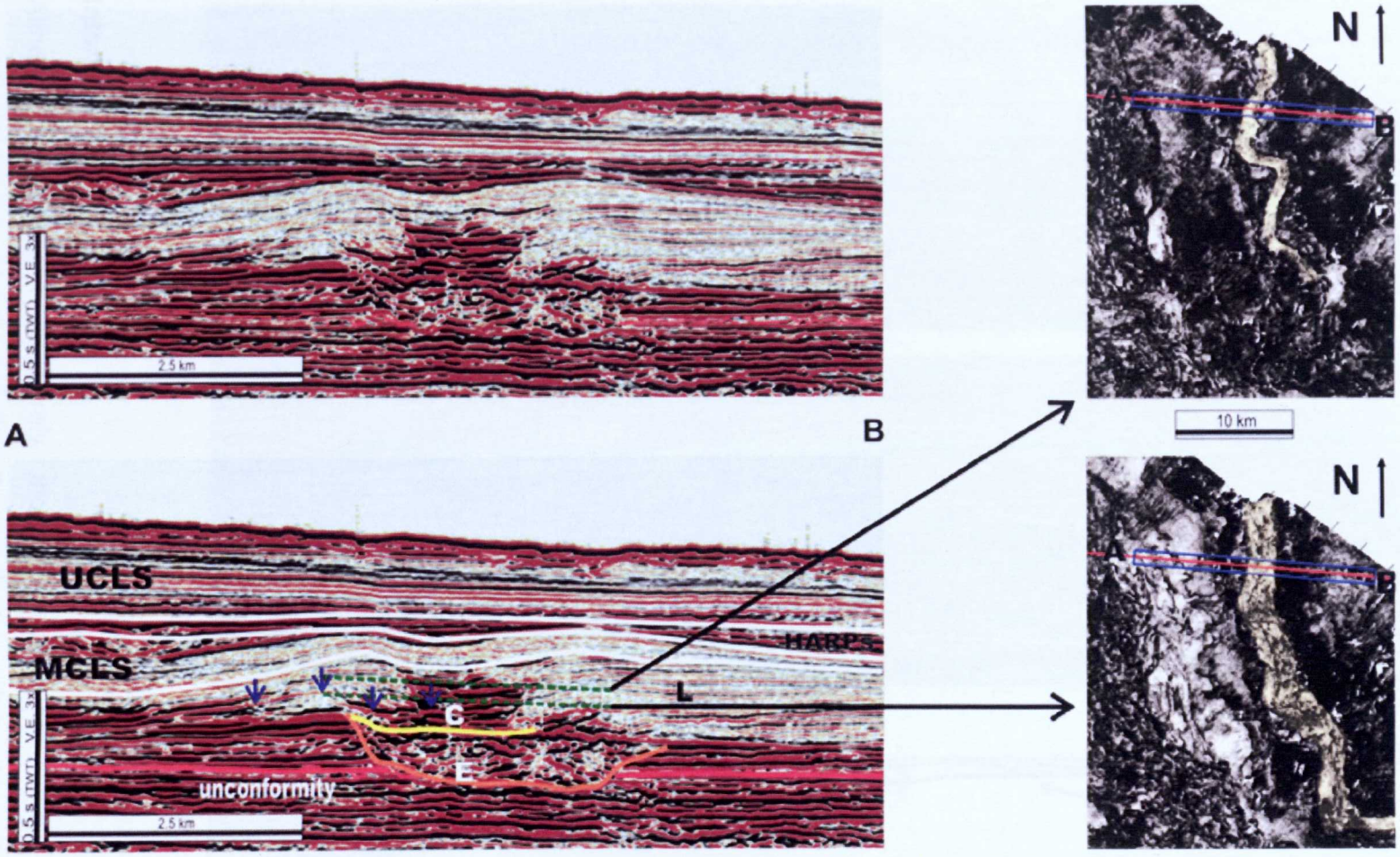

Figure 5-23 – Seismic section AB perpendicular to the channel axis in the Lower Channel-Levee System. The channel (C) is composed of the high amplitude reflections partially in continuity with enclosing low amplitude reflections of the levee (L). The two horizon slices of RMS coherence extractions, indicated in the cross section by the dashed green lines, show the channel narrower and more sinuous upwards. The orange horizon is the basal erosive channel. The blue arrows show the lateral continuity of a reflection from the channel fill to the levee.

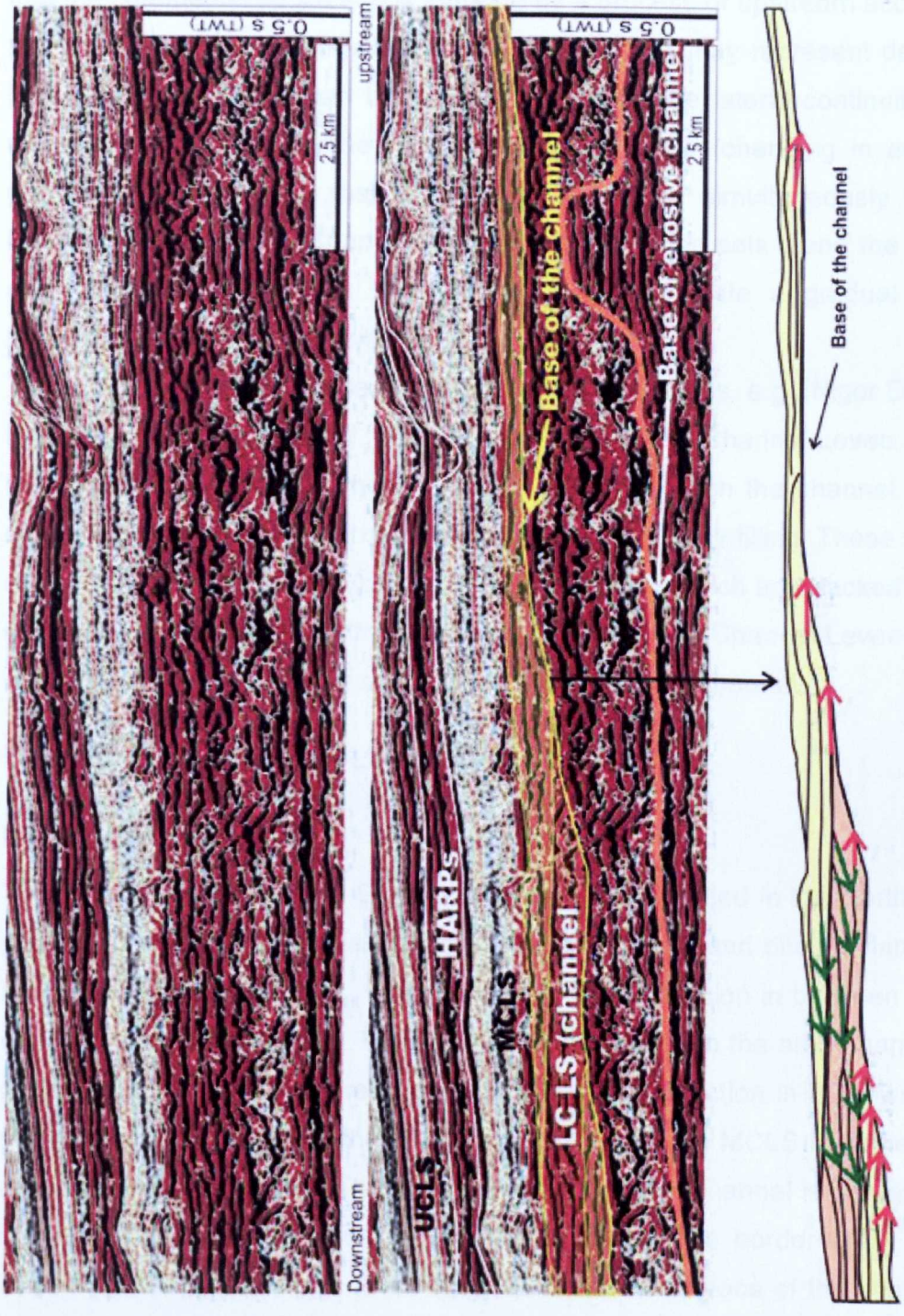

Figure 5-24 – Non-interpreted and interpreted seismic section along the channel axis in the Lower Channel-Levee System. The overlay figure exhibits sets of prograding reflections, downlaps toward downstream (green arrows), retreating (red arrows – onlaps on the channel thalweg) and pinching out upstream.

Interpretation

Although this system is barely included within the area, important considerations are raised regarding its architecture elements and formation processes. The overall onlap character of the channel fill reflections suggests

that the channel-levee system is evolving by a process of upstream accretion of the system. The downstream prograding reflections may represent deposition in a higher frequency than the overall retreating. The lateral continuity of the reflections passing from the channel fill to the levee (changing in amplitude character) may indicate that the channel was filled simultaneously with the levee build-up. The upstream pinching out of reflection sets along the channel axis characterizes a back fill style which may indicate a gradual upward retreating of the sand deposition.

Many other channel-levee systems of different fans, e.g., Niger Delta and Indus Fan (Deptuck et al., 2003) and the Upper Channel-Levee System (described further in this Chapter) show a style in which the channel is wider near the base and narrower near the top, ending with clay filling. These systems are composed of widening upward channel elements which are stacked within a narrowing upward succession. Contrastingly, the Lower Channel-Levee System of this study is composed of a single narrowing upward channel.

5.5.4 – Middle Channel-Levee System

Description

The Middle Channel Levee System (MCLS) is also located in the Northeastern part of the seismic survey, and has deposited upslope and directly flanking on the left margin of the LCLS. There is no HARPs deposition in between the two channel-levee systems (Fig. 5.18). The channel bends in the area change from a NE orientation in its upstream segment to a NW direction in its downstream segment. Contrasting with the LCLS, the channel in the MCLS becomes wider and less sinuous upward. The fill of the aggradational channel is characterized by sub-horizontal continuous high amplitude reflections bordered by the low amplitude reflections of the levee (Fig 5.25).The reflections of the channel fill, however, do not have lateral continuity with the low amplitude reflections of the levee; on the contrary, they onlap the internal levee wall (Fig 5.25 and 5.26).

The Middle Channel-Levee System can be divided into two distinct segments. In the upstream segment, the levee height may reach 380 m and the channel width range from 160 to 2600 m, with the channel fill composed of longitudinally continuous sub-parallel reflections (Fig. 5.26). In the downstream

segment only the basal half of the levees is preserved whereas the upper half has collapsed and/or been eroded (Fig. 5.26, cross section AB). Cross section AB (Fig. 5.26) shows an erosive surface (in blue) cutting across the levees and the channel fill of the MCLS. HARPs onlap this surface. In general, the channels are more sinuous and thinner downstream than upstream (Fig. 5.26).

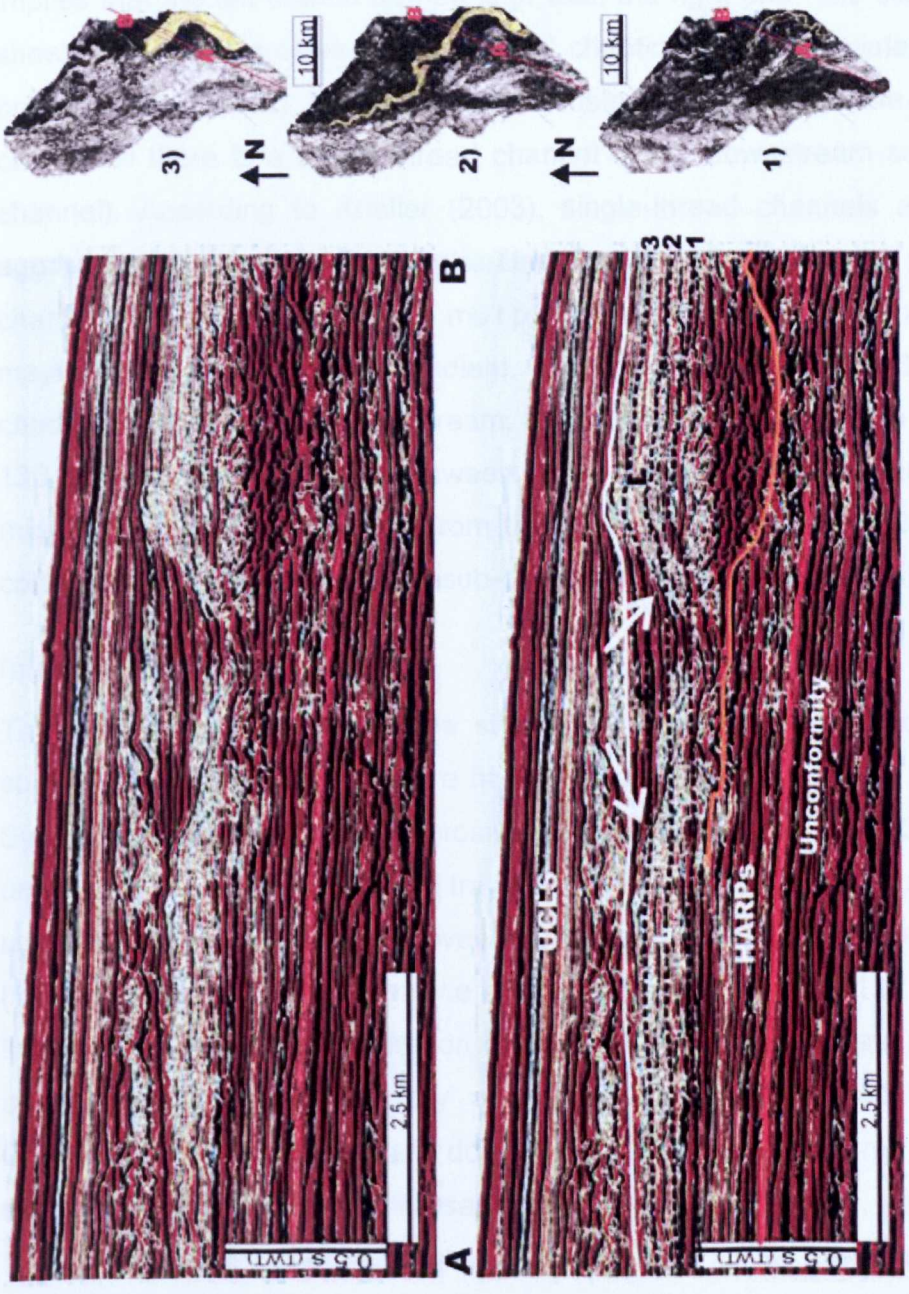

Figure 5-25 – Seismic section (AB) transverse to the channel axis in the Middle Channel-Levee System (non-interpreted and interpreted). Three horizon slices produced by extracting RMS of coherence (maps on the right) are represented by dashed lines in cross section. They show the channel widening and reducing sinuosity upwards. The arrows in the channel (C) point out the fill reflections onlapping the levee limbs.

The sequential analysis of horizon slices of RMS coherence extraction, taken from the base to the top across this system (from horizon slice 350 ms to

50 ms below the datum, which is the base of the UCLS levee), shows the upward and longitudinal transition from a chaotic to multi thread channel and subsequently to a single-thread channel (Fig. 5.27).

The horizon slice at 350 ms (Fig. 5.27) shows the basal erosive channel (in which the coherence character of the channel fill is chaotic) dispersing almost northwardly (yellow arrow), and disconnected from the left branch. This implies that the left branch formed later than the right one. The slice at 300 ms shows the basal erosive channel, with chaotic fill, now deviated to the left branch (yellow arrow). In the same slice, instead of a wide erosive channel with chaotic fill there is a single thread channel in the downstream segment (blue channel). According to Kneller (2003), single-thread channels are typical of aggradational submarine channels. The slice at 220 ms shows a single thread channel (yellow) passing into a multiple thread channel (in which the channel maybe close to equilibrium gradient, according to Kneller (2003) and into a chaotic channel towards downstream. From the slice at 200 ms up to the one at 130 ms, the transition point between single thread to multiple thread channel migrates downstream. Finally, from the slice at 120 ms up to 50 ms the light colours represent the organized sub-parallel reflections of the HARPs.

Interpretation

The sequence of horizon slices shows a combined upward (temporal) and spatial change in the architecture of the channels from the Lower to the Middle System starting from the basal erosive channel. From the slice at 350 ms to the one at 300 ms there is a vertical transition from the basal erosive channel to the agradational Lower Channel-Levee system and the avulsion of the left levee (view downstream). From the slice at 220 ms up to the one at 130 ms there is a longitudinal downstream migration of the transition from agradational to erosive channel form. This may imply a progradation of the agradational Middle Channel-Levee System toward downstream. From slice 120 ms up to 50 ms the deposition of the sheet-like sand rich deposits occurs, i.e., an interchannel lobe resulting from channel avulsion as described in the literature of the ODP Leg 155 (Flood and Piper, 1997; Pirmez et al., 1997). The complete description of the evolution of the MCLS is presented in Chapter 6.

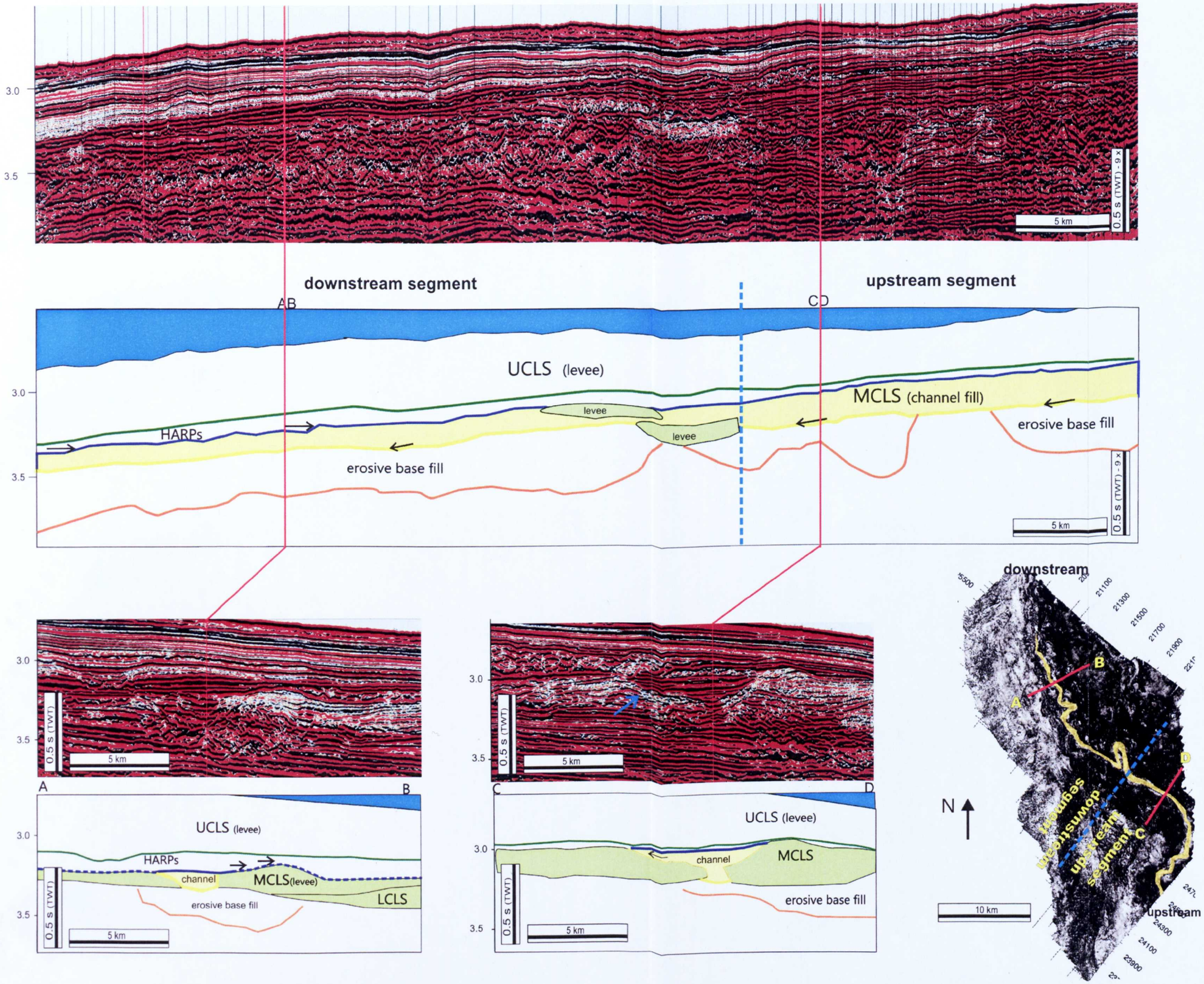

Figure 5-26 – Seismic line along the channel axis of the MCLS, outlined in yellow in the horizon slice (150 ms below the datum – i.e., the base of the UCLS green horizon). The channel fill is the set of the high amplitude reflections between the yellow horizon in the base and the dark blue horizon on the top. The channel fill reflections are sub-parallel and relatively continuous and if not sub-parallel they slightly downlap the channel base. The upstream and downstream segments are outlined by the dashed blue line. The cross section AB shows the eroded levees of the downstream segment. The cross section CD shows the upstream segment better preserved but with the internal walls of the channel partially eroded, characterized by the truncation of the levee reflections (blue arrow), seen in the cross section CD.

Legend:

UCLC – Upper channel-levee complex

MCLS – Middle channel-levee system

HARPs – High amplitude reflexion packet

Green horizon – base of UCLC

White horizon - Top of channel fill

Yellow horizon – Base of the channel

Orange horizon – Erosive channel base

Dashed blue horizon – outline of downstream and upstream segments of MCLS

Dashed white horizon – erosive surface on the top of the downstream portion of the MCLS.

Time slices (two-way-travel time) through the Medium Channel-Levee System, from the base to the top

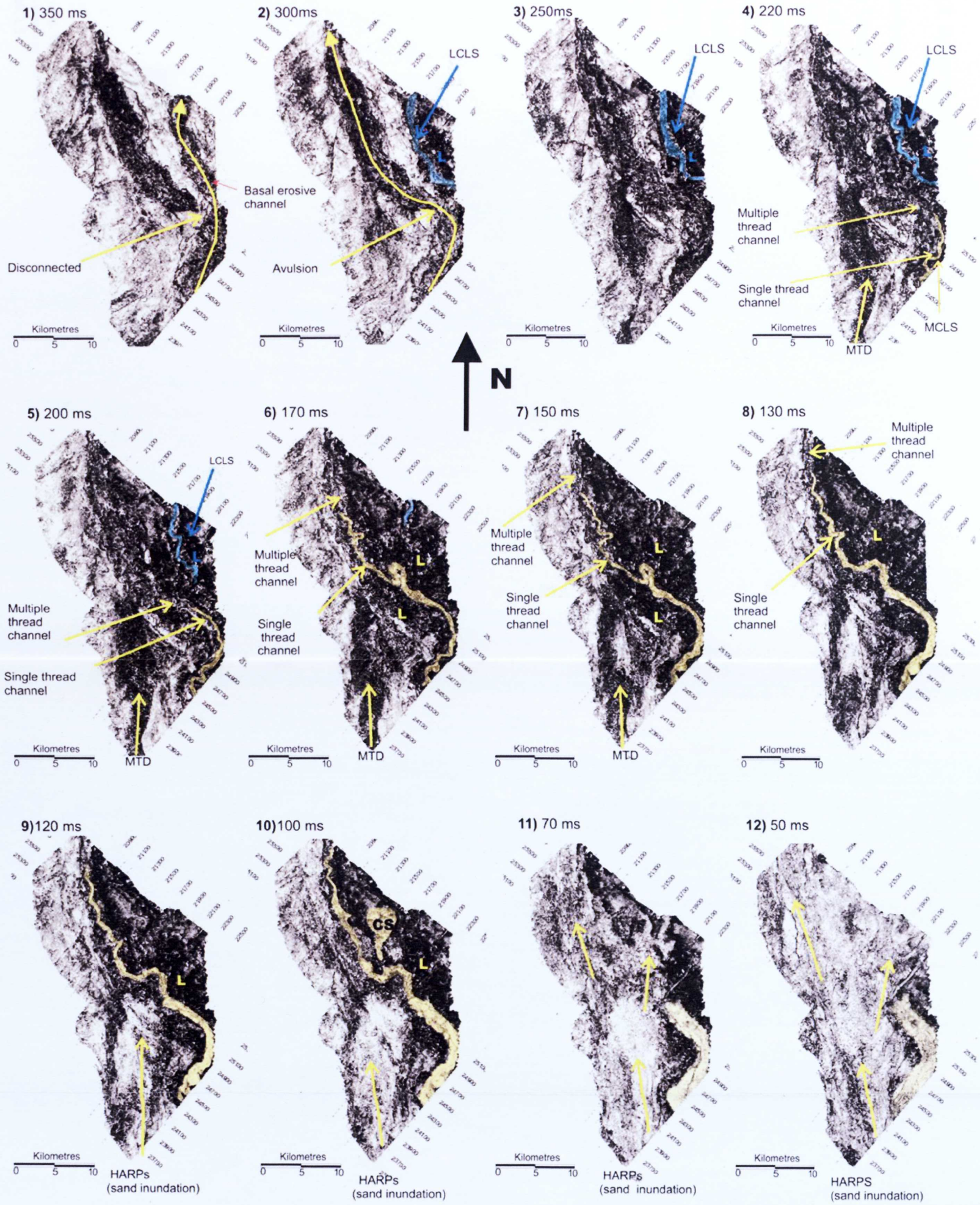

Legend: blue highlighted channel (LCLS) yellow highlighted channel (MCLS) L - levee (dark grey) CS - crevasse splay

Figure 5-27 - Horizon slices showing the RMS of cohence extractions in a range of 20 ms, using the base of the UCLS right levee as datum. The sequential images show the depositional history from the initial erosive channel base up to HARPs deposition. The number of ms shown on the top of each image represents two-way-travel time from the slice to the datum. The horizon slices are organized from the base to the top showing: from image 1 to 2 – avulsion of erosive channel due to LCLS emplacement; from image 3 to 10 – downstream migration of the transition point between erosive/graded to channel-levee. This is characterised by the transition from multiple thread to single thread channel; from image 11 to 12 – erosion of the downstream portion of the channel and HARPs deposition. Notice that from images 4 to 8 the MTD between the slope and the levee backlimb is pointed out.

5.5.5 Upper Channel-Levee System

Description

The Upper Channel-Levee System (UCLS), also located in the Northeastern part of the seismic survey, and was deposited upslope of the MCLS, and after the HARPs deposition (Fig. 5.18). In the study area, the UCLS is confined between an upslope bathymetric high generated by an anticline and a downslope high due to MCLS emplacement (Fig. 5.28). Similarly to the other two systems, the UCLS evolved upward from a basal erosive channel to an aggradational channel-levee.

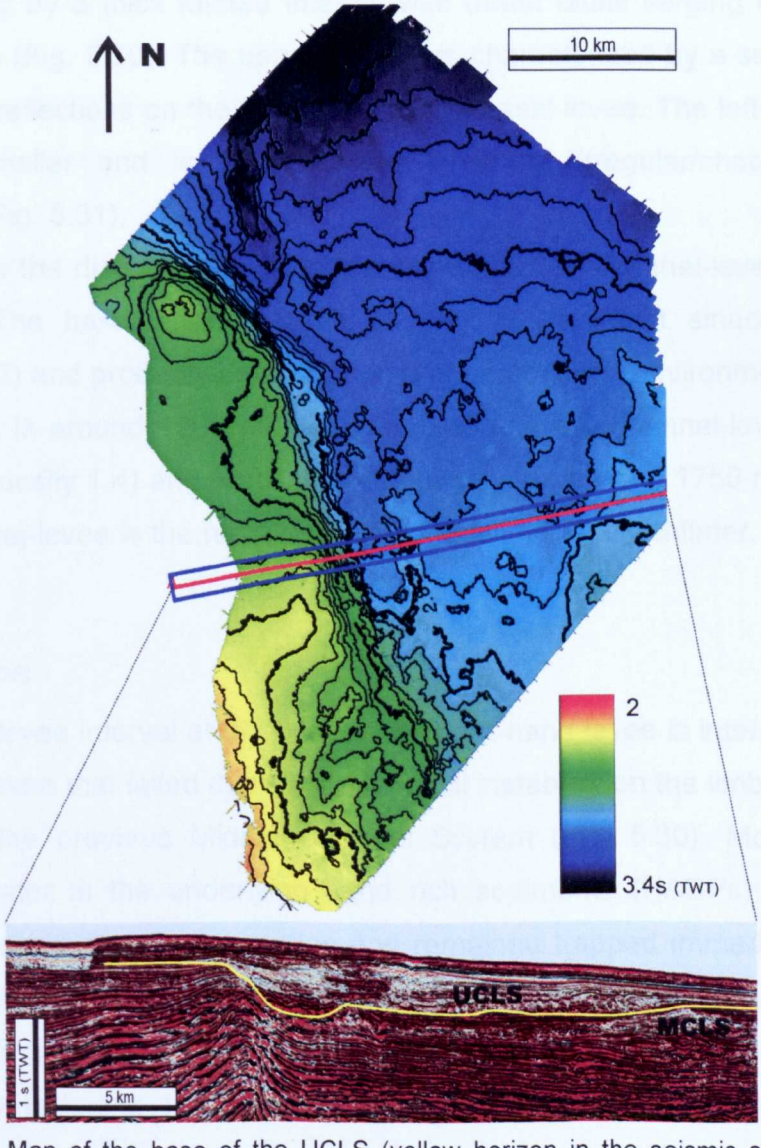

Figure 5-28 – Map of the base of the UCLS (yellow horizon in the seismic section) whose development was confined between an upslope anticline and the downslope relief formed by the MCLS.

The UCLS is composed of a sub-vertical stacking of 4 channel-levee elements. The system can be divided vertically into two intervals by an internal discontinuity (Fig. 5.29). This discontinuity is a pervasive surface across the system, and may represent a small break in sedimentation. In the larger levee, on the right-hand side (looking downstream), the discontinuity consists of a high amplitude downlap reflector.

At the base of the interval, under the discontinuity, there is a leveed erosive channel. This basal erosive channel is partially filled by ordered high amplitude reflections and partially by chaotic reflections (Fig. 5.29). The right-hand levee can be subdivided into two intervals. The lower interval is characterized by a thick faulted interval with thrust faults verging towards the channel axis (Fig. 5.30). The upper interval is characterized by a set of regular downlaping reflections on the top of the faulted basal levee. The left-hand levee is much smaller and is characterized by more irregular/chaotic internal reflections (Fig. 5.31).

Above the discontinuity there are three stacked channel-levee elements (Fig. 5.32).The basal channel-levee element is the least sinuous channel (sinuosity 1.2) and probably developed in a more confined environment than the other two. It is around 1200 m wide. The intermediate channel-levee is more sinuous (sinuosity 1.4) and wider than the basal one, around 1750 m wide. The upper channel-levee is the most sinuous (sinuosity 1.7) and thinner, around 450 m wide.

Interpretation

The faulted levee interval at the base of the right-hand levee is interpreted to be a slumped levee that failed due to gravitational instability on the limb of the relief formed by the previous Middle Channel System (Fig. 5.30). Moreover, the formation water in the underlying sand rich sediments (HARPs) could have migrated upward due to compaction and remained trapped immediately under the clay rich levee. Therefore, a fluid layer on the contact between the HARPs and the sealing levee may possibly have become overpressured and worked as lubricant by reducing the effective strength at the contact, favouring the overlying levee package to slump towards the channel. This process is analogous to the gravity tectonics that occur within thick packages of sediments

in the slope, described in Chapter 2 (section 2.2) and earlier in this chapter (section 5.4), but at smaller scale. The contact between the sands of the underlying HARPs and the clays of the levee above worked as a detachment surface. On the left levee, underneath the internal discontinuity of the UCLS, the adjacent growing anticline could have promoted instability and slumping of the levee generating the chaotic facies.

Figure 5.32 also shows that the three stacked channel-levee elements of the Upper Channel-Levee System exhibit a distinct amplitude contrast between the channel fill and the enclosing levee. Considering that in the lower channel-levee element, the channel has higher amplitude reflection and smaller sinuosity, it is thought to be sandier than the two higher channels. By way of contrast, the uppermost channel is thinner, more sinuous and with the smallest amplitude contrast in relation to the levee, hence the channel fill is thought to be more clay rich. Channel narrowing upward in aggradational leveed channels has been documented in other systems (Deptuck et al., 2003; Stelting, 1985) and is considered to be related to the tendency of the flow becoming smaller and muddier with time (Kneller, 2003).

In Chapter 7, further discussion and analysis regarding the characteristics and development of the Upper Channel-Levee System are provided.

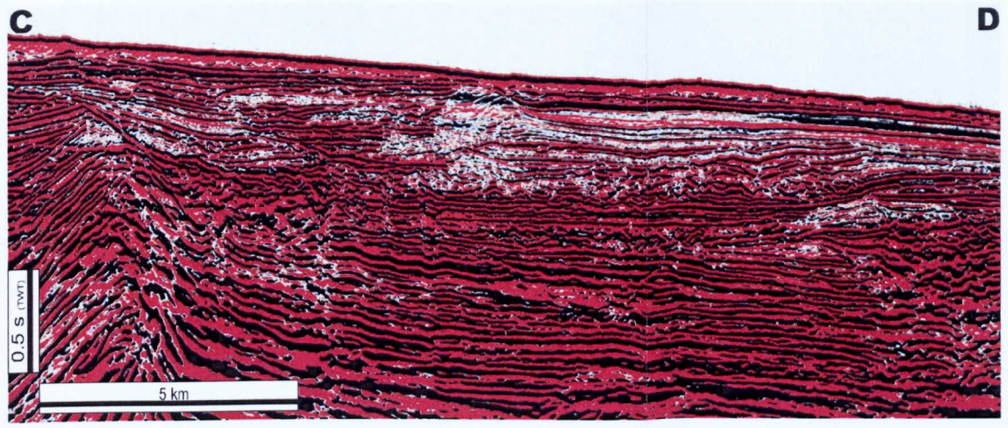

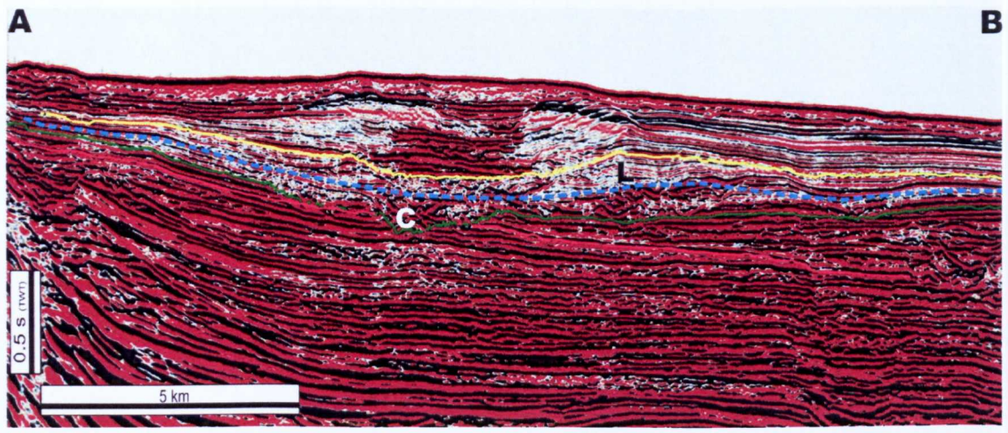

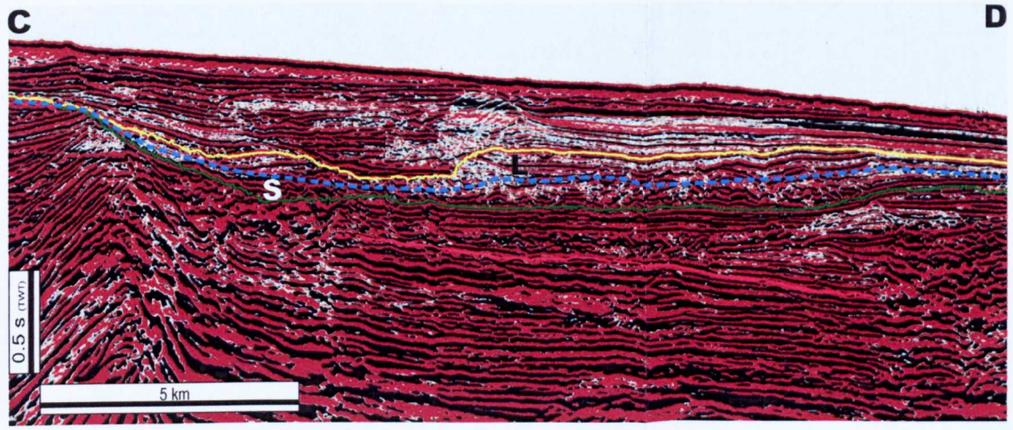

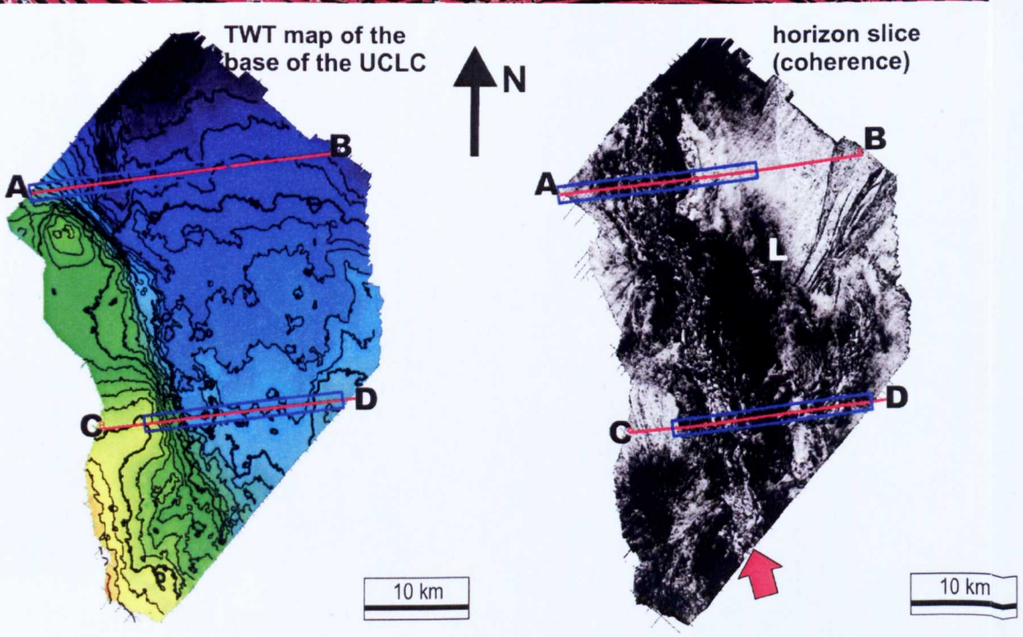

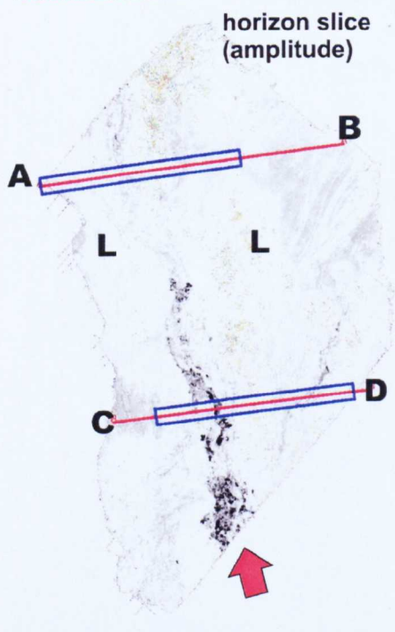

Legend:

yellow hozizon - discontinuity across the UCLS

green horizon - base of the UCLS

red horizon - unconformity underneath

dashed blue line - isoproportional horizon slice between the discontinuity and the base of the UCLS

L - levee

C - chaotic channel fill reflections

S - channel fill with sigmoid reflections

AB - downstream section across the UCLS

CD - upstream section across the UCLS

red arrow - indicates the channel

Figure 5-29 – Interpreted and non-interpreted seismic reflection sections downstream (AB) and upstream (CD) across the Upper Channel-Levee System (UCLS). Notice the upstream channel fill exhibits sigmoidal reflections with higher amplitude whereas the downstream channel fill presents chaotic reflections with lower amplitude. The black and white maps are isoproportional horizon slices between the base and the UCLS and the internal discontinuity (yellow),extracting coherence and amplitude within a time window of 20 ms. The amplitude map show the upstream segment of the channel with higher amplitude (dark gray) than the lower one (light gray), which is very similar to the amplitude of the surrounding levee.

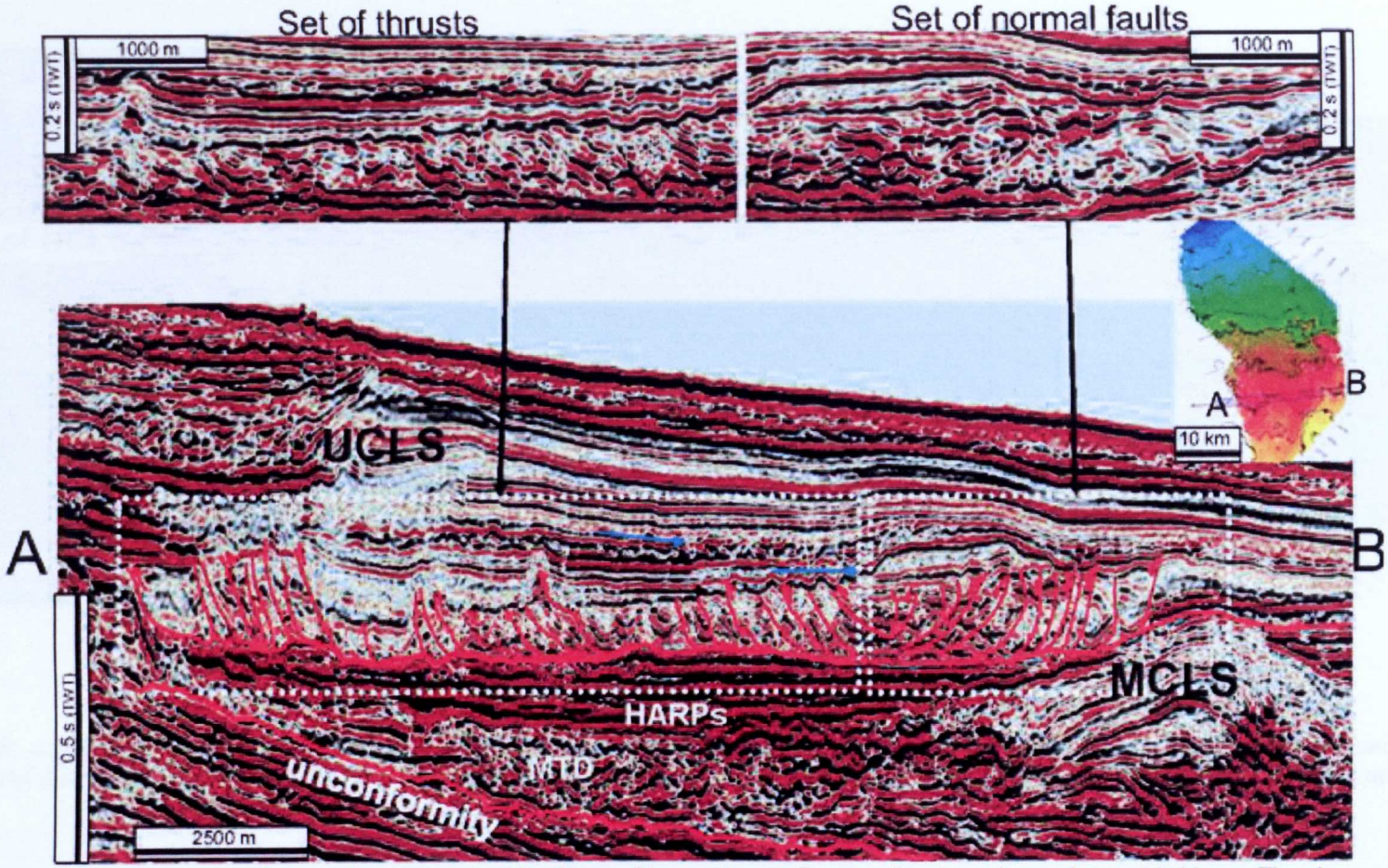

Figure 5-30 – Right levee (looking downstream) of the Upper Channel-Levee System showing a large slump at its' base. The slump exhibits an extensional portion characterized by a set of normal faults and a compressional portion characterized by thrust faults. The slump initiated on relief formed by the underlying MCLS toward the thalweg of the channel of the UCLS. The horizon at the top of the slumped levee represents a time gap in the deposition of the system as there is a sequence of onlap reflections above it (red arrows). The erosive surface on the top of the slump represents a gap in the sedimentation as it is a downlap surface (blue arrow).

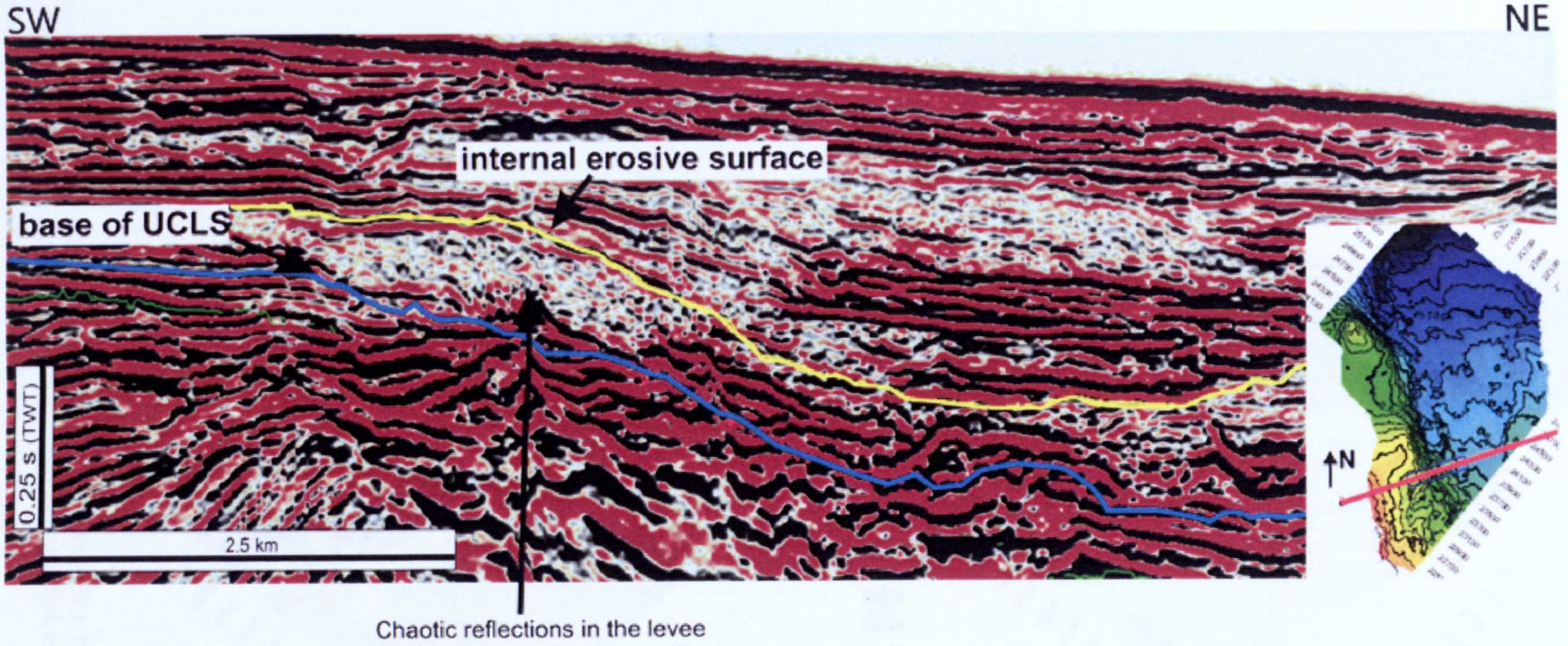

Figure 5-31 – Left-hand levee of the Upper Channel-Levee System underneath the internal unconformity (yellow horizon). Instead of a sequence of semi-parallel downlapping reflections, there are chaotic reflections that may indicate syn-depositional or immediately post-depositional uplift of the levee.

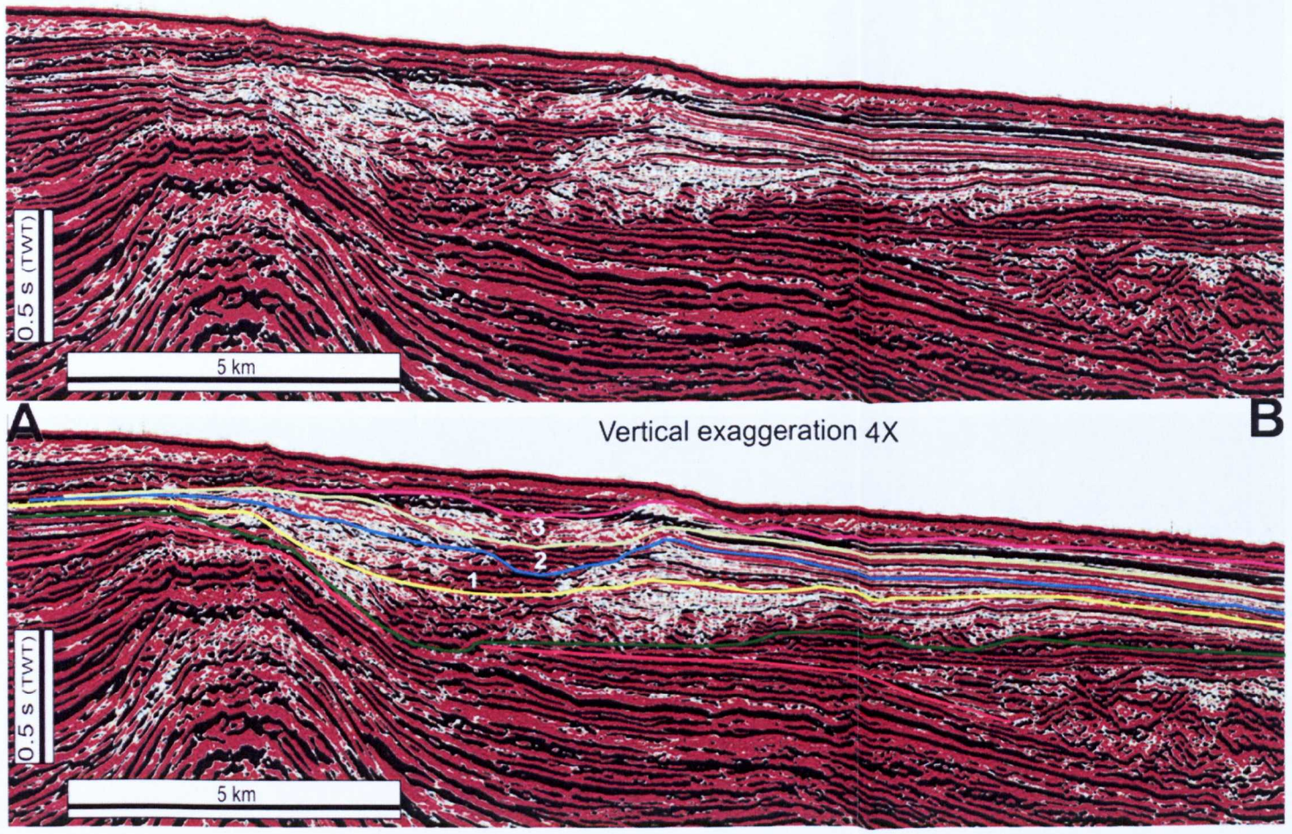

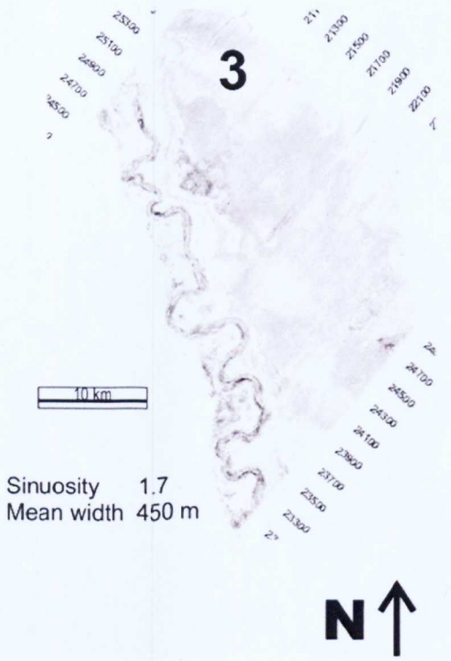

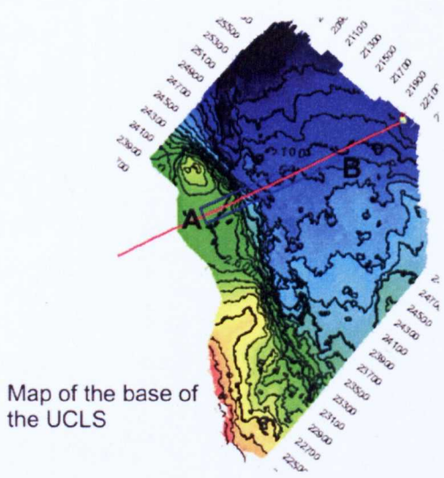

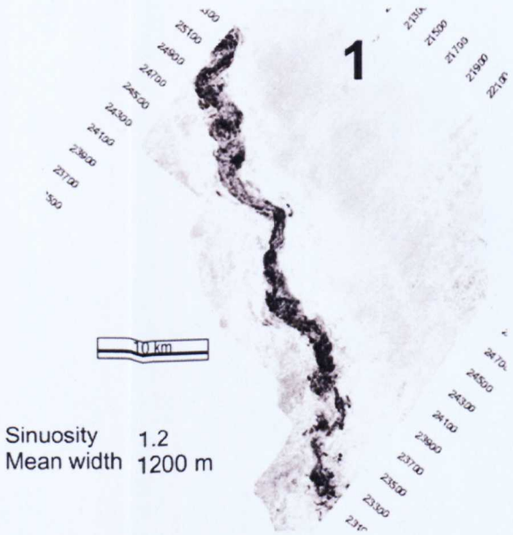

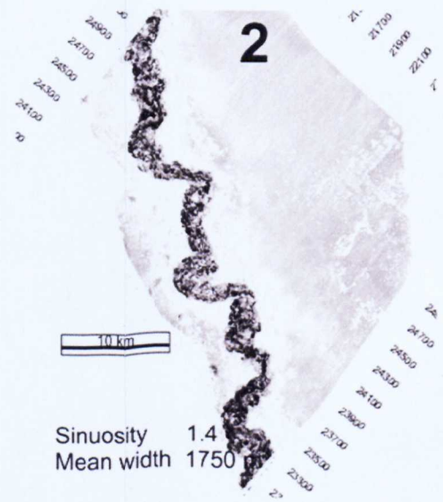

Figure 5-32 – Horizon slices exhibiting RMS amplitude extractions of the three stacked channel-levees above the inner unconformity (yellow horizon) in the Upper Channel-Levee System. The horizon slices were taken using a 20ms window in the mean surface between the base and the top maps of each channel-levee (1, 2 and 3), highlighted in the seismic section. The channels are more sinuous and clay rich upward, as there is less amplitude contrast between the channel and the levee in the upper channel-levee (3).

6 SPATIO-TEMPORAL EVOLUTION OF CHANNEL-LEVEE ARCHITECTURE

6.1 Introduction

Submarine channel-levee architecture can yield important evidence on the behaviour of turbidity currents at the time when the channel was active. Previous studies on deep-sea fans have discussed submarine channel-levee architecture and its evolution considering issues such as flow character parameter control on channel levee-architecture (e.g., Kneller, 2003; Peakall et al., 2007; Peakall et al., 2000) and avulsions and their causes (e.g., Flood and Piper, 1997; Pirmez and Flood, 1995). Furthermore, a large number of channel architecture descriptions and inferred evolutionary histories based on studies of 3D seismic data can be found in the literature (Abreu et al., 2003; Deptuck et al., 2003; Deptuck et al., 2007; Gee and Gawthorpe, 2006; Heiniö and Davies, 2007; Kolla et al., 2001; Pirmez et al., 2000; Posamentier and Kolla, 2003). Although the characteristics of channel-levee systems and the controls upon their evolution have commonly been discussed, many studies nevertheless do not discuss in detail how a channel-levee evolves spatially over time. With this in mind, the objective of this chapter is to characterise styles of evolution of channel-levee architectures in deep marine clastic systems and relate them to interpreted forcing mechanisms. The analysis of the spatio-temporal evolution of channel-levee presented here is based on the contrasting architectures of the Pleistocene Lower and Middle Channel-Levee Systems on the upper slope of Amazon Fan within the 3D study coverage area. These systems represent two different architectural morphotypes in cross section which can be related to distinct patterns of spatio-temporal evolution of the channel-levee, namely upstream vs. downstream accretion.

6.2 Upstream-accreting channel-levee system

This style of channel-levee development is characterized by an upstream accretion of the system. The characteristics of the channel planform, channel fill and levee style and the final abandonment of the channel are described here.

Particular focus is given to the way in which channel architectural parameters evolve through time and space.

6.2.1 Planform evolution

In order to evaluate the vertical changes in channel morphology, a quantitative analysis was performed by measuring the channel width, sinuosity, meander arc height, channel length and meander length of channel meanders observed in five horizon slices taken across the LCLS (Fig. 6.1). The values of the measured parameters (Fig. 6.1) for each meander along the channel of the LCLS are presented in Table 6.1. The range of measured channel widths varies between approximately 0.3 and 1.5 km and of measured sinuosities between 1.1 and 1.4; these values are similar to the values previously measured in the late Pleistocene channels in the middle and lower Amazon Fan of 0.3 – 1.4 km and 1.1 – 2.9, for width and sinuosity respectively (Flood and Damuth, 1987; Flood et al., 1991; Pirmez and Flood, 1995).

The concept of sinuosity used here is the same of Kane (2007) i.e., the ratio between the channel length along its axis and the meander length. Meander length is the distance between two consecutive inflection points (Fig. 6.2), whereas meander-arc height (MAH) is the measure of the distance between the line that connects successive inflection points and the channel bend (Wood and Mize-Spansky, 2009). Meander-arc height is typically used as a measure of bend symmetry (Brice, 1984 in: Wood and Mize-Spansky, 2009).

There is a weak inverse correlation between the sinuosity and the width of the channel (Fig. 6.3), such that the narrower channels are more sinuous. The correlation is possibly not very good because the width may vary with the position on the channel bend. Hence, the same sinuosity can be associated with different width values depending where it was measured on the bend. The measured averages of each parameter by horizon slice show how the channel properties vary vertically (Fig. 6.4). The measurements show an upward reduction of the channel width and an upward increase in channel sinuosity.

Therefore, this morphotype is characterized by the upward tendency of the channel planform to become narrower and more sinuous (Fig. 6.5). Most of the aggradational channel-levee was built up above the level of and after the filling of the erosional channel base, as highlighted in Figure 6.5.

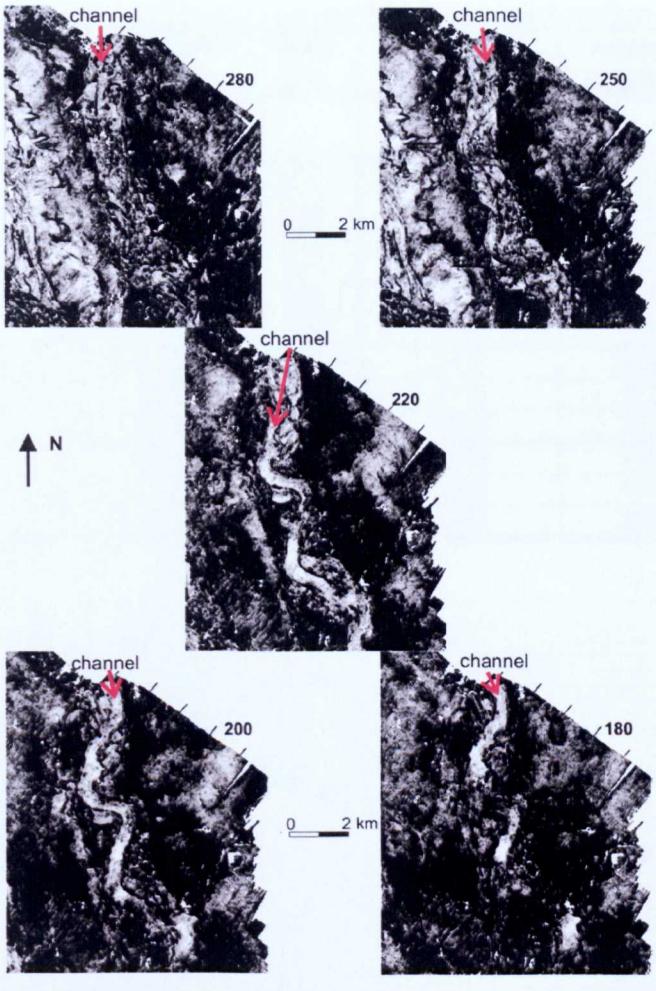

Figure 6-1 – Horizon slices of the LCLS where the channel parameters were measured as shown in table 6.1. The numbers attached to each slice represent the time (ms) below the datum (base of the UCLS) where the slices were taken. The slices are organized in sequence from the bottom to the top of the LCLS.

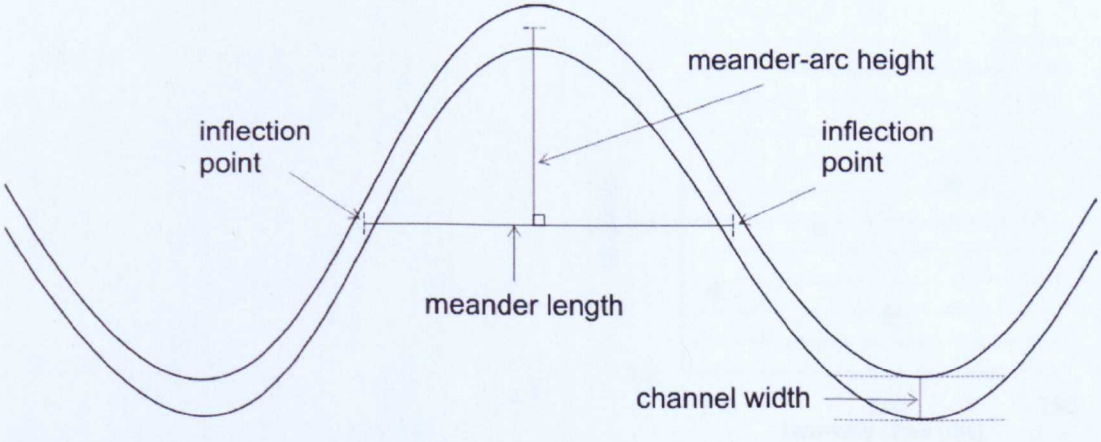

Figure 6-2 – Schematic diagram exhibiting geometrical meaning of the measures of channel width, meander-arc height, meander length (adapted from Wood and Mize-Spanky (2009).

Table 6-1 – Measured parameters for the channel meanders in each horizon slice of the LCLS

horizon slice (ms)	Meander No.	width (m)	MAH (m)	channel length (m)	meander length (m)	sinuosity
280	straight channel	1493				1.00
250	1	424	921	3217	2534	1.27
	2	912	681	2925	2603	1.12
220	1	512	722	2447	1964	1.25
	2	590	811	3023	2544	1.19
	3	337	669	2241	1652	1.36
	4	482	600	1902	1371	1.39
200	1	472	677	2867	2448	1.17
	2	540	704	2315	1732	1.34
	3	518	571	2558	2122	1.21
180	1	406	866	2809	2187	1.28
	2	422	588	1901	1330	1.43
	3	522	682	2847	2255	1.26

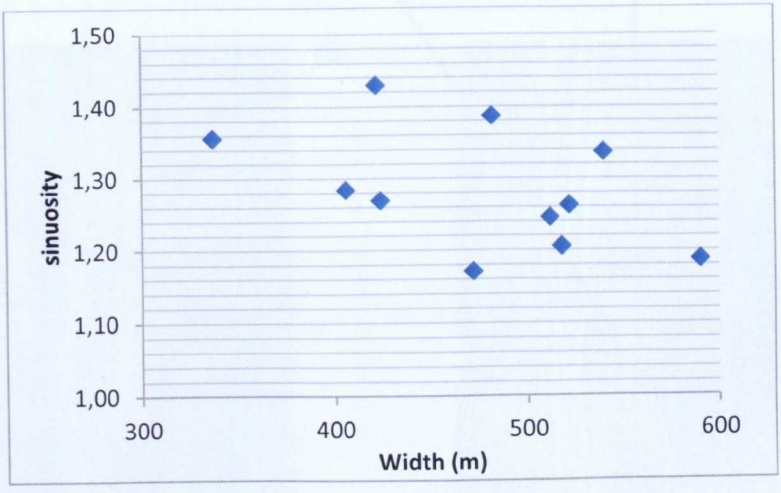

Figure 6-3 – Diagram showing a weak inverse correlation between sinuosity and channel width in the LCLS.

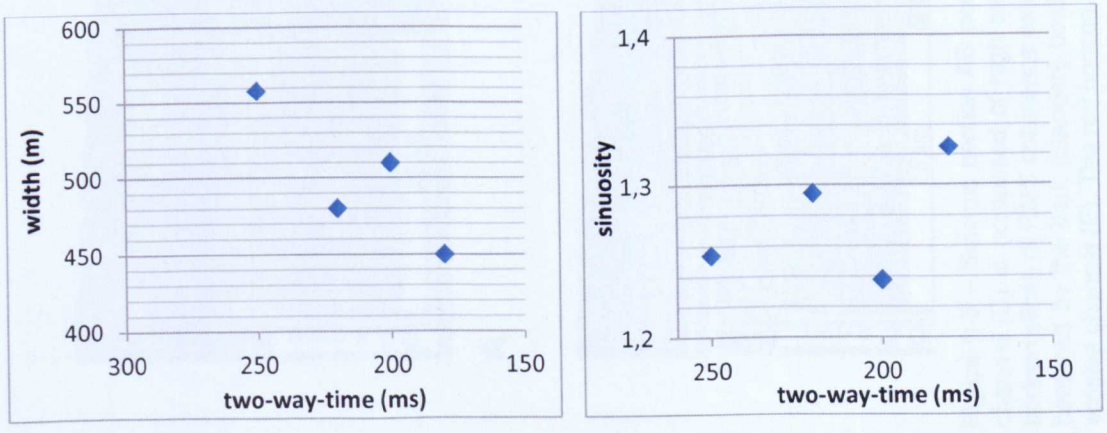

Figure 6-4 – Diagrams showing the average values of sinuosity and channel width obtained for each horizon slice across the LCLS. The x-axis represents the depth in time from the datum to the channel.

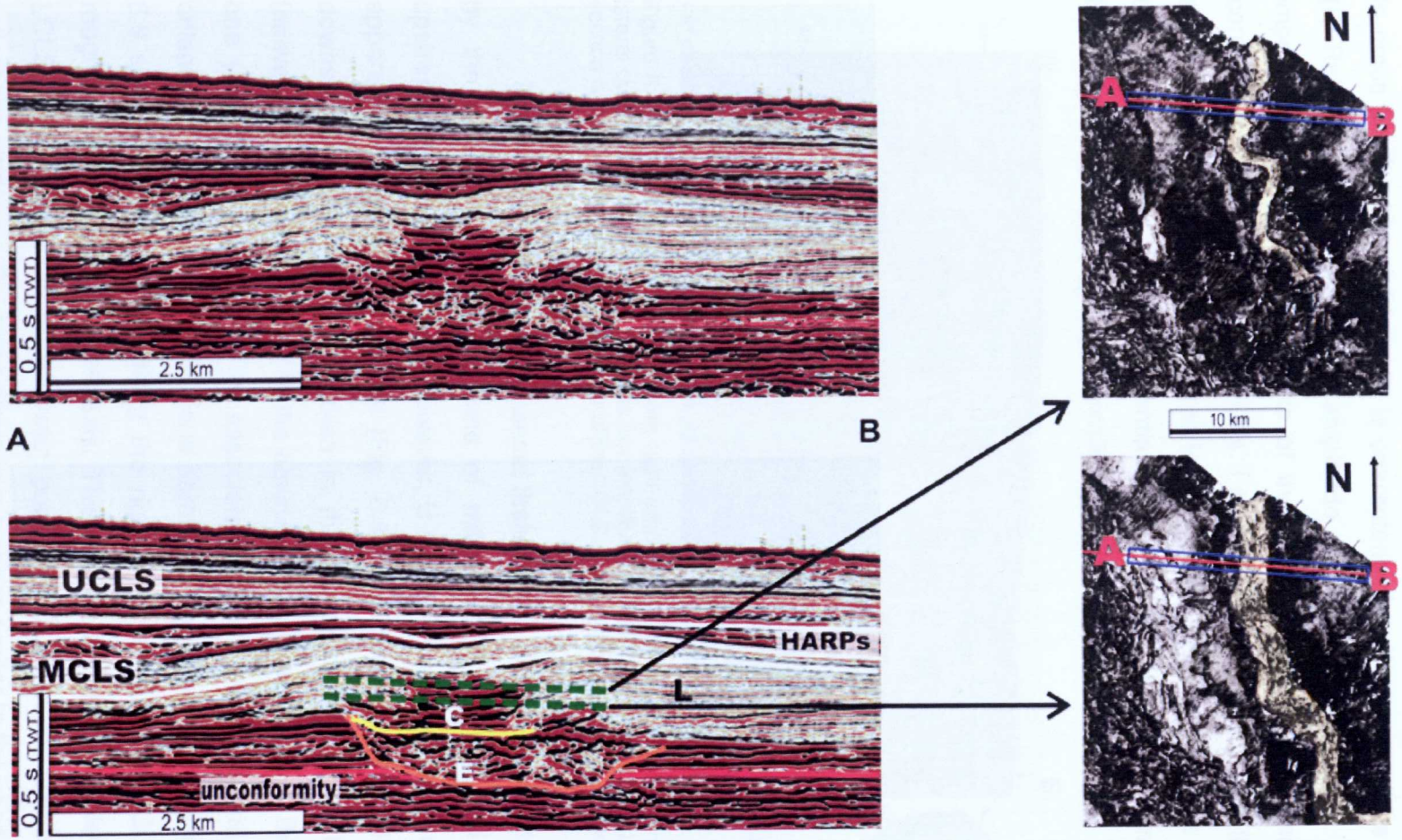

Figure 6-5 – Seismic section AB perpendicular to the channel axis in the Lower Channel-Levee System (non-interpreted and interpreted). The channel (C) is composed of high amplitude reflections partially in continuity with enclosing low amplitude reflections of the levee (L). The two horizon slices of RMS coherence extractions, indicated in the cross section by the dashed green lines, show the channel highlighted in yellow and bordered by the dark (blackish) bordering levees. The channel becomes narrower and more sinuous upwards. The orange horizon is the basal erosive channel (E). The red horizon below the LCLS is the pervasive unconformity that occurs in the area.

6.2.2 Channel fill and levee style

In cross section, the channel fill is characterized by high amplitude reflections (HARs) enclosed by the lower amplitude reflections (levee) (Fig. 6.5). It is important to note that the HARs of the channel fill are apparently laterally continuous with the levee reflections. Figure 6.6 shows the lateral transition of an individual reflection from high to low amplitude, moving from the channel to the levee position. This levee continuity may indicate that the channel fill and the corresponding levee were deposited simultaneously.

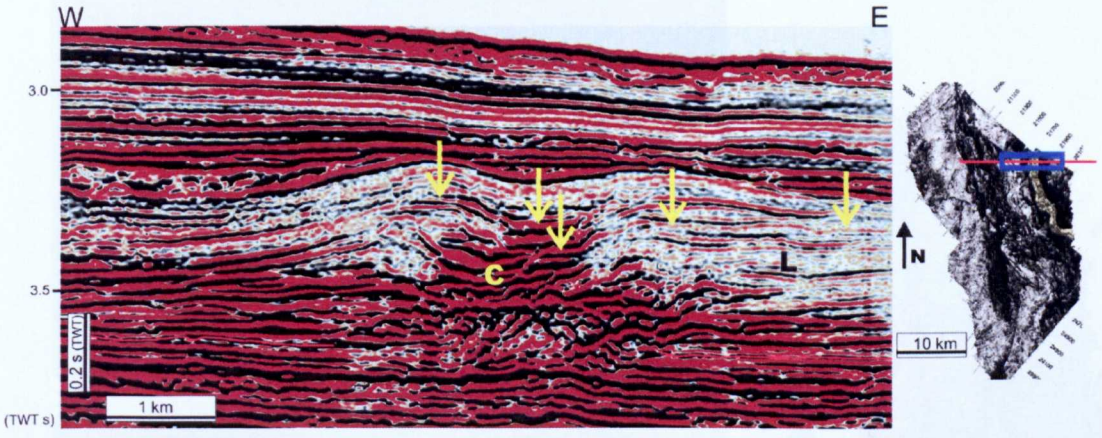

Figure 6-6 – Detail of the LCLS showing high amplitude reflections of the channel fill (C) in lateral continuity (yellow arrows) with the low amplitude reflections of the levee (L). The seismic section is transverse to the channel axis of the LCLS, highlighted in yellow in the horizon slice.

In the section along the channel thalweg, the channel fill is characterized by the stacking of retreating sets of reflections that onlap and pinch out upstream (Fig. 6.7). Each set, however, is formed by a group of discontinuous, apparently prograding reflections (Fig. 6.8). The channel fill is thicker in the downstream channel segment than in the upstream segment. The channel thalweg also appears steeper in the downstream segment than in the upstream one (Fig. 6.7, position 3). The associated levee exhibits internal reflections onlaping the paleo-slope in sections parallel to the mean channel axis. Figure 6.9 shows a cross section along the right-hand levee of the LCLS which is roughly parallel to the channel axis. This section sampled both levees of the LCLS and the MCLS. The lower portion (LCLS levee) exhibits internal reflections onlapping the paleo-slope in a manner similar to the channel fill. The upstream thinning of both channel fill (Fig. 6.8) and levee (Fig. 6.9) characterize an upslope pinching out of the system.

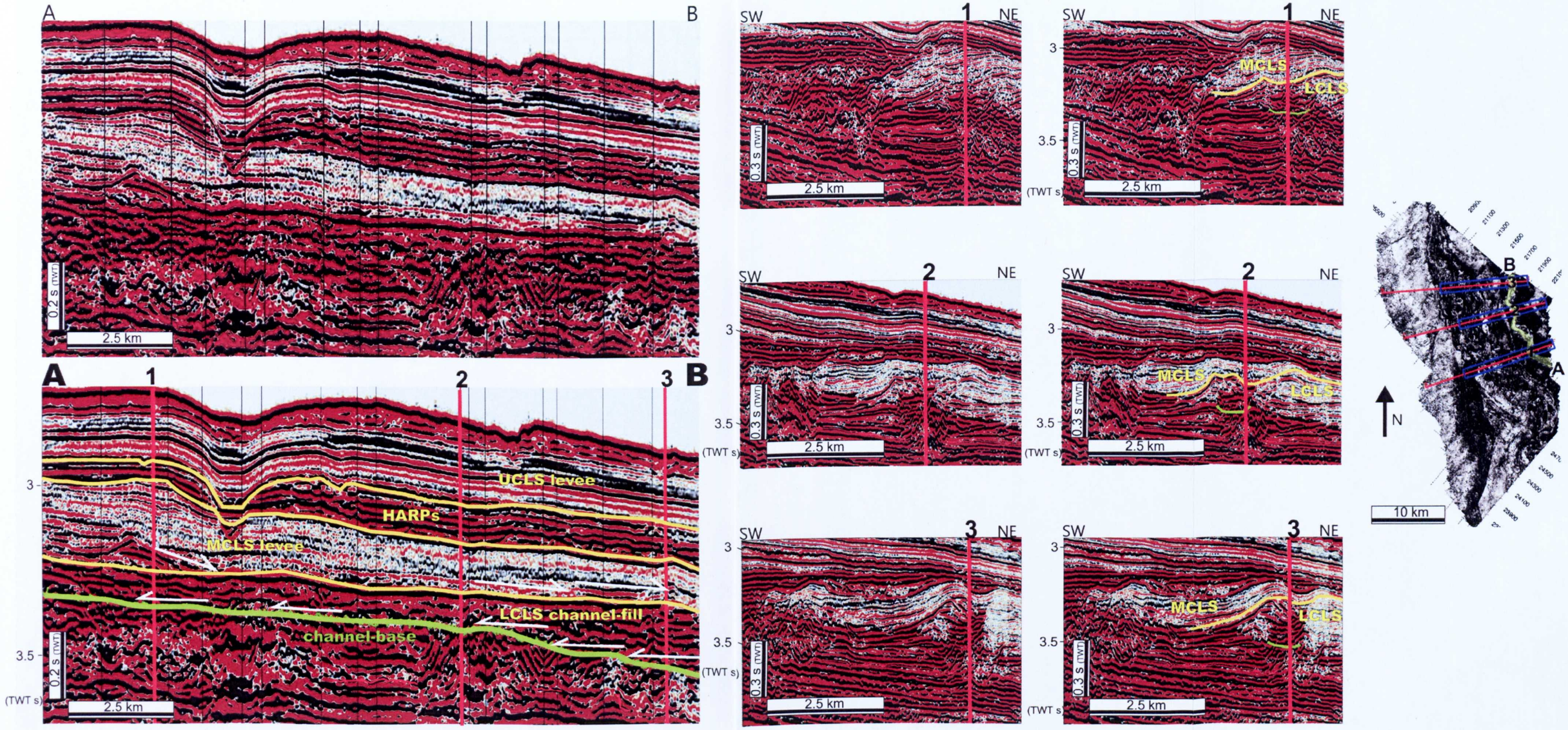

Figure 6-7 – Seismic sections cutting across the Lower Channel-Levee System. The section along the channel axis (AB) shows the reflections of the channel fill onlapping the base of the channel and becoming thinner upward. The other cross sections are transverse to the channel axis and cut the channels in positions 1, 2 and 3. The yellow horizons are the boundaries between the recognized channel-levee systems and also between the CLS and the HARPs. The green horizon corresponds to the channel base of the LCLS. Every section is duplicated showing the interpreted and its non-interpreted counterpart. Vertical exaggeration 8 x.

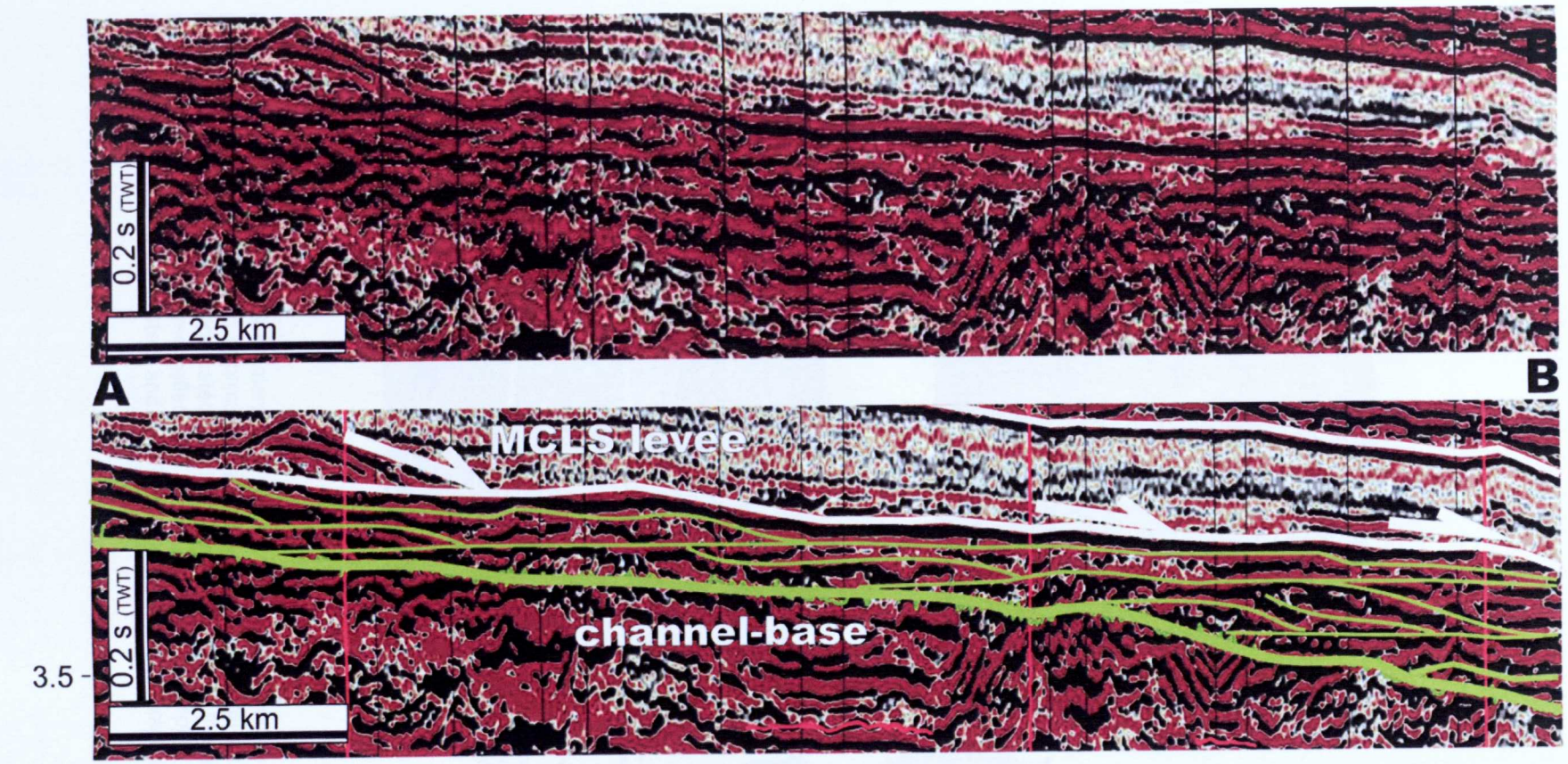

Figure 6-8 – Non-interpreted and interpreted seismic section (AB), detail of figure 6.7. The channel fill or the LCLS is formed by retreating sets of prograding reflections (highlighted in the thinner green lines). Vertical exaggeration 8 x.

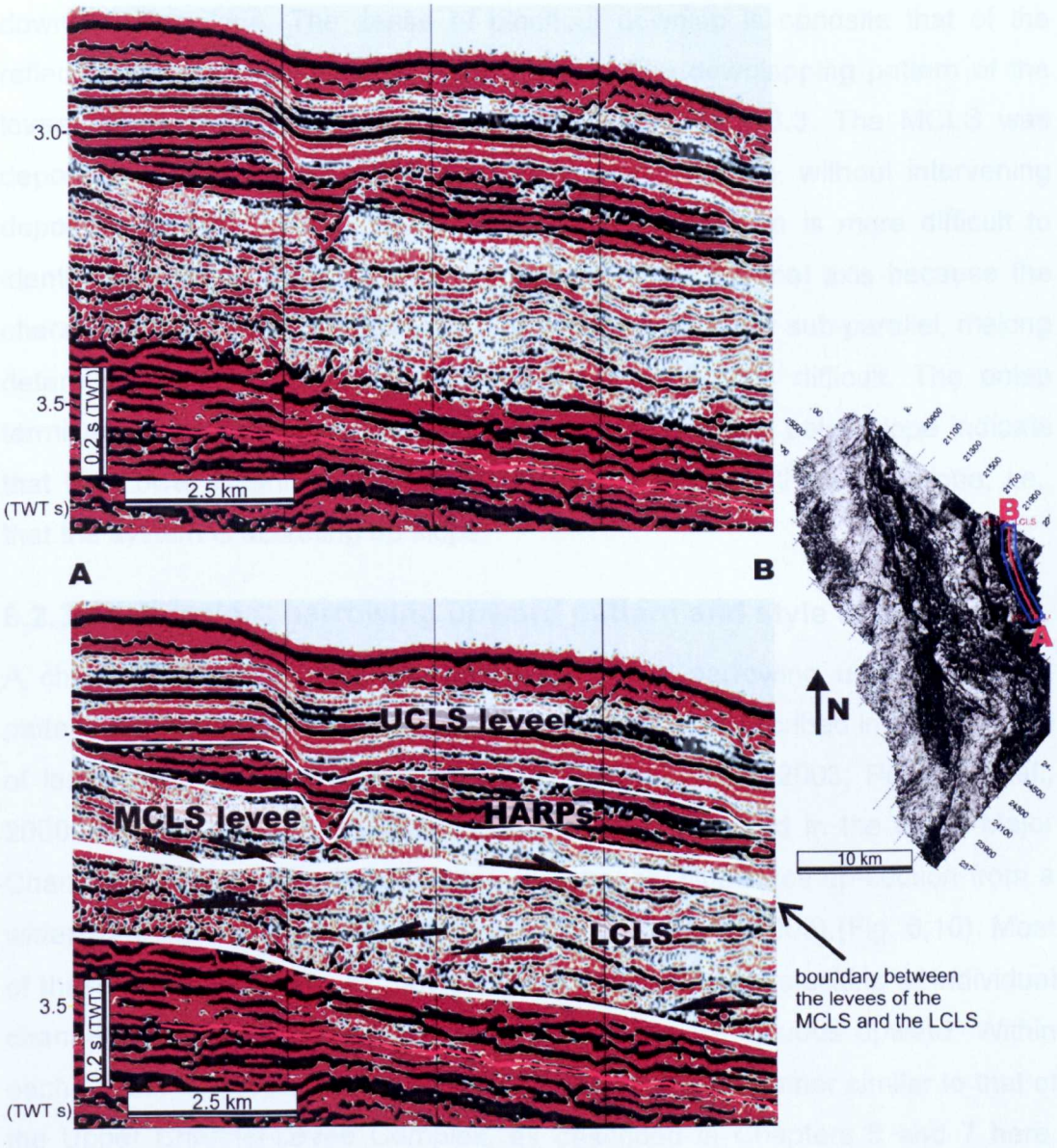

Figure 6-9 – Non-interpreted and interpreted seismic section (AB) across the right levee of the Lower Channel-Levee System approximately parallel to the channel axis. The levees of the MCLS and the LCLS are amalgamated with the levee reflections of the MCLS downlapping on the top of the LCLS. The levee reflections of the LCLS are onlapping upstream. The white horizons correspond to the system and HARP boundaries. Vertical exaggeration 8 x.

By way of contrast, the upper portion of the low amplitude reflections interpreted as part of the right-hand levee of the following Middle Channel-Levee System seen in the section (Fig. 6.9) exhibits reflections that appear to downlap downslope. The sense of pinchout downlap is opposite that of the reflections in the underlying package (LCLS). The downlapping pattern of the levee reflections in the MCLS is discussed in section 6.3. The MCLS was deposited directly on the LCLS with levee amalgamation, without intervening deposition of HARPs (Fig. 6.9). The levee amalgamation is more difficult to identify in cross sections that are transverse to the channel axis because the characteristic reflection orientations of the two systems are sub-parallel, making determination of the boundary between the two levees difficult. The onlap terminations of the channel fill and the levee against the paleo-slope indicate that the Lower Channel-Levee System is back stepping the paleo-slope, i.e., that the system is accreting up slope.

6.2.3 Discussion: narrowing upward pattern and style of channel fill

A channel-levee architecture characterized by a narrowing upward channel pattern in aggradational leveed channels is commonly described in the literature of large muddy systems (Deptuck et al., 2003; Kneller, 2003; Peakall et al., 2000; Stelting, 1985). For instance, in the Indus Fan and in the Benin-Major Channel-Levee System (Niger Delta), the channel fill passes up-section from a wider zone into narrower zone of HARs (Deptuck et al., 2003) (Fig. 6.10). Most of these literature examples, however, describe a vertical stacking of individual channel-levee phases narrowing and becoming more sinuous upward. Within each phase, however, the channels widen upward in a manner similar to that of the Upper Channel-Levee Complex, as described in Chapters 5 and 7 here. The LCLS apparently is composed of one phase of development and not a stacking of channel-levees (Deptuck et al., 2003) (Fig. 6.10). Similar progressive narrowing upward was also identified in the youngest Mississipi Fan channel and was attributed to a reduction in discharge with time during fourth-order cycles (approximately 100 ka) (Kneller, 2003). The onlap character of the channel fill and the levee reflections on channel thalweg and slope indicates that the channel-levee accreted upstream.

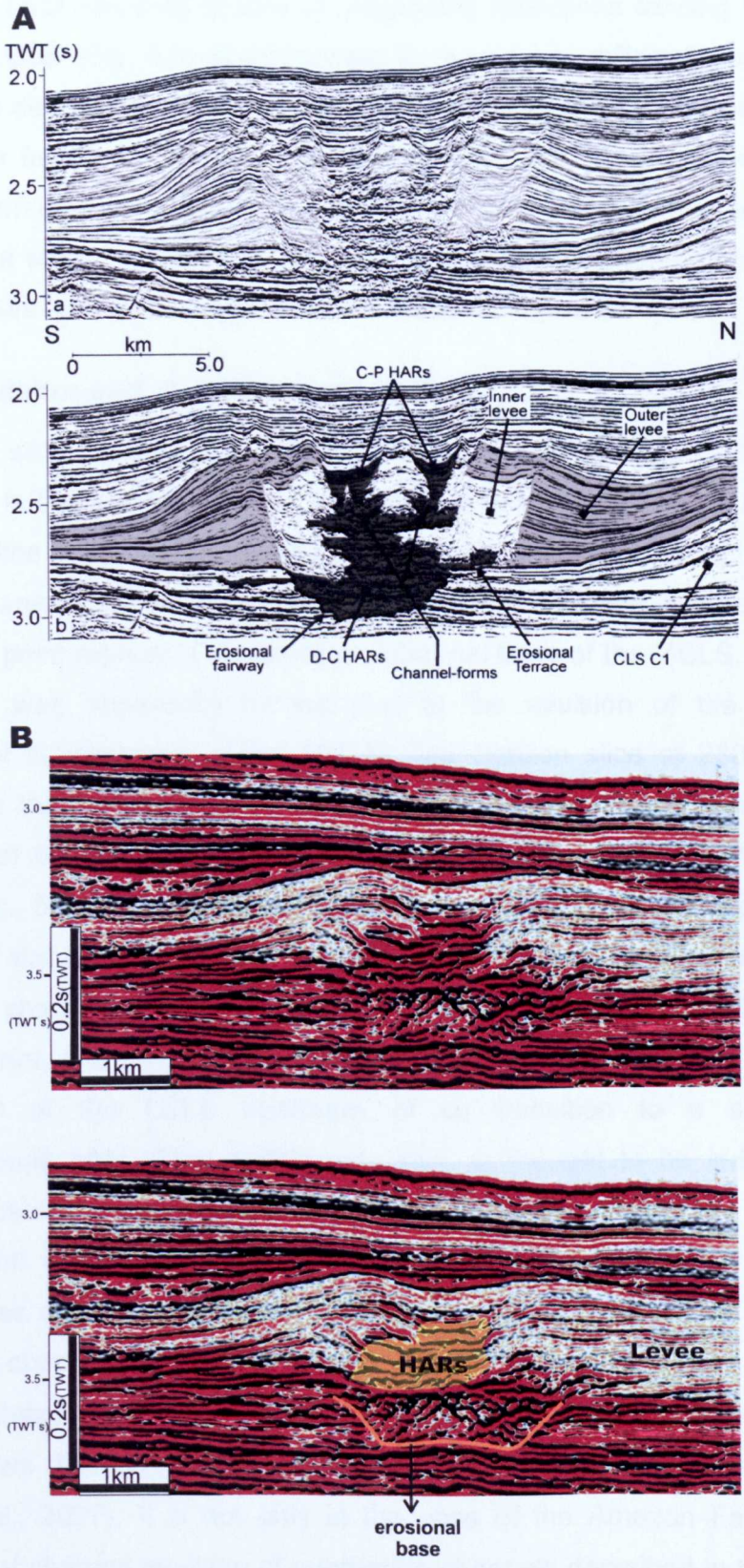

Figure 6-10 – Non-interpreted and interpreted seismic sections: A) A channel-levee system in Indus fan (Deptuck et al., 2003). Notice the stacking of individual bodies of HARs, each one widening upward. The top set of HARs (C-P) however are narrower than the underlying HARs. B) LCLS with the aggradational channel composed of narrowing upward HARs.

The back stepping of sets of prograding reflections forming the channel fill of the LCLS (Fig. 6.8) is interpreted to record two different frequencies of controls on deposition. The prograding reflections represent deposition dictated by a higher frequency control within a framework of a lower frequency control which determines the pattern of retreat. This may indicate that although the system as a whole is retreating, in a minor scale it is prograding. Therefore, the turbidite flows were occurring in smaller and smaller pulses.

6.2.4 Avulsion and abandonment of the LCLS

A horizon slice through the LCLS at 350 ms (TWT) (Fig. 6.11) shows a bifurcation in the erosive channel, with the left-hand branch disconnected from the bifurcation point. The right-hand branch is the erosional channel base of the LCLS, whereas the left-hand branch and the segment upstream of the bifurcation point represent the erosional channel base of the MCLS. Hence, this bifurcation was apparently formed due to the avulsion of the LCLS and subsequent development of the MCLS. The horizon slice at 280 ms (TWT) shows that the avulsed channel is multi-thread immediately downstream and upstream of the bifurcation point, whereas the abandoned channel is single thread (Fig. 6.11). The single thread channel represents the aggradational channel of the LCLS whereas the multi-thread channel is interpreted to be a composite channel, comprising a new, multithread section, downstream of the avulsion point, and an old, multithread section that was formerly a multithread component of the LCLS upstream of its transition to a single-thread (aggradational) style. The multithread style is thought to be indicative of a channel close to an idealized equilibrium profile (Kneller, 2003).

In the Quaternary of the Amazon Fan, channel avulsion is generally described as an abrupt process associated with levee breaches or wall failures of perched channels, on the outer-bend, induced by sand rich flows, resulting in sand inundation (HARPs) and deposition of sheet like deposits in the inter-channel lows (Damuth et al., 1983a; Flood et al., 1991; Pirmez et al., 1997; Wynn et al., 2007). It is not only in the case of the Amazon Fan, but most examples of channel avulsion of submarine channels described in the literature refer to perched, levee bordered channels. In the study case, however, the avulsion of the parent channel and abandonment of the LCLS occurred without

subsequent HARP formation (Fig. 6.7 and 6.9) but rather with the immediate development of a graded/erosional channel instead, and later development of the MCLS (Fig. 6.11).

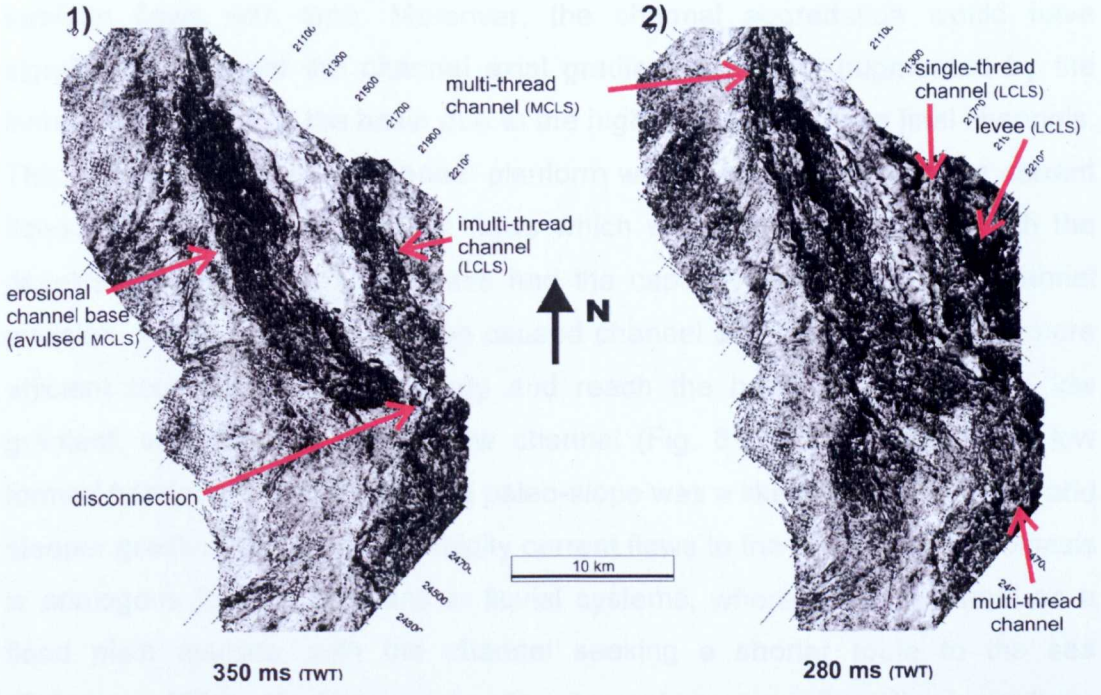

Figure 6-11 – The horizon slices showing the avulsion and LCLS abandonment. 1) Deeper horizon slice, at 350 ms (TWT) below the datum. The slice shows the bifurcation but with the left-hand branch disconnected from the parent channel. 2) Shallower horizon slice, at 280 ms (TW) below the datum. The slice shows the avulsion of the multi-thread channel. The abandoned LSLS is characterized by the single thread channel and levee, both of which are identified in the figure.

Avulsion of a multi-thread submarine channel has not been described in the literature of turbidite systems and there are apparently no models to describe this process in the literature. If the multi-thread style is indicative of low accommodation space (Kneller, 2003), then a multi-thread channel may be relatively shallow, without well developed levees which would favour avulsion. In addition, because multi-thread channels may show little or no aggradation (Kneller, 2003), they may be unlikely to become perched and, consequently, there may be no significant paleo-bathymetric difference between the channel base and the adjacent area. This small height difference may imply that there would be only minor accommodation space in which to aggrade a HARP. The avulsed flow would, therefore, be more likely to bypass or erode.

The channel avulsion may be related to the development of the LCLS downstream from the eventual avulsion point together with an abrupt increase

in flow size. Thus the aggradation and upward increase of sinuosity and decrease in channel width of the LCLS may represent the channel form progressively moving towards an equilibrium with the gradual change in turbidite flows with time. Moreover, the channel aggradation would have significantly reduced the channel axial gradient, an effect augmented by the increased distance to the basin due to the higher sinuosity of the final channels. This inference is that this channel planform was in equilibrium with the current flows. Therefore, larger turbidite flows which were not in equilibrium with the developed channel form may have had the capacity to have caused channel avulsion. These flows would have caused channel avulsion by seeking a more efficient route to dissipate energy and reach the basin compared to a low gradient, very sinuous and narrow channel (Fig. 6.12). The bathymetric low formed between the LCLS and the paleo-slope was a likely straighter, wider and steeper gradient pathway for turbidity current flows to the basin. This hypothesis is analogous to what happens in fluvial systems, where a river channel on a flood plain avulses, with the channel seeking a shorter route to the sea (Schumm, 1993). In other words, the channel-levee configuration may have become meta-stable. The transition from erosional to aggradational channel is a likely place for avulsion because at this point the channel would have been less well confined. Unfortunately, the relationship between the abandoned LCLS and the upstream avulsed channel could not be visualised because the avulsion point is just outside the seismic data.

In summary, three main points must be considered to explain the avulsion of the LCLS: an interpreted strong increase in flow magnitude, no longer in equilibrium with the relatively low gradient, sinuous and narrow channel form; the metastable equilibrium of the multithread channel at the transition from upstream erosional to downstream aggradational channel; and the steeper gradient on the back levee slope/continental slope. This type of avulsion can occur for example in the following context. An increase in relative sea level would favour the dispersion of sediments on the shelf and consequent reduction of the amount of sediment captured by the Amazon Canyon and delivered to the slope, resulting in the observed narrowing-upward channel architecture. A subsequent sea level fall would reactivate the turbidite system on slope eventually forcing the avulsion of the channel.

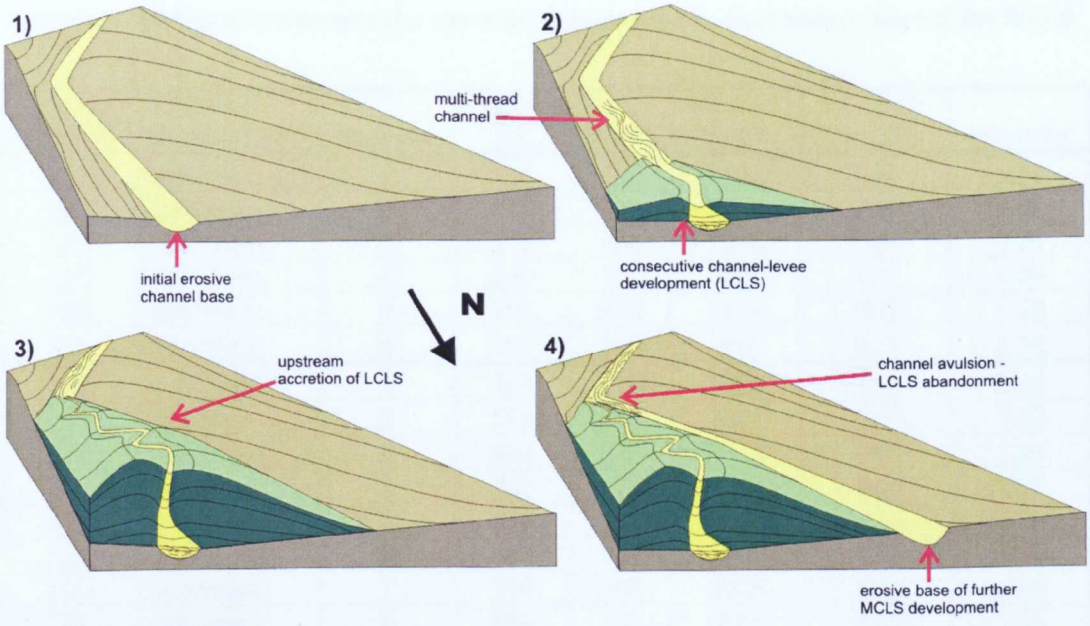

Figure 6-12 – Schematic block diagrams representing the model of upstream development of a channel-levee and subsequent avulsion. The evolution phases of the LCLS and subsequent avulsion are: 1) initial channel incision; 2) aggradation of the channel-levee and accretion from downstream to upstream; 3) channel-levee onlapping the paleo slope and upward tendency of the channel to become narrower, more sinuous and of lower gradient; 4) abandonment of the LCLS and avulsion. Notice that multi-thread channel (at grade) is represented at the transition from erosional to aggradational. The view of the diagrams is upstream.

6.3 Downstream-stepping channel-levee system

The evolution of this channel-levee is characterized by a downstream accretion of the system. The characteristics of the channel planform, channel fill and levee style and the final abandonment of the channel are described here. The ways controlling parameters may have evolved through time and space are discussed in order to establish an evolutionary model.

6.3.1 Planform evolution

In order to evaluate the vertical changes in channel morphology, a quantitative analysis was performed by measuring the channel width, sinuosity, meander arch height, channel length and meander length of channel meanders observed in eight horizon slices taken across the MCLS. The values of the measured parameters for each meander along the channel of the MCLS are presented in Table 6.2.

Table 6-2 – Measured parameters for the channel meanders in each horizon slice of the MCLS

horizon slice (ms)	Channel segment	meander	width (m)	MAH	channel length	meander length	sinuosity
220	upstream	1	268	642	1731	884	1.96
220	upstream	2	313	603	2075	1400	1.48
220	upstream	3	218	458	1945	1430	1.36
220	upstream	4	230	170	790	722	1.09
220	upstream	5	209	453	1866	1560	1.20
220	upstream	6	211	246	847	623	1.36
200	upstream	1	344	819	2069	841	2.46
200	upstream	2	360	617	2067	1460	1.42
200	upstream	3	432	613	1978	1481	1.34
200	upstream	4	233	279	1173	964	1.22
200	upstream	5	332	341	1474	1246	1.18
200	upstream	6	333	202	923	759	1.22
200	upstream	7	267	148	1026	935	1.10
200	upstream	8	133	78	870	818	1.06
200	upstream	9	324	355	3209	3144	1.02
200	upstream	10	168	246	1086	834	1.30
200	upstream	11	194	430	1715	1293	1.33
180	upstream	1	271	437	1565	1128	1.39
180	upstream	2	286	460	1381	1061	1.30
180	upstream	3	329	560	1822	1331	1.37
180	upstream	4	380	290	1882	1773	1.06
180	upstream	5	322	232	1021	885	1.15
180	upstream	6	233	247	1236	1072	1.15
180	upstream	7	279	707	4222	3930	1.07
180	upstream	8	381	398	1786	1536	1.16
180	upstream	9	400	413	1552	1233	1.26
180	upstream	10	221	389	1295	1011	1.28
170	upstream	1	470	590	2160	1695	1.27
170	upstream	2	424	387	1263	1029	1.23
170	upstream	3	285	502	1588	1089	1.46
170	upstream	4	468	631	2001	1480	1.35
170	upstream	5	548	252	1721	1609	1.07
170	upstream	6	426	387	1472	1194	1.23
170	upstream	7	406	196	996	927	1.07
170	upstream	8	417	451	3395	3192	1.06
170	upstream	9	437	368	2149	2013	1.07
170	upstream	10	528	435	1694	1307	1.30
170	upstream	11	334	408	1614	1276	1.26
170	upstream	12	617	1152	3814	1099	3.47
150	upstream	1	476	453	1421	1143	1.24
150	upstream	2	311	551	1671	1195	1.40
150	upstream	3	312	477	1342	946	1.42
150	upstream	4	478	285	1874	1700	1.10
150	upstream	5	395	385	1567	1294	1.21
150	upstream	6	189	166	1076	978	1.10
150	upstream	7	218	195	1260	1187	1.06
150	upstream	8	518	169	5134	4961	1.03

150	downstream	9	567	2049	5997	1091	5.50
150	downstream	10	570	1299	3055	1066	2.87
150	downstream	11	391	475	1832	1552	1.18
150	downstream	12	315	334	1296	949	1.37
150	downstream	13	323	579	2595	2047	1.27
150	downstream	14	359	580	1660	705	2.35
150	downstream	15	347	453	1737	1257	1.38
150	downstream	16	330	371	1930	1578	1.22
130	upstream	1	1020	3113	10876	8680	1.25
130	upstream	2	1006	871	3465	2902	1.19
130	downstream	3	814	1459	4999	2938	1.70
130	downstream	4	585	855	2649	1750	1.51
130	downstream	5	751	914	5350	4473	1.20
130	downstream	6	552	890	2049	696	2.94
130	downstream	7	409	793	2220	1418	1.57
130	downstream	8	636	637	2248	1509	1.49
130	downstream	9	516	429	1546	1293	1.20
130	downstream	10	540	447	2221	2006	1.11
130	downstream	11	397	373	1645	1375	1.20
130	downstream	12	450	460	2061	1826	1.13
120	upstream	1	1334	3056	12185	9624	1.27
120	upstream	2	1019	873	3461	2984	1.16
120	downstream	3	801	1523	4879	3273	1.49
120	downstream	4	837	1849	6741	5279	1.28
120	downstream	5	517	1000	2253	900	2.50
120	downstream	6	486	596	2062	1365	1.51
120	downstream	7	573	624	2120	1666	1.27
120	downstream	8	447	503	1661	1259	1.32
120	downstream	9	573	476	2234	1965	1.14
120	downstream	10	472	363	1375	1241	1.11
120	downstream	11	362	550	2256	2004	1.13
100	upstream	1	2055	4128	14292	11043	1.29
100	upstream	2	1350	986	3877	3221	1.20
100	downstream	3	715	1309	4726	3386	1.40
100	downstream	4	481	502	2209	2042	1.08
100	downstream	5	389	292	1483	1200	1.24
100	downstream	6	259	373	1212	804	1.51
100	downstream	7	212	373	1463	1171	1.25

The range of measured channel widths is from 0.2 to 2.0 km and of measured sinuosities between 1.0 and 5.5. Only one width measurement was 2.0 km; the others were in the range previously measured in the middle and lower fan of the Amazon Fan, that is from 0.3 to 1.4 km (Flood and Damuth, 1987; Flood et al., 1991; Pirmez and Flood, 1995). Most of the measured values of sinuosity were in the interval 1.1 – 2.9 as described previously in the literature of the Amazon Fan (Flood and Damuth, 1987; Flood et al., 1991; Pirmez and Flood, 1995), with only 3 values greater than 2.9.

The MCLS exhibits two distinct segments in the study area. In the upstream segment the channel can develop larger dimensions than in the downstream segment (Table 6-2). The channel parameters, therefore, were measured taking into account whether they occurred in downstream or in upstream segments. The transition between these two segments is marked by a strong reduction in channel width and by a sinuosity increase. The channel planform also changes vertically very often in the transition from the upstream to the downstream segments, with strongly variable sinuosity (see Fig. 6.13).

A scatter chart (Fig. 6.14) does not show a clear relationship between the sinuosity and the channel width measured in each meander (Fig. 5.27). Very high values of sinuosity in the downstream segment are located close to the transition to the upstream segment, where the thalweg gradients are interpreted to have been smaller. The scatter plots in Figure 6.15 show that sinuosity reduces upward whereas width increases. The scatter plots clearly show different trends between the two channel segments. Generally, in the same horizon slice, the channels are more sinuous and thinner downstream than upstream (Fig. 6.15). It is worth mentioning that there are no measured values for the downstream channel segment in the deepest slices because the measurements were performed only in single-thread channels and in these slices the downstream channel segment was still a multi-tread channel. Therefore, the Middle Channel Levee System is characterized by the upward tendency of the channel planform to become wider and less sinuous (Fig. 6.16). Most of the aggradational channel-levee was built up above and after the filling of the erosional channel base, as is highlighted in Figure 6.16.

The occurrence of two distinct segments of developments (downstream and upstream) is thought to reflect differing evolutionary histories. Most of the upstream segment is above the point of avulsion of the LCLS (which is close to and outside the border of the seismic data). The point of avulsion does not coincide exactly with the transition from the upper to the downstream segment which is slightly downstream. Therefore, the whole downstream segment comprises a new channel pathway that resulted from avulsion. This channel, in the downstream segment, is thought probably to have had an initial gradient different from the upstream parent channel and, therefore, a different evolutionary history until some equilibrium may have been reached. There is a

net reduction in the apparent channel gradient in the passage from the upstream to downstream segment (Fig. 6.17) that could correspond to the abrupt increase in channel sinuosity in the transition from upstream to downstream segment shown in Figure 6.13.

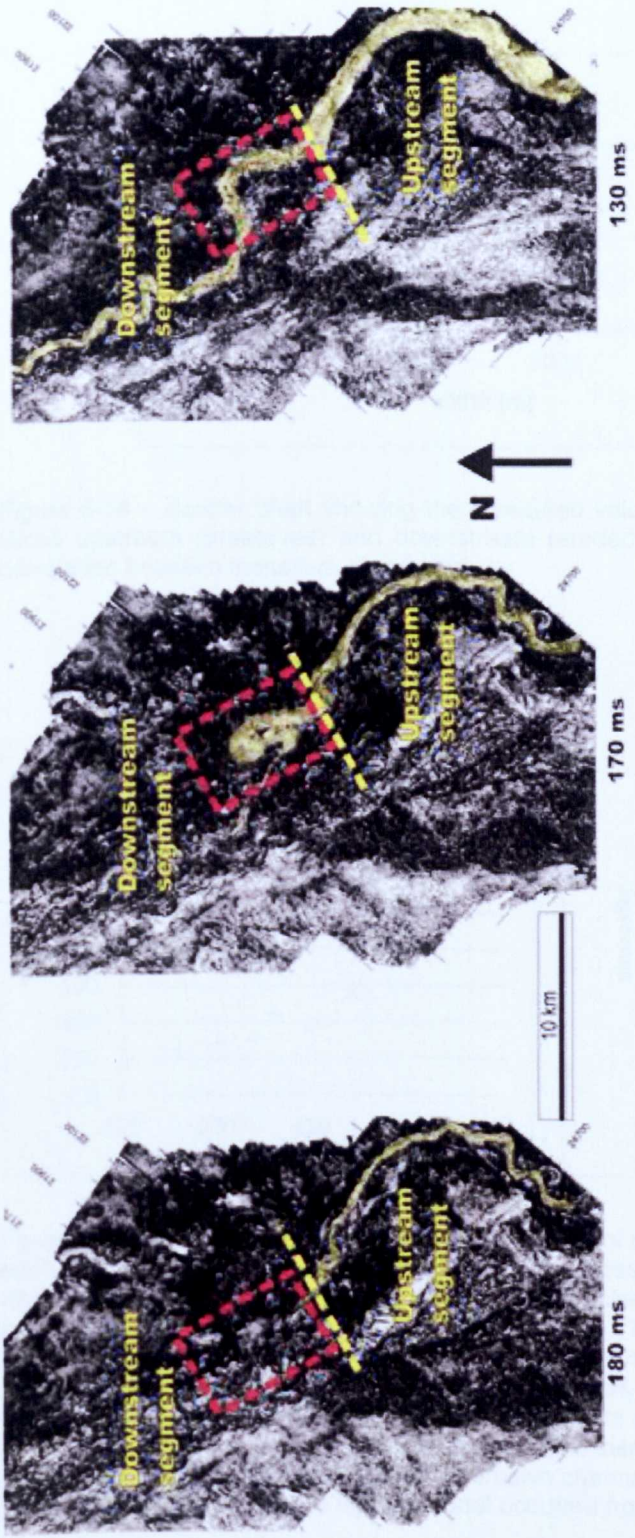

Figure 6-13 – Three horizon slices extracted at 180, 170 and 130 ms below the datum. On the maps, the channel is highlighted and the two segments: up and downstream. These slices were extracted very close to each other (10 and 40 ms) and show a dramatic change in the channel sinuosity in the portion immediately downstream from the vertical separations of the transition between the two segments in the area, highlighted with the dashed red box.

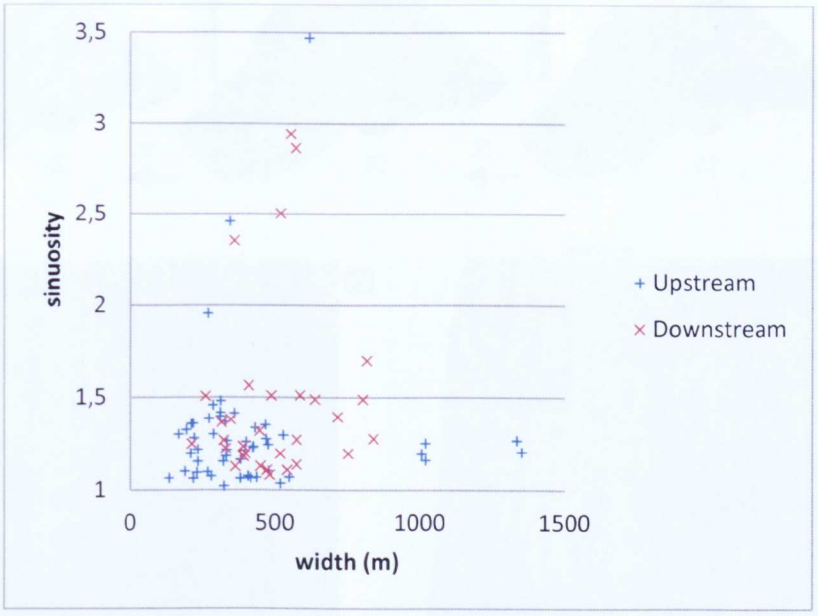

Figure 6-14 – Scatter chart showing the measured values of sinuosity and width in all horizon slices upstream (preserved) and downstream (eroded) channel segment. There is no clear correlation between these two parameters.

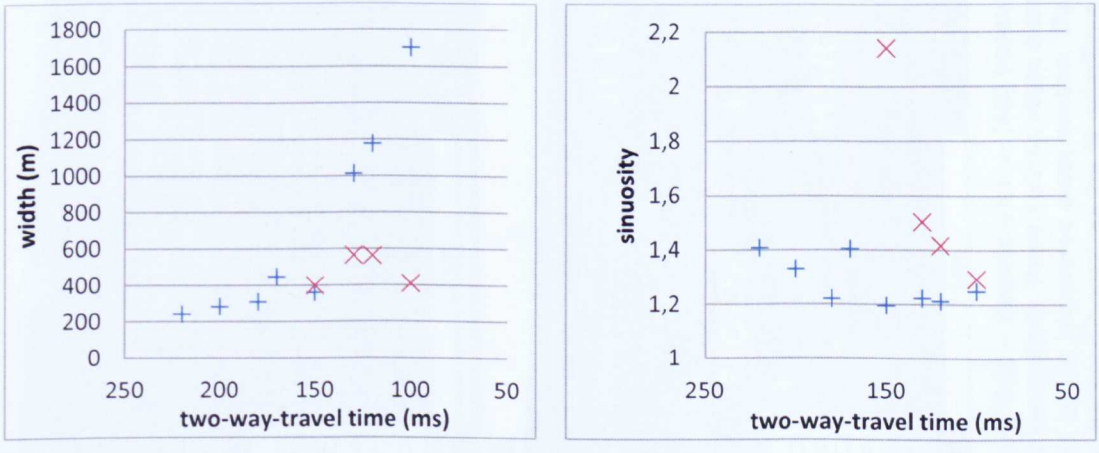

Figure 6-15 – Diagrams showing the average values of sinuosity and channel width obtained for each horizon slice across the MCLS. The x-axis represents the time underneath the datum at which the RMS of coherence horizon slice was extracted. Therefore, the greater the time value, the closer to the base of the channel-levee system. The upstream values (+) represent the measurements on the non-eroded channel-levee portion (upstream segment) whereas the downstream values (x) represent the measurements on the eroded channel-levee portion (downstream segment). There are no measurements of the channel in the deepest horizon slices (TWT greater than 150) because at this point there were no single-thread (aggradational) channels formed yet, only multi-thread or erosive channels in this segment, in the deeper slices. The transition from erosive to aggradational occurred from upstream to downstream.

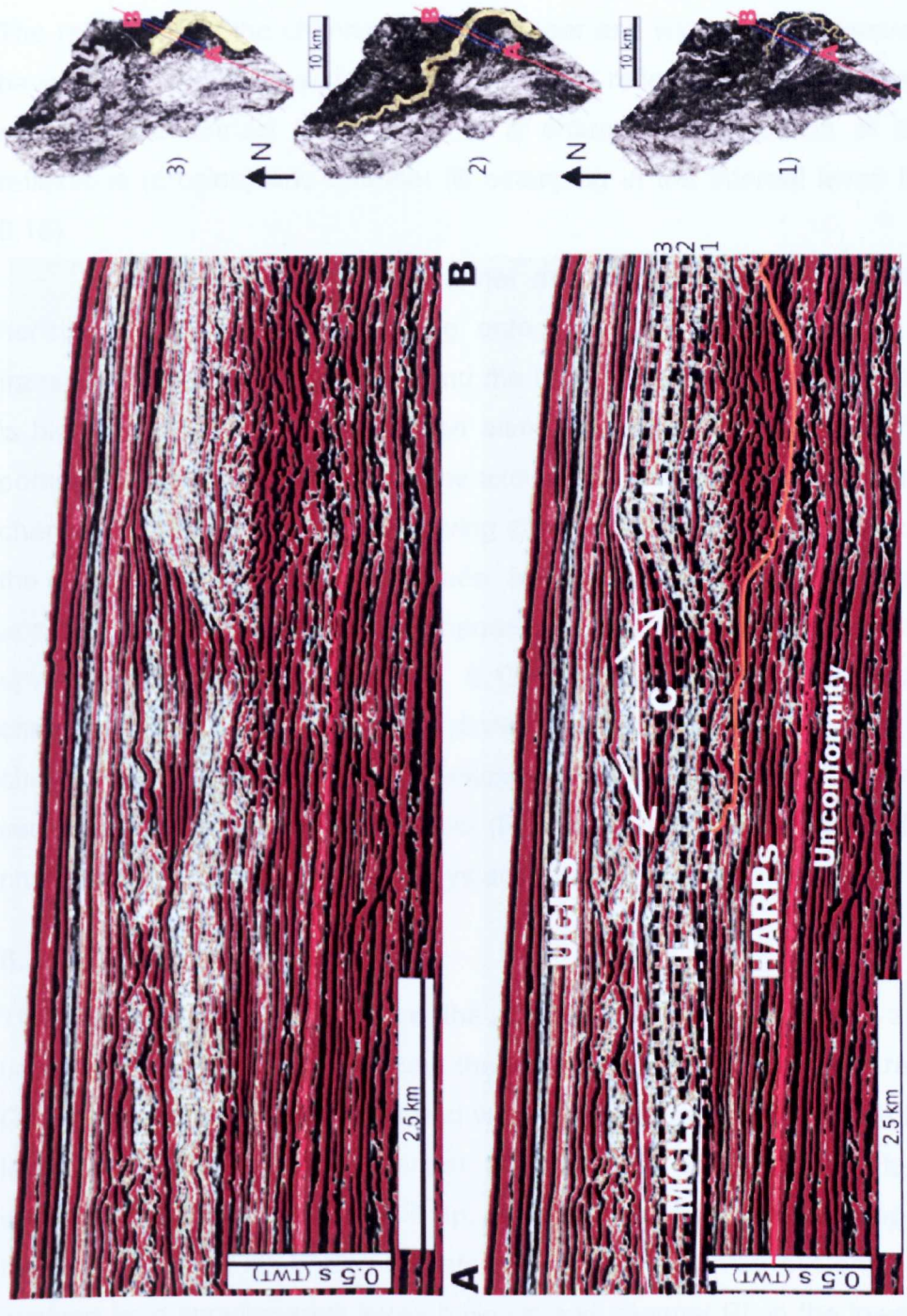

Figure 6-16 – Seismic section (AB) transverse to the channel axis in the Middle Channel-Levee System (non-interpreted and interpreted). Three horizon slices extracting RMS of coherence (maps on the right) are represented by dashed black lines on the interpreted cross section. They show the channel widening and reducing sinuosity upwards. The arrows in the channel (C) point out the fill reflections onlapping the levee limbs.

6.3.2 Channel fill and levee style

The fill of the aggradational channel is characterized by high amplitude reflections (HARs) bordered by the low amplitude reflections of the levee (Fig. 6.18). In cross section, the channel fill in the upstream segment can be divided into two parts. Close to the base of the channel, in its narrowest portion, the

reflections appear to be in lateral continuity with the levee reflections (Fig.6.18). The reflections of the channel fill in the upper and widest part, however, do not have lateral continuity with the low amplitude reflections of the levee. On the contrary, the contact between them is sharp, with truncation of the levee reflections (erosion) and channel fill onlapping in the internal levee limb (Fig. 6.18).

In a section along the channel axis, the channel fill reflections are horizontal, or slightly downlapping onto the channel base (Fig. 6.17). The transition between the upstream and the downstream segments of the channel is highlighted in blue in the section along the channel axis (Fig.6.17). In this portion, the vertical section along the axis could not be taken so as to show only channel fill (HARs) due to the evolving channel sinuosity through time; similarly the levee reflections (low amplitude reflections) bordering the channel will appear in the section, as the channel position changes frequently, moving upwards in a vertical section (Fig. 6.13). Although in transverse sections the channel-levee presents an aggradational character, in longitudinal sections the channel levee reflections are downlapping upon the slope. Two longitudinal sections, one along the levee crest (Fig. 6.19) and other sub-parallel to the channel axis (Fig. 6.17) show the system development downstream.

6.3.3 Erosion of the MCLS

The lower and narrower portion of the channel fill and the levee were apparently deposited simultaneously because they present lateral continuity of reflections. On the other hand, in the upper and wider channel portion, the truncation of the levee reflections and the channel fill reflections onlapping the levee limb suggest that after the levee built up, there was erosion and later deposition of the channel fill (Fig. 6.20). Therefore, the channel-levee system apparently evolved from simultaneous levee build up and channel fill, in the lower portion, to levee build up, erosion and bypass of coarser sediments in the upper portion and, finally, to channel fill in the enlarged channel. In the downstream segment of the channel-levee only the basal portion of the system appears to be preserved.

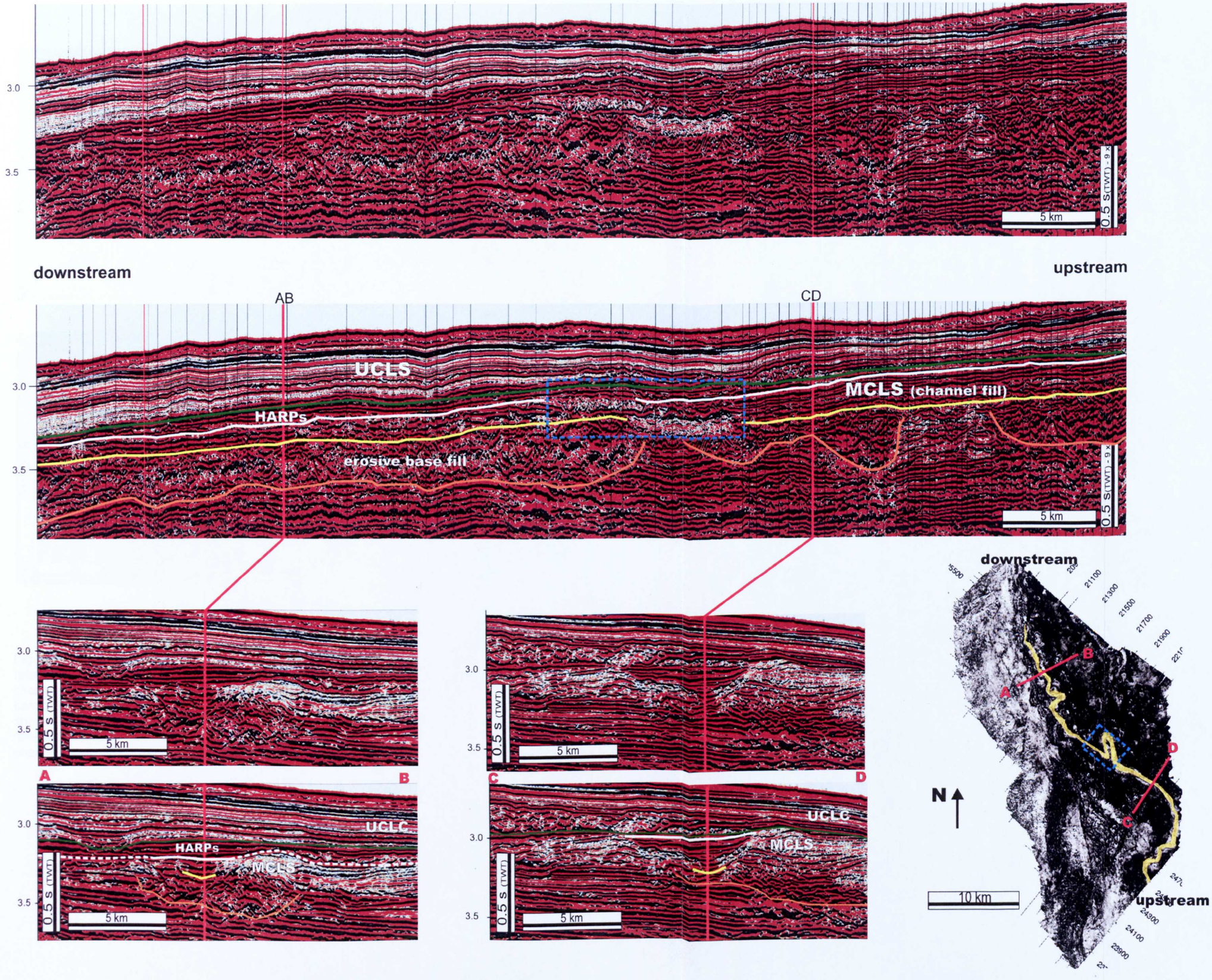

Figure 6-17 – Seismic line along the channel axis of the MCLS, outlined in yellow in the horizon slice (150 ms below the datum – base of the UCLS green horizon). The channel fill is the set of the high amplitude reflections between the yellow horizon in the base and the white horizon on the top. The reflections are sub-parallel and relatively continuous and if not sub-parallel they slightly downlap the channel base. The area in the intermediate portion of the channel with low amplitude reflection and delimitated by the dashed blue line corresponds to the area where the channel gradient is thought to reduce significantly and the sinuosity of the channel increases significantly downstream. From this area, the MCLS was strongly eroded as shown by a dashed white horizon in the cross section AB whereas the MCLS is better upstream preserved. Although the upstream segment of the MCLS is relatively well preserved, the internal walls of the channel were eroded, characterized by the truncation of the levee reflections, seen in the cross section CD.

Legend:
UCLS – Upper channel-levee system
MCLS – Middle channel-levee system
HARPs – High amplitude reflexion packet
Green horizon – base of UCLC
White horizon - Top of channel fill
Yellow horizon – Base of the channel
Orange horizon – Erosive channel base
Dashed blue horizon – intermediate area with lower gradient and channel planform with frequent vertical variatiion.
Dashed white horizon – erosive surface on the top of the downstream portion of the MCLS.

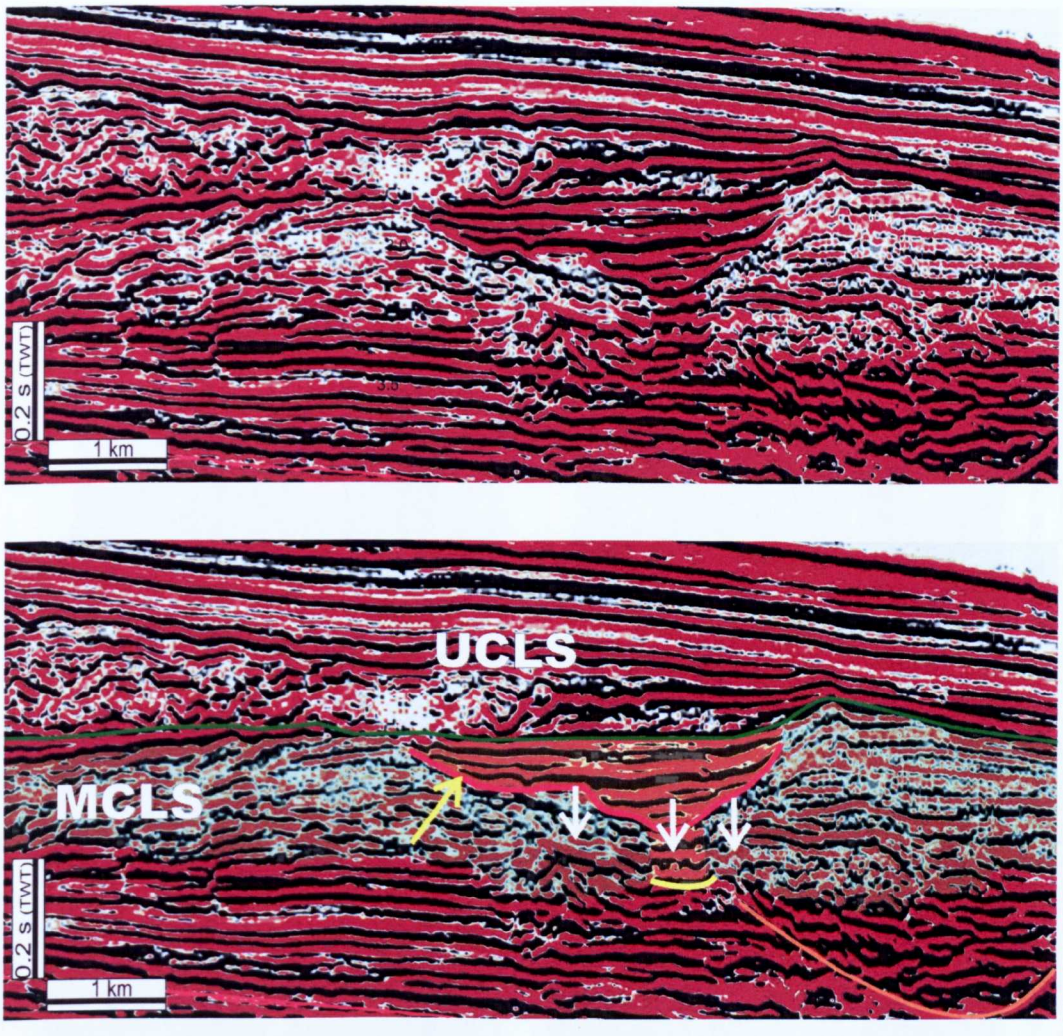

Figure 6-18 – Non-interpreted and interpreted section across MCLS, showing the relationship between the channel fill and levee reflections. In upper zones of the channel the channel fill reflections onlap the internal levee limb (yellow arrow). In the lowest zones, the same high amplitude reflection changes laterally from high to low amplitude, from the channel fill to the levee (white arrows). Red horizon = erosive surface truncating the levee reflections; yellow horizon = base of aggradational channel; orange horizon = erosive channel base; and green horizon = base of UCLS.

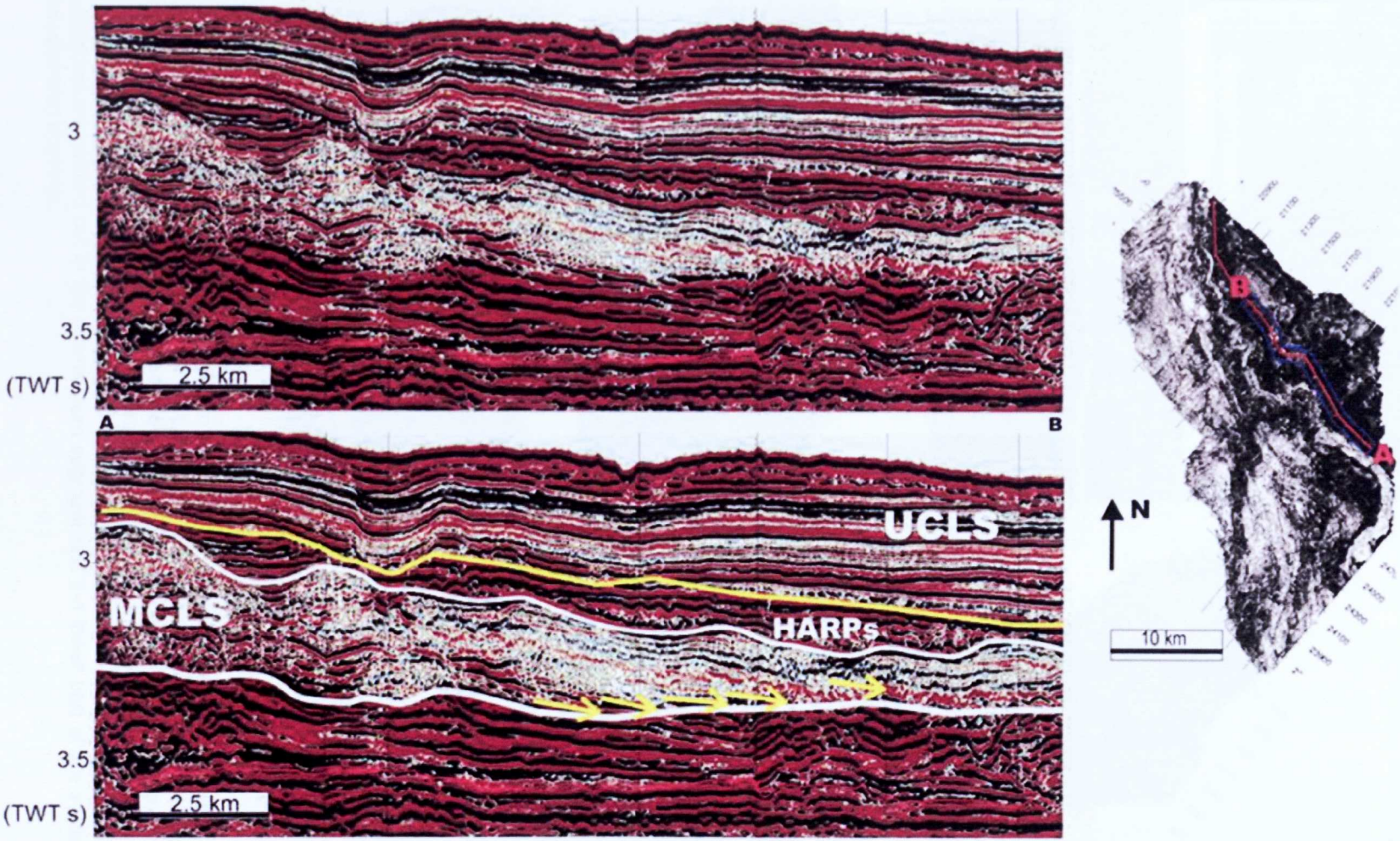

Figure 6-19 – Non-interpreted and interpreted seismic section (AB) cutting across the crest of the right levee of the Middle Channel-Levee System. The levee reflections are downlapping upon the slope as indicated by the yellow arrows. Vertical exaggeration 8 x.

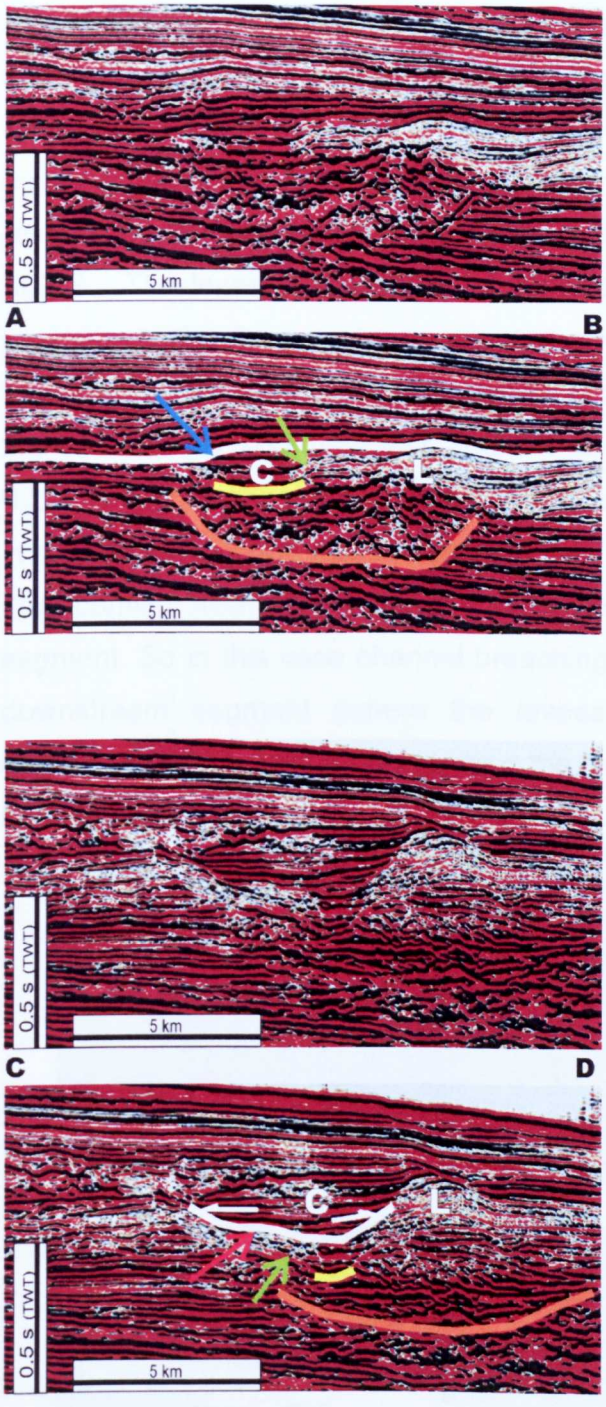

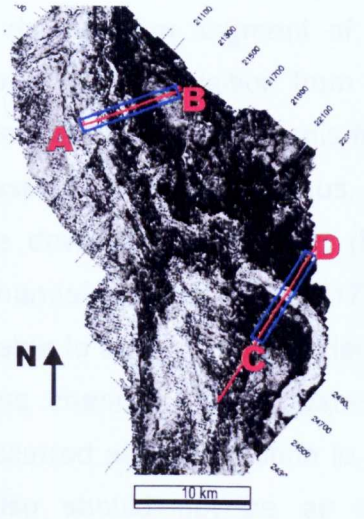

Legend:

C - channel
L - levee

horizons:
orange - erosive channel base
yellow - gradational channel base
white - erosive surface

arrows:
green - channel fill and levee reflections continuity
blue - channel fill truncation
red - levee reflections truncation

Figure 6-20 – Two sections perpendicular to the channel axis across the downstream (AB) and the upstream (CD) segments of the MCLS. Notice that in the downstream segment only the lower portion of the system was preserved. The upper portion of the system was eroded (blue arrow and white surface). In the upstream segment (CD), the levees are preserved but with some erosion in the internal limbs (red arrow). The continuity of channel fill and levee reflections are pointed out in the downstream segment and the lower part of the system in the upstream segment.

It seems likely that the internal levee erosion shown in the upstream segment is an equivalent event to the pervasive erosion of the upper portion of the downstream segment. It is possible that the same flows that eroded the internal levee limbs in the upstream segment of the MCLS were responsible for the pervasive erosion of the downstream segment of the MCLS. The levee collapse (Fig. 6.21) observed at the transition from the upstream to the downstream segment may have happened due to a mis-fit of the channel form at the time of a strong increase in the flow size. Thus, the higher sinuosity and narrower channel of the downstream segment (Fig. 6.21) in association with a reduction of the channel gradient (Fig. 6.17) is interpreted to indicate that the channel was unable to accommodate a larger flow coming from the wider and less sinuous channel of the upstream segment. So in this case channel breaching occurred at the transition to the downstream segment (where the levees also should not be as well developed as the upstream one since the sinuosity often reduced in younger horizon slices).

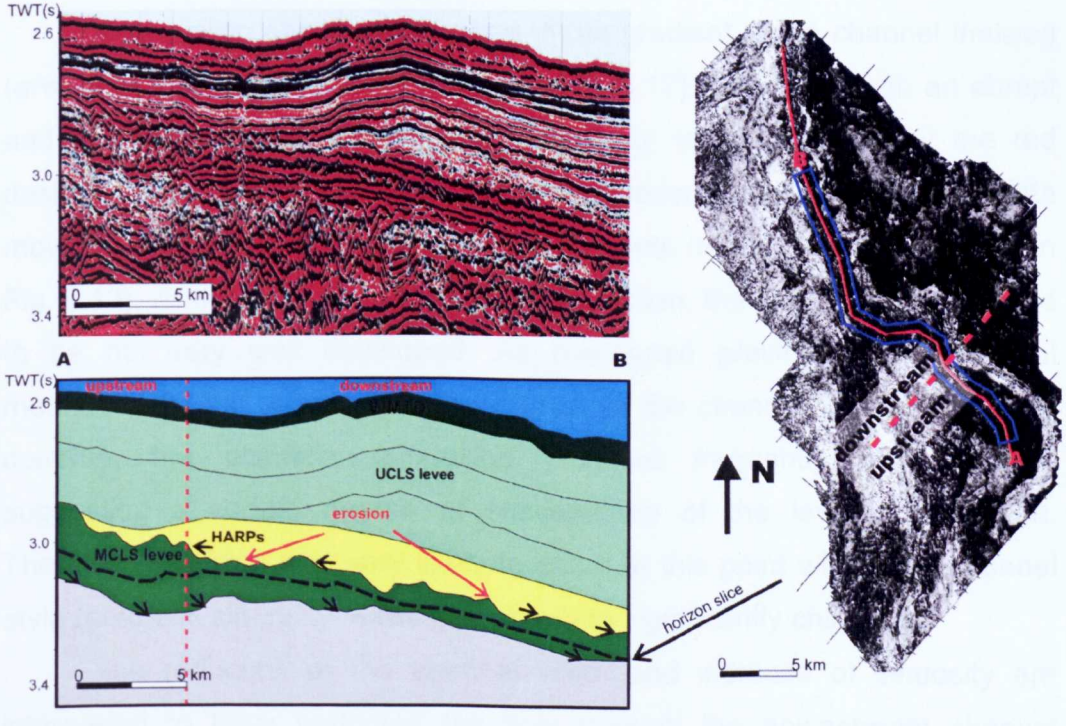

Figure 6-21 – Seismic section (AB) along the left-hand levee (view downstream) of the MCLS with exaggeration of the vertical scale (~16 x). On the transition from the upstream to the downstream segment (red dashed line) the levee thickness reduces significantly and shows an eroded top. The horizon slice (RMS coherence) is outlined in the section with a black dashed line. HARPs occur preferentially above the eroded levee of the downstream segment. The black arrows in the interpreted section show the downlapping character of the MCLS and onlapping character of the HARPs.

6.3.4 Initiation and progradational pattern of the MCLS

The evolution of the MCLS has been interpreted based on the analysis of channel planform, channel fill pattern and levee reflection terminations. In map view, the horizon slices of RMS coherence (Fig. 5.27) show also distinct channel features: blurry chaotic facies bounded by large scale erosive incision, and both multiple-thread and single-thread channels (Fig. 6.22). The sequential analysis of the horizon slices, from the base to top across the MCLS system, shows the upward and downstream transition from a multi-thread channel to single-thread channel form (Fig. 5.27). Single-thread channels are associated with agradational channel-levees. There, the channel axis commonly remains more or less fixed in position as the system aggrades, whereas the multiple-thread channels appear to migrate laterally on what is interpreted to be an equilibrium surface and are therefore interpreted to be "at grade" or "in equilibrium" channels. These associations between the planform and the channel types were previously described by Peakall et al. (2000) and Kneller (2003).

There is an apparent reduction in the gradient of the channel thalweg (area delimited by blue dashed area in Fig. 6.17) associated with an abrupt and strong increase in the channel sinuosity (area delimited by the red dashed line in Fig. 6.13). There is also a reduction in the channel width moving from upstream to downstream segments (horizon slice at 130 ms in Fig. 6.13). At the point of channel width reduction, the levees are interpreted to be not very well developed. As mentioned previously, the channel meanders did not remain fixed in position as the channel aggraded, on the contrary, the planform (sinuosity) changed frequently and abruptly, suggesting a certain degree of susceptibility of the levees to erosion. Therefore, avulsion was very likely to occur at this point where the channel style (gradient, sinuosity, levee height, width) significantly changed.

The reduction of the channel width and increase of sinuosity are interpreted to have restricted the flow through the downstream channel segment. Such restrictions added to the relative levee weakness and to a possible strong increase in the flow size may have promoted levee collapse at the outer bends of the channel (Fig. 6.13, slice 130 ms) and erosion of the

upper part of the channel-levee system in the downstream segment of the MCLS.

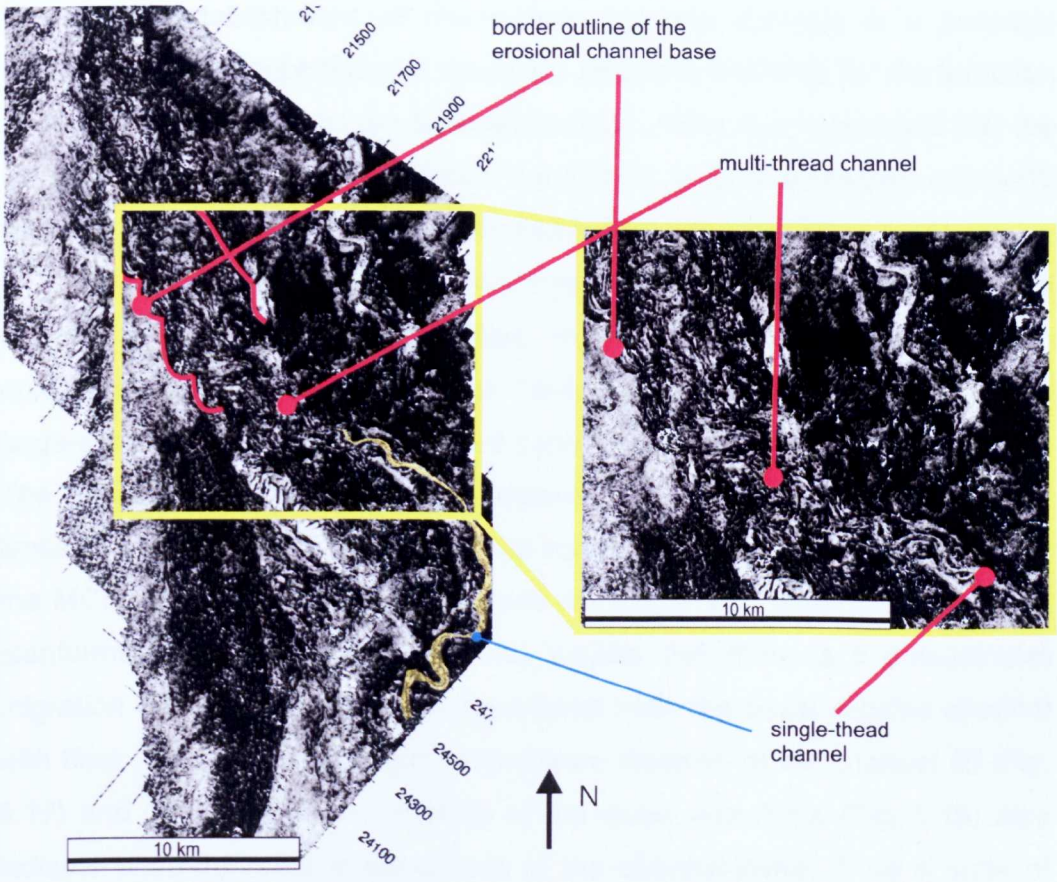

Figure 6-22 – Horizon slice (200 ms below the datum) showing in planview the transition between single-thread (yellow) and multi-thread channel. Notice the crescent shaped borders of the erosional channel base (red). A zoomed view of the yellow area highlights the features but without interpretation.

The basal erosive channel of the MCLS cuts through sheet-like deposits (HARPs) which were deposited before the LCLS. These sheet-like deposits onlap the unconformity and were deposited prior to the three studied channel levee systems as shown in Figure 6.16. Thus, there is no evidence of HARP deposition between the LCLS and MCLS (Figs. 6.7 and 6.9). Therefore, the initiation of the MCLS apparently took place with the incision of a basal erosive channel. Conversely, earlier studies using ODP Leg 155 in

Amazon Fan data described the initiation of the channel-levee system as always occurring via avulsion of a parent channel, followed by sand inundation and deposition sheet-like deposits in adjacent unconfined areas (Flood et al., 1995; Lopez, 2001; Normark et al., 1997; Pirmez et al., 1997). The direct establishment of channelized turbidity currents is a possible alternative to the deposition of sheet-like deposits (HARPs) for the initiation of the turbidite system on the submarine slope. Here, it is interpreted that the incision of the channel that initiated the MCLS, in its downstream segment, was due to avulsion forced by the development of the LCLS.

The orientation of the erosive base is thought to have dictated the direction of the channel-levee system. In cross section, the transition from erosive to aggradational is roughly marked by the passage from a basal large-scale channel cut to an upward constructive channel-levee (Figs. 6.16). The aggradational channel-levee, however, can start to develop inside the limits of the erosive incision. From the basal to the top horizon slice across the MCLS, the transition point between the single and multi-thread channel planforms migrates downstream. This implies that there is a downstream migration of the agradational channel-levee over the basal erosive channel with time (Fig. 6.23). The slight downstream downlap of the channel fill (Fig. 6.17) and the downstream downlap of the levee reflections (Fig. 6.19) also indicate a downstream development of the channel-levee. Thus a suite of related features can be recognized which are indicative of this style of channel-levee development. An interesting idea to pursue is that recognition of any of these features might allow prediction of the others.

6.3.5 Avulsion of MCLS

Contrasting with the transition from LCLS to MCLS deposits which amalgamated without intervals of other types of deposition in the transition from the MCLS to the younger UCLC sheet-like HARPs occur similar to those already described in the literature of the Amazon Fan (Lopez, 2001; Pirmez et al., 1997) and others submarine fans, e.g., Zaire Fan (Droz et al., 2003). These HARPs have been described as product of avulsion of the channel where the flow becomes unconfined and loses its competence, depositing sheet-like sand deposits (Flood et al., 1995; Lopez, 2001;

Normark et al., 1997; Pirmez et al., 1997). In the study case, the HARPs occur onlapping outer limb of the levee in the upstream segment and onlapping/covering the erosive surface in the downstream segment (Fig. 6.24). The possible point of channel avulsion and possible source of the sand inundation that formed the HARPs is upstream toward S/SW, but outside the seismic survey limits, as suggested by the HARPs reflections that are dipping toward NE (Fig.6.24). Further possible evidence of upstream avulsion is the occurrence of a mass transport deposit (MTD) immeditately underneath the HARPs (Fig 6.24). This MTD is tongue-shaped in plan-view and flanks the MCLS. It shows internal structures with NE vergence, which suggests that the MTD slumping may have been from S/SW toward N/NE. Therefore, it is inferred that the MTD may be the result of an upstream levee collapse which led to the channel avulsion and sand inundation forming the HARPs (Fig.6.25). This levee collapse is suggested to have been to the South, upstream and outside the seismic survey area.

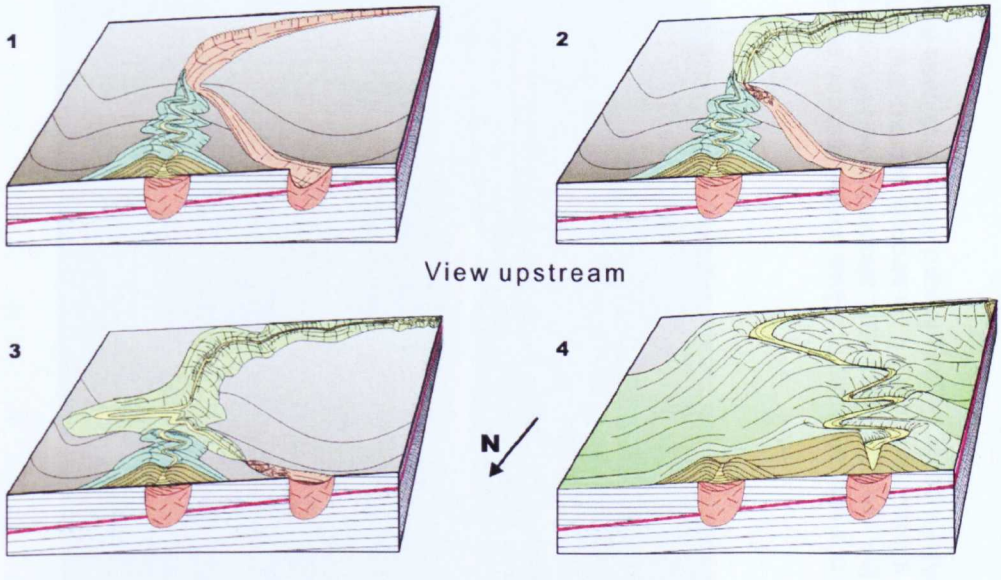

Figure 6-23 - Block diagrams summarizing the evolution of the Middle Channel-Levee System. 1 – After aggradation of the LCLS and further avulsion of the parent channel, incision of the downstream segment of the LCLS. 2 to 4 - The erosive channel started to evolve to a channel-levee system with the transition point between single and multi-thread form migrating downstream.

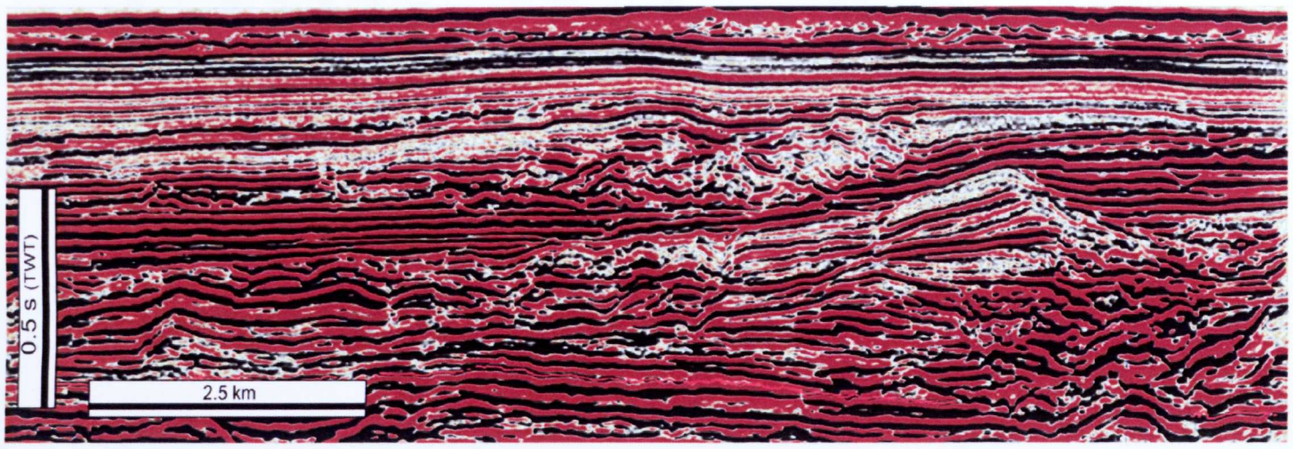

A B

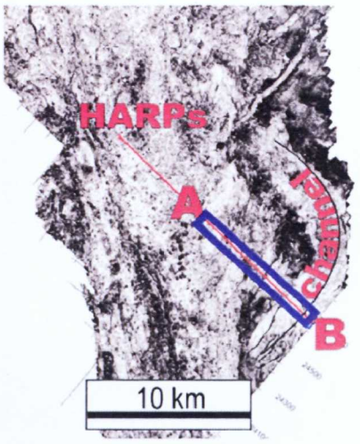

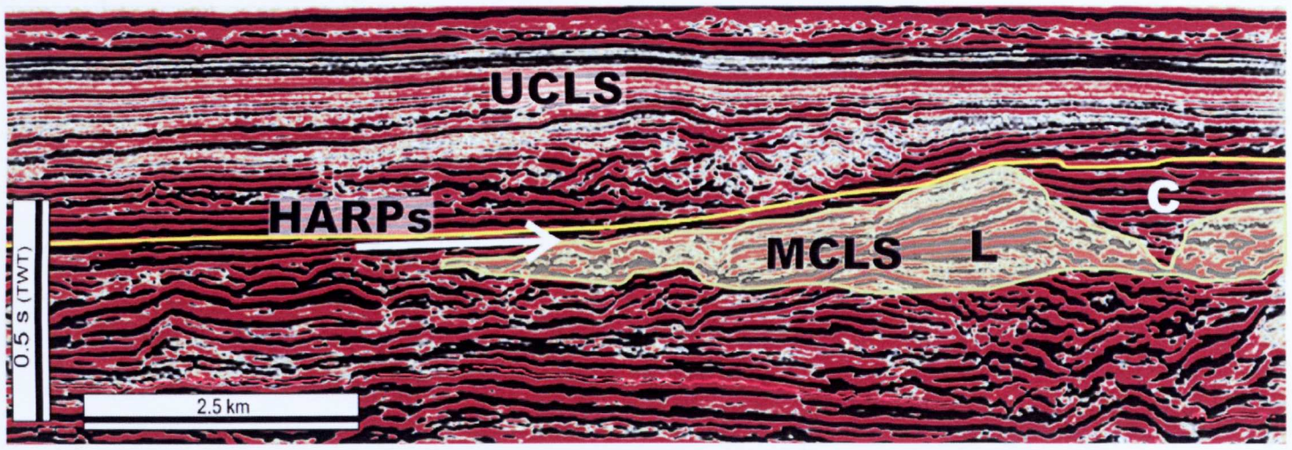

N

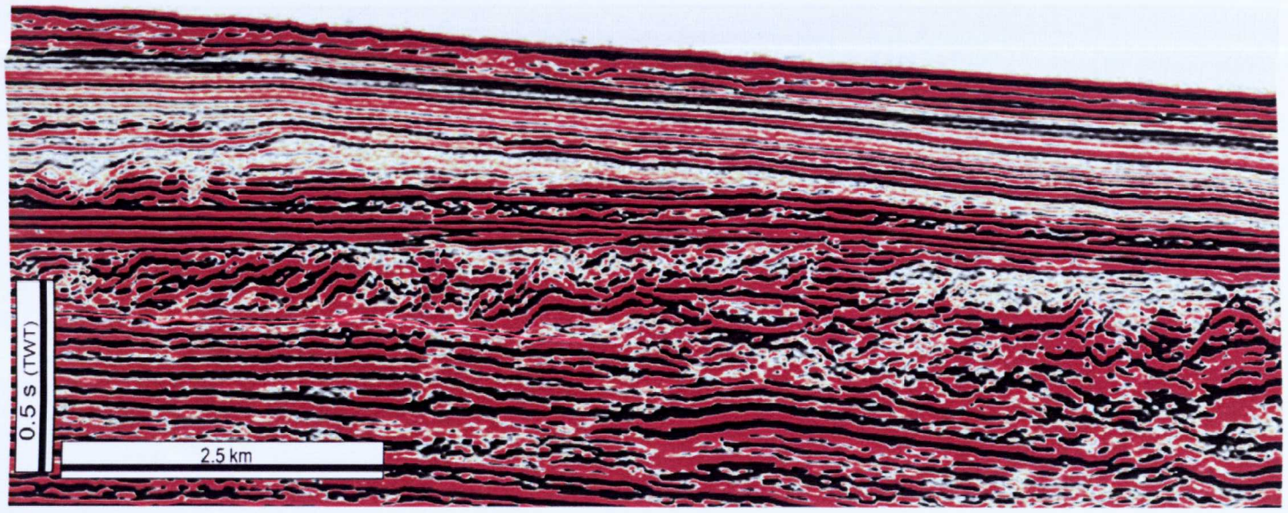

C D

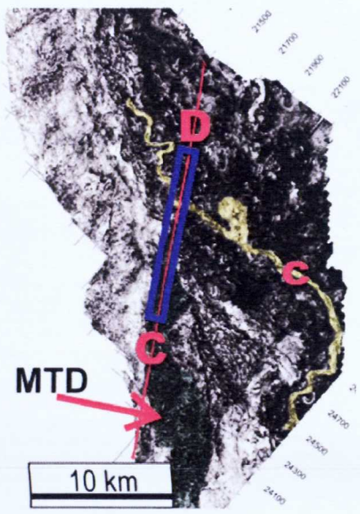

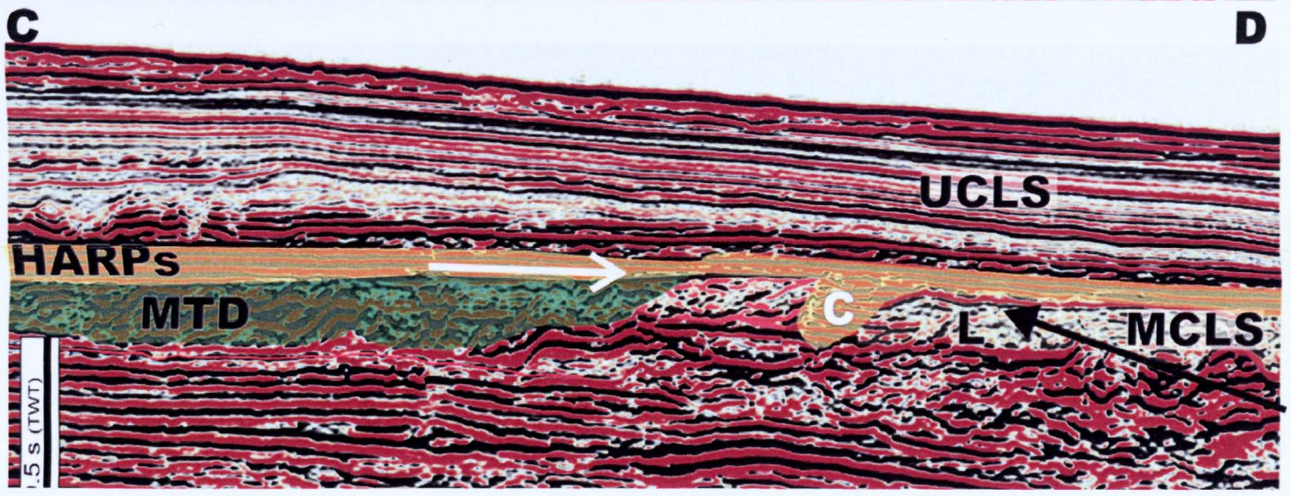

levee erosion

Figure 6-24 – Two pairs of interpreted and non-interpreted sections across the channel in the upstream and downstream segments of the MCLS. Section AB, located in the upstream segment, shows the HARPs onlapping the base of the external levee limb and also the spill out of the channel fill. Section CD shows top of the MCLS strongly eroded, the MTD flanking the MCLS and the HARPs onlapping the top of the MTD and the MCLS. Notice the HARPs gently dipping toward N/NE. The base map of the section CD shows the MTD alongated from South (upstream) to North (downstream).

The avulsion of the MCLS and associated deposition of what are interpreted to be sand rich HARPs as well as the event of levee collapse and extensive erosion of the downstream segment of the MCLS (described in section 6.3.3) indicate probable peaks in high magnitude (catastrophic) flows that triggered the avulsion (Pirmez and Flood, 1995; Pirmez et al., 1997). At least when associated with the HARPs, these peak flows are thought likely to have been sand-rich and, therefore, to have deposited in a sand sheet.

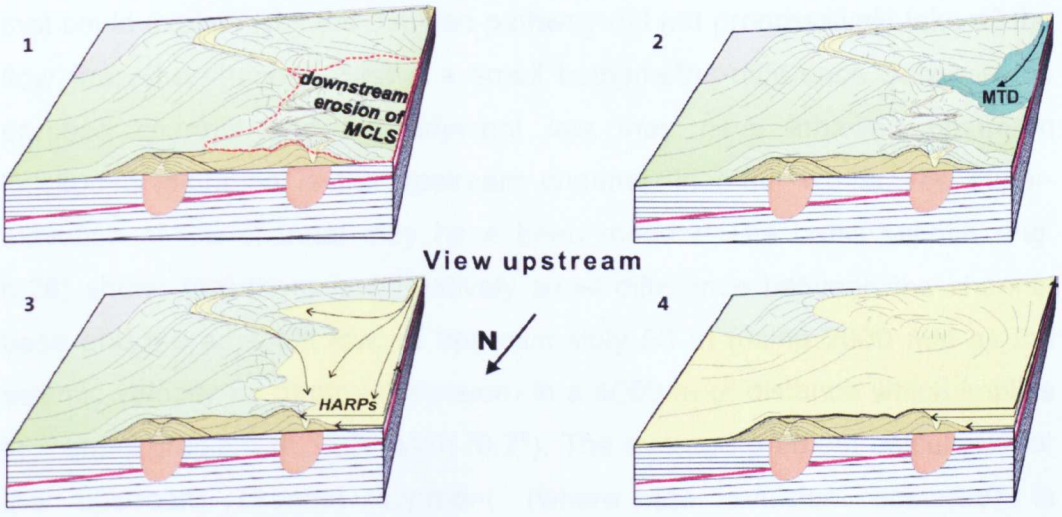

Figure 6-25 - Block diagrams summarizing part of the evolution of the Middle Channel-Levee System. 1 – Levee collapse and pervasive erosion of the downstream segment of the MCLS. 2 – Upstream levee collapse and slumping of MTD. 3 and 4 – Sand inundation and HARPs formation.

6.3.6 Stable bifurcation: channel fill and HARPs formation

The channel fill in the upstream segment of the MCLS appears also to spill out of the channel and contributes to the formation of adjacent HARPS (Fig. 6.24). This relationship implies that at least some of the HARPs intervals, from the base up to the continuous reflection that covers the top of the channel over the levees, and into the HARPs, formed simultaneously to the channel fill. It follows that HARP deposition did not occur due to complete channel avulsion. The simultaneous deposition of channel fill and HARPs is thought to have occurred via a partial avulsion of the channel, leading to a flow bifurcation (Fig. 6.25). This would reduce the flow efficiency of each branch of flow and promote the deposition both of the channel fill and the

sand inundation, forming HARPs in the adjacent low between the MCLS and the paleoslope.

The avulsion and complete abandonment of the channel would happen if, after the levee break-through, the subsequent flows gradually escape from a perched channel through the levee aperture such that a nickpoint gradually migrates upstream, capturing the flow entirely.

Synchronous deposition of the channel fill and the HARPs implies the development of a stable flow bifurcation. Two possible causes are suggested that could explain why the avulsed pathway did not progressively take all the flow from the channel. Firstly, a small bathymetric difference between the perched channel and the adjacent low may have inhibited upstream knickpoint migration in the upstream channel. In other words, the super-elevation of the channel may have been modest. The cross section (Fig. 6.26) shows that there is a relatively small difference between the channel base and the adjacent low, of approximately 50 m (using 2000 m/s as the seismic velocity for depth conversion) in a 4000 m of distance which implies in a small gradient of 12.5 m/km (0.7°). The average gradient calculated for the upstream channel segment (where the avulsion occurred) is approximately 9.5 m/km (0.5°), on the same basis. Taking into account that the gradient from the channel to the adjacent low measured here is not exactly the gradient of the point of avulsion because it is upstream and outside the area of seismic coverage, the calculation can, nevertheless, give a rough estimative. Therefore, the gradient difference between the channel thalweg and the potential avulsed pathway is at least 3 m/km (0.2°), which is quite low in comparison with the gradients measured in the Late Pleistocene of the Amazon Fan by Pirmez and Flood (1995) (Tab. 6.3). These authors estimated the gradient of the parent channel and calculated the gradients from the tops of the parent channel thalwegs to the bases of avulsed channels. The gradient of the potential avulsion course in the study area is only 1.3 times bigger than the channel gradient whereas the in the channels of the Late Pleistocene of the Amazon Fan it can range approximately from 3.5 to 8 times the gradient of the parent channel.

Secondly, an inner bend avulsion may not have experienced the same loss of flux as an equivalent outer-bend avulsion due to centripetal effects.

However, the sinuous form of the channel at the point of avulsion is difficult to constrain in this case because the possible levee collapse occurred outside the area of seismic data coverage. Therefore, such a possible contributory mechanism is speculative, in this case.

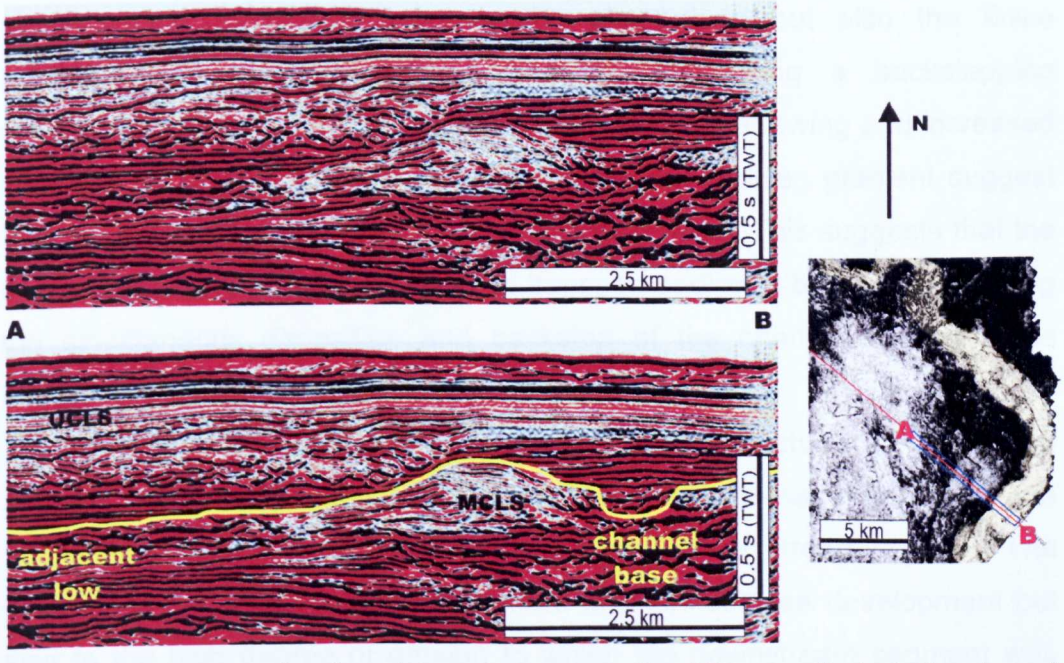

Figure 6-26 – Interpreted and non-interpreted cross section AB perpendicular to the channel axis in the MCLS. The section shows the height difference between the channel base and the adjacent low of approximately 50 m in 4000 m distance (very small gradient).

Table 6-3 – Upper and middle avulsions in the Late Pleistocene of Amazon Fan (adapted from Kolla)

Avulsion	Pre-avulsion Channel Gradient	Pre-avulsion sinuosity	Estimated gradient of the avulsed channel at the time of avulsion
Aqua	6.5 m/km (Purple)	1.3 (Purple)	24-36 m/km (Purple top to Aqua base)
Brown	4 m/km (Aqua)	2.3 (Aqua)	15-18 m/km (Aqua top to Brown base)
IF	1.5 m/km (Brown)	3.0 (Brown)	8.5-12 m/km (Brown base to IF base)

6.4 *Upstream vs. Downstream channel-levee development*

Although the seismic data coverage over the LCLS system is relatively poor, important considerations can be raised about its architectural elements and

their processes of formation. Thus, the whole LCLS pinches out upstream as the system thickness reduces significantly from downstream to upstream (Fig. 6.7). The sets of prograding reflections of channel fill that are onlapping the thalweg characterize back fill of the channel. In addition, the reflections of the channel fill are in continuity with the levee reflections indicating simultaneous deposition. Not only the channel fill but also the levee reflections are onlapping the paleoslope, suggesting a backstepping development. Finally, an upward pattern of channel narrowing and increased sinuosity as well as a significant reduction in the thalweg gradient suggest that the system became muddier and smaller upward. This suggests that the flows gradually reduced their ability to transport sediment basinward, causing the simultaneous deposition and backstep of the channel fill and levee buildup.

On the other hand, the MCLS presents architectural elements and possibly formation processes that are distinct from those exhibited by the LCLS. The MCLS is thicker in its upstream than in downstream segment. The differences not only relate to the pattern of channel-levee development but also to the high degree of erosion to which the downstream segment was submitted. Additionally, the downlap pattern of the levee reflections suggests that the system pinches out downstream (Fig. 6.19). Contrasting with the LCLS, the MCLS presents a downstream pattern of accretion with the channel widening and becoming less sinuous upward. This suggests that the system became more efficient and possibly sandier. Therefore, the MCLS has a more complex evolution than the lower system as it presents two different processes of channel fill: simultaneously with the levee buildup in its lower portion and after some erosion in its upper portion.

It is inferred that the way the study channels attempted to evolve towards an equilibrium profile during their evolution may have determined their architectural style and thus their distinct upstream and downstream patterns of development. The evaluation of the controls on the development of these two distinct channel-levee architectures should take into account differences and changes in flow parameters and also in the paleo-topography of the slope. Therefore, models for flow efficiency and equilibrium profile controls on each of the two architecture models are described below. Finally,

the auto-cyclic vs. allo-cyclic nature of the controls on channel-levee development can be discussed.

6.5 *Equilibrium profile controls*

6.5.1 Upstream development of channel-levee systems

Two models could account for the upstream development style of channel-levee aggradation on the slope. The system may have aggraded filling a bathymetric low inherited from previous slope deposits or may have been induced to aggrade due to changes in the equilibrium profile along the channel thalweg.

In the first case, the system aggrades and fills the topographic low, filling the accommodation space. The channel profile tends to reach the equilibrium gradient by eroding upstream and by bi-directional aggradation in its downstream segment (Figs. 6.27 and 6.28). During aggradation, the system could onlap upstream and downlap downstream filling the accommodation space. The putative downstream downlaps, however, were not sampled by the study seismic data because the seismic data only clips the LCLS.

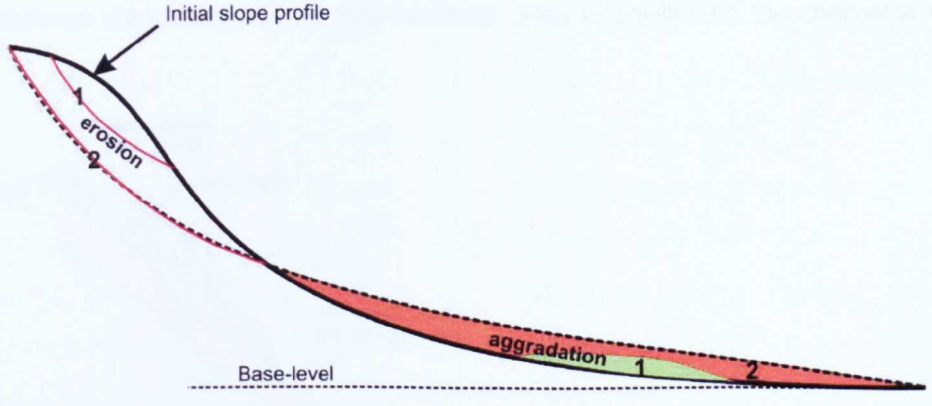

Figure 6-27 – Relationship between of submarine slope profile and equilibrium profile (adapted from Kneller 2003).

In the second case, although most of the slope deformation of the area took place before the establishment of the study channel-levee systems as described in Chapter 5, some later small scale uplifts could have disrupted the equilibrium profile during system development. As the channel-levee systems are located downslope from the thrust-fold belt that affected the

slope of Amazon Fan, an uplift of the upstream anticline would move the equilibrium profile upward, increasing the downstream accommodation space. The accommodation increment could induce the channel-levee to aggrade, onlapping the paleoslope (Fig. 6.29).

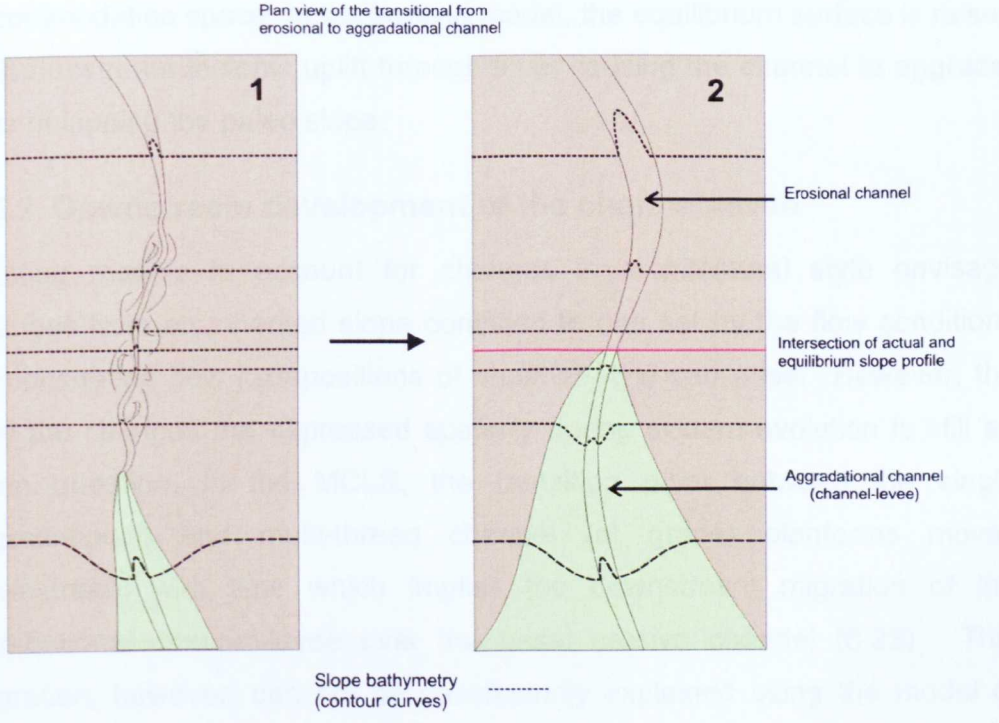

Figure 6-28 – Plan view of the upstream development of the channel-levee. Notice that in the area between the erosive and the aggradational, close to equilibrium, the channel is multi-thread.

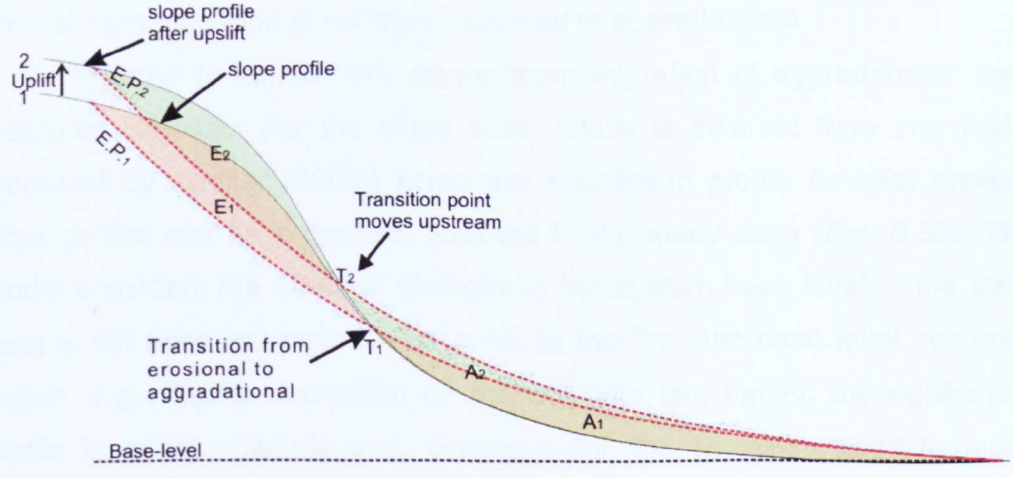

Figure 6-29 – Schematic diagram of equilibrium profile adapted from Kneller (2003) for the study case. Changes in equilibrium profile due to upstream uplift. There are two stages of slope evolution before and after upstream uplift: the initial slope profile 1 and equilibrium profile (E.P.1) with potential erosion E_1 (orange) and accommodation A_1 (orange); and the post-uplift slope profile 2 and equilibrium profile (E.P.2) with potential erosion E_2 (green) and accommodation A_2 (green). Notice that, after the uplift, the transition point migrates upstream, from T_1 to T_2.

Thus in summary, two models can account for the upstream development of the LCLS characterized by the onlap pattern of the seismic reflections. In the first model, the equilibrium profile is not affected by the external factors and the channel-levee simply aggrades to infill the accommodation space. In the second model, the equilibrium surface is raised by an upstream tectonic uplift through time, causing the channel to aggrade, thus onlapping the paleo slope.

6.5.2 Downstream development of the channel-levee

Existing models to account for changes in architectural style envisage changes from an inherited slope condition to one set by the flow conditions demonstrating how juxtapositions of channel style can arise. However, the way the changes are expressed spatially during system evolution is still an open question. In the MCLS, the transition point between the single (agradational) and multi-thread channel (at grade) planforms moves downstream with time which implies the downstream migration of the agradational channel-levee over the basal erosive channel (6.23). This migration, however, can not be satisfactorily explained using the model of equilibrium profile proposed by Kneller (2003) because his model is based in the occurrence of an upslope area of potential erosion passing into a downslope area with accommodation space and, in the study system, the downstream migration is not from incisional to aggradational.

In order to explain this downstream migration of aggradational over incisional channels (for the study case, which is different from the model proposed by Kneller (2003)) using the equilibrium profile concept another slope profile can be proposed, adapted to the study case (Fig. 6.30). The model considers the effect of changes in the system base level. If the base level is not fixed two possibilities arise. In the first, the base level becomes higher, e.g., due to deposition on the downdip fan, forcing the equilibrium profile to move upwards and, consequently, the transition point to move downstream (Fig. 6.30). In the second, the base level can become lower, e.g., due to downstream avulsion or erosion of the downdip fan with bypass, forcing the equilibrium profile to move downwards and, consequently, the transition point to move upstream (Fig. 6.30). In the case where the base

level did not migrate, an upstream uplift of the anticlines, forcing the equilibrium profile to move upwards, would also create accommodation and cause the downward migration of the transition point (Fig. 6.31).

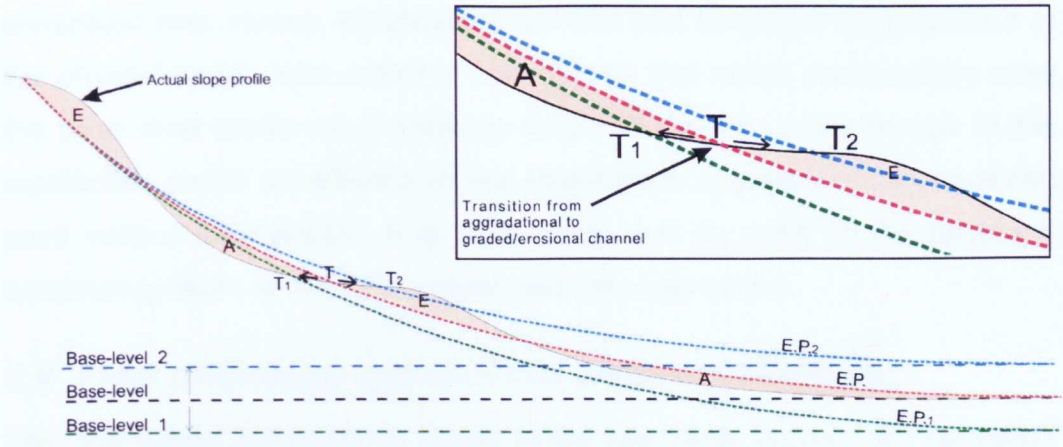

Figure 6-30 - Schematic diagram of equilibrium profile adapted from Kneller (2003) for the study case. Changes in equilibrium profile are due to changes in base level. If the base level moves downward, the equilibrium profile (E.P.) also moves downward (E.P.1) forcing the transition point between aggradational and erosive channel to migrate upstream (from T to T_1). If the base level moves upward, the equilibrium profile (E.P.) moves upward (E.P.2) forcing the transition point between aggradational and erosive channel to migrate downstream (from T to T_2). In this diagram, the areas between the actual slope profile and the equilibrium profile (highlighted in orange) represents accommodation (A) and potential erosion (E).

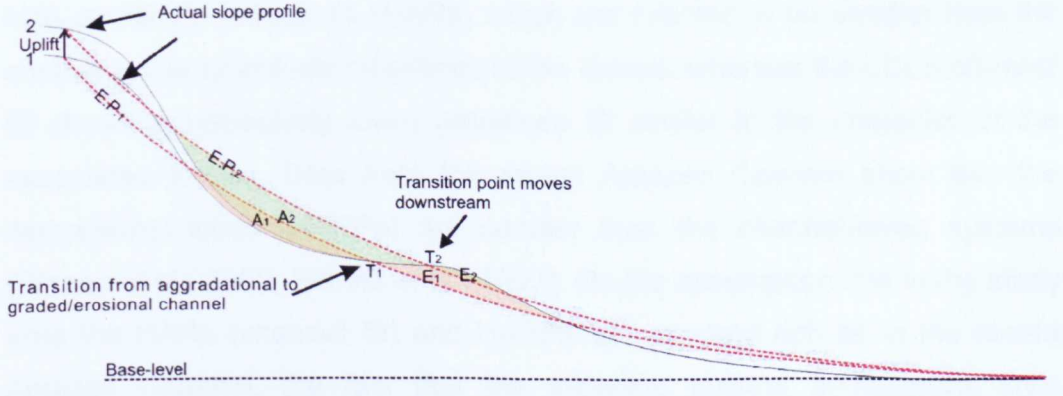

Figure 6-31 - Schematic diagram of equilibrium profile adapted from Kneller (2003) for the study case. There is change in the equilibrium (E.P.1) profile due to upstream uplift. The equilibrium profile curve also moves upward causing a downstream migration of the transition point from T1 to T2. In the diagram, A is accommodation and E is potential erosion.

Of the three models described above, only two would explain the downstream migration of the transition point between aggradational and erosional styles: i.e. base level rise and upstream uplift. However, it is worth

mentioning that larger and clay rich fans like the Amazon, Mississipi or Zaire tend to develop channel-mouth lobe complexes that are very small compared to the whole fan (Jegou et al., 2008). They are very far from the coast, in very deep water, occurring on relatively low gradients compared to small and sand dominated fans. Hence, significant deposition and consequent aggradation of the channel-mouth lobe complex to a degree that would meaningfully raise the base level would not commonly occur. Therefore, if the change in the equilibrium profile contributed to the longitudinal migration of the transition point toward downstream, it is most likely that an uplift of the upstream anticlines present on the upper slope was the main cause.

6.6 Flow properties and channel-levee development

The contrasting architectures styles in the two study cases, i.e., narrowing and becoming more sinuous upward in the LCLS and widening and becoming less sinuous upward in the MCLS, could represent opposite tendencies in changes in turbidite current character through time. Indeed, the widening-upward system is interpreted to be associated with an increase in flow sand/mud ratio upward whereas the narrowing upward system is thought to be associated with a decrease. Thus, the MCLS channel fill consists of high amplitude reflections (HARs) which are inferred to be sandier than the enclosing low amplitude reflections of the levees, whereas the LCLS channel fill shows progressively lower amplitude fill similar to the character of the associated levees. Data from the recent Amazon Channel show that the depositional lobes (HARPs) are sandier than the channel-levee systems (Pirmez et al., 2000; Pirmez et al., 1997). On the assumption that in the study area the HARs (channel fill) and HARPs are as sand rich as in the recent Amazon Channel, the fact that the widening upward architectural style presents volumetrically more channel fill toward the top and also ended up with the spill out of the channel forming part of the HARPs indicates that the flows that built this channel-levee system (MCLS) evolved to become sandier with time. In contrast, it follows that the flows which built up the narrowing upward LCLS most likely became gradually muddier with time. The sinuosity evolution with time in both systems also suggests changes in sand/mud ratio of the turbidity flow. Thus, the upward reduction of sinuosity indicates an

increase in sand/mud ratio in the flow whereas the upward increase of sinuosity indicates a decrease. The literature of submarine channels is rich in examples of high sinuousity mud rich channels like the Amazon, Indus and Zaire fans and the Niger Delta (Babonneau et al., 2002; Deptuck et al., 2003; Droz et al., 1996; Hiscott et al., 1997; Kolla and Coumes, 1987), also with some examples of low sinuous sand rich channels like Northwest Atlantic Mid-Ocean Channel (NAMOC) (Klaucke et al., 1997).

In conclusion, successive turbidite currents are thought to have evolved differently during the development of these two channel-levee architectures. It remains challenging, however, to make a comprehensive link between flow character and architectural style. Changes in flow properties such as flow size, density and/or grain size of suspended sediment may have caused erosion, bypassing or deposition, depending on the position of the actual channel profile in relation to the equilibrium profile (Kneller, 2003). These processes may determine the erosive or aggradational nature of the submarine channel character.

Erosion, bypass and deposition are associated with the ability of the flow to transport sand basinward, which is a property of flow efficiency (Al Jaaidi et al., 2004; Mutti, 1992). The controls on the efficiency of turbidity flows have been described in the literature (Al Jaaidi et al., 2004; Bouma, 2000; Gladstone et al., 1998; Mutti, 1992; Mutti and Normark, 1987; Normark, 1978; Normark and Piper, 1991) the main controls considered to be the grain-size composition of the suspended sediment load and the flow volume (Al Jaaidi et al., 2004; Mutti, 1992).

In order to analyze the possible flow characteristics during the evolution of each of the study channel-levee, a conceptual model is built incorporating the relative grain size variation of the suspended sediment, the flow magnitude and the resultant flow efficiency (Fig. 6.32). This analysis is qualitative and based on relative changes of these parameters deduced from the architecture styles identified in the interpretation of seismic data. The green arrow illustrates a possible evolution of the turbidite flows with time in the channel of the LCLS. From the initial position 1 to final position 2, the flows passing along the channel of the LCLS may have become muddier but

smaller with time, such that the flow efficiency was reducing. The increasing mud content of the flow should, by itself, result in increased flow efficiency.

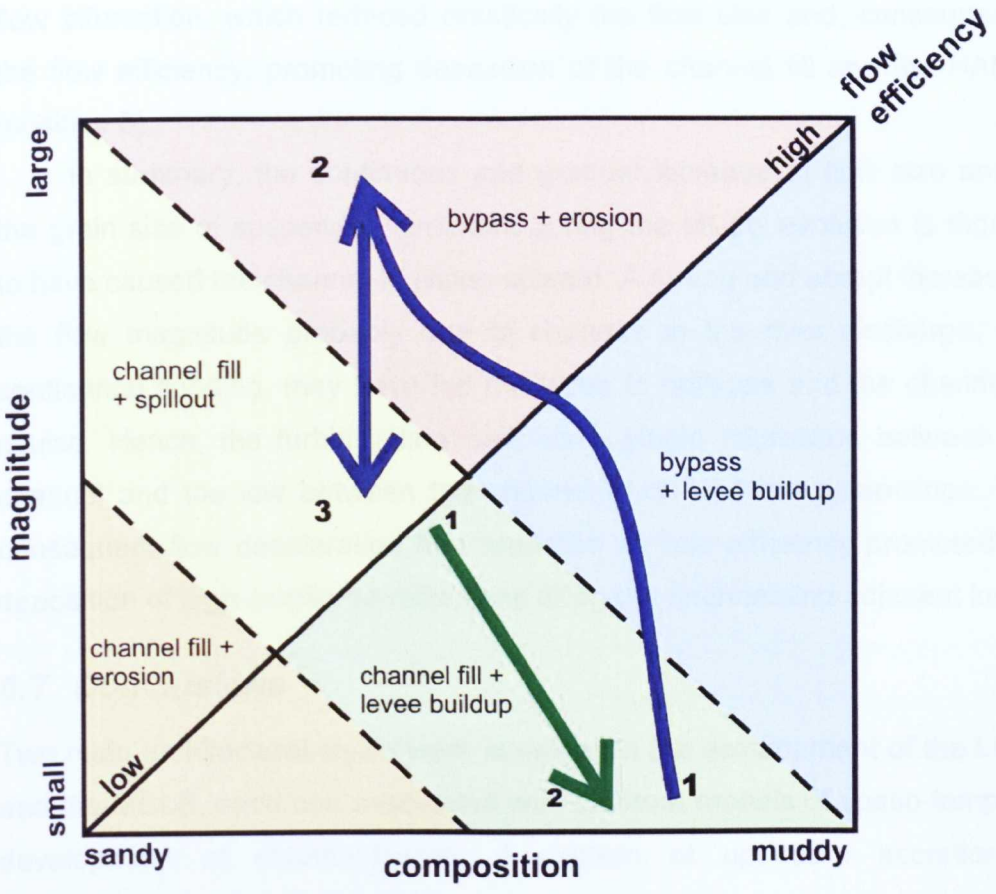

Figure 6-32 – Conceptual model illustrating possible evolution of the of the turbidite currents along the evolution of the LCLS (green arrow) and MCLS (blue arrow), taking in account the flow magnitude, the grain size of the suspended sediment and the corresponding flow efficiency.

The associated reduction in magnitude must be invoked to explain the inferred reduction in flow efficiency. On the other hand, the MCLS presents a much more complex flow development during system evolution (dark blue arrow). From an inferred initial position 1 to position 2, the flows passing along the channel of the MCLS become sandier and larger with time. As the flows become larger and sandier, it is thought that the channel-levee evolved underwent four stages of development. It started from the simultaneous deposition of channel fill and levee buildup (green area) which corresponds to the lower portion of the MCLS and evolved to a possible long duration stage of levee buildup and sand bypass (blue area). Later, larger and sandier flows eroded the internal levee walls in the upstream segment and the upper

part the downstream segment of the MCLS up to position 2 after which an upstream avulsion of the channel occured with the development of a stable flow bifurcation, which reduced drastically the flow size and, consequently, the flow efficiency, promoting deposition of the channel fill and the HARPs (position 3).

In summary, the continuous and gradual increase of flow size and of the grain size of suspended sediment during the MCLS evolution is thought to have caused the channel to widen upward. A strong and abrupt increase in the flow magnitude probably due to changes in the river discharge, e.g. continental flooding, may have led the levee to collapse and the channel to avulse. Hence, the turbidity flow split via a stable bifurcation between the channel and the low between the channel-levee and the paleo-slope. The consequent flow deceleration and reduction of flow efficiency promoted the deposition of high amplitude reflections filling the channel and adjacent lows.

6.7 Conclusions

Two main architectural styles were identified in the development of the LCLS and the MCLS, each one associated with different models of spatio-temporal development of channel-levees. A pattern of upstream accretion is associated with the channel narrowing and becoming more sinuous upward, with a continuous evolutionary history until channel avulsion. The apparent back stepping of the system due to the onlap of the channel and levee reflections can be related either to passive infill of an inherited topographic low or to a creation of accommodation due to upstream uplift resulting from slope tectonics.

The downstream accretion style of channel-levee development is associated with the channel widening and becoming less sinuous upward. In the case studied here, a more complex evolutionary history can be inferred than for the upstream-accretion case. This evolution involves more stages, e.g., internal erosion of the internal levee limbs, later channel filling and deposition of HARPs in the paleo-bathymetric low adjacent to the channel-levee system. The apparent fore-stepping of the system was evidenced by the downstream migration of the transition point between multi-thread and single-thread channel planforms and the downlap of channel and levee

reflections. This migration could have occurred due to accommodation generated by upstream uplift.

There are a suite of features that can be recognized in seismic and can be used to predict each of the two styles of channel-levee development (upstream and downstream accretion). The slope onlap of reflections associated with possible narrowing and more sinuous upward architecture may correspond to the style of upstream channel-levee accretion. The slope downlap of reflections of both levee and channel fill associated with widening and becoming less sinuous upward may correspond to the style of downstream channel-levee accretion.

The analysis of the probable flow magnitude and the grain-size of the suspended sediment suggests that the sequences of turbidity currents responsible for building up the two different architectures had contrasting styles of evolution during the channel-levee growth. These different styles of flow evolution may explain the patterns of vertical deposit development (i.e. sandier vs. muddier development of each system) and also the occurrence of erosive events and the formation of HARPs. In the upstream accretion style of channel-levee development, the tubidite flows were interpreted as becoming gradually muddier and smaller, whereas in the downstream accretion style of channel-levee development, the flows were interpreted as becoming sandier and larger with time.

The two models have important consequence for prediction of sand prone areas (here interpreted to be represented by HARPs). Not all avulsions resulted in HARP formation or in the direct build-up of the next system (without the HARPs deposition at the base of the system). HARPs are thought to comprise sand-rich sheet deposits and thus require a parental sand rich flow. The levee breach interpreted to have caused the partial avulsion is thought to have been caused by a large flow. Therefore, the avulsion event and the deposition of a large volume of sand rich deposits (HARPs and the channel-fill) suggest a tendency of the turbidite flows to become larger and sandier with time in the evolutionary history of the MCLS. In the avulsion of the lower system where there was no HARP formation, the flow responsible for the channel avulsion was probably not sand rich, as suggested by the architecture of the avulsed channel immediately prior to

avulsion (which is narrowing and interpreted to be becoming muddier upward). The cause of avulsion in this case is thought to be an outsize muddy flow/s or spontaneous levee collapse. Instead of HARPs formation, the next system initiated with incisional channel development.

The changes in flow type during the evolution of the two distinct architectures can be attributed to both allocyclic and auto cyclic processes. In the case of the flows becoming muddier and smaller continuously with time (LCLS) at least three causes can be postulated. Firstly, an autocyclic gradual (progressive) upstream avulsion of the system could promote a gradual reduction of sediment flow in the channel. Secondly, an allocyclic increase in relative sea level could gradually trap and/or disperse the sediments brought by the river on the shelf until the complete abandonment of the turbidite slope system. Thirdly there could be allocyclic decrease of sediment discharge brought by the river due to changes in climate. In the second and third cases a later increase in the flow magnitude to produce misfit flow in late stage sinuous, narrow LCLS would be necessary to promote the avulsion of the system. Here relative sea level fall and/or the increase of sediment discharge by the Amazon River would be able to increase significantly the flow magnitude and consequently force the avulsion of the LCLS. The longitudinal transition point from erosional to aggradational channel style would be a likely place for avulsion because in this position the flow is inferred to be in a meta-stable equilibrium with the channel (which is close to the equilibrium profile).

In the case of the flows becoming sandier with time (MCLS) at least 2 causes can be postulated. Relative sea level fall with gradual increase in sediment flow in the channel or gradual increase in sediment discharge by the river could theoretically drive this evolution of flows on the slope channels until the channel avulsion. The mechanisms of flow evolution due to relative changes in sea level are not likely to have occurred in the study area. This is because each of the "levee-complexes" grouping the channel-levee systems in sets separated by maximum flooding surfaces (carbonate rich muds) are related to a single glacial period (Flood and Piper, 1997). Therefore, the flow evolution and avulsions of individual channel-levee systems might be related to auto-cyclic processes or to changes in the river discharges.

Finally, the mechanisms that may have driven development of these contrasting channel-levee architectures might have resulted due to the interaction between the style of accommodation space and the different styles of evolution of the flows on the slope. The channel can aggrade (downstream or upstream) simply to infill an inherited topographic low or an accommodation space created due to upstream uplift. A narrowing and more sinuous upward or a widening and less sinuous upward channel style would then develop depending on whether the flows became sandier or muddier with time.

7 CONTROLS ON PATTERNS OF CHANNEL DISTRIBUTION

Different patterns of channel distribution were identified on slope in the study area. The essentially erosive canyon-like channels that occur in the pre-unconformity interval (described previously in Chapter 5) appear to have different direction and controls on their distribution than the channel-levee systems on the post-unconformity interval above. Underneath the unconformity, the channels are oriented towards the NE and were apparently strongly affected during their evolution by growing anticlines. Above the unconformity, the channels are oriented towards the N/NW and appear to be relatively unaffected by slope tectonics. In detail, the post-unconformity channel-levee systems exhibit two styles of stacking pattern: a slope-oblique pattern, which results from a sequential upslope stacking after channel avulsion, and a sub-vertical stacking pattern.

These observations raise the question: what are the controls on channel dispersion and channel stacking pattern on slope? As turbidite channels cross the slope they are naturally susceptible to some control on their geometry and orientation due to the effect of contemporaneous bathymetry. Thus on many slope systems, salt or shale diapirism and fold and thrust belts associated with slope gravity tectonics create seafloor relief which may affect the channel geometries (Clark and Cartwright, 2009; Mayall et al., 2006; Mayall and Stewart, 2000; Morgan, 2004). The way these structures dictate the channel directions and stacking on slope is still, however an issue that requires deeper study.

The purpose of this chapter is to review the apparent controls on the different styles of submarine channels present in the 3D seismic data of the Amazon Fan. The reasons why the channels underneath the unconformity (basal interval) are dipping roughly in the same direction as the mean slope dip (NE) in the area and the channels above the unconformity are oblique to the mean slope dip will be discussed.

The post-unconformity channels are below the current sea floor and above the unconformity (Fig. 5.21); the unconformity can be considered a former

palaeoslope before which the development of the aggradational channel-levee systems took place. Both sea floor and unconformity dip towards the NE. The post-unconformity channels dispersing in a NW direction are, therefore oblique to these surfaces.

A post-depositional tilting of the surfaces could be considered to be a cause of this difference of dip directions between the channels and the slope and/or palaeoslope, as there is a thrust and fold belt upslope from the studied channels. Some considerations, however, militate against considering any post-depositional changes of the slope to be due to tectonic tilting. Firstly, as described in Chapter 5, the rate of deformation after the unconformity was eroded, was low. Secondly, all the three channel-levee systems are downslope from the anticlines in the study area and Figure 5.2b shows that at least the LCLS is relatively distant from the effect of uplift on these structures. The 2D seismic line also shows cross sections (SW-NE) through two extra channel levee-systems downslope from the LCLS, further from the influence of the upslope anticlines (Figs. 5.2b and 5.4). Thirdly, the fact that the two surfaces (sea floor and unconformity) which enclose the studied channels, dip in the same direction (NE) with similar dips (1.5° and 1.4°, respectively) reduces the chances that a post depositional tilting could have changed the main slope dip from towards NW to the current direction. Given these considerations it was not deemed necessary to pursue a backstripping analysis because the probability that a tilt on slope due to tectonic activity changed the main slope dip from the time of the deposition of the channels to the current slope dip is considered small.

7.1 Structural controls on development of erosional channels

The objective of this section is to evaluate the structural controls on the development of the erosive channels present in the basal interval (defined in Chapter 4 and described in Chapter 5) (Fig. 5.7).

Unlike the post-unconformity channel-levee systems, that were only slightly deformed by the slope tectonics, the pre-unconformity erosive channels divert and/or deflect, as defined by Clark and Cartwright (2009) (Fig. 2.53), from the palaeo-seafloor relief formed by the growth of the thrust-cored hangingwall anticlines. Some channels also cut through the anticlines (Fig. 5.15, channel 2).

Incised channels are the only channel type in the pre-unconformity interval whereas in the post-unconformity interval erosive channels evolved upwards to become aggradational channel-levee systems.

The two-way-time maps of the base and the top of the basal interval (Fig. 5.7) show the anticlines A, B, C and D. Anticline C only slightly affects these two horizons. The upslope-most anticline (E) shown in the cross section is not shown on the maps because mapping of these horizons across the anticline could not be achieved. The yellow crescent shaped features are two sections of the same erosive channel (Chapter 2). In cross section this channel seems to be affected by growing anticlines (see below).

There is no apparent difference between the amplitude of the channel fill and the enclosing sediments present in the basal interval (Fig. 5.7). However, the channel fill reflections can be more irregular than the monotonous subparallel reflections of the background. Bearing this in mind, two horizon slices showing RMS coherence in a time interval of 20 ms were extracted parallel to the base of the basal interval in order to cut across the channels and show their planform distribution (Fig. 7.1). Channel 2 exhibits a different planform position in slice (1), which is centred 100 ms above the base of the basal interval, and in slice (2), 200 ms above the base of the basal interval. Channel 1 appears to have been disrupted by the tear fault and shows an approximate dextral offset of 2 km (Fig. 7.1). The cross section (Fig. 7.2) shows the channels 2a, 2b and channel 3. Channel 2a occurs cutting across only the basal layers of the interval whereas channels 2b and 3 cut essentially the whole interval. This indicates that channels 2b and 3 are younger than 2a.

The isochron map of the basal interval shows that there is thinner sediment cover on the folds crests, mainly on the top of anticlines A and C (Fig. 5.15). The cold colours (green-blue) in the map indicate shorter two-way-travel time, indicating smaller sediment thickness than the hot colours (red-orange). The thicker elongate features correspond to the channels identified in the RMS coherence horizon slices (Fig. 7.1). The green/blue colours represent the thinner sediment packages coincident to the bathymetric highs generated by the growing anticlines and transpression on the bend of the tear fault (Fig. 5.15). This thin sediment packages on the anticline crests suggests that the anticlines

were growing structures with uplift rates lower than the sedimentation rates during the deposition of the basal interval.

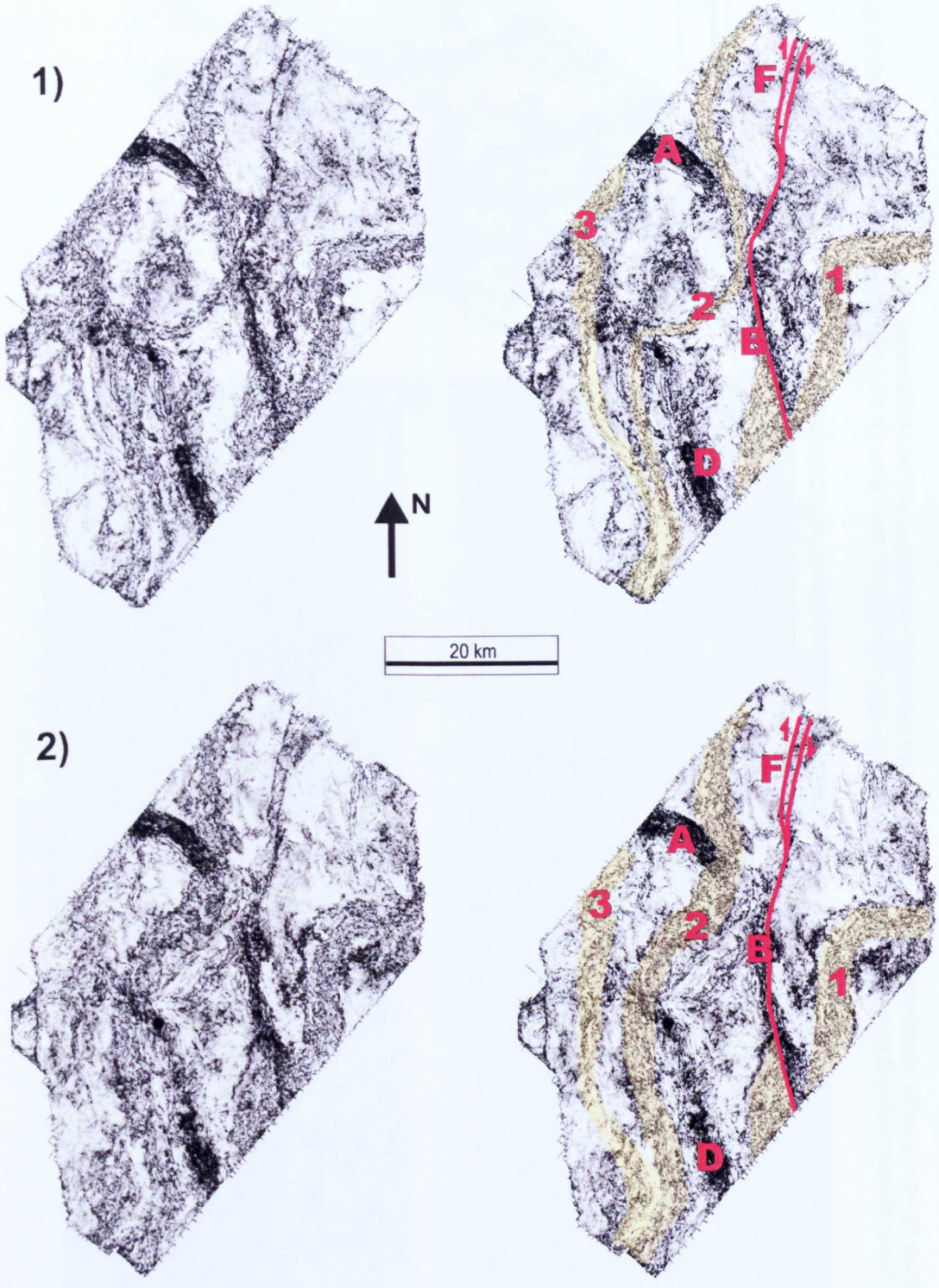

Figure 7-1– Two horizon slices (1 and 2) extracting RMS coherence in an interval of 10 ms parallel to the base of the basal interval (non-interpreted and interpreted). There are at least 3 erosive channels, 1, 2 and 3 roughly dipping toward N/NE. The anticlines A, B and D identified in Figure 5.15 are highlighted and also the tear fault (F).

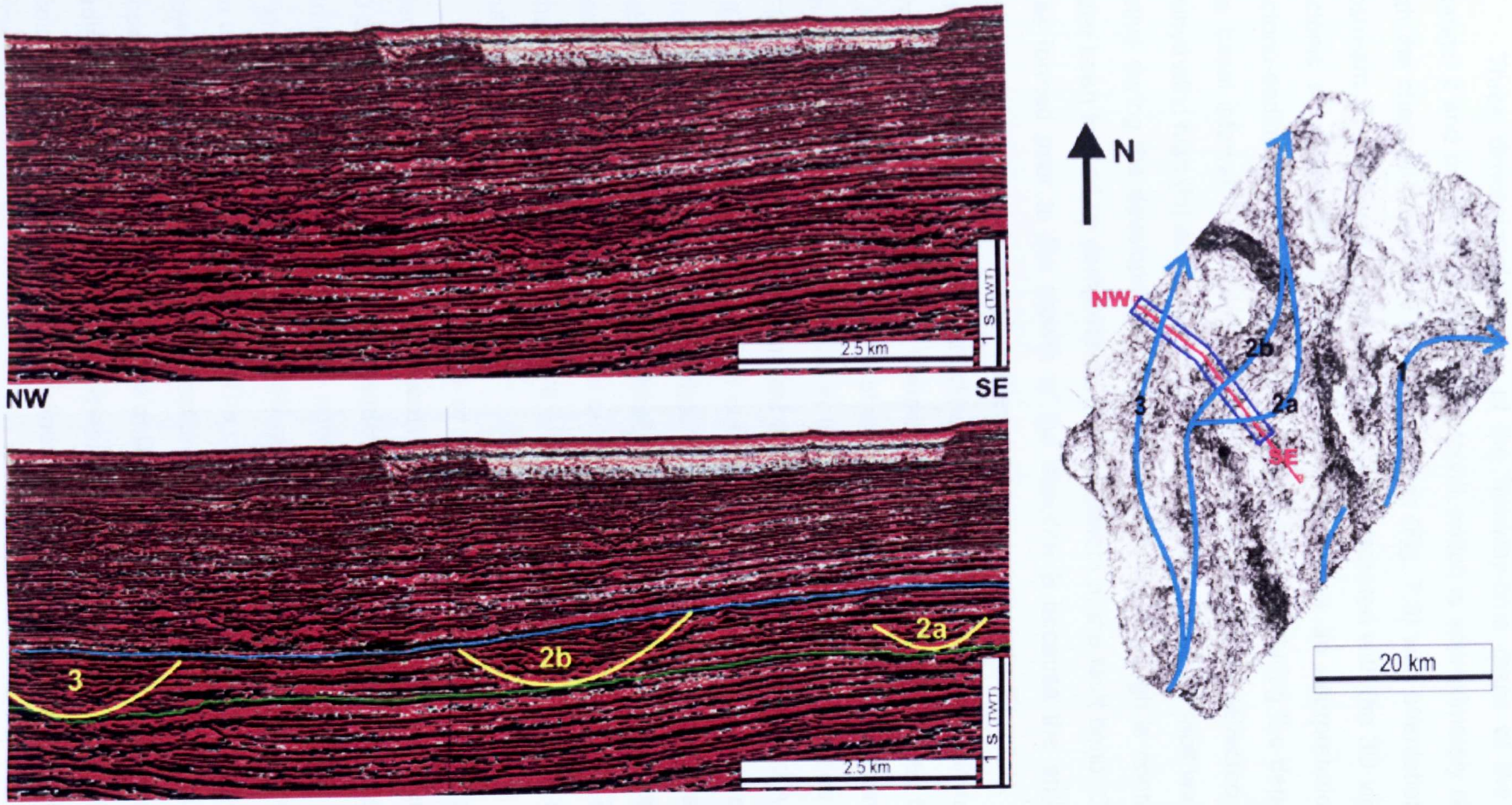

Figure 7-2 – Cross section showing three channels in the Basal Interval. Channel 2a is older than 2b as it cuts through only the basal layers of the interval whereas channel 2b cuts through almost the whole interval, as does channel 3. Interpreted and non-interpreted.

Three dimensional images of the two-way-time maps of the base of channel 2 and the base of the basal interval, which is approximately coincident with the channel base, were plotted together (Fig. 7.3) with orientation looking upstream. The analysis of the isochron map integrated with the 3D view of the tectonic structures and the erosive channels allows an interpretation of the tectono-sedimentary sequence of events that occurred during the deposition of the basal interval. Channel 1 and channel 2 appear to be deflected from the bathymetric high (H) on the tear fault bend, indicating that the fault was already active during the development of these channels as this high is considered to have been formed by compression (transpression) at the fault bend. Channel 1 was formed prior to the growth of the anticline B because the anticline lies between the downstream and upstream channel segments (Fig. 7.1). Channel 2a seems to be deflected by anticline B towards the north and also uplifted by anticline C. Channel 2b occurs downslope from 2a and is not uplifted by C (Fig. 7.3.2). This indicates that growth of anticline C may have forced channel 2a to change its course to channel 2b in the segment between anticlines D and A (Fig. 7.3.2). Moreover, it implies that the growth of anticlines D and A occurred after C because channel 2, which cuts across D and A, was active during the growth of anticline C. The eventual growth of anticline D appears to have pushed later turbidite currents laterally towards the NW, forming channel 3. It seems that the development of the anticline A occurred only after the incision of channel 3, otherwise it would have blocked or deflected it, whereas channel 3 cuts across it.

In summary, the sequence of fold growth in the study area during the deposition of the basal interval seems to have occurred in the sequence: B, C, D and A. The channels show a tendency of lateral migration towards NW with time, apparently controlled by the sequence of anticline growth (Fig. 7.4). The Figure 7.2 shows the lateral channel migration from 2a to 3 toward the NW due to uplift of anticline C in the SE. The channel flow directions are approximately towards the N/NE but show deflection along their course due to the growing topographic barriers formed by the anticline structures. Where the channels are adjacent to the NW oriented anticlines, they are deflected towards N/NW to the point that they cut through the anticlines and then are redirected towards the NE (Fig. 7.1).

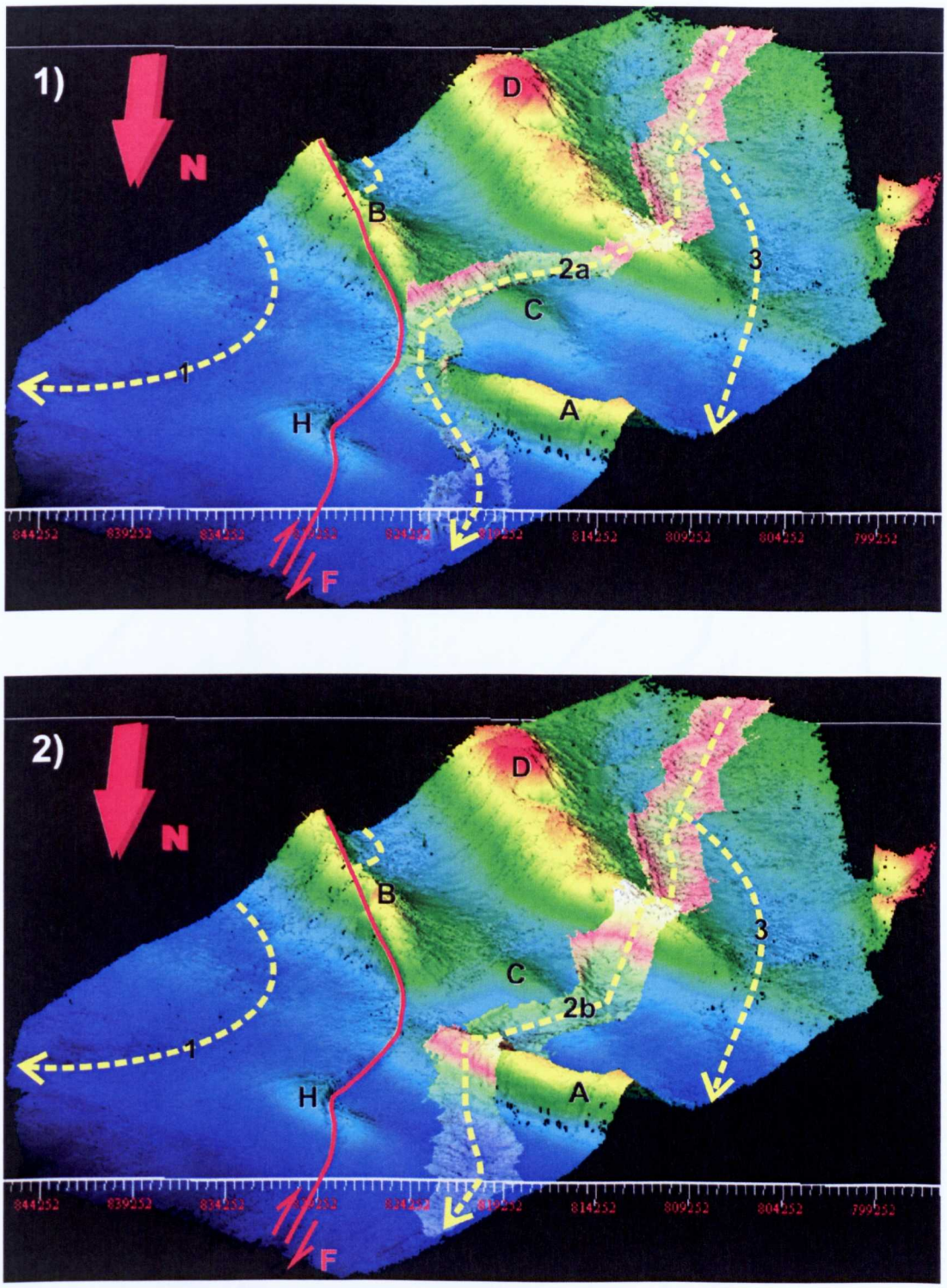

Figure 7-3 – 3D view of the mapped base of the basal interval and the base of channel 2 (a and b). The view is upstream – towards the SE. The images exhibit the 4 bathymetric highs formed by the growing tectonic structures: anticlines A, B, C and D and the high (H) formed at the tear fault (F) bend. Images 1 and 2 show the mapped channel 2 with different planforms (a and b). Channels 1 and 3 are indicated by the dashed yellow arrows.

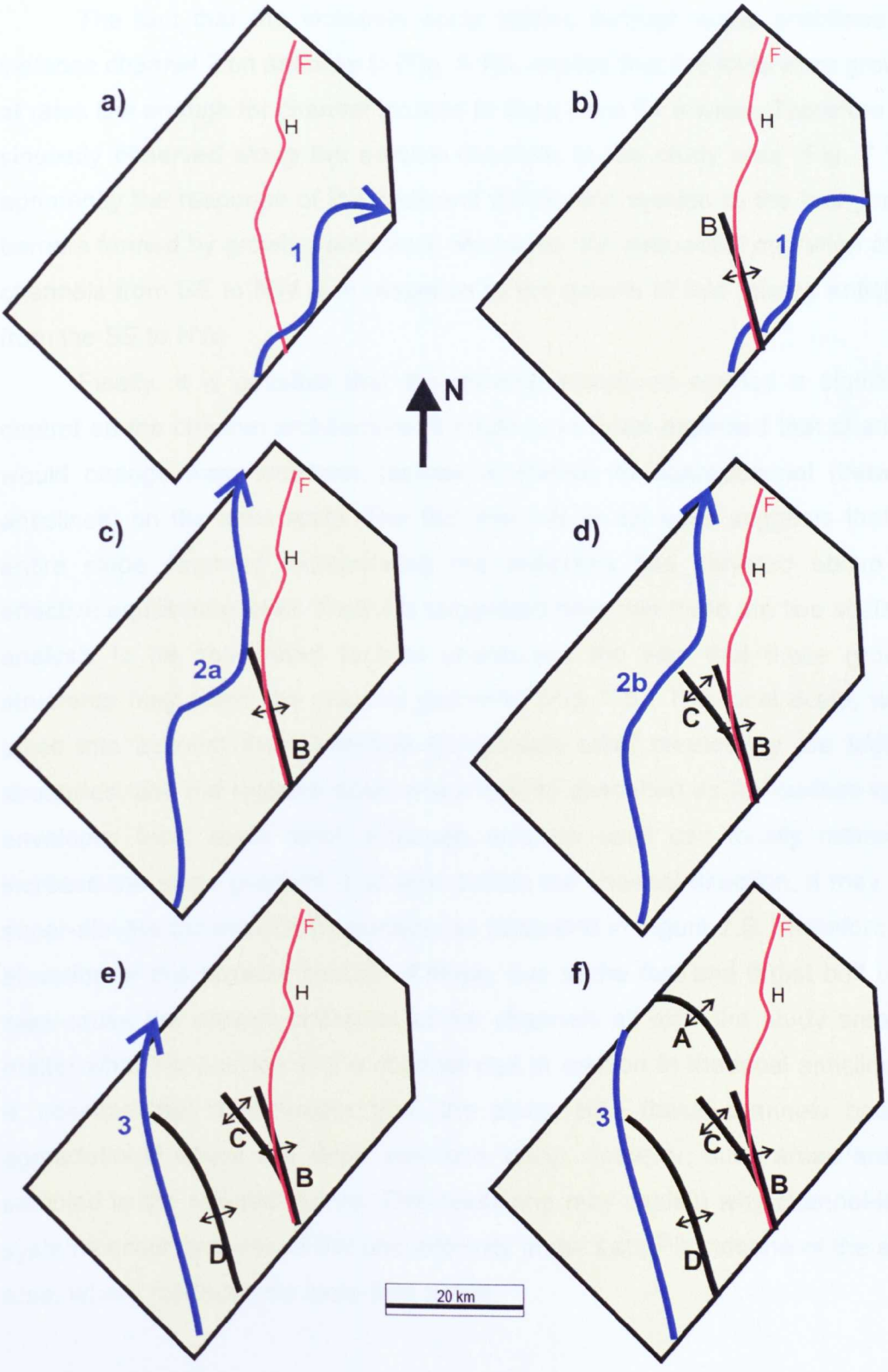

Figure 7-4 – Schematic diagrams showing the sequence of growing structures and erosive channel development: a) channel 1 diverted from the topographic high (H) formed at the fault (F) bend; b) anticline B growth blocking the channel 1; c) channel 2a diverted from anticline B and H; d) anticline C growth deflecting channel 2b; e) anticline D growth deflecting channel 3, f) anticline A growth possibly blocking channel 3.

The fact that the channels occur cutting through some anticlines, for instance channel 2 on anticline D (Fig. 5.15), implies that the folds were growing at rates low enough for channel incision to keep pace for a while. Therefore, the sinuosity observed along the erosive channels in the study area (Fig. 7.1) is apparently the response of the sediment distribution system to the bathymetric barriers formed by growing anticlines. Moreover, the sequential migration of the channels from SE to NW is in response to the growth of fold related anticlines from the SE to NW.

Finally, it is possible that the growing structures exerted a significant control on the channel architecture. It might have been expected that channels would change from incisional (across anticlines) to aggradational (between anticlines) on the local scale. The fact that this is not seen suggests that the entire slope segment incorporating the anticlines has elevated above the effective equilibrium level. Thus it is suggested here that there are two scales of analysis to be considered to best understand the way that these growing structures may affect the channel geometry (Fig. 7.5). The local scale, which takes into account the immediate bathymetric relief created by the tectonic structures, and the regional scale which can be described as the surface which envelopes local scale relief. Although anticline uplift can locally reduce or increase the slope gradient, and also deflect the channel direction, it may also super-elevate the enveloping surface, as illustrated in Figure 7.5. Therefore, the elevation of this broader section of slope, due to the fold and thrust belt uplift, may cause the erosive character of the channels all over the study area, no matter what the position of the channel was in relation to the local anticlines. It is possible that downstream from the study area these channels became aggradational where the slope was less steep, however, such areas are not sampled in the seismic survey. This reasoning may explain why channel-levee systems occur only above the unconformity in the Late Pleistocene of the study area, where the tectonics were less active.

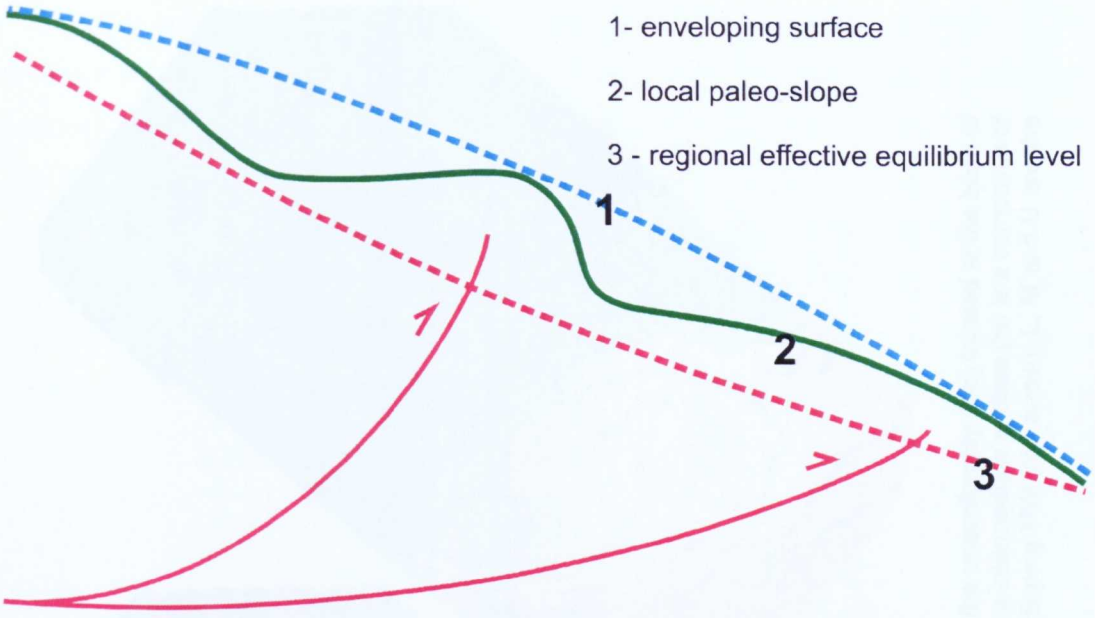

Figure 7-5 – Schematic diagram illustrating the two different possible scales of analysis of the slope paleobathymetry: variable slope gradient created by each anticline uplifts (2), and the overall gradient increase (steepening of the enveloping surface), due to the overall uplift the fold and thrust belt (1).

7.2 Oblique channel orientation with respect to the slope dip

Channels in the interval above the unconformity disperse towards the N/NW, a direction oblique to the steepest dip of the present-day slope (~1.5°), which dips towards the NE (Fig. 7.6), as does the unconformity (~1.4°) which is the other palaeo-slope candidate (Fig. 7.6). Between these two surfaces the deposition of the turbidite systems occurred as erosive channels, channel-levee systems or intra-slope lobes (HARPs). Each one of the deposits created relief on the slope which in turn affected the deposition of later deposits. Therefore, the palaeoslope bathymetry for each channel-levee system in the study area (which is small if compared with the whole area of the Amazon Fan) is dynamic in time, changing after the deposition of each one of these deposits and it is therefore difficult to choose a unique paleoslope datum. Hence, for analytical purposes the unconformity already described in Chapter 5 and exhibited in Figures: 5.2, 5.4, 5.5 and 5.18 is considered the palaeoslope for the deposition of the whole package of channel-levee systems and associated deposits (MTDs and HARPs). The objective of this section is to evaluate why these channels are oblique to the palaeoslope in the study area, and in particular to ascertain if there is a structural control on channel orientation.

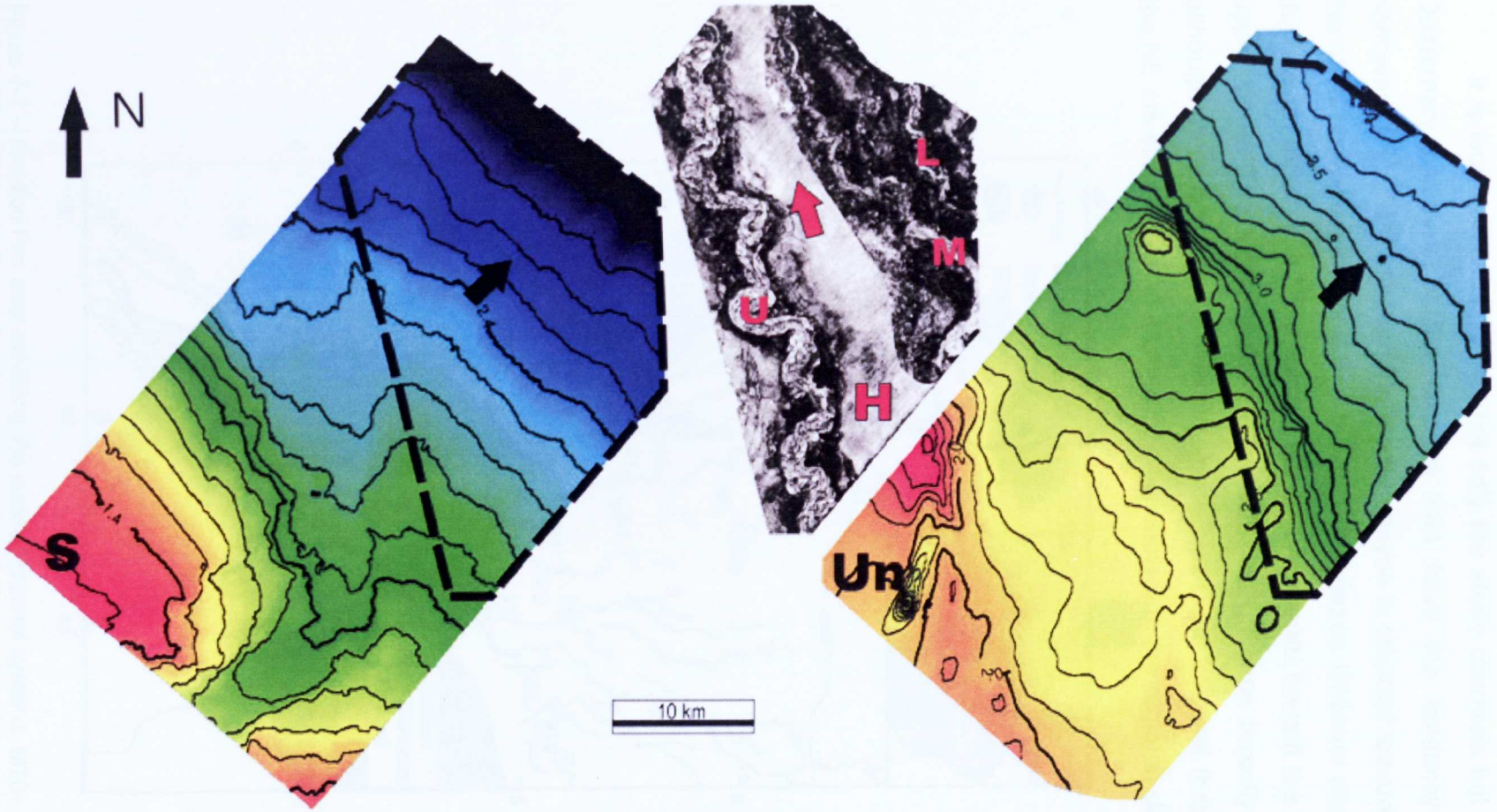

Figure 7-6 – Schematic diagram showing the two-way-time maps of the sea floor (S) and the unconformity (Un) located at the base of the channel-levee systems identified in the study area, both dipping NE (black arrows). The intermediate surface (H) is a composite of three horizon slices (RMS coherence) across the three systems, showing the channels dipping NW (red arrow). L, M and U are the channels of the LCLS, MCLS and UCLS, respectively.

It is worth mentioning that not only the study channels but most of the Quaternary channels of the Amazon Fan have the tendency to deviate northward (Fig. 7.7). Although the feeder canyon is oriented towards the NE on the shelf border/upper slope and the recent Amazon Channel disperses from the canyon mouth in a NE direction, the channel bends toward the north on the upper slope. The other avulsed channels also disperse broadly northwards although there is a spread. Nevertheless even these channel that disperse to the NE are still oblique (in an anticlockwise sense) to the regional slope dip.

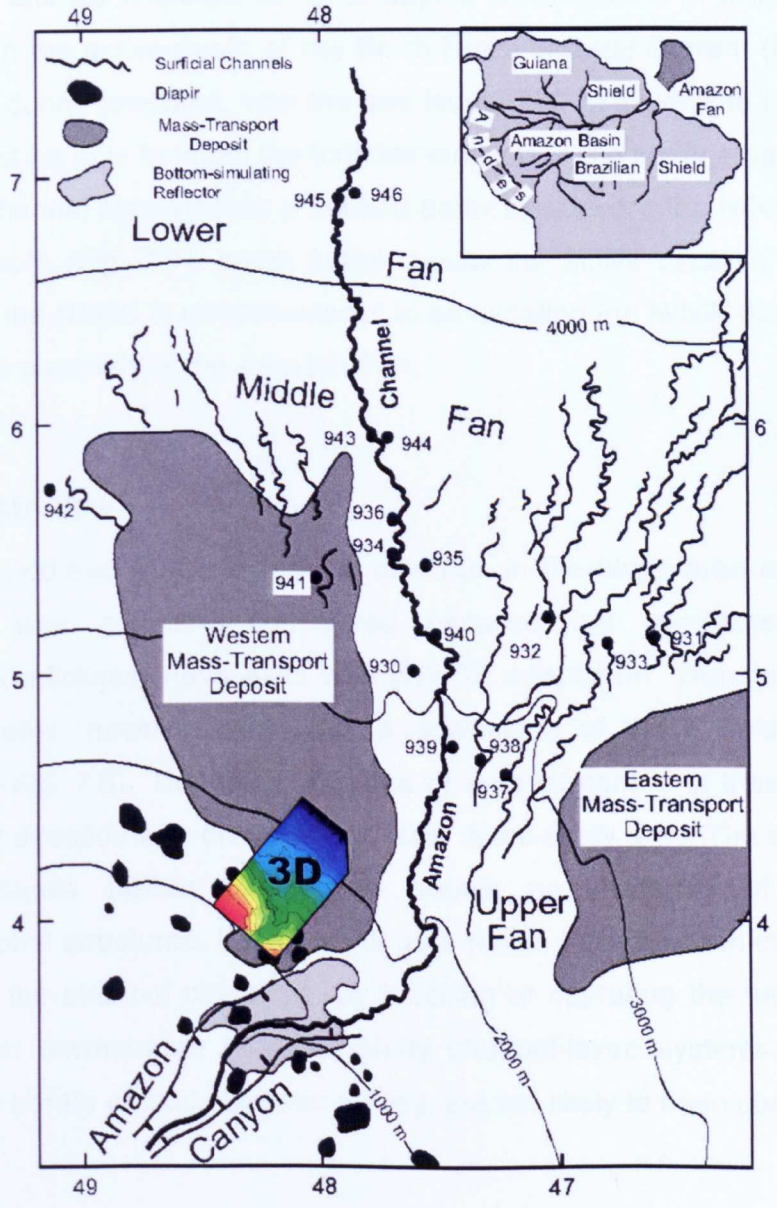

Figure 7-7 – Amazon Fan map exhibiting the surficial channel systems, MTDs, the location of the Leg155 sites and of the study seismic survey. Notice the northward growing direction of the fan. Adapted from Normark et al. (1997).

Possible controls on the channels evolution include the influence of marine currents, tectonics (through changing the paleoslope topography) and directional inheritance from the previous channel-levee. These controls could have contributed individually or jointly to causing the oblique flow direction on slope.

7.2.1 Marine currents

The studied channels occur at depths around 2000 m which are much deeper than the active depth of the North Brazil Coastal Current (NBCC) (Fig. 3.6). Even during lowstand, with the sea level ~100 m lower, the NBCC would probably not be able to affect the turbidite currents in the study area. The recent Amazon Channel also exhibits a marked deflection toward the N/NW at around 2000 m depth (Fig. 7.7), much further below the active depth of the NBCC. Therefore, the NBCC is not considered to be dictating the N/NW direction of the Pleistocene channels of the Amazon Fan.

7.2.2 Tectonics

The hypothesis that the channel direction in the study area is structurally controlled was originally considered because the compressional slope structures (anticlines) have axes with NW-SE orientation. The study channel-levee systems, however, are located downslope of these (fold-thrust belt) structures (Fig. 7.8). Therefore, the idea of a direct control of these structures on channel direction was discarded, at least in the study area. The study 2D line (which extends further downslope) shows no evidence of downslope compressional structures. It is thought, as a result, that other structures directly controlling the channel directions, by blocking or capturing the turbidite flows, and located downstream from the study channel-levee systems beyond the downslope border of study seismic survey, are not likely to have been present.

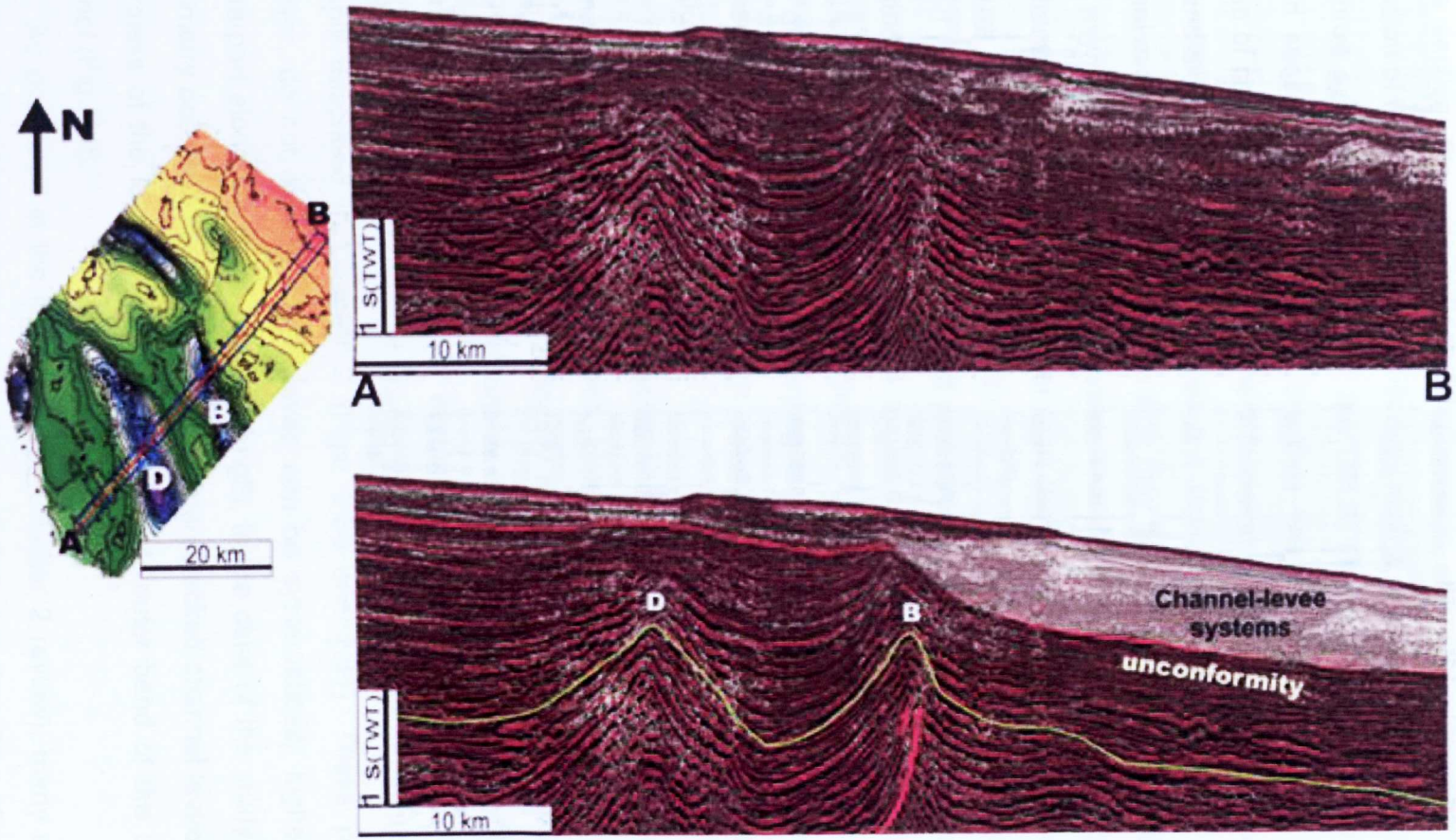

Figure 7-8 – Non-interpreted and interpreted seismic sections (AB) across the area showing the downslope position of the channel-levee systems in relation to the fold-thrust belt. The location of the section is plotted in the TWT map of the green horizon in which are highlighted the folds D and B.

7.2.3 Inheritance of direction from older channel-levee deposits

In this section, the contribution of bathymetric inheritance resulting from the deposition of the previous systems in determining channel direction is analysed. The three systems identified, i.e., the LCLS, MCLS and base of UCLS, are formed sequentially upslope and are thus laterally stacked due to recurrent phases of channel-levee development following systemic avulsions through the left-hand side of the channel (viewed in a downstream direction). The recurrent channel avulsion through the same side may have been favoured by the strong levee asymmetry of the channel-levees. This asymmetry is characterized by the right-hand levee being much larger than the left one in all of the three study systems (e.g. Fig. 7.9). Therefore, any abrupt increase in the flow size, to exceed the channel capacity would probably force a break through the weaker left-hand levee to cause channel avulsion. Consequently, the next channel would initially align along the bathymetric low between the slope and backside levee of the previous channel, inheriting its direction. In this case, therefore, the succeeding channel-levee system would have inherited the approximate direction of the abandoned one.

Levee asymmetry is considered an important characteristic determining channel avulsion in the study cases. However, levee asymmetry is a feature known more commonly to occur locally at the bend of a submarine channel rather than along its entire extensions as is observed in the study systems. The preferential occurrence of levee asymmetry at a channel bend is due to overbanking of channelized flow related to processes of flow stripping or inertial overspill described in Chapter 2 (Figs. 2.30 and 2.31). These processes, however, do not explain how a levee can be systematically higher than its counterpart along the entire channel length. In the case of the study area, the asymmetry occurs along the channels of three stacked channel-levee systems, regardless of the levee location at the inner or outer bend of the submarine channel (Fig. 7.9).

As described in the literature (see Chapter 2 review), many submarine channels exhibit levee asymmetry which is attributed to the effect of the Coriolis Force, e.g., North Atlantic Mid-Ocean Channel (NAMOC), Danube Deep-Sea Fan, Bengal and Indus Fan (Curray et al., 2003; Klaucke et al., 1997; Kolla and

Coumes, 1987; Popescu et al., 2001) (Fig. 2.38). Thus, these channels are located in higher latitudes where the Coriolis force can be more effective. These authors attributed this levee asymmetry to be an effect of the Coriolis force acting on the flow overspill along the channel systematically causing overbank deposition on the right side, if the channel is located in North Hemisphere. However, the Amazon Fan is located in very low latitudes (3 – 8° N), very close to the Equator, where the Coriolis force should be negligible, but nevertheless presents levee asymmetry.

Although the Amazon channel-levees present strong levee asymmetry in the study area, previous studies in Amazon Fan (e.g., ODP Leg 155 Proceedings) did not mention this characteristic. The levees of the Amazon Channel, however, can be asymmetric, with asymmetry decreasing basinward (Fig. 7.10). Most of the data analysed by the ODP Leg 155 are in the Middle and Lower Fan. Therefore, the fact that the systems analysed by ODP do not have strong asymmetry can be related to their Middle and Lower Fan location where the slope dip tends to be lower. Thus, in the Upper Fan, the levee asymmetry of the Amazon Channel is more conspicuous. In the Bengal Fan, for instance, the levee-asymmetry was stronger in the upper and middle fan but less evident in the lower fan (Wynn et al., 2007). These authors, however, suggest that the proximity to the Equator causes the asymmetry reduction in the lower fan, because the Bengal Fan grows southward, to lower latitudes (Fig. 7.11). If the proximity to the Equator was determining the levee asymmetry in the Amazon Channel, however, the asymmetry would be expected to increase downstream (N), as this is further from the Equator. On the contrary, the channel-levees tend to become relatively more symmetric downstream.

The bathymetric high already created by the deposition of each previous downslope system may be another possible cause of the levee asymmetry. In this case, although the depositional rate from the overbank flows on both sides of the channel may be the same, the right levee would be always higher because it was already a high when the levees started to grow (growing on the left-hand levee of the predecessor channel). However, Figure 7.9 shows that the right levee of the UCLS is volumetrically much larger than the left one, and in any case is offset from the relatively small relief previously created by deposition of the left-hand levee of the MCLS. Moreover, the limb of the left-

hand levee is steeper than the right-hand one (Fig. 7.9) further indicating some difference in depositional flow process.

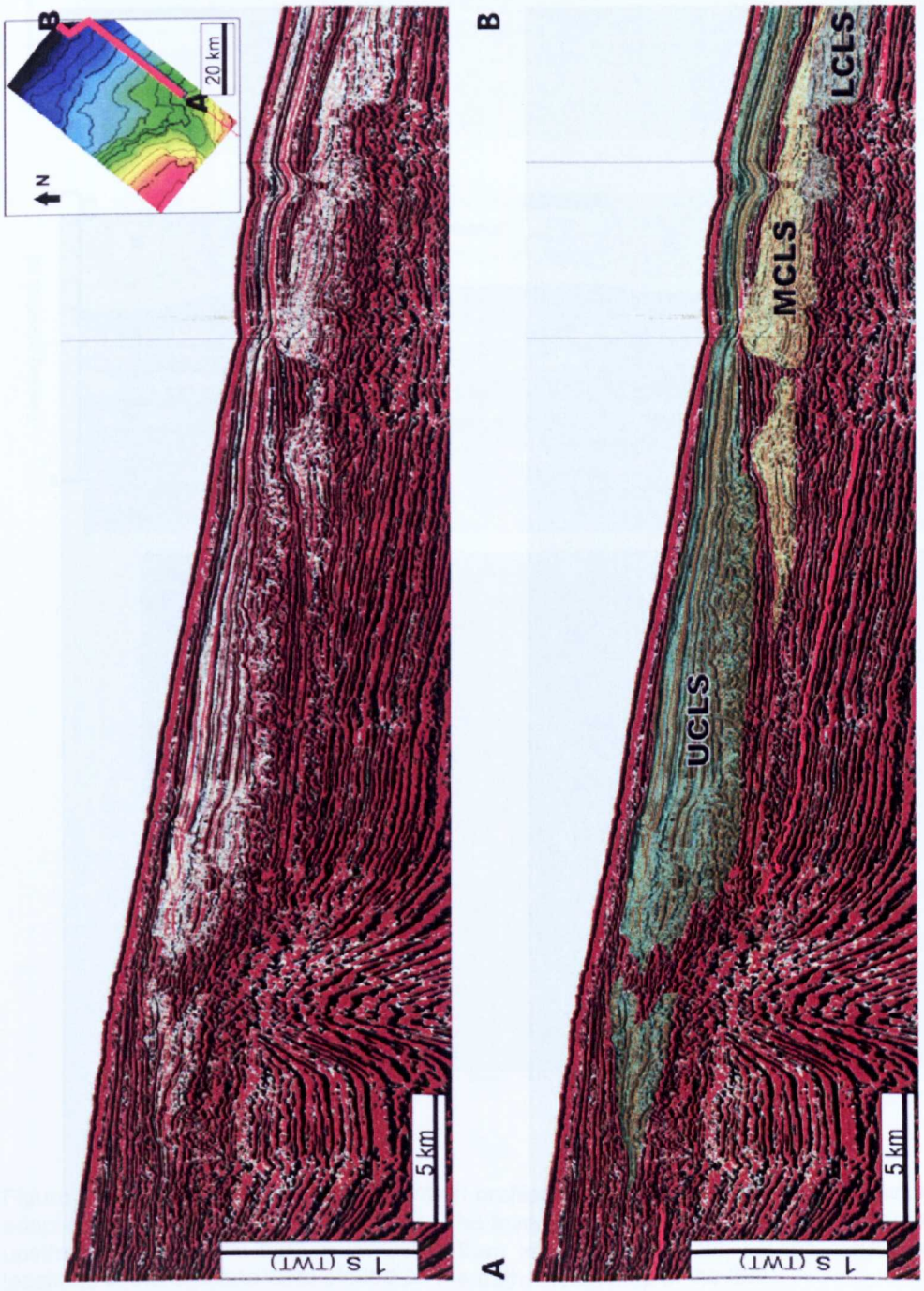

Figure 7-9 – Section across the study area showing the highlighted levees of the stacked channel-levee systems (LCLS, MCLS and UCLS) with downlope/right-hand levee much larger than the upslope/left-hand one. This section is viewed toward the downstream direction. The location of the section AB is given on the above seafloor map.

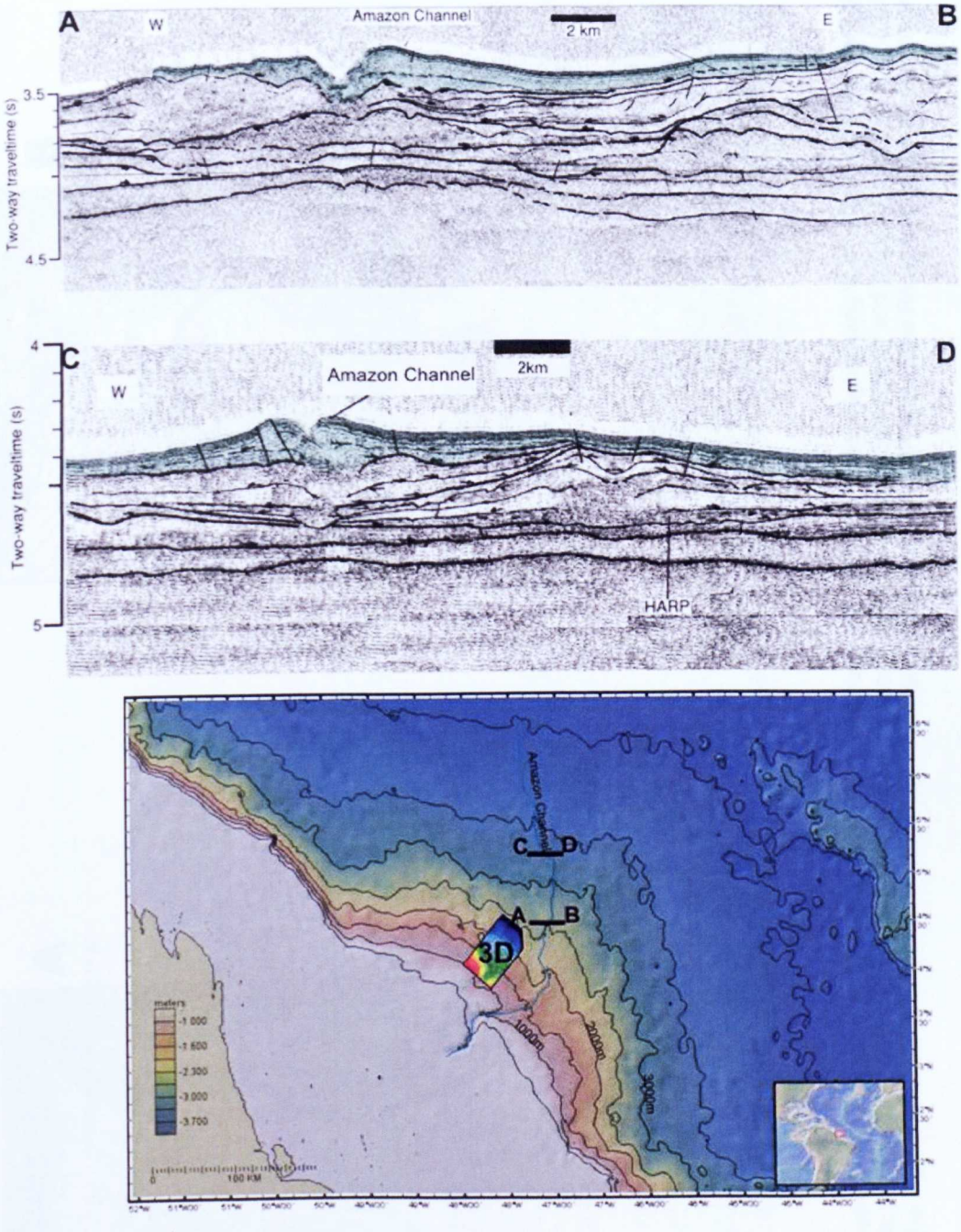

Figure 7-10 – Interpreted seismic reflection profiles (AB) and (CD) across the Amazon channel adapted from Pirmez and Flood (1995). The levees (highlighted in green) of the channel in its upstream section are more asymmetric than in the downstream section. The approximate locations of the sections were plotted on the bathymetric map of the fan.

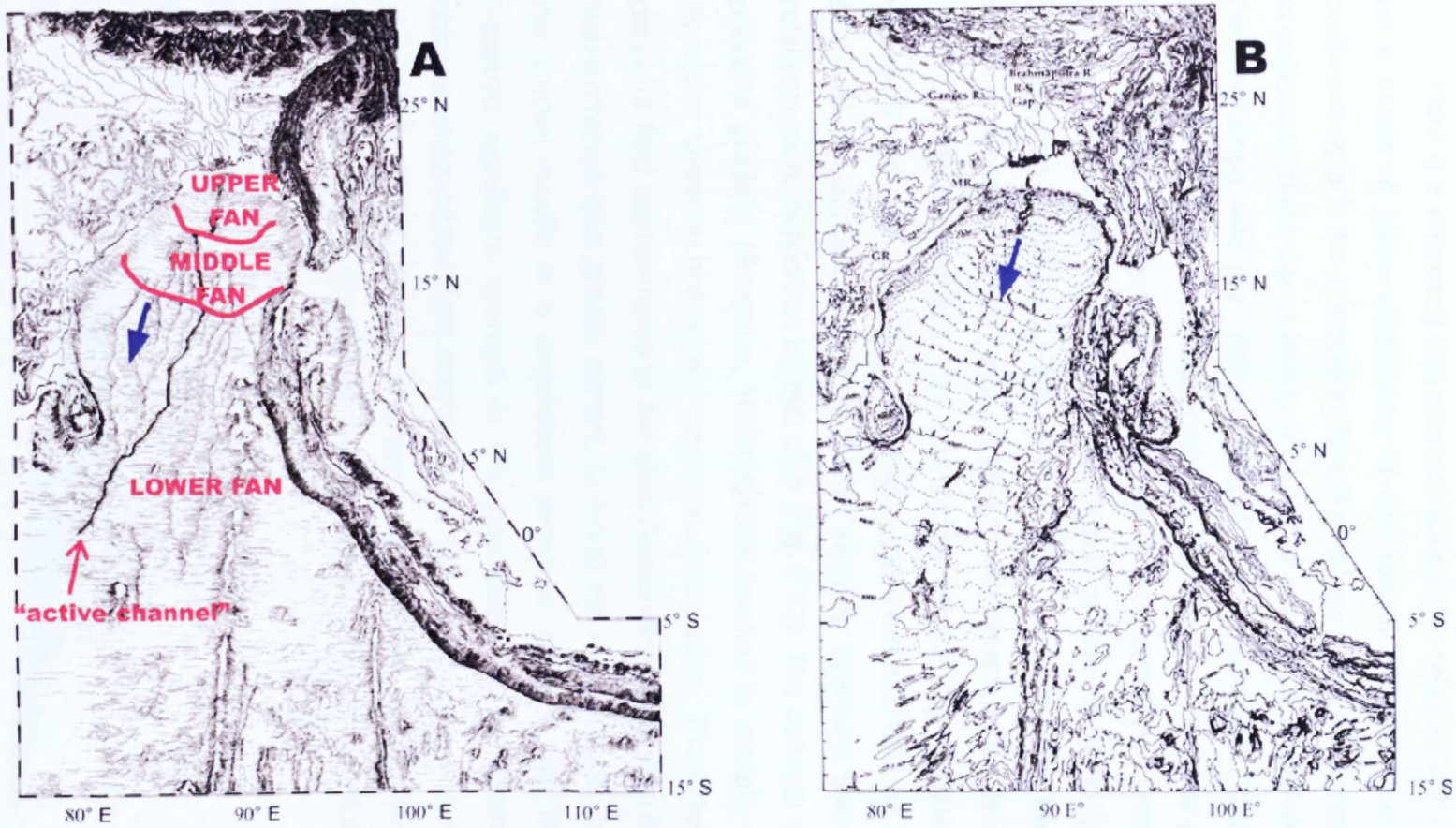

Figure 7-11 – A) Physiographic diagram of the northeastern Indian Ocean and adjacent lands, highlighting the fan subdivisions, the "active channel" and the main slope dip (blue arrow). B) Bathymetry and topography of northeastern Indian Ocean and adjacent land areas, in corrected meters. R-S Gap is the Rajmahal-Shillong Gap; MR is Mahanadi River; Gr is Godavari River; KR is Krishna River. Both maps are adapted from Curray et al. (2003).

Here it is proposed that channel obliquity in relation to the slope dip may be a cause of levee asymmetry. It can readily be seen that gravity would preferentially pull the overspilling flow downslope in the case where the channel is oblique to slope dip, resulting in a higher volume of overbank sediments on the downslope side (i.e., right-hand side in the study case) than the up-slope side of the channel. The fact that the asymmetry increases proximally (the levees of the middle/lower fan channels are relatively more symmetrical) suggests that slope gradient, which is higher upslope, is a principal control. The overbank flow thickness on the upslope side may be smaller because the flow became ponded between the slope and the levee backside, thus reducing relative rates of overbank loss and hence resulting in deposition of smaller sediment thickness. On the other hand, the overbank flow on the downslope side was not ponded, favouring greater rates of overbank loss and ultimately relatively more deposition on that side (Fig. 7.12). The concept of an intra flow pressure gradient (Simpson, 1997) can be invoked to explain the lateral flow direction, under a hydrostatic pressure assumption. Thus the cross stream pressure field approximates to the axial (longitudinal) pressure field in a classic lock-exchange-type gravity current, in which the overall upper surface slope of the current results in a longitudinal pressure gradient that drives the flow. Because significant overspill in the downslope direction can occur in the oblique, channelized flow scenario (but not upslope), a similar cross-stream slope will develop resulting in a pressure gradient laterally (higher up slope, lower down slope) that will drive the lateral flow of overspilling fluid.

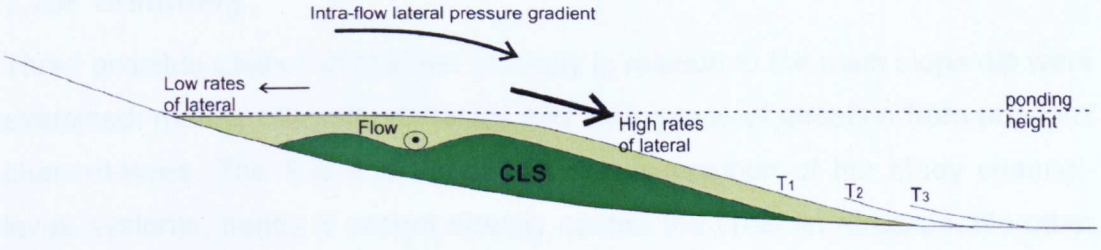

Figure 7-12 – Schematic model explains levee asymmetry in the case of oblique dispersal down the slope. Internal lateral pressure gradient favour greater rates of overbank loss downslope, hence greater levee volumes.

Therefore, the model of levee asymmetry development due to channel obliquity in relation to slope dip can be applied to explain levee asymmetry both in the Amazon Channel and also in the Bengal Fan (Wynn et al., 2007) which shows the levees becoming more symmetrical downstream. The "active channel" in the Bengal Fan (Fig. 7.11) is slightly oblique to the main slope dip, bending to the left on the Middle Fan, which would explain the higher right-hand levee on this channel segment. The upstream segment of the channel-levee systems in the Indus Fan immediately after the feeder canyon mouth (Fig. 7.13) is also oblique to the main slope dip. In both cases the channel obliquity to the main slope dip could be responsible for the levee asymmetry identified in these fan positions (Figs. 7.11 and 7.13).

On the other hand, the "active channel" of Zaire Fan has approximately the same dip direction of the main slope dip (Fig. 7.14) and has been described as having very symmetrical small levees (Migeon et al., 2004). Therefore, channel obliquity in relation to the mean slope dip can to be crucial to the development of asymmetrical levees on slope channels.

In summary several processes were proposed to explain levee asymmetry in the study channel-levee systems. Coriolis force was discarded as a main force due to its negligible effect close to the Equator. Flow stripping and inertial overspill can explain the levee asymmetry only locally when it occurs at the channel bends. Although the origin of levee asymmetry along the whole extension of the channel is still not fully understood, the obliquity of the channel on the slope is the most probable cause, at least in the study area and possibly elsewhere.

7.2.4 Summary

Three possible causes of channel obliquity in relation to the main slope dip were examined: marine currents, tectonics and inheritance of direction from previous channel-levee. The fold and thrust belt occurs upslope of the study channel-levee systems, hence it cannot directly control the channel direction. No other tectonic structures were identified downslope of the study channel-levee systems in the 3D survey or in the 2D line across the slope. Therefore, there is no apparent structural control dictating the channel directions.

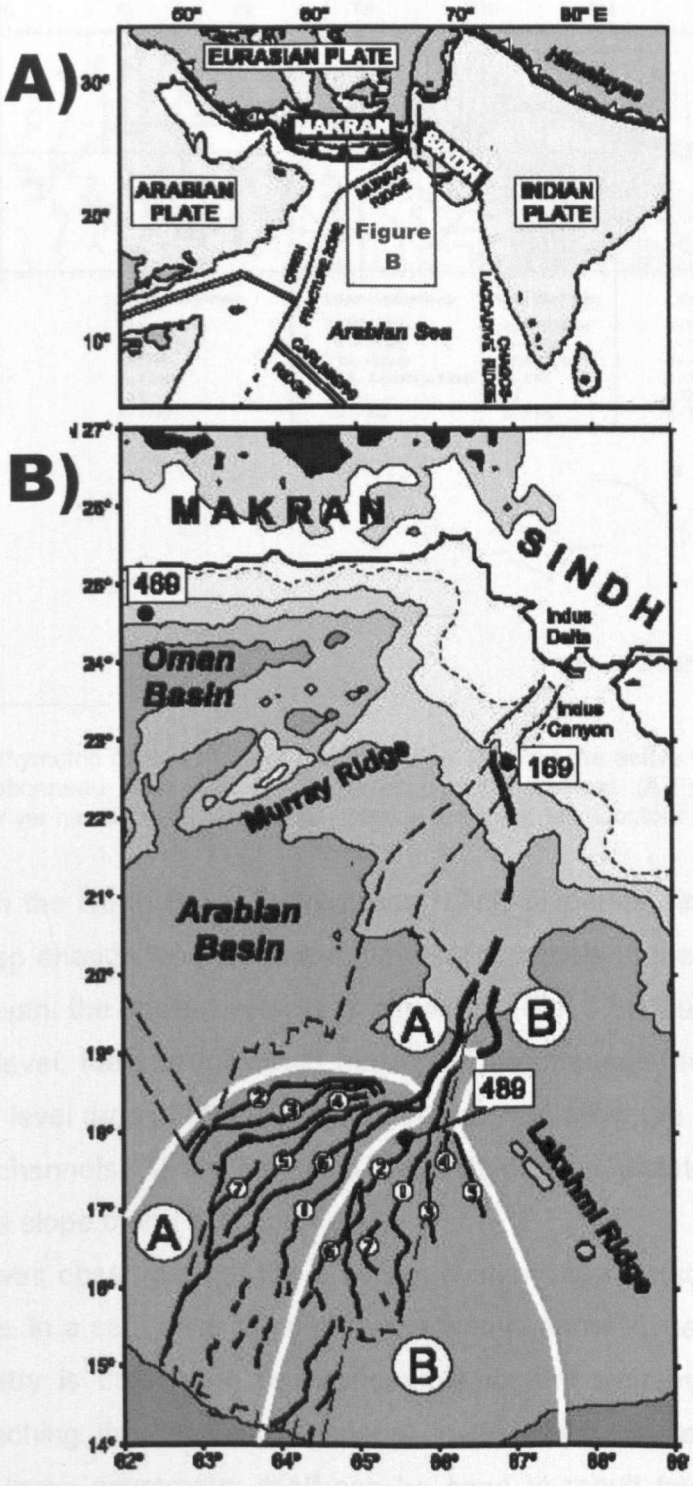

Figure 7-13– Maps adapted from Prins and Postma (2000). Geomorphic setting of Makran and Indus Fan turbidite systems. A) Tectonic setting of Makran and Sindh continental margins showing the location of Figure B. B) Localities of the Indus canyon and part of the complex of associated large channel-levee systems (A younger than B), and small channel-levee systems (e.g. A1 is younger than A2. Topography contour interval is 500 m and bathymetry contour interval is 1000 m (dashed contour line is 125 m). Notice in the upper fan, immediately following the canyon mouth, the channel is oblique to the main slope dip.

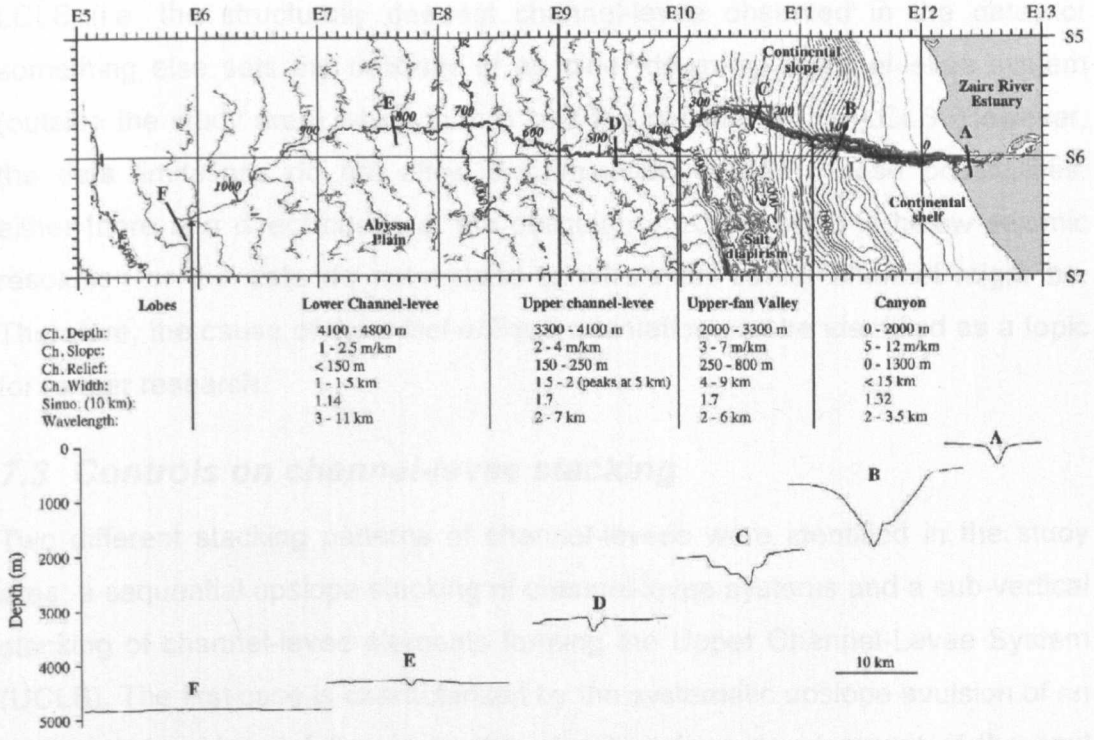

Figure 7-14 – Bathymetric contour map of the Zaire Fan showing the active Canyon/Channel, adapted from Babonneau et al. (2002). Bathymetric cross sections (A-F) show changing morphology from river mouth down to the distal lobe on the lower fan. Contour interval is 100 m.

Although the North Brazil Current has N/NW dispersal direction, it does not extend deep enough to affect the submarine channels in the Amazon Fan, as at 800 m depth, the current velocity is almost nil (Fig. 3.6). During periods of lowstand sea level, the current would not affect the channels evolution either, because a sea level drop of 100 m is still not enough to allow the marine current to reach the channels. Thus, the NBC (NBCC) did not dictate the channel direction on the slope of the Amazon Fan.

Finally, it was observed that the previous system may dictate the direction of the next one, in a sequence of upslope stacked channel-levee systems. The levee asymmetry is thought to be responsible for the systematic pattern of avulsions breaching the left-hand (upslope) levee which causes the upslope stacking. The levee asymmetry itself can be seen to result from the channel obliquity to the main slope dip. The lateral pressure gradient from upslope to downslope would account for the building up of a larger downslope levee due to greater rates of overbank loss on that side.

This raises the question of what causes the first oblique orientation. There are two possibilities: there is an unknown mechanism setting the obliquity of the

LCLS (i.e. the structurally deepest channel-levee observed in the data) or something else sets the obliquity of an older down-dip channel-levee system (outside the study area) which in turn sets the obliquity of the LCLS. However, the data limitations do not allow discrimination between these possibilities: either there is a direct cause of the obliquity of LCLS, but it is below seismic resolution or the data do not extend to where an earlier channel might be. Therefore, the cause of the initial oblique orientation can be identified as a topic for further research.

7.3 Controls on channel-levee stacking

Two different stacking patterns of channel-levees were identified in the study area: a sequential upslope stacking of channel-levee systems and a sub-vertical stacking of channel-levee elements forming the Upper Channel-Levee System (UCLS). The first case is characterized by the systematic upslope avulsion of an earlier channel-levee followed by the lateral upslope development of the next system, as discussed previously. The evaluation of the causes of the sub-vertical stacking of the UCLS is discussed as follows.

7.3.1 UCLS stacking

The UCLS is composed of a stack of at least four channel-levee elements. The lowest channel-levee element evolved from the top of the underlying HARPs up to an erosive surface (described in Chapter 5) (Fig. 7.15). This erosive surface is identified in both left and right-hand levees of the UCLS and may represent an important depositional gap in the evolution of the channel-levee system.

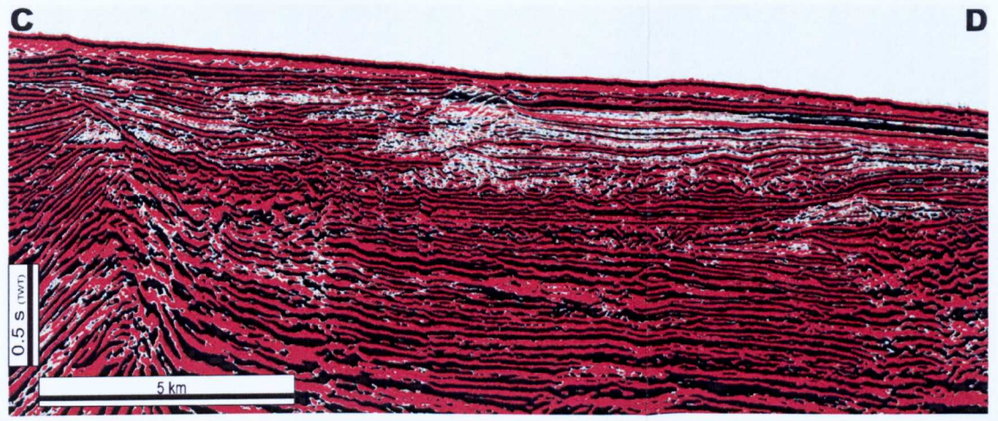

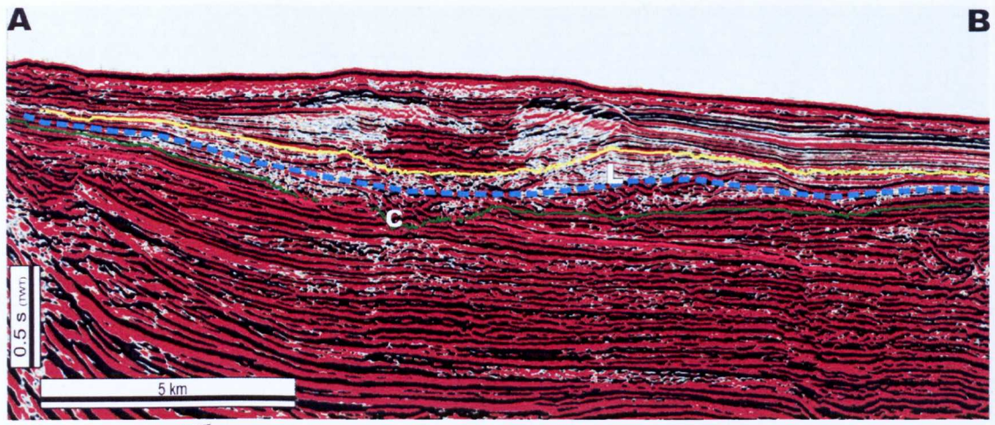

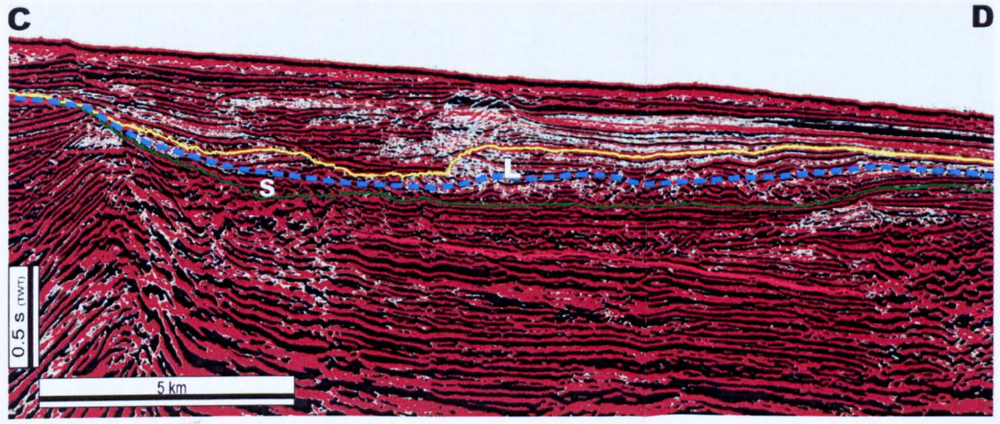

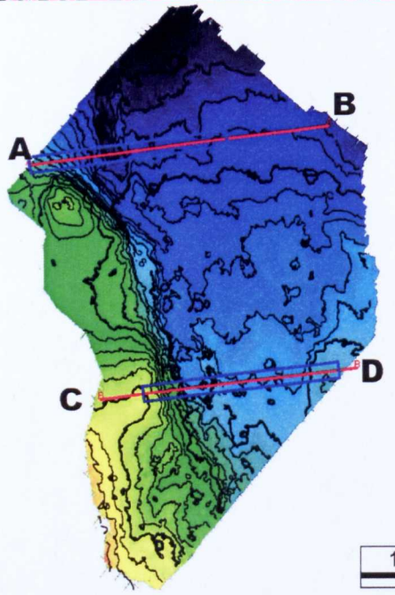

TWT map of the base of the UCLS

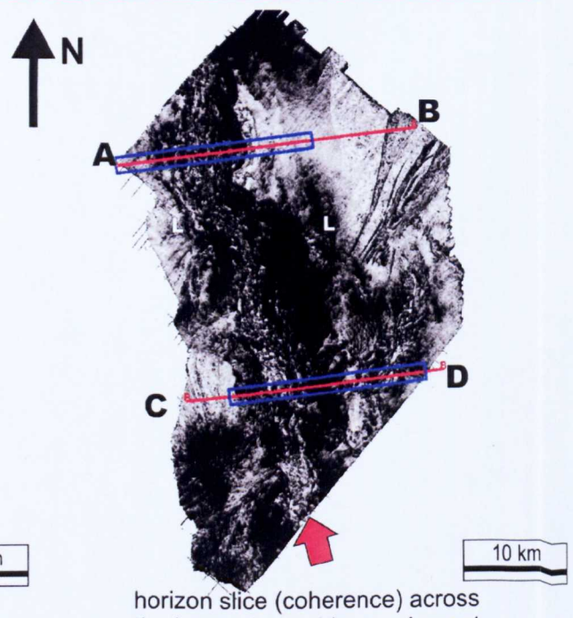

horizon slice (coherence) across the lower channel-levee element

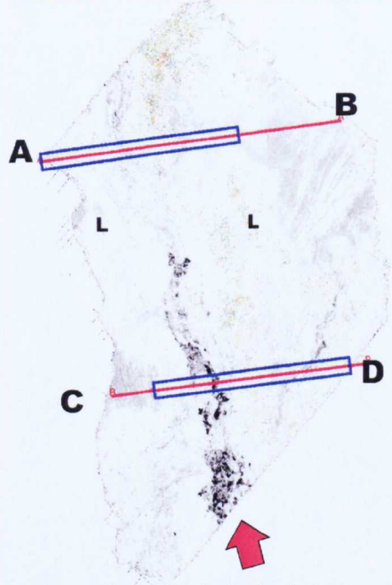

horizon slice (amplitude) across the lower channel-levee element

Legend:

yellow hozizon - erosive surface across the UCLS

green horizon - base of the UCLS

red horizon - unconformity underneath

dashed blue line - isoproportional time slice between top and base of the lower CL element

L - levee

C - chaotic channel fill reflections

S - channel fill with sigmoid reflections

AB - downstream section across the UCLS

CD - upstream section across the UCLS

red arrow - indicates the channel

Figure 7-15 – Interpreted and non-interpreted seismic reflection sections downstream (AB) and upstream (CD) across the Upper Channel-Levee System (UCLS). Notice the upstream channel fill presents sigmoidal reflections with higher amplitude whereas the downstream channel fill presents chaotic reflections with lower amplitude. The black and white maps are isoproportional horizon slices across the lower channel-levee extracting coherence and amplitude in a time window of 20 ms. The amplitude map shows the upstream segment of the channel with higher amplitude (dark gray) the lower one (light gray), which is very similar to the levee amplitude.

The channel fill of this lowest interval varies from chaotic low amplitude reflections to ordered high amplitude reflections. The high amplitude reflections are sub-horizontal and/or have sigmoid shape (Fig. 7.15). On the base of the right-hand levee, there is an interval of deformed sediments showing sets of thrust duplets and as their updip counterpart, normal faults verging toward the channel axis (Fig. 5.30). The vergence of the structures indicates a sliding direction from the SE toward the NW, i.e., into the axis of the new channel. The seismic reflections in this direction do not have the same organized downlapping pattern of the enclosing levee, but they have similar amplitude. The amplitude similarity of the reflections of the remobilized sediments to the levee reflections suggests that the slide is result of remobilization of levee sediments (Fig. 5.30). This slide is interpreted to have occurred as a result of the instability of the basal levee layers due to the relief caused by the underlying MCLS. In the lower channel-levee element of the UCLS, the levee buildup is characterized by levee reflections downlapping at the upper surface of the MTD. This depositional interval extends vertically from the top of the MTD up to the erosive surface mentioned above. It exhibits the downlapping pattern typical of levee build up.

Above the erosive surface, three channel-levee systems are sub-vertically stacked. Within this sequence, the channels become more sinuous and narrower from the basal to top system although within each individual system the channels widen upward (Fig. 7.16). In a section across the channel (Fig. 7.16), the channel fill of the two lowest systems is roughly sub-horizontal. The uppermost channel-levee element is described in detail by Nakajima et al. (2009). This channel includes channel fill elements in the form of offlapping point bars, described as "outer-bank bars" for the first time, which onlap the channel border. The channels of the three systems above the erosive surface exhibit different sinuosity, which increases toward the top system (Fig. 7.16). In parallel, the amplitude of the seismic wavelets showing the channel fill reduces toward the top of the system. The channel fill of the uppermost system exhibits similar reflection amplitude to that of its related levee. This similarity indicates that the lithology of the channel fill is similar to that of the enclosing levee, and is therefore probably silt dominated.

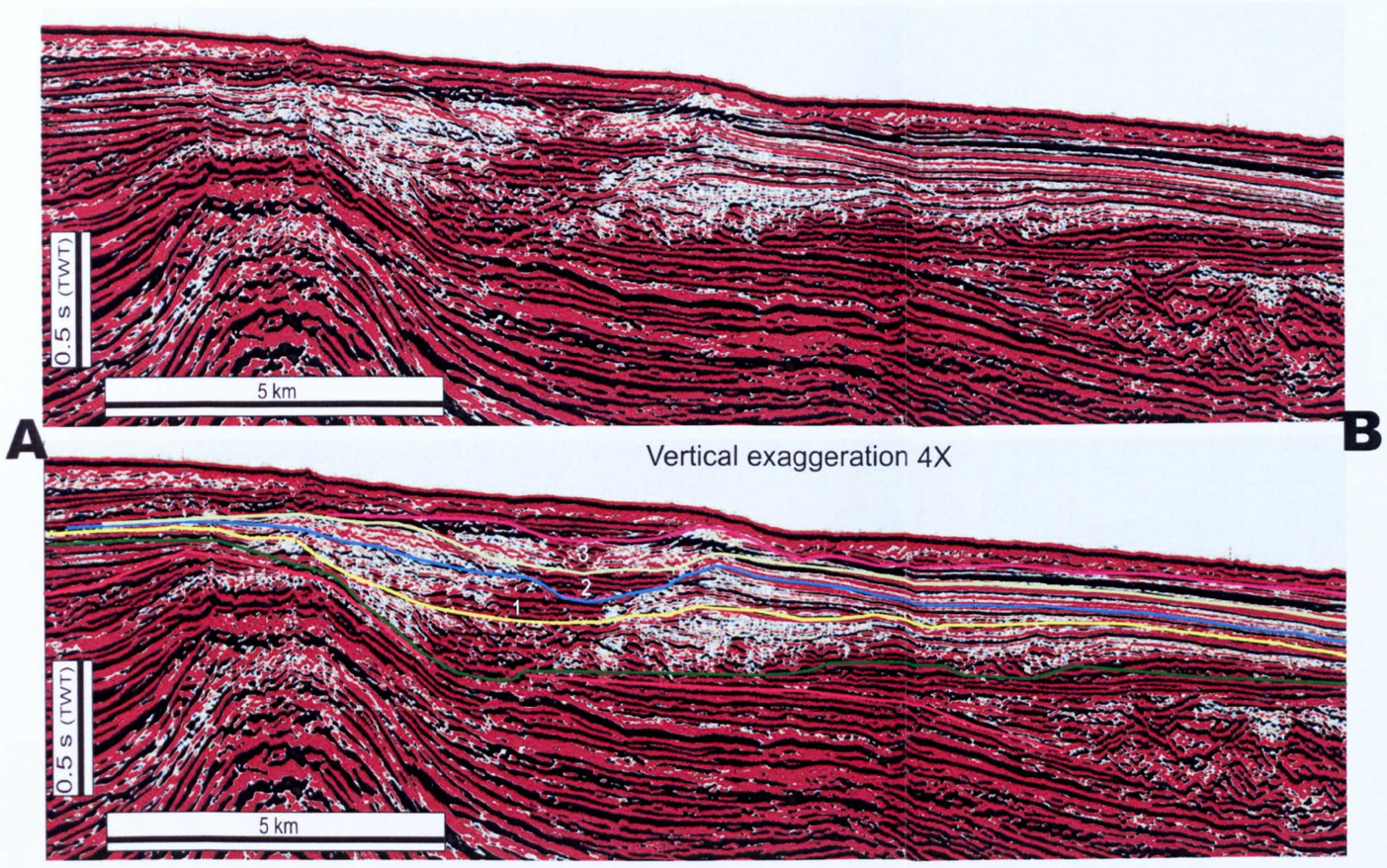

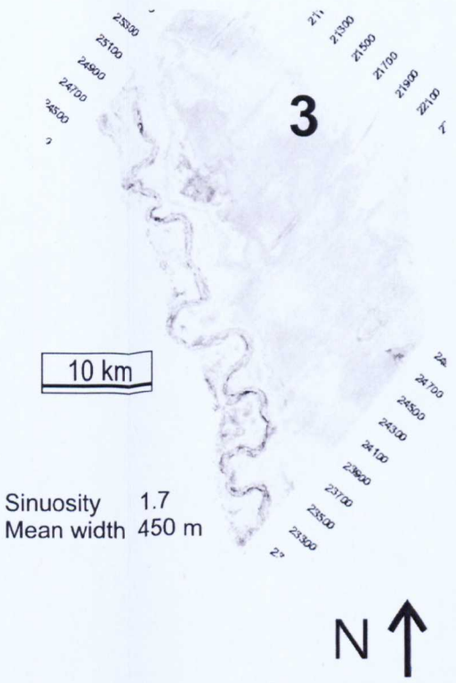

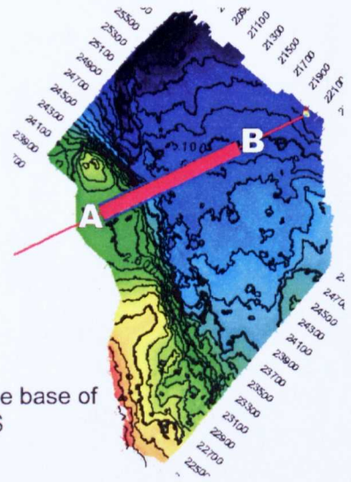

N

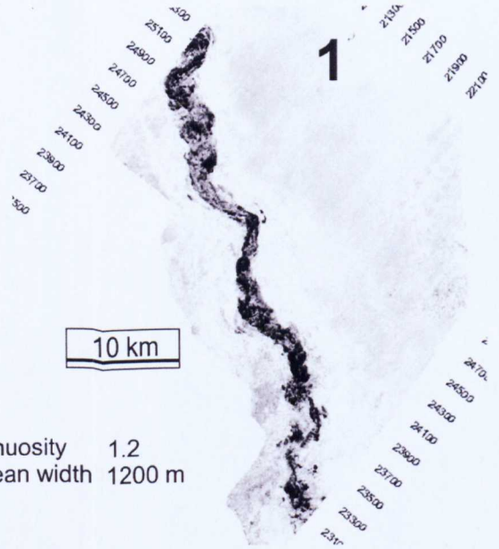

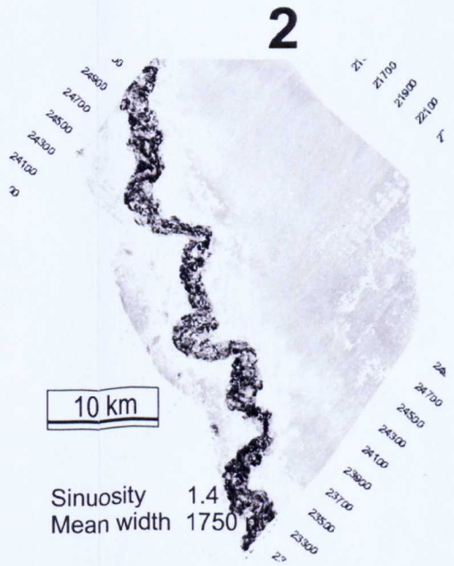

Figure 7-16 – Horizon slices exhibiting RMS amplitude extractions of the three stacked channel-levees above the inner unconformity (yellow horizon) in the Upper Channel-Levee System. The horizon slices were taken using a 20 ms window in the mean surface between the base and the top maps of each channel-levee (1, 2 and 3), highlighted in the seismic section. The channels are more sinuous and clay rich upward, as there is less amplitude contrast between the channel and the levee in the upper channel-levee (3).

It follows that the channel fill is inferred to be siltier/muddier in the uppermost channel than in the underlying channels of the lower systems that comprises the UCLS. These changes in channel characteristics can be related to changes in flow properties (Kneller 2003) and have been described in the literature (Deptuck et al., 2003). Kneller (2003) notes that the flows within aggradational channel-levee systems may become both smaller and muddier with time which may respond to three main controls (i.e. grain-size, flow size and flow density). As discussed in Section 7.2, the cause of the lateral and upslope stacking of channel levees from the LCLS to the base of the UCLS was inferred to be the systematic upslope avulsion of each system. By way of contrast, in the sub-vertical stacking of the UCLS, there no avulsion was identified in the study area. The absence of avulsion is discussed below.

The strong levee asymmetry of UCLS arose due to the channel obliquity in relation to the slope, as discussed Section 7.2 (Fig. 7.9). The outsized right-hand levee developed along the whole system in the study area, and prevented the channel from avulsing downslope. In contrast to the MCLS and LCLS, no bathymetric low was created between the perched aggradational channel and the slope that could favour channel avulsion (Fig. 7.17). On the contrary, the updip growing anticline actually uplifted part of the up-slope levee, resulting in an absence of space into which channels could avulse. In other words, the surface expression of the anticline effectively ponded the channel margin of the UCLS, effectively acting as a levee, (Fig. 7.17).

Therefore, the sub-vertical stacking of four channel-levee systems in the study area may be attributed to its confinement between the outsize right-hand levee developed downslope, building over the previous MCLS and the upslope anticline. The widening-upward characteristic of each channel of the stacked systems suggests that the flows in each channel became larger and sandier upward with time, as discussed in the evolution of the MCLS in Chapter 6, which culminated in the channel avulsion. These two bathymetric highs, upslope folding and downslope levee, however, did not allow the channel to avulse in the study area, as in the previous MCLS and LCLS. Avulsion might have occurred somewhere during the evolution of the stacked channel-levee elements of the UCLS, but downstream and outside of the study area.

Another instance of vertical stacking occurs in the "Upper Levee Complex" (Late Pleistocene) of the Amazon Fan (Flood et al., 1995), as shown in seismic sections presented by Pirmez and Flood (1995) (Fig. 7.18). The sections are located upstream from the bifurcation points of the channels, i.e., upstream of the points of channel avulsion. Figure 7.18 shows the stacking of three channel-levee systems, from the base to the top: the "Aqua", "Brown" and the "Amazon". They represent the youngest channel-levee systems of the Late Pleistocene deposition in the Amazon Fan. This section is located upstream of the point of avulsion of the Aqua Channel and the subsequent development of the Brown System, leading the three channel-levee systems to stack vertically. In this case of the Late Pleistocene channels of the Amazon Fan, the channel stacking is not related to the confinement between upslope structure and downslope large levee. It is possible that the symmetrical levees provided enough confinement to permit sub-vertical channel stacking, such that the avulsion occurred in a downstream position, e.g. an outer bend. Therefore, it is possible to infer vertically stacked channel-levee systems are more likely to occur in relatively upstream positions in the absence of inferred tectonic and/or obliquity controls, for instance, in the MCLS.

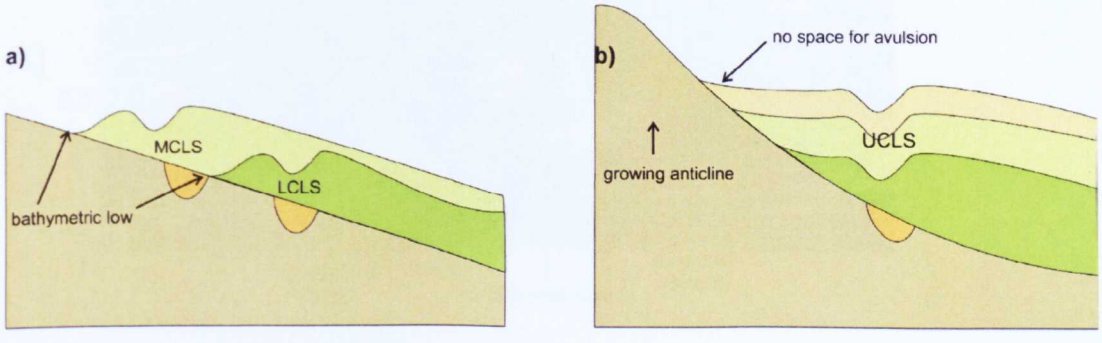

Figure 7-17 – Schematic diagrams the two patterns of channel-levee stacking in the studied area: a) the outsized right-hand levee forced avulsion trough the left-hand one and the upslope stacking of the channel-levee systems; b) the confinement of the channel between the outsized right-hand levee and the upslope anticline favour the sub-vertical stacking of channel-levee elements (UCLS).

The Indus Fan and the Niger Delta show similar vertical stacking of channel-levees in the upper slope, close to the feeder canyon mouth, similar to the location of the study channel-levee system (Deptuck et al., 2003) (Fig. 7.19). These channel-levee systems, however, are not confined between the upslope structure and the downslope large levee. In a similar manner to the

study area, these stacked channel-levee elements are probably imaged upstream from the points of avulsion. Hence, these units possibly represent the upstream segment of each avulsed channel, being the uppermost one relative to the earliest active channel-levee.

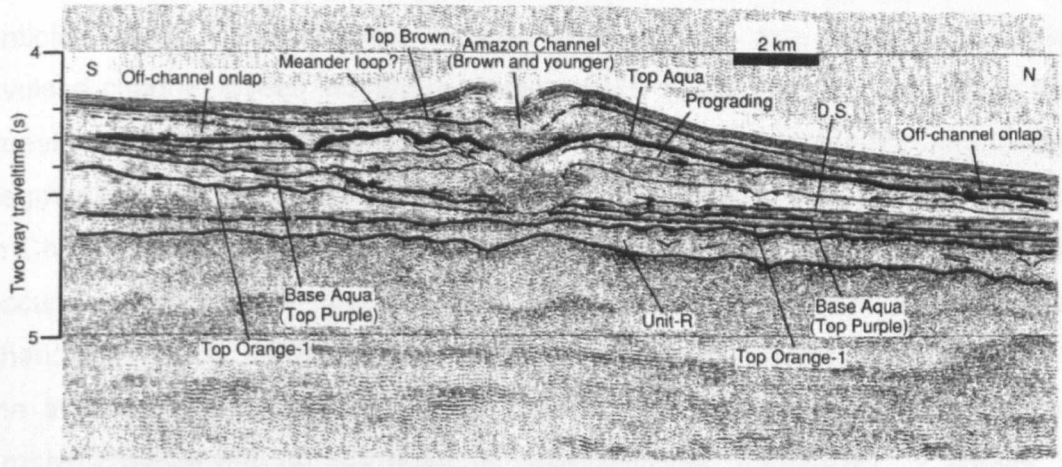

Figure 7-18 – Interpreted seismic reflection section cutting across the Amazon Channel and other channel-levees are included in the Upper Levee Complex deposited during the Late Pleistocene (Flood et al., 1995), adapted from Pirmez and Flood (1995). Notice the vertical stacking of channel-levee systems, Aqua, Brown and Amazon Channel. This seismic is located upstream of the bifurcations (i.e. avulsion points) that separate these channels

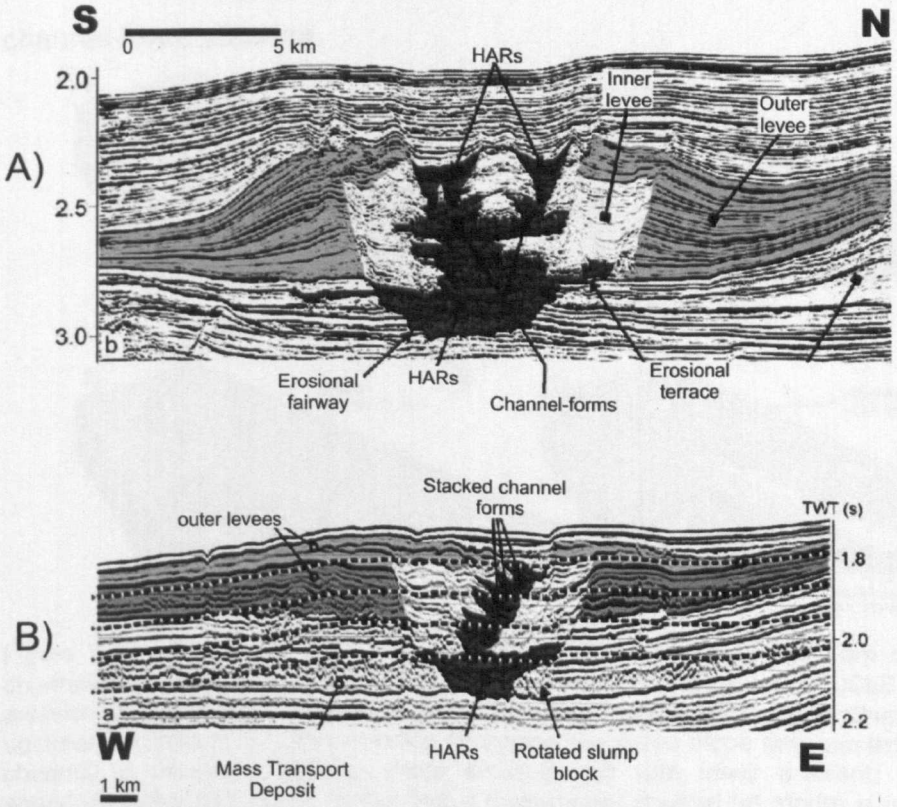

Figure 7-19 – Interpreted seismic profiles across channel-levees in Indus Fan (A) and Niger Delta/Benin-major (B), from Deptuck et al. (2003). Similarly to the study data, these channel-levees are located in the upper slope close to the canyon mouth.

7.3.2 Discussion about channel-levee stacking

The sub-vertical stacking of four channel levees forming the Upper Channel-Levee System (UCLS) is interpreted to have been due to the confinement of the channel between the outsize downslope levee and the upslope high formed by anticline uplift. Each stacked channel-levee system may represent distinct avulsed channel-levees located upstream of any avulsion point. This raises the question why no vertical stacking of channel-levee systems was recorded in the segment of MCLS upstream from the point of avulsion of the LCLS, discussed in Chapter 6. A possible explanation is that because the avulsion of the LCLS occurred upstream of the transition point from erosional to aggradational channel style (Fig. 7.20), the LCLS was expressed as an erosive channel above the avulsion node. Therefore, the following MCLS developed directly on the erosive channel with no aggradational channel-levee to stack on. Moreover, it may imply that if other downstream avulsions in both MCLS and LCLS happened they may have been during the graded ("equilibrium") or erosive phase of the channel development, which resulted in the absence of upstream channel-levee stacking.

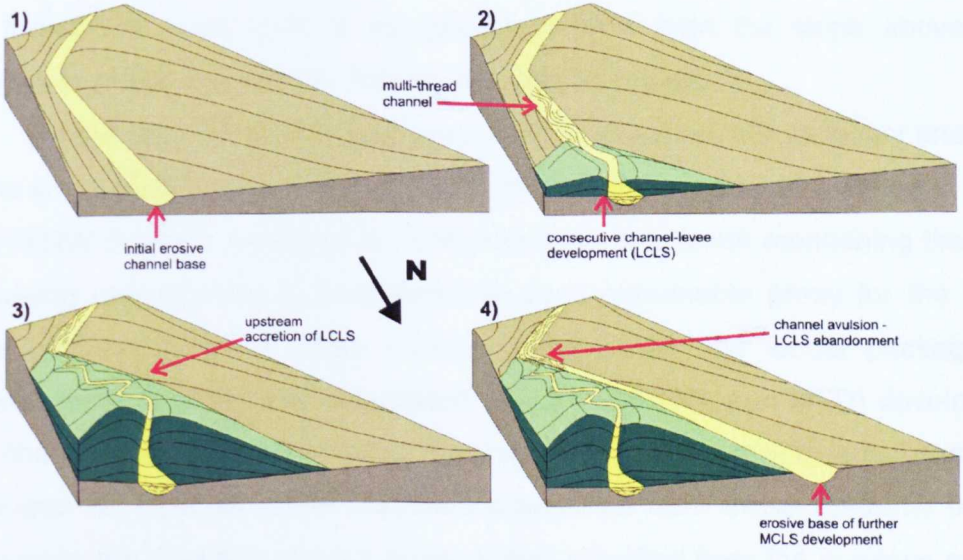

Figure 7-20 –Schematic block diagrams represent the model of upstream development of a channel-levee and subsequent avulsion. The evolution phases of the LCLS and subsequent avulsion are proposed: 1) initial incisional channel; 2)aggradation of the channel-levee and its upstream accretion; 3) channel-levee onlapping the paleo slope and upward tendency of the channel to become narrower, more sinuous and with lower gradient; 4) avulsion and abandonment of the LCLS. Notice that a multi-thread channel (at grade) is represented in the transition from erosional to agradational. The view of the diagrams is upstream.

7.4 Conclusions

Three aspects of channel distribution on slope were discussed: structurally controlled erosive channels; channels obliquely oriented on slope with lateral and upslope stacking; and confined channels vertically stacked. In each of these patterns of channel distribution the external controls on channel architecture and direction were analysed.

The pre-unconformiy erosional channels are dipping approximately toward the NE, in contrast to the post-unconformity aggradational channels which are dipping toward the N/NW. The difference of channel directions between these two intervals is thought to be due to different controls on channel development. Thus the pre-unconformity channels are strongly affected by the growing anticlines during their evolution. These anticlines (with N/NW-S/SE oriented axes) dictated the channels' orientation on slope, creating some sinuosity but without affecting the overall north-easterly channel dispersal direction. The sequence of anticline growth promoted a successive northwestward channel migration in time. The erosive character of the channels seems to be controlled by the super-elevation due to the uplift of the whole fold and thrust belt. This uplift is interpreted to have kept the slope above the equilibrium profile in the area, forcing the channels to erode.

On the other hand, the post-unconformity channels are obliquely oriented on the slope but not due to a direct control by tectonic structures although they have N/NW direction similar to the anticline axes. It is worth mentioning that the underlying unconformity is considered to be a reasonable proxy for the local slope because it is an onlap surface above which the whole package of channel-levee systems and associated deposits (HARPs and MTD) developed. The channel-levee systems occur downslope from the growing anticlines and there was no other structure identified downslope from these systems. In the study area, the direction of each channel was inherited from the previous one in a sequence of upslope stacking after systematic avulsion through the left-hand levee (viewed toward downstream). The question of what caused the first oblique channel orientation is intriguing and remains open.

The vertical stacking of channel-levee systems seems to be related to the confinement of the channel between the outsize downslope levee and the

upslope anticline which did not readily allow channel avulsion (as seen in the earlier LCLS and MCLS). Similar vertical stacking patterns have also been identified in other fans, e.g., the Late Pleistocene systems of the Amazon Fan (Pirmez and Flood, 1995), the Indus Fan and the Niger Delta (Deptuck et al., 2003). In these cases, however, the channels are not confined by external features such as tectonic structures. The channels have levees that are relatively more symmetrical, i.e., well-developed levees on both sides, which can represent a simple self confinement. The points of avulsion in these cases occurred downstream. Indeed, in the Late Pleistocene of the Amazon Fan, each stacked element of channel-levee represents a downstream channel avulsion (Pirmez and Flood, 1995). Therefore, based on this example, it is possible to infer that the studied UCLS, the Indus Fan and Niger Delta are examples of channel-levee segments upstream from avulsion points, with each stacked channel-levee element possibly representing a downstream avulsed channel. However, not all parent channel of downstream avulsions must have stacked systems because, if the avulsion occurred while the channel was still erosive or at grade, only the following aggradational phase will be present, as is shown in the evolution of the MCLS.

8 DISCUSSION

8.1 Tectonics

The studied submarine channels are located on the upper slope immediately downslope of anticlines formed by gravity driven tectonics. Therefore, understanding the structural framework of the area was important because one of the objectives of the thesis is to determine if these structures affected the slope bathymetry where the submarine channels evolved and if so, how they controlled the channel dispersion and architecture on the slope.

Some previous studies describe the gravity tectonics of the Amazon Fan (Silva, et al., 1999; Cobbold et al. 2004; and Reis et al., 2010) and many others describe the architecture and evolution of the channel-levee systems of the Quaternary of the Amazon Fan (Damuth et al., 1983a; Damuth and Kowsmann, 1998; Damuth and Kumar, 1975; Flood et al., 1991; Flood and Piper, 1997; Flood et al., 1995; Lopez, 2001; Manley and Flood, 1988; Pirmez et al., 2003). However, this is apparently the first work to establish a genetic relationship between the tectonics and channel development on the Amazon Fan.

Two tectonic styles were identified in the study area (represented by the set of thrust-cored anticlines and the tear fault). Their formation and genetic relationship are the focus of the following discussion. The set of thrust cored anticlines were interpreted to be formed by gravity tectonics because: although the seismic data are relatively shallow (down to 5 s, two-way-time travel) and do not show where the thrusts are rooted, the studied 2D line could be correlated with the section presented by Reis et al. (2010) which extends down to 10 s (Fig. 3.17). Therefore, it can be seen that compressional tectonics, characterised by a set of thrust-cored folds, occurred in response to the seaward gliding of a thick package of sediments along large listric normal faults, formed due to extension on the shelf border (Fig. 5.2), as described by previous studies on the Amazon Fan (Cobbold et al., 2004; Reis et al., 2010; Silva et al., 1999).

A style of syn-depositional growth of the anticlines was proposed after analysing the inter-relationship between the anticlines and the erosive channels present in the lower interval. The isochron map of the lower package shows that

there are thinner sediment covers on the fold crests (Fig. 5.15). These thin sediments on the anticline crests suggest that the anticlines did not grow only after the deposition of the lower package, since, if they had done the package thickness would remain approximately the same on the anticlines and synclines. Moreover, some channels cut through the anticlines (Fig. 5.15) further implying that the folds were growing during the channel development rather than pre-existing as a bathymetric barrier. Therefore, the anticlines were growing structures with sedimentation rates greater than the rates of uplift during the deposition of the lower package. If the sedimentation rates were lower than the uplift, the deposition would have occurred preferentially on the synclines with the strata pinching out towards the limb of the anticlines.

A detailed description of the relationship between erosive canyon-like channels and the growing structures with the implications for slope evolution can be found in Chapter 7. Analysis shows that the growth of the anticlines began with the outer anticline (B) then the inner anticline (D) and a later the growth of anticline (A). This indicates that the sediment glided toward downslope with heterogeneous displacement rates which varied laterally, leading to a distinct timing of anticlinal fold growth. The heterogeneity of the sediment displacement towards the NE may have favoured the development of a tear fault.

The tear fault direction changes along its trace in the study area (Figs. 5.13 and 5.14). It exhibits two fault segments with NE orientation and clearly associated extensional features whereas the fault segments with NW directions may represent compressive features with some degree of extension retained (Fig. 5.13). These observations suggest that the major compressive stress axis ($\sigma 1$) is NE whereas the extensional stress axis ($\sigma 3$) is NW (Fig. 5.14). This implies that the two blocks separated by the fault are tearing apart in a NW-SE direction (Fig. 5.13). The bathymetric high in the fault bend suggests an initial compression causing the sediment layers to fold until they ruptured and the sediments began tear apart. The fact that the same faulted block can behave as both a hanging wall and a foot wall indicate that block rotation occurred. Moreover, the tear fault has both strike and dip offsets which indicate oblique movements between the east and west fault blocks (Fig. 5.13). The dip-slip

orientation of the normal faults in segments 1-2 and 3-4 are opposite to each other (Fig. 5.13 a and c) and may indicate that the faulted blocks rotated with a rotational axis located approximately within the area of segment 2-3 (Fig. 5.14).

Analysis of the growth strata shows that the structures were active before the deposition of the lower package and were mainly active during the deposition of middle package (Fig. 5.7). Rather than being driven by thrust and fold development which mainly uplifted during the middle package deposition, most of the transpressional uplift at the fault bend occurred during the deposition of the lower package as evidenced by the development of growth strata (Fig. 5.13b). The fault tearing occurred after the transpressional uplift as it is seen to split the sediments of the lower package (Fig. 5.13b). Therefore, there is a correlation between the timing of the maximum fold activity and the tear fault formation which occurred during the deposition of the middle package. This may imply that the tear fault is related to the same process of thrusting and folding due to gravitational sediment gliding on slope.

8.2 Stratigraphy

The key horizon in the tectono-stratigraphic analysis of the seismic data is the unconformity that extends from the shelf to the upper slope (Fig. 5.2). It represents an interruption (time gap) in the deposition of the sub-parallel reflections of the pre-unconformity package before the recurrence of sedimentation with the onlapping strata of the post-unconformity package. It also marks the deactivation of most of syn-depositional tectonics and it is erosive on the anticline crests.

Subsequently a series channel levee systems (in the studied area) which are part of a "levee complex" (i.e., a group of channel-levee systems separated by maximum flood surface or mass transport deposit) are deposited as described by Flood and Piper (1997). Previous studies (Damuth, 1977; Damuth et al., 1988; Flood and Piper, 1997; Flood et al., 1995) concluded that the most of the deposition during the Quaternary on slope in the Amazon Fan occurred during sea level lowstand because during highstand the sediments were trapped on the shelf. Hence, the "levee complexes" represent lowstand system tracts deposited above the unconformity, due to the direct connection of the river to the upper slope during lowstand. Therefore, in the studied case, the

unconformity is interpreted to represent a fragment of the former palaeo-slope on which the Quaternary levee complexes developed.

The unconformity also separates the seismic data into two separate packages of sediments each with different levels of deformation and distinct styles of channel architecture. In the pre-unconformity interval erosive channels are strongly affected by tectonics, whereas in the post-unconformity interval channel-levee systems evolved only slightly affected by tectonics. These observations raise the question of whether a relationship between the channel architecture, erosive and/or aggradational exists, and if so, how the tectonic activity influenced it.

8.3 Erosional vs. agradational channel

The erosive channels of the pre-unconformity interval show similar amplitude to those of the enclosing rocks. For this reason, it was not possible to infer different compositions based on the amplitude character. This is unlike the post-unconformity channel-levees, where it is interpreted that the mud rich levees present low amplitude reflections and the sand-rich channel fill and HARPs present high amplitude reflections. However, the erosive channels may develop a lenticular shape (Fig. 5.16) and may have convex upper boundaries which might suggest differential compaction between the channel fill and the surrounding sediments. This characteristic implies that the channel fill may possibly have been formed by coarser-grained sediments than the surrounding host sediments because sand-rich sediments are more resistant to compaction effects than mud-rich sediments (although their reflections present similar amplitude intensity) (Kosa, 2007). Erosional channels, furthermore are frequently associated with coarse grained turbidite currents (Clark and Pickering, 1996b).

As was discussed in Chapter 7, it is very likely that the growing folds, which were more active during deposition of the pre-unconformity package of sediments, induced the development of a steep local slope topography that was always above the equilibrium profile (Fig. 7.5). This may have inhibited the development of large aggradational channel-levee systems in the pre-unconformity package, since, in order to aggrade, accommodation space is required (e.g. Kneller 2003).

In the post-unconformity package, characterised by less active tectonics and lower slope gradients, channel-levee systems developed downslope from the fold and thrust belt (e.g., Figs. 5.2 and 5.7). In the studied area these channel-levee systems however, evolved from a basal erosive channel which was not described in previous studies on the Amazon Fan (Damuth, 1977; Damuth et al., 1988; Flood and Piper, 1997; Flood et al., 1995; Lopez, 2001; Pirmez et al., 1997).

The chaotic low amplitude reflections of the basal erosive channel fill can be associated with slump deposits, which maintain close proximity to the channel base, whereas the chaotic high amplitude reflections resemble products of remobilization of the enclosing HARPs (Fig. 5.22). The chaotic and high amplitude reflection seismic facies can also be associated with coarse-grained thalweg deposits from laterally migrating channels, as interpreted in Indus Fan erosive channels (Deptuck et al., 2003). The ordered high amplitude reflectors may represent channel axis deposits, and the laterally dipping reflections (Fig. 5.22) are possibly lateral accretion packages (Abreu et al., 2003) that developed when the channel was in equilibrium, i.e., without aggrading or eroding, and instead, meandered laterally (Kneller, 2003). The filling of this kind of initial erosive channel has been described by previous workers as involving complex alternations of channel architectures and facies, but often ending up with an aggradational channel levee (Kneller, 2003; Mayall and Stewart, 2000; Samuel et al., 2003).

Previous studies (Damuth, 1977; Damuth et al., 1988; Flood and Piper, 1997; Flood et al., 1995; Lopez, 2001; Pirmez et al., 1997) suggested that the initiation of a channel levee system in the Amazon Fan occurred with channel avulsion and the deposition of sheet-like sand bodies (HARPs) in the adjacent inter-channel lows. Afterwards, the upward transition from the HARPs to channel-levee would be due to the waning of HARPs deposition and return of the channel axis to a graded longitudinal profile with levees growing down-fan to confine the sand-rich basal parts of turbidite currents to a narrow channel axis leading to subsequent channel-levee development (Lopez, 2001).

Deptuck et al. (2003) attribute the origin of the basal erosive channel (erosional fairway) to the interval when sea level was falling, when the sediment supply to the slope was at a maximum; the development of under-fit narrower

channels, flanked by inner levees (Fig. 8.1) thus corresponds to periods of reduced sediment supply during rising sea level. If this interpretative scheme is correct it operated only in the upper fan of the Amazon fan where the studied area is located, because the basal erosive channels were not identified in the base of the previously studied channel-levee systems that occur on the middle fan (Damuth, 1977; Damuth et al., 1988; Flood and Piper, 1997; Flood et al., 1995; Lopez, 2001; Pirmez et al., 1997). Therefore, it is probable that the occurrence of the basal erosive channel in the studied systems is related to its' position on the upper slope. At this position steeper gradients and more efficient turbidity currents are more likely to occur than in the Middle Fan (where most of previous works are located).This is because the flow tends to become less efficient moving down the slope, farther from the source. The studied channel-levee systems are located in the transition between the canyon and the strictly aggradational channel-levee systems. They are also a transition between the strictly erosive channels of the pre-unconformity interval and the strictly aggradational channel-levees of the Middle Fan. Therefore, the reason why there was no erosive channel base in the channel-levee systems analyzed by ODP Leg 155 is because they occur downstream of the current study area and further away from the Amazon Canyon mouth.

This style of slope incision (i.e., basal erosive channel style in the studied area) corresponds to the erosional fairway of Deptuck et al. (2003) and the "slope valley" of Samuel et al. (2003). The "slope valley" incision was thought to create accommodation for the channel-levee to aggrade in the case of the Nile Delta (Samuel et al., 2003). The studied systems of the Amazon Fan, however, are more similar to channel-levee systems of the Indus Fan and Niger Delta than to the Nile Delta. As noted above, in the Nile Delta the necessary accommodation for channel-levee aggradation was created by the erosion of the slope valley (Fig. 8.2). On the other hand, in the Amazon Fan, Indus Fan (Fig. 7.19) and Niger Delta, most of the channel-levee systems rise above the erosive base which suggests that the accommodation space for channel aggradation might not have been created merely by the erosion. The analysed channel-levee systems in the Indus Fan, which also exhibit a basal erosive channel (erosional fairway) (Deptuck et al., 2003) are also located on the upper slope and close to structural highs (Fig. 8.1). This suggests that the location

and/or the presence of growing structures played an important role in the development of these channel levee systems as they did in the Amazon Fan.

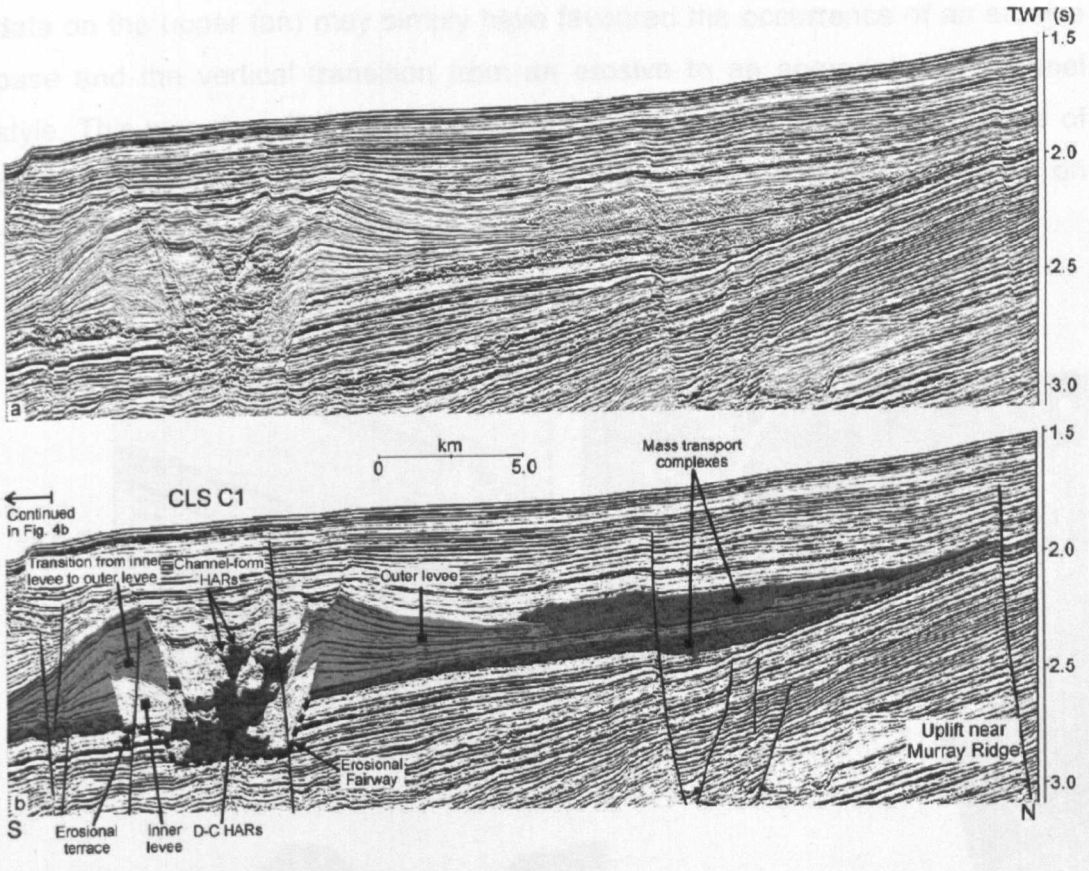

Figure 8-1 - Channel-levee system of the Indus Fan showing a basal erosive channel (erosional fairway) located in an analogous position of the studied channel-levee systems of the Amazon Fan, i.e., close to uplifted structures (Murray Ridge). From Deptuck et al. (2003).

Understanding the cause of the vertical transition from erosive channel to aggradational channel-levee is hindered because of the lack of rock data and age control in the study area. However, it is known from the literature that the vertical evolution from erosive to aggradational may reflect an interaction of different parameters. The combination of changing sea level and evolving sediment source characteristics (sediment supply and grain size, etc.) are believed to have caused changes in gravity flow character though time (including flow composition, size, erosiveness, frequency and maybe triggering mechanisms – Piper and Normark, 2001). For instance, this architectural transition in the Niger Delta is apparently due to the decrease in the gravity flow size with time and erosion level (Deptuck et al., 2003). In the studied case on the upper Amazon Fan, aside from the relative sea level change and the flow

parameter variation, the increase of accommodation space (due to local tectonics) and the proximity to the canyon mouth (i.e., the location of the study data on the upper fan) may simply have favoured the occurrence of an erosive base and the vertical transition from an erosive to an aggradational channel style. This was described in Chapters 6 and 7. However, the precise nature of changes in the gravity flow or accommodation space and resultant impact on channel-levee architecture still needs further investigation.

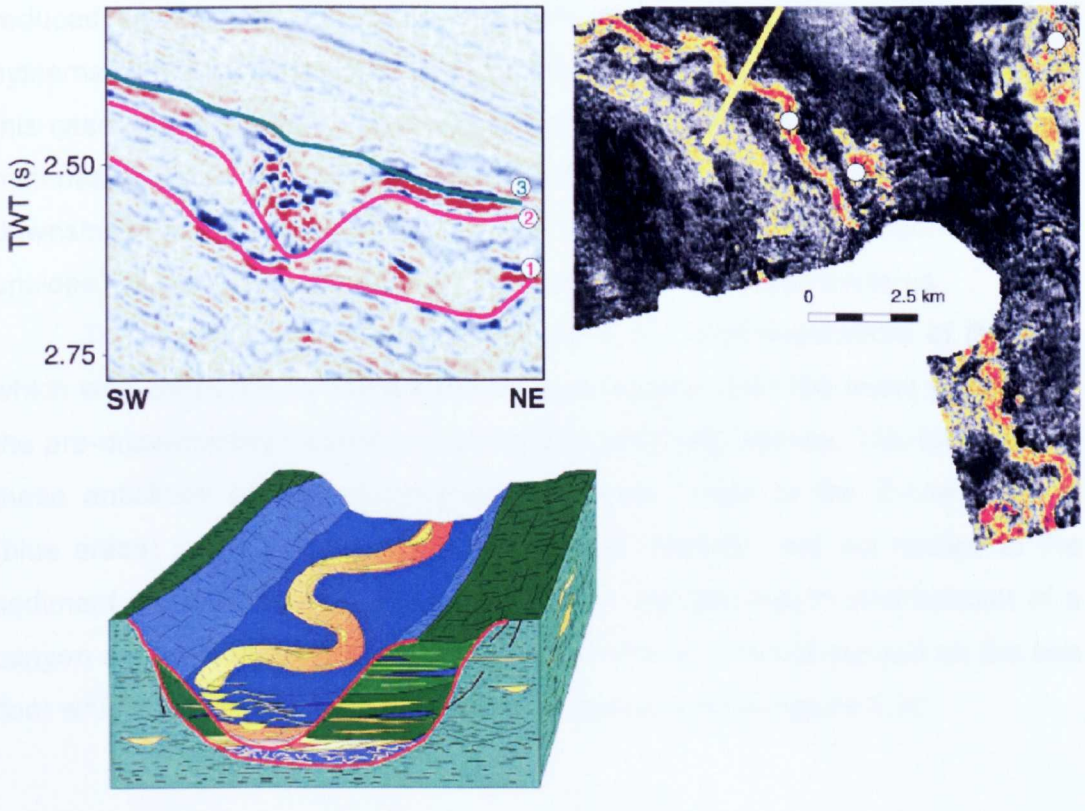

Figure 8-2 - Seismic section, map and block diagram showing the infill of the "slope valley" in the Nile Delta. Notice the aggradation the channel levee confined in the erosive valley and due to the accommodation created by the erosion. From Samuel et al. (2003)

8.4 Transition from the pre- to the post-unconformity interval

The isochron maps of the lower-middle packages in the pre-unconformity interval, and the isochron map of the post-unconformity interval show that sediment dispersion within the study area varied with time (Fig. 8.3). In the pre-

unconformity interval, during the deposition of the lower package, the structures were already active and locally deflecting the channel direction on the slope, while still allowing the gravity currents to flow downslope, approximately toward the NE (Fig. 8.3a). Consequently, deposition was distributed across the slope, with major thicknesses along the channels and minor thicknesses on the top of the growing structures. During the deposition of the middle package, the uplift rate was higher and caused the trapping of sediments upslope of the anticlines, in synclines (mini-basins) between the anticlines (Fig. 8.3b).

During the post-unconformity interval, the uplift rates of the anticline reduced significantly and the subsequent development of the channel-levee systems allowed the accumulation of major sediment thicknesses (Fig. 8.3c). In this case, the local depocentre moved seawards after the filling of the upslope mini-basins. This location was favoured by accommodation space generated downslope on the palaeo-seafloor due to the thrust-folding (which occurred upslope) allowing the aggradation of following channel-levee systems.

To summarise, there was a change in the local depocentre of the area which was controlled by the growth of the anticlines, from the lower package of the pre-unconformity interval to the post-unconformity interval. The formation of these anticlines created accommodation space. Most of the thinnest layers (blue areas) in the post unconformity interval, however, are not related to the sediment dispersion at the time of deposition, but are due to later erosion of a canyon on the seafloor (Fig. 8.4). Figure 8.4 shows a recent canyon on the sea floor which coincides with the lowest thicknesses seen in Figure 8.3c.

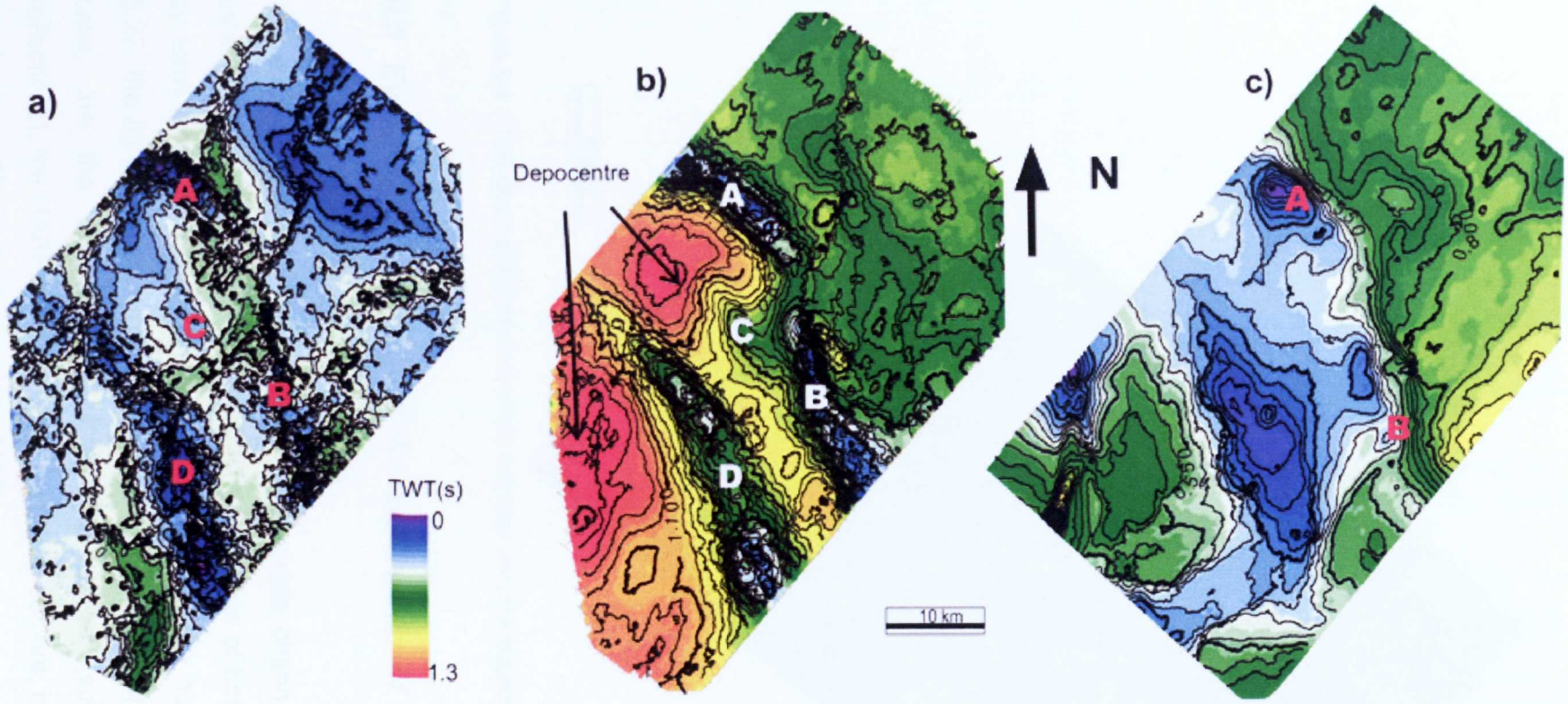

Figure 8-3 – Isochron maps of the lower (a) and middle (b) packages in the pre-unconformity interval and of the post-unconformity interval (c). The anticlines A, B, C and D are located on the maps.

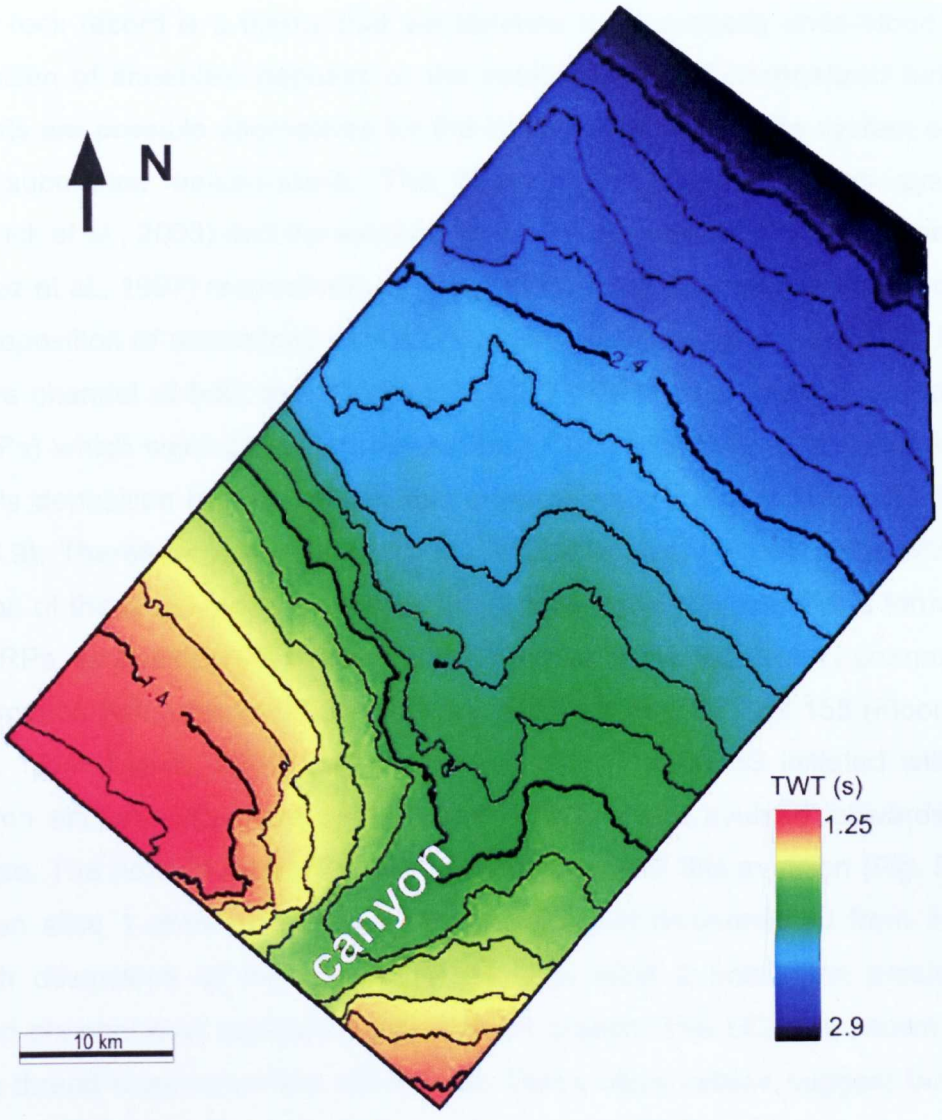

Figure 8-4 – Two-way-travel time map of the sea floor with the location of the canyon.

8.5 Evolutionary history of the deposition of the channel-levee systems in the studied area

The evolutionary history of the lower and middle channel-levee systems was established based on the analysis of the sequence of horizon slices across the systems interpreted through time (Fig. 5. 27). In the horizon slices of Figure 5.27, the light grey colours represent more coherent reflections, which in this case, are the pre-unconformity seismic facies (sub-parallel continuous reflections), the HARPs or the HARs. The dark colours, however, represent the erosive base fill, the levees and the MTD.

The manner in which initiation of the turbidite flows on slope is expressed in the rock record is a theme that yet remains to be properly understood. The deposition of sheet-like deposits or the establishment of channelized turbidity currents are possible alternatives for the initiation of the turbidite system on the local submarine palaeo-slope. The Niger Delta and Indus Fan systems (Deptuck et al., 2003) and the systems of the middle portion of the Amazon Fan (Pirmez et al., 1997) respectively are examples of initiation with channel incision and deposition of unconfined sands first, then incision by a channel. The basal erosive channel of both the LCLS and MCLS cuts through sheet-like deposits (HARPs) which were deposited before the LCLS, and there is no evidence of HARPs deposition between these two channel-levee systems (Figs. 5.18, 6.7 and 6.9). Therefore, the initiation of the MCLS apparently took place with the incision of the basal erosive channel rather than sand inundation and formation of HARPs, as has been described in the literature of the Quaternary channels of the Amazon Fan, mainly based in the proceedings of ODP Leg 155 (Flood and Piper, 1997; Lopez, 2001; Pirmez et al., 1997). The MCLS initiated with the avulsion and abandonment of the LCLS. The channel avulsed leftwards and upslope. The horizon slices 1 and 2 show evidence of this avulsion (Fig. 5.27). Horizon slice 1 shows the former erosive channel disconnected from its left branch downslope of the bifurcation. Horizon slice 2 shows an erosive or graded channel now connected with the left branch. The LCLS is shown as a single thread channel on the left branch. These observations suggest that the avulsion occurred above or at the point of longitudinal transition from aggradational to erosional in the precursor LCLS. The block diagrams 1 to 3 in Figure 8.5 illustrate the initial incision of the basal erosive channel, aggradation of LCLS and the avulsion above the transition point between aggradational and erosional channel sections.

The MCLS had a complex evolution which includes a transition from a basal erosive channel to an aggradational channel-levee system, then to levee collapse, avulsion and sand inundation in adjacent lows (Fig. 5.27). In cross section, the transition from erosive to aggradational is roughly marked by the passage from a basal large-scale channel cut upward to a constructive channel-levee (Figs. 6.16, 6.17 and 6.18). In map view, the horizon slices of the RMS coherence (Fig. 5.27) show also distinct channel features: blurry chaotic facies

inside the large scale erosive incision, with both multiple-thread and single-thread channels. The single-thread channel is associated with the agradational channel-levee where the channel axis commonly remains more or less fixed in position as the system aggrades, whereas the multiple-thread channel is associated with what are interpreted to be graded i.e., equilibrium channels, with meanders migrating laterally on what is thought to be an equilibrium surface. These associations between the planform and the channel types have previously been described by Kneller (2003) and Peakall et al. (2000). In the study area, the transition point between this single and multi-thread channel planforms migrates downstream, and implies the downstream migration of the agradational channel-levee over the basal erosive channel.

In the case of the MCLS, most of the levee buildup occurred prior to the channel fill because the high amplitude reflections of the channel fill onlap the internal limbs of the levees (Fig. 6.18). Only the narrowest and basal portion of the channel seems to have deposited simultaneously with the levee formation, because at this level the channel fill high amplitude reflections have some lateral continuity with the low amplitude reflections of the levee (Fig. 6.18).

In the downstream part of the system, however, only the basal portion of the aggradational channel-levee is preserved (Fig. 6.17, section AB, Fig. 6.20, section AB and Fig. 6.21). This suggests that there was levee collapse and a high degree of associated erosion. The flow that eroded the downstream portion of the channel-levee also partially eroded the inner levee walls of the upstream segment of the MCLS (Figs. 618 and 6.20, section CD). The reduction in the thalweg gradient, the higher sinuosity and abrupt reduction of channel width immediately downstream of the boundary between the upstream and downstream segments of the MCLS may have favoured an outer-levee collapse (see channel plan view in Fig. 5.26). These restrictions to the flow through the downstream channel segment combined with the relative levee weakness and a strong increase in sediment flux possibly promoted the levee collapse and erosion of the downstream upper part of the MCLS.

Another levee collapse is suggested southward, upstream and outside the seismic survey area, closer to the feeder canyon mouth. This possible collapse may have promoted the partial avulsion of the channel, leading to a flow bifurcation which would reduce the flow efficiency and promote the

deposition of the channel fill and the sand inundation forming HARPs in the adjacent low between the MCLS and the palaeo-slope. An upstream levee collapse is suggested because of the occurrence of a mass transport deposit (MTD) underneath the HARPs (Fig. 5.27, slices 4 to 8). The MTD is assumed to be a product of an upstream levee collapse because it slumped along the low between the levee and the palaeo-slope extending from upstream channel-levee portion (outside the seismic data) (Fig. 5.27, slices from 4 to 8).

After the levee collapse, the flow bifurcation allowed the simultaneous deposition of the channel fill (MCLS) and the HARPs (discussed in Chapter 6). This interpretation is based on the evidence that the reflections of the upper portion of the channel fill (MCLS) onlap the eroded inner channel walls, HARPs onlap the erosive surface on top of the downstream segment, and the internal erosion of the channel is the same erosive surface on the top of the downstream segment. Flow bifurcation was proposed assuming that there was no significant bathymetric difference between the abandoned channel floor and the adjacent area between the channel-levee system and the palaeoslope (such a difference might have favoured the migration of the knickpoint upstream in the channel capturing the flow completely).

The depositional evolution on the slope, from the initiation of the LCLS to the HARPs deposition is illustrated in Figure 8.5, in block diagrams 1 to 10. The sequence of block diagrams illustrates the initial incision, the upstream accretion of the LCLS, avulsion and incision of a channel followed by the downstream development of the MCLS, partial erosion of the downstream segment of the MCLS, upstream levee breach with associated MTD slumping and final channel fill and HARPs deposition. The details of the avulsions, MCLS erosion, HARPs deposition, channel fill, channel plan form and the possible causes the distinct style of development of the two systems are discussed in Chapter 6.

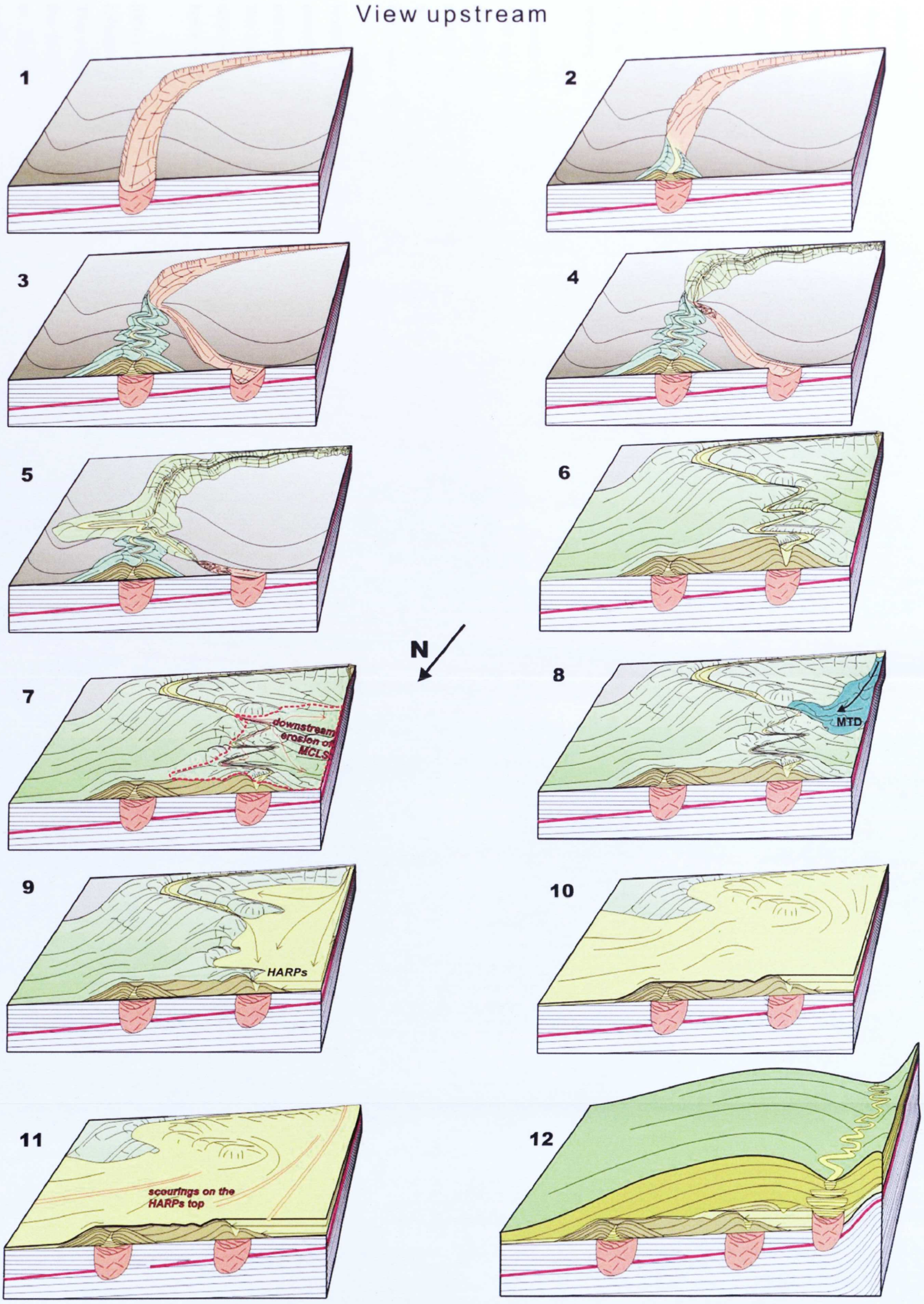

Figure 8-5 - Block diagrams summarizing the slope evolution of in the study area: 1 - initiation with an erosive channel cutting through previous HARPs; 2 – upstream development of the LCLS; 3 – avulsion at the point of transition from erosional to aggradational channel; 4 to 6 – downstream development of the MCLS; 7 – levee collapse and downstream erosion of MCLS; 8 - upstreaml channel avulsion (MTD associated); 9 to 10 – channel filling and sand inundation in the low between the system and the paleoslope, with HARPs formation; 11 – scouring of the top of the HARPs; 12 –development of the UCLS.

The UCLS started with the incision of an erosive channel in the HARPs deposited after the avulsion the MCLS. The transition from unconfined deposition of HARPs to confined erosive channel is not yet fully understood. Some authors interpret HARPs as being deposited during equilibrium readjustment following disruption due to avulsion, with HARP construction decreasing when the channel thalweg returned to a graded longitudinal profile (Lopez, 2001; Pirmez et al., 1997). However, in the study area of these authors, which is in the middle Amazon Fan, there is no erosive channel base cutting through the HARPs but a vertical transition from HARPs to an aggradational channel-levee system. In the study area, on the top of the HARPs, there are some scours (in addition to the erosive channel base that evolved to the UCLS (Fig. 8.5)). This may indicate that before the tubidite flow focused into the main erosive channel axis, erosional turbidite flows scoured the HARPs top.

This system presents a complex evolution, with an internal gap in deposition (discontinuity) marked by a downlap surface (yellow horizon in figs. 7.15 and 7.16) which clearly divides the system into two main packages with distinctive evolution. The uplifted left-hand underlying levee (Figs. 5.32) can sometimes be seen with disruption of the internal reflections (Fig. 5.31) which suggests that the anticline was active after and possibly during the deposition of the lower interval of the UCLS.

The complexity of the channel fill below the internal discontinuity (yellow horizon, Figs. 7.15 and 7.16) which shows portions with either regular fill or with chaotic and clay rich material, may also be related to the adjacent uplift and consequent slumping of material from the levee into the channel. The slump in the base of the right-hand levee with apparent movement direction toward the channel axis also suggests that the channel was uplifted after the levee slump because it is now topographically higher than the right-hand levee base.

The three stacked channel-levees in the upper package of the UCLS have varied depositional characteristics. For instance, the sinuosity is quite different for each of the three channels and increases from the base to the top. The channels become narrower and more sinuous upward (Fig. 7.16), similar to the stacked channel-levee elements in Niger Delta and Indus Fan (Deptuck et al., 2003). These changes in channel characteristics can be related to changes in flow properties (Kneller, 2003). An increase in the clay content of the channel

fill from the base to the top could also have developed – an interpretation based on the reduction in the contrast of amplitude between the channel fill and the levee, possibly associated with the increase in channel sinuosity (Fig. 7.16).

The vertical stacking of channel-levee systems may be attributed to their confinement between the large right-hand levee which developed downslope, covering the previous MCLS, and the upslope folding related to the slope tectonics. These two highs did not allow the channel to avulse as it did in the previous MCLS and LCLS. Therefore, channel avulsion was inhibited in the study area but, downstream, where there was less influence of the thrust and fold belt and the slope gradient was less steep, channel avulsion could have occurred. If so, each stacked channel-levee element composing the UCLS may represent the upstream segment of a downstream avulsed channel-levee. The relationship between the UCLS evolution and the slope deformation, channel asymmetry and avulsion are more fully described in Chapter 7.

8.6 Initiation of turbidite system on slope

The study of the evolution of the three channel-levee systems raised the discussion of how turbidite systems can initiate on slope. In the literature two possibilities are considered: initiation with an incision (basal erosive channel) or with a slope lobe (HARPs). For instance, Pirmez et al. (1997) considered that the initiation of the channel-levee systems of the Amazon Fan is related to channel avulsion and deposition of an intra-slope lobe which evolves vertically to a channel-levee system. On the other hand, Deptuck et al. (2003) considered the initiation of the channel-levee systems in Niger Delta and Indus Fan to occur with the development of an erosional fairway which is equivalent to the basal erosive channels described in this thesis.

In the studied area, all three studied channel-levee systems evolved from a basal erosive channel. The UCLS, however, cuts HARPs deposited after partial avulsion of MCLS whereas the MCLS evolved from an incision created after avulsion of the LCLS (there are no HARPs deposited between LCLS and MCLS). The occurrence of an erosive channel may be related to the position on the fan. In the studied area, close to the feeding canyon, the turbidite flows reaching the slope are more erosive and efficient, favouring the occurrence of a basal incision. This does not happen in the downslope channel-levee systems

in the Middle Amazon Fan where the flows may lose their efficiency and erosive character, thus the systems do not develop a basal erosive channel.

The occurrence of the HARPs seems to be associated with the inferred evolution of the turbidite flows which built the previous system together with the way in which the channel avulsed (see detailed discussion in Chapter 6). The different evolutions of the flows led to distinctly different channel-levee architectures (e.g., LCLS and MCLS). If so, the identification of the two architectures can be predictive in respect of the likelihood of later HARP development. The evolution of the LCLS suggests a general tendency of gradual reduction in the magnitude and the sand content of the flows. The evolution of the MCLS indicates a general tendency of gradual increase the magnitude and the sand content of the flows. Therefore these two occurrences may be associated with the occurrence of the HARPs at the end of the MCLS deposition and the absence of HARPs at the end of the LCLS deposition.

The initiation of the UCLS occurs with the incision of the basal erosive channel in the HARPs deposited at the end of the MCLS deposition. Therefore, there was a marked change in the character of the turbidite flows from essentially depositional (HARPs deposition) to essentially erosional.

8.7 Relevance of the results for depositional facies prediction and industrial application

Although no significant hydrocarbon accumulation has yet been found in the Amazon Fan, the studied data were nevertheless fruitful because the analyses of the seismic volume allowed the relationship between the interpreted depositional facies and their probable evolutionary history to be established. Thus the understanding of the evolutionary history of the fan components can help to predict the depositional facies distribution in the fan. Although the studied depositional history is exclusive to the Amazon Fan some general tendencies can be used to understand the depositional architectures of channel-levee systems of other similar slope areas. Therefore, these studies can help the prediction of petroleum system components such as reservoir rocks and caprocks in less studied areas.

The two important channel-levee architectural morphotypes identified (widening upward (MCLS) and narrowing upward (LCLS)) are associated with two distinct spatio-temporal evolutions or channel-levee style: downstream and upstream accretion, respectively. The models of upslope and downslope accretion may indicate sand prone areas; as was discussed in the last section, the relation of the two different evolutionary histories may relate to the occurrence or not of the HARPs. This is important because the intraslope or avulsion lobes (HARPs) are recognized as sand-rich sheet deposits (Pirmez et al., 1997 and Lopez, 2001). Furthermore if the HARPs are also located underneath a mud-rich channel-levee system, e.g. as in this study, where the HARPs are underneath the UCLS, the HARPs present a potential oil reservoir because the mud-rich sediments may form a caprock, providing a trap.

The identification of stacked channel-levee elements, e.g. UCLS, may indicate downslope avulsion. These avulsions may be associated with possible intra-slope lobe development. If the channel-levee element, component of the UCLS has a widening upward morphotype it might be related to the occurrence of a downslope avulsion lobe (HARPs). On the other hand, if the channel-levee element has a narrowing upward morphotype it might not be related to the occurrence of a downslope avulsion lobe. Therefore, the occurrence of the three different channel-levee architectures described in this thesis can give suggestions on the likelihood of occurrence of downslope sand prone areas.

8.8 Channel obliquity to the main slope

One of the initial motivations of this research was to understand the reason why the Quaternary submarine channels in the study area are oblique to the current main slope dip. As was discussed in Chapter 7, this obliquity is now thought to result from the recurrent avulsion through the left-hand levee as a result of levee asymmetry. This asymmetry is characterized by the outsized right-hand (downslope) levee. The outsized levee, however, seems to result from the channel obliquity to the main slope dip. A pressure gradient within flows acting across the channel axis and down the slope could account for the building up of downslope larger levee. Such a difference of pressure gradient is more likely to occur on the upper slope where the slope gradients are steeper. On the middle/lower slope the slope gradient is very low, reducing the effect of the

pressure gradient. This explains why the levee asymmetry is more commonly observed in the upper fan (the study area) than in the middle/lower fan (the area studied by ODP Leg 155).

Although any interpretation of what causes the first oblique orientation of the former channel on slope that dictated the N/NW direction of the following channels is speculative, some ideas can be suggested. Firstly, the levee asymmetry is more likely to occur on the upper slope, so the recurrent channel avulsions causing upslope stacking would therefore only occur in this area. Secondly, even if the former channel had a NE direction, which is approximately the same direction as the main slope dip, if the first avulsion occurred on the upper slope such that the new channel course becomes oblique to the slope, an outsized downslope levee would develop (Fig. 8.6). Therefore, any following sequence of avulsions may be progressively more likely to occur through the left-hand and upslope levee due to this levee asymmetry. This may be more likely to take place on the upper slope where the gradients are higher (Fig. 8.6). On the other hand, in the middle/lower slope there is not likely to be a preferential direction of avulsion because the levees tend to be symmetrical.

8.9 Further work

The Lower Package and the Post-Unconformity interval were reasonably well studied in this project but the Middle Package (see Fig. 4.6) was not investigated. The characterization of the architectures and the understanding of the distribution of the erosive channels present in the Middle Package in relation to the growth strata and the structures could be compared with the channels in the Lower Package and with channel-levee systems in the Post Unconformity Interval. A possible focus for study could be the analysis of the effects of tectonics in the channel development, for instance, to determine if they were able to erode through the growing anticlines or if the anticlines were able to pond the turbidite flows. These combined results would give a more integrated idea of the evolution of the tectono-sedimentation on slope from the point of deposition of the Lower Package up to the Recent. In order to study this interval, a similar method of analysis could be taken, extracting a sequence of horizon slices of coherence only because there is no significant contrast of amplitude between the reflections in the Middle Package.

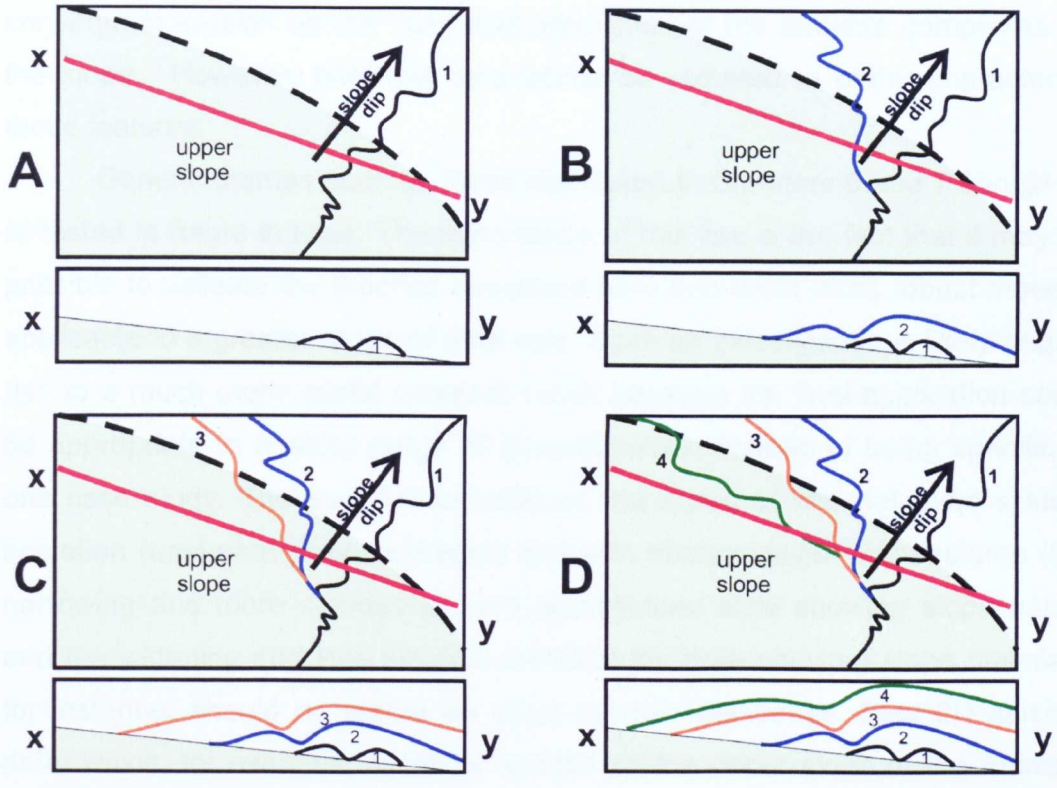

Figure 8-6 – The schematic diagrams show a sequence of channel avulsions (from channel 1 to 4) in plan and cross section view. Channel 1 has approximately the same direction (NE) of the main slope dip. The sequence of avulsed channels oblique to the slope dip on the upper slope (green area) favours the development of levee asymmetry and the consequent sequence of left-hand levee breakthroughs.

The filling of the erosive channels of the Lower Package and of the erosive base of the systems in the Post-Unconformity Interval were not well visualized. Therefore, the evolution of these channels and the transition to the later channel-levee systems could not be described with a high level of confidence in this thesis. In order to understand the way the erosive channels in the lower package and on the base of the channel-levee systems of the post-unconformity interval were filled, extraction of horizon slices of spectral decomposition could be done. This attribute measures the frequency of amplitude and could possibly improve the visualization of the internal arrangement of the channel fill reflections.

Another line of enquiry would be to check if there is correlation between the erosive surfaces identified in the shelf border (Fig. 5.3) and the "Levee Complexes" described in the ODP Leg 155 Procedures (Fig. 3.9). These

surfaces may represent sequence boundaries associated with sea level fall, consequent erosion on the shelf and deposition of the turbidite complexes on the slope. However, borehole data would be required to better characterize these features.

Generic themes such as those discussed in Chapters 6 and 7 should be re-tested in future studies. The importance of this lies in the fact that it may be possible to validate the theories described here and erect more robust models, applicable to a greater range of data sets. Such an investigation is likely to give rise to a much more useful research result because the final application could be appropriate to a wider range of general cases, instead of being specific to one case study. The association between the styles of channel-levee system accretion (upstream or downstream) and with channel-levee architectures (the narrowing and more sinuous upward architectural style showing slope onlap; and the widening and less sinuous architectural style showing slope downlap) for instance, should be tested on other seismic databases. New 3D seismic data, which, for example, could be located on the upper slope of the Amazon Fan or on the upper slope of another mud rich fan (e.g., the Indus or Bengala) should also be analyzed, and the association between styles of system accretion (development) and channel-levee architecture ought to also be investigated. Furthermore, outcrop analogs may be investigated in order to demonstrate evidence of the relationships discovered (e.g., channel-levees of Rosario Formation, Baja California, Mexico, described in Kane et al., 2007).

The occurrence of channel orientations oblique to the main slope was not completely understood. The idea proposed here that the occurrence of avulsion on the upper slope, where there are steeper gradients, would favour a downslope oversized levee which would lead to the avulsion to the same side (i.e. upslope) repeating in a sequence of avulsions, could be checked in future studies. The investigation of other 3D data sets imaging the upper fan and lower fan of this or other deep water systems with the purpose of examining the occurrence of levee asymmetry/symmetry and its' relation with recurrent avulsions toward the same side and consequent channels obliquity on slope would support the model proposed in this thesis, and therefore would also be a valuable subject for further work.

9 CONCLUSIONS

9.1 Introduction

This thesis primarily describes and analyzes the evolution of a range of channel architectures of Pleistocene age developed on the upper slope of the Amazon Fan, as described in Chapter 5. The interpretation of the slope channels' evolution includes different scales and types of analysis: placing the study 3D survey into its regional tectono-stratigraphic context by matching the data to a large scale regional 2D seismic dip line; structural analysis; the examination of the interaction between the two main channel styles (erosive/canyon-like channels and aggradational/channel-levees) and slope deformation; and the assessment of the contrasting styles of development of the channel-levee systems. Two conceptual themes emerged from the analysis of the slope channel evolution in the area: the spatio-temporal evolution of channel-levees (Chapter 6) and the controls on patterns of channel distribution on slope (Chapter 7). The objective of this chapter is to present a summary of the original work detailed in Chapters 5, 6 and 7, and the conclusions obtained from the study.

9.2 Slope evolution

9.2.1 Tectono-stratigraphy

The study area (i.e., the area covered by the 3D seismic data) was significantly affected by fold and thrust belt activity. This activity is characterized by the development of thrust-cored anticlines, which can be genetically related to listric normal faults on the shelf margin. These structures were formed by the gravity gliding of thick packages of sediments from the shelf margin towards the ocean. Locally, the sliding of these sediments towards the basin (NE) caused heterogeneous displacements that led to the division of the package into two blocks by a strike-slip fault of approximate N-S strike orientation. The majority of the tectonic activity is interpreted to have been syn-depositional, and characterized by the occurrence of growth strata on both the upper slope and the shelf edge.

The study data are subdivided into two main intervals by a pervasive unconformity which can be traced up to the shelf. The unconformity may represent an important gap in the deposition on the slope because it separates the underlying strongly deformed sediments from overlying slightly deformed sediments. It thus marks the timing of accentuated reduction of deformation.

The post-unconformity channel-levee systems were interpreted to be part of the "Middle Levee Complex", defined by Flood et al. (1995) as a group of laterally shingled channel-levee systems deposited during the Middle Pleistocene on the Amazon Fan, due to its position on the fan, depth of occurrence and the orientation of the channels.

9.2.2 Channel architecture and development

Two different styles of channel architecture were developed in the post and the pre-unconformity intervals: canyon-like erosive channels in the pre-unconformity interval and channel-levee systems in the post-unconformity interval. The development of the canyon-like channels was mostly syn-tectonic whereas the development of the channel-levee systems was mostly post-tectonic, although they were still slightly affected by relatively minor tectonic activity.

The post-unconformity deposition evolved as a succession of upslope stacked channel-levee systems, intercalated with HARPs and MTDs. Three main channel-levee systems were identified in the area: LCLS, MCLS and UCLS. These systems were deposited with a tendency of the younger channel-levees to initiate upslope and on the left-hand side (looking downstream) of the earlier one.

Both HARPs and the MTD (flanking the MCLS levee) were interpreted as being related to the channel avulsion. The MTD is considered to have occurred due to upstream levee collapse. HARPs are considered sand rich sheet-like deposits and occur in the space between the upslope levee and the regional paleo-slope after channel avulsion, in agreement with the published literature on the Amazon Fan (Pirmez et al., 1997).

The three channel-levee systems described in the post-unconformity interval present three different architectures which reflect three distinctive evolutional histories. In the LCLS, the channel narrows and becomes more sinuous upward whereas in the MCLS, the channel widens and becomes less

sinuous upward. The UCLS is composed of four stacked channel-levee elements, each with widening upward channel characteristics.

9.2.3 Evolutionary history of the Post-Unconformity Interval

The evolutionary history of the interval above the unconformity, during the Middle Pleistocene in the study area, started with the incision of an erosive channel, infill, and then the development of the LCLS. The aggradational component of the LCLS developed through a process of upstream accretion. Channel avulsion through the left-hand side (looking downstream) and abandonment initiated another incision between the backlimb of the levee and the paleoslope. This erosive channel evolved upward through a process of downstream accretion to become the MCLS. Upstream avulsion caused channel infill and HARP formation onlapping the up-dip levee slope. Later, turbidite flows became focused and incised a channel in the HARPs which evolved upward to become the UCLS. This system grew by stacking of at least four channel elements due to the confinement between the upslope anticline and the outsize down-slope levee.

9.3 Spatio-temporal evolution of channel-levee/architecture

9.3.1 Architectural styles

Two models of spatio-temporal development of channel systems were identified: upstream and downstream accretion of the aggradational channel-levee. These two models of development resulted in two different architectural styles of channel-levee systems. The differences between the two architectural styles can be noticed in the plan form evolution with time, in the channel shape in cross section and in the terminations and amplitudes of the reflections of the channel fill and levee.

The upstream accretion of the channel-levee is associated with an upward narrowing and more sinuous channel style. In cross section, the high amplitude reflections of channel fill change laterally to the low amplitude reflections in the levee. In a section along the channel axis, the channel fill reflections onlap the paleo-thalweg. The levee reflections also onlap the paleoslope.

The downstream-accretion channel-levee development style is associated with an upward widening and less sinuous channel style. In cross section, the high amplitude reflections of the channel fill onlap the internal levee at least in the wider channel. In a section along the channel axis, the channel fill reflections occur sub-parallel to or slightly downlapping onto the paleo-thalweg. The levee reflections downlap onto the paleoslope.

9.3.2 Controls on channel-levee development

The interaction between the slope bathymetry and flow properties, expressed by the changes in the equilibrium profile and in the flow magnitude and grain size of suspended sediment may have accounted for the upstream and downstream development styles of the channel-levees. The changes in the equilibrium profile may have worked differently during the evolution of the two channel-levee models, bearing in mind the caveats of this conceptual scheme described in Chapter 6. In the upstream development of a channel-levee, there are two possibilities of changes in equilibrium profile that could contribute to the upstream migration of the system. In the first, the equilibrium profile does not change with time, and the channel-levee develops filling an inherited bathymetric low on the slope. In the second, due to upstream uplift of the anticlines, the equilibrium profile moves upward causing an increase in the accommodation downstream, favouring upstream channel-levee accretion. In the case of downstream development of a channel-levee, the upward displacement of the equilibrium profile may also cause downstream migration, probably due to the upstream uplift. In this case the accommodation space would also increase downstream (Fig. 6.31).

The changes in the equilibrium profile, however, can only favour or inhibit one and/or another style of channel-levee development. The nature of the turbidite flows themselves causes the distinctive styles of channel-levee growth. Thus the flows that built up the two channel-levee styles may have experienced different evolutionary pathways. Two flow parameters were considered in the analysis of the impact of flow efficiency on the two channel-levee styles: flow magnitude and grain-size composition. In the case of upstream development of a channel-levee, the flows may have gradually become muddier and smaller with time, reducing the flow efficiency. This may account for the simultaneous

deposition of the channel fill and levee during the channel evolution up to the time of channel abandonment. In the downstream development of a channel levee, the flows may have had a more complex evolution (Fig. 6.32). In general they are thought to have become sandier and larger with time, increasing consequently flow efficiency (i.e. with the flow magnitude contribution to flow efficiency out-weighing the reduction to flow efficiency caused by increased grain size), until the moment of levee breach. With the levee breach the flow split, with reduced flow efficiency in each branch of flow, promoting channel fill and HARPs deposition.

9.4 Controls on patterns of channel distribution on slope

Slope channels were analyzed taking in account possible controls on their distribution by tectonic structures and by the depositional environment.

The difference in channel direction between the pre unconformity channels and the post-unconformity channels is due to distinct controls on channel development. The pre-unconformity channels are strongly affected by the growing anticlines during their evolution. These anticlines (with N/NW-oriented axes) diverted the channel directions on slope, creating some sinuosity but without affecting the overall channel direction toward the NE. Anticline growth promoted a successive northwestward channel migration in time. The erosive character of the channels seems to be controlled by the steepening of the overall slope dip due to the uplift of the entire fold and thrust belt. This uplift would keep the slope above the equilibrium profile in the area, forcing the channels to erode.

The post-unconformity channels are obliquely oriented with N/NW-oriented direction, similar to the anticlines axes. The channel orientation, however, is not directly related to the anticlines. The channel-levee systems occur downslope from the growing anticlines and there were no other structures identified downslope from the systems that could have caused their slope-oblique orientation. Although the marine currents (NBCC) occurring on the shelf have a northwestward direction, they also probably did not affect the slope channel direction because they were not deep enough to affect the slope sedimentation, even during sea level lowstand. Thus the initial cause of mis-orientation is not directly constrained.

The direction of each channel was inherited from the previous one in a sequence of upslope stacking after systematic avulsion through the left-hand levee (viewed toward downstream). Although the cause of the oblique orientation of the first of these channels is not satisfactorily established, a hypothesis can be proposed. Even if the former channel had a NE direction, which is approximately the same direction as the main slope dip, if the first avulsion occurs on the upper slope such that the new channel course becomes oblique to the slope, an outsized downslope levee would develop. Therefore, any following sequence of avulsions may be progressively more likely to occur through the left-hand and upslope levee due to this levee asymmetry. This would keep the channels oblique to the main slope dip.

The vertical stacking of channel-levee systems is related to the confinement of the channel between the outsize downslope levee and the upslope anticline which inhibited channel avulsion. The vertical stacking pattern has also been identified in many other fans, e.g., the Late Pleistocene systems of the Amazon Fan (Pirmez and Flood, 1995), Indus Fan and Niger Delta (Deptuck et al., 2003), but contrasting with the study case, these channels are not confined by external features such as a tectonic structure. In the Late Pleistocene of the Amazon Fan, each stacked element of the channel-levee system represents a downstream channel avulsion (Pirmez and Flood, 1995). Therefore, based on this example, it is possible to infer that the UCLS study section, the Indus Fan and the Niger Delta are examples of channel-levee segments upstream from avulsion points, with each stacked channel-levee element representing a downstream avulsed channel. However, not all parent channels of downstream avulsions build stacked systems because, if the avulsion occurred while the channel was still erosive or at grade, only the following aggradational phase will be present, as is thought to have occurred in the evolution of the MCLS.

REFERENCES

Abreu, V., Sullivan, M., Pirmez, C., and Mohrig, D., 2003, Lateral accretion packages (LAPs): an important reservoir element in deep water sinuous channels: Marine and Petroleum Geology, v. 20, p. 631-648.

Adeogba, A.A., McHargue, T.R., and Graham, S.A., 2005, Transient fan architecture and depositional controls from near-surface 3-D seismic data, Niger Delta continental slope.AAPG Bulletin, v. 89, p. 627-643.

Al Jaaidi, O.S., McCaffrey, W.D., and Kneller, B.C., 2004, Factors influencing the deposit geometry of experimental turbidity currents; implications for sand-body architecture in confined basins: Geological Society Special Publications, v. 222, p. 45-58.

Arnott, R.W.C., 2007, Stratal architecture and origin of lateral accretion deposits (LADs) and conterminuous inner-bank levee deposits in a base-of-slope sinuous channel, lower Isaac Formation (Neoproterozoic), East-Central British Columbia, Canada: Marine and Petroleum Geology, v. 24, p. 515-528.

Babonneau, N., Savoye, B., Cremer, M., and Bez, M., 2004, Multiple terraces within the deep incised Zaire Valley (ZaiAngo Project); are they confined levees?: Geological Society Special Publications, v. 222, p. 91-114.

Babonneau, N., Savoye, B., Cremer, M., and Klein, B., 2002, Morphology and architecture of the present canyon and channel system of the Zaire deep-sea fan: Marine and Petroleum Geology, v. 19, p. 445-467.

Baztan, J., Berné, S., Olivet, J.L., Rabineau, M., Aslanian, D., Gaudin, M., Réhault, J.P., and Canals, M., 2005, Axial incision: The key to understand submarine canyon evolution (in the western Gulf of Lion): Marine and Petroleum Geology, v. 22, p. 805-826.

Beaubouef, R.T., 2004, Deep-water leveed-channel complexes of the Cerro Toro Formation, Upper Cretaceous, southern Chile. 10.1306/06210403130: AAPG Bulletin, v. 88, p. 1471-1500.

Berryhill, H.L.J., 1981, Ancient buried submarine though, north west Gulf of Mexico: Geo-Marine Letters, v. 1, p. 105-110.

Booth, J.R., Dean, M.C., DuVernay, A.E., III, Styzen, M.J., and Mutti, E., 2003, Paleo-bathymetric controls on the stratigraphic architecture and reservoir development of confined fans in the Auger Basin; central Gulf of Mexico slope, *in* Steffens, G.S., Pirmez, C., Orlando, M., and Roberts, D., eds., Marine and Petroleum Geology, Volume 20: Oxford, Elsevier, p. 563-586.

Bouma, A.H., 2000, Coarse-grained and fine-grained turbidite systems as end member models: applicability and dangers: Marine and Petroleum Geology, v. 17, p. 137-143.

Bouma, A.H., Normark, W.R., and Barnes, N.E., 1985, Submarine fans and related turbidite systems: New York, NY, United States, Springer-Verlag, 343 p.

Brandao, J.A.S.L., and Feijo, F.J., 1994, Bacia da Foz do Amazonas: Bol. Geoci. Petrobras, v. 8, p. 91-100.

Bucher, W.H., 1940, Submarine valleys and related geologic problem sof the North Atlantic: Geological Society of America Bulletin, v. 51, p. 489-512.

Castro, J., Miura, K., and Braga, J.A.E., 1978, Stratigraphic and structural framework of the Foz do Amazonas Basin, 10th Annual Offshore Technology conference, Volume 1843-1847.

Chough, S., and Hesse, R., 1976, Submarine meandering thalweg and turbidity currents flowing for 4,000 km in the Northwest Atlantic Mid-Ocean Channel, Labrador Sea: Geology (Boulder), v. 4, p. 529-533.

Clark, I.R., and Cartwright, J.A., 2009, Interaction between submarine channel systems and deformation in deepwater fold belts: examples from the Levant Basin, eastern Mediterranean Sea: Marine and Petroleum Geology, v. 26, p. 1465-1482.

Clark, J.D., Kenyon, N.H., and Pickering, K.T., 1992, Quantitative analysis of the geometry of submarine channels: Implications for the classification of submarine fans: Geology, v. 20, p. 633-636.

Clark, J.D., and Pickering, 1996a, Submarine Channels - Processes and Architecture, Vallis Press, p. 231pp.

Clark, J.D., and Pickering, K.T., 1996b, Architectural elements and growth patterns of submarine channels; application to hydrocarbon exploration: American Association of Petroleum Geologists Bulletin, v. 80, p. 194-221.

Cobbold, P.R., Mourgues, R., and Boyd, K., 2004, Mechanism of thin-skinned detachment in the Amazon Fan: assessing the importance of fluid overpressure and hydrocarbon generation: Marine and Petroleum Geology, v. 21, p. 1013-1025.

Corredor, F., Shaw, J.H., and Bilotti, F., 2005, Structural styles in the deep-water fold and thrust belts of the Niger Delta 10.1306/02170504074: AAPG Bulletin, v. 89, p. 753-780.

Cramez, C., and Jackson, P.A., 2000, Superposed deformation stradding the continental-oceanic transition in deep-water Angola: Marine and Petroleum Geology, v. 17, p. 1095-1109.

Crans, W., Mandl, G., and Haremboure, J., 1980, On the theory of growth faulting; a geomechanical delta model based on gravity sliding: scientific Press, Beaconsfield, p. 265-307.

Cronin, B.T., Hartley, A.J., Celik, H., Hurst, A., Turkmen, I., and Kerey, E., 2000a, Equilibrium profile development in graded deep-water slopes; Eocene, eastern Turkey: Journal of the Geological Society of London, v. 157, p. 943-955.

Cronin, B.T., Hurst, A., Celik, H., and Turkmen, I., 2000b, Superb exposure of a channel, levee and overbank complex in an ancient deep-water slope environment: Sedimentary Geology, v. 132, p. 205-216.

Curray, J.R., Emmel, F.J., and Moore, D.G., 2003, The Bengal Fan: morphology, geometry, stratigraphy, history and processes: Marine and Petroleum Geology, v. 19, p. 1191-1223.

Daly, R.A., 1936, Origin of submarine "canyons": American Journal of Science, v. 31, p. 401-420.

Damuth, J.E., 1977, Late Quaternary sedimentation in the western equatorial Atlantic: Geological Society of America Bulletin, v. 88, p. 695-710.

—, 1994, Neogene gravity tectonics and depositional processes on the deep Niger Delta continental margin: Marine and Petroleum Geology, v. 11, p. 320 - 346.

Damuth, J.E., and Embley, R.W., 1981, Mass-transport processes on Amazon Cone: western equatorial Atlantic: AAPG Bulletin, v. 65, p. 629-643.

Damuth, J.E., and Flood, R.D., 1983, Morphology, sedimentation processes, and growth pattern of the Amazon Deep-Sea Fan: Geo-Marine Letters, v. 3, p. 109-117.

—, 1985, Amazon Fan, Atlantic Ocean, *in* Bouma, A., Normark, W.R., and Barnes, N.E., eds., Submarine fans and related turbidite systems: New York, Springer-Verlag, p. 97-106.

Damuth, J.E., Flood, R.D., Kowsmann, R.O., Belderson, R.H., and Gorini, M.A., 1988, Anatomy and growth pattern of Amazon deep-sea fan as revealed by long-range side-scan sonar (GLORIA) and high resolution seismic studies: American Association of Petroleum Geologists Bulletin, v. 72, p. 885-911.

Damuth, J.E., Kolla, V., Flood, R.D., Kowsmann, R.O., Monteiro, M.O., Gorini, M.A., Palma, J.J.C., and Belderson, R.H., 1983a, Distributary channel meandering and bifurcation patterns on the Amazon deep-sea fan as revealed by long-range side-scan sonar (GLORIA): Geology (Boulder), v. 11, p. 94-98.

Damuth, J.E., and Kowsmann, R.O., 1998, New evidence for extensive sand distribution in "mud-rich" submarine fans; insights and fan models based on ODP drilling of Amazon Fan, *in* Anonymous, ed., AAPG international conference and exhibition; abstracts., Volume 82; 10: AAPG Bulletin: Tulsa, OK, United States, American Association of Petroleum Geologists, p. 1907.

Damuth, J.E., Kowsmann, R.O., Flood, R.G., Belderson, R.H., and Gorini, M.A., 1983b, Age relationships of distributary channels on Amazon deep-sea fan: implications for fan growth pattern: Geology, v. 11, p. 470-473.

Damuth, J.E., and Kumar, N., 1975, Late Quaternary depositional processes on continental rise of western equatorial Atlantic; comparison with western North Atlantic and implications for reservoir-rock distribution: AAPG Bulletin, v. 59, p. 2172-2181.

Damuth, J.E., and Normark, W.R., 1991, Seismic facies and sedimentary processes of modern submarine fans and turbidite systems; introduction, *in* Weimer, P., and Link, M.H., eds., Seismic facies and sedimentary

processes of submarine fans and turbidite systems.: New York, NY, United States, Springer-Verlag, p. 319-322.

Demercian, S., Szatmari, P., and Cobbold, P.R., 1993, Style and pattern of salt diapirs due to thin-skinned gravitational gliding, Campos and Santos basins, offshore Brazil, *in* Cobbold, P.R., ed., New insights into salt tectonics; collection of invited papers reflecting the recent developments in the field of salt tectonics. : Amsterdan, Elsevier, p. 393-433.

Demyttenaere, R., Ibrahim, A., Tromp, J.-P., Zulkifli, B.A., and Anonymous, 2000, Brunei deep water exploration; from sea-floor images to depositional models in a slope turbidite setting, AAPG international conference and exhibition; abstracts, Volume 84: Tulsa, American Association of Petroleum Geologists, p. 1418.

Deptuck, M., W, P.D.J., Savoye, B., and Gervais, A., 2008, Dimensions and architecture of late Pleistocene submarine lobes off the northern margin of East Corsica: Sedimentology, v. 55, p. 869-898.

Deptuck, M.E., Steffens, G.S., Barton, M., and Pirmez, C., 2003, Architecture and evolution of upper fan channel-belts on the Niger Delta slope and in the Arabian Sea Turbidites; models and problems v. 20, p. 649-676.

Deptuck, M.E., Sylvester, Z., Pirmez, C., and O'Byrne, C., 2007, Migration-aggradation history and 3-D seismic geomorphology of submarine channels in the Pleistocene Benin-major Canyon, western Niger Delta slope: Marine and Petroleum Geology, v. 24, p. 406-433.

Droz, L., Marsset, T., Ondreas, H., Lopez, M., Savoye, B., and Spy-Anderson, F.-L., 2003, Architecture of an active mud-rich turbidite system; the Zaire Fan (Congo-Angola margin Southeast Atlantic); results from ZaiAngo 1 and 2 cruises: AAPG Bulletin, v. 87, p. 1145-1168.

Droz, L., Rigaut, F., Cochonat, P., and Tofani, R., 1996, Morphology and Recent evolution of the Zaire turbidite system (Gulf of Guinea): Geological Society of America Bulletin, v. 108, p. 253-269.

Duval, B., Cramez, C., and A, J.P., 1992, Raft tectonics in the Kwanza Basin, Angola: Marine and Petroleum Geology, v. 9, p. 389-404.

Emmel, F.J., and Curray, J.R., 1981, Dynamic events near the upper and mid-fan boundary of the Bengal Fan: Geo-Marine Letters, v. 1, p. 201-205.

Eschard, R., Albouy, E., Deschamps, R., Euzen, T., Ayub, A., and Mutti, E., 2003, Downstream evolution of turbiditic channel complexes in the Pab Range outcrops; Maastrichtian, Pakistan, *in* Steffens, G.S., Pirmez, C., Orlando, M., and Roberts, D., eds., Marine and Petroleum Geology, Volume 20: Oxford, Elsevier, p. 691-710.

Escutia, C., Eittreim, S.L., Cooper, A.K., and Nelson, C.H., 2000, Morphology and acoustic character of the antarctic Wilkes Land turbidite systems; ice-sheet-sourced versus river-sourced fans: Journal of Sedimentary Research, Section A: Sedimentary Petrology and Processes, v. 70, p. 84-93.

Ferry, J.N., Mulder, T., Parize, O., and Raillard, S., 2005, Concept of equilibrium profile in deep-water turbidite systems; effects of local physiographic

changes on the nature of sedimentary process and the geometries of deposits Submarine slope systems; processes and products v. 244, p. 181-193.

Figueiredo, J., Hoorn, C., van der Ven, P., and Soares, E., 2009, Late Miocene onset of the Amazon River and the Amazon deep-sea fan: Evidence from the Foz do Amazonas Basin: Geology, v. 37, p. 619-622.

Figueiredo, J.J.P., Zalan, P.V., and Soares, E.F., 2007, Bacia do Foz do Amazonas: Bol. Geoci. Petrobras, v. 15, p. 299-309.

Fildani, A., and Normark, W.R., 2004, Late Quaternary evolution of channel and lobe complexes of Monterey Fan: Marine Geology, v. 206, p. 199-223.

Flood, R.D., and Damuth, J.E., 1987, Quantitative characteristics of sinuous distributary channels on the Amazon deep-sea fan: Geological Society of America Bulletin, v. 98, p. 728-738.

Flood, R.D., Manley, P.L., Kowsmann, R.O., Appi, C.J., and Pirmez, C., 1991, Seismic facies and late Quaternary growth of Amazon submarine fan, *in* Weimer, P., and Link, M.H., eds., Seismic facies and sedimentary processes of submarine fans and turbidite systems.: New York, NY, United States, Springer-Verlag, p. 415-433.

Flood, R.D., and Piper, D.J.W., 1997, Amazon Fan Sedimentation: the relationship to equatorial climate change, continental denudation, and sea-level fluctuations, *in* Flood, R.D., Piper, D.J.W., Klaus, A., and Peterson, L.C., eds., Proceedings of the Ocean Drilling Program, Scientific Results, Volume 155, p. 653-675.

Flood, R.D., Piper, D.J.W., Klaus, A., and al., e., 1995, Proceedings Ocean Drilling Program, Initial Reports: College Station, TX, v. 155.

Franzinelli, E., and Potter, P.E., 1983, Petrology, chemistry and texture of modern river sands, Amazon River System: The Journal of Geology, v. 91, p. 23-39.

Galloway, W.E., 1986, Growth faults and fault-related structures of prograding terrigenous clastic continental margins: Gulf Coast Association of Geological Societies Transactions, p. 121-128.

Gardner, M.H., Borer, J.M., and Anonymous, 2000, Submarine channel architecture along a slope to basin profile, Brushy Canyon Formation, West Texas American Association of Petroleum Geologists 2000 annual meeting v. 2000, p. 52.

Garrison, L.E., Kenyon, N.H., and Bouma, A.H., 1982, Channel systems and lobe construction in the Mississippi fan: Geo-Marine Letters, v. 2, p. 31-39.

Gaullier, V., and Vendeville, B.C., 2005, Salt tectonics driven by sediment progradation: Part II--Radial spreading of sedimentary lobes prograding above salt 10.1306/03310503064: AAPG Bulletin, v. 89, p. 1081-1089.

Gee, M.J.R., and Gawthorpe, R.L., 2006, Submarine channels controlled by salt tectonics: Examples from 3D seismic data offshore Angola: Marine and Petroleum Geology, v. 23, p. 443-458.

Gervais, A., Savoye, B., Mulder, T., and Gonthier, E., 2006, Sandy modern turbidite lobes: A new insight from high resolution seismic data: Marine and Petroleum Geology, v. 23, p. 485-502.

Gibbs, R.J., 1967, The Geochemistry of the Amazon River System: Part I. The Factors that Control the Salinity and the Composition and Concentration of the Suspended Solids: Geological Society of America Bulletin, v. 78, p. 1203-1232.

Gladstone, C., Phillips, J.C., and Sparks, R.S.J., 1998, Experiments on bidisperse, constant-volume gravity currents; propagation and sediment deposition: Sedimentology, v. 45, p. 833-843.

Grando, G., and McClay, K., 2004, Structural evolution of the Frampton growth fold system, Atwater Valley-Southern Green Canyon area, deep water Gulf of Mexico: Marine and Petroleum Geology, v. 21, p. 889-910.

Grecula, M., Flint, S., Potts, G., Wickens, D., and Johnson, S., 2003, Partial ponding of turbidite systems in a basin with subtle growth-fold topography; Laingsburg-Karoo, South Africa: Journal of Sedimentary Research, v. 73, p. 603-620.

Hallworth, M.A., Phillips, J.C., Huppert, H.E., and Sparks, R.S.J., 1993, Entrainment in turbulent gravity currents: Nature (London), v. 362, p. 829-831.

Hampton, M.A., 1972, The role of subaqueous debris flow in generating turbidity currents: Journal of Sedimentary Petrology, v. 42, p. 775-793.

Hay, A.E., 1987, Turbidity currents and submarine channel formation in Rupert Inlet, British Columbia; 2, The roles of continuous and surge-type flow: Journal of Geophysical Research, C, Oceans, v. 92, p. 2883-2900.

Heezen, B.C., 1952, Turbidity currents and submarine slumps, and the 1929 Grand Banks, earthquake.

Heinio, P., and Davies, R.J., 2006, Degradation of compressional fold belts: Deep-water Niger Delta 10.1306/11210505090: AAPG Bulletin, v. 90, p. 753-770.

Heiniö, P., and Davies, R.J., 2007, Knickpoint migration in submarine channels in response to fold growth, western Niger Delta: Marine and Petroleum Geology, v. 24, p. 434-449.

Hesse, R., 1995, Continental slope and basin sedimentation adjacent to an ice margin: a continuous sleeve-gun profile across the Labrador-Slope, Rise and Basin, *in* Pickering, K.T., Hiscott, R.N., Kenyon, N.H., Lucchi, F.R., and Smith, R.D.A., eds., Atlas of Deep Water Environments; Architectural Style in Turbidite systems. Chapman & Hall, p. 14-18.

Hickson, T.A., and Lowe, D.R., 2002, Facies architecture of a submarine fan channel-levee complex: the Juniper Ridge Conglomerate, Coalinga, California: Sedimentology, v. 49, p. 335-362.

Hiscott, R.N., Hall, F.R., and Pirmez, C., 1997, Turbidity-current overspill from the Amazon channel: texture of the silt/sand load, paleoflow from anisotropy of magnetic susceptibilty and implications for flow process, *in*

Flood, R.D., Piper, D.J.W., Klaus, A., and Peterson, L.C., eds., Proceedings of the Ocean Drilling Program, Scientific Results, Volume 155, p. 53-78.

Hodgson, D.M., and Haughton, P.D.W., 2004, Impact of syndepositional faulting on gravity current behaviour and deep-water stratigraphy; Tabernas-Sorbas Basin, SE Spain, *in* Lomas, S.A., and Joseph, P., eds., Confined turbidite systems, Volume 222: London, Geological Society of London, p. 135-158.

Hoorn, C., Guerrero, J., Sarmiento, G.A., and Lorente, M.A., 1995, Andean tectonics as a cause for changing drainage patterns in Miocene northern South America: Geology, v. 23, p. 237-240.

Horn, D.R., Ewing, M., Horn, B.M., and Delach, M.N., 1971, Turbidites of the Hatteras and Sohm abyssal plains, western North Atlantic: Marine Geology, v. 11, p. 287-323.

Hubbard, R.J., Pape, J., and Roberts, D.G., 1985, Depositional sequence mapping as a technique to establish tectonic and stratigraphic framework and evaluate hydrocarbon potential on a passive continental margin, Memoir 39: Seismic Stratigraphy II: An Integrated Approach to Hydrocarbon Exploration, Volume 39, p. 79-91.

Huyghe, P., Foata, M., Deville, E., Mascle, G., Cagna, R., Callec, Y., Desaubliaux, G., Ellouz, N., Griboulard, R., Guerlais, S.H., Lallemant, S., Lebrun, F., Mascle, A., Mugnier, J.L., Padron, C., Prinzhofer, A., Schmitz, J., and Wendenbaum, E., 2004, Channel profiles through the active thrust front of the southern Barbados prism: Geology, v. 32, p. 429-432.

Imran, J., G, P., and Pirmez, C., 1999, A numerical model of flow in meandering submarine and sub-aerial channels Journal of Fluid Mechanics, v. 400, p. 295-331.

Jegou, I., Savoye, B., Pirmez, C., and Droz, L., 2008, Channel mouth lobe complex of the recent Amazon Fan: The missing piece: Marine Geology, v. 252, p. 62-77.

Johns, W., Lee, T., Beardsley, R., Candela, J., Limeburner, R., and Castro, B., 1998, Annual cycle and variability of the North Brazil Current: Jounal of Physical Oceanography, v. 28, p. 103-128.

Kane, I.A., 2007, Architecture and sedimentology of submarine channel-levee systems: insights from the Upper Cretaceous Rosario Formation, Baja California, Mexico, and from laboratory experiments: Leeds, University of Leeds.

Kane, I.A., Kneller, B.C., Dykstra, M., Kassem, A., and McCaffrey, W.D., 2007, Anatomy of a submarine channel-levee: An example from Upper Cretaceous slope sediments, Rosario Formation, Baja California, Mexico: Marine and Petroleum Geology, v. 24, p. 540-563.

Kane, I.A., McCaffrey, W.D., and Peakall, J., 2008, Controls on sinuosity evolution within submarine channels: Geology, v. 36, p. 287-290.

Kastens, K.A., and Shor, A.N., 1985, Depositional processes of a meandering channel on Mississippi Fan: AAPG Bulletin, v. 69, p. 190-202.

—, 1986, Evolution of a channel meander on the Mississippi deep-sea fan: Marine Geology, v. 71, p. 165-175.

Kenyon, N.H., Amir, A., and Cramp, A., 1995, Geometry of the younger sediment bodies of the Indus Fan, *in* Pickering, K.T., Hiscott, R.N., Kenyon, N.H., Lucchi, F.R., and Smith, R.D.A., eds., Atlas of Deep Water Environments; Architectural Style in Turbidite systems. Chapman & Hall, p. 89-93.

Kenyon, N.H., Belderson, R.H., and Stride, A.H., 1978, Channels, canyons, and slump folds on the continental slope between southwest Ireland and Spain: Oceanologica Acta, v. 1, p. 369-380.

Kenyon, N.H., and Millington, J., 1995, Contrasting deep sea depositional systems in the Bering Sea, *in* Pickering, K.T., Hiscott, R.N., Kenyon, N.H., Lucchi, F.R., and Smith, R.D.A., eds., Atlas of Deep Water Environments; Architectural Style in Turbidite systems. Chapman & Hall, p. 196-202.

Khripounoff, A., Vangriesheim, A., Babonneau, N., Crassous, P., Dennielou, B., and Savoye, B., 2003, Direct observation of intense turbidity current activity in the Zaire submarine valley at 4000 m water depth: Marine Geology, v. 194, p. 151-158.

Klaucke, I., and Hesse, R., 1996, Fluvial features in the deep-sea: new insights from the glacigenic submarine drainage system of the Northwest Atlantic mid-ocean channel in the Labrador Sea: Sedimentary Geology, v. 106, p. 223-234.

Klaucke, I., Hesse, R., and Ryan, W.B.F., 1997, Flow parameters of turbidity currents in a low-sinuosity giant deep-sea channel: Sedimentology, v. 44, p. 1093-1102.

Klaucke, I., Masson, D.G., Kenyon, N.H., and Gardner, J.V., 2004, Sedimentary processes of the lower Monterey Fan channel and channel-mouth lobe: Marine Geology, v. 206, p. 181-198.

Kneller, B., 2003, The influence of flow parameters on turbidite slope channel architecture: Marine and Petroleum Geology, v. 20, p. 901-910.

Kneller, B., and Buckee, C., 2000, The structure and fluid mechanics of turbidity currents: a review of some recent studies and their geological implications: Sedimentology, v. 47, p. 62-94.

Kneller, B., and McCaffrey, W., 1999, Depositional effects of flow nonuniformity and stratification within turbidity currents approaching a bounding slope; deflection, reflection, and facies variation: Journal of Sedimentary Research, v. 69, p. 980-991.

—, 2003, The interpretation of vertical sequences in turbidite beds: the influence of longitudinal flow structure: Jounal of Sedimentary Research, v. 73, p. 706-713.

Kneller, B.C., 1995, Beyond the turbidite paradigm: Physical models for deposition of turbidites and their implications for reservoir prediction: Characterisation of Deep Marine Clastic Systems, Geological Society of London Special Paper, v. 94, p. 29-46.

Kneller, B.C., Bennett, S.J., and McCaffrey, W.D., 1997, Velocity and turbulence structure of density currents and internal solitary waves; potential sediment transport and the formation of wave ripples in deep water: Sedimentary Geology, v. 112, p. 235-250.

Kolla, V., 2007, A review of sinuous channel avulsion patterns in some major deep-sea fans and factors controlling them: Marine and Petroleum Geology, v. 24, p. 450-469.

Kolla, V., Bourges, P., Urruty, J.-M., and Safa, P., 2001, Evolution of Deep-Water Tertiary Sinuous Channels Offshore Angola (West Africa) and Implications for Reservoir Architecture: AAPG Bulletin, v. 85, p. 1373-1405.

Kolla, V., and Coumes, F., 1987, Morphology, internal structure, seismic stratigraphy, and sedimentation of Indus Fan: AAPG Bulletin, v. 71, p. 650-677.

Kolla, V., Posamentier, H.W., and Wood, L.J., 2007, Deep-water and fluvial sinuous channels--Characteristics, similarities and dissimilarities, and modes of formation: Marine and Petroleum Geology, v. 24, p. 388-405.

Kosa, E., 2007, Differential subsidence driving the formation of mounded stratigraphy in deep-water sediments: Paleocene, central North Sea: Marine and Petroleum Geology, v. 24, p. 632-652.

Kuehl, S.A., Hariu, T.M., and Moore, W.S., 1989, Shelf sedimentation off the Ganges-Brahmaputra river system; evidence for sediment bypassing to the Bengal Fan: Geology, v. 17, p. 1132-1135.

Kumar, N., 1978, Sediment distribution in western Atlantic off northern Brazil - structural controls and evolution: AAPG Bulletin, v. 62, p. 273-294.

Leeder, M., 1999, Sedimentology and Sedimentary Basins - From Turbulence to Tectonics, Blackwell Science Ltd., 592 p.

Loncke, L., Gaullier, V., Mascle, J., Vendeville, B., and Camera, L., 2006, The Nile deep-sea fan: An example of interacting sedimentation, salt tectonics, and inherited subsalt paleotopographic features: Marine and Petroleum Geology, v. 23, p. 297-315.

Lopez, M., 2001, Architecture and depositional pattern of the Quaternary deep-sea fan of the Amazon: Marine and Petroleum Geology, v. 18, p. 479-486.

Manley, P., Pirmez, C., Busch, W., and Cramp, A., 1997, 3. Grain-size characterization of Amazon Fan deposits and comparison to seismic facies units, *in* Flood, R.D., Piper, D.J.W., Klaus, A., and Peterson, L.C., eds., Proceedings of the Ocean Drilling Program, Scientific Results, Volume 155.

Manley, P.L., and Flood, R.D., 1988, Cyclic sediment deposition within Amazon deep-sea fan: AAPG Bulletin, v. 72, p. 912-925.

Marr, J.G., Harff, P.A., Shanmugam, G., and Parker, G., 2001, Experiments on subaqueous sand gravity flows; the role of clay and water content in flow dynamics and depositional structures: Geological Society of America Bulletin, v. 113, p. 1377-1386.

Martinsen, O.J., Lien, T., Walker, R.G., Collinson, J.D., and Mutti, E., 2003, Facies and sequential organisation of a mudstone-dominated slope and basin floor succession; the Gull Island Formation, Shannon Basin, western Ireland, *in* Steffens, G.S., Pirmez, C., Orlando, M., and Roberts, D., eds., Marine and Petroleum Geology, Volume 20: Oxford, Elsevier, p. 789-807.

Maslin, M., 1998, Equatorial western Atlantic Ocean circulation changes linked to the Heinrich events: deep-sea sediment evidence from the Amazon Fan: Geological Society, London, Special Publications, v. 131, p. 111-127.

Maslin, M., Mikkelsen, N., Vilela, C., and Haq, B., 1998, "Sea-level and gas-hydrate"controlled catastrophic sediment failures of the Amazon Fan: Geology, v. 26, p. 1107-1110.

Mauduit, T., Guerin, G., Brun, J., and H, L., 1997, Raft tectonics; the effects of basal slope angle and sedimentation rate on progressive extension: Pergamon, Oxford-New York, p. 1219-1230.

Mayall, M., Jones, E., and Casey, M., 2006, Turbidite channel reservoirs--Key elements in facies prediction and effective development: Marine and Petroleum Geology, v. 23, p. 821-841.

Mayall, M., and Stewart, I., 2000, The architecture of turbidite slope channels, *in* Weimer, P., Slatt, R.M., Coleman, J.L., Rosen, N., Nelson, C.H., Bouma, A.H., Styzen, M., and Lawrence, D.T., eds., Global Deep-Water Reservoirs, GCSSEPM, Foundation 20th Annual Bob F Perkins Research Conference, p. 578-586.

McCaffrey, W.D., Gupta, S., and Brunt, R., 2002, Repeated cycles of submarine channel incision, infill and transition to sheet sandstone development in the Alpine foreland basin, SE France: Sedimentology, v. 49, p. 623-635.

Meade, R.H., Dunne, T., Richey, J.E., Santos, U.d.M., and Salati, E., 1985, Storage and remobilization of suspended sediment in the lower Amazon River of Brasil: Science, v. 228, p. 488-490.

Middleton, G.V., 1966a, Experiments on density and turbidity currents; [Part] 1, Motion of the head: Canadian Journal of Earth Sciences = Journal Canadien des Sciences de la Terre, v. 3, p. 523-546.

—, 1966b, Experiments on density and turbidity currents; [Part] 2, Uniform flow of density currents: Canadian Jour, v. Earth Sci., p. 627-637.

—, 1967, Experiments on density and turbidity currents; [Part] 3, Deposition of sediment: Canadian Jour, v. Earth Sci., p. 475-505.

—, 1993, Sediment deposition from turbidity currents: Annual Review of Earth and Planetary Sciences, v. 21, p. 89-114.

Migeon, S., Savoye, B., Babonneau, N., and Spy-Andersson, F.-L., 2004, Processes of sediment-wave construction along the present Zaire deep-sea meandering channel; role of meanders and flow stripping: Journal of Sedimentary Research, v. 74, p. 580-598.

Migeon, S., Savoye, B., and Faugeres, J.C., 2000, Quaternary development of migrating sediment waves in the Var deep-sea fan; distribution, growth pattern, and implication for levee evolution: Sedimentary Geology, v. 133, p. 265-293.

Mikkelsen, N., Maslin, M., Jackes, G., and William, S., 1997, Biostratigraphy and sedimentation rates of the Amazon Fan, *in* Flood, R.D., Piper, D.J.W., Klaus, A., and Peterson, L.C., eds., Proceedings of the Ocean Drilling Program, Vol. 155, p. 577-593.

Milliman, J.D., and Meade, R.H., 1983, World-wide delivery of river sediment to oceans: Journal of Geology, v. 91, p. 1-21.

Milliman, J.D., Summerhayes, C.P., and Barretto, H.T., 1975, Quaternary Sedimentation on the Amazon Continental Margin: A Model: Geological Society of America Bulletin, v. 86, p. 610-614.

Mitchell, N.C., 2005, Interpreting long-profiles of canyons in the USA Atlantic continental slope: Marine Geology, v. 214, p. 75-99.

Mitchum, R.M., Sangree, J., Vail, P.R., and Wornardt, W.W., 1994, Recognizing sequences and systems tracts from well logs, seismic data, and biostratigraphy: Examples from the Late Cenozoic of the Gulf of Mexico, *in* Weimer, P., and Posamentier, H.W., eds., Siliciclastic sequence stratigraphy: recent developments and applications, American Association of Petroleum Geologists Memoirs 58, p. 163-197.

Mohrig, D., Marr, J.G., and Mutti, E., 2003, Constraining the efficiency of turbidity current generation from submarine debris flows and slides using laboratory experiments, *in* Steffens, G.S., Pirmez, C., Orlando, M., and Roberts, D., eds., Marine and Petroleum Geology, Volume 20: Oxford, Elsevier, p. 883-899.

Moore, D.G., 1965, Erosional channel wall in La Jolla Sea-Fan Valley seen from bathyscaph Trieste II: Geological Society of America Bulletin, v. 76, p. 385-391.

Morgan, R., 2004, Structural controls on the postioning of submarine channels on the lower slopes of the Niger Delta, *in* Davies, R.J., Cartwright, J.A., Stewart, S.A., Lappin, M., and Underhill, J.R., eds., 3D Seismic Technology: Application to the Exploration of Sedimentary Basins, Volume 29, Geological Society, London, Memoirs, p. 45-51.

Morley, C.K., 2007, Development of crestal normal faults associated with deepwater fold growth: Journal of Structural Geology, v. 29, p. 1148-1163.

Morley, C.K., and Guerin, G., 1996, Comparison of gravity-driven deformation styles and behavior associated with mobile shales and salt: Tectonics, v. 15, p. 1154-1170.

Mulder, T., and Alexander, J., 2001, The physical character of subaqueous sedimentary density flows and their deposits: Sedimentology, v. 48, p. 269-299.

Mulder, T., and Syvitski, J.P.M., 1995a, Modelling of erosion and deposition by sediment gravity flows generated at river mouths: Journal of Sedimentary Research, v. 68, p. 124-137.

—, 1995b, Turbidity currents generated at river mouths during exceptional discharges to the world oceans: Journal of Geology, v. 103, p. 285-299.

Mutti, E., 1992, Turbidite Sandstones, 275 p.

Mutti, E., and Normark, W.R., 1987, Comparing examples of modern and ancient turbidite systems; problems and concepts, *in* Leggett, J.K., and Zuffa, G.G., eds., Marine clastic sedimentology; concepts and case studies.: London, United Kingdom, Graham and Trotman, p. 1-38.

—, 1991, An integrated approach to the study of turbidite systems, *in* Weimer, P., and Link, M.H., eds., Seismic facies and sedimentary processes of submarine fans and turbidite systems.: New York, NY, United States, Springer-Verlag, p. 75-106.

Nakajima, T., Peakall, J., McCaffrey, W.D., Paton, D.A., and Thompson, P.J.P., 2009, Outer-Bank Bars: A New Intra-Channel Architectural Element within Sinuous Submarine Slope Channels: Journal of Sedimentary Research, v. 79, p. 872-886.

Nigro, F., and Renda, P., 2004, Growth pattern of underlithified strata during thrust-related folding: Journal of Structural Geology, v. 26, p. 1913-1930.

Nittrouer, C.A., Kuehl, S.A., Demaster, D.J., and Kowsmann, R.O., 1986, The deltaic nature of Amazon shelf sedimentation: Geological Society of America Bulletin, v. 97, p. 444-458.

Normark, W.R., 1978, Fan Valleys, channels, and depositional lobes on modern submarine fans; characters for recognition of sandy turbidite environments: AAPG Bulletin, v. 62, p. 912-931.

Normark, W.R., Damuth, J.E., and Group, L.S., 1997, Sedimentary facies and associated depositional elements of the Amazon Fan, *in* Flood, R.D., Piper, D.J.W., Klaus, A., and Peterson, L.C., eds., Proceedings of the Ocean Drilling Program, Scientific Results, Volume 155, p. 611-651.

Normark, W.R., Hess, G.R., Stow, D.A.V., and Bowen, A.J., 1980, Sediment waves on the Monterey Fan levee; a preliminary physical interpretation: Marine Geology, v. 37, p. 1-18.

Normark, W.R., and Piper, D.J.W., 1991, Initiation processes and flow evolution of turbidity currents; implications for the depositional record, *in* Osborne, R.H., ed., From shoreline to abyss; contributions in marine geology in honor of Francis Parker Shepard., Volume 46: Special Publication -

Society of Economic Paleontologists and Mineralogists: Tulsa, OK, United States, SEPM (Society for Sedimentary Geology), p. 207-230.

Normark, W.R., Piper, D.J.W., and Hiscott, R.N., 1998, Sea level controls on the textural characteristics and depositional architecture of the Hueneme and associated submarine fan systems, Santa Monica Basin, California: Sedimentology, v. 45, p. 53-70.

O'Grady, D.B., Syvitski, J.P.M., Pratson, L.F., and Sarg, J.F., 2000, Categorizing the morphologic variability of siliciclastic passive continental margins: Geology, v. 28, p. 207-210.

Paull, C.K., Mitts, P., Ussler, W., III, Keaten, R., and Greene, H.G., 2005, Trail of sand in upper Monterey Canyon: Offshore California

10.1130/B25390.1: GSA Bulletin, v. 117, p. 1134-1145.

Peakall, J., Amos, K.J., Keevil, G.M., William Bradbury, P., and Gupta, S., 2007, Flow processes and sedimentation in submarine channel bends: Marine and Petroleum Geology, v. 24, p. 470-486.

Peakall, J., Best, J., McCaffrey, W., Kneller, B., and Kirkbride, A.D., 1998, Flow processes in meandering submarine channel bends.

Peakall, J., McCaffrey, B., and Kneller, B., 2000, A process model for the evolution, morphology, and architecture of sinuous submarine channels: Journal of Sedimentary Research, v. 70, p. 434-448.

Peel, F.J., Travis, C.J., and Hossack, J.R., 1995, Genetic Structural Provinces and Salt Tectonics of the Cenozoic Offshore U. s. Gulf of Mexico: A Preliminary Analysis, *in* Jackson, M.P.A., Roberts, D.G., and Snelson, S., eds., Salt Tectonics: A Global Perspective: AAPG Memoir 65, p. 153-175.

Pickering, K., Coleman, J., Cremer, M., Droz, L., Kohl, B., Normark, W.R., O' Connell, S., Stow, D., and Meyer Wright, A.A., 1986, A high sinuosity, laterally migrating submarine fan channel-levee-overbank; results from DSDP Leg 96 on the Mississippi Fan, Gulf of Mexico: Marine and Petroleum Geology, v. 3, p. 3-18.

Pickering, K.T., and Hiscott, R.N., 1985, Contained (reflected) turbidity currents from the Middle Ordovician Cloridorme Formation, Quebec, Canada; an alternative to the antidune hypothesis: Sedimentology, v. 32, p. 373-394.

Pickering, K.T., Hiscott, R.N., and Hein, F.J., 1989, Deep Marine Environments: Clastic Sedimentation and Tectonics: London, Unwin Hyman, 416pp p.

Piper, D., and Normark, W.R., 1983a, Turbidite depositional patterns and flow characteristics, Navy Submarine Fan, California Borderland: Sedimentology, v. 30, p. 681-694.

Piper, D.J.W., and Deptuck, M., 1997, Fine-grained turbidites of the Amazon Fan: Facies characterisation and interpretation, *in* Flood, R.D., Piper, D.J.W., Klaus, A., and Peterson, L.C., eds., Proccedings of the Ocean Drilling Program, Scientific Results, Volume 155, p. 79-107.

Piper, D.J.W., Flood, R.D., Cisowski, S., Hall, F., Manley, P.L., Maslin, M., Mikkelsen, N., and Showers, W.J., 1997, Synthesis of stratigraphic

correlations of the Amazon Fan, *in* Flood, R.D., Piper, D.J.W., Klaus, A., and Peterson, L.C., eds., Proceedings of the Ocean Drilling Program, Scientific Results Volume 155, p. 595-609.

Piper, D.J.W., Hiscott, R.N., and Normark, W.R., 1999, Outcrop-scale acoustic facies analysis and latest Quaternary development of Hueneme and Dume submarine fans, offshore California: Sedimentology, v. 46, p. 47-78.

Piper, D.J.W., and Normark, W.R., 1983b, Turbidite depositional patterns and flow characteristics, Navy submarine fan, California Borderland: Sedimentology, v. 30, p. 681-694.

—, 2009, Processes that inititate turbidity currents and their influence on turbidites: a marine geoloby perspective: Journal of Sedimentary Research, v. 79, p. 347-362.

Pirmez, C., 1994, Growth of a submarine meandering channel-levee system on the Amazon Fan.

Pirmez, C., Beaubouef, R.T., Friedmann, S.J., and Mohrig, D.C., 2000, Equilibrium profile and base level in submarine channels: examples from late Pleistocene systems and implications for the architecture of deep-water reservoirs, *in* Weimer, P., Slatt, R.M., Coleman, J., Rosen, N.C., Nelson, H., Bouma, A.H., Styzen, M.J., and Lawrence, D.T., eds., Deep-Water Reservoirs of the World, Volume III, G.C.S.S.E.P.M., p. 782-805.

Pirmez, C., and Flood, R.D., 1995, Morphology and structure of Amazon Channel, *in* Flood, R.D., Piper, D.J.W., Klaus, A., and al., e., eds., Proceedings of the Ocean Drilling Program, Initial Reports 155, Ocean Drilling Program, College Station, TX, p. 23-45.

Pirmez, C., Hiscott, R.N., and Kronen, J.D., Jr., 1997, Sandy turbidite successions at the base of channel-levee systems of the Amazon Fan revealed by FMS logs and cores: unraveling the facies architecture of large submarine fans, *in* Flood, R.D., Piper, D.J.W., Klaus, A., and Peterson, L.C., eds., Proceedings of the Ocean Drilling Program, Scientific Results, Volume 155, p. 7-33.

Pirmez, C., Imran, J., and Mutti, E., 2003, Reconstruction of turbidity currents in Amazon Channel, *in* Steffens, G.S., Pirmez, C., Orlando, M., and Roberts, D., eds., Marine and Petroleum Geology, Volume 20: Oxford, Elsevier, p. 823-849.

Popescu, I., Lericolais, G., Panin, N., Wong, H.K., and Droz, L., 2001, Late Quaternary channel avulsions on the Danube deep-sea fan, Black Sea: Marine Geology, v. 179, p. 25-37.

Posamentier, H.W., 2003, Depositional elements associated with a basin floor channel-levee system; case study from the Gulf of Mexico Turbidites; models and problems v. 20, p. 677-690.

Posamentier, H.W., and Kolla, V., 2003, Seismic geomorphology and stratigraphy of depositional elements in deep-water settings: Journal of Sedimentary Research, v. 73, p. 367-388.

Posamentier, H.W., and Mutti, E., 2003, Depositional elements associated with a basin floor channel-levee system; case study from the Gulf of Mexico, *in* Steffens, G.S., Pirmez, C., Orlando, M., and Roberts, D., eds., Marine and Petroleum Geology, Volume 20: Oxford, Elsevier, p. 677-690.

Posamentier, H.W., and Vail, P.R., 1988, Eustatic controls on clastic deposition II - sequence and systems tract models, *in* Wilgus, C.K., ed., Sea level channges: An intergrated approach, Volume 42, SEPM Special Publications, p. 125-154.

Prather, B.E., 1998, A Gulf of Mexico based depositional process model for above-grade slopes, *in* Anonymous, ed., AAPG international conference and exhibition; abstracts., Volume 82; 10: AAPG Bulletin: Tulsa, OK, United States, American Association of Petroleum Geologists, p. 1953.

—, 2003, Controls on reservoir distribution, architecture and stratigraphic trapping in slope settings: Marine and Petroleum Geology, v. 20, p. 529-545.

Pratson, E.L., Pirmez, C., Goldberg, D., and Ocean Drilling Program, L., Shipboard Scientific Party, College Station, Tx, United States,, 1994a, Refining lithologic interpretation through mineral inversion on the Amazon Fan, *in* Anonymous, ed., AGU 1994 fall meeting., Volume 75; 44 Suppl.: Eos, Transactions, American Geophysical Union: Washington, DC, United States, American Geophysical Union, p. 315.

Pratson, L.F., and Coakley, B.J., 1996, A model for the headward erosion of submarine canyons induced dy downslope-eroding sediment flows: Geological Society of America Bulletin, v. 108, p. 225-234.

Pratson, L.F., and Haxby, W.F., 1996, What is the slope of the U.S. continental slope?: Geology, v. 24, p. 3-6.

Pratson, L.F., Ryan, W.B.F., Mountain, G.S., and Twichell, D.C., 1994b, Submarine canyon initiation by downslope eroding sediment flows: evidence in the late Cenozoic strata on the New Jersey continental slope: Geological Society of America Bulletin, v. 106, p. 395-412.

Prins, M.A., and Postma, G., 2000, Effects of climate, sea level, and tectonics unraveled for last deglaciation turbidite records of the Arabian Sea: Geology, v. 28, p. 375-378.

Prior, D.B., Adams, C.E., and Coleman, J.M., 1983, Characteristics of a deep-sea channel on the middle Mississippi Fan as revealed by a high-resolution survey, *in* Bogard, M.B.E., and Fritts, J., eds., Transactions, Gulf Coast Association of Geological Societies, a section of the American Association of Petroleum Geologists., Volume 33: Transactions - Gulf Coast Association of Geological Societies: New Orleans, LA, United States, Gulf Coast Association of Geological Societies, p. 389-394.

Raillard, S., Vendeville, B.C., Guerin, G., Mauduit, T., and Anonymous, 1997, Causes and structural characteristics of thin-skinned inversion during gravity gliding or spreading above salt or shale, American Association of Petroleum Geologists 1997 annual convention, Volume 6: Tulsa, OK, American Association of Petroleum Geologists and Society of Economic Paleontologists and Mineralogists, p. 95.

Reading, H.G., and Richards, M., 1994, Turbidite systems in deep-water basin margins classified by grain size and feeder system: AAPG Bulletin, v. 78, p. 792-822.

Reis, A.T., Perovano, R., Silva, C.G.V., B C , Araujo, E., Gorini, C., and Oliveira, V., 2010, Multi-gravitational collapse in the Amazon Deep-sea Fan: a coupled system of gravity tectonics and mass wasting processes: Journal of the Geological Society, v. 167, p. 593-604.

Richards, M., and Bowman, M., 1998, Submarine fans and related systems II: variability in reservoir architecture and wireline log character: Marine and Petroleum Geology, v. 15, p. 821-839.

Richards, M., Bowman, M., and Reading, H., 1998, Submarine-fan systems i: characterization and stratigraphic prediction: Marine and Petroleum Geology, v. 15, p. 689-717.

Ridente, D., Foglini, F., Minisini, D., Trincardi, F., and Verdicchio, G., 2007, Shelf-edge erosion, sediment failure and inception of Bari Canyon on the Southwestern Adriatic Margin (Central Mediterranean): Marine Geology, v. In Press, Corrected Proof.

Rowan, M.G., Peel, F.J., and Vendeville, B.C., 2004, Gravity-driven fold belts on passive margins, *in* McClay, K.R., ed., Thrust tectonics and hydrocarbon systems, AAPG Memoir 82, Volume 82, p. 157-182.

Samuel, A., Kneller, B., Raslan, S., Sharp, A., and Parsons, C., 2003, Prolific deep-marine slope channels of the Nile Delta, Egypt: AAPG Bulletin, v. 87, p. 541-560.

Schumm, S.A., 1993, River Response to Baselevel Change: Implications for Sequence Stratigraphy: The Journal of Geology, v. 101, p. 279-294.

Schwenk, T., Spie, V., Breitzke, M., and Hubscher, C., 2005, The architecture and evolution of the Middle Bengal Fan in vicinity of the active channel-levee system imaged by high-resolution seismic data: Marine and Petroleum Geology, v. 22, p. 637-656.

Schwenk, T., Spiess, V., Huebscher, C., and Breitzke, M., 2003, Frequent channel avulsions within the active channel-levee system of the middle Bengal Fan; an exceptional channel-levee development derived from Parasound and Hydrosweep data: Deep-Sea Research. Part II: Topical Studies in Oceanography, v. 50, p. 1023-1045.

Shanmugam, G., 1996, High-density turbidity currents; are they sandy debris flows?: Journal of Sedimentary Research, Section A: Sedimentary Petrology and Processesj, v. 66, p. 2-10.

—, 2003, Deep-marine tidal bottom currents and their reworked sands in modern and ancient submarine canyons: Marine and Petroleum Geology, v. 20, p. 471-491.

Shanmugam, G., and Moiola, R.J., 1991, Types of submarine fan lobes; models and implications: AAPG Bulletin, v. 75, p. 156-179.

Shaw, J.H., Connors, C.D., and Suppe, J., 2005, Seismic interpretation of contractional fault-related folds: an AAPG seismic atlas, AAPG studies in geology #53: Tulsa, Oklahoma, U.S.A.

Shepard, F.P., 1933, Submarine valleys: Geographical Review, v. 23, p. 77-89.

Silva, S.R.P., Maciel, R.R., and Severino, M.C.G., 1999, Cenozoic tectonics of Amazon Mouth Basin: Geo-Marine Letters, v. 18, p. 256-262.

Simpson, J.E., 1997, Gravity Currents in the Environment and the Laboratory: New York, Cambridge Univ. Press.

Skene, K.I., Piper, D.J.W., and Hill, P.S., 2002, Quantitative analysis of variations in depositional sequence thickness from submarine channel levees: Sedimentology, v. 49, p. 1411-1430.

Smith, R., 2004a, Silled sub-basins to connected tortuous corridors; sediment distribution systems on topographically complex sub-aqueous slopes: Geological Society Special Publications, v. 222, p. 23-43.

—, 2004b, Turbidite systems influence by structurally induced topography in the multi-sourced Welsh Basin: Geological Society Special Publications, v. 222, p. 209-228.

Spathopoulos, F., 1996, An insight on salt tectonics in the Angola Basin, South Atlantic, *in* Alsop, G.I., Blundel, D.J., and I, D., eds., Salt tectonics, Geological society (London) Special Publication 100, p. 153-174.

Spinelli, G.A., and Field, M.E., 2001, Evolution of Continental Slope Gullies on Northern California Margin: Journal of Sedimentary Research, v. 71, p. 237-245.

Sprague, A.R., Sullivan, M.D., Campion, K.M., Jensen, G.N., Goulding, F.J., Sickafoose, D.K., and Jennette, D.C., 2002, The physical stratigraphy of deep-water stratal a hierarchical approach to the analysis of genetically–related stratigraphic elements for improved reservoir prediction, AAPG Annual Convention Abstracts: Houston, TX, p. 10-13.

Stelting, C.E., 1985, Migratory characteristics of a mid-fan meander belt, Mississippi Fan, *in* Bouma, A.H., Normark, W.R., and Barnes, N.E., eds., Submarine fans and related turbidite systems.: New York, NY, United States, Springer-Verlag, p. 283-290.

Stelting, C.E., Pickering, K.T., Bouma, A.H., Coleman, J.M., Cremer, M., Droz, L., Meyer, W.A.A., Normark, W.R., O, C.u., Stow, D.A.V., and Deep Sea Drilling Project, L.S.S., United States,, 1985, Drilling results on the Middle Mississippi Fan, *in* Bouma, A.H., Normark, W.R., and Barnes, N.E., eds., Submarine fans and related turbidite systems.: New York, NY, United States, Springer-Verlag, p. 275-282.

Stow, D.A.V., Reading, H.G., and Collinson, J.D., 1996, Deep seas, *in* Reading, H.G., ed., Sedimentary environments; processes, facies and stratigraphy.: Oxford, United Kingdom, Blackwell Science, p. 395-453.

Straub, K.M., Mohrig, D., McElroy, B., Buttles, J., and Pirmez, C., 2008, Interactions between turbidity currents and topography in aggrading

sinuous submarine channels: A laboratory study: Geological Society of America Bulletin, v. 120, p. 368-385.

Sultan, N., Voisset, M., Marsset, B., Marsset, T., Cauquil, E., and Colliat, J., 2007, The Potential role of compressional structures in

generating submarine slope failures in the Niger Delta: Marine Geology, v. 237, p. 169-190.

Suppe, J., Chou, G.T., and Hook, S.C., 1992, Rates of folding and faulting determined from growth strata, *in* Mcclay, K.R., ed., Thrust Tectonics: London, Chapman and Hall, p. 105-121.

Swarbrick, R.E., Osborn, M.J., and Yardley, G.S., 2002, Comparison of overpressure magnitude resulting from the main generating mechanisms, *in* Huffman, A.R., and Bowers, G.L., eds., Pressure regimes in sedimentary basins and their prediction.: Tulsa, American Association of Petroleum Geologists, p. 1-12.

Sykes, T.J.S., Ramsay, A.T.S., and Kidd, R.B., 1998, Southern hemisphere Miocene bottom-water circulation: a palaeobathymetric analysis, *in* CRAMP, A., MACLEOD, C.J., LEE, S.V., and JONES, E.J.W., eds., Geological Evolution of Ocean Basins: Results from the Ocean Drilling Program, Volume 131, Geological Society, London, Special Publications, p. 43-54.

Twichell, D.C., and Roberts, D.G., 1982, Morphology, distribution, and development of submarine canyons on the United States Atlantic continental slope between Hudson arid Baltimore Canyons: Geology, v. 10, p. 408-412.

Twichell, D.C., Schwab, W.C., Nelson, C.H., Kenyon, N.H., and Lee, H.J., 1992, Characteristics of a sandy depositional lobe on the outer Mississippi fan from SEAMARC 1A sidescan sonar images: Geology, v. 20, p. 689-692.

Vail, P.R., 1987, Seismic stratigraphy interpretation using sequence stratigraphy, *in* Bally, A.W., ed., Atlas in seismic stratigraphy:AAPG studies in geology, Volume 27 Part I.

Vendeville, B.C., 2005, Salt tectonics driven by sediment progradation: Part I--Mechanics and kinematics, Volume 89, p. 1071-1079.

Wagoner, V., Mitchum, R.M., Campion, K.M., and Rahmanian, V., 1990, Siliciclastic sequence stratigraphy in well logs, cores, and outcrops American Association of Petroleum Geologists, Methods in Exploration Series 7.

Walker, R.G., 1985, Comparison of shelf environments and deep basin turbidite systems, *in* Tillman, R.W., Swift, D.J.P., and Walker, R.G., eds., Shelf sands and sandstone reservoirs., Volume 13: SEPM Short Course: Tulsa, OK, United States, Society of Sedimentary Geology, p. 465-502.

Weaver, P.P.E., Rothwell, R.G., Ebbing, J., Gunn, D., and Hunter, P.M., 1992, Correlation, frequency of emplacement and source directions of megaturbidites on the Madeira abyssal plain, *in* Middelburg, J.J., and Nakashima, S., eds., The geochemistry of North Atlantic abyssal plains.,

Volume 109; 1-2: Marine Geology: Amsterdam, Netherlands, Elsevier, p. 1-20.

Weber, M.E., Wiedicke, M.H., Kudrass, H.R., Huebscher, C., and Erlenkeuser, H., 1997, Active growth of the Bengal Fan during sea-level rise and highstand: Geology (Boulder), v. 25, p. 315-318.

Weimer, P., 1990, Sequence stratigraphy, facies geometries, and depositional history of the Mississippi Fan, Gulf of Mexico: AAPG Bulletin, v. 74, p. 425-453.

—, 1991, Seismic facies, characteristics, and variations in channel evolution, Mississippi Fan (Plio-Pleistocene), Gulf of Mexico, *in* Weimer, P., and Link, M.H., eds., Seismic facies and sedimentary processes of submarine fans and turbidite systems.: New York, NY, United States, Springer-Verlag, p. 323-347.

Winker, C.D., 1981, Cenozoic shelf margins, northwestern Gulf of Mexico basin. Recognition of shallow-water versus deep-water sedimentary facies in growth-structure affected formations of the Gulf Coast Basin; program and abstracts.: Society of Economic Palaeontologists and Mineralogists, Gulf Coast Section, p. 74-82.

Winker, C.D., and Booth, J.R., 2000, Sedimentary dynamics of the salt-dominated continental slope, Gulf of Mexico; integration of observations from the seafloor, near-surface, and deep subsurface American Association of Petroleum Geologists 2000 annual meeting v. 2000, p. 158.

Wood, L.J., and Mize-Spansky, K.L., 2009, Quantitative seismic geomorphology of a Quaternary leveed-channel system, offshore eastern Trinidad and Tobago, northeastern South America: AAPG Bulletin, v. 93, p. 101-125.

Worrall, D., and Snelson, S., 1989, Evolution of the nothern Gulf of Mexico, with emphasis on Cenozoic growth faulting and the role of salt, *in* Bally, A., and Palmer, A., eds., The Geology of North America: an overview. , Geological Society of America, p. 97-138.

Wynn, R.B., Cronin, B.T., and Peakall, J., 2007, Sinuous deep-water channels: Genesis, geometry and architecture: Marine and Petroleum Geology, v. 24, p. 341-387.

Wynn, R.B., Kenyon, N.H., Masson, D.G., Stow, D.A.V., and Weaver, P.P.E., 2002, Characterization and Recognition of Deep-Water Channel-Lobe Transition Zones: AAPG Bulletin, v. 86, p. 1441-1462.

Zalan, P.V., 2004, End members of gravitacional fold and thrust belts (GFTBs) in the deep waters of Brazil, *in* Mcclay, K.R., ed., Seismic Interpretation of contractional fault-related folds, AAPG Seismic Atlas . Studies in Geology 53.

Zaragosi, S., Auffret, G.A., Faugeres, J.C., Garlan, T., Pujol, C., and Cortijo, E., 2000, Physiography and Recent sediment distribution of the Celtic deep-sea fan, Bay of Biscay: Marine Geology, v. 169, p. 207-237.